

**Aggregation of Small Molecules in Cryogenic Matrices and
Reaction of Aryl Radicals with Small Molecules
Matrix Isolation and Computational Studies**

Dissertation
for the Degree of
Doktor der Naturwissenschaften (Dr. rer. nat.)
Ruhr-Universität Bochum

Artur Mardyukov

2010

Partial results of this work were already published in the following contributions:

Publications:

1. "Furan-Formic Acid Dimers: An ab Initio and Matrix Isolation Study."

Sanchez-Garcia, Elsa; Mardyukov, Arthur; Studentkowski, Marc; Montero, Luis A., Wolfram Sander. *Journal of Physical Chemistry A* (2006), 110(51), 13775-13785.

2. "Formamide Dimers: A Computational and Matrix Isolation Study."

Mardyukov, Artur; Sanchez-Garcia, Elsa; Rodziewicz, Pawel; Doltsinis, Nikos L.; Sander, Wolfram. *Journal of Physical Chemistry A* (2007), 111(42), 10552-10561.

3. "Ab initio and matrix isolation study of the acetylene-furan dimer."

Sanchez-Garcia, Elsa; Mardyukov, Artur; Tekin, Adem; Crespo-Otero, Rachel; Montero, Luis A.; Sander, Wolfram; Jansen, Georg. *Chemical Physics* (2008), 343(2-3), 168-185.

4. "Matrix Isolation and Ab Initio Study of the Noncovalent Complexes between Formamide and Acetylene."

Mardyukov, Artur; Sanchez-Garcia, Elsa; Sander, Wolfram. *Journal of Physical Chemistry A* (2009), 113(6), 1086-1095.

5. "Matrix isolation and spectroscopic characterization of the phenylperoxy radical and its rearranged products."

Mardyukov, Artur; Sander, Wolfram. *Chemistry--A European Journal* (2009), 15(6), 1462-1467.

6. "Interaction and Reaction of the Phenyl Radical with Water: A Source of OH Radicals."

Mardyukov, Artur; Sanchez-Garcia, Elsa; Crespo-Otero, Rachel; Sander, Wolfram. *Angewandte Chemie, International Edition* (2009), 48(26), 4804-4807,

7. "Photochemistry and reactivity of the phenyl radical – water system: A matrix isolation and computational study"

Mardyukov, Artur; Crespo-Otero, Rachel; Sanchez-Garcia, Elsa; Sander Wolfram. *Chemistry--A European Journal* (2010) accepted.

8. "Matrix Isolation and IR Characterization of the Benzoyl and Benzoyl Peroxy Radicals"

Mardyukov, Artur; Sander Wolfram. *European Journal of Organic Chemistry* (2010), 15, 2904-2909.

Poster contributions:

1. "Aggregation of small molecules in cryogenic matrices. Non-covalent complexes of Formamide-Acetylene and Formamide-Formic Acid"

Mardyukov, Artur; Sanchez-Garcia, Elsa; Sander, Wolfram. At the International Symposium of Reactive Intermediates and Unstable Molecules (ISRIUM 2007), Ascona, Switzerland, (19-24 August 2007).

2. "Matrix Isolation and Photochemistry of Phenyl Peroxy Radical"

Artur Mardyukov, Wolfram Sander. 19th IUPAC Conference on Physical Organic Chemistry, The Royal University of Santiago de Compostela, Spain, (13-18 July 2008).

3. "Matrix-Isolated Spectra of Phenyl Peroxy Radical"

Artur Mardyukov, Wolfram Sander. 7th International Conference of Low Temperature Chemistry, Helsinki, Finland, (24-29 August 2008).

4. "Photochemistry of N-methylformamide: Monomers, Dimers"

Mardyukov, Artur; Sanchez-Garcia, Elsa; Sander, Wolfram. On non-covalent interactions in chemistry and biochemistry. Czocha castle, Poland (21-28 September 2008) (**oral presentation**).

5. "Complete Story of the Reaction of Phenyl Radical with Water: A Matrix Isolation Study."

Mardyukov, Artur; Sanchez-Garcia, Elsa; Sander, Crespo-Otero, Rachel; Sander, Wolfram. At the International Symposium of Reactive Intermediates and Unstable Molecules (ISRIUM 2009), Liblice Castle near Prague, Czech Republic, (5-10 July 2009).

6. "Matrix Isolation and Photochemistry of Phenyl Radical – Water System"

Mardyukov, Artur; Sanchez-Garcia, Elsa; Sander, Crespo-Otero, Rachel; Sander, Wolfram. 7th Seminars of Advanced Studies on Molecular Design and Bioinformatics: Molecular Interactions, Havana, Cuba, (22-28 August 2009).

Workshops:

1. Workshop Forschergruppe 618. Ruhr-University Bochum, 13 February 2006 (Oral presentation).
2. Workshop Forschergruppe 618. Ruhr-University Bochum, 06 November 2006 (Oral presentation).
3. Workshop Forschergruppe 618. Ruhr-University Bochum, 12 October 2007 (Oral presentation).
4. Workshop Forschergruppe 618. Ruhr-University Bochum, 10 February 2010 (Oral presentation).

This work was carried out between October 2005 and April 2010 under the supervision of Prof. Dr. Wolfram Sander, Department of Organic Chemistry II, Ruhr University Bochum.

First of all I would like to record my sincere gratitude to Prof. Dr. Wolfram Sander for his supervision, advice, and guidance from the very early stage of this research as well as giving me extraordinary experiences throughout the work. Above all and the most needed, he provided me unflinching encouragement and support in various ways. I am also very thankful for providing me the research facilities and the financial support.

First Referee: Prof. Dr. Wolfram Sander

Second Referee: Prof. Dr. Martina Havenith

Dissertation submitted on:

Disputation on:

To my family

Abstract	i
Chapter 1. General Introduction of H-Bond	1
1.1. Van der Waals interactions.....	1
1.2. Hydrogen bond.	1
1.3. Historical and prospective aspects of the Hydrogen Bond.....	2
1.4. Intermolecular and Intramolecular Hydrogen bonds.....	3
1.5. Classification of H-bonds.	4
1.6. Application of H-bonds	8
1.7. Some experimental methods of studying hydrogen bonds.....	9
1.8. Experimental Evidences of Hydrogen Bond Presence	12
1.9. H/D Substitution in H–bonds	13
1.10. Proton Transfer or H–atom Transfer	13
Chapter 2. Concepts and Theoretical insight	15
Chapter 2.1. Technique and equipment.....	15
2.1.1. Matrix Isolation	15
2.1.2. Equipment.....	15
2.1.3. Precursors and deposition methods	16
2.1.4. The generation of reactive intermediates.....	17
2.1.5. Matrix effects.....	18
Chapter 2.2. Quantum chemical methods.....	20
2.2.1. Calculation of Molecular Energy	20
2.2.2. Density Functional Theory (DFT).....	21
Chapter 3. Noncovalent complexes of Formamide	22
Chapter 3.1. Aggregation of formamide.....	22
3.1.1. Introduction	22
3.1.2. Results and Discussion	24
3.1.2.2. Argon matrix	28
3.1.2.2. Xenon Matrix.....	32
3.1.3 Conclusion.....	33
Chapter 3.2. Formamide - Acetylene.....	36
3.2.1. Introduction	36
3.2.2. Results and Discussion	37

3.2.2.1. Experimental results	37
3.2.2.1.1. Argon Matrix	37
3.2.2.1.2. Nitrogen Matrix	42
3.2.2.2. Computational results	47
3.2.2.2.1. Dimers	47
3.2.2.2.2. Trimers	49
3.2.2.3. Comparison of Calculated and Experimental Vibrational	52
3.2.2.3.1. Frequencies: Dimers A and B	52
3.2.2.4. Comparison of Calculated and Experimental Vibrational Frequencies: Trimers	58
3.2.2.5. Conclusions	60
Chapter 3.3. Formamide and Formic Acid Dimers	61
3.3.1. Introduction	61
3.3.2. Result and Discussion	61
3.3.2.1. Experimental Results	61
3.3.2.2. Comparison of calculated and experimental vibrational frequencies.	64
Chapter 4. Furan – Formic Acid Dimers	68
4.1. Introduction	68
4.2. Matrix Isolation Studies	68
4.3. Conclusion	76
Chapter 5. Acetylene – Furan	77
5.1. Introduction	77
5.2. Results and Discussion	77
5.2.1. Vibrational assignments	82
5.2. Conclusion	86
Chapter 6. N-methylformamide: Monomers and Dimers	87
Chapter 6.1. N-methylformamide-Monomers	87
6.1.1. Introduction	87
6.1.2. Results and Discussion	90
6.1.2.1. FT-IR Spectra of N-methylformamide in Rare Gas Matrices	90
6.1.2.2. Photochemistry of NMF. Photoconversion of the <i>trans</i> - conformer to the <i>cis</i> - conformer	91
6.1.2.3. Formation of N-methylformimidic acid	97

6.1.2.4. Formation of $\text{H}_2\text{NCH}_3:\text{CO}$ and $\text{HNCO}:\text{CH}_4$ complexes	102
6.1.3. Conclusion	104
Chapter 6.2. NMF–Dimers: Aggregation and Photochemistry	105
6.2.1. Introduction	105
6.2.1.1. Computational Results	105
6.2.1.2. Matrix Isolation Experiments	109
6.2.1.3. Conclusion	115
6.2.1.3. <i>Trans–Cis</i> Photoisomerization in dimer of NMF	116
Chapter 6.3. NMF – Methanol	120
6.3.1. Introduction	120
6.3.2. Results and discussion	120
6.3.2.1. Computational results	120
6.3.2.2. Experimental results	123
6.3.3. Comparison of the Computed and the Experimental Vibrational Frequencies	129
6.3.3.4. Conclusion	136
Chapter 7. Interaction and Reaction of Phenyl Radical with small molecules	137
7.1. Introduction (Phenyl Radical)	137
Chapter 7.2. Phenyl Peroxy Radical	143
7.2.1. Introduction	143
7.2.2. Results and Discussion	146
7.2.3. Summary	160
Chapter 7.3. Benzoyl Radical	162
7.3.1. Introduction	162
7.3.2. Results and Discussion	163
7.3.3. Summary	177
Chapter 7.4. Phenyl Radical - Water	178
7.4.1. Introduction	178
7.4.2. Results and Discussion	179
7.4.2.1 Matrix Isolation Studies the phenyl radical –water system	179
7.4.2.2. Computational studies the phenyl radical –water dimers	187
7.4.2.3 Photochemistry of the phenyl radical – water complex	192

7.4.2.4. Computational studies the Benzene – OH dimers.....	198
7.4.2.5. Photochemistry of the Benzene – OH dimer.....	201
7.4.2.6. Calculation of the ring opening.....	205
7.4.3. Summary	217
Chapter 8. Pyridyl Radicals	220
8.1. Introduction.....	220
8.2. Molecular and electronic structure.....	222
8.3. Matrix Isolation Study.....	226
8.3.1. <i>o</i> -Pyridyl Radical (24).....	226
8.3.2. <i>o</i> -Pyridyl Peroxy Radicals (28a and 28b)	228
8.4.1. <i>p</i> -Pyridyl Radical (26).....	237
8.4.2. <i>p</i> -Pyridyl Peroxy Radical (32).....	241
8.5.1. <i>m</i> -Pyridyl Radical (25).....	245
8.5.2. <i>m</i> - Pyridyl Peroxy Radicals (34a and 34b).....	247
8.4. Summary	253
9. General Summary	254
9.1. Aggregation of formamide in inert matrices at low temperature conditions	254
9.2. Formamide –Acetylene complexes	255
9.3. Furan–Formic Acis	256
9.4. Acetylene-Furan.....	257
9.5. N-methylformamide: Monomers and Dimers.....	258
9.6. NMF–Methanol.....	260
9.7. Phenyl Peroxy Radical	261
9.8. Benzoyl Radical	262
9.9. Phenyl radical –water. A pre-reactive complex	262
9.10. Pyridyl radicals.....	263
Chapter 10. Methods and matherials	265
10.1. Synthesis.....	265
10.2. Analytical equipments.....	265
10.3. Matrix Isolation Set-up.....	265
10.3.1. Apparatus	265
10.3.2. Deposition	265
10.3.3. Flash vacuum pyrolysis (FVP).....	266

10.3.4. IR- and UV- spectrometers.....	266
10.3.5. Light Sources.....	266
10.4. Quantum chemical calculations.....	266
Chapter 11. Synthesis.....	267
Chapter 12. Appendix.....	268
12.1. Quantum chemical calculations.....	268
Chapter 13. References.....	282
<u>PERSONA DATA</u>.....	298

Abstract

Hydrogen bonds range from the very strong, comparable with covalent bonds, to the very weak, comparable with van der Waals forces. Most hydrogen bonds are weak interactions with a binding strength about one-tenth of that of a normal covalent bond. Nevertheless, they are very important. Without them, biological systems would not exist, and all living things would disintegrate into lifeless matter.

The description of properties of noncovalent bonds starts with that of the exceptional features it displays in its vibrational spectra. IR spectroscopy in combination with the matrix isolation technique appears is a precise tool to observe H-bonds.

Matrix isolation infrared spectroscopy and quantum chemical calculations were carried out to investigate H-bonded complexes of closed shell as well open shell species. Dimers and larger aggregates of formamide, N-methylformamide, formamide – acetylene, furan – formic acid, phenyl radical – water were obtained under low temperature conditions. Experimental data (IR frequencies and frequency shifts) compared to the calculated frequencies allowed us to characterize the trapped species. The photochemistry of monomers and dimers were also investigated. Particularly, N-methylformamide undergoes a *trans- cis-* isomerization under irradiation with a 248 nm laser. Prolonged irradiation results in complete decomposition of the monomeric forms of NMF, while dimers do not undergo photodissociation under UV irradiation.

We also have isolated and characterized complexes between the phenyl radical and water and between the hydroxyl radical and benzene for the first time. We observed light-driven hydrogen-atom transfer from water to the phenyl radical within these complexes. Our results demonstrate the importance of radical complexes for the understanding of radical reactivity. We expect that this phenomenon is also of importance for the understanding of radical reactions in biological media.

Chapter 1. General Introduction of H-Bond

1.1. *Van der Waals interactions.*

When two identical molecules come in close proximity they, nevertheless, undergo residual electrostatic interactions called Van der Waals interactions. Energies of Van der Waals interactions are typically of the order of about 0.01 eV (1 eV= 23.06037 kcal/mol) for small molecules, which is at least two orders of magnitude smaller than the energies of covalent bonds. Vdw complexes play a fundamental role in fields as diverse as supramolecular chemistry, structural biology, polymer science, nanotechnology, surface science, and condensed matter physics.^[1]

1.2. *Hydrogen bond.*

Hydrogen Bond^[1] occur between molecular groups, most often O–H or N–H, which carries an H atom and exhibits a marked electrical dipole moment, and O– or N– atom another molecule. This latter atom is characterized by the presence of at least one nonbonding orbital that can point towards the H-atom of the polar group of the first molecule and is filled with a lone pair of electrons.^[1-3]

In addition, there is a nonnegligible electron density transfer from a proton acceptor to a donor.^[4] Electron density is transferred from the proton acceptor (lone pair) to the σ^* -antibonding orbital of the X–H bond, which causes a weakening and elongation of this bond and a decrease in the X–H stretch frequency. The electrostatic character of H-bonds was described first by Pauling.^[5] Some H-bonds also have charge-transfer character and the H...Y link can also be partly covalent. The electrostatic character is dominating generally in the O–H...N, N–H...O, O–H...O bonds.^[2]

This H-bond “acceptor site” may also be an extended π electron cloud such as found with aromatic rings, also filled with electron pairs that point towards this H-atom. The “donating” molecular groups, (O–H or N–H) made of covalently bound atoms, retain their identities upon formation of this H-bond (Figure 1.1).^[2, 6, 7] The polar group that carries the H-atom is called “donor”, while the group O or N with a nonbonding orbital is called the “acceptor”. This designation leads for definition that H-bond acceptor acts as an electron donor, and a H-bond donor as a acceptor.^[1]

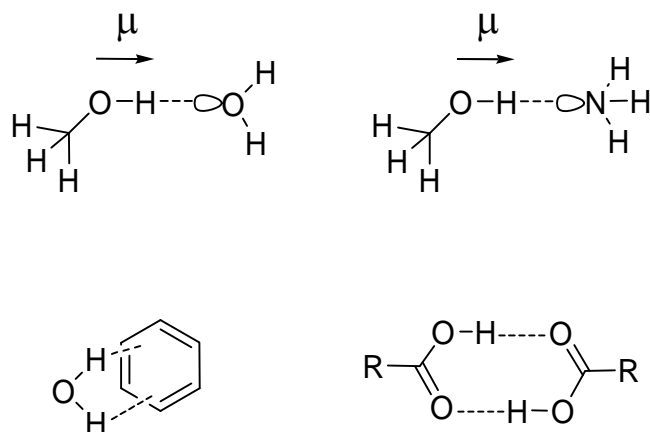


Figure 1.1. H-bonds X–H...Y between various molecules.

In classical H-bonding there is a shortening of the X...Y distance if X–H is H-bonded to Y. The distance between X...Y is less than the sum of the van der Waals radii of the two atoms X and Y. H-bonding interactions lead to an increase in the X–H bond distance. As a consequence, a substantial red shift (of the order of 100 cm^{-1}) is observed in the fundamental X–H stretching vibrational frequencies. The O...O distance between two O-atoms of an OH...O bond is shorter than the distance defined by Van der Waals radii. It is typically 2.8 Å for an OH...O bond, but may vary between 2.5 and 3 Å depending on OH and Y.^[8] The enthalpy of formation of such kind of H-bond is 0.1 eV for a weak H-bond and can reach 0.7 eV for a strong H-bond.^[2] These enthalpies are between the enthalpies of covalent and Van der Waals bonds.

1.3. Historical and prospective aspects of the Hydrogen Bond.

The concept of the H-bond slowly emerged in the 20th century and took some time to be fully accepted. In 1902, Werner^[9] described an interaction which is now called the H-bond. He suggested that hydrated ammonium NH_4OH should be better written as H-O-H...NH_3 . He called this interaction *Nebenvalenzbindung*. Later, in 1911, Hantzsch^[10] described the existence of such kind of a bond in acetoacetic acid ester. In 1920, Latimer and Rodebus,^[11] postulated that if an H-atom lies between two electronic octets, a weak bond appears. At that time the H-bond was recognized as responsible for the anomalous properties of liquid water.

The concept “hydrogen bond” was developed after 1930 and described in the famous book “*Nature of the Chemical Bond*” written by Pauling.^[5] According to Pauling the hydrogen bond is described as follows: “*Under certain conditions an atom of hydrogen is attracted by rather strong forces to two atoms instead of only one, so it may be considered*

to be acting as a bond between them. This is called a hydrogen bond” and “A hydrogen atom with only one stable orbital cannot form more than one pure covalent bond and the attraction of the two atoms observed in hydrogen bond formation must be due largely to ionic forces”.

The first comprehensive compilation of the basic properties of H-bonds, mainly thermodynamic, structural and spectroscopic properties was written by Pimentel and McClellan.^[12] They give a more general definition of hydrogen bond: “A hydrogen bond exists between the functional group, A-H, and an atom or a group of atoms B, in the same or different molecules when (a) there is evidence of bond formation (association or chelation), (b) there is evidence that this new bond linking A-H and B specifically involves a hydrogen atom already bonded to A”. It is important to realize that the Pimentel and McClellan definition makes no assumptions about the nature of the A and B atoms, and that it enables an evaluation of the hydrogen bonding potential of groups like C-H and π acceptors.

In 1997, Jeffrey^[1] wrote a textbook “An Introduction to Hydrogen Bonding”, with a focus on the structural aspects of H-bonds.

Recently, Desiraju suggested the term hydrogen bridge to represent the H-bond.^[2] Since the H-bonding strength ranges from van der Waals to covalent limit, hydrogen bridge is a better description of the interaction without any borders. The description of H-bond is follows: “A hydrogen bond, X-H...A, is an interaction wherein a hydrogen atom is attracted to two atoms, X and A, rather than just one and so acts like a bridge between them. It was recognized from early times that this attraction always increases with the increasing electronegativity of X and A, and the electrostatic nature of all hydrogen bonds is accepted without question. It is important to note that the term “electrostatic” is used here to refer to interactions that have an r^{-1} to r^{-3} energy/distance dependence or thereabouts, so that dipole-dipole interactions are included”.

1.4. Intermolecular and Intramolecular Hydrogen bonds.

Most H-bonds X-H...Y that are formed between two independent X-H and Y molecules as represented in Figure 1.1 are classified as “intermolecular H-bonds”. Another category of H-bonds are the “intramolecular H-bonds”, where molecular groups X-H and Y are both parts of a same molecule. The intramolecular H-bonds include quite a large variety of H-bonds. Two typical examples are shown in Figure 1.2.^[13]

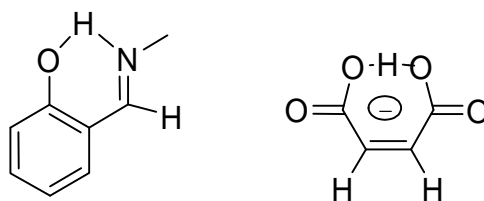


Figure 1.2. Two intramolecular H-bonds in an aromatic Schiff (left drawing) and in maleate anion (right drawing).

An intramolecular H-bond involves a single molecule, while an intermolecular H-bond involves two molecules that become independent upon disruption of the H-bond. Consequently, intermolecular H-bonds, which establish relatively strong interactions between molecules in a liquid, are known to strongly influence the boiling temperature and heat of evaporation of a liquid.^[14] The best example is liquid water. In contrast, intramolecular H-bonds do not modify the interactions between molecules. The gas phase, intermolecular H-bonds are at the origin of deviations from perfect gas law, which is not so for intramolecular H-bonds. Also, in an intermolecular H-bond the relative positions of the donor and acceptor groups, X–H and Y, are only controlled by the H-bond interaction.^[2] The other groups of the molecule have almost no influence on these relative positions, as shown in Figure 1.1. This is not the case with an intramolecular H-bond. Thus, the relative positions of the three atoms that form the –O–H...N– or –O–H...O– bonds in Figure 1.2 are first governed by the surrounding covalent bonds that are predominated and imposed their own steric conditions.^[15]

1.5. Classification of H-bonds.

The hydrogen bond energy, E_{HX} , is not physically observable and therefore it is not directly measurable.^[1] In the case of intermolecular hydrogen bond, E_{HX} is the difference between the energy of the adduct and the sum of the energies of the separate component molecules by a long distance and consequently do not establish H-bonds. According to the values of enthalpies of formation the H-bond, H-bonds are roughly divided into three categories: strong, intermediate (moderate) and weak H-bonds.

The strength of the strong H-bonding interactions ranges from 15.0 to 40 kcal/mol. For the moderate and weak H-bonds, the strengths vary from 4 – 15 to 1 – 4 kcal/mol, respectively. The strength of H-bonded interactions in different molecular systems has been classified by many authors.^[1, 2, 16] The three types of H-bonding interactions which

are most often discussed in literature are weak, moderate, and strong. The properties of these three types are listed in Table 1.^[16]

Table 1.1. Strong, moderate, and weak hydrogen bonds following the classification of Jeffrey.^[1]

	Strong	Moderate	Weak
interaction type	strongly covalent	mostly electrostatic	electrostat./ dispers.
bond lengths [Å]			
H...A			
lengthening of X–H [Å]	1.2 – 1.5	1.5 – 2.2	> 2.2
X–H versus H...A	0.08 – 0.25	0.02 – 0.08	< 0.02
X...A [Å]	X–H ≈ H...A	X–H < H...A	X–H << H...A
directionally	strong	moderate	weak
bond angles [°]	170 – 180	> 130	> 90
bond energy [kcal mol ⁻¹]	15 – 40	4 – 15	< 4
relat. IR shift $\Delta\nu_{\text{XH}}$ [cm ⁻¹]	25 %	10 – 25 %	< 10 %
¹ H downfield shift	14 – 22	< 14	

Weak H-bonds

Weak H-bonds are for example “ π hydrogen bonds” that have acceptors that are not atoms with the nonbonding orbital, but a set of atoms with polarized orbitals such as π -orbitals (π =Ph, $\text{C}\equiv\text{C}$, $\text{C}=\text{C}$, Py, etc.). A simple example of such a complex is the complex between water as donor and benzene as acceptor with both H-atoms of the H_2O molecule pointing towards the benzene ring.^[17] It has been shown by microwave spectroscopy that the strength of the H-bonding interaction in the Water – Benzene dimer is 2 kcal/mol.^[18] X–H... π H-bonds occur in many different fields of chemistry such as structural^[19] and biological chemistry.^[20] *Ab initio* MO calculations were performed to study the interactions of benzene with a variety of molecules with binding enthalpies in the order $\text{N–H}^+ > \text{O–H} > \text{N–H} > \text{sp}^3 \text{ C–H} > \text{sp}^1 \text{ C–H}$.^[19] A particularly interesting group is $\text{C}\equiv\text{C–H}$, because it can interact as a donor and π -acceptor simultaneously. These interactions have similar energies and geometries than van der Waals complexes, however, differ from the latter by a directional involvement of the X–H bond.^[1]

The second most common types of weak H-bonds with C–H groups as donors are reported in literature.^[21–23] Formerly considered as “unusual” or “nonconventional” discussed frequently in structural chemistry and biology. In contrast to classical H-bonds the C–H bond gets compressed and the corresponding X–H stretching vibration is shifted to a higher frequency. The experimental evidence for blue shift was observed by Arnold

and coworkers who measured the blue shift of the C–H stretch of the chloroform–triforylmethane complex.^[24] In 1997, Boldeshul et al. have reported the blue shift in the H-bonded complexes of chloroform with various proton acceptors.^[25] The first theoretical study on blue shifted H-bonded systems has been performed by Hobza et al.^[26] Subsequently, numerous theoretical studies have been carried out to understand the blue shifted H-bonding interaction.^[27-30] According to theoretical calculations,^[30, 31] a blue-shift of C–H indicates a different kind of electronic interaction in the hydrogen bond: electron density of the acceptor is not mainly transferred into the antibonding σ^* orbital of the donor X–H, but into remote parts of the donor molecule (such as the C–Cl part of CHCl_3). This transfer of electron density is also associated with a shortening of the X–H bond. The term “improper blue-shifting” hydrogen bonds was introduced to distinguish these interactions from “proper” hydrogen bonds.

The importance of weak hydrogen bonds (< 4 kcal/mol), particularly those involving C–H donor groups, has been established and is recognized to be of importance in crystal engineering.^[2] The absolute abundance of C–H donor groups in organic compounds and thus organic ligands necessitates that C–H...Y hydrogen bonds (particularly $Y = \text{O}, \text{N}$) must be considered. Such hydrogen bonds often support stronger hydrogen bonds.

Medium-strength H-bonds

The absolute values of enthalpies of medium-strength H-bonds extend from 5 to 10 kcal/mol. Two typical examples of such intermediate H-bonds are shown in Figure 1.3. The first is the centrosymmetric cyclic dimer of carboxylic acids that are found in vapours of these acids,^[32-34] and in argon matrices at low temperatures.^[35] These dimers are stable, with a well-defined structure. They are excellent models of H-bonds. The enthalpies of formation of acetic acid dimers was determined to -14 kcal/mol.^[36] A second example is given by phenol-amine bonds O–H...N -. For phenol - triethylamine, the enthalpies of formation has been found of -9 kcal/mol.^[37]

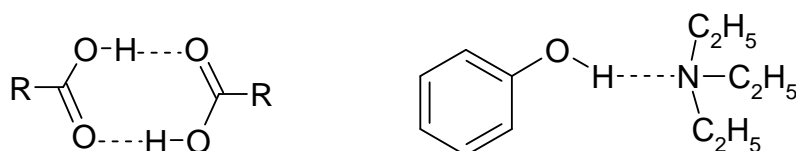


Figure 1.3. Examples of intermediates H-bonds.

Strong H-bonds

Strong H-bonds with the strength greater than 10 kcal/mol are rare. Unlike moderate and weak H-bonds, strong H-bonds are quasi-covalent in nature.^[38] They often imply charged acceptor groups and have been observed in crystals. Thus acid salts of either carboxylic or carbonic acids strength that varies between 10 and 20 kcal/mol. Their structure is drawn in Figure 1.4. A neutral form of trichloroacetic acid as a donor and trioctylphosphine oxide as an acceptor has also been reported to display an enthalpy of formation of -29 kcal/mol.^[39] Other strong H-bonds imply F–H in various forms. The strongest H-bond ever detected is F–H...F[−] which displays strength of H-bond equal to about -37 kcal/mol.^[1, 2] It is the energy of a covalent bond and the electronic structure of this complex that make it a molecule where the H-atom is indeed divalent. More recently, strong H-bonds implying F–H and some noble gases such as Ar, Kr or Xe have been identified.^[40]

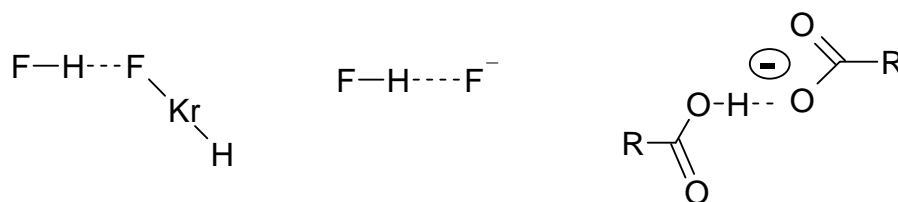


Figure 1.4. Examples of strong H-bonds.

While many authors classify hydrogen bonds as “strong” and “weak”, the borderline between these classes, usually described in terms of hydrogen bond energies, often varies depending on the context in which hydrogen bonding is being discussed. The classifications provided by Desiraju,^[2] which are assigned in the context of the utility of hydrogen bonds in supramolecular chemistry, to classify broad range of interaction that lies between the extremes of half-covalent (with much electrostatic character), a pure electrostatic interaction, and a pure van der Waals interaction. These are documented in Figure 1.5. He used terms “very strong”, “strong”, “weak” and “very weak” terms for classification of H-bonds.

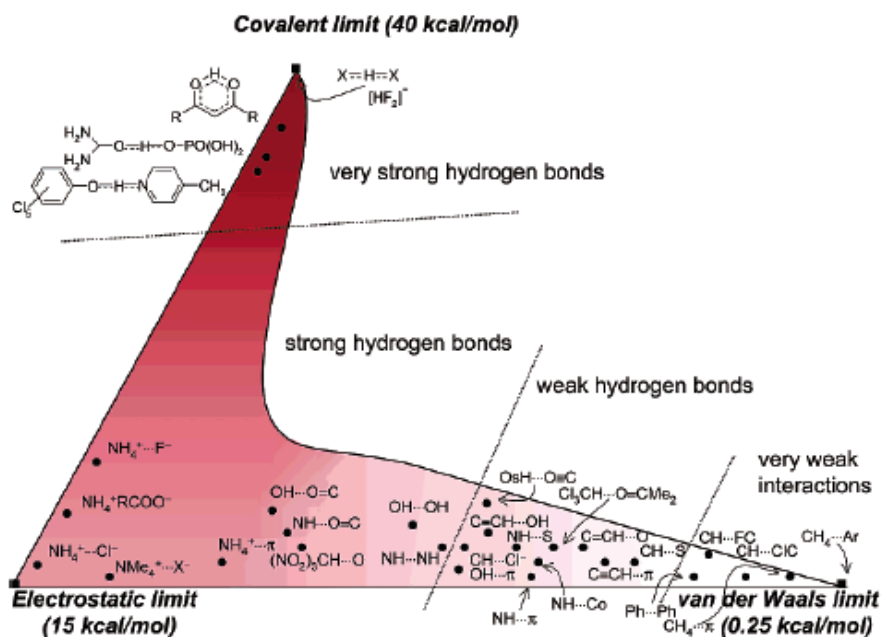


Figure 1.5: Desiraju's classification of hydrogen bonds. This figure has been taken from "Hydrogen Bridges in Crystal Engineering: Interactions without Borders" by G. R. Desiraju.^[2]

1.6. Application of H-bonds

It is well documented that the H-bonding interaction is important for the structure and function of biomolecules. H-bonding in α -helical and β -sheet structures in proteins by Pauling et al.,^[41] DNA base pairs by Watson and Crick.^[42] The H-bonding interactions in nucleic acids play a crucial role in the double helical structure of DNA and RNA along with stacking interactions facilitating molecular recognition via replication processes and protein synthesis.^[43] Extensive theoretical methods have been used to derive information about the H-bonding in DNA base pairing.^[44-50] The representative H-bonded G...C and A...T DNA base pairs are shown in Figure 1.6. The *ab initio* calculation on the G...C and A...T pairs provides the required information about the strength of H-bonding in these systems and the respective binding energies are 20.0 and 17.0 kcal/mol respectively, as calculated by Hobza and et al.^[47]

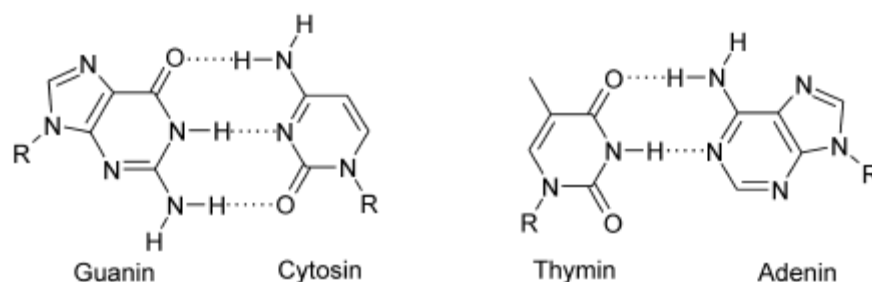


Figure 1.6. Hydrogen-bonded G...C and A...T DNA base pairs.

H-bonding is the most important interaction governing protein structure, folding, binding, enzyme catalysis, and other properties. The basic secondary structural elements in protein structure are α -helix, β -sheet, etc., which are stabilized by H-bonding interactions.^[1, 22]

Crystal structure arises as a result of intermolecular interactions and packing. The packing interaction is important of a large number of strong and weak interactions, each of which influences the other closely.^[22] Small changes in the molecular structure lead to observable changes in the crystal structure. In crystal engineering, attempts have been made to design molecular systems which could throw light on how molecular structure is related to crystal structure. Both the strong and weak H-bonded interactions play a dominant role in engineering of crystals. The role of weak H-bonded interactions in various molecules and crystals has been discussed in great detail by Desiraju and Steiner.^[22]

1.7. Some experimental methods of studying hydrogen bonds

Many methods have been used and will be used in the future to study H-bond interactions. Here we described briefly some of them.

According to Jeffrey^[1] three types of properties are particularly important for H-bonds: thermodynamics, geometry and dynamics.

(1) Thermodynamics quantities, such as enthalpies ΔH , may be directly measured by calorimetry on simple H-bonds found in systems that exhibit ideally a single type of H-bonds. These enthalpies ΔH may also be obtained from IR, Raman or NMR spectroscopy, in the case, for instance, where H-bonded complexes $X-H\cdots Y$ coexist with their free $X-H$ and Y components and variation of their relative proportions can be induced by variations of temperature, of concentration, or of any other external parameter.

(2) Geometrical quantities rely on three basic methods: rotational spectroscopy, X-ray or neutron diffraction, and IR spectroscopy. Rotational spectroscopy in the microwave region is a highly precise method, but it works only in gases at low pressures and low temperatures, which considerably reduces the number of H-bonds that can be studied.

(3) Dynamic quantities such as spectroscopic constants (frequencies of various vibrations) are obtained from IR or Raman spectra. IR spectroscopy is a precise method to measure such quantities related to intramonomer vibrations such as vibrations of X–H component, which contain a lot of information on H-bonds themselves. Raman spectra are more useful for intermonomer vibrations that are found in a region of smaller wavenumbers, where the quality of IR spectra becomes poorer.

Microwave spectroscopy

The energy levels that absorb photons with wavenumbers typically of 1 cm^{-1} have energies typically of 10^{-4} eV . These energies are those of rotations of isolated molecules or of isolated H-bonded complexes in gases.^[51, 52] Microwave spectroscopy of H-bonds consists of inducing transitions between rotational levels of isolated H-bonded molecular complexes found in the gas phase. Such transitions occur when these H-bonded complexes have permanent electric dipole moments.

A typical microwave spectrum thus consists of numerous narrow bands. Separating them requires having a great resolution. With modern techniques, the resolution at which frequencies of bands are determined may indeed be great, of the order of 1 Hz in the GHz region. However, this great resolution is useless if too many overlapping bands are present, as assigning them then becomes most difficult because of a great number of rotational levels are populated at room temperature. In consequence, many transitions can be induced from these populated levels. Having a small number of populated rotational levels only, and consequently a smaller number of transitions in the spectra, requires lowering the temperature down to some K. This cannot be simply done, because all gases at these temperatures condense into solids with vapour pressures nearly equal to 0. The solution consists then of observing gases at such temperatures when they are out of equilibrium. One of the most used techniques to do this consists of inducing an adiabatic cooling of this gas diluted in an inert gas such as argon. This adiabatic cooling is obtained by expanding the gas, through a nozzle, from a cell at a temperature where the vapour tension is still appreciable,^[51, 53] into an evacuated chamber that forms the microwave cavity. Before this

gas condenses when hitting the walls of the chamber, it acquires a supersonic speed and no collision or exchange of energy between the various molecular complexes that compose it occurs. This is equivalent to having an effective temperature of this expanding gas of some K only.^[53]

Microwave spectroscopy therefore appears to be a highly precise technique that conveys a lot of fundamental data not only on the geometry of H-bonds,^[54, 55] but also on transfers of protons through H-bonds that are mechanisms at the origin of all acid–base chemistry.^[56] The requirement that such measurements can only be performed in gases limits its interest. The studied systems are consequently made of simple molecules only. The data obtained using these techniques nevertheless constitute highly useful starting points for more complicated systems that are not observable in the gas phase.

NMR spectroscopy

H-bonds established by small or medium size molecules can be characterized by their chemical shifts. Various groups of molecules are characterized by their various chemical shifts δ_G . Chemical shifts allow one to characterize H-bonds in NMR spectroscopy, because the screening of the spin of the proton of an O–H group is not the same when this O–H group is free or when it establishes an H-bond.^[41, 57] However these do not convey enough original information on H-bonds to become a general method to observe H-bonds. Nevertheless, NMR spectroscopy remains one of the most precise, basic methods in chemical physics and analytical chemistry, due to its ultrahigh spectral resolution and the precisely known spin–spin interaction dependence on distances. In these domains it has for long been a pioneering method for establishment of an H-bond in liquid phase.^[1] In NMR spectroscopy they allow to establish precise correlations between various groups of a macromolecule, leading to “structural constraints” that convey useful complementary information to obtained data by other structural methods such as X-ray or neutron scattering methods.

IR Spectroscopy

Among many experimental methods that are used to observe H–bond, IR spectroscopy plays an essential role due to its great sensitivity to the presence of H-bonds.^[58]

IR spectra in the mid-IR region, that is with wavenumbers (ν/c , with ν the frequency of the IR wave and c the velocity of light) which are in the region $400\text{--}4000\text{ cm}^{-1}$. When another spectral region is considered, as FIR (far infrared region) for below 400 cm^{-1} or NIR (near infrared region) for $4000\text{--}12.500\text{ cm}^{-1}$. For H-bonds, mainly *intramonomer* vibrations appear in the mid-IR region, that is, vibrations that mainly occur either in the X–H molecule or in the Y molecule that constitute the X–H...Y, H-bonded complex. The formation of H-bonds often induce the changes of the intensity of ν_s is due to the relatively small displacement of electrons that accompanies an increase of the X–H distance in X–H...Y, thus creating an important electric dipole moment. *Intermonomer* vibrations due to H-bonds that appear in the FIR region due to the relative vibrations of the two parts X–H and Y of an H-bond X–H...Y appear. These bands disappear when these H-bonds disrupt consequently provide a lot of information on H-bonds.^[59]

1.8. Experimental Evidences of Hydrogen Bond Presence

From the experimental point of view, the existence of a hydrogen bridge can be easily recognized by some specific changes in the molecular geometry and in some chemical–physical properties are discussed by many authors.^[1, 2, 16] In particular:

(a) The X–H bond length becomes longer than the common X–H bonds, whereas the X...Y and H...Y distances are shorter than the sum of the van der Waals radii of the X, Y and H atoms involved in the hydrogen bridge.

(b) The X–H...Y angle is mostly in the range $140\text{--}150^\circ$ for hexatomic chelate rings and in the range $115\text{--}130^\circ$ for the pentatomic ones.

(c) In presence of a conventional hydrogen bridge, the frequencies of the X–H (and C=O) stretching mode vibration are red-shifted with respect to the corresponding values recorded in a hydrogen bonded free compound. The entity of the shift is strictly related to the strength of the hydrogen bridge. On contrary, in presence of a non-conventional hydrogen bond, shortening of the X–H bond length and a blue shift of its vibration frequency are observed.

(d) Proton experiencing hydrogen bond undergoes deshielding, which, in turn, causes a downfield of its chemical shift. For many compounds, it has been found that deshielding increases linearly with $r_{0..0}$ decreasing whilst the potential function changes from a double to a single minimum well. Very useful correlations between the experimental (and/or

theoretical) hydrogen bond distances or hydrogen bond strength and NMR chemical shifts have been also found.^[60-64]

1.9. H/D Substitution in H–bonds

The H-atom can be easily replaced by its isotopic equivalent, the deuterium D-atom. The difference is only that the two nuclei have different mass: that a D is twice than of an H, but they have the same charge. Consequently the electronic structures of both H and D atoms remains are exactly the same. The H/D isotope effect displays a dramatic influence on reactivity and geometry of H-bonds. This existence of slightly different values of X...Y distances has thus been originally measured using this technique by Ubbelohde and Gallagher^[65] and has been called the “Ubbelohde effect”. This is thought to be a result of the zero-point vibrational energy of the O–D relative to the O–H, which makes O–D bond more stable.^[16] Mootz and Schilling^[66] shown that trifluoroacetic acid tetrahydrate tolerate strict structural changes upon isotope exchanges. Particularly, it has ionic structure $\text{CF}_3\text{COO}^- \cdot 3\text{H}_2\text{O} \cdot \text{H}_3\text{O}^+$ for undeuterated, whereas perdeuterated tetrahydrate has been found to be molecular $\text{F}_3\text{COOD} \cdot 4\text{D}_2\text{O}$ structure have been confirmed by X-ray analysis

Marechal has concluded^[14] that the geometry and the enthalpy of formation of a D-bond are slightly different from those of the corresponding H-bond. H-bonds are shorter than D-bonds by somewhat less than 0.05 Å for a medium-strength H–bond, a distance that is in principle measurable, but has been actually scarcely measured, and by <0.05 Å for a weak H-bond. They have greater enthalpies than enthalpies of corresponding D-bonds by a few percents. These are small differences that are hard to put into evidence due to the relative imprecision of corresponding measurements.

As mentioned above that isotopic effects displayed by H-bonds are comparable small for concerns thermodynamics and geometry. For dynamic properties of H–bonds it has huge influence, particularly transfers of protons dramatically vary when a D–atom replaces the H–atom of an H–bond.^[14]

1.10. Proton Transfer or H–atom Transfer

Proton transfer or H–atom transfer is an important part of the flexibility molecular structures, which are essential in biology. Proton transfers are of practical importance in chemistry and biology.^[67-70] They also appear more occasionally, as for instance, in the chemistry of the atmosphere.^[71, 72] Also these transfers are fundamental mechanisms in the

reactivity of biochemical processes such as photosynthesis or vision. H-bonds form a very efficient path to transfer protons or H-atoms between two molecules. Two fundamental molecular mechanisms in ordinary chemistry have been given, particularly that part of chemistry that deals with ionization mechanism of acid/base reactions and proton transfers in electronic excited states.

(a) Ionization mechanism of an acid or a base

Dissociation of an acid or a base in water is definitely one of the most spectacular manifestations of proton transfers and is documented in classical chemistry.^[73] As well known that on mixing hydrogen chloride with liquid water, leads dissociation of HCl molecules into Cl^- and H_3O^+ ions strongly diluted among H_2O molecules, which clearly indicates that protons have been transferred from HCl molecules to water molecules.^[74, 75] And the whole reaction that leads to dissociation of HCl requires at least two steps, with two different kinds of transfer of protons: ionization and diffusion of ions. To understand in great detail the ionization process how many various parameters influence on such as concentration of acid/base in water, intermolecular distance of hydrogen bond different experimental methods have been employed.^[56, 73, 75]

(b) Proton transfer in the electronic excited state

Proton transfers that occur after excitation of an electronic level, display some interest of their own with respect to proton transfers in the ground electronic state. Such transfers are often labelled ESPT (excited states proton transfers).^[76] They occur as a relaxation mechanism of the electronic excitation of a molecule that follows absorption of a visible or UV photon. The interest of studying these systems is that the dynamics of proton transfer is more accurately measured using time-resolved spectroscopy, than for proton transfers in the ground state; excitation starts with a laser flash that excites the molecule at time $t=0$, which can then be defined with a resolution better than psec. Time-resolved IR spectroscopy or pump-probe spectroscopy or any other “two-photon spectroscopy” may then be applied to convey original information on the dynamics of the proton transfer and the various parameters that govern it. This is not possible for ordinary proton transfers in the ground state. Also the intramolecular proton transfer responsible for keto-enol isomerization in the excited state of conjugated aromatic rings has been shown to be occurs in its excited state.^[77]

Chapter 2. Concepts and Theoretical insight

Chapter 2.1. Technique and equipment

2.1.1. Matrix Isolation

Matrix isolation comprises a range of experimental techniques in which guest molecules are trapped in rigid host materials and are thereby prevented from undergoing diffusion, and cannot undergo bimolecular reactions, except with host.^[78] The matrix isolation technique was first invented by George Pimentel.^[79] This technique is a modified and extended version of organic glasses, where solvent mixtures or polymer host materials are replaced by solidified inert (or occasionally reactive) gases for trapping unstable species. Chemical inertness of rare gases, complete transparency throughout the UV-visible-IR regions and the tendency to form clear glasses are main advantages of using rare gases as host. The other important advantage is the availability of various spectroscopic techniques such as IR, UV, in combination with matrix isolation. On the other hand, many odd electron species (radicals, triplet biradicals and carbenes, radical ions) can be characterized by electron spin resonance (ESR) methods. This provides a great opportunity to characterize a reactive species by more than one form of spectroscopy.

Another important application of the matrix isolation technique is the study of weakly bound systems like H-bonded, charge transfer, molecular conformations and van der Waals complexes that can be isolated in low temperature matrices, despite they dissociate under normal temperature conditions due to the weak intermolecular forces. The IR bands of the components of these complexes are significantly perturbed respect to the isolated monomers which provides an insight into the intermolecular interactions. Therefore, matrix isolation, combined with spectroscopic methods such as infrared spectroscopy, is a very important tool for the study of hydrogen bonding.

2.1.2. Equipment

The important equipments needed for matrix isolation technique are shown schematically in Figure 2.1.

a refrigerator system (cryostat for cooling) (either a two-stage or a three-stage closed cycle helium gas cryostat for 10 K and 3 K, respectively)

a vacuum-pumping unit (oil diffusion pump, turbo molecular pump etc.)

a spectroscopic target unit (CsI window for IR, quartz window for UV-visible and copper rod for ESR. They should be in thermal contact with cryostat, normally using indium wire.)

a vacuum chamber

a thermal shield to protect cold target units

a sample holder

a means of measuring and controlling the cold window

a gas-handling systems (gas container connected with manometers, flow controller and gas lines leads to vacuum chamber)

methods of generating the species of interest (e.g. UV irradiation or pyrolysis)

methods of analyzing the matrices (IR, UV, ESR etc.)

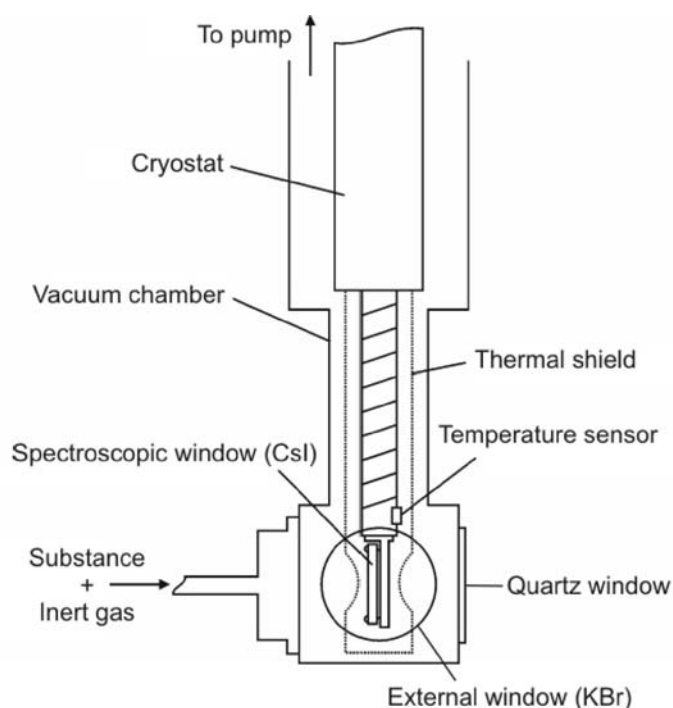


Figure 2.1.1. Schematic view of matrix isolation infrared spectroscopic set-up

2.1.3. Precursors and deposition methods

For matrix isolation of the right precursor in gas matrices should be highly pure and volatile so that they can be premixed at high dilution with rare gases before deposition. If the substance has low volatility, they can be deposited from a side-arm into the vacuum chamber containing cold window (or spectroscopic target). The most important criterion

for any precursor is its deposition temperature that should be below its decomposition point. All three types of precursors (solid, liquid and gaseous substance) can be used for deposition. Co-deposition of two streams of materials can also be done. Despite isolation of molecules in gas matrices, aggregation is one of the most unwanted phenomena that can be avoided by using pulsed deposition method. Majority of the experiments are carried out by slow deposition, however, the duration of deposition varies with spectral techniques to be used.

2.1.4. The generation of reactive intermediates

Roughly there are four general ways that reactive species can be generated and trapped in low temperature matrices:^[78]

(1) deposition of a matrix containing a stable precursor, followed by irradiation of the matrix, for instance with UV light, X-ray, or an electron beam;

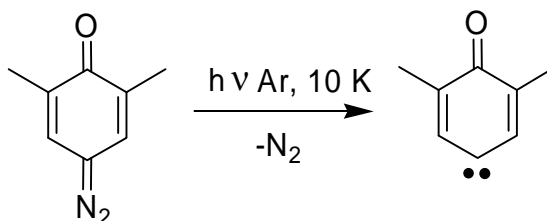
(2) external generation of the reactive species in the gas phase, for instance by photolysis, pyrolysis, or microwave excitation, followed by deposition in a stream of the host gas;

(3) co-condensation of two stream of material on to the cold window, for instance (i) a stream of azobenzene throughout of quartz tube (ii) a mixture of oxygen and host gas, followed by reaction at the matrix surface during deposition;

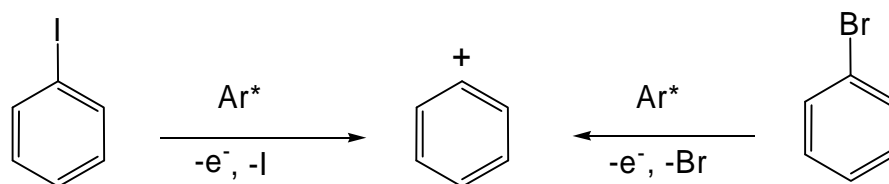
(4) a reactive species already generated by one of the methods listed above, to undergo a thermal reaction within the matrix, either with a reactive host (CO, N₂), or with another guest species.

Examples of these four approaches are shown in scheme 1.1

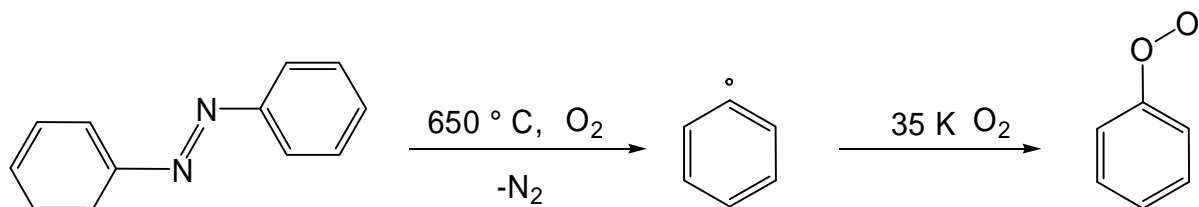
(1) Matrix photolysis: (Photolysis of 2,6-dimethylcyclohexa-2,5-dien-1-on-4-ylidene).^[80]



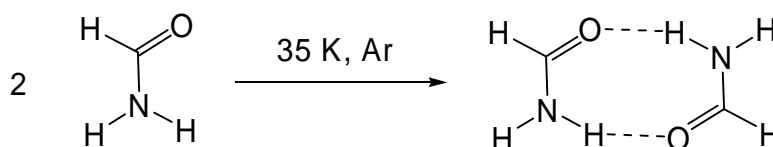
(2) External Generation (Microwave discharge, FVP): (formation of phenyl cation).^[81]



(3) Co-condensation: (Reaction of phenyl radical with oxygen).^[82]



(4) Matrix reaction: (Dimerization of formamide).^[83]



2.1.5. Matrix effects

In matrix isolation, it is important to consider the effects in which matrix host will have on the guest molecules. These host–guest interactions relatively are very weak interactions between host and guest molecules that can easily be understood from frequency shifts in infrared spectra (from gas–phase values). The matrix host, however, influence the diffusion and rotational motion of the guest species. In an extreme case, the host atoms can even react, if the trapped species are reactive, like metal atoms. Many infrared spectra of matrix isolated species show small sub-bands, which can be termed as “matrix splitting” or “site effect”. There are three main causes of splitting in the IR spectra.

Variable host-guest interactions (This arises due to geometrical factors and environment of guest molecules)

Guest-guest interactions (This molecular aggregation can arise from various interactions such as van der Waals association, dipole-dipole alignments, hydrogen bonding, complexation etc).

Fermi resonance.

The most obvious effect of the host matrix is to prevent diffusion and rotation of the guest species in where its (host) acts as a cage and also as clamp. In fact, usually the IR

bands of matrix isolated species are often very narrow ($<1\text{ cm}^{-1}$). It makes spectra more clear, especially when several different species are present. But it is not true that the matrix host will always stop guest molecules rotating. For example H_2O is always rotating in the matrix cage.^[84] Fermi resonance (an intrinsic property of the molecule), also influence the number of signals in an infrared spectrum. Fermi resonance is unavoidable, whereas the other two interactions can be avoided or minimized either by dilution or by changing the host.

Apart from these physical effects, few chemical effects can be deliberately introduced by mixing or using a pure reactive gas like CO as host matrix. Another important effect caused by matrices is “cage effect”. Whenever a pair of radical is produced within the same cage by photolysis, they have less probability for reacting together, (e.g. dimerization or disproportionation), before leaving each other, unlike in viscous solvents. They can either recombine or stay apart within the cage. These recombinations can be minimized by using precursors with a unreactive leaving group (such as CO_2 , N_2 etc.) or making two radical species separated again by a unreactive group.

Chapter 2.2. Quantum chemical methods

Computational Chemistry has emerged as a powerful tool for chemists to solve many problems such as electronic structure, potential energy surfaces, reaction pathways, H-bonding interactions etc.^[85, 86] A variety of theoretical methodologies are employed at different theoretical levels and accuracy. Different quantum chemical methods used to analyze H-bonding interactions have been systematically discussed in literature.^[87] Starting from semi-empirical molecular orbital methods up to coupled-cluster method are widely used methodologies to investigate H-bonding interactions etc.

2.2.1. Calculation of Molecular Energy

In quantum chemistry, the calculation of the energy of a molecule implies the solution of the well-known Schrödinger equation:^[85, 88]

$$\hat{H}\Psi = E\Psi \quad (2.2.1)$$

Where H is the Hamiltonian operator and Ψ is the wave function obeying to the restrictions required by the quantum mechanics postulates. The operator H is the sum of the kinetic (T) and potential (V) energies; therefore it represents the total energy of the system. The Hamiltonian for a single-particle three-dimensional system in cartesian coordinates is:

$$\hat{H} = T + V = -\frac{h^2}{8\pi^2m} \left(\frac{\partial^2}{\partial x^2} + \frac{\partial^2}{\partial y^2} + \frac{\partial^2}{\partial z^2} \right) + V(x, y, z) \quad (2.2.2)$$

h being the Plank constant and m the mass of the particle. The differential operator in parentheses in equation 2.2.2 is the Laplacian operator that can simply written as

$$-\frac{h^2}{8\pi^2m} \nabla^2 \Psi + V(x, y, z) \Psi = E\Psi \quad (2.2.3)$$

For n -particles three-dimensional system above equation becomes

$$-\sum_{i=1}^n \frac{h^2}{8\pi^2m_i} \nabla^2 \Psi + V(x_1, y_1, z_1, \dots, x_n, y_n, z_n) \Psi = E\Psi \quad (2.2.4)$$

The above equation is the time-independent Schrödinger equation for the considered system. The above equation cannot be analytically solved and only approximate solutions are possible.

2.2.2. Density Functional Theory (DFT)

DFT method approach is based on a strategy of modelling electron correlation through general functions of electron density. The foundation for the use of DFT methods in computational chemistry is the introduction of orbital, as suggested by Kohn and Sham. Following their work, the approximate functionals employed by current DFT methods partition the electronic energy into several terms.^[88]

$$E = E^T + E^V + E^J + E^{XC} \quad (2.2.5)$$

Where E^T is the kinetic energy term, E^V is the term of the potential energy between electron-nuclear attraction and repulsion between pairs of nuclei, E^J is the electron-electron repulsion term E^{XC} is the exchange-correlation term that also involves the remaining part of the electron-electron interaction.

All term beside the nuclear-nuclear repulsion are functions of ρ , where ρ is electron density. $E^T + E^V + E^J$ correspond to the classical energy of the charge distribution, and E^{XC} is resolved by the electron density. Hohenberg and Kohn divided the E^{XC} term into separate parts (exchange and correlation parts)

$$E^{XC}(\rho) = E^X(\rho) + E^C(\rho) \quad (2.2.6)$$

In these homogeneous electron gas models, E_{XC} is expressed as a function of the exchange-correlation energy per particle. Use of the LDA (local density approximation) generally overestimates binding energies and underestimates exchange energy.

To improve the correlation functional, GGA (generalized gradient approximation) formalisms have been developed. Becke has developed functionals which include a mixture of Hatree-Fock and DFT exchange, where E^{XC} is defined as:

$$E^{XC}_{\text{hybrid}} = c_{\text{HF}} E^X_{\text{HF}} + c_{\text{DFT}} E^{XC}_{\text{DFT}} \quad (2.2.7)$$

Several other exchange functionals have also been developed, which are similar to Becke. Some of most used functionals are BP86, BLYP and BPW91. Apart from these methods, there are some other functionals like B3PW91 and B3LYP that incorporates both HF and DFT exchange; they are called *hybrid functional methods or adiabatic connection methods*. Normally, the choice of any of these methods is only based on the agreement of the results with experimental data for the system of interest or closer analogs. Some DFT methods like BLYP and B3LYP are widely used particularly to study properties of molecules like structural parameters, vibrational frequencies and electrostatic potentials, etc.

Chapter 3. Noncovalent complexes of Formamide

Chapter 3.1. Aggregation of formamide

3.1.1. Introduction

The peptide bond is among the most important binding motifs in biochemistry. It links amino acids together, provides rigidity to the protein backbone, and contains the two essential docking sites for hydrogen-bond-mediated protein folding and protein aggregation, namely, the C=O acceptor and the N–H donor unit. Formamide (FMA) complexes are simple models of larger systems such as proteins or nucleic acids to study weak intermolecular interactions. The N–H...O=C and C–H...O=C interactions in the formamide dimer and the double intermolecular proton transfer were studied extensively both by theoretical and experimental methods.^[89-98]

Vargas et al. identified five different FMA dimer structures as local minima using the using Møller-Plesset second-order perturbation theory (MP2).^[89] These structures were also studied by Frey and Leutwyler^[99] using resolution of identity Møller-Plesset second-order perturbation theory (RIMP2) and the coupled cluster with singles, doubles, and perturbative triples (CCSD(T)) method. Three structures called linear, zig-zag and cyclic dimers were studied by Bende, Vibók et al. at the Hartree-Fock (HF) and MP2 levels of theory. They compared the results after using the a posteriori counterpoise (CP) method to correct the basis set superposition error (BSSE) with the results of the a priori chemical hamiltonian approach (CHA).^[100]

Four formamide dimers were studied by Papamokos and Demetropoulos^[95] in the assessment of the PW91XC functional with the 6-31+G* basis set for the vibrational spectra of amide dimers. Gómez Marigliano and Varetti calculated one cyclic and one open dimer of FMA with the B3LYP functional and 6-31G(d,p) or 6-31++G(d,p) basis sets as part of their experimental and quantum chemistry study of the self-association process of formamide in carbon tetrachloride solutions.^[94]

Grabowski et al. analyzed the N–H...O hydrogen bonds in the formamide dimer at the MP2/6-311++G(d,p) level of theory and applied the Bader theory to explain the nature of these interactions.^[101] An ab initio molecular-dynamics study of liquid formamide was reported by Tsuchida,^[102] and Cabaleiro-Lago and Ríos developed an intermolecular potential function for interactions in formamide clusters based on ab initio calculations.^[90]

The association of formamide in argon was studied using matrix isolation techniques by Räsänen^[93] who found that both “open” and cyclic structures are formed upon diffusion-controlled association in the matrix. However, the dimers trapped from the gas phase consisted predominantly of the “open” structure. The most stable dimer of formamide is generated in pulsed supersonic jet expansions and detected by FTIR spectroscopy in the gas phase by Albrecht et al.^[98]

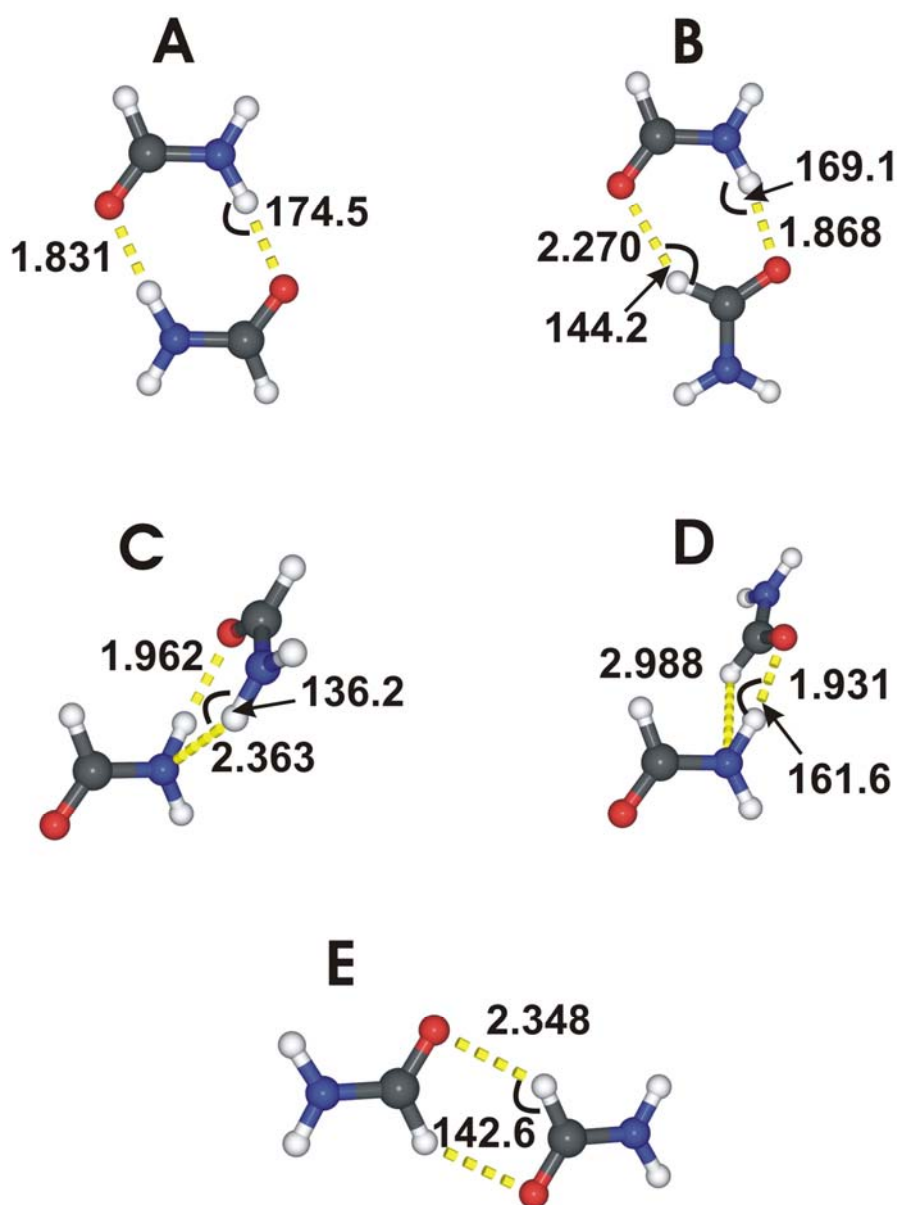


Figure 3.1.1. The calculated structures with hydrogen bond lengths (Å) of the FMA dimers **A** - **E** at the MP2/cc-pVTZ level of theory.

Here the matrix isolation experiments of formamide aggregation are presented in argon and xenon matrices. The calculations of the spectra of the various minima allow the assignment and interpretation of the results of the matrix isolation experiments. A systematic computational study using the MMH^[103] method produces five dimers **A** – **E** which are

minima at the MP2/cc-pVTZ level of theory. With a calculated dimerization energy of -10.4 kcal/mol **A** is, as expected, the most stable dimer found.^[83, 103]

3.1.2. Results and Discussion

3.1.2.1. Matrix Isolation experiments (Computational Results by Elsa Sanchez-Garcia)

There are four basic interactions in the FMA dimers (Figure 3.1.1):

- (1) N–H...O interaction between the amide hydrogen atom of one FMA molecule and the carbonyl oxygen atom of the other FMA molecule.
- (2) C–H...O interaction between the CH hydrogen atom of one FMA molecule and the carbonyl oxygen atom of the other FMA molecule.
- (3) N–H...N interaction between the amide hydrogen atom of one FMA molecule and the nitrogen atom of the other FMA molecule.
- (4) C–H...N interaction between the CH hydrogen atom of one FMA molecule and the nitrogen atom of the other FMA molecule.

The most stable dimer **A** (–10.41 kcal/mol) is a cyclic C_{2h} complex stabilized exclusively by the N–H...O interaction (1) at 1.831 Å. (Figure 3.1.1 and Table 3.1.1) The cyclic C_s dimer **B** (–6.54 kcal/mol) shows interaction (1) at 1.868 Å and interaction (2) at 2.270 Å hydrogen bond distance.

Dimers **C** (–4.74 kcal/mol) and **D** (–4.37 kcal/mol) show interesting structural similarities because they both stabilize due to interaction (1) and additionally, one FMA nitrogen atom is directly involved in a hydrogen bond. However, dimer **C** is additionally stabilized by interaction (3), whereas complex **D** shows the weaker interaction (4). The least stable FMA dimer is the cyclic C_{2h} complex **E** (–2.94 kcal/mol), which is stabilized exclusively by interaction (2).

The IR spectra of the FMA monomer **M** and the FMA dimers generated under various conditions of deposition and annealing of the matrices were compared with spectra calculated at the MP2/cc-pVTZ level of theory (Table 3.1.2). The formation of dimers and other molecular aggregates results in characteristic shifts of some of the vibrations of **M**. These shifts can be used to identify the dimers by comparison of the experimental with calculated data. To facilitate this comparison the calculated frequencies were scaled with individual factors to achieve for the monomer **M** an exact match of calculated and experimental IR frequencies (**M**: Table 3.1.2, dimers **A**, **B** and **C**: Table 3.1.3, dimers **D** and **E** calculated frequencies: Table 3.1.4).

Table 3.1.1. Calculated binding energies of the FMA dimers **A-E** at the MP2/cc-pVTZ basis sets including ZPE and BSSE corrections compared to the DFT/PBE plane wave results^a

	MP2/ cc-pVTZ				DFT/PBE pw
	ΔE	BSSE	ZPE	$\Delta E_{(BSSE+ZPE)}$	ΔE
A	-15.59	2.52	2.66	-10.41	-14.01
B	-10.66	2.06	2.06	-6.54	-9.12
C	-8.86	1.99	2.13	-4.74	-6.67
D	-7.82	1.70	1.75	-4.37	-8.03
E	-5.65	1.53	1.18	-2.94	-3.59

[a] All energies are given in kcal/mol

Table 3.1.2. Calculated and experimental vibrational frequencies (cm^{-1}) of the FMA Monomer **M**

Argon			Xenon			Assignment
M exp.	M calc.^a	Factor of correction	M exp.	M calc.^a	Factor of correction	
3547.4	3787.1	0.937	3536.7	3787.1	0.933	$\nu_{\text{as}}(\text{NH}_2)$
3426.6	3634.7	0.943	3411.3	3634.7	0.938	$\nu_{\text{s}}(\text{NH}_2)$
2882.9	3017.2	0.955	2851.4	3017.2	0.945	$\nu(\text{C-H})$
1739.1	1811.0	0.960	1731.0	1811.0	0.955	$\nu(\text{C=O})$
1575.8	1618.7	0.973	1574.3	1618.7	0.972	$\delta(\text{NH}_2)$
1260.4	1285.0	0.980	1267.2	1285.0	0.986	$\nu(\text{C-N})$
678.2	645.4	1.050	702.4	645.4	1.088	$\tau(\text{NH}_2)$

[a] Vibrational frequencies of the formamide monomer calculated at the MP2/cc-pVTZ level of theory.

Table 3.1.3. Calculated and experimental vibrational modes of the formamide dimers **A**, **B** and **C**

MP2/cc-pVTZ (with Ar corrections)						Argon matrix				MP2/cc- pVTZ (with Xe corrections)		Xenon matrix		assignment
A		B		C		A		C		A		A		
$\nu\text{ cm}^{-1}$	<i>I</i>	$\nu\text{ cm}^{-1}$	<i>I</i>	$\nu\text{ cm}^{-1}$	<i>I</i>	$\nu\text{ cm}^{-1}$	<i>I</i>	$\nu\text{ cm}^{-1}$	<i>I</i>	$\nu\text{ cm}^{-1}$	<i>I</i>	$\nu\text{ cm}^{-1}$	<i>I</i>	
3494.2	16	3544.7 3498.6	10 16	3523.4 3452.3	32 27	3515.1	13	3521.6	12	3479.2	16	3498.6	14	$\nu_{\text{as}}(\text{NH}_2)$
3170.0	100	3424.2 3193.3	9 100	3379.8 3266.0	41 79	3130.6	10	3353.1 3219.1	7 3	315 3.1	100	3158.2	10	$\nu_{\text{s}}(\text{NH}_2)$
2902.0	19	2944.0 2879.5	2 20	2912.3 2883.2	24 19	-				2871.6	19	2863.6	2	$\nu(\text{C-H})$
1730.2	55	1729.8 1694.1	95 24	1731.3 1714.4	98 100	1728.0	100	1730.8 1720.7	100 86	172 1.2	55	1719.2	100	$\nu(\text{C=O})$
1321.2	12	1312.3 1274.1	15 25	1292.2 1256.4	26 32	1312.9	11	1296.0	12	132 9.3	12	1305.4	17	$\nu(\text{C-N})$
904.8	5	847.2 700.7	5 1	831.2 754.9	31 9	818.7	4	834.6 769.2	7 4	937 .6	5	797.4	9	$\tau(\text{NH}_2)$
										466.3 ^a	17	478.2	16	$w(\text{NH}_2)$
[a]Unscaled.														

[a]Unscaled.

Table 3.1.4. Calculated and predicted experimental vibrational frequencies (cm⁻¹) of the FMA dimer **D** and **E**^a

MP2/cc-pVTZ									
Calculated frequencies and shifts in the complex									Assignment
M calc	Dimer D without correction		Dimer D corrected		Dimer E without correction		Dimer E corrected		
1811.0	1789.4 ^b	(-21.6)	1717.8	(-20.7)	1795.9	(-15.1)	1724.1	(-14.5)	ν(C=O)
	1803.4 ^c	(-7.6)	1731.3	(-7.3)					
3017.2	3050.6 ^b	(+33.4)	2913.3	(+31.9)	3065.0	(+47.8)	2927.1	(+45.6)	ν (C-H)
	3006.9 ^c	(-10.3)	2871.6	(-9.8)					
3634.7	3629.7 ^b	(-5)	3422.8	(-4.7)	3632.2	(-2.5)	3425.2	(-2.4)	vs (NH ₂) ^b
	3495.9 ^c	(-138.8)	3296.6	(-130.9)					
3787.1	3780.3 ^b	(-6.8)	3542.1	(-6.4)	3785.6	(-1.5)	3547.1	(-1.4)	vas (NH ₂) ^c
	3714.7 ^c	(-72.4)	3480.7	(-67.8)					

[a] The frequency shifts in **D** and **E** compared to FMA (monomers **M**) are given in parentheses.

[b] FMA molecule which is out of plane vibration. [c] FMA molecule which is in plane vibration.

3.1.2.2. Argon matrix

The IR spectrum of monomer **M**, matrix-isolated in argon at 10 K, agrees very well with the spectrum reported in literature.^[97] The aggregation of FMA in inert gas matrices was already studied by Räsänen et al.^[92] They reported IR absorptions of two aggregates in the N-H stretching region and between 700 and 300 cm⁻¹. It was concluded that upon diffusion-controlled aggregation of **M** both “open” and cyclic dimers were formed in the matrix.

In our experiments the aggregation of **M** was induced by either warming the matrix (argon or xenon) from 10 K to 40 K with a rate of approximately 1 K min⁻¹ (free warm-up) or by annealing the matrix at a defined temperature between 20 and 40 K for up to 60 min. In free warm-up experiments the intensity of the carbonyl stretching vibration of **M** at 1739.1 starts to decrease at a temperature of 25 K, and simultaneously new bands at 1730.8, 1728.0 and 1720.7 cm⁻¹ increase in intensity. At 25 K the band at 1728.0 cm⁻¹ gains intensity faster than the bands at 1730.8 and 1720.7 cm⁻¹, indicating that two different species are formed. By comparison with *ab-initio* calculations (MP2/cc-pVTZ) the band at 1728.0 cm⁻¹ is assigned to the carbonyl vibration mode of dimer **A** and the bands at 1730.8 and 1720.7 cm⁻¹ are assigned to dimer **C** (Figure 3.1.2, Table 3.1.3). Under both conditions – free warm-up and annealing of the matrix – mixtures of dimers **A** and **C** are formed. Dimer **A** corresponds to the cyclic dimer and **C** to the “open” dimer described by Räsänen et al.^[93]

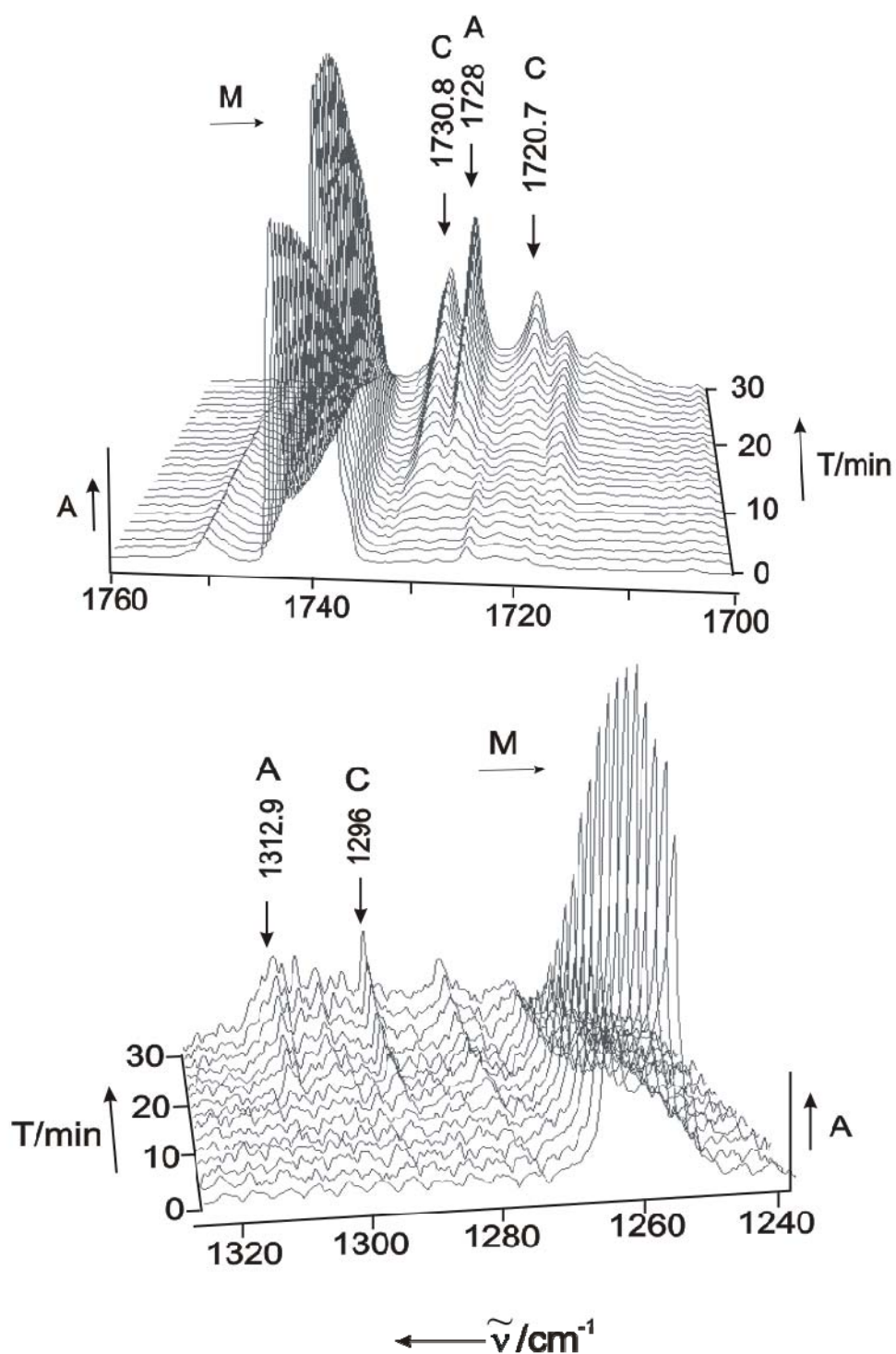


Figure 3.1.2. IR spectra of an argon matrix containing formamide during the slow warm up from 10 K ($t = 0$ min) to 40 K ($t = 30$ min). Bands assigned to monomeric formamide **M**, dimer **A**, and dimer **C**

As mentioned above, the C=O stretching vibration observed in argon at 10 K at 1728 cm^{-1} is in good agreement with the theoretical prediction (MP2/cc-pVTZ, scaled) for dimer **A** at 1730.2 cm^{-1} . Due to its symmetry, only one C=O stretching vibration is expected whereas the other dimers with lower symmetry should exhibit two different C=O stretching vibrations. For dimer **B** these vibrations are predicted at 1729.8 and 1694.1 cm^{-1} and for dimer **C** at 1731.3 and 1714.4 cm^{-1} . Thus, for dimer **B** one of the C=O str. vibrations are calculated to be shifted more than 40 cm^{-1} , while for dimer **C** no shift larger than 25 cm^{-1} is predicted. Since in the experiment no new absorptions are found below 1710 cm^{-1} (Figure 3.1.3), we assign the second dimer observed in the matrix to dimer **C** and discard the formation of dimer **B**.

The C-N stretching mode of monomer **M** is found at 1260.4 cm^{-1} . On warming the matrix this band decreases in intensity and bands at 1312.9 and 1296 cm^{-1} increase in intensity. The band at 1312.9 cm^{-1} is assigned to the C-N stretching vibration mode of dimer **A**, which is blue shifted from the unperturbed molecule by 52.5 cm^{-1} . MP2/cc-pVTZ predicts a band at 1321.2 cm^{-1} which is in reasonable agreement with the experimental value (Table 3.1.3). The band found at 1296 cm^{-1} is in good agreement with a vibration at 1292.2 cm^{-1} predicted for dimer **C**. For dimer **B** the corresponding vibrations are predicted to be at 1312.3 and 1274.1 cm^{-1} , respectively (Table 3.1.3).

As described by Räsänen,^[92] annealing of a matrix containing **M** leads to new broad bands in the NH stretching region (Figure 3.1.3, Tables 3.1.3 and 3.1.4). Annealing results in a decrease of $\nu_{\text{as}}(\text{NH}_2)$ of **M** at 3547.4 cm^{-1} and formation of an intense broad band at 3515.1 cm^{-1} and a less intense band at 3521.6 cm^{-1} . In agreement with the results of Räsänen et al.^[93] the band at 3515.1 cm^{-1} is assigned to $\nu_{\text{as}}(\text{NH}_2)$ of **A** and the band at 3521.6 cm^{-1} to $\nu_{\text{as}}(\text{NH}_2)$ of **C** (Table 3.1.4).

In **M** $\nu_{\text{s}}(\text{NH}_2)$ is found at 3426.6 cm^{-1} which after annealing is shifted to a set of broad bands in the range 3450-3050 cm^{-1} . Although due to the broadness it is difficult to make clear assignments, some bands can be assigned to dimers **A** and **C**. The most intense band at 3130.6 cm^{-1} corresponds to **A**, and bands at 3353.1 and 3219.1 cm^{-1} to **C** (Table 3.1.3).

The NH_2 twisting vibration $\omega(\text{NH}_2)$ of **M** appears at 678.2 cm^{-1} (Figure 3.1.3). In **A** this vibration is shifted to 818.7 cm^{-1} (Table 3.1.3). Weak bands at 834.6 and 769.2 cm^{-1} correspond to dimer **C**, in excellent agreement with the predictions from ab initio calculations (831.2 and 754.9 cm^{-1}). Additional weak bands at 1717 and 1281 cm^{-1} are assigned to a FMA- H_2O complex formed by water contaminations in the matrix.^[59]

Comparison of the experimental spectra with spectra calculated for the dimers **D** and **E** did not give any hint for the formation of these dimers (Table 3.1.4).

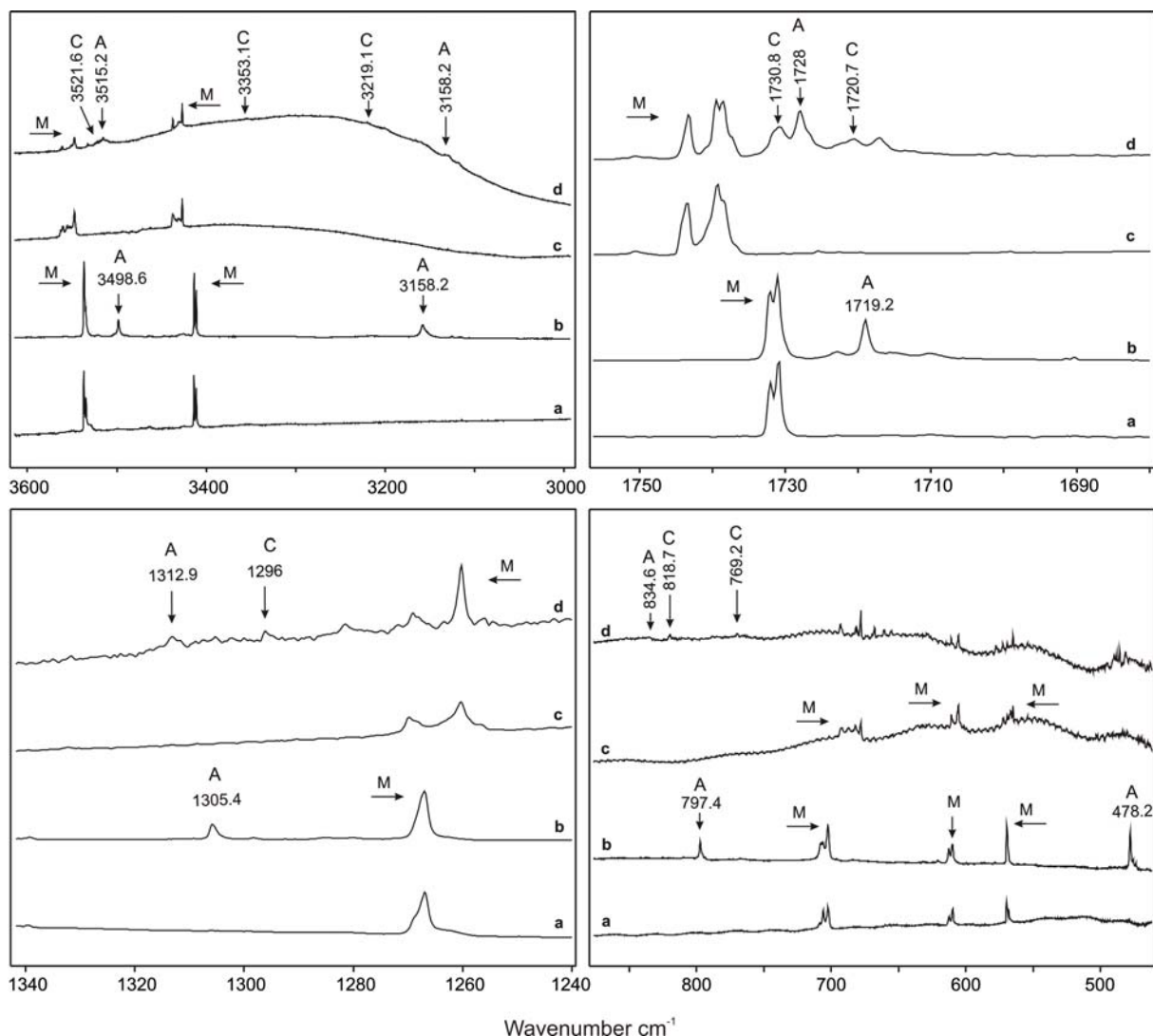


Figure 3.1.3. IR spectra of FMA in different sets of experiment. (a) Deposition of FMA at 15 K in xenon (sample temperature -50°C). (b) Deposition of FMA at 30 K in xenon (sample temperature -30°C). (c) Deposition of FMA at 10 K in argon (sample temperature -50°C). (d) Changes after annealing at 35 K. Bands assigned to **M**, **A** and **C** are labeled in the spectra

3.1.2.2. Xenon Matrix.

The spectrum of **M**, matrix-isolated in xenon, is in very good agreement with the spectra reported in the literature (Tables 3.1.2 and 3.1.3).^[92, 97] However, the composition of the matrices very much depends on the sublimation temperature of FMA. Two types of experiments were performed: (i) FMA was sublimed from a sample kept at -50°C and deposited with a large excess of xenon at a temperature of 15 – 30 K. Under these conditions, monomer **M** was found almost exclusively by IR spectroscopy (Figure 3.1.3). (ii) If FMA was sublimed at -30°C , where its vapor pressure is considerably higher, monomer **M** and additional bands assigned to dimers were found.

Annealing of a xenon matrix containing mainly **M** from 30 K to 65 K results in the formation of sharp bands at 3498.6, 3158.2, 1719.2, 1305.4, 797.4 and 478.2 cm^{-1} showing identical kinetic behavior assigned to dimer **A**. This assignment was confirmed by comparison with the spectra obtained in argon and with results from MP2/cc-pVTZ calculations (Table 3.1.3). Except for the $\tau(\text{NH}_2)$ mode, the calculated vibrational modes are in good agreement with the experimental frequencies. The asymmetric NH_2 vibration of **A** appears as a sharp band at 3498.6 cm^{-1} , above 10 cm^{-1} from the band described by Räsänen et al.^[93] (Table 3.1.5). However, the other bands assigned to **A** agree very well with the literature data. In addition, several very broad bands, presumably due to other aggregates, are observed which are difficult to assign.

If higher concentrations of FMA are deposited in the matrix, **M** and all bands assigned to **A** are found at 30 K without annealing the matrix. Additional weak bands are found at 1722.1, 1690.3, 1298.2, and 766.5 cm^{-1} . These additional bands proved to be labile and completely disappear during annealing at 50 K. Comparison with the results of MP2 calculations gives a reasonable agreement with the predicted spectrum of **B**. Thus, we tentatively assign the thermolabile compound to dimer **B**. Several other broad bands already formed after the deposition change shape and intensity during the annealing. Again, these bands could not be definitely assigned, although it is tempting to assume that **C** is formed as in the matrix. The broadness of these bands might result from the conformational flexibility of **C** and equilibria between **C** and **D**.

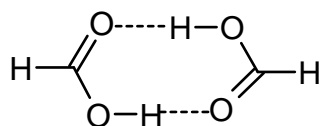
Table 3.1.5. Vibrational frequencies of the normal modes of formamide dimers experimentally found in our work compared to the values of the literature

Ar matrix				Xe matrix		Assignment
A ^[83]	A ^[93]	C ^[83]	Open Dimer ^[93]	A ^[83]	A ^[93]	
3515.1	3515	3521.6		3498.6	3510	$\nu_{\text{as}}(\text{NH}_2)$
3130.6	3216 3195	3353.1 3219.1	3369 3355	3158.2	3158	$\nu_{\text{s}}(\text{NH}_2)$
-	-		-	2863.6	-	$\nu(\text{C-H})$
1728.0	-	1730.8 1720.7	-	1719.2	-	$\nu(\text{C=O})$
-	-	1598.7 1586.0	-	-	-	$\delta(\text{NH}_2)$
1312.9	-	1296.0	-	1305.4	-	$\nu(\text{C-N})$
818.7	819	834.6 769.2	769	797.4	797	$\tau(\text{NH}_2)$

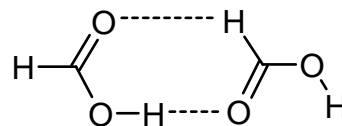
3.1.3 Conclusion

The dimerization of FMA monomer **M** in argon matrices leads to two products: the thermodynamically more stable dimer **A** with two strong NH...O hydrogen bonds and the less stable **C/D** with only one strong hydrogen bond. In solid xenon evidence for an additional labile dimer **B** is found. A systematic computational study using the MMH method produces five dimers **A – E** which are minima at the MP2/cc-pVTZ level of theory. With a calculated dimerization energy of –10.4 kcal/mol **A** is, as expected, the most stable dimer found. In dimer **B** one of the FMA molecules is rotated in a way that a strong NH...O interaction is replaced by a weaker CH...O interaction reducing the complex stabilization compared to **A** by about 4 kcal/mol. These two FMA dimers correspond to the two most stable dimers of formic acid, the well known symmetrically bridged dimer **F** (corresponding to FMA dimer **A**) and the less stable asymmetrical dimer **G** (corresponding to FMA dimer **B**).^[104, 105] In the case of formic acid the less stable dimer **G** is primarily formed under conditions of matrix isolation, but rearranges to the more stable dimer **F** on annealing the matrix. With FMA dimer **B** is not observed after annealing and instead the

even less stable (-4.7 kcal/mol) dimer **C/D** is formed. Dimer **E** with a calculated dimerization energy of -2.9 kcal/mol is not observed in the experiment and, according to the ab initio molecular dynamics simulations, predicted to be not stable. The dynamics simulations also reveal that the structurally and energetically similar dimers **C** and **D** rapidly interconvert even at low temperature. Thus, just three distinct dimers are remaining: **A**, **B**, and **C/D**, which are indeed observed in the experiment, **B** having been observed before annealing when high FMA concentrations had been deposited.

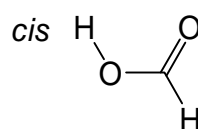
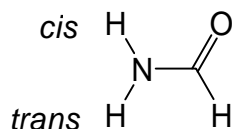


Dimer F



Dimer G

This leaves us with the question why besides the most stable dimer **A** only **C/D** but not **B** are formed during annealing of matrices (both argon and xenon) containing **M**, whereas **B** is formed in small quantities after deposition of high concentrations of FMA in xenon. In contrast, annealing of matrices containing the monomer of formic acid results in the formation of a dimer corresponding to **B** with one strong OH...O and one weak CH...O hydrogen bridge.^[105] This formic acid dimer on further annealing rearranges to the more stable symmetrical dimer with two strong OH...O hydrogen bridges (corresponding to FMA dimer **A**). The difference between formic acid and FMA is (i) the lower acidity of the NH proton leading to less stable hydrogen bonds and (ii) the availability of two acidic NH hydrogen atoms in each FMA molecule (labeled *cis* and *trans*) increasing the structural possibilities for the formation of FMA dimers compared to formic acid dimers. In formic acid the *cis* conformer is the only conformer found after deposition in an inert gas matrix from the gas phase.



The formation of both dimers **A** and **C/D** in the argon matrix is a consequence of the first step of the dimerization of **M** in which the carbonyl oxygen atom of one FMA molecule interacts with an amino hydrogen atom of the second molecule. There are two possible arrangements for this interaction leading to different dimers: (i) The *trans* hydrogen atom of the first FMA molecule interacts with the carbonyl oxygen atom of the second molecule. This can only lead to dimers **C** or **D**. (ii) The *cis* hydrogen atom of one FMA molecule interacts with the carbonyl oxygen atom of the second molecule leading to

dimers **A** or **B**. The rearrangement of **C/D** to **A** or **B** requires breaking the strong N- $H_{cis} \cdots O$ hydrogen bond, which is energetically not possible under the conditions of matrix isolation. Thus, once one strong $NH \cdots O$ hydrogen bond is formed, the further reaction leads either to **C/D** or **A/B** which do not interconvert. In case (ii) obviously the energetically more stable complex **A** is formed rather than **B**.

Chapter 3.2. Formamide - Acetylene^[106]

3.2.1. Introduction

Amides play an essential role in biochemistry and organic chemistry. Formamide (FMA) is the simplest molecule containing the amide bond which is the basis of peptide chemistry.^[107, 108] The structure and spectroscopic properties of formamide have been studied in detail. The monomer and dimers of formamide in inert gas matrices were studied by Räsänen.^[92, 93] The interactions of formamide with water,^[59] hydrogen fluoride^[109] and the isocyanat anion^[110] have been studied using matrix isolation spectroscopy and *ab initio* methods. Selective UV irradiations of the isolated formamide monomer at 193 nm have been performed by Lundell et al. leading to the formation of the CO...NH₃ and HNCO...H₂ complexes as photoproducts in an argon matrix.^[97] Alternatively, the UV irradiations at 248 nm in an argon matrix led to the formation of formimidic acid (H(OH)C=NH), a tautomer of formamide.^[111]

The weak CH...O and CH... π interactions are gaining more attention in recent years because of their significant role in determining the shapes and stabilities of proteins and crystal structures. The CH...X complexes where X can be a proton acceptor such as O, N, halogens or a π system have been studied experimentally and theoretically.^[112-114] Ault and co-workers^[115-117] extensively studied the hydrogen-bonded complexes of alkynes and alkenes with several oxygen and nitrogen atom-containing bases by the matrix isolation technique.

In this chapter, we investigate the formamide and acetylene complexes (FMA – acetylene) using matrix isolation techniques and *ab initio* calculations. Three FMA – acetylene dimers stabilized by the NH_{FMA}... π , C-H_{acet}...C=O_{FMA}, and C-H_{FMA}... π interactions are identified by *ab initio* calculations. The geometries, binding energies and spectroscopic properties of the dimers are discussed here. The assignment of the complexes is achieved by comparison of the experimental and calculated frequencies. The geometries, energies and vibrational frequencies of selected 1:2 FMA – acetylene complexes are also described here.^[106]

3.2.2. Results and Discussion

3.2.2.1. Experimental results

Infrared spectra of FMA isolated in rare gas matrixes have been reported previously.^[92, 118] Our reference infrared spectra of FMA and acetylene (Ac) in argon and nitrogen matrices are in good agreement with the data reported in literature.^[92, 118-121] The matrix isolation of FMA as well as acetylene has been studied by several groups.^[93, 120, 122-124] Mixed aggregates (mainly dimers) were produced by matrix isolation of mixtures of FMA and Ac in argon or nitrogen at 10 K and subsequent annealing of these matrices at temperatures up to 40 K. Under the conditions of high dilution in either argon or nitrogen and slow deposition of the matrices at 10 K mainly the monomers of FMA and Ac are isolated. At 10 K these matrices are very rigid and diffusion of trapped molecules is efficiently inhibited, whereas at higher temperatures (approximately 1/3 of the melting point of the matrices) small molecules start to diffuse and intermolecular reactions become possible. This technique allows to directly monitor the aggregation via IR spectroscopy.

3.2.2.1.1. Argon Matrix.

The asymmetric and symmetric N–H stretching modes of FMA are strongly affected by the formation of complexes (Figure 3.2.1). In the presence of both FMA and Ac in argon, new bands are observed at 3536.2 and 3399.1 cm^{-1} assigned to FMA – Ac complexes. Compared to the unperturbed N–H stretching vibrations of the FMA monomer at 3547.4 and 3426.6 cm^{-1} these bands are red shifted by 11.2 and 27.5 cm^{-1} , respectively.

The C=O stretching vibration of FMA shows also characteristic shifts induced by the formation of FMA – Ac complexes (Figure 3.2.2). The band at 1739.1 cm^{-1} is assigned to the C=O stretching vibration of the FMA monomer.^[92] Matrix site effects cause a splitting of this band. After annealing the matrix at 30 K for several minutes, new absorptions appear at 1730.9, 1724.2, and 1722.3 cm^{-1} . These bands are red-shifted by 8.2, 14.9 and 16.8 cm^{-1} , respectively, compared to the C=O stretching vibration of the FMA monomer. Increasing the Ac concentration and annealing the matrix for several minutes to allow diffusion of the trapped species results in an increase of the intensity of these bands. Since the new bands appear only in the presence of both FMA and Ac they are assigned to a FMA – Ac complexes. The peaks at 1730.9 cm^{-1} and 1724.2 cm^{-1} are also observed at low

concentrations of either FMA or Ac, and therefore are assigned to dimers of FMA – Ac and not to higher aggregates.

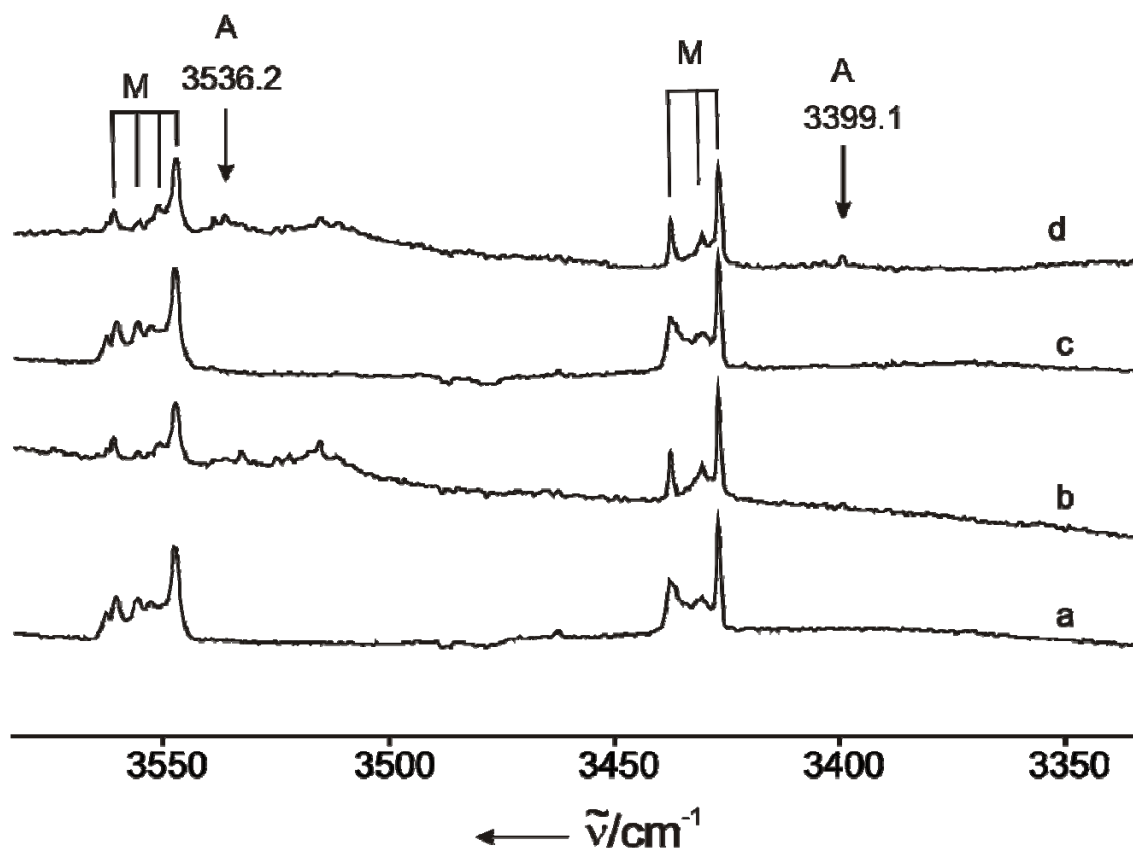


Figure 3.2.1. IR spectra in the range 3550 – 3350 cm^{-1} of FMA/Ac mixtures, matrix-isolated in argon: (a) FMA:Ac:Ar ratio 1:1:600, 10 K; (b) FMA:Ac:Ar ratio 1:1:600, after annealing at 30 K; (c) FMA:Ac:Ar ratio 1:3:600, 10 K; (d) FMA:Ac:Ar ratio 1:3:600 after annealing at 30 K. Vibrational modes were assigned to FMA/Ac complexes, respectively.

The doublet peaks at 1269.8 and 1260.4 cm^{-1} (Figure 3.2.3) correspond to the C–N stretching vibration of FMA monomer. A blue shift of the C–N stretching vibration is characteristic of FMA in hydrogen bonded complexes.^[59, 109] After annealing the matrix for several minutes at 30 K a new band at 1273.1 cm^{-1} appears, simultaneously the monomer bands start to decrease. On co-deposition of FMA with Ac and Ar (1:3:600 molar ratios), the peak at 1273.1 cm^{-1} can be observed even without annealing (Figure 3.2.3 spectrum c). After annealing the matrix at 30 K this band gains in intensity, as expected for a FMA – Ac complex. Even at low concentrations of FMA or Ac the peak at 1273.1 cm^{-1} is found, and is therefore assigned to the C–N stretching mode of a 1:1 FMA – Ac complex. Another

weak band is observed at 1276.9 cm^{-1} , blue-shifted by 16.5 cm^{-1} from the unperturbed FMA.

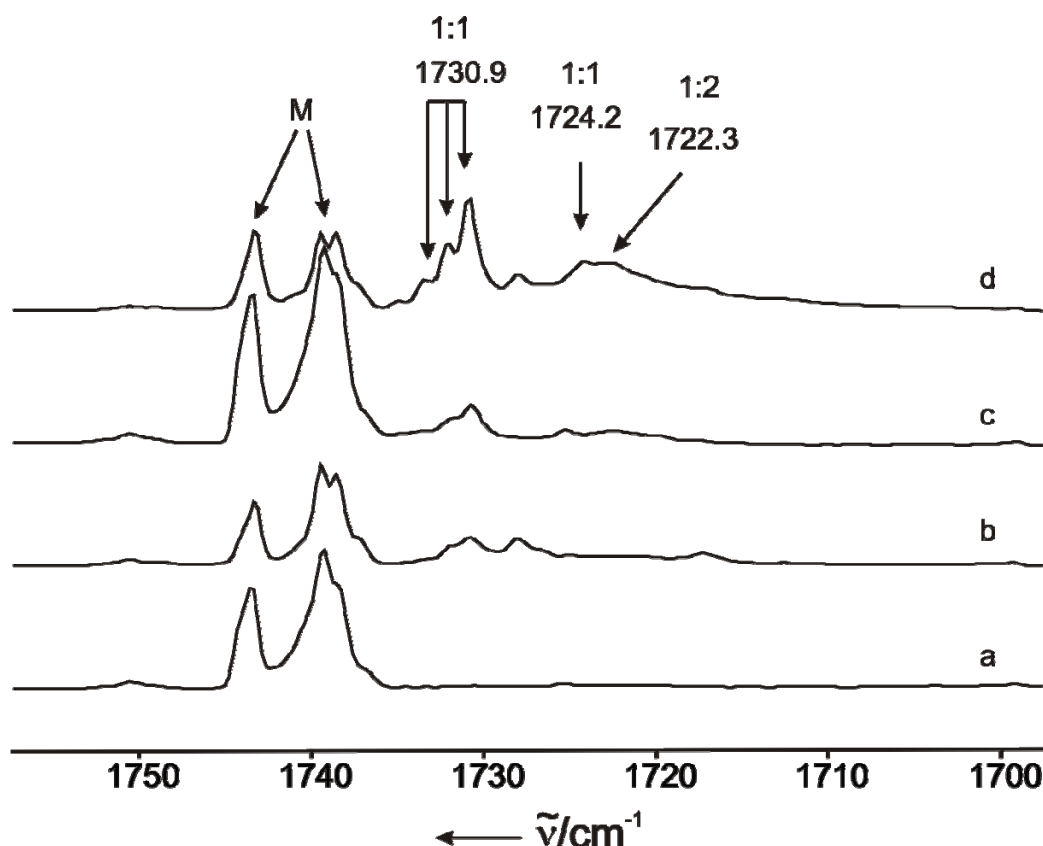


Figure 3.2.2. IR spectra in the range $1760 - 1700\text{ cm}^{-1}$ of FMA/Ac mixtures, matrix-isolated in argon: (a) FMA:Ac:Ar ratio 1:1:600, 10 K; (b) FMA:Ac:Ar ratio 1:1:600, after annealing at 30 K; (c) FMA:Ac:Ar ratio 1:3:600, 10 K; (d) FMA:Ac:Ar ratio 1:3:600 after annealing at 30 K. Vibrational modes were assigned to FMA/Ac complexes, respectively.

The vibrational modes of Ac are also perturbed in the presence of FMA. The C–H stretching mode (ν_3) of Ac monomer is observed at 3288.8 cm^{-1} and the ($\nu_2 + \nu_4 + \nu_5$) mode is found at 3302.9 cm^{-1} .^[119] Additional weak bands appear around 3285, 3269, and 3265 cm^{-1} assigned to Ac dimers (Figure 3.2.4).^[119, 120, 122] The weak band at 3240 cm^{-1} has been assigned to a complex between Ac and water by Engdahl and Nelander.^[125] When Ac and FMA are co-deposited, new bands are observed at 3205.5, 3210.5, 3215.5, and 3232.2 cm^{-1} . The intensity of these absorptions depends on the FMA concentration, indicating the formation of FMA – Ac complexes. In the C–H bending region of Ac the doubly degenerated ν_5 mode is observed at 736.8 cm^{-1} with two satellites at 744.7 and 750.8 cm^{-1} (Figure 3.2.5).^[120, 121] After co-deposition of FMA with Ac new bands appear at 784.3,

790.4 cm^{-1} , 795.7 and 819.3 cm^{-1} . The intensities these absorptions depend on the concentrations of FMA and Ac, are assigned to a 1:1 complexes.

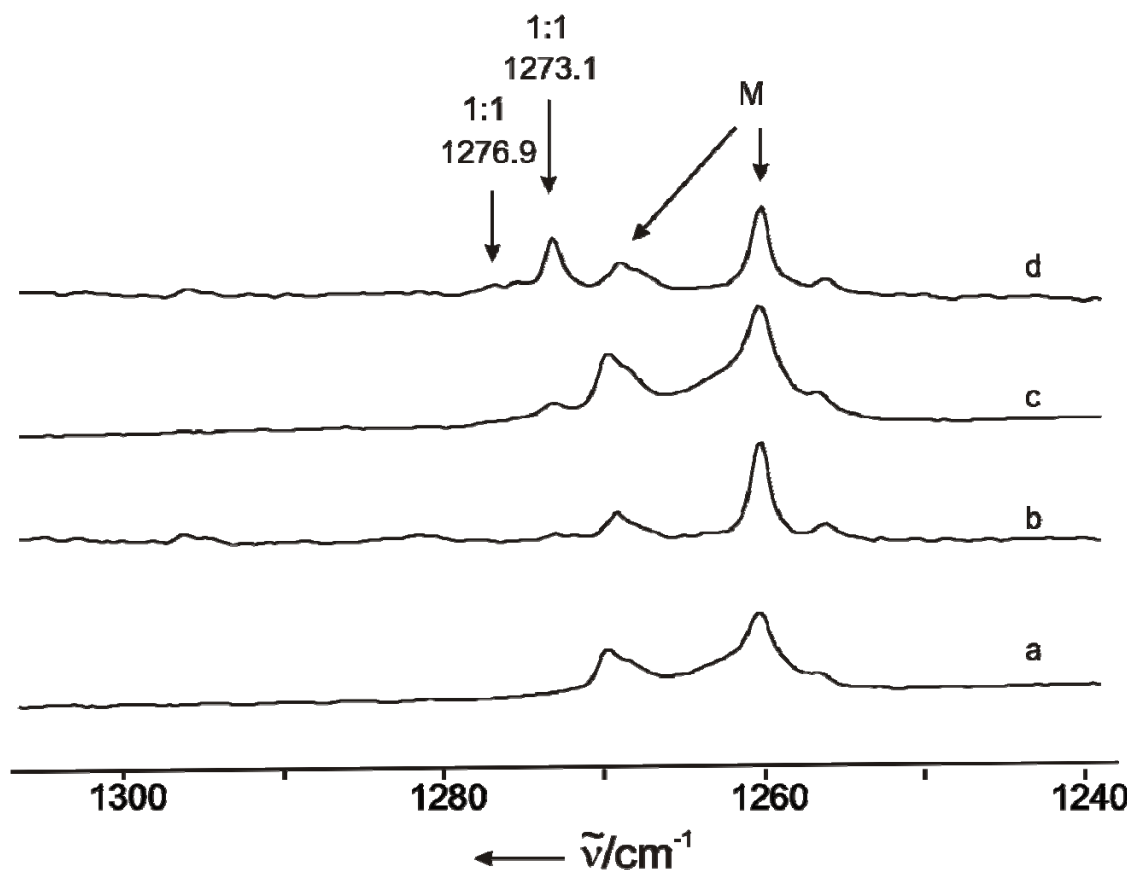


Figure 3.2.3. IR spectra in the range $1300 - 1240\text{ cm}^{-1}$ of FMA/Ac mixtures, matrix-isolated in argon: (a) FMA:Ac:Ar ratio 1:1:600, 10 K; (b) FMA:Ac:Ar ratio 1:1:600, after annealing at 30 K; (c) FMA:Ac:Ar ratio 1:3:600, 10 K; (d) FMA:Ac:Ar ratio 1:3:600 after annealing at 30 K. Vibrational modes were assigned to FMA/Ac complexes, respectively.

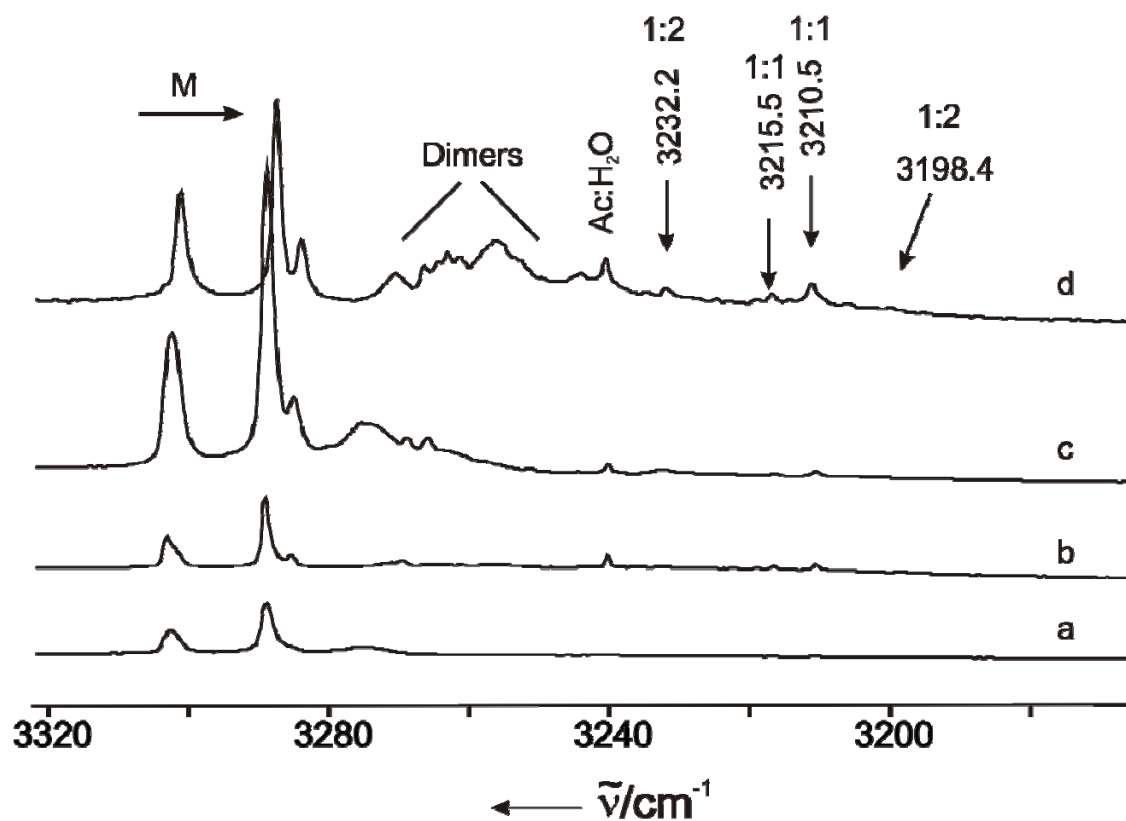


Figure 3.2.4. IR spectra in the range $3200 - 3180 \text{ cm}^{-1}$ of FMA/Ac mixtures, matrix-isolated in argon: (a) FMA:Ac:Ar ratio 1:1:600, 10 K; (b) FMA:Ac:Ar ratio 1:1:600, after annealing at 30 K; (c) FMA:Ac:Ar ratio 1:3:600, 10 K. (d) FMA:Ac:Ar ratio 1:3:600 after annealing at 30 K. Vibrational modes were assigned to FMA/Ac complexes, respectively.

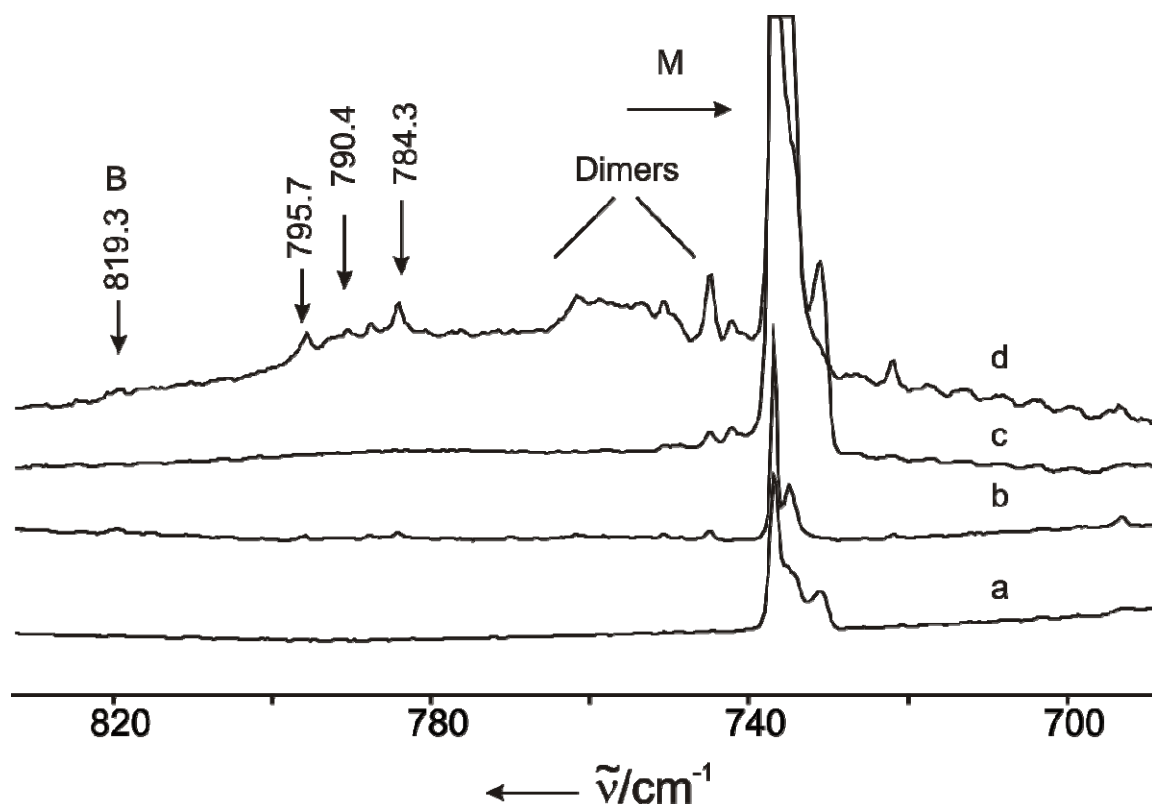


Figure 3.2.5. IR spectra in the range $830 - 700 \text{ cm}^{-1}$ of FMA/Ac mixtures, matrix-isolated in argon: (a) FMA:Ac:Ar ratio 1:1:600, 10 K; (b) FMA:Ac:Ar ratio 1:1:600, after annealing at 30 K; (c) FMA:Ac:Ar ratio 1:3:600, 10 K. (d) FMA:Ac:Ar ratio 1:3:600 after annealing at 30 K. Vibrational modes were assigned to FMA/Ac complexes, respectively.

3.2.2.1.2. Nitrogen Matrix

To investigate the influence of the matrix host, the FMA/Ac experiments were performed in nitrogen matrix. In the N–H stretching region the strong bands at 3553.2 and 3430.5 cm^{-1} are assigned to the asymmetric and symmetric N–H stretching modes of the FMA monomer, in good agreement with the values previously reported by Räsänen.^[92] The bands at 3517.6 , 3513.9 and 3511.7 cm^{-1} are due to the formation of FMA dimers in the nitrogen matrix (Figure 3.2.6).^[93]

In the presence of both FMA and Ac new bands are observed at 3540.7 , 3428.4 and 3405.7 cm^{-1} . The intensity of these bands increases with the concentration of both FMA and Ac, since these bands appeared at low concentrations of FMA and Ac, indicating the formation of a 1:1 complexes.

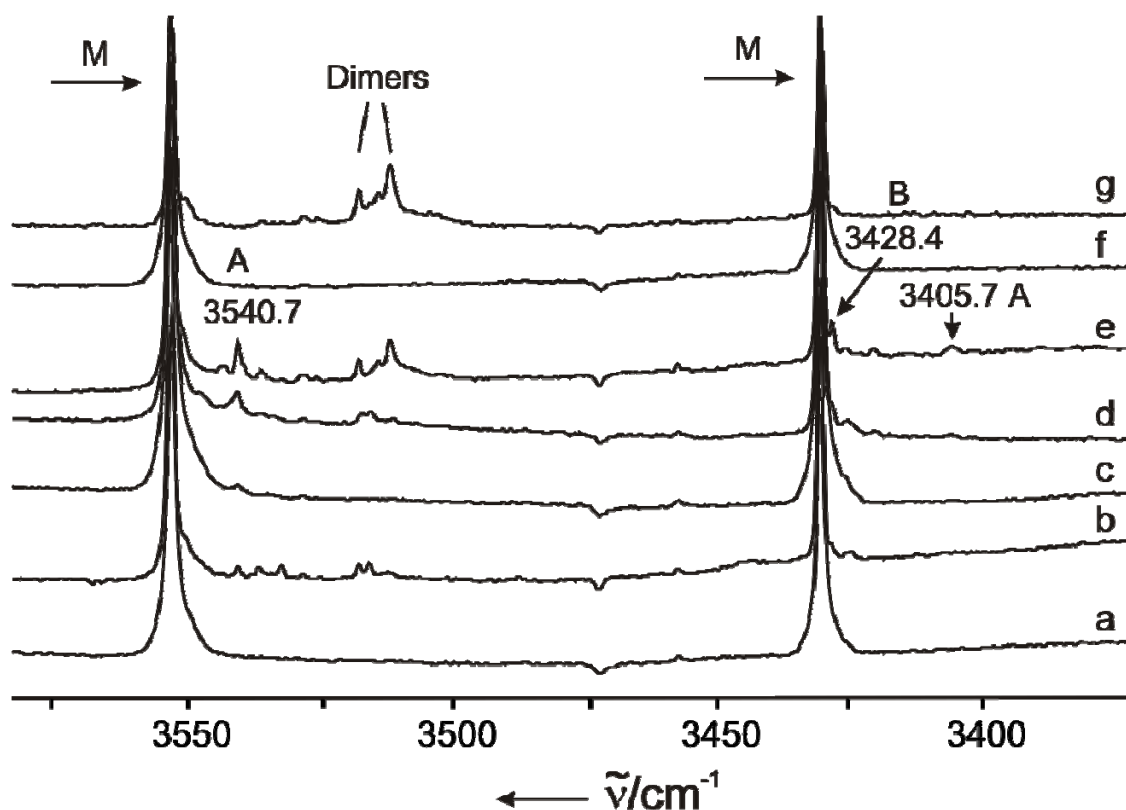


Figure 3.2.6. IR spectra in the range $3600 - 3350 \text{ cm}^{-1}$ of FMA/Ac mixtures, matrix-isolated in nitrogen: (a) FMA:Ac:N₂ ratio 1:1:600, 10 K; (b) FMA:Ac: N₂ ratio 1:1:600, after annealing at 30 K; (c) FMA:Ac: N₂ ratio 1:3:600, 10 K; (d) FMA:Ac: N₂ ratio 1:3:600 after annealing at 25 K; (e) FMA:Ac: N₂ ratio 1:3:600 after annealing at 30K; (f) FMA: N₂ ratio 1:600, 10 K; (g) FMA: N₂ ratio 1:600, after annealing at 25 K; Vibrational modes were assigned to FMA/Ac complexes , respectively.

In the nitrogen matrix the C=O stretching mode of the FMA monomer appears at 1736.1 cm^{-1} (Figure 3.2.7).^[92] In the presence of both FMA and Ac new bands appear at 1729.3 , 1726.0 , and 1721.9 cm^{-1} , which are assigned to the C=O stretching vibrations of a FMA – Ac complexes. The bands at 1729.3 and 1726.0 cm^{-1} can be observed at low concentrations of Ac and FMA and are thus assigned to dimers and not to higher aggregates. In contrast, the band at 1721.9 cm^{-1} appears only at high concentrations of Ac. Therefore, this band can be assigned to a 1:2 FMA – Ac complex.

A few new bands are observed at 1274.9 , 1267.5 , and 1260.8 cm^{-1} , the region of C–N stretching vibrations of FMA (Figure 3.2.8). These bands are blue shifted from the unperturbed C–N stretching vibration mode at 1246.5 cm^{-1} .

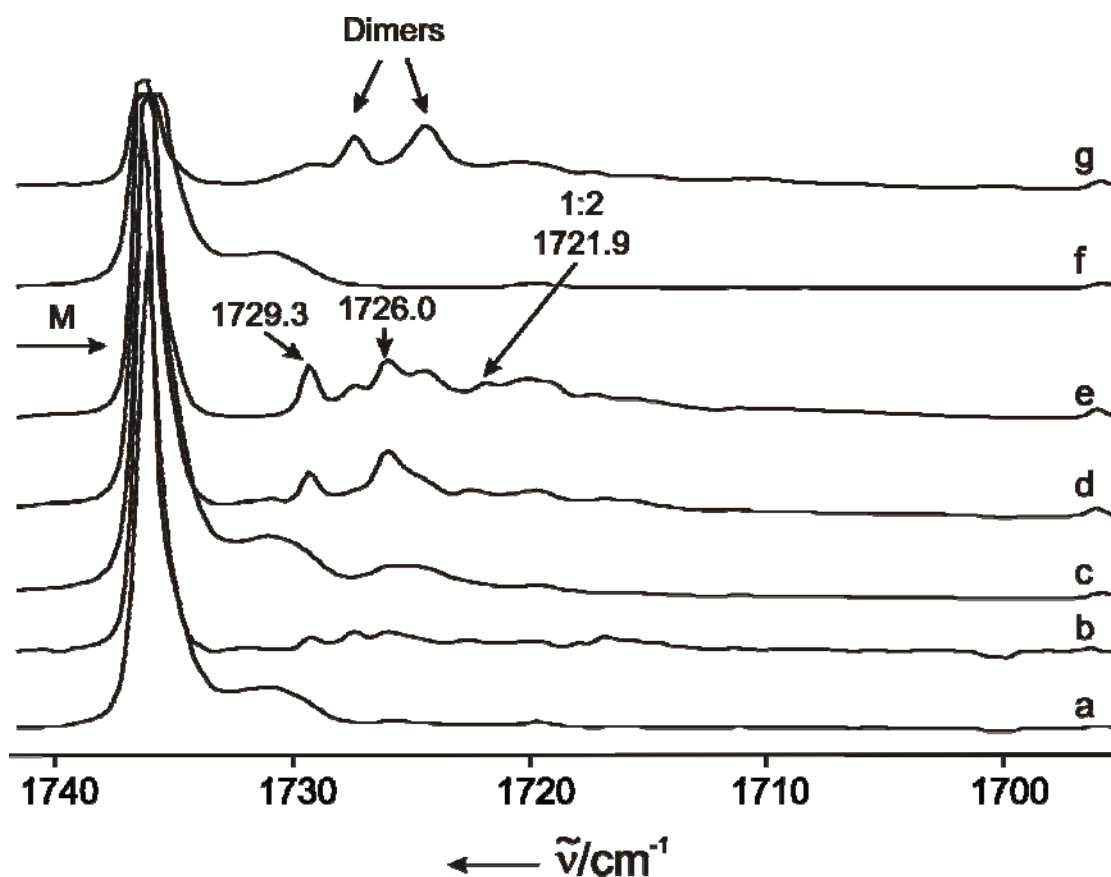


Figure 3.2.7. IR spectra in the range 1740 – 1700 cm^{-1} of FMA/Ac mixtures, matrix-isolated in nitrogen: (a) FMA:Ac: N_2 ratio 1:1:600, 10 K; (b) FMA:Ac: N_2 ratio 1:1:600, after annealing at 30 K; (c) FMA:Ac: N_2 ratio 1:3:600, 10 K; (d) FMA:Ac: N_2 ratio 1:3:600 after annealing at 25 K; (e) FMA:Ac: N_2 ratio 1:3:600 after annealing at 30K; (f) FMA: N_2 ratio 1:600, 10 K; (g) FMA: N_2 ratio 1:600, after annealing at 25 K; Vibrational modes were assigned to FMA/Ac complexes , respectively.

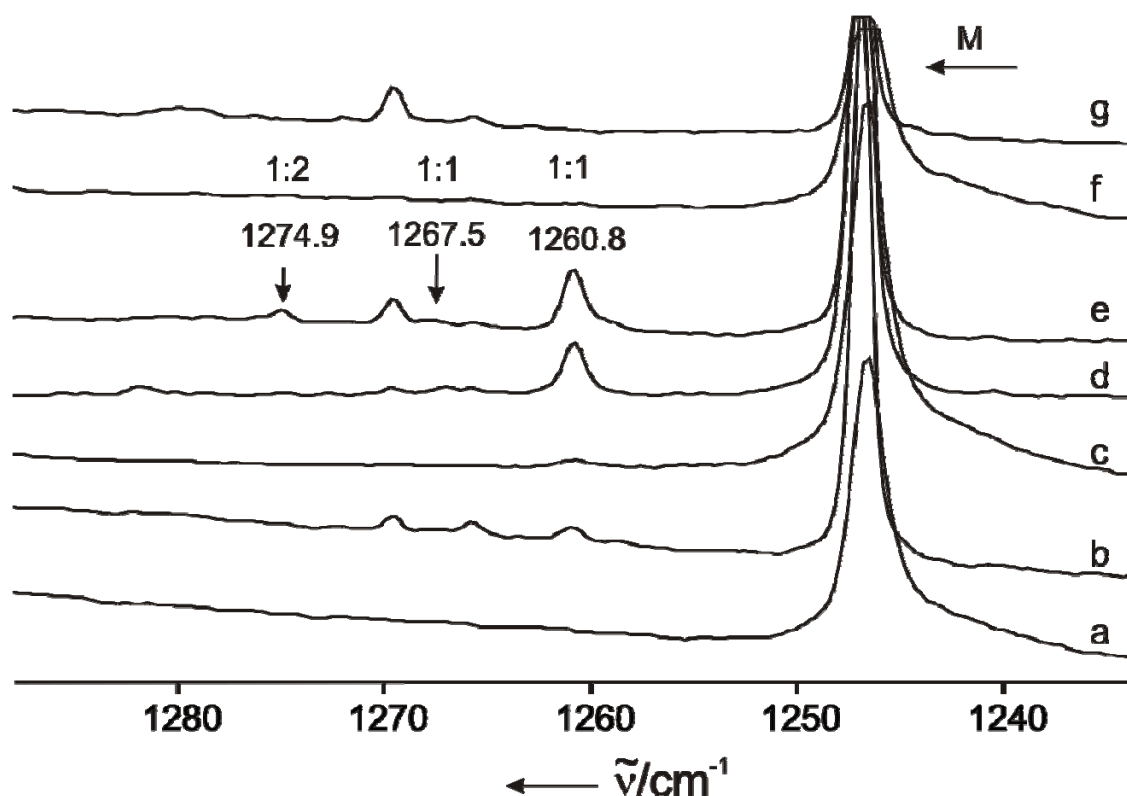


Figure 3.2.8. IR spectra in the range 1280 – 1240 cm^{-1} of FMA/Ac mixtures, matrix-isolated in nitrogen: (a) FMA:Ac: N_2 ratio 1:1:600, 10 K; (b) FMA:Ac: N_2 ratio 1:1:600, after annealing at 30 K; (c) FMA:Ac: N_2 ratio 1:3:600, 10 K; (d) FMA:Ac: N_2 ratio 1:3:600 after annealing at 25 K; (e) FMA:Ac: N_2 ratio 1:3:600 after annealing at 30K; (f) FMA: N_2 ratio 1:600, 10 K; (g) FMA: N_2 ratio 1:600, after annealing at 25 K; Vibrational modes were assigned to FMA/Ac complexes , respectively.

The unperturbed C–H stretching vibration of Ac in solid nitrogen appears at 3283.0 cm^{-1} and 3311.0 cm^{-1} , the latter with very low intensity.^[121] Bands at 3218.5 and 3225.7 cm^{-1} are assigned to the Ac – H_2O complex and bands at 3258.0 and 3279.2 cm^{-1} to the Ac dimer.^[126]

When Ac and FMA are co-deposited in nitrogen and the matrix is subsequently annealed, new bands appear at 3226.1, 3221.4 cm^{-1} and barely visible at 3215.5 cm^{-1} . These bands correspond to the ν_3 stretching vibration of Ac in a FMA – Ac complexes (Figure 3.2.9).

The CC–H bending mode occurs as a doublet at 747.6 and 742.1 cm^{-1} (Figure 3.2.10).^[121] After co-deposition of FMA with Ac new bands at 796.4, 791.1 and 787.7 cm^{-1} are observed. From the dependence of the intensities of these absorptions on the concentrations of both monomers we conclude that a 1:1 complexes of FMA and Ac are formed.

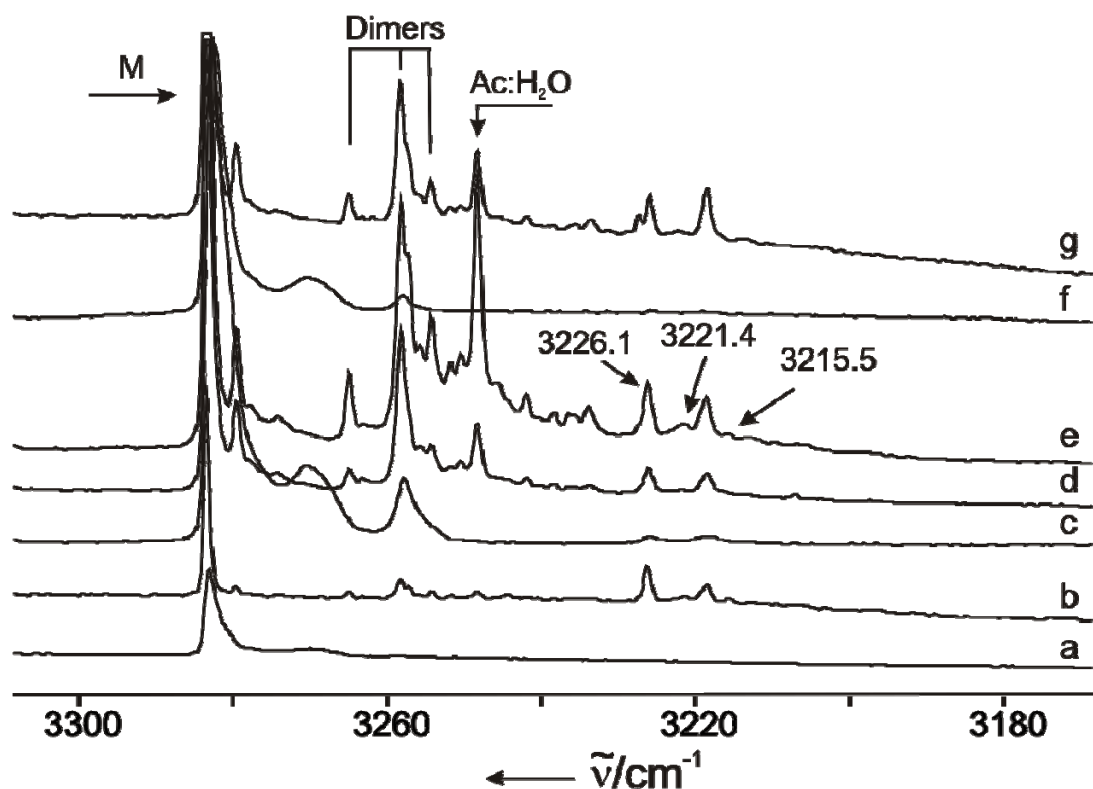


Figure 3.2.9. IR spectra in the range $3300 - 3200 \text{ cm}^{-1}$ of FMA/Ac mixtures, matrix-isolated in nitrogen: (a) FMA:Ac:N₂ ratio 1:1:600, 10 K; (b) FMA:Ac: N₂ ratio 1:1:600, after annealing at 30 K; (c) FMA:Ac: N₂ ratio 1:3:600, 10 K; (d) FMA:Ac: N₂ ratio 1:3:600 after annealing at 25 K; (e) FMA:Ac: N₂ ratio 1:3:600 after annealing at 30 K; (f) FMA: N₂ ratio 1:600, 10 K; (g) FMA: N₂ ratio 1:600, after annealing at 25 K; Vibrational modes were assigned to FMA/Ac complexes, respectively.

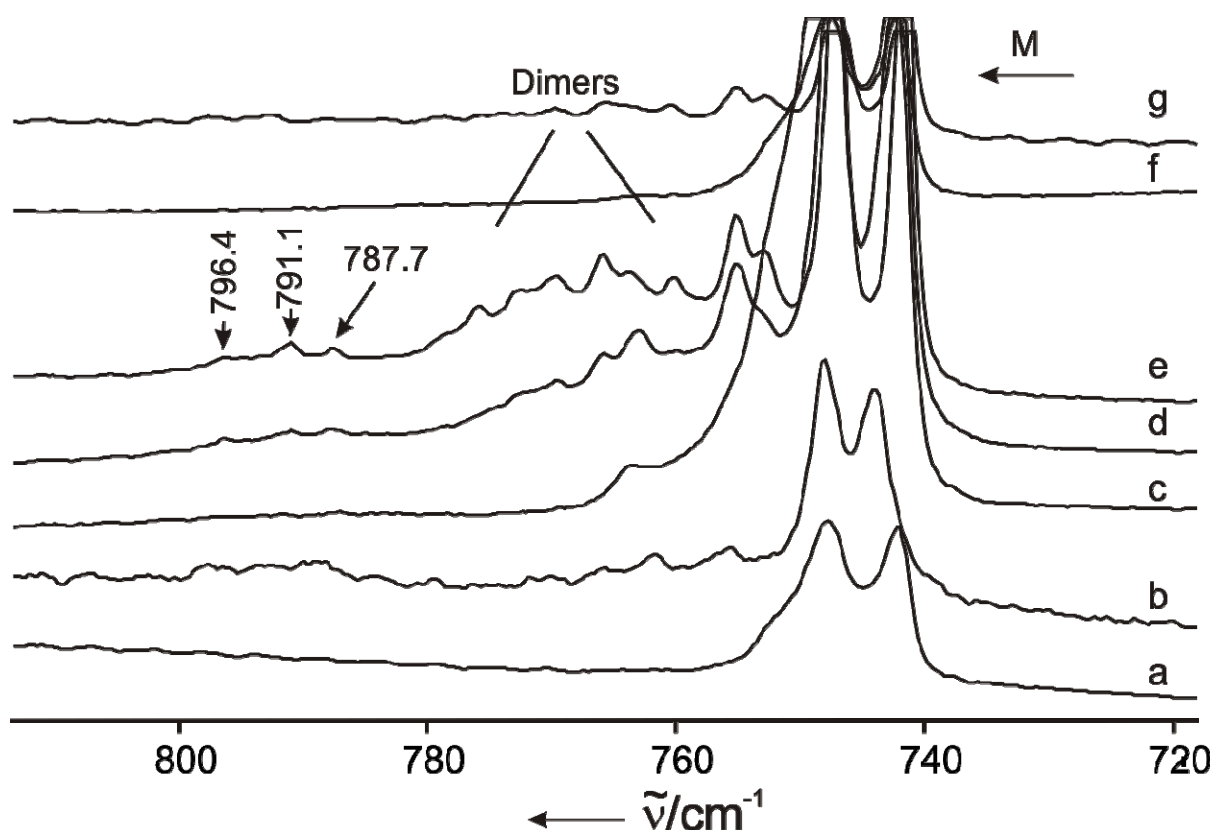


Figure 3.2.10. IR spectra in the range 810 – 720 cm^{-1} of FMA/Ac mixtures, matrix-isolated in nitrogen: (a) FMA:Ac: N_2 ratio 1:1:600, 10 K; (b) FMA:Ac: N_2 ratio 1:1:600, after annealing at 30 K; (c) FMA:Ac: N_2 ratio 1:3:600, 10 K; (d) FMA:Ac: N_2 ratio 1:3:600 after annealing at 25 K; (e) FMA:Ac: N_2 ratio 1:3:600 after annealing at 30K; (f) FMA: N_2 ratio 1:600, 10 K; (g) FMA: N_2 ratio 1:600, after annealing at 25 K; Vibrational modes were assigned to FMA/Ac complexes , respectively.

3.2.2.2. Computational results (by Elsa Sanchez-Garcia)^[103]

3.2.2.2.1. Dimers

Three FMA – Ac dimers were localized at the MP2 level of theory with the aug-cc-pVDZ and cc-pVTZ basis sets. The geometries and ZPE+BSSE corrected binding energies of the dimers are discussed here at the MP2/cc-pVTZ level of theory only, since there is a very good agreement between the calculated geometries and binding energies with both basis sets (Figure 3.2.11 and Table 3.2.1).

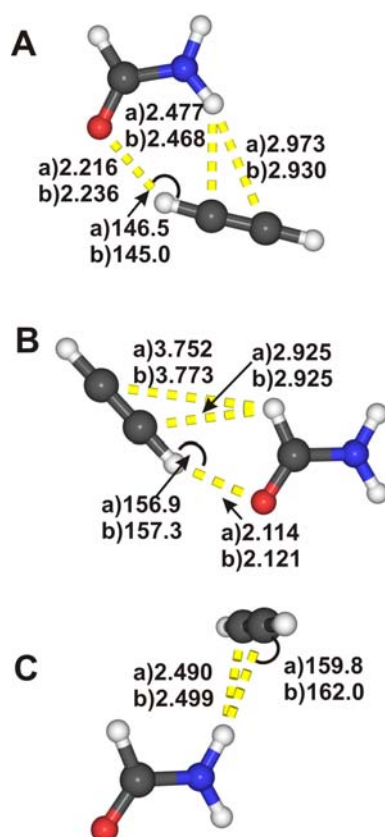


Figure 3.2.11. The calculated structures with hydrogen bond lengths (Å) of the FMA – acetylene dimers A, B and C at the a) MP2/cc-pVTZ and b) MP2/aug-cc-pVDZ levels of theory.

There are three basic interactions between the FMA and acetylene molecules in the dimers:

- (1) $\text{N-H}_{\text{FMA}} \dots \pi$ interaction between the amide hydrogen atom of FMA and the π system of acetylene.
- (2) $\text{C=O}_{\text{FMA}} \dots \text{H}_{\text{acet}}$ interaction between the carbonyl oxygen atom of FMA and one hydrogen atom of acetylene.
- (3) $\text{C-H}_{\text{FMA}} \dots \pi$ interaction between the CH hydrogen atom of FMA and the π system of acetylene.

The most stable dimer **A** (-2.96 kcal/mol) is stabilized by the $\text{N-H}_{\text{FMA}} \dots \pi$ interaction (1) with distances of 2.447 and 2.973 Å to both carbon atoms of acetylene. The $\text{C=O}_{\text{FMA}} \dots \text{H}_{\text{acet}}$ interaction (2) at 2.216 Å additionally stabilizes dimer **A** which is 0.50 kcal/mol more stable than complex **B** (-2.46 kcal/mol). (Figure 11 and Table 1)

In dimer **B** the interaction (2) shows a shorter hydrogen bond distance (2.114 Å) compared to dimer **A**. Complex **B** is additionally stabilized by a very weak $\text{C-H}_{\text{FMA}} \dots \pi$ interaction (3) with 2.925 and 3.752 Å distance to both acetylene carbon atoms. This

shows the importance of the contribution of interaction (2) to the stabilization of both dimers **A** and **B**. In dimer **B**, albeit interaction (3) is very weak, it also contributes to define the shape of the complex. Dimer **C** is a very weakly interacting complex (-1.79 kcal/mol) which is only stabilized by interaction (1) with a $\text{N-H}_{\text{FMA}} \cdots \text{C}_{\text{acet}}$ distance of 2.490 Å to both acetylene carbon atoms.

Table 3.2.1. Calculated binding energies (kcal/mol) of the FMA – acetylene dimers **A**, **B** and **C** at the MP2 level of theory

	MP2/aug-cc-pVDZ				MP2/cc-pVTZ			
	ΔE	BSSE	ZPE	$\Delta E_{(\text{BSSE}+\text{ZPE})}$	ΔE	BSSE	ZPE	$\Delta E_{(\text{BSSE}+\text{ZPE})}$
A	-5.59	1.32	1.27	-3.00	-5.20	1.10	1.14	-2.96
B	-4.84	1.16	1.12	-2.56	-4.62	1.06	1.10	-2.46
C	-3.67	1.10	0.80	-1.77	-3.12	0.59	0.74	-1.79

3.2.2.2.2. Trimers

Eight 1:2 FMA – Ac trimers (**T-A** to **T-H**) were localized at the MP2/aug-cc-pVDZ level of theory, using the MMH approach and starting from 200 randomly generated geometries (Figure 3.2.12).

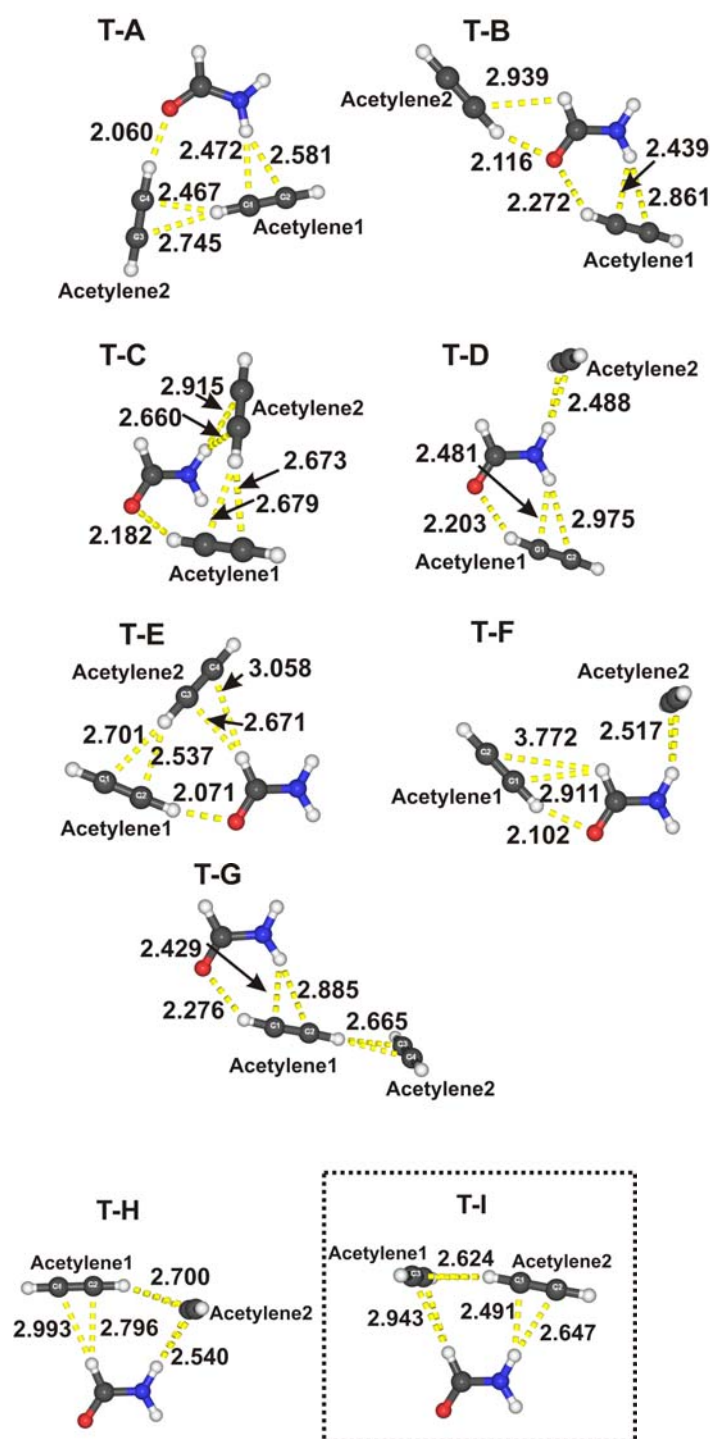


Figure 3.2.12. The calculated structures with hydrogen bond lengths (Å) of the FMA – acetylene trimers T-A to T-I at the MP2/aug-cc-pVDZ level of theory.

Similarly to the dimers, the 1:2 FMA – Ac complexes are stabilized by interactions (1), (2) and (3), but there is also the $\text{C-H}_{\text{acet}} \dots \pi$ interaction (interaction (4)) between both molecules of acetylene. Trimers T-A and T-B are the most stable complexes and, with -5.44 and -5.54 kcal/mol, respectively, very close in energy (for the trimers, all energies discussed here are at the MP2/aug-cc-pVDZ + BSSE + ZPE level of theory, Table 3.2.2).

The trimer **T-A** is stabilized by the $\text{N-H}_{\text{FMA}}\dots\pi$ interaction (1) of FMA with the first acetylene molecule Ac1, the $\text{C=O}_{\text{FMA}}\dots\text{H}_{\text{acet}}$ interaction (2) FMA – Ac2 and the $\text{C-H}_{\text{acet}}\dots\pi$ interaction (4) between both molecules of Ac resembling the well established “T” shaped acetylene dimer.^[127-134]

In complex **T-B** the two molecules of Ac do not interact with each other. Instead, the oxygen atom of FMA interacts with the hydrogen atoms of both molecules of Ac (interaction (2)) and one of the FMA N-H hydrogen atoms interacts with the π system of Ac1 (interaction (1)). The position of Ac2 with respect to the FMA molecule indicates a very weak $\text{C-H}\dots\pi$ interaction (3), which also has been found in the 1:2 formic acid – Ac trimers.^[135]

At this point, it is very interesting to compare the geometries of the 1:2 FMA – Ac **T-A** and **T-B** trimers with the two most stable 1:2 formic acid – Ac complexes (**F-A** and **F-B**) previously studied in our group (Figure 3.2.13).^[135] It is remarkable that, starting from completely randomly generated geometries without any previous chemical assumptions, the 1:2 FMA and the formic acid complexes with Ac show very similar structures. The 1:2 formic acid – Ac trimer **F-A** is stabilized by the $\text{O-H}_{\text{FA}}\dots\pi$ interaction involving one molecule of Ac, and the $\text{C=O}_{\text{FA}}\dots\text{H}_{\text{acet}}$ interaction involving the second molecule of Ac, together with the acetylene – acetylene $\text{C-H}_{\text{acet}}\dots\pi$ “T” interaction, similarly to the 1:2 FMA – Ac complex **T-A**.

Table 3.2.2. Calculated binding energies (kcal/mol) of the FMA – acetylene trimers **T-A** to **T-I** at the MP2/aug-cc-pVDZ level of theory

	MP2/aug-cc-pVDZ			
	ΔE	BSSE	ZPE	$\Delta E_{(\text{BSSE}+\text{ZPE})}$
T-A	–11.08	3.26	2.38	–5.44
T-B	–10.44	2.60	2.30	–5.54
T-C	–9.71	2.97	2.01	–4.73
T-D	–9.47	2.55	2.03	–4.89
T-E	–9.46	2.95	2.00	–4.51
T-F	–8.82	2.37	1.88	–4.57
T-G	–8.16	2.44	1.87	–3.85
T-H	–6.96	2.83	1.51	–2.62
T-I^a	–7.22			

[a] T-I does not represent a minimum at this level of theory.

Similar to the 1:2 FMA – Ac complex T-**B**, the formic acid – Ac trimer F-**B** also does not show any interaction between the two molecules of acetylene. F-**B** is stabilized by the $\text{O-H}_{\text{FA}} \cdots \pi$ interaction with Ac1 and $\text{C=O}_{\text{FA}} \cdots \text{H}_{\text{acet}}$ interactions with both molecules of acetylene. In both T-**B** and F-**B** the second molecule of Ac stabilizes the trimer via a $\text{C-H}_{\text{FA(FMA)}} \cdots \pi$ interaction.

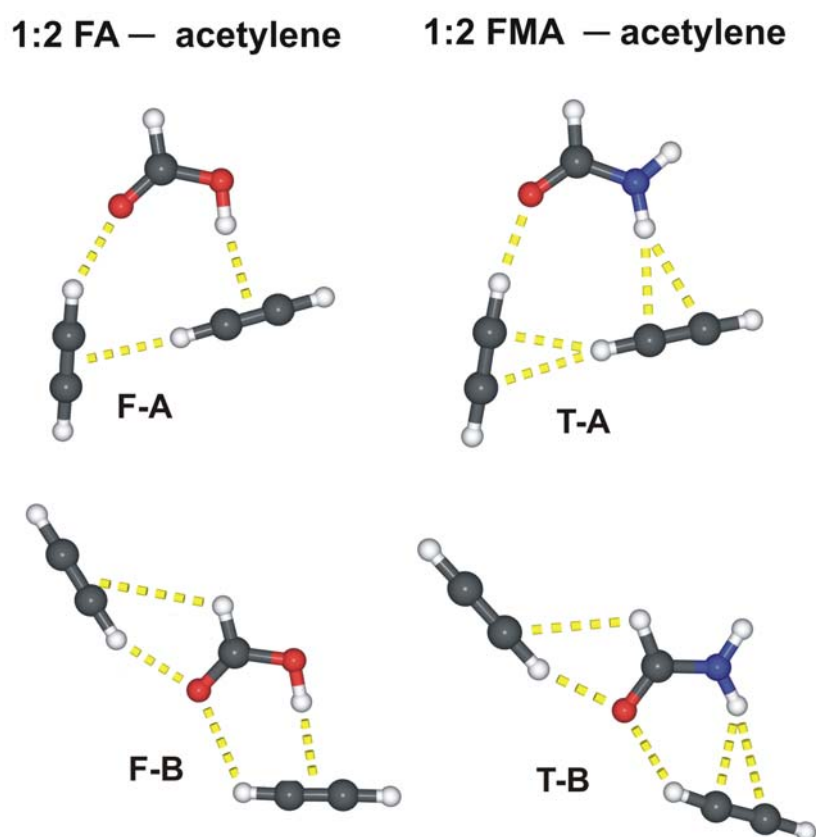


Figure 3.2.13. FMA – acetylene trimers T-A and T-B and FA – acetylene trimers F-A and F-B^[135] MP2/cc-pVTZ level of theory.

3.2.2.3. Comparison of Calculated and Experimental Vibrational

3.3.2.3.1. Frequencies: Dimers A and B

The experimental vibrational frequencies of the FMA – Ac dimers were compared to MP2/cc-pVTZ calculations (Tables 3.2.4-3.2.6). The deviations between the experimental and calculated modes are attributed to matrix shifts as well as deficiencies of the theoretical model (e. g. not considering the anharmonicity of the vibrations). Scaling

factors for each vibrational mode of the FMA and acetylene monomers were calculated to correct for these deviations. These scaling factors, by definition, exactly reproduce the experimental values of the monomers (Table 3.2.3). Applying the scaling factor to the modes of the complexes allows to reliably predict the band positions for the complexes.

N–H and Acetylene C–H Stretching Vibrations. Our experimental data in argon and nitrogen matrices indicate the formation of two cyclic FMA – acetylene complexes **A** and **B**. In the N–H stretching region in argon new bands at 3399.1 (–27.5) and 3536.2 (–11.2) cm^{-1} are observed, in good agreement with the predictions from the MP2/cc-pVTZ calculations for complex **A** (scaled, Table 3.2.4). In nitrogen a similar agreement between experiment and calculation was found. In dimer **B** the NH group of FMA is not engaged in hydrogen bonding (Figure 3.2.11), and thus the NH stretching vibration of the FMA subunit in **B** shows only small shifts compared to the FMA monomer band. In argon the shift was too small to be detected whereas in nitrogen a new band at 3428.4 cm^{-1} (red shift –2.1 cm^{-1}) is assigned to the symmetric stretching vibration mode of FMA in dimer **B**.

The large shifts in the C–H stretching and bending modes of acetylene show that the acetylene hydrogen atoms are the hydrogen bond donors. The shift of the ν_3 mode of acetylene is a good indicator of the hydrogen bond strength.^[136, 137] According to our calculations the largest shifts are expected for the C–H stretching vibration of acetylene in complex **A**, which after scaling is predicted at 3220.1 cm^{-1} and 3213.4 cm^{-1} in argon and nitrogen, respectively (Table 3.2.4, the difference is due to different scaling factors in argon and nitrogen). For dimer **B** the C–H stretching vibration is calculated to 3199.0 cm^{-1} (argon, Figure 3.2.4, Table 3.2.4). The C–H stretching vibration calculated for complex **A** at 3220.1 cm^{-1} (argon) agrees well with both experimentally observed bands at 3215.5 and 3210.5 cm^{-1} . The difference between the experimental bands (3215.5 and 3210.5 cm^{-1}) is only 5 cm^{-1} , the difference calculated for the two dimers in argon 21.1 cm^{-1} . It is therefore not possible to make a clear assignment of the C–H stretching vibrations of acetylene to dimer **A** or **B**.

The C–H stretching vibration of monomeric acetylene in a nitrogen matrix is found at 3283.0 cm^{-1} together with a weak doublet at 3227.4 and 3225.7 cm^{-1} (Figure 3.2.9). A singlet at 3218.5 cm^{-1} is assigned to the well known acetylene – water complex.^[126] In the presence of both FMA and acetylene an additional band at 3226.1 cm^{-1} is found. For dimer **A** the calculations (MP2/cc-pVTZ) predict this band at 3213.4 cm^{-1} (red-shifted by 67.3 cm^{-1} from the monomer), quite close to the experimental value (Table 3.2.4). For dimer **B**

this band is expected at 3192.2 cm^{-1} (red-shifted by 86.4 cm^{-1} from the monomer) in less agreement with the experiment.

Acetylene C–H Bending Vibrations. An additional criterion for the hydrogen bond formation in acetylene complexes is the blue shift of the C–H bending modes of the acetylene unit. The C–H bending modes in complex **A** are predicted (MP2/cc-pVTZ, scaled) at $795.7 (+59.3)$ and $794.5 (+58.1)\text{ cm}^{-1}$ in argon and at $803.8 (+59.8)$ and $802.6 (+58.7)\text{ cm}^{-1}$ in nitrogen, respectively, thus showing the expected blue shifts (Table 3.2.4). For complex **B** bands are predicted at $833.2 (+96.7)$ and $797.6 (+61.1)\text{ cm}^{-1}$ in argon and at $841.6 (+97.7)$ and $805.7 (+61.7)\text{ cm}^{-1}$ in nitrogen. The band observed at 819.3 cm^{-1} in argon with the large blue shift of $+82.5\text{ cm}^{-1}$ is thus been assigned to complex **B**, whereas the other three bands at $795.7 (+58.9)$, $790.4 (+53.6)$, and $784.3 (+47.5)\text{ cm}^{-1}$ could either belong to **A** or **B** (Figure 3.2.5). In nitrogen only three bands at 796.4 , 791.1 and 787.7 cm^{-1} are observed.

C=O Stretching Vibrations. The presence of two shifted C=O stretching vibrations at 1730.9 and 1724.2 cm^{-1} in argon and at 1729.3 and 1726.0 cm^{-1} in nitrogen indicates that two complexes are formed with the carbonyl group as hydrogen bond acceptor. For complexes **A** and **B** the C=O stretching vibrations are calculated (scaled) to 1724.8 and 1724.9 cm^{-1} , respectively, in argon, and 1721.2 cm^{-1} and 1721.3 cm^{-1} , respectively, in nitrogen (Table 3.2.4). Since the C=O stretching vibrations in both complexes are very close, a definitive assignment was not possible.

C–N Stretching Vibrations. The formation of FMA – Ac complexes results in blue shifts of the C–N stretching vibrations (Figures 3.2.3 and 3.2.8). In argon a weak band at 1276.9 and a strong band at 1273.1 cm^{-1} are assigned to FMA – Ac complexes. In nitrogen, new bands in this region are observed at 1274.9 (probably more than one acetylene molecule involved), 1267.5 and 1260.8 cm^{-1} .

The C–N stretching mode of **A** is calculated (MP2/cc-pVTZ, scaled) to 1279.2 cm^{-1} in argon and 1263.5 cm^{-1} in nitrogen, and that of **B** to 1275.0 cm^{-1} in argon and 1259.4 cm^{-1} in nitrogen, respectively. We therefore assign the bands at higher frequency to dimer **A** and that at lower frequency to dimer **B**.

The comparison between our calculated and experimental spectra shows that we are able to trap both dimer **A** and **B** in argon and nitrogen matrices whereas complex **C** is not observed (Table 3.2.5). Since the expected shifts for many bands in **A** and **B** are small or very similar, the assignments can only be tentative in these cases.

Table 3.2.3. Calculated and experimental vibrational frequencies (cm^{-1}) of the FMA and acetylene monomers.

MP2/cc-pVTZ		Argon		Nitrogen		Assignment
Mode	Calc.	Exp.	Factor of correction	Exp.	Factor of correction	
Formamide (FMA)						
6	1285.1	1260.4	0.981	1246.5	0.969	ν (C–N)
9	1811.0	1739.1	0.960	1736.1	0.958	ν (C=O)
10	3017.2	2882.9	0.955	2871.2	0.951	ν (C–H)
11	3634.7	3426.6	0.943	3430.5	0.943	ν_s (NH ₂)
12	3787.1	3547.4	0.937	3553.2	0.938	ν_{as} (NH ₂)
Acetylene (Ac)						
5	753.0	736.8	0.978	742.1 747.6	0.988	δ (CCH)
3	3446.1	3288.8	0.954	3283.0	0.952	ν_{as} (C–H)

Table 3.2.4. Experimental and calculated vibrational frequencies and shifts (cm^{-1}) of the FMA – acetylene dimers **A** and **B**.

Experimental		MP2/cc-pVTZ						Experimental		MP2/cc-pVTZ		
Argon	Rel. Int.	Dimer A uncorrect.	Dimer A correct.	Rel. Int.	Dimer B uncorrect.	Dimer B correct	Rel. Int.	Nitrogen	Rel. Int.	Dimer A correct.	Dimer B correct	Assingnment
Formamide (FMA) ^a												
1273.1 (+12.7)	9	1304.0	1279.2	32	1299.7	1275.0	27	1260.8 (+14.3)	20	1263.5	1259.4	v (C–N)(v ₆)
1276.9 (+16.5)	2	(+18.9)	(+18.5)		(14.6)	(+14.3)		1267.5 (+21.0)	2	(+18.3)	(+14.1)	
1724.2 (–14.9)	30	1796.7	1724.8	99	1796.8	1724.9	100	1726.0 (+10.1)	100	1721.2	1721.3	v(C=O)(v ₉)
1730.9 (–8.2)	100	(–14.3)	(–13.7)		(–14.2)	(–13.6)		1729.3 (+6.8)	92	(–13.7)	(–13.6)	
3399.1 (–27.5)	3	3603.6	3398.2	31	3631.9	3424.9	16	3405.7 (–28.4)	5	3398.2	3424.8	v _s (NH ₂)(v ₁₁)
		(–31.1)	(–29.3)		(–2.8)	(–2.6)		3428.4 (–2.1)	14	(–29.3)	(–2.6)	
3536.2 (–11.2)	4	3767.9	3530.5	30	3783.7	3545.3	15	3540.7 (–12.5)	17	3534.3	3550.0	v _{as} (NH ₂)(v ₁₂)
		(–19.2)	(–18.0)		(–3.4)	(–3.2)				(–18.0)	(–3.2)	
Acetylene (Ac) ^a												
784.3 (+47.5)	7	812.4 ^b	794.5 ^b	22	815.5 ^b	797.6 ^b	16	787.7 (+43.4)	16	802.6 ^b	805.7 ^b	δ(CCH)(v ₅)
790.4 (+53.6)	4	(+5)	(+58.1)		(+62.5)	(+61.1)		791.1 (+46.8)	18	(+58.7)	(+61.7)	
795.7 (+58.9)	8	813.6	795.7	39	851.9	833.2	27	796.4 (+52.1)	10	803.8	841.6	
819.3 (+82.5)	2	(+60.6)	(+59.3)		(+98.9)	(+96.7)				(+59.8)	(+97.7)	
3210.5 (–78.3)	21	3375.4	3220.1	60	3353.2	3199.0	77	3221.4 (–61.6)	20	3213.4	3192.2	v _{as} (C–H)(v ₃)
3215.5 (–73.3)	13	(–70.7)	(–67.4)		(–92.9)	(–88.6)		3226.1 (–56.9)	50	(–67.3)	(–86.4)	

[a] The frequency shifts in **A** compared to FMA and Ac (monomers M) are given in parentheses (Table 3.2.3).

[b] Out of plane mode.

Table 3.2.5. Calculated (MP2/cc-pVTZ) vibrational frequencies (cm^{-1}) of the FMA – acetylene dimer **C**.

Dimer C without correction		Corrected Argon		Corrected Nitrogen		Relative Intensity	Assignment
Formamide (FMA) ^a							
1288.4	(+3.3)	1263.9	(+3.2)	1248.4	(+1.9)	25	$\nu(\text{C-N})(\nu_6)$
1806.5	(−4.5)	1734.2	(−4.3)	1730.6	(−5.5)	99	$\nu(\text{C=O})(\nu_9)$
3608.2	(−0.6)	2880.8	(−0.57)	2868.8	(−2.4)	21	$\nu(\text{C-H})(\nu_{10})$
3608.2	(−26.5)	3402.5	(−25.0)	3402.5	(−25.0)	33	$\nu_s(\text{NH}_2)(\nu_{11})$
3759.7	(−27.4)	3522.8	(−25.7)	3526.5	(−26.7)	40	$\nu_{as}(\text{NH}_2)(\nu_{12})$
Acetylene (Ac) ^a							
756.1 ^b	(+3.1)	739.5 ^b	(+3.0)	747.0 ^b	(+2.7)	21	$\delta(\text{CCH})(\nu_5)$
762.5	(+9.5)	745.7	(+9.3)	753.3	(+9.5)	26	
3436.0	(−10.1)	3277.9	(−9.6)	3271.1	(−11.9)	29	$\nu_{as}(\text{C-H})(\nu_3)$

[a] The frequency shifts in **C** compared to FMA and Ac (monomers **M**) are given in parentheses (Table 3.2.3). [b] Out of plane mode

3.2.2.4. Comparison of Calculated and Experimental Vibrational Frequencies: Trimers

Table 3.2.6 shows the calculated vibrational frequencies for trimers T-**A** and T-**B** (MP2/aug-cc-pVDZ). Experimentally, at higher concentrations of acetylene new peaks, which cannot be assigned to the parent species or to the dimers, appear in different regions. The intensities of these absorptions increase with the acetylene concentration. In argon, the weak absorption at 1722.3 cm^{-1} is assigned to the carbonyl stretching mode of FMA in the T-**B** trimer in argon. In nitrogen, the absorption at 1721.9 cm^{-1} is assigned to the carbonyl stretch of FMA in the trimer T-**B**. The good agreement between the experimental frequency shifts (16.8 cm^{-1} in argon and 14.2 cm^{-1} in nitrogen), and the calculated values (15.3 cm^{-1} in an argon and a nitrogen), could be an indication of the presence of trimer T-**B** in the matrix. However, it does not allow us to discard the formation trimer T-**A** instead.

In argon, other weak absorptions in the C-H stretching region of acetylene are found at 3232.2 and 3198.4 cm^{-1} , red shifted by 56.6 and 90.4 cm^{-1} , respectively (Figure 3.2.4). These are in good agreement with the calculated values for the both trimers T-**A** and T-**B** (see Table 3.2.6) The calculated frequency shifts are 48.1 and 85.2 cm^{-1} for complex T-**A** and 54.1 and 87.9 cm^{-1} for complex T-**B**, respectively. No additional peaks that can be assigned to the corresponding trimers were found. In nitrogen, in the C-H stretching region a weak absorption is found at 3215.5 cm^{-1} , which is red-shifted by 67.5 cm^{-1} . This can be assigned to either dimer **A** or dimer **B** (Table 3.2.4).

In the nitrogen matrix, a new band at 1274.9 cm^{-1} was found at high concentration of acetylene, which is in agreement with the calculated values both trimers T-**A** and T-**B** (Table 3.2.6)

Table 3.2.6. Experimental and Calculated Vibrational Frequencies and Shifts (cm⁻¹) of the FMA – Acetylene 1:2 Complexes T-A and T-B

Experimental			MP2/Aug-cc-pVDZ						Experimental		MP2/Aug-cc-pVDZ		Assingnment
Argon	Rel. Int.	M	Trimer A uncorrect.	Trimer A correct. ^c	Rel. Int.	Trimer B uncorrect.	Trimer B correct. ^c	Rel. Int.	Nitrogen	Rel. Int.	Trimer A correct. ^d	Trimer B correct. ^d	
Formamide (FMA) ^a													
1722.3 (−16.8)	100	1273.8	1299.6 (+25.8)	1285.5 (+25.5)	21	1305.7 (+31.9)	1291.3 (+31.5)	33	1274.9 (+28.3)	15	1271.7 (+25.2)	1276.9 (+31.4)	v (C-N)(v ₆)
		1763.3	1755.8 (−7.5)	1731.7 (−7.4)	100	1747.7 (−15.6)	1723.2 (−15.3)	99	1721.9 (−14.2)	100	1728.7 (−7.4)	1719.7 (−15.3)	v(C=O)(v ₉)
		3604.4	3553.6 (−50.8)	3378.7 (−47.8)	48	3567.1 (−37.3)	3388.7 (−35.1)	36			3382.1 (−47.9)	3392.3 (−35.2)	v _s (NH ₂)(v ₁₁)
		3763.6	3734.6 (−29.0)	3517.9 (−28.0)	23	3740.0 (−23.6)	3523.1 (−22.4)	29			3525.8 (−27.6)	3530.5 (−22.4)	v _{as} (NH ₂)(v ₁₂)
Acetylene (Ac) ^a													
3198.4 (−90.4) 3232.2 (−56.6)	15	703.2	758.2 ^b (+55.0)	794.4 ^b (+57.6)	12	753.2 ^b (+50.0)	788.6 ^b (+52.3)	31			802.2 ^b (+58.2)	796.8 ^b (+52.9)	δ(CCH)(v ₅)
			768.8 ^b (+65.6)	804.9 ^b (+68.7)	20	763.7 ^b (+60.5)	799.6 ^b (+63.3)	18			813.4 ^b (+69.4)	807.9 ^b (+64.0)	
			805.0 (+101.5)	842.8 (+106.2)	20	776.8 (+73.6)	813.3 (+77.1)	23			851.7 (+107.4)	821.8 (+77.8)	
			805.3 (+102.3)	843.1 (+107.1)	20	800.5 (+97.3)	838.1 (+101.8)	32			852.0 (+108.2)	846.9 (+102.9)	
	10	3431.4	3342.9 (−89.0)	3202.5 (−85.2)	75	3339.6 (−91.8)	3199.3 (−87.9)	99	3215.5 (−67.5)	10	3195.8 (−85.1)	3192.6 (−87.7)	v _{as} (C-H)(v ₃)
			3381.1 (−50.3)	3239.1 (−48.1)	65	3374.9 (−56.5)	3233.1 (−54.1)	40			3232.3 (−48.1)	3226.4 (−54.0)	

[a] The frequency shifts in Trimers T-A and T-B compared to FMA and acetylene monomers. [b] Out of plane mode. [c] Factors of correction for the MP2/aug-cc-pVDZ level of theory (argon) : Formamide C-N stretching: 0.989, C=O stretching: 0.986, N-Hsym stretching: 0.942, N-Has stretching: 0.95. Acetylene C-H bending: 1.047, C-H stretching: 0.958. ^d Factors of correction for the MP2/aug-cc-pVDZ level of theory (nitrogen): Formamide C-N stretching: 0.978, C=O stretching: 0.984, N-Hsym stretching: 0.944, N-Has stretching: 0.951. Acetylene C-H bending: 1.058, C-H stretching: 0.956.

3.2.2.5. Conclusions

Using matrix isolation techniques and *ab initio* calculations, we found that FMA – acetylene dimers are formed in the matrix and there is an evidence of the formation of one FMA – acetylene trimer when increasing the acetylene concentration.

Three stable FMA – acetylene dimers were identified at the MP2 level of theory with the aug-cc-pVDZ and cc-pVTZ basis sets. Their binding energies are between -2.96 and -1.79 kcal/mol.(MP2/cc-pVTZ +ZPE+BSSE) The most stable dimer **A** is stabilized by the N-H_{FMA}... π and C=O_{FMA}...H_{acet} interactions between FMA and acetylene. Dimer **B** shows the C-H_{FMA}... π and C=O_{FMA}...H_{acet} interactions while dimer **C** is stabilized only by the N-H_{FMA}... π interactions. By comparing the experimental and calculated frequencies, the dimers **A** and **B** were identified in argon and nitrogen matrices. In both complexes the stronger C=O_{FMA}...H_{acet} interaction occurs as it is evidenced by the large shifts of the \equiv C-H stretching modes.

Eight, 1:2 FMA – acetylene trimers (T-**A** to T-**H**) with binding energies between -5.44 and -2.62 kcal/mol were identified (MP2/aug-cc-pVDZ + ZPE +BSSE). The trimers T-**A** and T-**B** are close in energy. Weak bands observed under matrix isolation conditions at higher concentrations of acetylene suggest the formation of a trimer. Nevertheless, the spectra could not be clearly assigned as corresponding to the trimer T-**B** or T-**A**.

Chapter 3.3. Formamide and Formic Acid Dimers

3.3.1. Introduction

Formic acid (FA) is one of the simplest molecules forming hydrogen bonds in the gaseous, liquid and solid states. The proton transfer mechanism in FA dimers has been extensively described and studied.^[138-140] Matrix isolation studies of the complexes between FA and acetylene, water, and dimethyl ether have been carried out in our laboratory in combination with computational methods.^[135, 141-143] IR spectra of monomeric formic acid is also described in literature.^[35, 144, 145] Lundell and co-workers reported that multiphoton IR irradiation of *trans*- formic acid led to the *cis*- conformer at low temperatures.^[145]

Hydrogen bonded complexes formed between FA and FMA have been prepared in argon matrix and characterized by FTIR spectroscopy coupled with *ab initio* computation. Computations at the MP2/aug-cc-pVTZ level of theory show the existence of nine energetically stable complexes with binding energies between -3,47 and -14,41 kcal/mol.^[146] The experimentally observed results are compared with calculated frequencies of the most stable complexes, that are stabilized by the interactions $\text{NH}_{\text{FMA}} \dots \text{C}=\text{O}_{\text{FA}}$ and $\text{C}=\text{O}_{\text{FMA}} \dots \text{OH}_{\text{FA}}$.

3.3.2. Result and Discussion

3.3.2.1. Experimental Results

Infrared spectra of formic acid and formamide isolated in several rare gas matrices were reported earlier.^[35, 83, 92, 145] In order to identify the spectra of FA – FMA complexes, infrared spectra of FA and FMA were recorded independently. The reference spectra of matrix isolated FA and FMA are in good agreement with those reported in literature. The experiments were performed by codeposition of mixtures of FA and FMA with an excess of argon at 10 K. Under these conditions of high dilution in argon and slow deposition mainly the monomers of FA and FMA are formed. Subsequent annealing of the matrix containing FA and FMA monomers up to 40 K led to the formation of several complexes. Some of these complexes were easily identified (FA and FMA dimers) based on the previous reports.^[35, 83] After careful analysis of the IR spectra, we observed new bands that could not be assigned to any of the previously known species.

The C=O stretching modes of FA and FMA monomers are strongly perturbed by the formation of complexes. The bands at 1767.1 and 1764.8 cm^{-1} belong to the C=O stretching mode of the FA monomer. The weak absorptions at 1744.8 and 1728.3 cm^{-1} are assigned to the acyclic and cyclic forms of the formic acid dimers (Figure 3.3.1 spectrum a).^[35] Even at high dilution of the formic acid, these characteristic dimer bands are observed. The splitted bands at 1745 and 1739 cm^{-1} are attributed to the C=O stretching mode of FMA monomer (Figure 3.3.1. spectrum b). In the presence of both FA and FMA in argon, new bands are observed at 1716.8 at 1679 cm^{-1} and assigned to the C=O stretching modes of FA and FMA in a FA – FMA complex (Figure 3.3.1 spectrum d). These bands at 1716.8 at 1679 cm^{-1} are also observed at low concentration of either of FA or FMA, and therefore are assigned to a 1:1 dimer of FA – FMA and not to higher aggregates.

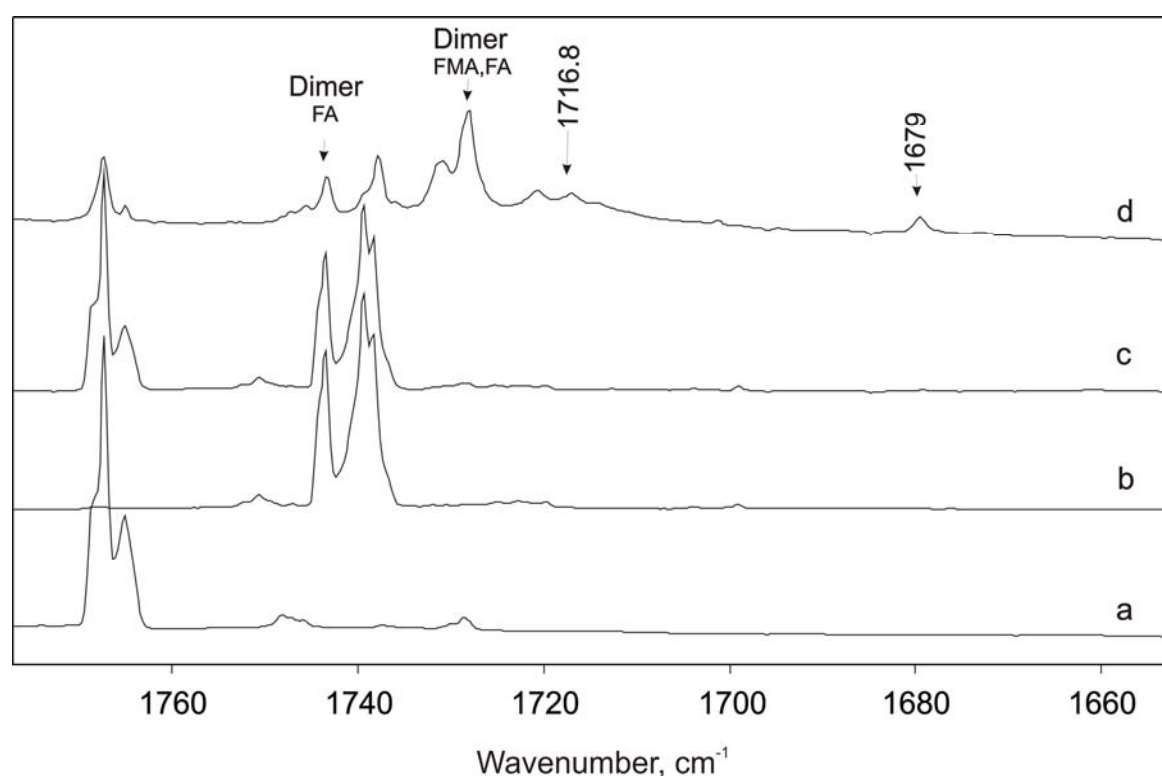


Figure 3.3.1. FTIR spectra of matrix isolated FA, FMA, and FA/FMA mixtures in argon (in the C=O stretching region). (a) FA:Ar ratio 1:1000 at 9 K. (b) FMA:Ar ratio 1:1000 at 9 K. (c) FA:FMA:Ar ratio 1:1:1000, 9 K. (d) FA:FMA:Ar ratio 1:1:1000 after annealing up to 40 K.

The C–N stretching mode of FMA is found at 1261 cm^{-1} with a site splitting at 1270 cm^{-1} (Figure 3.3.2 spectrum b). In the presence of both FA and FMA in argon new bands are observed that grow in the intensity after annealing up to 40 K. The band at 1324 cm^{-1} is assigned to the C–N stretching mode of the formamide in a 1:1 of FA – FMA complex (Figure 3.3.2 spectrum d). Formic acid does not exhibit any absorption in this region.

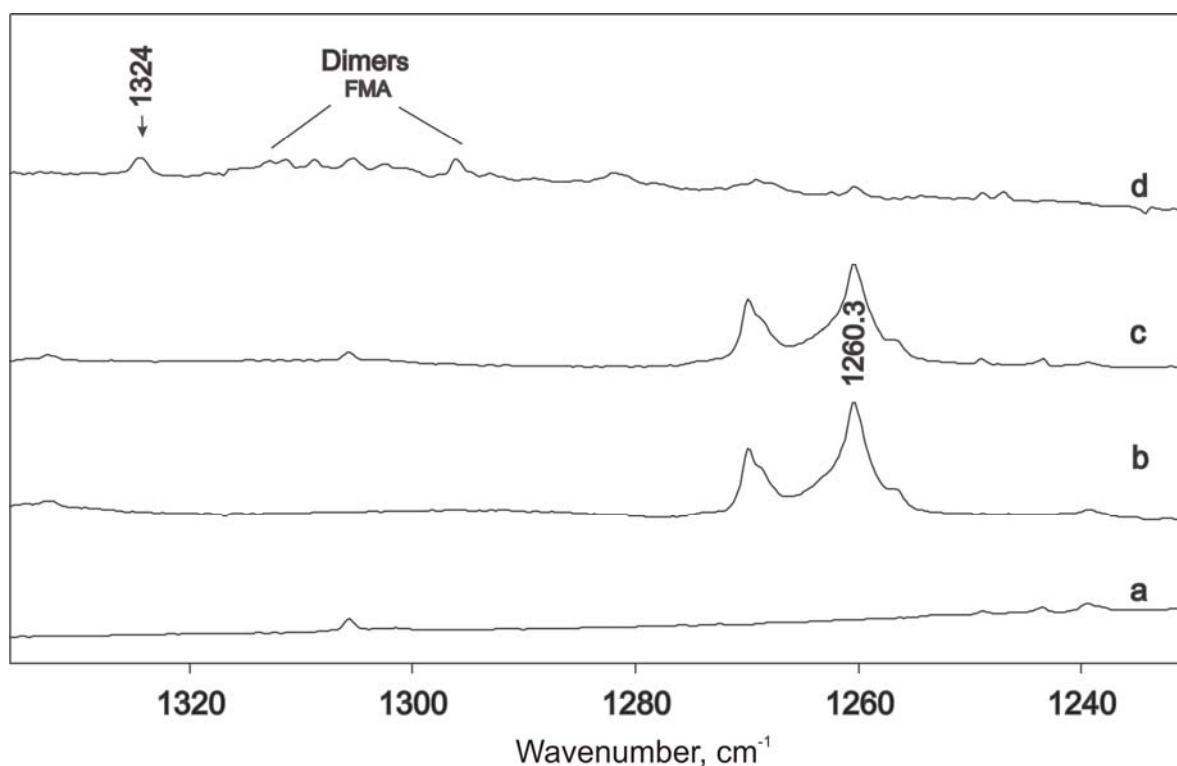


Figure 3.3.2. FTIR spectra of matrix isolated FA, FMA, and FA/FMA mixtures in argon (in the C–N stretching region). (a) FA:Ar ratio 1:1000 at 9 K. (b) FMA:Ar ratio 1:1000 at 9 K. (c) FA:FMA:Ar ratio 1:1:1000, 9 K. (d) FA:FMA:Ar ratio 1:1:1000 after annealing up to 40 K.

The C–O stretching mode of FA in the FA – FMA dimer is observed at 1200.5 cm^{-1} (Figure 3.3.3 spectrum d), which is 96.8 cm^{-1} blue shifted from the unperturbed C–O stretching mode of monomeric FA at 1103.4 cm^{-1} . The peak at 1215 cm^{-1} is due to the $\delta(\text{COH})$ vibration mode of monomeric form of FA, and the band at 1184 cm^{-1} is attributed to the rocking mode of FMA (Figure 3.3.3 spectrum a and b).^[92]

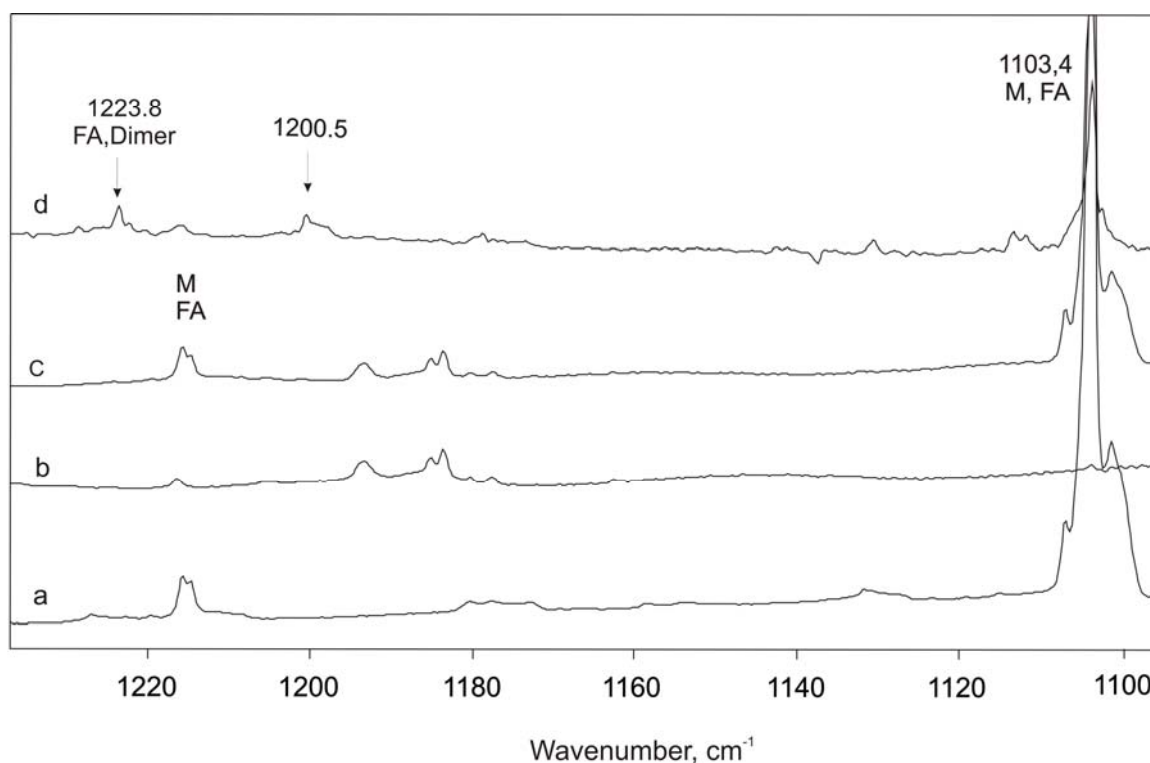


Figure 3.3.3. FTIR spectra of matrix isolated FA, FMA, and FA/FMA mixtures in argon (in the C–O stretching region). (a) FA:Ar ratio 1:1000 at 9 K. (b) FMA:Ar ratio 1:1000 at 9 K. (c) FA:FMA:Ar ratio 1:1:1000, 9K. (d) FA:FMA:Ar ratio 1:1:1000 after annealing up to 40 K.

3.3.2.2. Comparison of calculated and experimental vibrational frequencies.

The geometries and binding energies of 1:1 formic acid and formamide complexes were calculated by quantum chemical procedures and have been discussed in detail in literature. We address them only briefly to compare our experimentally observed frequencies with the calculated frequencies at the MP2/cc-pVTZ level of theory.

Our experimental data reveal the existence of one complex between FA and FMA. On other hand, computational calculations show the existence of two energetically stable complexes, **A** and **B**, with binding energies, -14.41 and -11.18 kcal/mol, respectively (Figure 3.3.4). Complex **A** is stabilized by $\text{NH}_{\text{FMA}} \cdots \text{O}=\text{C}_{\text{FA}}$ and $\text{C}=\text{O}_{\text{FMA}} \cdots \text{HO}_{\text{FA}}$ interactions, whereas the complex **B** is stabilized by $\text{CH}_{\text{FMA}} \cdots \text{O}=\text{C}_{\text{FA}}$ and $\text{C}=\text{O}_{\text{FMA}} \cdots \text{HO}_{\text{FA}}$ interactions.^[146] The IR spectra of the FA – FMA dimers were calculated at the MP2/cc-pVTZ level of theory (Table 3.3.1).

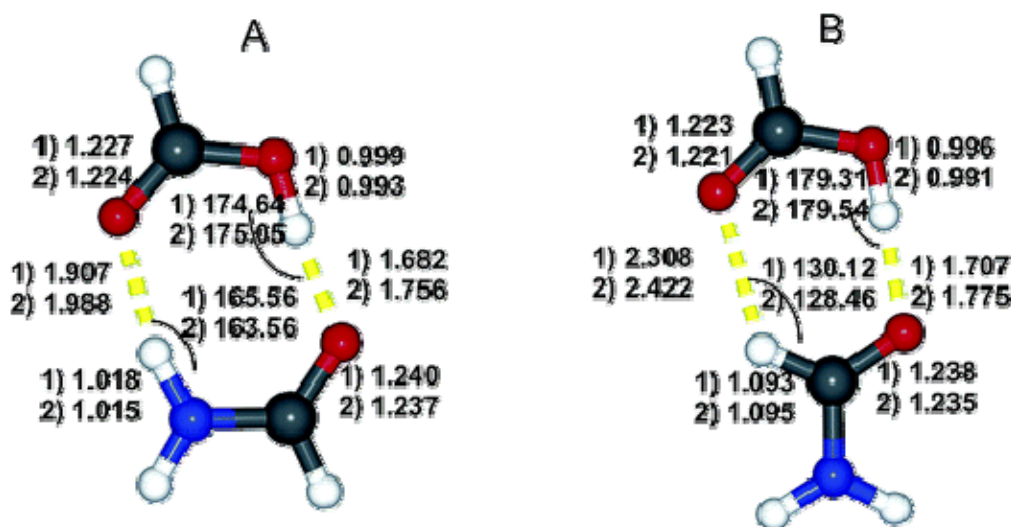


Figure 3.3.4. MP2/cc-pVTZ geometries with inter- and intramolecular lengths (angstrom) and hydrogen bond angles (deg) of dimers A and B: (1) optimized without BSSE corrections; (2) optimized with BSSE corrections. This figure has been taken from reference.^[146]

Bohn and Andrews have used matrix isolation method to study a binary complex between hydrogen fluoride and formamide. They interpreted their results as evidence for a cyclic complex structure.^[109] The infrared spectrum of the water-formamide complex in argon matrix has been recorded from 10 to 4000 cm^{-1} . The interaction energy of the complex forming molecules has been calculated from a theoretical potential energy surface. One global and three different local minima have been found for this PES. Intermolecular vibrational frequencies have been calculated for each minimum. The results were compared with the experimentally observed far infrared spectrum, that revealed the presence of two different complexes with closed and open structures in argon matrix.^[59]

One of the characteristic features of the formation of complexes between FMA and FA is the red shift of the C=O stretching vibrations. Bohn and Andrew observed a red shift -18 cm^{-1} , for the C=O stretch in the HF – FMA complex, whereas in the FMA – H₂O complex the shift is -21 cm^{-1} .

In the symmetrical doubly bridged dimer of formic acid the C=O stretching vibration is shifted by -38.6 cm^{-1} , and in the complex with water (FA – Water) is shifted by -30.4 cm^{-1} .^[35] Computations at MP2/cc-pVTZ level of theory predict a red shift of -46.4 cm^{-1} and -73.9 cm^{-1} , respectively, for the C=O stretching vibration of FA and FMA in complex A. In complex B, the predicted frequency shifts are -37.7 cm^{-1} , and -71.5 cm^{-1} , respectively.

In the C=O stretching region perturbed modes of FA and FMA are found at 1718.8 and 1679 cm^{-1} , are shifted by -50.3 cm^{-1} (FA) and -60.1 cm^{-1} (FMA) from parent modes at 1767.1 and 1739.1 cm^{-1} (Figure 3.3.1). The experimentally observed frequency shifts for the C=O stretching modes of the FA – FMA complex are in good agreement with calculated shifts.

The formation of hydrogen-bonded complex of FA – FMA results a blue shift of the C–N stretching vibration mode found at 1260.3 cm^{-1} for the unperturbed molecule (Figure 3.3.2). The bands at 1296 cm^{-1} and 1312 cm^{-1} due to formamide dimers.^[83, 93] The new band at 1324.0 cm^{-1} is assigned to a previously unknown FA – FMA complex. Predicted frequency shift in complex **A** is blue-shifted by 80.7 cm^{-1} (MP2/cc-pVTZ), whereas in complex **B**, it is only by 29.6 cm^{-1} . The experimentally observed blue shift is 63.7 cm^{-1} , which is in good agreement with complex **A**.

Another characteristic absorption of monomeric FA is the very strong $\nu(\text{C–O})$ vibration mode at 1104 cm^{-1} (Figure 3.3.3). After annealing the matrix up to 40 K we found a new band at 1200.5 cm^{-1} which is assigned to $\nu(\text{C–O})$ vibration mode of FA in the FA – FMA complex. The calculated frequency shifts for the corresponding mode in dimers **A** and **B** are blue-shifted by 131.5 cm^{-1} , and 105.6 cm^{-1} , respectively (Table 3.3.1). The experimentally observed blue-shift is 90.5 cm^{-1} .

Table 3.3.1. Experimental and calculated vibrational frequencies and shifts of FA-FMA dimers.

MP2/cc-pVTZ									Assignment
Experimental frequencies (shifts)			Calculated frequencies and shifts in the complex						
M exp ^a	Dimer A		M calc.	Dimer A		Dimer B			
Formamide									
1260.3	1324.0	(63.7)	1267.9	1348.6	+80.7	1297.5	+29.6	v (C–N)	
1739.1	1679	(–60.1)	1803.8	1729.9	–73.9	1732.3	–71.5	v(C=O)	
3426.6	-	-	3579.9	3348.5	–231.4	3679.4	–0.5	vs (NH ₂)	
3547.4	-	-	3718.2	3675.5	–42.7	3715.8	–2.4	vas (NH ₂)	
Formic Acid									
3549.9	-	-	3722.1	3044.8	–677.3	3136.7	–585.4	v (O–H)	
1767.1	1716.8	(–50.3)	1826.2	1779.8	–46.4	1788.5	–37.7	v(C=O)	
1103.4	1200.5	(97.1)	1125.0	1256.5	+131.5	1230.6	+105.6	v(C–O)	

[a] The frequency shifts in dimers **A** and **B** compared to FMA and **FA** (monomers **M**) are given in parentheses.

Due to a large number of absorptions in the region of the OH/CH stretching modes, the definitive assignment is not possible. All bands that are assigned to the FA – FMA complex show the same kinetic behavior upon annealing and nicely match the calculated spectra for complex **A**.

Chapter 4. Furan – Formic Acid Dimers^[147]

4.1. Introduction

Furan and its aggregates, and complexes with small molecules have been subject to many experimental and theoretical studies.^[148-152] The complexes of furan with hydrogen halides and alkynes have been investigated by Ault^[153] and DeLaat and Ault^[116] using matrix isolation spectroscopy. The excited states of furan and the rotational spectra of some of its complexes with halides were also investigated.^[151, 152, 154] Matrix isolation spectroscopy allowed us to record the IR spectrum of aggregates between FA and furan. By comparison of the experimental IR spectrum with calculated IR spectra of a variety of complexes, it was possible to identify the most stable furan-FA dimer as the major product of the aggregation.

4.2. Matrix Isolation Studies

Matrix isolation experiments were performed in order to identify aggregates between FA and Fu. The experiments were performed by matrix isolation of mixtures of FA and Fu in argon at 10 K. Under these conditions (high dilution in argon and slow deposition) mainly the monomers of FA and Fu were matrix-isolated. Subsequent annealing of the matrix at temperatures up to 35 K resulted in the formation of complex mixtures of aggregates. The main constituents of these mixtures were identified as the FA dimer, which has been extensively described in literature,^[35, 104, 155] and complex between Fu and FA.

The annealing experiments show new sets of IR bands, which are only produced in the presence of both Fu and FA, which are thus assigned to mixture of FA/Fu aggregate. One set is formed on depositing a matrix of FA, Fu, and argon in a 1: 1: 1500 ratios. On annealing at 30 K the intensities of these bands slightly increase (Figures 4.1 – 4.5). By comparison with the calculated spectra of several aggregates is assigned to complex **A** (Figure 4.6 and Table 4.1). Further annealing matrix at 35 K the IR bands of aggregates increase. In order to avoid the formation of formic acid dimers in the matrix experiments were performed with various concentrations of FA and Fu. In the case of 1:3:1500 (FA:Fu:Ar) after annealing of the matrix at 35 K main part in the matrix FA – Fu complex formed (Figure 4.1 – 4.5).

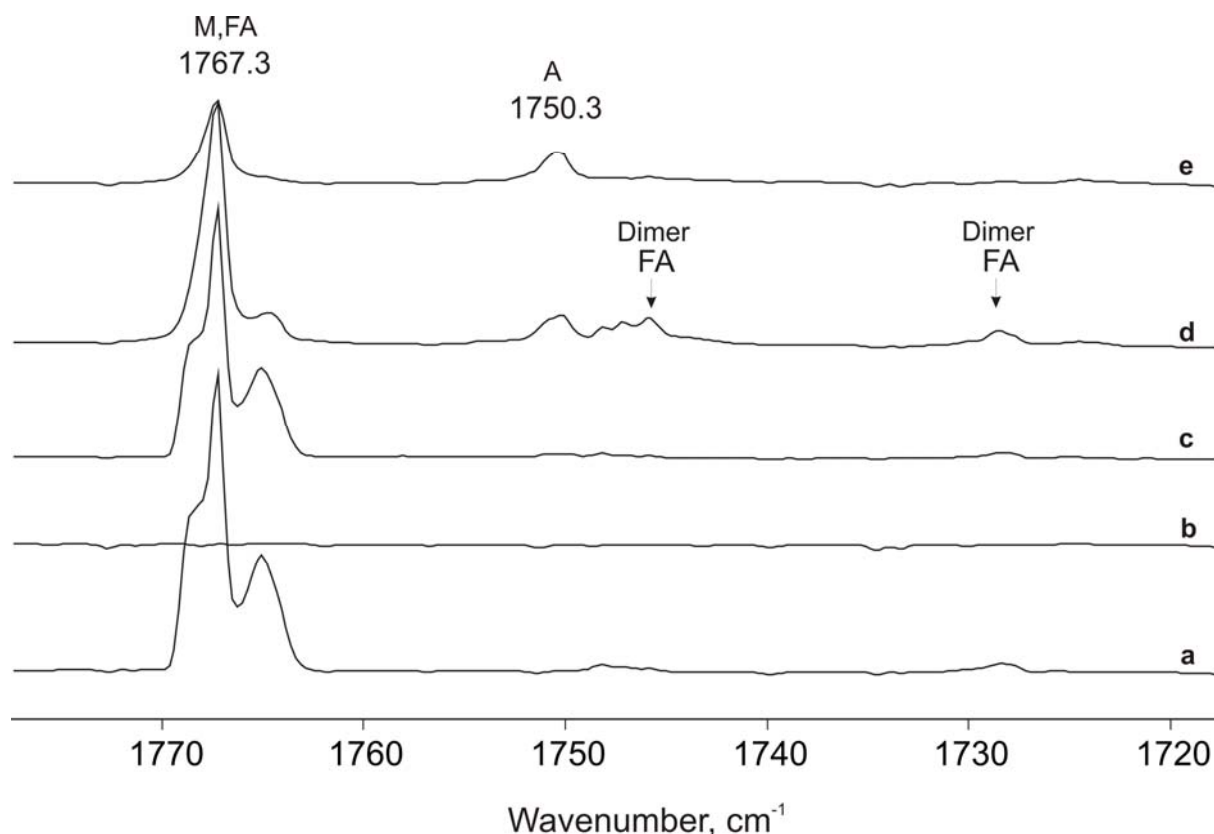


Figure 4.1. IR spectra in the range 1800 – 1720 cm^{-1} of FA, Fu, and FA – Fu mixtures, matrix-isolated in argon. a) FA:Ar ratio 1:1500, 10 K. b) Fu:Ar ratio 1:1500, 10 K. c) FA:Fu:Ar ratio 1:1:1500, 10 K. d) FA:Fu:Ar ratio 1:1:1500 after annealing at 30 K. e) FA:Fu:Ar ratio 1:3:1500 after annealing at 35 K. Vibrational modes assigned to FA/Fu complex is assigned A, respectively (see Tables 4.1 and 4.2).

The IR spectra of complex **A** were assigned by comparison with calculations at the MP2/Aug-cc-pVTZ and MP2/6-311++G(d,p) level of theories (Tables 4.1 and 4.2). Characteristic for the formation of complexes of FA is the red shift of the C=O stretching vibration found at 1767.3 cm^{-1} .^[35] In the symmetrical doubly bridged dimer of FA the C=O stretching vibration mode is shifted by -38.6 cm^{-1} ^[35] and in the complex with water by -30.4 cm^{-1} ^[156], in the complexes with diethyl ether the shifts are -31.4 cm^{-1} and -24.2 cm^{-1} correspondingly^[157]. In the complex **A** this shift is -17 cm^{-1} , respectively, and thus in the expected range (Figure 4.1). The experimental red-shift is in excellent agreement with the both of MP2 /Aug-cc-pVDZ and MP2 /6-311++G(d,p) calculations which predict shifts of -15.1 and -14.5 cm^{-1} , respectively, for complex **A**. The red-shifts in the C=O stretching vibration reflect the elongation of the C=O bond due to the formation of complex. For

complex **B** red shift -12.7 cm^{-1} , For complexes **C** and **D** red shifts are -13.2 and -13.5 cm^{-1} by MP2/Aug-cc-pVDZ level theory correspondingly.

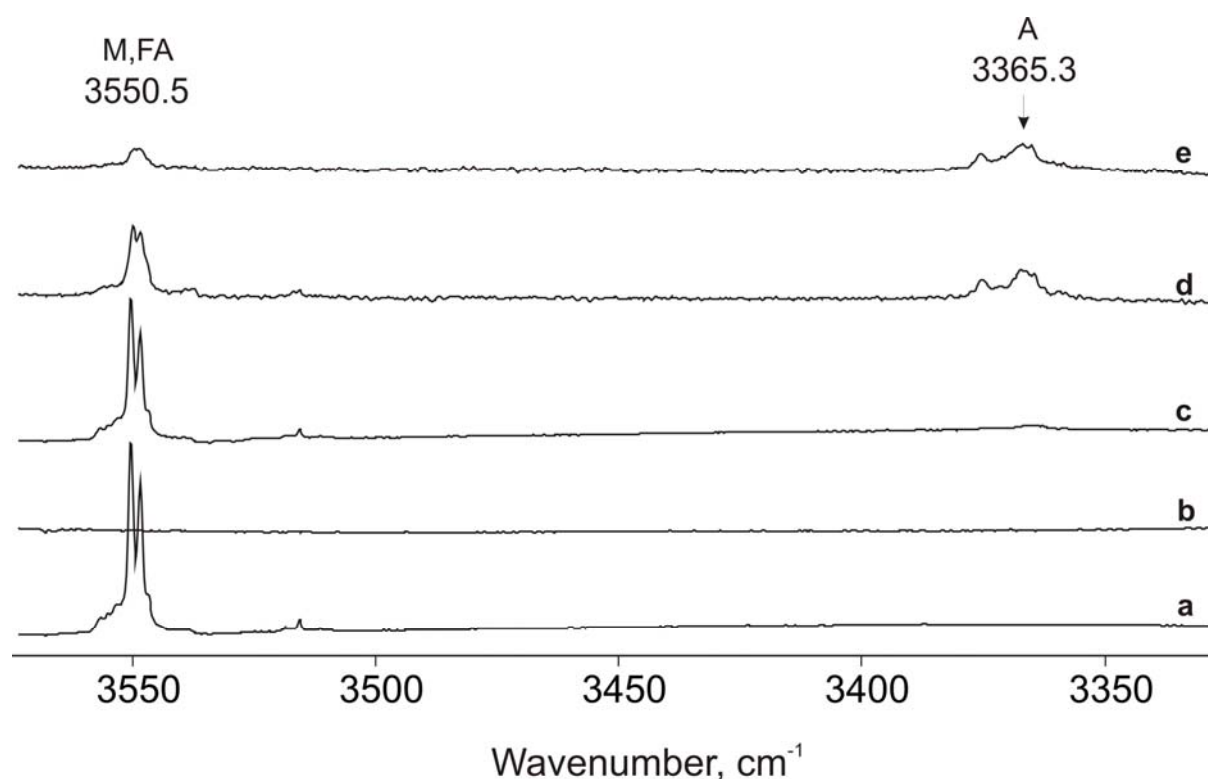


Figure 4.2. IR spectra in the range $3600 - 3300\text{ cm}^{-1}$ of FA, Fu, and FA – Fu mixtures, matrix-isolated in argon. a) FA:Ar ratio 1:1500, 10 K. b) Fu:Ar ratio 1:600, 10 K. c) FA:Fu:Ar ratio 1:1:1500, 10 K. d) FA:Fu:Ar ratio 1:1:1500 after annealing at 30 K. e) FA:Fu:Ar ratio 1:3:1500 after annealing at 35 K. Vibrational modes assigned to FA/Fu complex is assigned **A**, respectively (see Tables 4.1 and 4.2).

Figure 4.2 displays the OH stretching region of FA in four different sets of experiments. The peak observed at 3550.5 cm^{-1} is assigned to the O–H stretching vibration of formic acid.^[35] The splitting of this band is caused by site effects in the argon matrix^[158]. On co deposition of formic acid, furane, and argon in a 1:1:1500 molar ratio and annealing at 30 K, new distinct feature appears at 3365.3 cm^{-1} (Figure 4.2 spectrum d) red shift by -185.1 cm^{-1} from the unperturbed OH mode of formic acid. Increasing the furan concentration and annealing at 35 K for several minutes result in an increase in the intensity of this band (Figure 4.2 spectrum e). Computational calculations with the both of MP2/Aug-cc-pVDZ and MP2/6-311++G (d,p) level theories predict red shifts -182.7 cm^{-1} and -159.9 cm^{-1} for complex **A**, correspondingly.

Experimental observed frequency shift is -185.1 cm^{-1} for O–H stretching mode which is in excellent agreement with the calculated shift (-182.7 cm^{-1}) calculated at MP2/Aug-cc-pVDZ level of theory (Table 4.1). For complex **B** the calculated frequency shift is -145.8 cm^{-1} , in complexes **C** and **D** are -160.9 and -149.4 cm^{-1} , respectively (Table 4.2). The large shift of the O–H stretching vibrations allows discarding the FA – Fu complexes **B** – **D** where the O–H_{FA}...O_{Fu} interaction is lacking and thus the O–H stretching vibration of the FA molecule is much less perturbed (Figure 4.6).

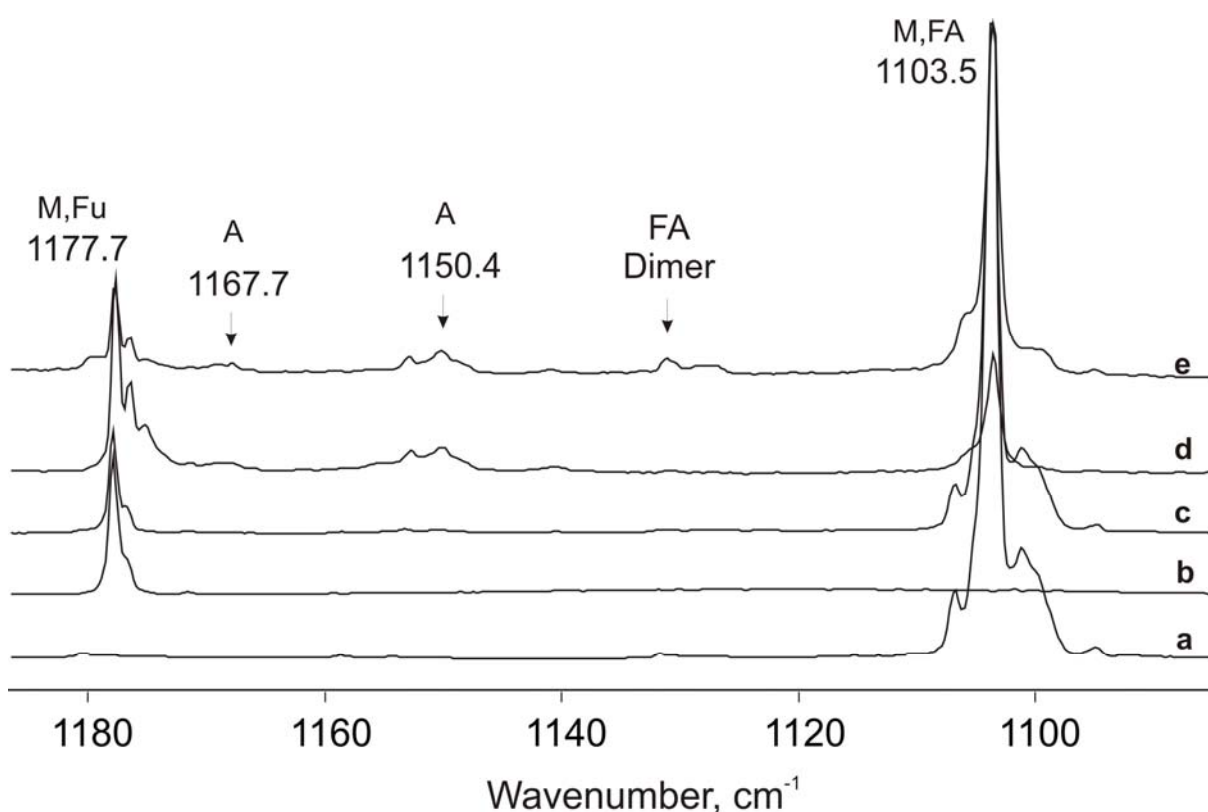


Figure 4.3. IR spectra in the range $1180 - 1080\text{ cm}^{-1}$ of FA, Fu, and FA – Fu mixtures, matrix-isolated in argon. a) FA:Ar ratio 1:1500, 10 K. b) Fu:Ar ratio 1:1500, 10 K. c) FA:Fu:Ar ratio 1:1:1500, 10 K. d) FA:Fu:Ar ratio 1:1:1500 after annealing at 30 K. e) FA:Fu:Ar ratio 1:3:600 after annealing at 35 K. Vibrational modes assigned to FA/Fu complexes is assigned **A**, respectively (see Tables 4.1 and 4.2).

The formation of hydrogen-bonded complexes of FA results in a contraction of the C–O bond and a blue shift of the C–O stretching vibration found at 1103.5 cm^{-1} in the unperturbed molecule. For complex **A** blue shift of 53.4 cm^{-1} is predicted at the MP2/Aug-cc-pVDZ of theory, which matches with experimental value ($+46.9\text{ cm}^{-1}$) (Figure 4.3). For complex **B** a shift of 19.1 cm^{-1} , for complex **C** a shift of 24.9 cm^{-1} , for complex **D** blue-shift 26.1 cm^{-1} are predicted (Table 4.2).

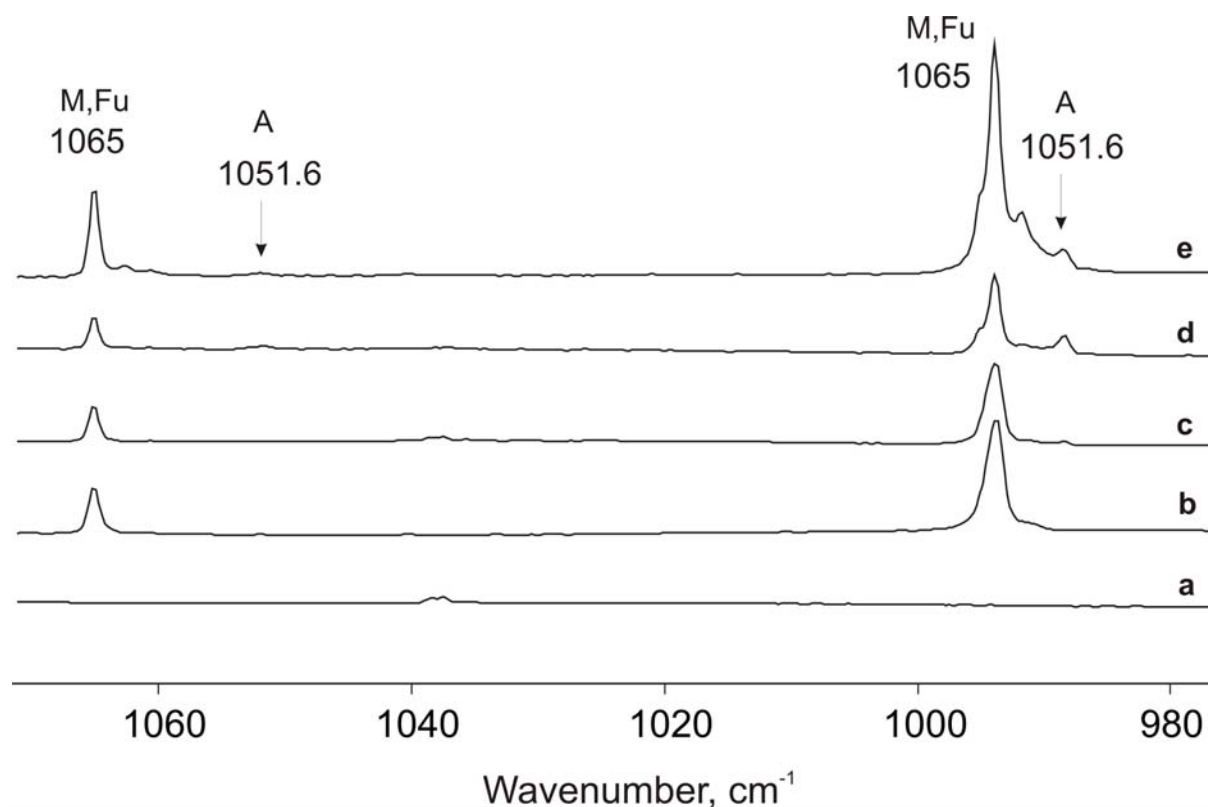


Figure 4.4. IR spectra in the range 1070 – 980 cm⁻¹ of FA, Fu, and FA – Fu mixtures, matrix-isolated in argon. a) FA:Ar ratio 1:1500, 10 K. b) Fu:Ar ratio 1:1500, 10 K. c) FA:Fu:Ar ratio 1:1:1500, 10 K. d) FA:Fu:Ar ratio 1:1:1500 after annealing at 30 K. e) FA:Fu:Ar ratio 1:3:600 after annealing at 35 K. Vibrational modes assigned to FA/Fu complexes are assigned **A**, respectively (see Tables 4.1 and 4.2).

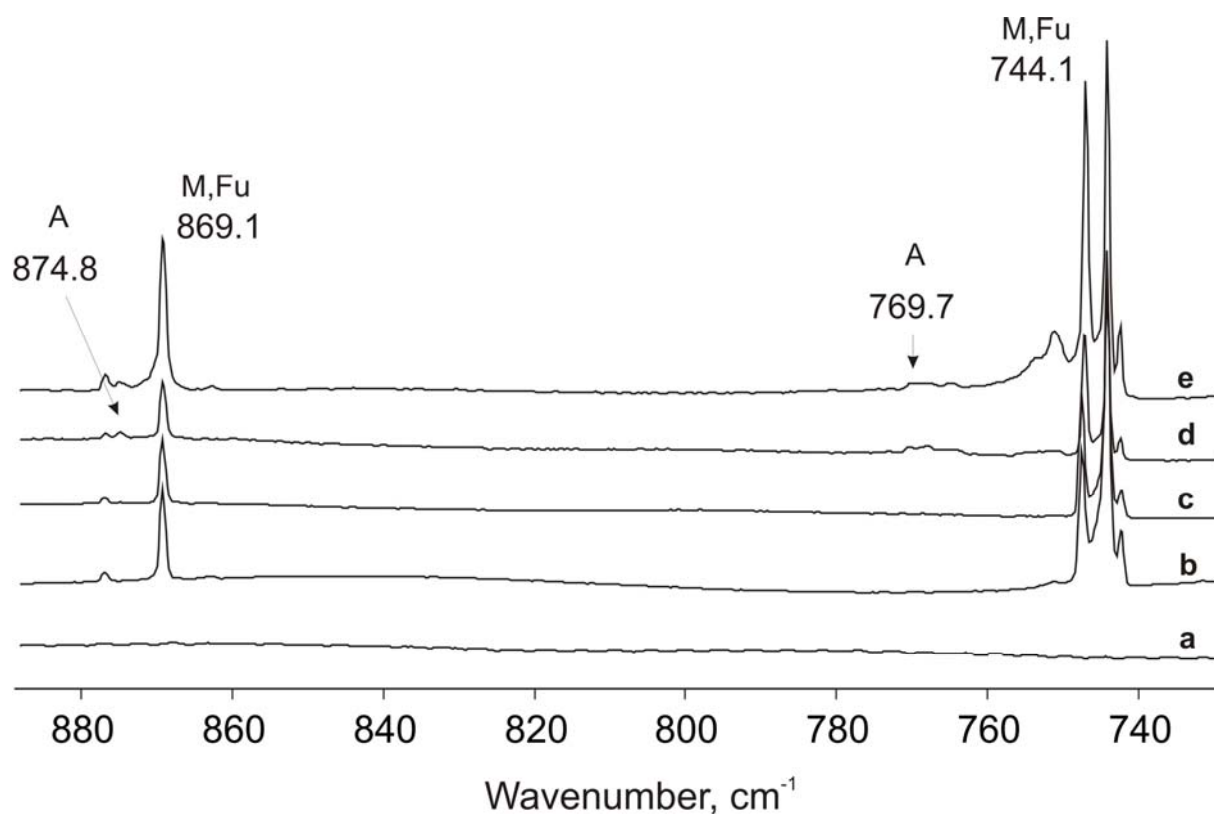


Figure 4.5. IR spectra in the range $890 - 740 \text{ cm}^{-1}$ of FA, Fu, and FA – Fu mixtures, matrix-isolated in argon. a) FA:Ar ratio 1:1500, 10 K. b) Fu:Ar ratio 1:1500, 10 K. c) FA:Fu:Ar ratio 1:1:1500, 10 K. d) FA:Fu:Ar ratio 1:1:1500 after annealing at 30 K. e) FA:Fu:Ar ratio 1:3:600 after annealing at 35 K. Vibrational modes assigned to FA/Fu complexes are assigned **A**, respectively (see Tables 4.1 and 4.2).

The furan molecule shows less pronounced shifts in IR spectrum due to the complex formation. The asymmetric and symmetric C–O–C stretching vibration of complex **A** could be identified. Experimentally observed values the asymmetrical C–O–C stretching vibration exhibits a red-shift of -10 cm^{-1} while the symmetrical vibration is shifted by -13.4 cm^{-1} respect to unperturbed molecule (Figure 4.4 and 4.5). This might be rationalized by the smaller distortion of the weak $\text{HOC(H)=O}\dots\text{HCCHCHOCH}$ hydrogen bonds during the asymmetrical vibration as compared to the symmetrical vibration. The experimental red-shifts are in excellent agreement with the calculated values (MP2/Aug-cc-pVDZ) (Table 4.1). The band at 993.6 cm^{-1} belongs to deformation vibration mode of CCH moiety of monomeric furan. Subsequent annealing matrix up to 35 K results of formation a new band at 988.5 cm^{-1} which is assigned to $\delta(\text{CCH})$ vibration mode in the complex **A** (Figure 4.5), which is in good agreement with calculated value (Table 4.1). For $\delta(\text{COH})$ and $\gamma(\text{CCH})$ vibration modes blue shifts are observed by $+5.7$ and $+25.6 \text{ cm}^{-1}$, correspondingly (Figure 4.5). Again experimental blue shifts are in good agreement with the calculated

shifts (MP2/Aug-cc-pVDZ), which predict shifts by +3.5 and +15.7 cm^{-1} , respectively for complex A (Figure 4.6).

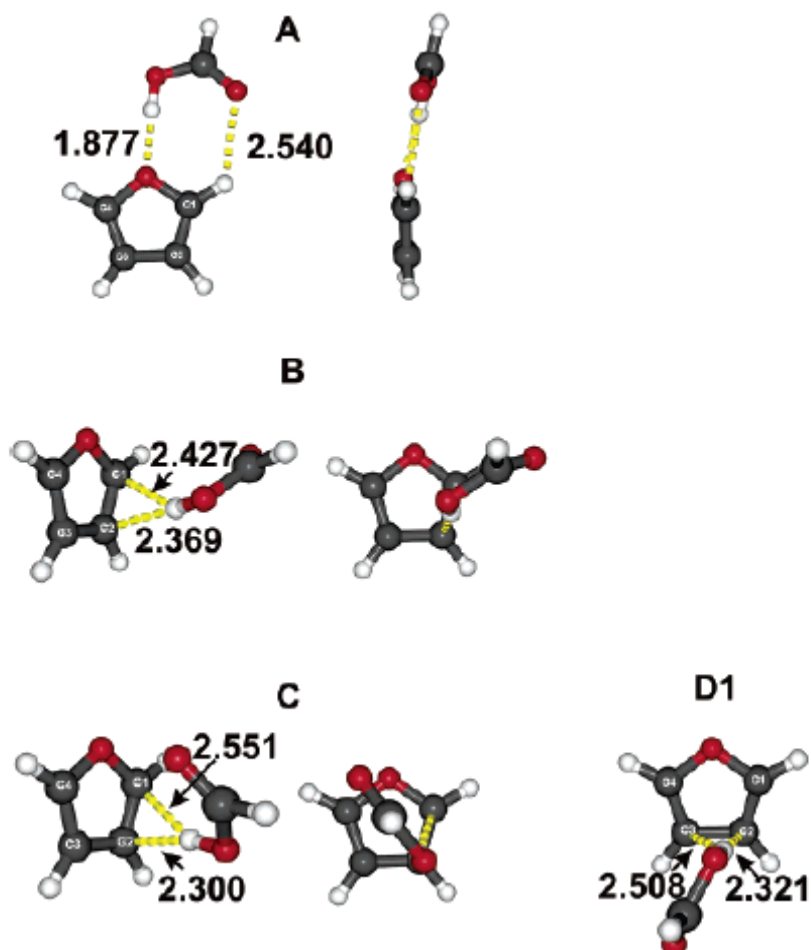


Figure 4.6. The calculated structures with hydrogen bond lengths (Å) of the type i furan-FA complexes A, B, C, and D1 at the MP2/6-311++G(d,p) level of theory.

Table 4.1. The experimental (Ar matrix at 10 K) and the calculated MP2 /Aug-cc-pVDZ and MP2 /6-311++G(d,p) unscaled vibrational frequencies (in cm^{-1}) of the FA/Fu complex **A**, along with the frequency shift (in brackets) in the complex, $\Delta\nu$, from the monomer (in parentheses).

Experimental			MP2 /Aug-cc-pVDZ			MP2 /6-311++G(d,p)			Assignment
Monomer	Complex A		Monomer	Complex A		Monomer	Complex A		
Formic Acid									
3550.5	3365.3	(−185.1)	3726.6	3543.9	(−182.7)	3797.6	3637.7	(−159.9)	ν_{36} : ν (O–H)
1767.3	1750.3	(−17.0)	1770.9	1755.8	(−15.1)	1807.6	1793.0	(−14.5)	ν_{30} : ν (C=O)
1103.5	1150.4	(+46.9)	1115.7	1169.1	(+53.4)	1142.7	1193.9	(+51.2)	ν_{21} : ν (C–O)
Furan									
1177.7	1167.7	(−10.0)	1218.8	1207.9	(−10.9)	1249.9	1236.2	(−13.7)	ν_{23} : ν_{as} (C-O)
1065.0	1051.6	(−13.4)	1093.9	1081.4	(−12.5)	1112.5	1095.7	(−16.8)	ν_{20} : ν_{s} (C–C)+ ν_{s} (C–O)
993.6	988.3	(−5.3)	1011.4	1006.2	(−5.2)	1025.5	1021.6	(−3.9)	ν_{17} : δ_{s} (CC–H)
869.1	874.8	(+5.7)	865.5	869.0	(+3.5)	879.9	885.7	(+5.9)	ν_{15} : δ_{s} (C–O–C)
744.1	769.7	(+25.6)	742.6	758.3	(+15.7)	732.4	748.8	(+16.4)	ν_{11} : γ (CC–H)

Table 4.2. Calculated vibrational frequencies (in cm^{-1}) of FA/Fu complexes **B-D** by MP2-FC/Aug-cc-pVDZ level theory, along with the frequency shifts (in brackets) in the complexes $\Delta\nu$, from the monomer (in parentheses).

MP2-FC/Aug-cc-pVDZ							Assignment
M	Complex B		Complex C		Complex D		
Formic Acid							
3726.6	3580.4	(−145.8)	3565.7	(−60.9)	3577.4	(−149.2)	ν_{36} : ν (O–H)
1770.9	1758.2	(−12.7)	1757.7	(−13.2)	1757.4	(−13.5)	ν_{30} : ν (C=O)
1115.7	1134.8	(+19.1)	1140.6	(+24.9)	1141.8	(+26.1)	ν_{21} : ν (C–O)
Furan							
1218.8	1218.4	(−0.4)	1222.8	(+4)	1217.2	(−1.6)	ν_{23} : ν_{as} (C–O)
1093.9	1094.6	(+0.7)	1099.2	(+5.3)	1094.5	(+0.6)	ν_{20} : ν_{s} (C–C)+ ν_{s} (C–O)
1011.4	1011.4	(0)	1013.2	(+1.8)	1011.6	(+0.2)	ν_{17} : δ_{s} (CC–H)
865.5	865.5	(0)	865.9	(0.4)	865.5	(0)	ν_{15} : δ_{s} (C–O–C)
742.6	746.8	(+4.2)	735.6	(−7)	744.4	(+1.8)	ν_{11} : γ (CC–H)

4.3. Conclusion

The binding energy of the most stable complex **A** is -3.91 kcal/mol (MP2/6-311++G(d,p) + PE+ BSSE). Although the OH...O interaction is dominating in dimer **A**, the secondary $\text{C}=\text{O}_{\text{FA}}\dots\text{H}_{\text{Fu}}$ interaction between the carbonyl oxygen atom of FA and the hydrogen atom of furan leads to an additional significant stabilization of this complex. The matrix isolation experiments reveal that dimer **A** is the major, if not only, complex formed if the two monomers are allowed to diffuse slowly in solid argon. The additional IR absorptions that appear in the matrix spectra under these conditions nicely match the theoretical predictions for complex **A**.

Chapter 5. Acetylene – Furan ^[159]

5.1. Introduction

The equilibrium structure of the acetylene dimer has been studied experimentally and is known to have a T-shaped geometry.^[132, 160-163] It is well understood that this dimer has a T-shaped minimum of C_{2v} symmetry and a C_{2v} transition state on the interconversion coordinate. This information came from both experimental and theoretical studies. Fraser et al.^[161] rationalized their microwave and infrared spectra in terms of an internal rotation-tunneling motion between four equivalent C_{2v} minima through four C_{2v} transition states. Alberts et al.^[164] performed *ab initio* self-consistent field (SCF) and Møller-Plesset perturbation theory (MP2) calculations to locate the minimum and transition state in agreement with the experimental observations. Prichard et al.^[165] observed infrared spectrum of acetylene trimer using pulsed molecular beam technique. Later Richard et al.^[166] confirmed by quantum chemical calculations that the global minimum of the trimer is of C_{3h} symmetry. High resolution IR spectroscopy of acetylene – furan in ultracold helium nanodroplets have been measured by Metzelthin et al.^[167] They have observed eight bands that can be attributed to acetylene-furan complexes.

In this chapter we presented the experimental results with the combination of quantum chemical calculations for the acetylene – furan dimer. Experimental results are obtained from matrix isolation infrared spectroscopy, computational results from various levels of *ab initio* theory such as second-order Møller-Plesset (MP2).^[103]

5.2. Results and Discussion (Computational Results by Elsa Sanchez-Garcia)

Five acetylene–furan dimer structures **A** – **E** with stabilization energies between – 0.75 and –1.77 kcal/mol were localized at the MP2/6-311++G(d,p) level of theory (Table 5.1). The three basic intermolecular interactions (1)–(3) determine their stability and shape (Figure 5.1):

(1) $CH_{Ac} \cdots O_{Fu}$ interaction between the hydrogen atom of acetylene and the oxygen atom of furan.

(2) $CH_{Ac} \cdots \pi_{Fu}$ interaction between the hydrogen atom of acetylene and the p system of furan.

(3) $\text{CH}_{\text{Fu}} \dots \pi_{\text{Ac}}$ interaction between the hydrogen atom of furan and the π system of acetylene.

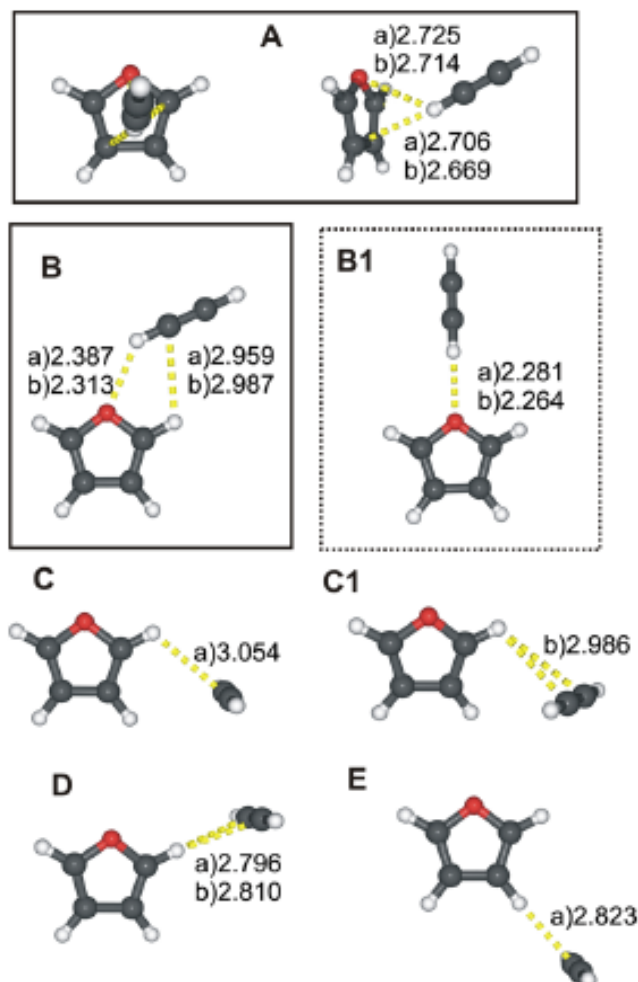


Figure 5.1. Calculated structures of the acetylene–furan complexes **A–E** with some intermolecular distances (Å) at the (a) MP2/6-311++G(d,p) and (b) MP2/cc-pVTZ levels of theory.

Dimer **A** is characterized by a $\text{CH}_{\text{Ac}} \dots \pi_{\text{Fu}}$ interaction. The geometry of dimer **A** has T-shaped geometry similar to benzene–acetylene dimer described by Steiner et al,^[168] in their crystallographic, spectroscopic, and quantum mechanical studies on the $\text{C–H} \dots \pi$ hydrogen bonding in terminal alkynes. The nearly isoenergetic structure **B** is characterized by a $\text{CH}_{\text{Ac}} \dots \text{O}_{\text{Fu}}$ interaction and an additional, presumably very weak, interaction of an α -hydrogen atom with the π system of the acetylene. **B1** is a C_{2v} symmetrical transition state (both with the 6-311++G(d,p) and the cc-pVTZ basis set) only slightly higher in energy than **B**. In structure B1 the $\text{C–H} \dots \text{O}$ hydrogen bond distance is shorter than in **B** and the

hydrogen bond angle is 180° (Figure 5.1). The less stable structures **C** – **E** with C_s symmetrical structures display $CH_{Fu} \dots \pi_{Ac}$ interactions according to *ab initio* calculation.

Table 5.1. Calculated stabilization energies of the acetylene–furan dimer structures **A** – **E** at the MP2 level of theory with the 6-311++G(d,p) and cc-pVTZ basis sets, including CP and ZPE corrections (in kcal/mol).

	MP2					
	6-311++G(d,p)			cc-pVTZ		
	E_{stab}	E_{stab}^{CP}	E_{stab}^{CP+ZPE}	E_{stab}	E_{stab}^{CP}	E_{stab}^{CP+ZPE}
A	–3.51	–1.77	–0.55	–3.11	–2.45	–2.00
B	–2.71	–1.76	–1.31	–2.60	–1.95	–1.46
B1	– ^a			– ^a		
C	–2.29	–1.08	–0.51	C1^b		
C1	C^b			–1.92	–1.45	–1.09
D	–1.98	–0.83	–0.35	–1.39	–1.09	–0.83
E	–1.91	–0.75	–0.28	C1^b		

[a] Transition state. [b] Geometry that was found after optimization.

Complexes between furan and acetylene are generated by co-deposition of furan and acetylene with a large excess of argon at 10 K. In highly diluted matrices mainly the monomers – acetylene and furan – are observed by IR spectroscopy. The monomers are easily identified by comparison with the literature data and pure samples of matrix-isolated acetylene^[119, 120, 136, 169] and furan.^[147] This also allows to identify complexes of furan and acetylene with water, a frequent contaminant in the matrices. Acetylene shows a high tendency of aggregation even in low temperature matrices. These aggregates have been extensively studied by IR spectroscopy.^[170]

Matrices containing higher concentrations of both acetylene and furan show IR absorptions which are absent in matrices containing only one of these components. These absorptions are thus assigned to mixed complexes between furan and acetylene. Annealing argon matrices containing furan and acetylene at temperatures above 25 K allows small trapped molecules to diffuse and results in an increase of the aggregates. Dilution experiments in addition allow to differentiate dimers from higher aggregates. A combination of the results of all these experiments allows to confidently assign sets of IR absorptions to mixed furan – acetylene dimers.

Figure 5.2 shows the C–H stretching region of acetylene in different sets of experiment. The spectrum marked (a) corresponds to the 1:1500 molar ratio of the acetylene and argon deposited at 10 K. In this spectral region acetylene has strong absorptions at 3302.9 and 3288.8 cm^{-1} , which have been assigned to the combination

bands ($\nu_2 + \nu_4 + \nu_5$) and ν_3 modes respectively. Furan has no absorption in this region. After annealing matrix for several minutes at 30 K new feature appear in the spectra at 3285.3, 3269.3, and 3264.4 cm^{-1} are due to acetylene dimers (Figure 5.2 spectrum b).^[119, 120, 170] When acetylene and furan were codeposited and then matrix annealed, result of new absorption band at 3265.7 cm^{-1} , which is red shift from unperturbed molecule by 23.1 cm^{-1} (Figure 5.2 spectrum c and d). This band appears only when both the reagents were codeposited. Furthermore, this band increased in the intensity as the concentration of either of the two reagents was increased (Figure 5.2 spectrum e).

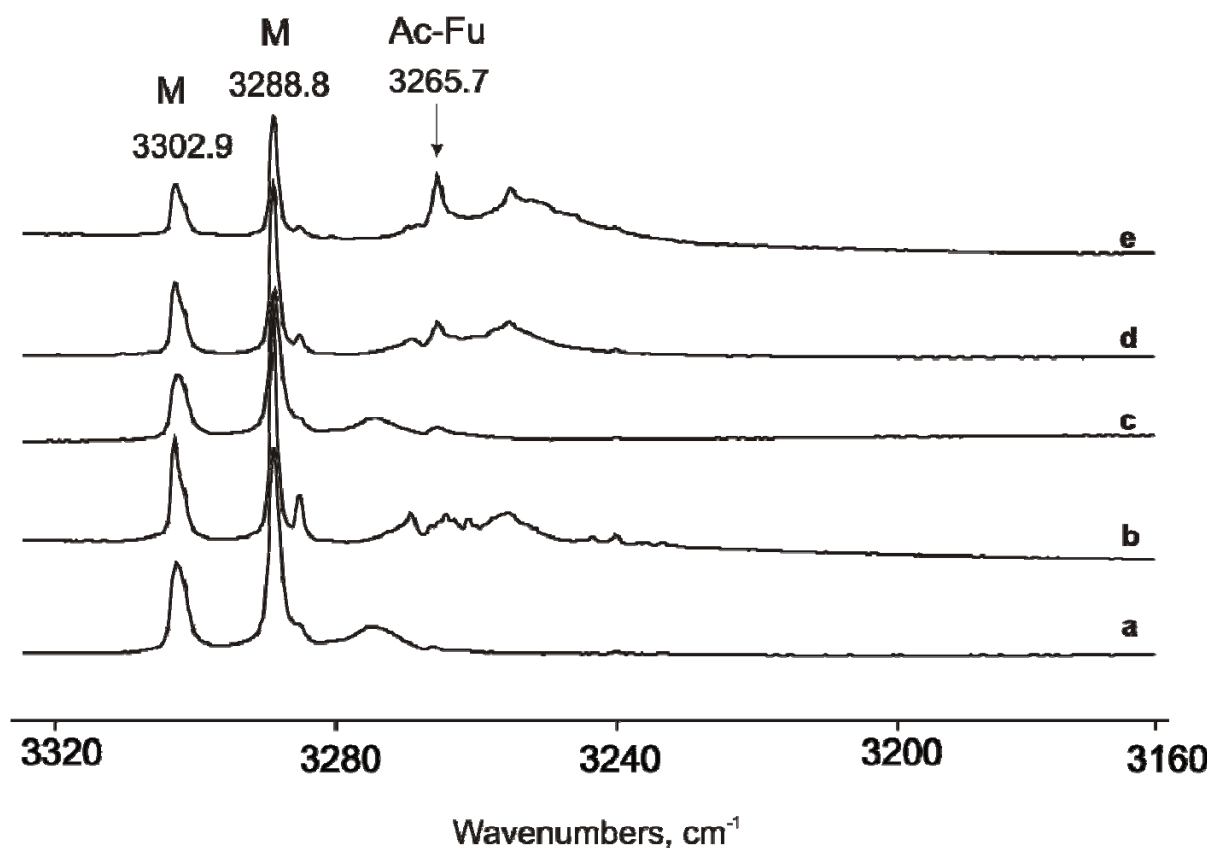


Figure 5.2. IR spectra in the range 3220 – 3200 cm^{-1} of acetylene, furane, and Acet/Fu mixtures, matrix-isolated in argon. a) Ac:Ar ratio 1:1500, 10 K. b) Ac:Ar ratio 1:1500, after annealing at 30 K. c) Ac:Fu:Ar ratio 1:1:1500, 10 K. d) Ac:Fu:Ar ratio 1:1:1500 after annealing at 30 K. e) Ac:Fu:Ar ratio 1:3:1500 after annealing at 35 K.

This clearly indicates that this feature can be attributed to a complex involving acetylene and furan. Since this band appears at low concentration of acetylene and furan, we believe that complex to be 1:1 type. The feature at 3265.1 cm^{-1} can be assigned to the ν_3 mode of acetylene submolecule in the Ac – Fu complex. We also observed a feature due to acetylene water complex at 3240 cm^{-1} , in excellent agreement with that reported in the

literature.^[125] Features corresponding to complex involving water appear, as water is an inevitable impurity in a matrix isolation experiment.

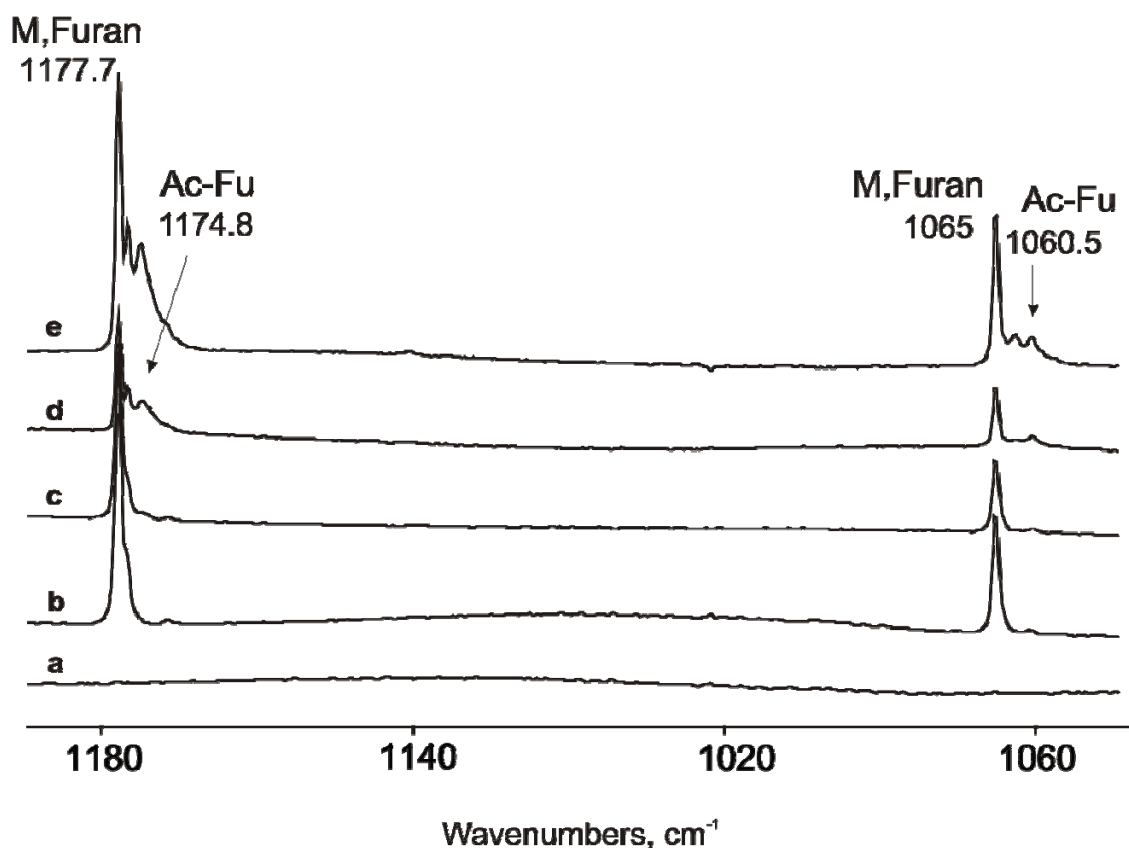


Figure 5.3. IR spectra in the range 1190 – 1050 cm^{-1} of acetylene, furane, and Acet/Fu mixtures, matrix-isolated in argon. a) Ac:Ar ratio 1:1500, 10 K. b) Fu:Ar ratio 1:1500, at 10 K. c) Ac:Fu:Ar ratio 1:1:1500, 10 K. d) Ac:Fu:Ar ratio 1:1:1500 after annealing at 30 K. e) Ac:Fu:Ar ratio 1:3:1500 after annealing at 35 K.

Figure 5.3 shows infrared spectra in the region between 1190 – 1050 cm^{-1} in different sets of experiment, where asymmetric and symmetric stretching modes of furan are observed. The asymmetric and symmetric vibration modes appear at 1177.7 and 1065 cm^{-1} , respectively, in isolated furan, and at 1174.8 and 1065.5 cm^{-1} , respectively, in the acetylene-furan complex (Figure 5.3 spectrum d and e). The formation of a complex only leads to a small red shift of -2.9 cm^{-1} and by -4.5 cm^{-1} , respectively.

5.2.1. Vibrational assignments

Vibrational frequencies were calculated at various theoretical methods and compared with experimentally observed frequencies (Tables 5.3 and 5.4). Deviations between calculated and observed vibrational modes result from matrix effects, anharmonicity of the vibrations, and deficiencies of the theoretical model. To correct for these deviations scaling factors for each vibrational mode of the monomers (furan and acetylene) were determined such that their application to the calculated modes of the monomers exactly reproduces the experimental matrix spectroscopical values of the monomers (Table 5.2) applying the scaling to modes of the complexes allows a most probable prediction of band positions of the complexes. A careful comparison between calculated and experimental spectra reveals that only one of the possible dimer structures was trapped in argon matrix (Tables 5.3 and 5.4).

Table 5.2. Calculated and experimental vibrational frequencies (cm^{-1}) of the furan and acetylene monomers. Factor of correction

MP2/6-311++G(d,p)			MP2/cc-pVTZ			Assignment
Monomer and factor of correction						
M exp.	M calc	Factor of corr.	M exp.	M calc	Factor of corr.	
Furan						
1177.7	1249.9	0.942	1177.7	1248.4	0.943	$\nu_{\text{as}}(\text{C}-\text{O}-\text{C})$ (ν_{13})
1065.0	1112.5	0.957	1065.0	1114.3	0.955	$\nu_{\text{s}}(\text{C}-\text{C})+\nu_{\text{s}}(\text{C}-\text{O})$ (ν_{11})
993.6	1025.5	0.968	993.6	1025.8	0.968	$\delta(\text{CC}-\text{H})$) (ν_9)
869.1	879.9	0.987	869.1	877.8	0.990	$\delta_{\text{s}}(\text{C}-\text{O}-\text{C})$)(ν_7)
744.1	732.5	1.015	744.1	761.5	0.977	$\gamma(\text{CC}-\text{H})$) (ν_4)
Acetylene						
3288.8	3457.5	0.951	3288.8	3446.1	0.954	$\nu_{\text{as}}(\text{C}-\text{H})$ (ν_3)
736.8	764.8	0.963	736.8	753.0	0.978	$\delta(\text{CC}-\text{H})$ (ν_5)

ν_3 Mode of Acetylene. As seen in Tables 5.3 and 5.4 most perturbed vibrational mode in complex **A** and **B** are the C–H stretching vibration of acetylene. The frequency shifts due to complexation calculated by MP2/cc-pVTZ level of theory are -21.7 and -17.8 cm^{-1} , respectively. With the 6-311++G(d,p) basis set, the corresponding frequency shifts for the C–H stretching mode are -11.6 and -14.4 cm^{-1} . As mentioned earlier, the ν_3 mode of

acetylene submolecule in the complex occurs at 3265.7 cm^{-1} which is red-shifted from unperturbed molecule by -23.1 cm^{-1} , which agrees well with the computed values of complexes **A** and **B** (Table 5.3 and 5.4).

The analysis of the experimental and computed shifts in the ν_3 mode of acetylene in other complexes of acetylene is in line with this observation. In the complexes where acetylene is a proton donor, the shifts in the ν_3 mode of acetylene submolecule are usually large. For instance, the ν_3 mode acetylene in the acetylene–water complex is red-shifted by $\approx 49\text{ cm}^{-1}$, where acetylene acts as proton donor.^[125] In the complexes where acetylene is the proton acceptor, the shifts in the ν_3 mode are comparatively small. For example the ν_3 mode of acetylene in the acetylene-chloroform complex where acetylene is the proton acceptor is red-shifted only by 5.9 cm^{-1} .^[122] In this study, ν_3 mode of the acetylene submolecule is red-shifted by 23.1 cm^{-1} indicating that acetylene acts as proton donor.

ν_5 Mode of Acetylene. Due to the formation of a complex the degenerate CCH bending mode ν_5 of acetylene is split into two components. Computed vibrational frequencies for the CC–H bending modes of the complexes **A** and **B** are listed in the Tables 5.3 and 5.4. Again computed frequency shifts for ν_5 modes of acetylene submolecule in the complexes **A** and **B** are close to each other. Calculations at the MP2/cc-pVTZ level of theory predict blue shifts of 24.5 and 10.8 cm^{-1} or the two vibrations in complex **A** and 31.9 and 16 cm^{-1} in complex **B**, respectively (Table 5.3 and 5.4). With the 6-311++G(d,p) basis set, the frequency shifts for the CC–H bending mode are 28.5 and 13.8 cm^{-1} for complex **A**, and 23.6 and 12 cm^{-1} for complex **B**.

In argon matrix the CC–H bending mode of acetylene is found at 736.8 cm^{-1} . The $\gamma(\text{CCH})$ mode of furan occur at 744.1 cm^{-1} . Thus, after co-deposition of acetylene with furan in argon two very strong absorptions appear in this spectral region. Annealing the matrices containing both acetylene and furan results in aggregation and leads to a number of new bands in this region which are difficult to assign. However, a new peak at 764.2 cm^{-1} , blue-shifted from the unperturbed molecule by 27.4 cm^{-1} , is in good agreement with the calculated value.

Table 5.3. Experimental, calculated and predicted experimental vibrational frequencies (cm^{-1}) of the Fu – acetylene complex **A**.^a

		MP2/6-311++G(d,p)			MP2/cc-pVTZ			
Experimental		Calculated frequencies and shifts in the complex						
M		M	Complex A		M	Complex A		Assignment
Exp.	Exp.	Calc.	wtc.	sc.	Calc.	wtc.	sc.	
Furan								
1177.7	1774.8 (−2.9)	1249.9	1248.7 (−1.2)	1176.2 (−1.5)	1248.4	1248.1 (−0.3)	1176.9 (−0.8)	$\nu_{\text{as}}(\text{C-O-C})$ (ν_{13})
1065.0	1060.5 (−4.9)	1112.5	1112.4 (−0.1)	1064.5 (−0.5)	1114.3	1115.0 (+0.7)	1064.8 (−0.2)	$\nu_{\text{s}}(\text{C-C})+$ $\nu_{\text{s}}(\text{C-O})(\nu_{11})$
993.6	-	1025.5	1025.8 (0.3)	992.7 (−0.9)	1025.8	1026.3 (+0.5)	993.4 (−0.2)	$\delta(\text{CC-H})$ (ν_9)
869.1	-	879.9	879.8 (−0.1)	868.3 (−0.8)	877.8	877.4 (−0.4)	868.6 (−0.5)	$\delta_{\text{s}}(\text{COC})$ (ν_7)
744.1	-	732.5	747.5 (+15.0)	758.7 (+14.6)	761.5	751.5 (−10.0)	734.2 (−9.9)	$\gamma(\text{CC-H})$ (ν_4)
Acetylene								
3288.8	3265.7 (−3.1)	3457.5	3445.9 (−11.6)	3277.0 (−11.8)	3446.0	3424.3 (−21.7)	3266.7 (−22.1)	$\nu_{\text{as}}(\text{C-H})(\nu_3)$
736.8	764.2 (+27.4)	764.8	793.3 (+28.5) 778.6 (+13.8) ^b	763.9 (+27.1) 749.7 (+12.9) ^b	753.0	775.5 (2+4.5) 763.8 (+10.8) ^b	758.4 (+21.6) 746.9 (+10.1) ^b	$\delta(\text{CCH})(\nu_5)$

[a] The frequency shifts in complex **A** compared to Fu and acetylene (monomers **M**) are given in parentheses. [b] Out of plane mode. wtc: without correction . sc: scaled

ν_{13} and ν_{11} modes of furan. The asymmetric and symmetric modes of furan also perturbed due to complexation. The experimentally observed bands in the acetylene-furan complex are found at 1174.8 and 1060.5 cm^{-1} those red-shifted by 2.9 and 4.5 cm^{-1} , respectively from unperturbed molecule at 1177.7 and 1065 cm^{-1} , correspondingly, for the asymmetric and symmetric stretching modes of furan (Figure 5.3).

Table 5.4. Experimental, calculated and predicted experimental vibrational frequencies (cm^{-1}) of the Fu – acetylene complex **B**.^a

MP2/6-311++G(d,p)					MP2/cc-pVTZ			
Experimental		Calculated frequencies and shifts in the complex						
M		M	Complex B		M	Complex B		Assignment
Exp.	Exp.	Calc.	wtc.	sc.	Calc.	wtc.	sc.	
Furan								
1177.7	1174.8 (-2.9)	1249.9	1245.3 (-4.6)	1173.1 (-4.6)	1248.4	1244.6 (-3.8)	1173.6 (-4.1)	$\nu_{\text{as}}(\text{C-O-C})$ (ν_{13})
1065.0	1060.5 (-4.9)	1112.5	1107.5 (-5.0)	1059.8 (-5.2)	1114.3	1108.8 (-5.5)	1058.9 (-6.1)	$\nu_{\text{s}}(\text{C-C})+$ $\nu_{\text{s}}(\text{C-O})(\nu_{11})$
993.6	-	1025.5	1024.3 (-1.2)	991.5 (-2.1)	1025.8	1024.9 (-0.9)	992.1 (-1.5)	$\delta(\text{CC-H})$ (ν_9)
869.1	-	879.9	881.3 (+1.4)	869.8 (+0.7)	877.8	878.7 (+0.9)	869.9 (+0.8)	$\delta_{\text{s}}(\text{COC})$ (ν_7)
744.1	-	732.5	727.6 (-4.9)	738.5 (-5.6)	761.5	760.9 (-0.6)	743.3 (-0.8)	$\gamma(\text{CC-H})$ (ν_4)
Acetylene								
3288.8	3265.7 (-3.1)	3457.5	3457.5 (-14.4)	3274.3 (-14.5)	3446.0	3428.2 (-17.8)	3270.5 (-18.3)	$\nu_{\text{as}}(\text{C-H})(\nu_3)$
736.8	764.2 (+27.4)	764.8	788.4 (+23.6) 776.8 (12.0) ^b	759.2 (+22.4) 748.0 (11.2) ^b	753.0	784.9 (+31.9) 770.0 (16.0) ^b	767.6 (+30.8) 753.0 (16.2) ^b	$\delta(\text{CCH})(\nu_5)$

[a] The frequency shifts in complex **B** compared to Fu and acetylene (monomers **M**) are given in parentheses. [b] Out of plane mode. wtc: without correction . sc: scaled

At the MP2/cc-pVTZ level of theory the frequency shifts in complex **A** are predicted to -0.3 and 0.7 cm^{-1} , and at the MP2/ 6-311++G(d,p) level of theory to -1.2 and 0.1 cm^{-1} , respectively (Table 5.3). At the same levels of theory, the frequency shifts in complex **B** are -3.8 , -5.5 cm^{-1} and -4.6 and -5 cm^{-1} , respectively (Table 5.4). The comparison of the experimental with the calculated frequency shifts suggests that structure **B** is formed in the matrix. Note, however, that the relevant calculated frequency shifts in structure **A** and **B**

are fairly similar, so that the existence of structure **A** rather than **B** cannot be excluded with certainty.

5.2. Conclusion

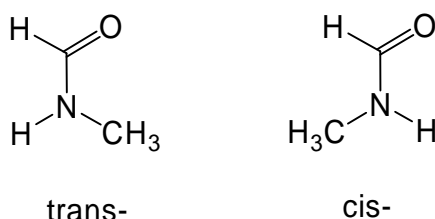
In conclusion, five structures were identified to be minima on the potential energy surface of the acetylene–furan dimer in MP2/6-311++G(d,p) geometry optimizations. Comparison between calculated and measured IR spectra of acetylene–furan deposited in an argon matrix, however, makes it likely that structure **B** is formed in the matrix.

Chapter 6. N-methylformamide: Monomers and Dimers

Chapter 6.1. N-methylformamide-Monomers

6.1.1. Introduction

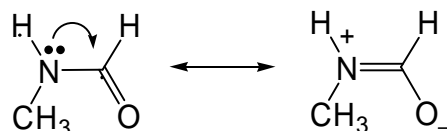
The amide group --CO--NH-- , is a unit of peptide linkage and the essential building block for the protein structure. The conformation of peptides about C–N bond has been extensively studied because of its significance to the backbone structure of polypeptides and proteins. N-methylformamide (NMF) is one of the simplest amide molecules that have rotational isomers. There are some confusions and inconsistencies about naming of conformers in literature. Some papers defined the naming for *trans*– and *cis*– conformers by the dihedral angle between C=O and N–CH₃ bonds around central OC–NC bond. We will follow to above mentioned definition such that *cis*– and *trans*– conformer is defined by the dihedral angle made by C=O and N–H bonds around the central CO–NH bond.



Scheme 6.1.1. Rotational isomers of the N-methyl formamide.

The matrix isolation infrared spectroscopy is a powerful tool for identifying the less stable conformers particularly by combining either the high-temperature nozzle technique or irradiation with ultraviolet or near-infrared light.^[171] Ataka et.al.^[172] used matrix isolation together with high-temperature nozzle technique and obtained the less stable *cis*– conformer of NMF and their variously deuterated species in nitrogen and argon matrices. The *cis*–*trans* isomerism of NMF has been reexamined by IR and NMR spectroscopic methods with the help of DFT calculation. The occurrence of the *cis*– form in the amide has been verified and the amount of the *cis*– form as a minor component was determined to be about 5% in the gas phase at room temperature by Shin and co-workers.^[173] *Ab-initio* studies attribute the instability of the *cis*– isomer to the repulsion between the aldehyde group and the hydrogen atoms of the N-methyl group.^[174] Matrix isolation infrared spectroscopy studies of NMF monomer showed that a larger amount of the *cis*– isomer can be only obtained via UV radiations or using techniques with hot nozzles.^[175] The barriers in the energy hypersurface are apparently too large to be overcome under annealing and

free-warm-up experiments, since the mobility and the rotation possibilities of the molecule are too small even in warm-up experiments. There is a high rotation barrier in the R_2N-COH bond, due to its partial double bond character.



Scheme 6.1.2. Partial double bond character of the R_2N-COH bond.

While amides are usually most stable in the *trans*- conformation, they can be converted into the *cis*- conformation by photoisomerization upon $\pi-\pi^*$ excitation. The photoisomerization of *N*-methylthioacetamide in different matrices have been studied by Tasumi^[172]. The Raman spectra of the transient species generated from *N*-methylthioacetamide under ultraviolet laser irradiation have been studied in water. Using the flow technique, the formation of the transient species was estimated to be 0,5 ms. Transient species was identified as the *cis*- isomer of *N*-methylthioacetamide.^[176]

In gas phase, the electronic spectra of amides have been well-characterized.^[177-181] The spectra have an intense band, often labeled V_1 , that corresponds to the $\pi_{nb}-\pi^*$ (nonbonding π orbital to antibonding π^* orbital) transition (Figure 6.1.1). This transition occurs in the range 6.2-7.4 eV. The addition of alkyl groups to the amide nitrogen atom considerably decreases the $\pi_{nb}-\pi^*$ excitation energy.^[182] The $n-\pi^*$ (lone pair on oxygen to π^* orbital) transition is termed the W band. This transition is much weaker and consequently more difficult to detect. However, it occurs typically in the region 5.5–5.8 eV.^[181] In addition, there are sharp bands that correspond to Rydberg transitions. In formamide, a further band at higher energy (~9 eV) called the Q-band was identified. The Q-band was originally assigned to the $\pi_b-\pi^*$ transition, but more recently it has been shown to arise from a superposition of Rydberg states^[183] while the $\pi_b-\pi^*$ (bonding π orbital to antibonding π^* orbital) transition energy is greater than 10 eV.^[179] At higher energy is a further transition corresponding to excitation from the second oxygen lone pair to the π^* orbital, denoted $n'-\pi^*$.

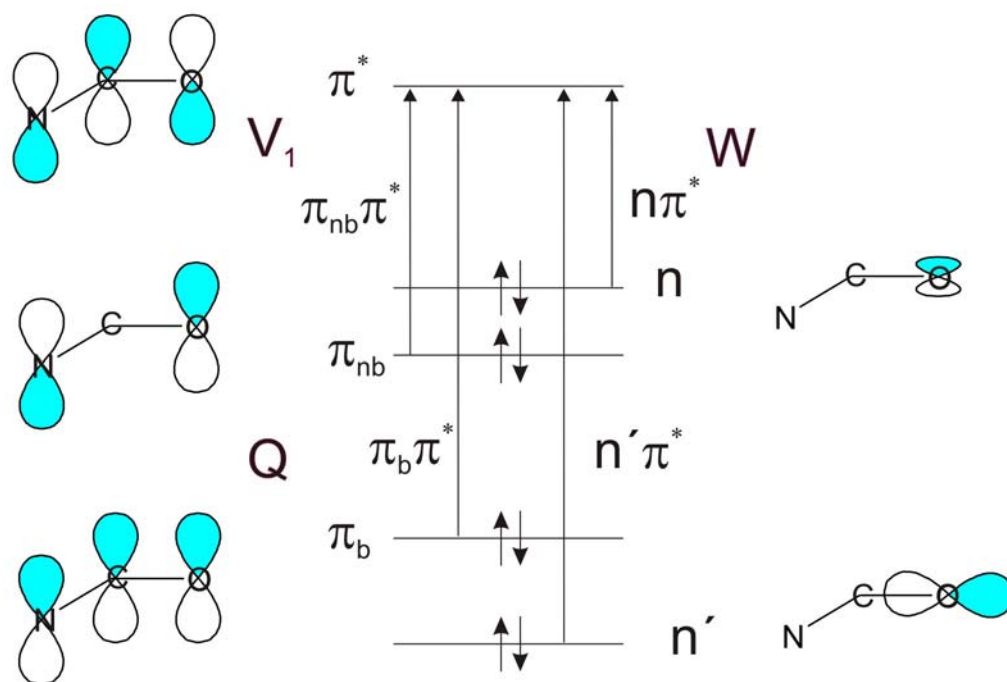


Figure 6.1.1. Valence molecular orbitals and electronic transitions of amides.

Solvents induce a number of changes in the electronic spectra of amides. The $\pi_{nb}\pi^*$ transition undergoes a red-shift. The magnitude of this shift varies for different amides and is dependent on the solvent. Experimental data indicate a red-shift of 0.40–0.5 eV for formamide^[180] and a smaller red-shift of ~ 0.1 eV for *N*-methylacetamide (NMA).^[184] The origin of the red-shift is considered to be largely electrostatic. Accurate determination of the effect of solvent on the $n\pi^*$ transition is difficult. In aqueous solution, a blue-shift of approximately 0.2–0.4 eV is observed. A blue-shift arises as a result of hydrogen bonding between the amide and solvent. The ground state forms stronger hydrogen bonds than the excited $n-\pi^*$ state, resulting in a blue-shift in the spectral band. However, the blue shift observed in carbonyl $n-\pi^*$ transitions has also been attributed to changes induced by hydrogen bonding in the geometry of the solute molecule.^[177, 185]

NMF complexes provide simple models for studying intermolecular interactions in larger system such as proteins and nucleic acids. Shin et.al.^[173] carried out IR spectroscopic investigation of aggregation of NMF in an argon matrix, and preliminary consideration on the conformations of the dimers has been made.

In this chapter we report infrared spectra of the *cis*- form of NMF generated by irradiation with light of wavelength $\lambda = 248$ nm from the *trans*- form in cryogenic matrices. On continuous irradiation at the same wavelength, it led to the transformation of the *cis*- form rearranged into *N*-methylformimidic acid, which is reported for the first time.

Under these irradiation conditions, the formation of photodecomposition products such as CO and methylamine has also been observed. We also investigated the aggregation of NMF using matrix isolation technique and DFT calculations. The geometries, binding energies and spectroscopic properties of the different types of dimers are discussed here. The assignment of the complexes is achieved by comparison of experimental and calculated frequencies.

6.1.2. Results and Discussion

6.1.2.1. FT-IR Spectra of N-methylformamide in Rare Gas Matrices

Experimental studies of NMF in the gas phase,^[173, 186, 187] in dilute solution of carbon tetrachloride,^[188] or isolated in rare gas matrices^[171-173] suggest the existence of two conformers, namely *trans*- and *cis*- forms. The *trans*- isomer is found to be the major, whereas the *cis*-form is the minor conformation. The vibrational spectra of NMF in liquid phase have been extensively studied by Suzuki.^[189] Using isotope labeling, he predicted the vibrational frequencies of NMF, and investigated the spectroscopic differences of two isomers. Gas electron diffraction experiments were carried out by Kitano and Kutchitsu^[190]. They estimated the presence of the *cis*- form and to be approximately 20 %. The IR spectra of NMF in argon and nitrogen matrices are shown in Figure 6.1.2, and their frequencies are tabulated along with its calculated infrared absorptions (Table 6.1.1 and 6.1.2). Our experimental spectra of NMF in argon and nitrogen matrices are in good agreement with those reported in literature^[172, 173]. As the earlier reports indicated, the *trans*- isomer is found to be the major isomer in rare gas matrices even at low temperature. The most intense bands, in both Ar and N₂ matrices, are due to the carbonyl stretching mode $\nu(\text{C}=\text{O})$ located at 1725.4 and 1719.6 cm⁻¹ (*trans*- form), and bands at 1730.6 and 1721.6 cm⁻¹ (*cis*- form) (Figure 6.1.2). Another strong absorption splitted to 3493.7 and 3488.9 cm⁻¹ is assigned to the NH stretching mode $\nu(\text{NH})$ of the *trans*- form. The $\nu(\text{NH})$ mode of the *cis*- form appears at 3456.4 and 3452.0 cm⁻¹.

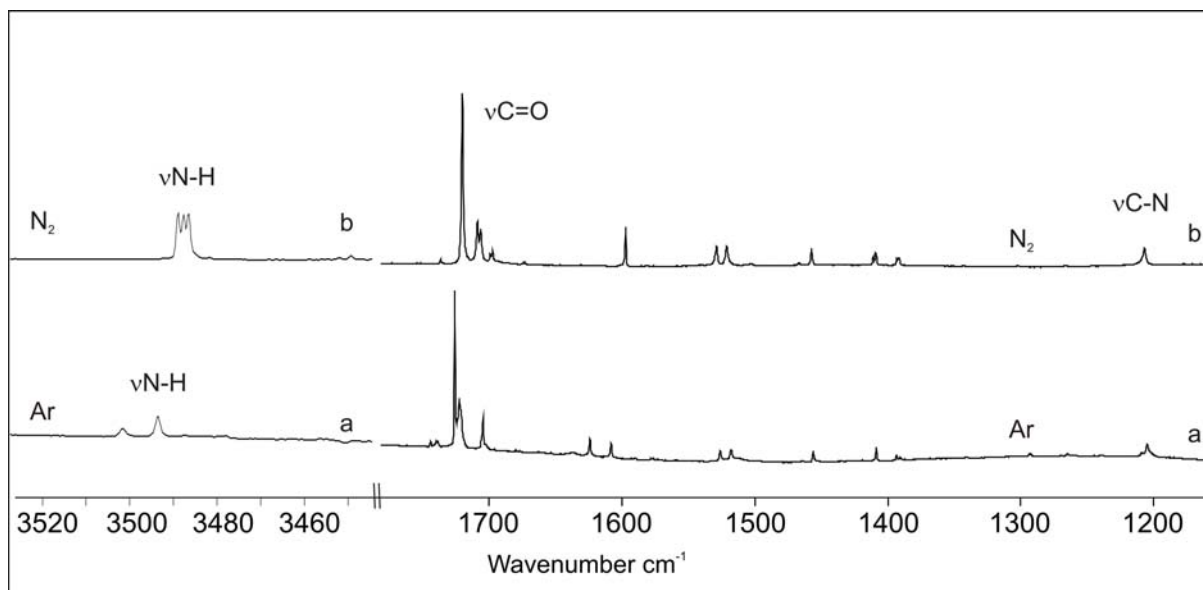


Figure 6.1.2. IR spectra of N-methylformamide (NMF) deposited at 20 K and recorded at 10 K (a) argon matrix (b) nitrogen matrix.

6.1.2.2. Photochemistry of NMF. Photoconversion of the *trans*-conformer to the *cis*-conformer

Ultraviolet irradiation might induce conformational isomerization if the molecule under study has an absorption in the ultraviolet region. Irradiation, in particular in the near-infrared region, has been used to induce conformational isomerizations in low temperature matrices.^[191-197] The effect of near-infrared irradiation for the *cis*–*trans* isomerization was first observed by Pizenrel in the case of nitrous acid.^[191] The mechanism involves absorption of radiation, followed by conversion into rotational modes by intramolecular energy transfer, where the energy of the internal rotational barrier is in the order of the energy of photon. In the NMF case photoisomerization of *trans*- to *cis*- requires a rotation around the C–N bond. The UV-irradiation should allow the photoisomerisation of the *trans*- conformer to the *cis*- required by overcoming the rotational barrier around C–N bond of NMF.

Table 6.1.1. Calculated and measured (Ar, N₂) IR data of *trans*- N-methylformamide

Mode	$\nu_{\text{calc.}}$ [cm ⁻¹] ^[a]	$I_{\text{rel,calc}}$ ^b	Sym	$\nu_{\text{exp.}}$ In Ar [cm ⁻¹]	$I_{\text{rel,calc}}$ _b	$\nu_{\text{exp.}}$ In N ₂ [cm ⁻¹]	$I_{\text{rel,calc}}$ ^b	Assignment
4	541.4	12	A''	535.5	7	570.0	9	NH wag.
6	951.8	5	A	947.7	11	950.5	6	C ^m N str
9	1161.2	7	A	1146.9	5	1148.2	3	HC ^m N def.
10	1218.7	25	A	1205.5	11	1207.0	10	CN str.
11	1422.5	1	A	1393.7	7	1393.1	4	CH bend
12	1443.9	6	A	1409.2	14	1409.1	7	CH ₃ def.
13	1493.3	9	A	1456.7	12	1457.6	10	CH ₃ def.
14	1502.9	1	A''	1464.5	2	1467.2	1	CH ₃ def.
15	1556.5	28	A	1518.2	11	1528.8	11	NH bend
16	1782.5	100	A	1725.4	100	1719.6	100	C=O str.
17	2933.5	35	A	2855.6	10	2857.9	3	CH str.
18	3028.5	13	A''	2940.4	1	2943.5	2	CH ₃ str.
19	3075.8	8	A	2963.3	1	2960.1	2	CH ₃ str.
21	3631.2	6	A	3493.7	20	3486.3 3488.9	18	NH str.

[a] Unscaled frequencies calculated at the B3LYP/cc-pVTZ level of theory. [b] Relative intensity based on the most intense absorption.

The UV irradiation at $\lambda = 248$ nm of NMF were performed from several minutes up to several hours in argon and nitrogen matrices at 10 K. The irradiation of NMF from several minutes (1 – 10 min) in the infrared spectra obtained of the destruction of the bands of precursor molecule (*trans*- form) suggests the presence of several new photoproducts. The longer irradiation led to the completely disappearance of the bands of the *trans*-conformer. We observed new bands in the typical region of OH stretching modes (3700 – 3500 cm⁻¹), carbon monoxide (2140 cm⁻¹), the bands correspond to deformation modes of NH and CH groups, and also few strong bands due to wagging mode of methylamine (830 – 750 cm⁻¹). Some peaks are shifted indicating the formation of hydrogen bonded complexes created in the matrix cage.

Table 6.1.2. Calculated and measured (Ar, N₂) IR data of *cis*- N-methylformamide.

Mode	$\nu_{\text{calc.}}$ [cm ⁻¹] ^[a]	$I_{\text{rel,calc}}$ ^b	Sym.	$\nu_{\text{exp.}}$ In Ar [cm ⁻¹]	$I_{\text{rel,calc}}$ ^b	$\nu_{\text{exp.}}$ In N ₂ [cm ⁻¹]	$I_{\text{rel,calc}}$ ^b	Assignment
4	611.7	2	A	586.4	6	608.4	8	OCN def.
5	622.8	22	A''	602.1	22	629.9	16	NH wag.
6	1008.6	8	A	1000.9	40	1002.0	21	HC ^m N def.
9	1158.4	6	A	1143.2	13	1144.9	7	C ^m N str
10	1301.7	23	A	1292.9	38	1301.2	5	CN str.
11	1398.5	1	A	1373.8	2			CH bend
12	1468.2	1	A	1435.1	6	1437.0	2	CH ₃ def.
13	1483.6	0	A					NH bend
14	1486.0	1	A''	1447.0	4			CH ₃ def.
15	1534.8	3	A	1499.1	4			CH ₃ def.
16	1791.4	99	A	1730.6	100	1721.6	100	C=O str.
17	2922.0	18	A	2858.3	7	2848.8	3	CH str.
18	3020.6	11	A''					CH ₃ str.
19	3066.3	6	A					CH ₃ str.
20	3107.9	2						CH ₃ str.
21	3595.9	4	A	3456.4	20	3452.0	10	NH str.

[a] Unscaled frequencies calculated at the B3LYP/cc-pVTZ level of theory. [b] Relative intensity based on the most intense absorption.

UV irradiation of NMF in cryogenic matrices at $\lambda = 248$ nm produced bands that are typical for the *cis*- NMF. (Figure 6.1.3) The strong bands at 1725.4 cm⁻¹ and 1719.6 cm⁻¹ are assigned to the carbonyl stretching mode of the *trans*- NMF (bands pointing downwards in Figure 6.1.3).^[171, 173] The splitting of this band is caused by matrix site effects. Irradiation of the matrix containing both *trans*- and *cis*- conformers of NMF led to disappearance of the bands the *trans*- conformer and growing of the bands of the *cis*- form. The peaks at 1730.6 cm⁻¹ and 1721.6 cm⁻¹ are assigned to the carbonyl stretching mode of the *cis*- NMF, and are in good agreement with the calculated data. Matrix isolation infrared spectroscopy in combination with the high temperature nozzle technique has been applied to identify rotational isomers of NMF and N-methylacetamide in nitrogen matrix by Ataka and co-workers.^[172] Shin and et. all.^[173] studied the population of *cis*-*trans* conformers of NMF by NMR and IR spectroscopic methods in combination with DFT calculations. The matrix isolated spectra of NMF in argon have been reported in the same paper. According to their assignment the carbonyl vibration mode of the *cis*- conformer of NMF appears at 1722 cm⁻¹ which differs from our assignment.

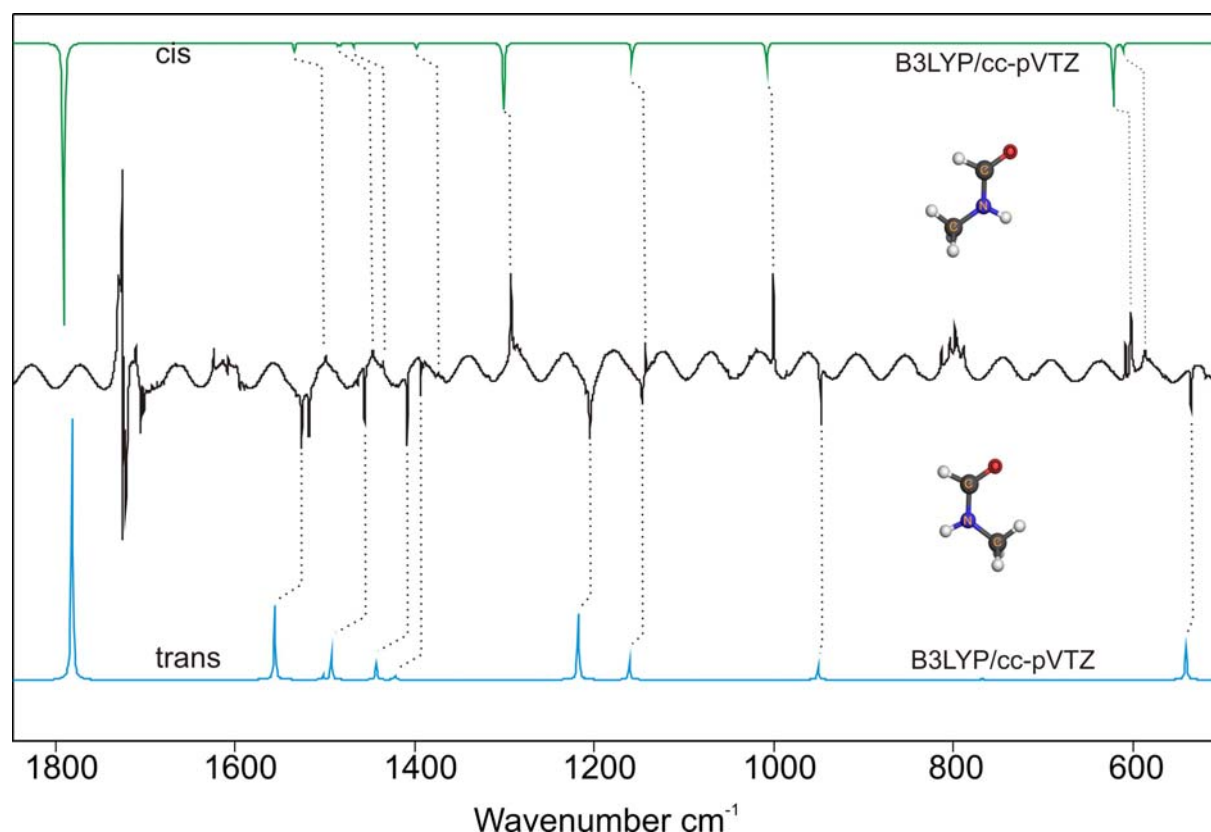


Figure 6.1.3. Difference FTIR spectra of NMF in argon matrix at 10 K after 15 min of irradiation at 248 nm (black curve).

The NH stretching mode (ν_{21}) of the *trans*- conformer of NMF appears at 3493.7 cm^{-1} in Ar, whereas in N_2 , it is split at 3486.3 , 3487.7 and 3488.9 cm^{-1} in N_2 . (Figures 6.1.3 and 6.1.4). Bands at 3456.4 cm^{-1} and 3452.0 cm^{-1} are assigned to the NH stretching mode of the *cis*- conformer in Ar and N_2 , respectively. The frequency shift between Ar and N_2 is less than -5 cm^{-1} . In dilute chloroform solution the NH stretching bands of the *trans*- and *cis*- forms of free NMF were found at 3466 and 3429 cm^{-1} respectively.^[198] The ν_{10} mode of *trans*- NMF appears at 1205.5 , 1207.7 cm^{-1} correspondingly. The ν_{10} mode of the *cis*- NMF appears at 1292.9 cm^{-1} and 1301.2 cm^{-1} . The ν_6 and ν_4 vibrational modes are located at 1146.9 and 947.7 cm^{-1} for the *trans*- conformer and 1144.9 and 1002 cm^{-1} for the *cis*- conformer, respectively (Figure 6.1.4, Tables 6.1.1 and 6.1.2). Moreover, it must be noted that the ν_6 modes is highly affected by the matrix environment, and the shift between Ar and N_2 is approximately 35 cm^{-1} for the *trans*- form and approximately 36 cm^{-1} for the *cis*-NMF.

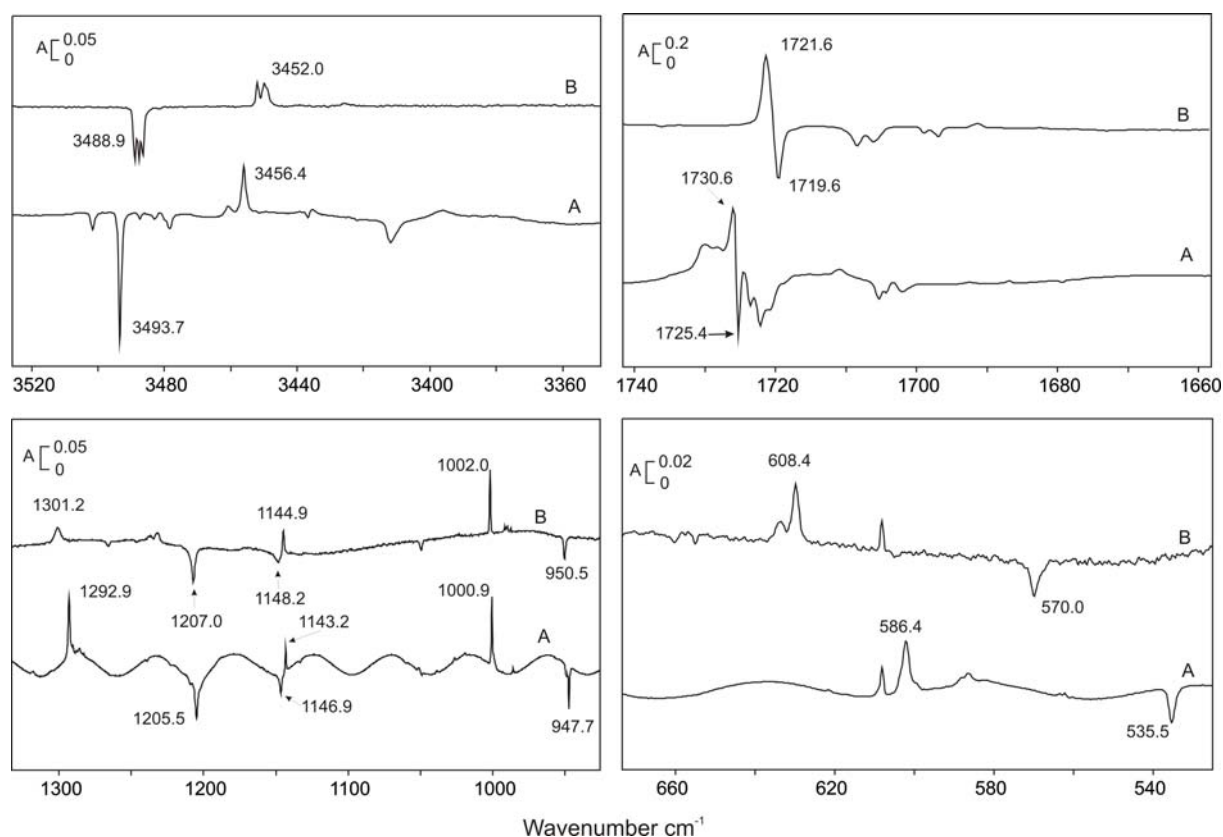
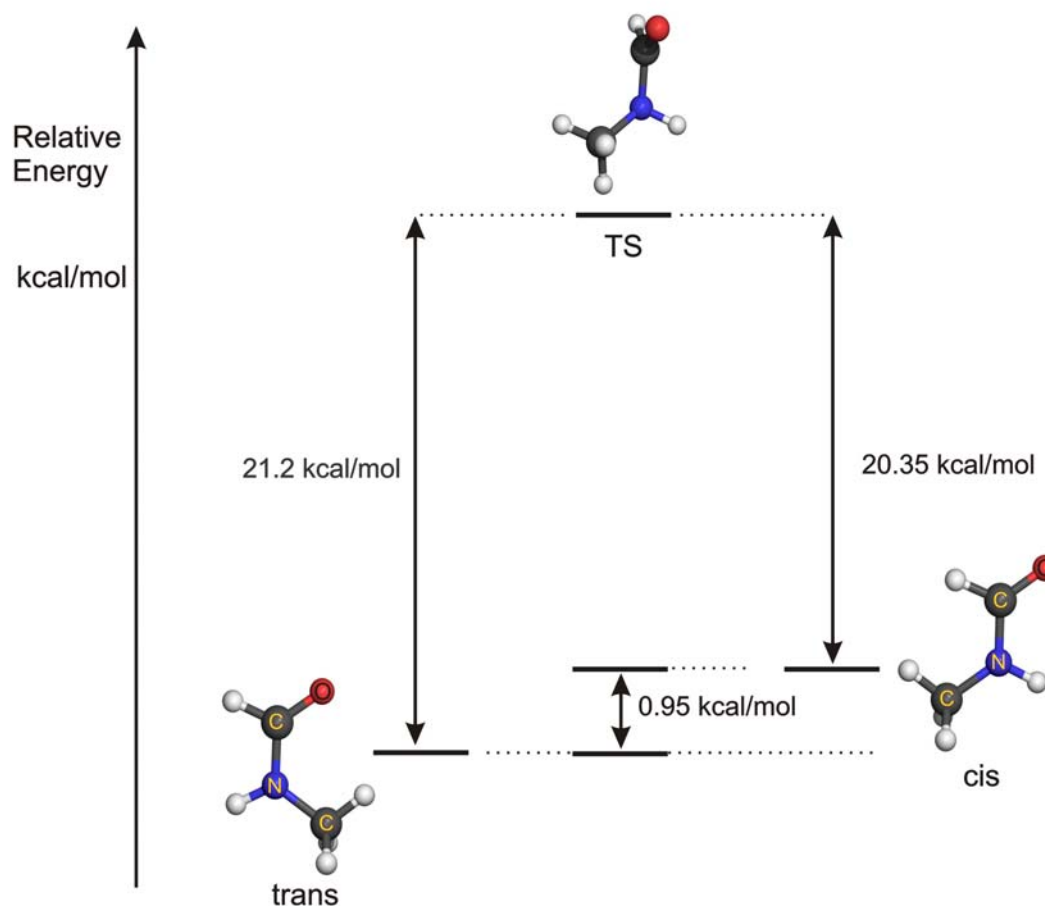


Figure 6.1.4. Difference FTIR spectra of NMF in argon matrix at 10 K after 15 min of irradiation at 248 nm (spectrum A). Difference FTIR spectra of NMF in nitrogen matrix at 10 K after 45 min of irradiation at 248 nm (spectrum B).

The ultraviolet irradiation of N-methyltioacetamide (NMTAA) was carried out by Tasumi et. al.^[172] They reported IR spectra of the *cis*- form of NMTAA generated from the *trans*- form in low temperature matrices. The reverse photoisomerization, from *cis*- to *trans*-, has also been found in low temperatures matrices. On the other hand, no reversible photochemistry has been observed from *cis*-NMF to the *trans*- form in argon matrix using variety of light sources. Irradiation using short wavelength UV light led only to decomposition products (CO and methylamine).

We calculated two possible structures of NMF (*trans*- and *cis*-), fully optimized using B3LYP with a cc-pVTZ basis set. According to the calculation, the *cis*- form is less stable than the *trans*- form by 0.948 and 0.88 kcal/mol, without and with ZPE correction, respectively. We located a transition state for the isomerization reaction between the two conformers. The reaction partway is represented in Scheme 6.1.3. According to B3LYP/cc-pVTZ level of theory, the transition state is 21.3 kcal/mol above than *trans*-isomer (ZPE by 20.57 kcal/mol) The transition state structure is found to be nonplanar, and has a HCNH dihedral angle of 118.9°.



Scheme 6.1.3. Isomerisation partway between two isomers of NMF. Stationary points and transition state were performed by use B3LYP/cc-pVTZ method

The peptide bond has attracted a great deal of attention relation to the understanding of the function of biomolecules and many theoretical calculations have been published^[199-201]. NMF as target one of the typical and simplest amides for theoretical calculation have been studied by Fantoni and Caminati.^[201] They performed geometry optimization at the HF and MP2 level of theory with the 6-31G** basis set, and estimated the relative concentration of the *cis*- form to be 10-15%. Robin et. al.^[202] studied the mechanism for the *trans*-*cis* isomerization of N-methylacetamide and its excited states using UHF method for triplets or with configuration interaction or with configuration interaction between all singly excited configurations (CIS). The likely mechanism for *trans*-*cis* isomerization of amides was as the excitation of *trans*- isomer to either S_1 or S_2 followed by rapid relaxation to the pyramidal and rotated S_1 states. Internal conversion of this state to S_0 or intersystem crossing to T_1 is fast, however, no fluorescence is observed in the cases of benzanilide and N-methylbenzanilide.^[203]

6.1.2.3. Formation of N-methylformimidic acid

Prolonged irradiation of NMF with light of wavelength $\lambda = 248$ nm in argon and nitrogen matrices leads to formation of new bands at 3563.5, 1691.6, 1159.5, 1119.5, 986.2, 562.2 cm^{-1} in argon matrix and bands at 3557.5, 1703.8, 1168.7, 990.1, 598.0 cm^{-1} in nitrogen matrix, respectively (Table 6.1.3, Figure 6.1.5). All these observed bands have been assigned to *N*-methylformimidic acid (scheme 6.1.5, **3a**), which is the tautomeric form of NMF. The location of these bands are compatible with the region of molecule behavior ν_{OH} stretching mode (3563.5, 3557.5 cm^{-1}), $\nu_{\text{C}=\text{N}}$ mode (1691.1, 1703.8 cm^{-1}), $\delta_{\text{CH/OH}}$ (1159.5, 1168.7 cm^{-1}), $\nu_{\text{CN}}+\delta_{\text{COH}}$ (986.2, 990.1 cm^{-1}) and τ_{OH} (562.2, 598.0 cm^{-1}) respectively (Figure 6.1.5).

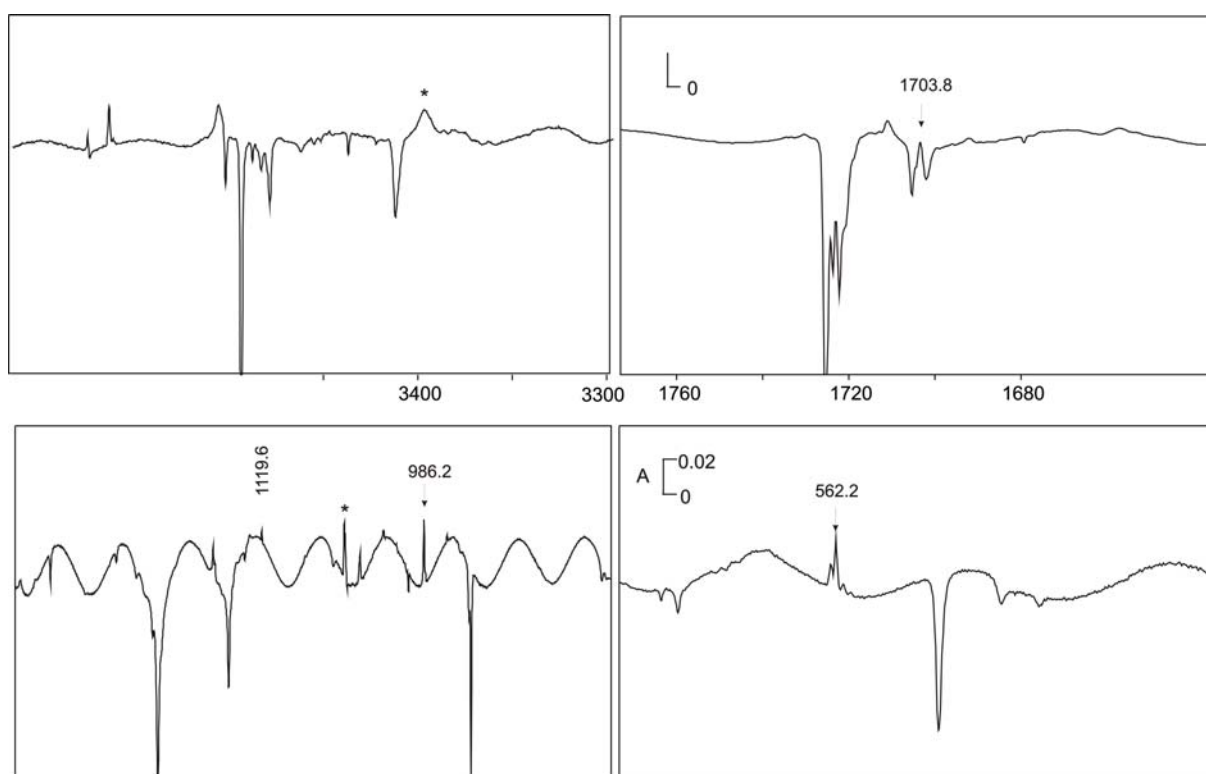


Figure 6.1.5. Difference FTIR spectra of NMF were recorded after 200 min of irradiation at 248 nm in argon matrix at 10 K. The peaks labeled with asterisk belong to methylamine (MA).

Maier and coworkers characterized^[111] the two energetically stable conformers of formidimic acid using matrix isolation technique. The formidimic acid forms during selective UV irradiation of formamide in argon matrices at $\lambda=248$ nm. Later by selective IR irradiation of their OH stretching mode of two conformers of formidimic acid to allow characterized the all of isomers of formimidic acid were carried out by Chiavassa^[204]. In the same way they also characterized the tautomer of urea, namely isourea^[205]

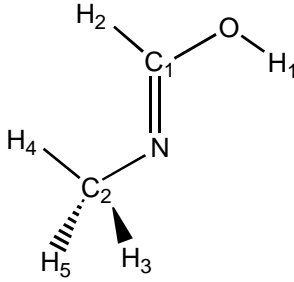
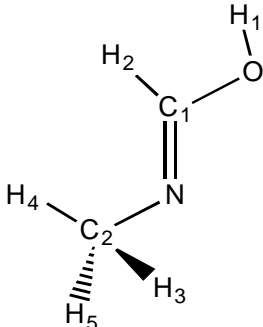
Table 6.1.3. Experimental and calculated IR frequencies of the two conformers of N-methylformimidic acid with in argon and nitrogen matrices respectively.

Mode	$\nu_{\text{calc.}}$ [cm ⁻¹] ^a	$I_{\text{rel,calc.}}$ ^b	$\nu_{\text{calc.}}$ [cm ⁻¹] ^a	$I_{\text{rel,calc.}}$ ^b	$\nu_{\text{exp.}}$ In Ar [cm ⁻¹]	$I_{\text{rel,calc.}}$ ^b	$\nu_{\text{exp.}}$ In N ₂ [cm ⁻¹]	$I_{\text{rel,calc.}}$ ^b
	3a		3b					
5	618.8	37	605.1	7	562.2	28	598.0	24
6	996.8	2	972.2	0				
7	1002.9	33	1012.1	5	986.2	38	990.1	53
9	1141.0	9	1140.1	0	1119.8	8		
10	1186.7	51	1192.7	9	1159.5	13	1168.7	23
11	1335.9	1	1295.0	99				
12	1394.2	4	1405.5	0				
13	1450.2	5	1449.3	4				
14	1483.1	1	1481.2	0				
15	1507.9	2	1506.8	3				
16	1762.6	99	1792.3	79	1703.8	100	1691.6	100
17	2974.0	22	2957.6	20				
18	3055.9	13	2989.8	27				
19	3071.9	7	3053.2	12				
20	3073.2	11	3071.6	7				
21	3737.1	14	3933.2	23	3563.5	19	3557.5	59

[a] Unscaled frequencies calculated at the B3LYP/cc-pVTZ level of theory. [b] Relative intensity based on the most intense absorption

The geometrical parameters and relative energies of two possible structures of N-methylformimidic acid fully optimized using B3LYP method with cc-pVTZ basis set are listed in Table 6.1.4. According to the calculations the **3a** stereoisomer is the most stable conformer. The **3b** stereoisomer is less stable by 5.17 kcal/mol with respect to **3a**. The two isomers show planarity of the NC₁OH₁ fragment. The values of angle NC₁H₂ fragment decrease from **3a** to **3b** by 1.7 degree, while the angle C₁NC₂ nearly remains constant.

Table 6.1.4. Geometrical Parameters of the two N-methylformidimic acid Stereoisomers calculated at the B3LYP/cc-pVTZ level of theory

		
parameter	(s-Z)-(E) 3a	(s-E)-(E) 3b
bond lengths (Å)		
R(OH ₁)	0.96	0.96
R(C ₁ O)	1.34	1.35
R(C ₁ H ₂)	1.09	1.09
R(C ₁ N)	1.25	1.25
R(C ₂ N)	1.44	1.44
R(C ₂ H ₃)	1.091	1.091
R(C ₂ H ₅)	1.091	1.091
R(C ₂ H ₄)	1.097	1.099
Bond angles (deg.)		
α(C ₁ OH ₁)	106.7	109.2
α(C ₁ NC ₂)	118.6	118.1
α(NC ₁ H ₂)	126.2	124.5
θ(NC ₁ OH ₁)	0	180.0
θ(C ₁ NC ₂ H ₃)	121.4	-121.5
θ(C ₁ NC ₂ H ₅)	-121.4	121.5
Energy (hartree)	-209.2670	-209.2588
<i>E</i> _{relative} (kcal/mol)	0	5.17

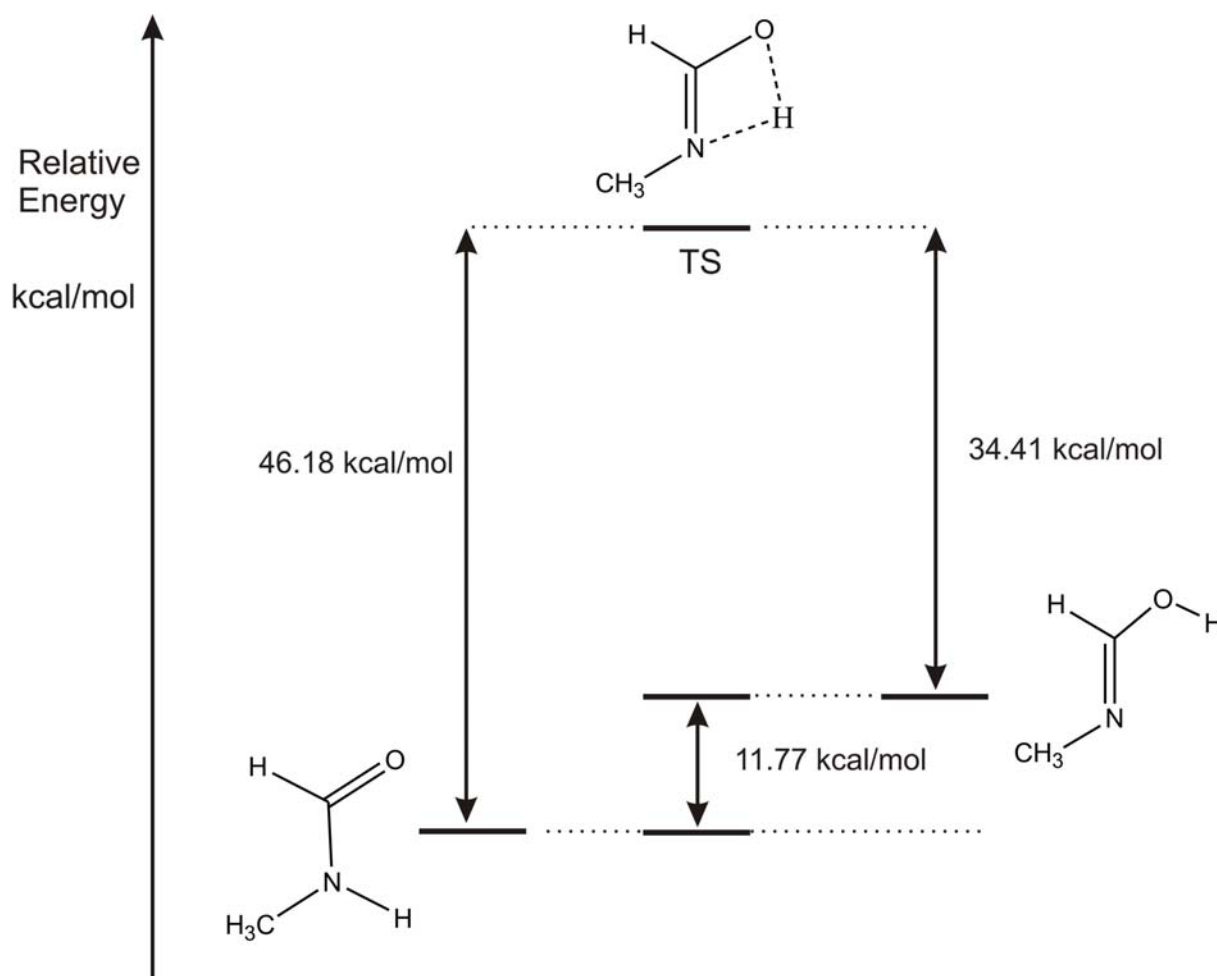
The computed vibrational frequencies of both conformers **3a** and **3b** have been obtained at the B3LYP/cc-pVTZ level of theory, which is known to be reliable predict the vibrational frequencies. The calculated harmonic frequencies of **3a** and **3b** stereoisomers are listed in Table 6.1.3. According to calculation the OH stretching mode of **3b** to be by 196.1 cm⁻¹ higher than the OH stretching mode of **3a**. The calculated frequency of the C=N stretching mode of **3b** is 29.6 cm⁻¹ more than for **3a** conformer. The relative intensity of ν₁₁ mode of **3a** conformer shows very low intensity in the contract to 3b which is most intense absorption according to the B3LYP/cc-pVTZ level of theory (Table 6.1.3). In the IR spectral region at 1350–1200 cm⁻¹, no peaks have been found that can be assigned to

either **3b** or **3a** conformers. The ν_{10} and ν_7 modes show frequency shifts of 5 cm^{-1} and 9 cm^{-1} between **3b** to **3a** in argon and nitrogen matrices, respectively. The ν_5 mode is higher by 13.7 cm^{-1} in **3a** compared to **3b**. We assume that stereoisomer **3a** is formed and characterized in cryogenic matrices. It is notable that the calculated relative intensities of **3a** and also in good agreement with the experimentally observed frequencies. On comparison with frequencies of the most stable conformer of formimidic acid in argon matrix,^[111] we observed more similarities. Maier and coworkers observed the $\nu_{\text{O-H}}$ mode at 3557.1 cm^{-1} , and we found this vibration at 3563.5 cm^{-1} . Similarly, the reported $\nu_{\text{C=N}}$ stretching mode at 1665.3 cm^{-1} , is observed at 1703.8 cm^{-1} . The $\delta_{\text{CH/OH}}$ mode of formimidic acid appears at 1168.4 cm^{-1} , which is close to our observed value located at 1159.5 cm^{-1} . The OH wagging mode of **3a** is observed at 562.2 cm^{-1} again close to a band observed at 577.7 cm^{-1} in an argon matrix by Maier.

We believe that the formation of **3a** occurs via an intermolecular proton migration from the amino group of NMF to the carbonyl oxygen atom. No studies have been reported in literature concerning the tautomerization of NMF to N-methylformimidic acid, however, the relationship between formamide and formimidic acid has been subject of several ab initio calculations.^[206, 207] The barrier estimated by ab initio calculations in the ground state for the conversion between formamide and formimidic acid is 31.9 kcal/mol higher than formamide.^[206] The energy needed to overcome this barrier can be provided by resonant excitation of the forbidden $n\text{-}\pi^*$ transition.^[208, 209] The electronic spectra of many amides have been well characterized in gas phase and by ab initio methods.^[210-214] The $n\text{-}\pi^*$ transition from the oxygen lone pair to the CO antibonding orbital was calculated as $\approx 5.5\text{ eV}$ for primary, secondary, and tertiary amides. Luis Serrano-Andres and Markus P. Fullscher studied the effect of the length of the alkyl chain and the center of substitution on the $n\text{-}\pi^*$ excitation energies that shows only slight change.^[211]

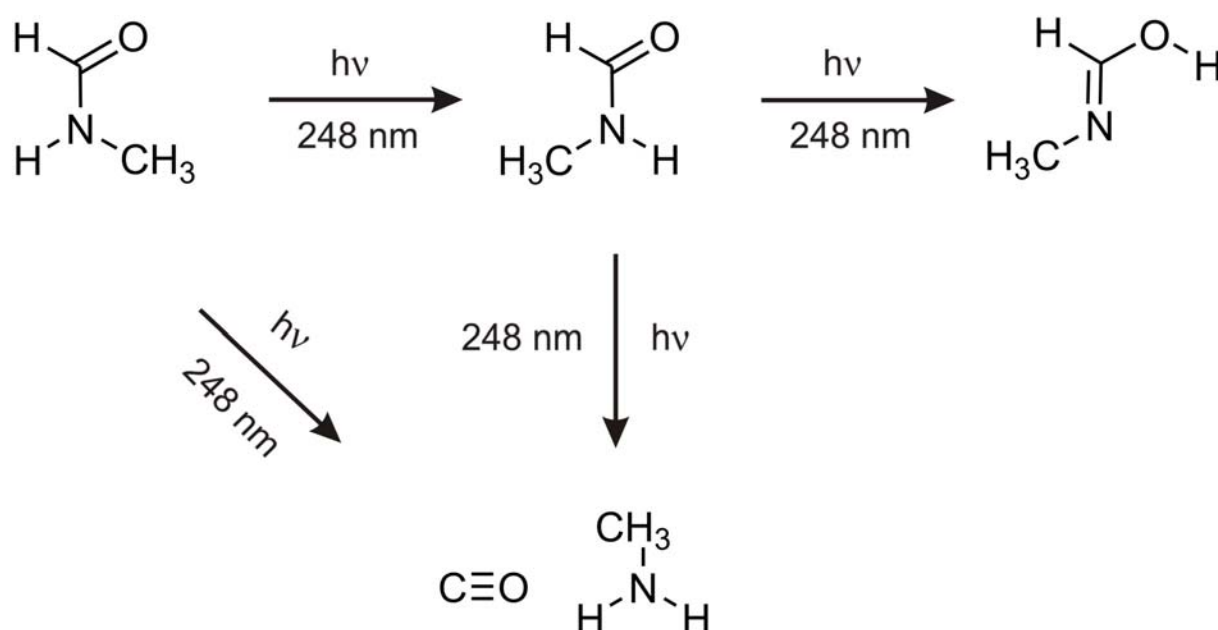
The N-methylformimidic acid is obtained well in both argon and nitrogen matrices. Its most stable stereoisomer with (s-Z)-(E) configuration is formed. The stereochemistry of this compound is similar to that observed during formamide irradiation at 248 nm , which led to the formation of formimidic acid, its most stable form. The electronic state involved in this transformation of formamide is S_1 , of $n\text{-}\pi^*$ character, which is lower in energy than S_2 . For NMF, both the $n\text{-}\pi^*$ and the $\pi\text{-}\pi^*$ transition energy are similar to formamide^[210, 211, 215] N-methylformimidic acid should be formed following an intramolecular H-atom shift,

which probably involves a four centered transition state, as it was shown by ab initio calculation for the similar cases of formamide and acetamide.^[216, 217]



Scheme 6.1.4. Isomerisation partway between two isomers of NMF. Stationary points and transition state were calculated at the B3LYP/cc-pVTZ method.

The relative energy of **3a** calculated by B3LYP is 12.72 and 11.77 kcal/mol higher than the *trans*- of NMF and the *cis*- of NMF, respectively. This clearly indicates proton transfer from nitrogen atom occurring from the *cis*- form of NMF. According to B3LYP/cc-pVTZ level of theory, the transition state of this reaction is 46.18 kcal/mol above that of the *cis*- (ZPE by 42.83 kcal/mol). The transition state is found to be a planar (Scheme 6.1.4).



Scheme 6.1.5. Photochemistry of N-methylformamide upon irradiation at wavelength $\lambda=248$ nm.

6.1.2.4. Formation of $\text{H}_2\text{NCH}_3:\text{CO}$ and $\text{HNCO}:\text{CH}_4$ complexes

After 2 hours irradiation at 248 nm of NMF in argon and nitrogen matrices produced vibrational bands that are typical for methylamine (MA) and carbon monoxide (CO), which show the same kinetics during the irradiation process. Strong bands are observed at 2140.3, 2138.6, 2136.6, 2135.3, 2133.3, 2130.3 cm^{-1} . The band at 2138.6 cm^{-1} belongs to unperturbed CO (Figure 6.1.6).

Methylamine has been studied in argon and nitrogen matrices by Purnell.^[218] Multiple bands with a maximum at 796 cm^{-1} are assigned to the NH_2 wagging mode of methylamine. The bands at 1140 and 1052 cm^{-1} are assigned to the CH_3 rocking and the CN stretching mode of the MA monomer, respectively. Also, broad bands have been observed in the region 3000-2800 cm^{-1} , which are assigned to the asymmetric and symmetric stretching modes of the NH_2 group of MA. The complex between of MA and CO had not yet studied by matrix isolation infrared spectroscopy. Lundell et al.^[97] studied the photodecomposition of formamide in argon and xenon matrices at 193 nm, which leads to the formation of NH_3-CO and $\text{HNCO}-\text{H}_2$ products. In argon matrix NH_3-CO binary system is the major product. Two different complexes have been found under matrix isolation conditions, which attributed to hydrogen bonded the carbon- and oxygen-attached complexes (NH_3-CO and NH_3-OC), respectively.^[219]

The mechanism of the photodecomposition of NMF can be explained by a similar way as the photochemistry of formamide.^[97] In solid argon, the $n-\pi^*$ excitation leads to the first excited singlet state, where probably a hot $\text{HCO} - \text{HNCH}_3$ radical pair is formed. The HCO radical donates its hydrogen to the HNCH_3 radical forming H_2NCH_3 . However, no radicals are observed in our experiment which indicates that radicals rapidly react in the matrix cage.

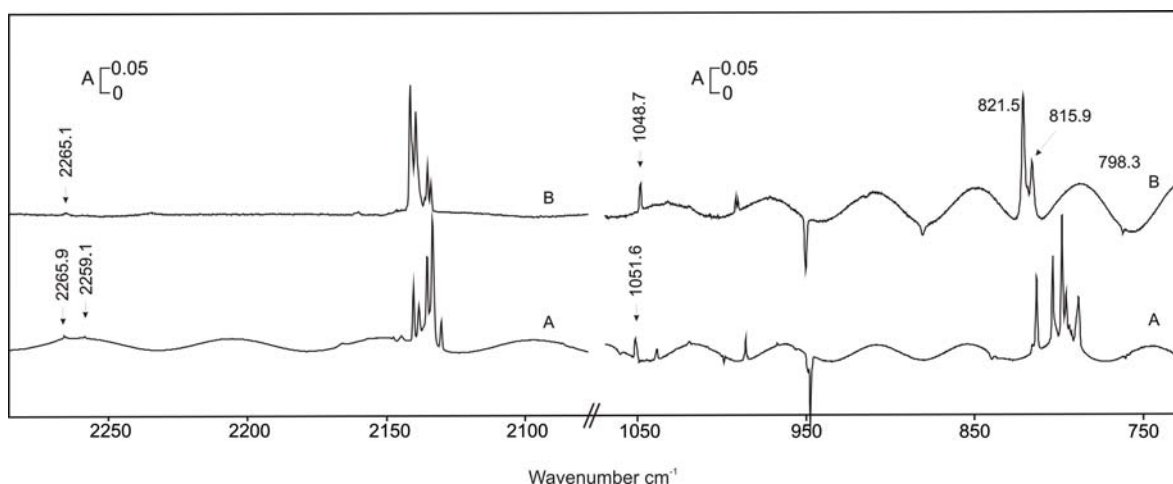


Figure 6.1.6. Difference FTIR spectra of NMF were recorded after 240 min of irradiation at 248 nm in argon matrix at 10 K (spectrum A), 270 min irradiation at 248 nm in nitrogen matrix at 10 K (spectrum B).

After irradiation of NMF new bands appear assigned to HNCO . Several studies reported the vibrational frequencies of HNCO in argon and neon matrices.^[220-222] According to those studies, the NCO asymmetric stretching mode (ν_2) at 2259.1 cm^{-1} is the strongest absorption in an argon matrix. This absorption can be observed in spite the low yield of HNCO in the matrix during the photodecomposition of NMF. During the formation of HNCO , also methane (CH_4) should be trapped in argon cage matrix with HNCO molecule. The peak at 2265.9 cm^{-1} which is due to the NCO asymmetric stretching mode is blue shifted from unperturbed molecule at 2259.1 cm^{-1} , indicates of the formation of the weakly interacted complex in the matrix cage.^[222] No previous data have been reported in the literature concerning noncovalent complexes between HNCO and CH_4 . However, the hydrogen bonded complex between HNCO and ammonia have been obtained by Raunier et al.^[223] Complex formation, the strong band at 2268 cm^{-1} and a weak band at 1330 cm^{-1} have been found that are due to the $\nu(\text{OCN})$ antisymmetric and symmetric stretching modes of HNCO , respectively. In our experiments a weak band at

1318.4 cm^{-1} was found in argon matrix during the photodecomposition and belongs to the symmetric stretching mode of the NCO group.

Many experimental and theoretical studies noncovalent complexes between $\text{CH}_4\text{-HX}$ (where $\text{X} = \text{Cl}, \text{F}, \text{CN}$) have been published.^[224-226] The antisymmetric vibration C–H stretch ν_2 mode of unperturbed methane appears at 3038 cm^{-1} , while the antisymmetric C–H bending mode ν_4 appears at 1305 cm^{-1} . Unfortunately, no peaks have been found that can be assigned to vibrational modes of methane.

6.1.3. Conclusion.

In summary, ultraviolet irradiation (wavelength $\lambda=248$ nm) of NMF in argon and nitrogen matrices at 10 K leads to the formation several primary photoproducts. According to B3LYP calculations the *cis*-NMF is less stable by 0.948 kcal/mol than the *trans*-NMF, was generated during irradiation from the *trans*- form of NMF. This *cis*- conformer is an intermediate in the ultraviolet photolysis, leading to intramolecular proton transfer from the amino group to the carbonyl oxygen atom in the formation of N-methylformimidic acid which is a tautomer of NMF. With the support of theoretical calculation we demonstrated that N-methylformimidic acid is isolated in argon and nitrogen matrices in its energetically most stable (s-*Z*)-(E) configuration. At the same time decompositions products such as $\text{H}_2\text{NCH}_3 - \text{CO}$ and $\text{HNCO} - \text{CH}_4$ have also been trapped in the matrix cage during the photolysis.

Chapter 6.2. NMF–Dimers: Aggregation and Photochemistry

6.2.1. Introduction

After detailed inspection of the matrix spectra of NMF in Figure 6.1.2, we observed that a few peaks can not be assigned to monomeric forms of NMF. They are mostly weak and appear near modes of both monomeric *trans*– and *cis*– forms of NMF. Those peaks are growing in intensity upon annealing which indicates the formation of oligomers of NMF in argon matrix. Due to this reason, we were tempted to investigate the structures of hydrogen-bonded complexes under matrix isolation conditions in the combination with the DFT method.

6.2.1.1. Computational Results

Here we focus on the dimers of NMF. There are four kinds of dimeric forms of NMF by combination of its *trans*– and *cis*– forms. We indicate them by the symbols **tt**, **tc**, **ct** and **cc**, where the letters **t** and **c** correspond to the isomeric forms of monomers, the *trans*– and *cis*– forms, respectively (Figures 6.2.1-6.2.3). For simplicity we define that the left part of the dimer acts as a hydrogen donor and the right side of the dimer acts as a hydrogen acceptor.

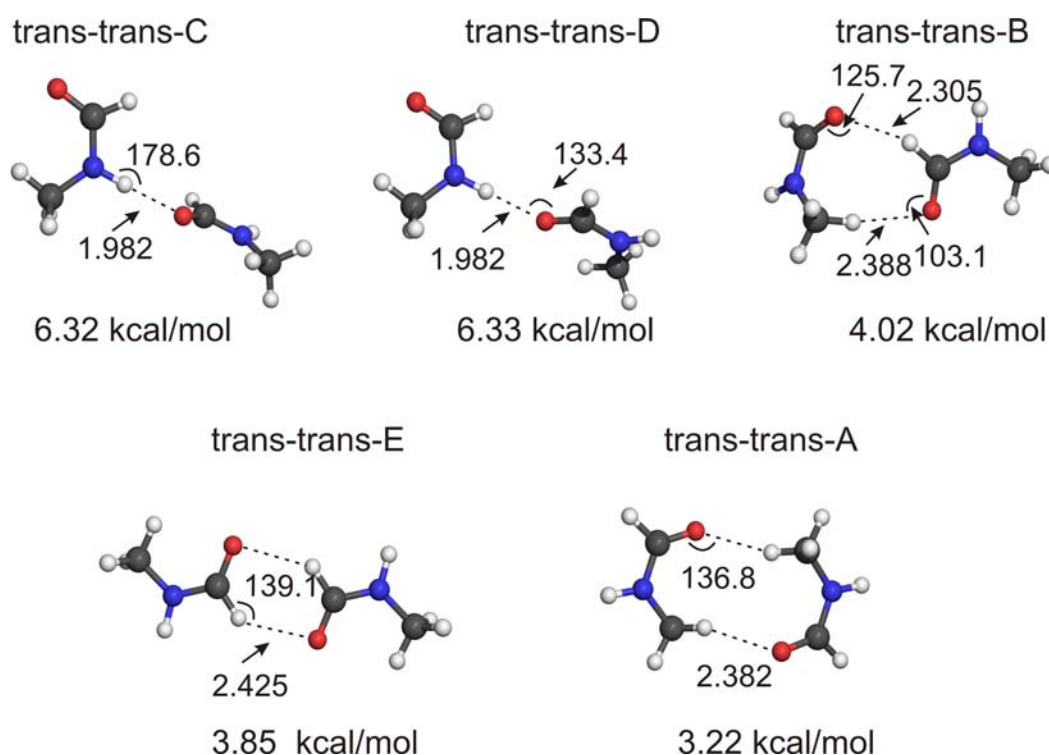


Figure 6.2.1. Calculated structures with hydrogen bonds lengths (Å°) of the *trans*–*trans* NMF dimers at the B3LYP/6-311++G(d,p) level of theory.

The structures of NMF dimers were calculated using DFT (B3LYP) method with 6-311++G(d,p) basis set. The stabilization energies were calculated by subtracting the energies of the monomers from those of the complexes and including zero-point energy (ZPE) corrections (Table 6.2.1). Five **t-t**, seven **t-c** and three **c-c** homo-dimers of NMF were localized at the B3LYP/6-311++G(d,p) level of theory.

Trans-trans- dimers. The most stable dimers **t-t-C** and **t-t-D** (both are -6.32 kcal/mol) show structural similarities because they are exclusively stabilized by the N-H...O interaction (Figure 6.2.11 and Table 6.2.1). The cyclic dimer **t-t-B** (-4.02 kcal/mol) is stabilized by the interactions $C^{met}H...O$ and $O...CH$, whereas the cyclic dimer **t-t-E** (-3.85 kcal/mol) is stabilized by the interaction $CH...O$. The least stable *trans-trans* dimer of NMF is the cyclic complex **t-t-A** (-3.22 kcal/mol), that is stabilized exclusively by the $C^{met}-H...O$ interaction.

Trans-cis- dimers. In the dimer **c-t-B** (-8.72 kcal/mol) (Figure 6.2.2), the main interaction is between the N-H hydrogen atom of the *cis*- NMF and the oxygen atom of the *trans*- conformer of NMF. Also, the structure **c-t-B** is stabilized by the interaction between the oxygen atom of the *cis*- conformer and the hydrogen atom of the C-H group of the *trans*- conformer.

The binding energy of dimer **t-c-A** is found to be -8.00 kcal/mol using B3LYP/6-311++G(d,p) level of theory. After ZPE correction the binding energy is reduced to -6.75 kcal/mol (Table 6.2.1). This dimer is stabilized by interaction between the oxygen atom of the C=O group of the *trans*- conformer and the hydrogen atom of the N-H group of the *cis*- conformer and the interaction between the hydrogen of the $C^{met}-H$ moiety of the *trans*- conformer and the oxygen atom of the C=O group of *cis*- conformer.

Dimers **t-c-D**, **t-c-D1** and **t-c-C** (-6.38, -6.37 kcal/mol) and (-6.24 kcal/mol) show interesting structural similarities with respect to the interaction of the hydrogen atom of the N-H group in the *trans*- with the oxygen atom of the C=O group in the *cis*- conformer. However, the dimer **t-c-C** is additionally stabilized by interaction of the hydrogen atom in the N-H group of the *cis*- with the nitrogen atom of the *trans*- conformer, whereas complexes **t-c-D** and **t-c-D1** show only a weak interaction (Figure 6.2.2).

Dimers **t-c-B** and **t-c-E** are weakly bonded complexes with binding energies -4.23 and -4.02 kcal/mol, respectively. After the ZPE correction the binding energies are reduced to -3.34 and -3.19 kcal/mol, respectively (Table 6.2.1). The dimers **t-c-B** and **t-c-E** have structural similarities with **t-t-B** and **t-t-E** dimers due to stabilization caused by similar interactions.

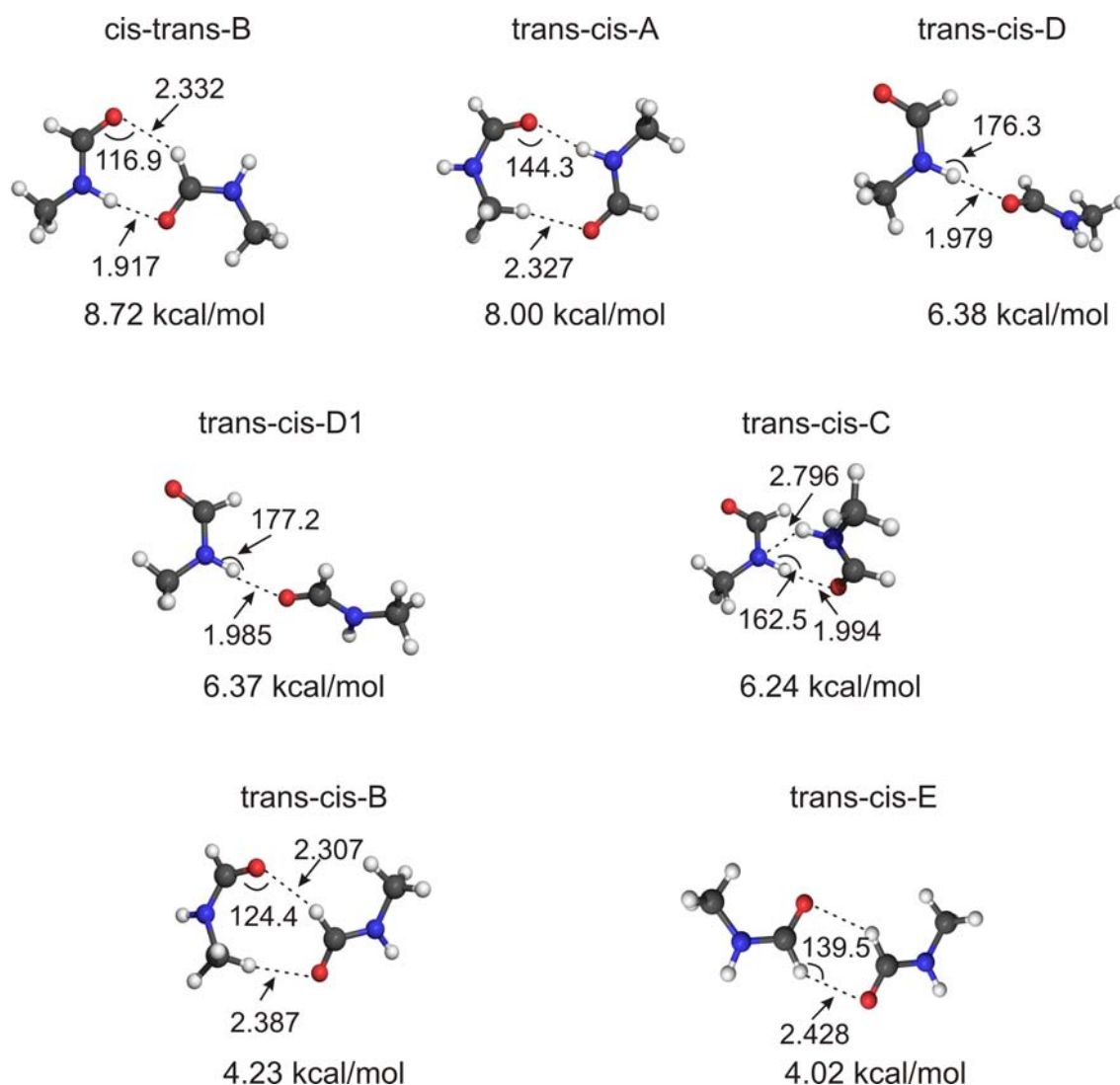


Figure 6.2.2. Calculated structures with hydrogen bonds lengths (Å) of the *trans-cis* NMF dimers at the B3LYP/6-311++G(d,p) level of theory.

***Cis-cis*– dimers.** Dimer **c-c-A** is the most stable one (stabilization energy –13.84 kcal/mol, ZPE corrected, Table 6.2.1) bearing a cyclic C_{2h} point group and the only structure that has been found as a global minimum. Dimer **c-c-A** is stabilized exclusively by the N–H...O interaction (Figure 6.2.3). The geometry of dimer **c-c-A** resembles the cyclic dimer of FMA which has been described in detail above.^[83]

The *cis*– form is expected to show a similar aggregation behavior as formamide,^[83] whereas the *trans*– form and also mixtures of the two isomers can only dimerize via a single but strong N–H...O=C interaction and relatively weak C–H...O interaction. The interesting twist is that the *trans*– form is more stable in the monomer, whereas the *cis*– form is expected to be more stable as dimer since it allows two strong hydrogen bonds.

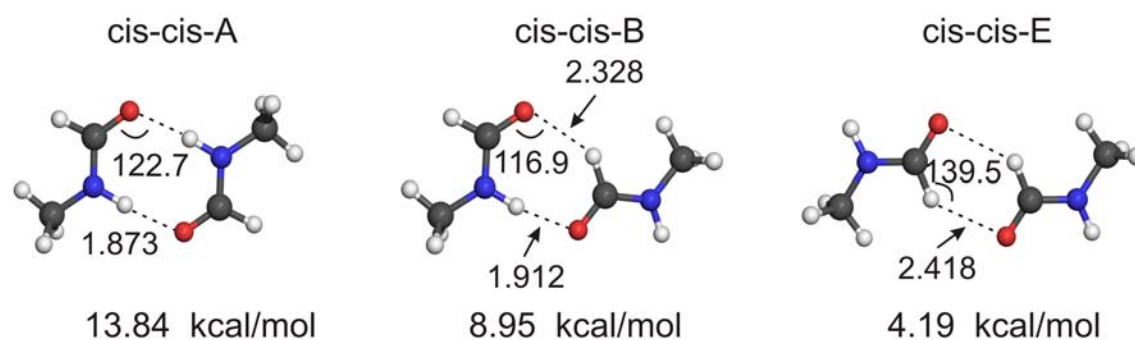


Figure 6.2.3. Calculated structures with hydrogen bonds lengths (Å) of the *cis-cis* NMF dimers at the B3LYP/6-311++G(d,p) level of theory.

Table 6.2.1. Calculated binding energies and ZPE corrections of the NMF dimers at the B3LYP/6-311++G(d,p) level of theory.

	B3LYP/6-311++G(d,p)	
	ΔE	ZPE
trans-trans-D	-6.32	-5.33
trans-trans-C	-6.32	-5.33
trans-trans-B	-4.02	-3.15
trans-trans-E	-3.85	-3.09
trans-trans-A	-3.22	-2.57
cis-trans-B	-8.72	-7.37
trans-cis-A	-8.00	-6.75
trans-cis-D	-6.38	-5.47
trans-cis-D1	-6.37	-5.44
trans-cis-C	-6.24	-5.15
trans-cis-B	-4.23	-3.34
trans-cis-E	-4.02	-3.19
cis-cis-A	-13.84	-12.13
cis-cis-B	-8.95	-7.58
cis-cis-E	-4.19	-3.33

Dimer **c-c-B** is stabilized by interactions between N-H...O and C-H...O of *cis*-NMF. The binding energy is -8.85 kcal/mol (B3LYP/6-311++G(d,p)), which is reduced after ZPE correction to -7.58 kcal/mol (Figure 6.2.3, Table 6.2.1). The comparison of the calculated binding energies shows that Dimer **c-c-B** is the second most stable complex of NMF dimers.

Finally, the cyclic dimer **c-c-E** is exclusively stabilized by interaction CH...O, and has a C_2 point group. The binding energy is -4.19 kcal/mol (B3LYP/6-311++G(d,p)), which is reduced after ZPE correction to -3.33 kcal/mol.

6.2.1.2. Matrix Isolation Experiments

We should also consider that even if the dimers of the *cis*- NMF would be more stable, they will not be produced by a rotation of the *trans*- isomer to the *cis*- isomers during the aggregation in the matrix. The amount of *cis*- NMF is very low, only 5%. For these reasons, we consider that mainly upon aggregation the *trans*- isomer of NMF produces dimers.

The IR spectra of the NMF monomer **M** and the NMF dimers generated under various conditions of deposition and annealing of matrices were compared with calculated spectra at the B3LYP/6-311++G(d,p) level of theory. The formation of dimers and other molecular aggregates results in characteristic shifts of some vibrations of **M**. These shifts can be used to identify the dimers by comparison of the experimental with calculated data. To facilitate this comparison the calculated frequencies were scaled with individual factors to achieve an exact match of calculated and experimental IR frequencies for the monomer **M** (**M**: Table 6.2.2, dimer **t-t-C**: Table 6.2.3, dimer **t-t-B**: Table 6.2.4, and **t-c-A**: Table 6.2.5).

Argon matrix. The IR spectrum of monomer **M**, matrix-isolated in argon at 10 K, agrees very well with the spectrum reported in literature.^[227] The aggregation of NMF in inert gas matrices was already studied by Shin et al.^[228] They reported IR absorptions of NMF aggregates in the region between 4000 and 400 cm^{-1} . It was concluded that upon diffusion-controlled aggregation of **M** several types of dimers were formed in the matrix with a predominant identification of *trans-trans* type dimers. They did not discriminate the particular dimer in their studies.

In our experiments the aggregation of **M** was achieved either by warming the matrix (argon) from 10 K to 40 K with a rate of approximately 1 K min^{-1} (free warm-up) or by annealing the matrix at a defined temperature between 20 and 40 K for up to 60 min. In free warm-up experiments the intensity of the carbonyl stretching vibration of **M** at 1725.4 starts to decrease at a temperature of 25 K, and simultaneously new bands at 1711.7, 1702.4 and 1688.9 cm^{-1} increase in intensity. At 25 K the band at 1711.1 and 1702.4 cm^{-1} gain intensity faster than the bands at 1688.9 cm^{-1} , indicating that two different species are

formed. By comparison with DFT calculations (B3LYP/6-311++G(d,p)) bands at 1711.7 and 1702.4 cm^{-1} are assigned to the carbonyl stretching mode of the dimer **t-t-C**, whereas the band at 1688.9 cm^{-1} is too broad and therefore an indication of existence of several species (Figures 6.2.4). Under both conditions – free warm-up and systematic annealing of the matrix – the dimer **t-t-C** is predominantly formed.

Table 6.2.2. Experimental and Calculated Vibrational Frequencies of the NMF monomers.

Mode	Monomers and Factor of Corections						Assignment
	<i>trans</i> –			<i>cis</i> –			
	M calc.	M exp.	Factor of Correction	M calc.	M exp.	Factor of Correction	
4	543.5	535.5	0.985	617.0	602.1	0.975	N–H wag.
6	950.0	947.7	0.997	1007.2	1000.9	0.993	C ^m –N str
10	1216.3	1205.5	0.991	1299.4	1292.9	0.994	C–N str
16	1770.0	1725.4	0.974	1777.6	1730.6	0.973	C=O str.
21	3628.5	3493.7	0.962	3596.3	3456.4	0.961	N–H str.

As mentioned above, the C=O stretching modes (1711.7 and 1702.4 cm^{-1}) observed in argon at 10 K are in good agreement with the theoretical predictions (after scaling) for the dimer **t-t-C** at 1713.6 and 1699.5 cm^{-1} , respectively. The band at 1688.9 cm^{-1} is red-shifted from the *trans*–**M** by 36.5 cm^{-1} and red-shifted from the *cis*–**M** by 41.7 cm^{-1} . The second energetically most stable *trans*–*trans* dimer is **t-t-B** for which the C=O stretching mode is predicted to have one small (–10.7 cm^{-1}) and one large (–37.0 cm^{-1}) red shifts (Table 6.2.4). Those predictions are in good agreement with the experimentally observed frequencies.

We have to consider that the *cis*– conformer also aggregates during annealing. The predicted frequencies of the carbonyl stretching mode of the **t-c-A** are 1716.7 (*cis*) and 1693.6 cm^{-1} (*trans*). The broad band at 1688.9 cm^{-1} can be attributed to the **t-t-B** and **t-c-A** dimers.

In the 1350–1200 cm^{-1} region the C–N stretching mode of monomers **M** are found at 1292.9 (*cis*–) and 1205.5 cm^{-1} (*trans*–). On warming the matrix, these bands decrease and simultaneously new bands at 1320.2, 1227.5 and 1219.2 cm^{-1} increase in intensity. The bands at 1227.5 and 1219.2 cm^{-1} are assigned to the ν_{10} vibrational modes of the dimer **t-t-C**,

which are blue shifted from the unperturbed molecule by 22 and 13.7 cm^{-1} . The calculated frequencies at 1241.4 and 1220.8 cm^{-1} are in a reasonable agreement with the experimental frequencies (Table 6.2.3). The band found at 1320.2 cm^{-1} is in good agreement with the calculated frequency of 1330.8 cm^{-1} predicted for the dimer **t-c-A**. For the dimer **t-t-B** the corresponding vibrations are predicted to be at 1223.1 and 1208.6 cm^{-1} (B3LYP/6-311++G(d,p)), respectively (Table 6.2.4). The band at 1209.2 is attributed to the **t-t-B** dimer.

Table 6.2.3. Experimental and Calculated Vibrational Frequencies and Shifts (in cm^{-1}) of the NMF Dimer **t-t-C**.

Experimental		B3LYP/6-311++G(d,p)				Rel. Int.	Assignment
Argon		unscaled		scaled			
952.9	+5.4	952.9	+2.9	950.0	+2.8	1	C ^m –N str
956.3	+8.8	962.4	+12.4	959.5	+12.3	1	
1219.2	+13.7	1231.9	+15.6	1220.8	+15.4	7	C–N str.
1227.5	+22	1252.7	+36.4	1241.4	+36.0	8	
1702.4	–23	1744.9	–25.1	1699.5	–24.4	99	C=O str
1711.7	–13.7	1759.4	–10.6	1713.6	–10.3	15	
3411.6	–82	3497.7	–130.8	3364.7	–125.8	63	N–H str.
3477.9	–15.8	3625.9	–2.6	3488.1	–2.5	3	

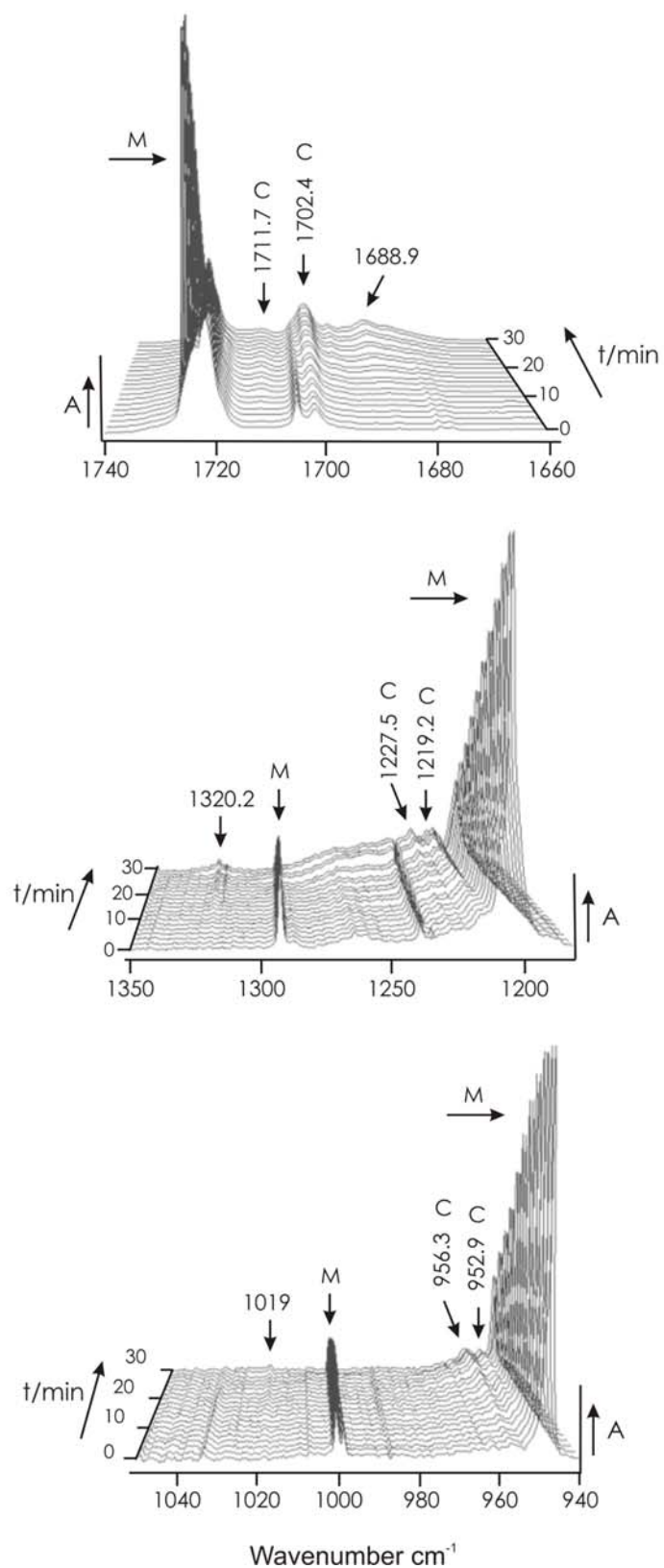


Figure 6.2.4. IR spectra of argon matrix containing NMF during slow warming from 10 K ($t=0$ min) to 40 K ($t=30$ min). Bands are assigned to monomeric NMF **M**, **t-t-C** (C).

The C^{meth}–N vibration modes of NMF monomers are found at 1000.9 and 947.7 cm⁻¹, respectively (Table 6.2.2). Annealing of an argon matrix containing mainly **M** from 10 K to 40 K results in the formation of new bands at 956.3 and 952.9 cm⁻¹ showing identical kinetic behavior are assigned to the dimer **t-t-C**. These assignments were confirmed by comparison with the spectra obtained in argon and with results from theoretical calculations (Table 6.2.3). For dimer **t-t-C** the corresponding vibrations are predicted to be at 959.5 and 950.0 cm⁻¹, respectively. The weak band at 1019.0 cm⁻¹ can be assigned to the ν_6 mode of the dimer **t-c-A**, which is blue shifted from the unperturbed molecule by 18.1 cm⁻¹. The band at 1019.0 cm⁻¹ is in an excellent agreement with the prediction from DFT calculations (1019.9 cm⁻¹). The calculation also predicts a small red shift for the ν_6 mode of the *trans*- conformer in the **t-c-A** dimer. The predicted value (B3LYP/6-311++G(d,p)) is 941.4 cm⁻¹. After annealing the matrix, formation of a small amount of the **t-c-A** dimer is observed, due to a band as a shoulder at 946.6 cm⁻¹.

Table 6.2.4. Experimental and Calculated Vibrational Frequencies and Shifts (in cm⁻¹) of the NMF Dimer **t-t-B**.

Experimental		B3LYP/6-311++G(d,p)				Rel. Int.	Assignment
Argon		unscaled		scaled			
946.6	−1.7	948.3	−1.7	945.4	−1.6	2	C ^m –N str
951.5	+3.8	953.7	+3.7	950.8	+3.6	4	
1209.2	+3.7	1219.6	+3.3	1208.6	+3.2	14	C–N str.
		1234.3	+18	1223.1	+17.8	5	
1688.9	−36.5	1732.0	−38	1686.9	−37.0	8	C=O str
		1759.0	−11	1713.2	−10.7	99	
		3629.2	+0.7	3491.2	+0.6	4	N–H str.
		3637.5	+9.0	3499.2	+8.6	4	

[a] Vibrational modes of the *cis*- conformer of NMF.

Annealing of the matrix containing **M** leads to the appearance new bands in the NH stretching region (Figure 6.2.5, Tables 6.3.3 – 6.3.5). Annealing results in a decrease of $\nu(\text{NH})$ of **M** at 3493.7 cm⁻¹ and formation of intense peaks at 3486.2, 3483.7, 3477.9 and 3411.8 cm⁻¹ and less intense bands at 3460.5, 3397.4, 3387.8 and 3329.9 cm⁻¹ those are in agreement with the results of Shin et al.^[228] The bands at 3477.9 and 3411.6 cm⁻¹ are

assigned to $\nu(\text{NH})$ mode of **t-t-C** dimer, which is red shifted from the unperturbed molecule by 15.8 and 82.0 cm^{-1} show the same kinetic behavior upon annealing.

DFT calculations for the NH stretching mode for **t-t-A**, **t-t-B** and **t-t-E** dimers predict only a blue shift due to complexation. The predicted frequencies of dimer **t-t-B** are 3499.2 and 3491.2 cm^{-1} , respectively (Table 6.2.4).

Table 6.2.5. Experimental and calculated vibrational frequencies and Shifts (in cm^{-1}) of the NMF Dimer **t-c-A**.

Experimental		B3LYP/6-311++G(d,p)				Rel. Int.	Assignment
Argon		unscaled		scaled			
946.6	−1.7	944.3	−5.7	941.4	−5.6	1	C ^m –N str
1019.0	+18.1	1027.1 ^a	+19.9	1019.9	+19.7	3	
		1239.8	+23.5	1228.6	+23.2	4	C–N str.
1320.2	+27.3	1338.8 ^a	+39.4	1330.7	+39.1	12	
1688.9	−36.5	1738.9	−31.1	1693.6	−30.2	12	C=O str
		1767.4 ^a	−13.2	1716.7	−12.8	100	
		3442.4 ^a	−153.9	3308.1	−147.8	55	N–H str.
		3627.8	−0.7	3489.9	−0.6	3	

[a] Vibrational modes of *cis*- conformer of NMF.

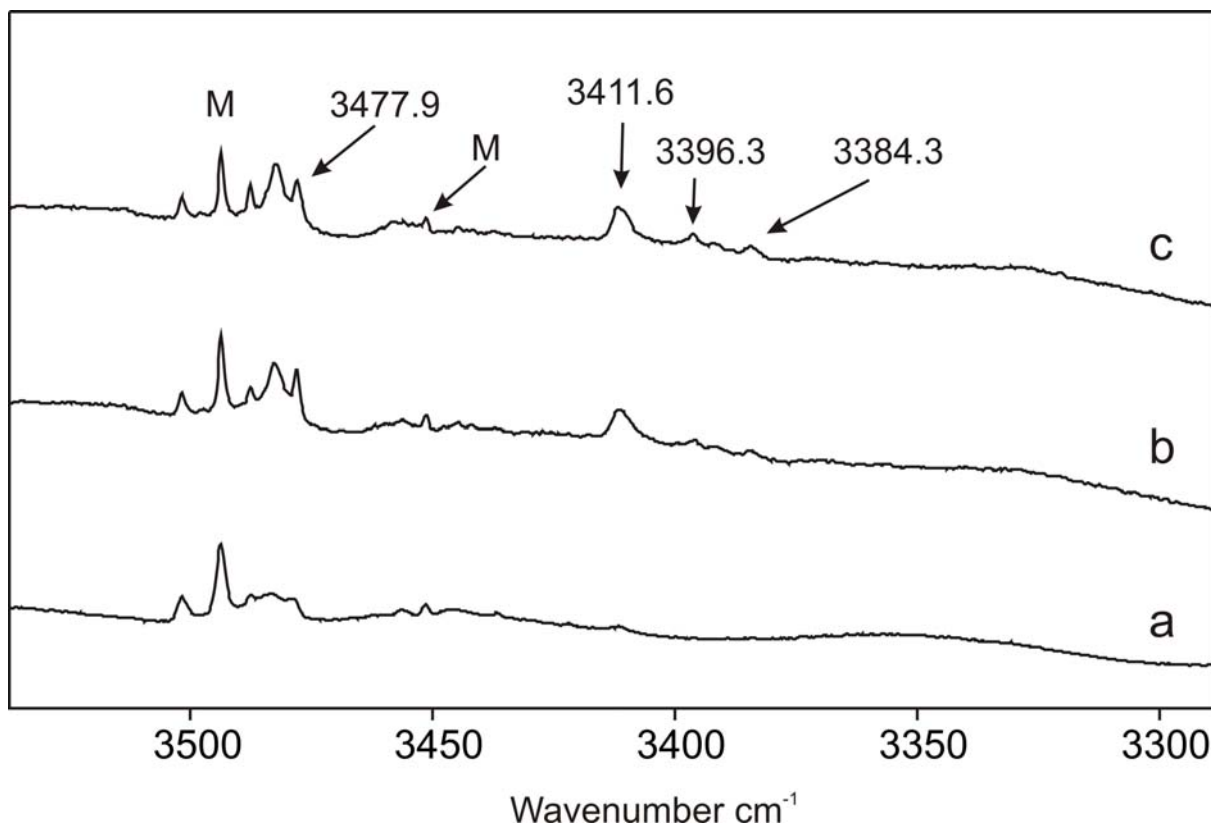


Figure 6.2.5. IR spectra in the range $3600 - 3300 \text{ cm}^{-1}$ of NMF, matrix-isolated in argon. (a) NMF:Ar ratio 1:1500, 10 K. (b) after annealing at 30 K. (c) after annealing at 35 K. Vibrational modes assigned to NMF **t-t-C** dimer.

6.2.1.3. Conclusion

In summary we have investigated the aggregation of the NMF in argon matrix in combination with DFT calculations that provide fruitful information to differentiate various dimers at low temperature conditions. After careful analyses of infrared spectra we are able to identify only one dimer (**t-t-C**). However, some weak bands that appear in the whole spectral region can be assigned to the *trans-cis-* types of dimers in argon matrix. The possibilities of finding the *cis-cis* type of dimers will be quite low in contrast to their large thermodynamic stability. These findings can be explained by the consideration that the population of the *cis-* conformer of the NMF is very low. Even if the dimers of the *cis-* NMF would be more stable, they will not be produced by rotation of the *trans-* to the *cis-* isomers during the aggregation at low temperature conditions. Therefore, upon annealing the *trans-* isomer of NMF mainly produces dimers.

6.2.1.3. *Trans–Cis* Photoisomerization in dimer of NMF.

Molecular conformation and molecular charge distribution play a crucial role in the selectivity and function of biologically active molecules. Peptide bonds in general prefer a *trans*– conformation by about 2.5 kcal/mol over the *cis*– isomeric form. As amino acids are polymerized into a polypeptide chain the more stable *trans*– peptide bond is formed. However, during the subsequent folding process the biologically active folded protein may require a *cis*– peptide bond in certain positions. As long as the forces that govern protein folding and stability are not completely understood there can be no exact explanation for this observation.

We showed that NMF can be found in two conformeric forms in agreement with results from previous studies,^[227, 228] where the less stable *cis*– form can be generated in high yields by irradiation of the *trans*– form of NMF. Computations predict that dimers of the *cis*– NMF are thermodynamically more stable in contrast to the *trans*– NMF.

The NMF dimers have been investigated theoretically and experimentally,^[98] experiments show that predominantly a *trans–trans*– type of dimers form. Here we present the first complex of the higher energy conformer (*cis*–) with the *trans*– conformer in solid argon. The *cis–trans*– heterodimer was generated by UV irradiation of a *trans–trans*– homodimer in argon matrix at low temperatures. In sharp contrast to both of *cis*– and *trans*– monomers, which undergo photodecomposition after prolonged irradiation at $\lambda=248$ nm (to methylamine and carbon monoxide), no decay of dimer is observed at low temperatures. This is most probably due to a strong N–H...O=C hydrogen bonding that can terminate photodissociation of NMF in dimers

Two types of experiments were performed: (i) NMF was sublimed from a sample kept at -50°C and deposited with a large excess of argon at a temperature of 15 – 30 K. Under these conditions, the monomer **M** was found almost exclusively by IR spectroscopy. (ii) If the NMF was sublimed at -20°C , where its vapor pressure is considerably higher, the monomer **M** and additional bands assigned to the **t-t-C** dimer were found (Figure 6.2.6 black curve). The presence of the **t-t-C** is evident from the C=O stretching absorptions at 1711.7 and 1702.4 cm^{-1} and other characteristic absorptions in the IR spectra. The complex formation induces shifts from the unperturbed molecule that are in good agreement with the theoretical data (Table 6.2.3).

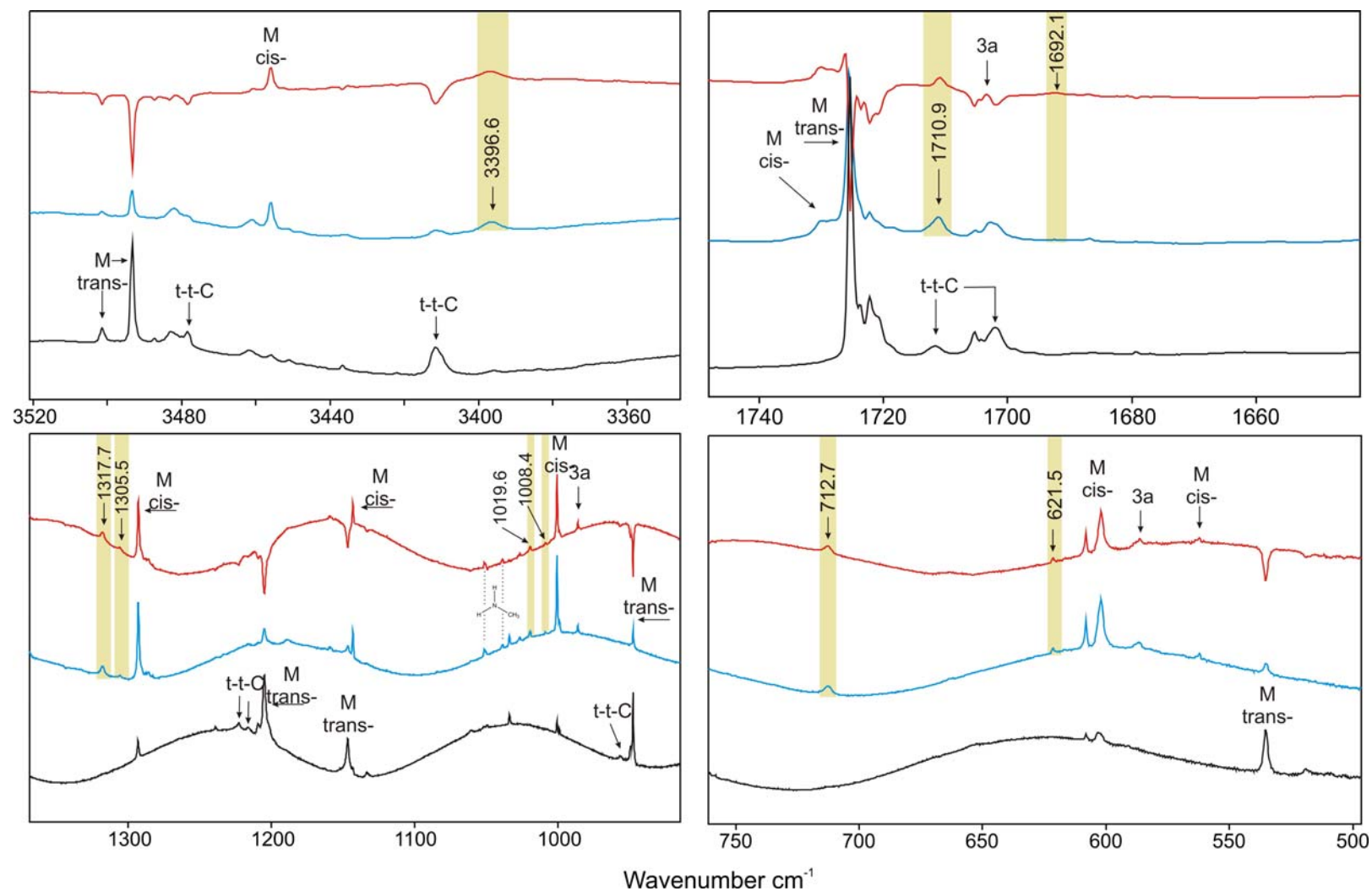


Figure 6.2.6 Matrix-isolated spectra of the NMF in argon 10 K, $T(\text{nmf}) = -20^\circ\text{C}$ (black curve); Matrix isolated spectra of the NMF in argon matrix at 10 K after 30 min of irradiation at 248 nm (blue curve); Difference FTIR spectra of the NMF in argon matrix at 10 K after 30 min of irradiation at 248 nm (red curve).

This dimer has also been observed in the gas phase.^[229-231] The other strong bands belong to the *trans*- monomeric form of NMF.

Figure 6.2.6 (curve b) shows that UV irradiation ($\lambda = 248$ nm) resulted in the bleaching both of the *trans*- monomer and the **t-t-C** dimer and promotes a number of new absorptions that have not been described previously, particularly, well defined bands at 3396.6, 1710.9, 1317.7, 1008.4, 712.7 and 621.5 cm^{-1} . Some of those bands appear near unperturbed vibrational modes of the *cis*- conformer on NMF, indicating the participation of the *cis*- NMF in complexation. These bands appear only in the presence of the **t-t-C** dimer in argon matrix and are assigned to the structure **t-c-D** (Figure 6.2.2). We have compared experimentally observed frequencies with all possible computed frequencies of NMF dimers. The **t-c-D** dimer is not the lowest energy dimer of NMF, however the experimentally observed frequencies and frequency shifts are in good agreement with the calculated frequencies (Table 6.2.6). This makes clear that the **t-t-C** \rightarrow **t-c-D** isomerization needs only the *trans*- to *cis*- conformational change in the dimer, while a more extensive changing of the system (for example **t-c-D** \rightarrow **t-c-A**) at 10 K is unlikely, especially taking into account the solid argon surrounding (Scheme 6.1.6).

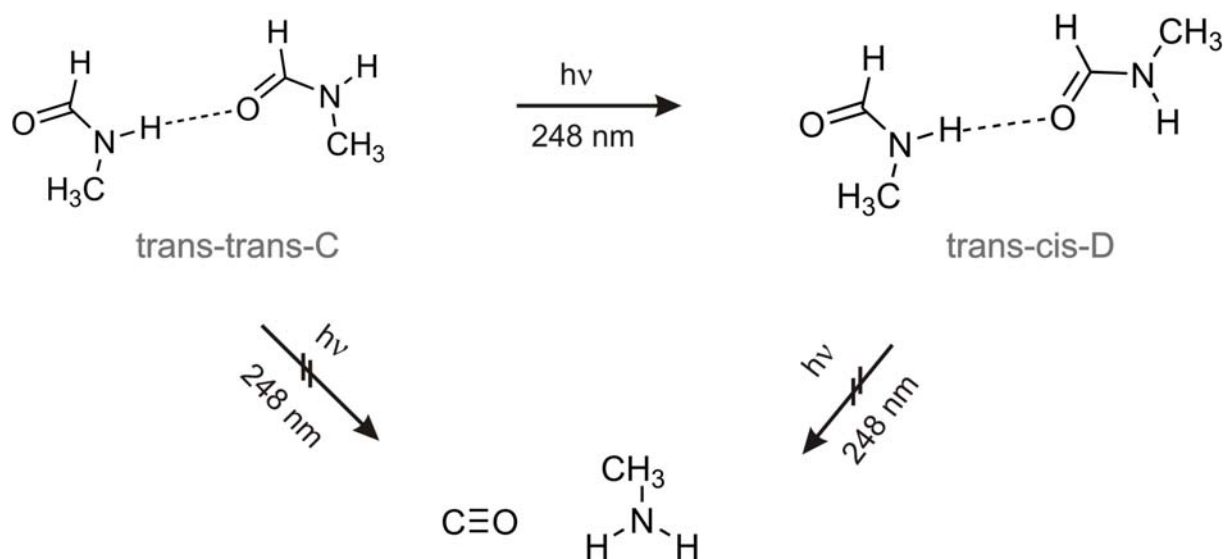
Table 6.2.6. Experimental and Calculated Vibrational Frequencies and Shifts (cm^{-1}) of the NMF Dimer **t-c-D**.

Experimental		B3LYP/6-311++G(d,p)				Rel. Int.	Assignment
Argon		unscaled		scaled			
621.5	+19.4	646.7 ^a	+29.7	630.5	+28.9	12	N-H wag.
712.7	+177.2	712.5	+169.0	701.8	+166.4	7	
967.1	+19.4	966.8	+16.8	963.8	+16.7	1	C ^m -N str
1008.4	+7.5	1011.2 ^a	+4.0	1004.1	+3.9	4	
		1257.8	+41.5	1246.4	+41.1	7	C-N str.
1317.7	+24.8	1320.4 ^a	+21.0	1312.4	+20.8	14	
1692.1	-33.3	1749.8	-20.2	1704.3	-19.6	99	C=O str
1710.9	-19.7	1763.6 ^a	-14.0	1745.1	-13.6	27	
3396.6	-97.1	3497.9	-130.6	3364.9	-125.6	62	N-H str.
		3590.8 ^a	-5.8	3450.7	-5.5	3	

[a] Vibrational modes of the *cis*- conformer of NMF.

Most notably, the **t-c-D** dimer is found to be very stable upon irradiation at $\lambda = 248$ nm, and it does not undergo decomposition to CO and methylamine. The stability of this complex under UV irradiation is very long. It undergoes no photochemistry even after

prolonged irradiation. The stabilization effect can be due to the strong N–H...O hydrogen bonding between *trans*– and *cis*– conformers of NMF.



Scheme 6.1.6. The mechanism of photochemistry of NMF dimer during ultraviolet irradiation at wavelength $\lambda=248$ nm

Chapter 6.3. NMF – Methanol

6.3.1. Introduction

The knowledge of the structure and internal dynamics of weakly bound complexes provides an insight into the molecular interactions in bioorganic and organic systems.^[173, 175, 186, 189, 190, 228, 232, 233] N-methylformamide (NMF) is the simplest molecule containing the N–C=O group, which is very important in peptide chemistry. The structure and spectroscopic properties of NMF have been intensively investigated.^[234-236]

To the best of our knowledge, the hydrogen-bonded complexes between NMF and methanol have not been studied before. The hydrogen bonding interactions of carbonyl compounds have been extensively studied using quantum chemical calculations^[59, 237-239] and matrix isolation infrared spectroscopy.^[234] Matrix isolation techniques in combination with *ab initio* computations provide useful information about the structure of the complexes and the strength of the molecular interactions in hydrogen bonded systems. Many complexes of carbonyl compounds adopt cyclic geometries in their most stable form,^[240-244] and molecules like the NMF are simple systems for investigating intermolecular forces and solvent effects in molecular scale. There are a number of matrix isolation studies on the molecular complexes between methanol and trifluoroacetic acid (TFA), water, acetone, dimethyl ether, acetonitrile, and pyridine.^[243, 244] In most of these complexes the methanol molecule acts as a proton donor.^[173, 175]

In this chapter we reported the complexes between NMF and methanol using matrix isolation techniques and *ab initio* calculations. The geometries and molecular interactions of the calculated dimers are discussed. The assignment of the complexes is achieved by comparison of the experimental and calculated IR frequencies.

6.3.2. Results and discussion

6.3.2.1. Computational results (by Elsa Sanchez-Garcia)

Four NMF – MeOH minima were found at the MP2/TZ2P level of theory. They show the following interactions (Figure 6.3.1):

(1) The O–H...O=C interaction between the hydroxyl hydrogen atom of methanol and the carbonyl oxygen atom of the N-methylformamide.

(2) The H–O...H(CH₃) interaction between the hydroxyl oxygen atom of methanol and one hydrogen atom of the methyl group in the N-methylformamide.

(3) The H–O...H(CO) interaction between the hydroxyl oxygen atom of methanol and the carbonyl hydrogen atom of the N-methylformamide.

(4) The H–O...HN interaction between the hydroxyl oxygen atom of methanol and the hydrogen atom linked to the nitrogen in the N-methylformamide.

(5) The C–H...O=C interaction between one hydrogen atom of the methyl group in the methanol molecule and the carbonyl oxygen atom of the N-methylformamide.

The most stable dimer is **A** with -5.45 kcal/mol binding energy (MP2/TZ2P + BSSE + ZPE). Dimer **B** is about half kcal/mol less stable (-4.92 kcal/mol). Both are cyclic complexes mainly stabilized by interaction (1) at 1.866 Å in dimer **A** and 1.868 Å in **B**. Both show also an additional weak H–O...H interaction. The difference is that in dimer **A**, the interacting hydrogen atoms belong to the methyl group of the NMF (interaction (2) at 2.738 Å), while in **B**, the interaction is via the carbonyl hydrogen atom (interaction (3) at 2.788 Å). (Table 6.3.1)

Due to the geometry of dimer **A** (C_s symmetry), the H–O...H interaction involves two of the hydrogen atoms of the NMF methyl group, which are both located at the same distance from the hydroxyl oxygen atom of methanol. This means an additional stabilization of complex **A** in comparison to **B** and shows the important role of weak interactions in defining the shape and stability of the complex.

C is an interesting complex (-4.41 kcal/mol), which is only stabilized by interaction (4) between the N–H hydrogen atom of NMF and the hydroxyl oxygen atom of methanol at 1.934 Å. In the less stable dimer **D** (-2.23 kcal/mol), the methyl group of the NMF does not play any role in the complexation. **D** shows a cyclic structure with interaction (3) at 2.356 Å and the interaction (5) at 2.446 Å between one hydrogen atom of the methyl group of methanol and the carbonyl oxygen of NMF.

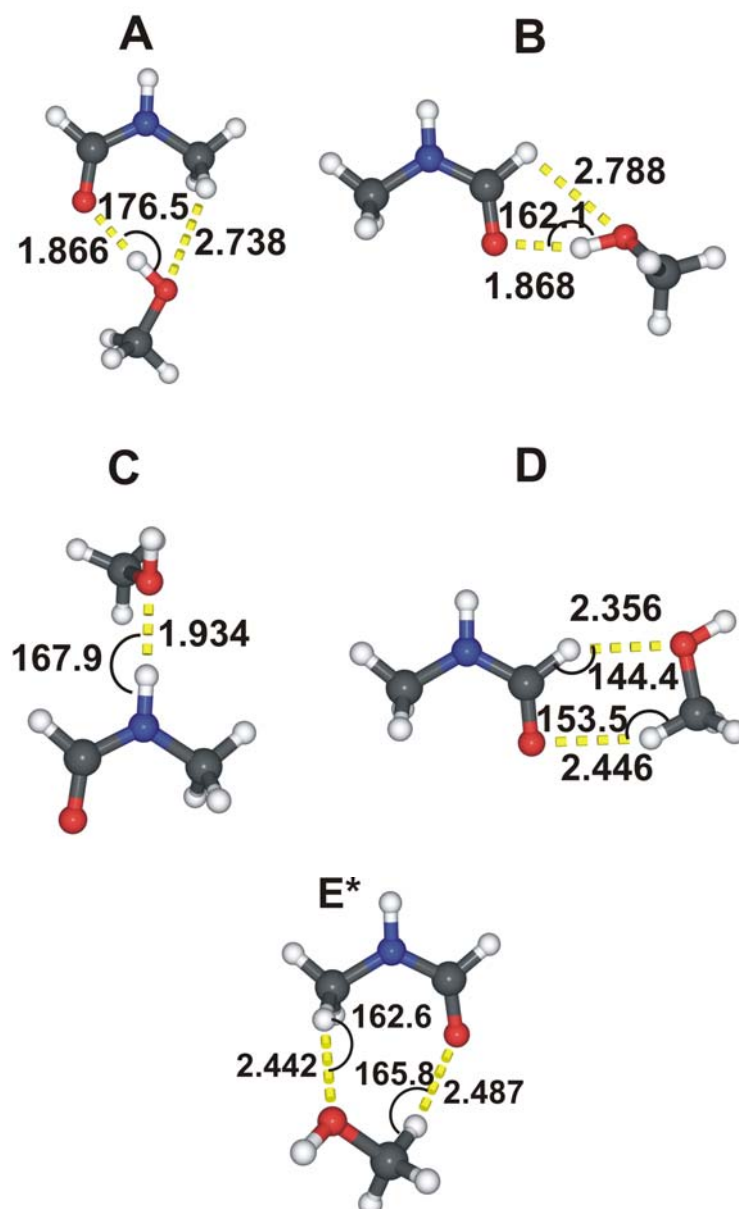


Figure 6.3.1. Trans-NMF – MeOH dimers **A** to **D** at the MP2/TZ2P level of theory. *E at the B3LYP/6-311++G(2d,2p)

An additional complex is found at the B3LYP/6-311++G(2d,2p) level of theory. Dimer **E** is a very weak interacting complex stabilized by interactions (2) and (5) at 2.442 and 2.487 Å, respectively. (B3LYP/6-311++G(2d,2p)) (Table 6.3.1, Figure 6.3.1)

At the MP2/TZ2P level of theory, the *trans*- NMF monomer is found in all complexes **A** – **D** in the staggered conformation, unlike at the B3LYP/6-311++G(2d,2p) level, where only **C** shows the staggered NMF. At the B3LYP/6-311++G(2d,2p) level, the NMF monomer adopts the eclipsed geometry in dimers **B** and **D** and a half-staggered conformation in complexes **A** and **E**. Therefore, in the B3LYP calculated structure of **A**,

the H-O...H interaction takes place with only one hydrogen atom of the methyl group, since the second is at more than 3 Å distance from the oxygen atom. In dimer **B**, the H-O...H(CO) interaction is also at more than 3 Å at the B3LYP/6-311++G(2d,2p) level of theory.

Table 6.3.1. Energies in kcal/mol of the NMF – MeOH dimers at the B3LYP/6-311++G(2d,2p) and MP2/TZ2P levels of theory.

	B3LYP/6-311++G(2d,2p)				MP2/TZ2P			
	ΔE	CP	ZPE	$\Delta E_{(CP+ZPE)}$	ΔE	CP	ZPE	$\Delta E_{(CP+ZPE)}$
A	-6.40	0.33	1.36	-4.72	-8.23	1.31	1.47	-5.45
B	-6.25	0.29	1.29	-4.67	-7.55	1.24	1.39	-4.92
C	-4.80	0.28	0.89	-3.63	-6.57	1.12	1.04	-4.41
D	-2.29	0.16	0.69	-1.44	-3.76	0.75	0.78	-2.23
E	-2.11	0.18	0.73	-1.20			-	

6.3.2.2. Experimental results

The infrared spectra of N-methylformamide isolated in nitrogen and argon matrices have been extensively investigated.^[245, 246] Several studies of methanol in argon and nitrogen matrices have also been reported.^[173, 175, 245, 246] The vibrational modes corresponding to the O–H and C–O stretching of methanol and the N–H, C=O and C–N stretching of NMF are used to identify the complex formation.

The infrared spectra of NMF and methanol were initially recorded independently, by premixing them in argon at matrix to sample ratios (M/A), ranging from 250 to 1000. At low matrix to sample ratios, absorptions due to aggregates of methanol and NMF are observed. All new spectroscopic features are closely associated with the fundamentals of either N-methylformamide or methanol. The reference spectra of the matrix-isolated NMF and methanol are in good agreement with the spectra reported in literature.^[247] New absorptions arising from the formation of NMF – MeOH complexes are shown in Figures 6.3.2–6.3.6.

Figure 6.3.2 shows the O–H stretching region of methanol and the N–H stretching region of NMF in different set of experiments. Details of the concentrations of individual spectra are described in the figure captions. A series of experiments were carried out by varying the concentrations of NMF and methanol. As seen in curves a and e, in addition to the monomer band at 3667.1 cm^{-1} , four other prominent bands at 3540.8 , 3533.1 , 3526.7 and 3518.3 cm^{-1} due to open chain methanol dimers are identifiable with all concentrations of methanol, even after deposition at 10 K .^[173] The observed fundamental absorptions of the isolated monomeric species of methanol and NMF are collectively summarized in Table 6.3.2, respectively, along with their spectral assignments. (Table 6.3.2)

When methanol was codeposited with NMF, new bands at 3536.3 and 3487.6 cm^{-1} appeared (Figure 6.3.2 curve b), which are 129.4 and 178.1 cm^{-1} red-shifted from the unperturbed O–H stretching vibration at 3665.7 cm^{-1} . When concentration of NMF was increased and annealing at 35 K for several minutes, the intensity of those peaks start to increase. The shifts and broadening were not observed when a matrix contained only methanol (Figure 6.3.2 e, f). That indicates that bands at 3536.3 cm^{-1} and 3487.6 due to NMF – MeOH complexes. The intensities of these absorptions depend on the concentrations of NMF and MeOH, are assigned to a 1:1 complexes.

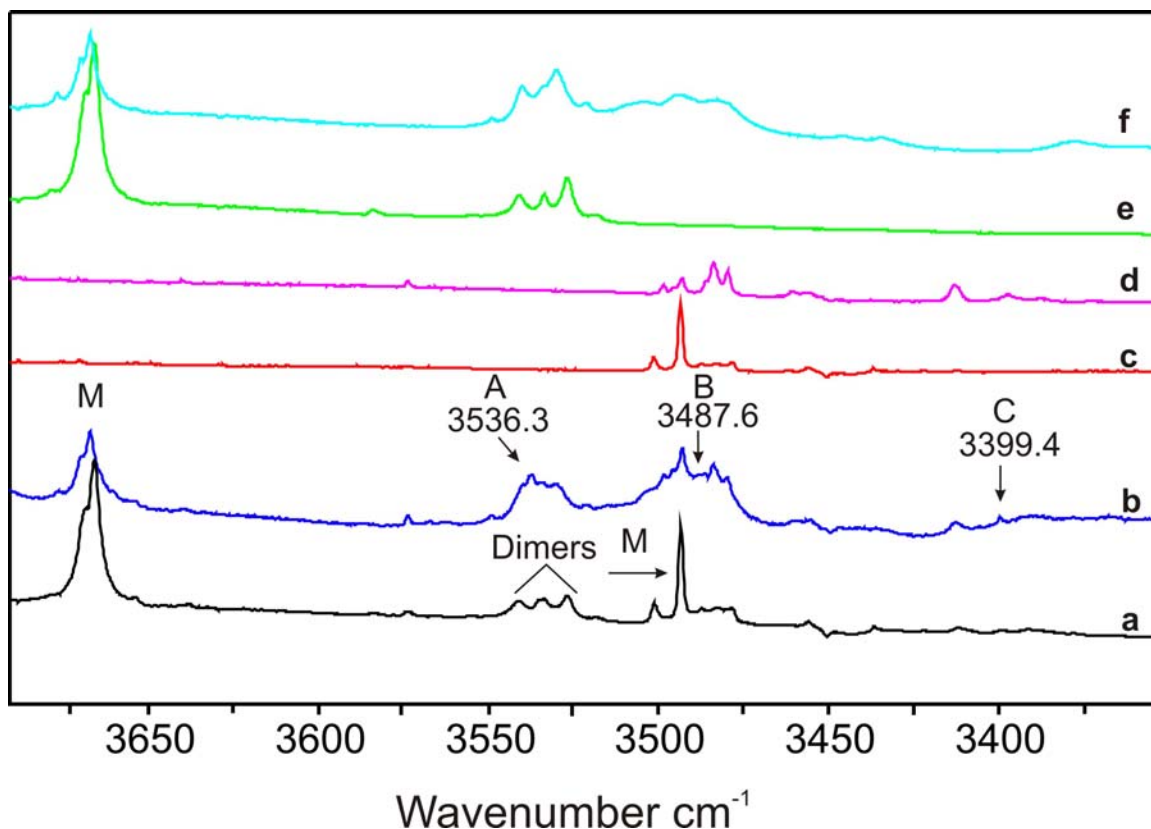


Figure 6.3.2. IR spectra in the range 3700 – 3300 cm^{-1} of NMF/MeOH mixtures, matrix-isolated in argon: (a) NMF:MeOH:Ar ratio 1:3:800, 10 K; (b) NMF:MeOH:Ar ratio 1:3:800, after annealing at 35 K; (c) NMF:Ar ratio 1:800, 10 K. (d) NMF:Ar ratio 1:800 after annealing at 35 K, (e) MeOH:Ar ratio 3:800, 10K, (f) MeOH:Ar ratio 3:800 after annealing at 35K. Vibrational modes were assigned to NMF/MeOH complexes, respectively

The N–H stretching region a new band at 3399.4 cm^{-1} is observed, which is red-shifted by 94.3 cm^{-1} from the unperturbed N–H mode of NMF at 3493.7 cm^{-1} (Figure 6.3.2).^[245] Increasing the methanol concentration and annealing the matrix at 35 K for several minutes, the band at 3399.4 cm^{-1} increases in intensity. This new absorption can be associated with the perturbation of the N–H stretching vibration of NMF in the complex.

Figure 6.3.3 (a-d) shows the IR spectra in the C=O stretching region for NMF/Ar, MeOH/Ar and NMF/MeOH/Ar mixtures after deposition at 10K in different set of experiments. The weak bands at 1711.7 and 1702.4 cm^{-1} are due to NMF dimers. These characteristic dimer absorptions were observed even at high dilution of NMF. On codepositing NMF, methanol, and argon in different molar ratios new bands appear at 1697.5 (sharp) and 1684.0 cm^{-1} (broad) (Figure 6.3.3 curve b). On increasing methanol concentration and after annealing the matrix at 35 K, these bands gain in intensity,

revealing that these spectral features are due to NMF – MeOH complexes, and hence they are attributed to a perturbed C=O stretching mode of a 1:1 complexes of NMF and methanol. Upon annealing the peak at 1697.5 cm^{-1} gains intensity faster than the peak at 1684.0 cm^{-1} , indicating that two different species are formed (Figure 6.3.3 curve b).

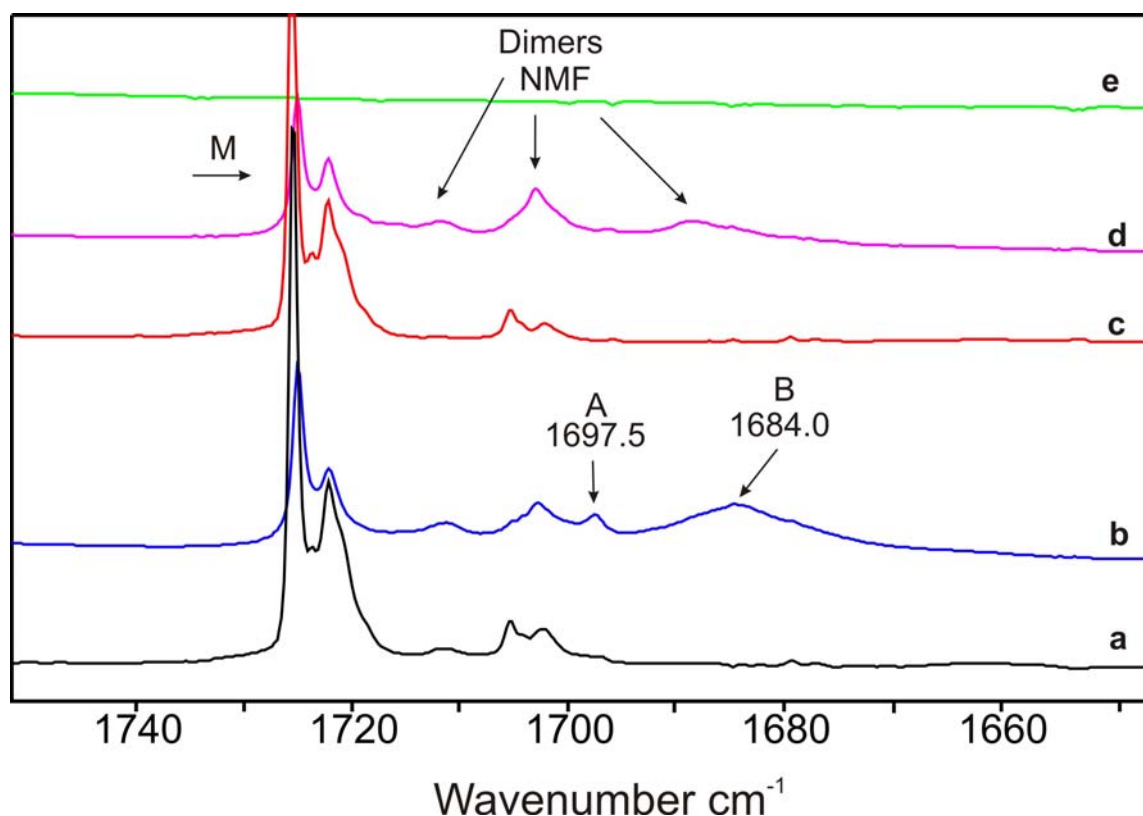


Figure 6.3.3. IR spectra in the range $1760 - 1640\text{ cm}^{-1}$ of NMF/MeOH mixtures, matrix-isolated in argon: (a) NMF:MeOH:Ar ratio 1:3:800, 10 K; (b) NMF:MeOH:Ar ratio 1:3:800, after annealing at 35 K; (c) NMF:Ar ratio 1:800, 10 K. (d) NMF:Ar ratio 1:800 after annealing at 35 K, (e) MeOH:Ar ratio 3:800, 10K. Vibrational modes were assigned to NMF/MeOH complexes, respectively.

In the C–O stretching region of methanol new bands are observed at 1056.5 and 1051.4 cm^{-1} (Figure 6.3.4 curve b), which are 22.9 and 17.8 cm^{-1} blue-shifted, respectively, from the unperturbed C–O stretching vibration at 1033.6 cm^{-1} . The relative intensity of two bands varies slightly depending on the experimental conditions. The band at 1051.4 cm^{-1} is always found to be the strongest, the band at 1056.6 cm^{-1} appears as a shoulder with the band of the methanol dimer at 1053.2 cm^{-1} and it is weak. The intensity of these new absorptions depends on the NMF concentration, indicating that these bands

correspond to the NMF – MeOH complexes. The spectra of the methanol dimers in argon matrix have been described in detail.^[240]

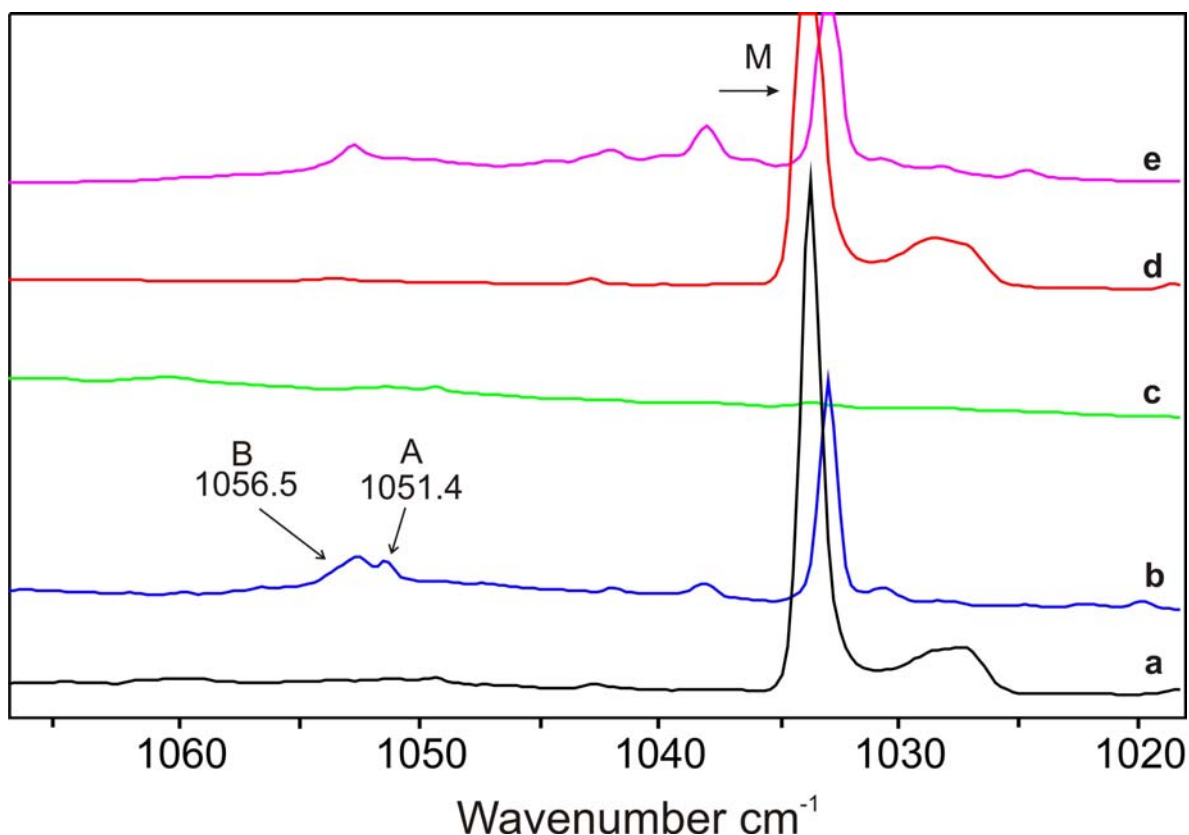


Figure 6.3.4. IR spectra in the range 1060 – 1020 cm^{-1} of NMF/MeOH mixtures, matrix-isolated in argon: (a) NMF:MeOH:Ar ratio 1:0.3:800, 10 K; (b) NMF:MeOH:Ar ratio 1:0.3:800, after annealing at 35 K; (c) NMF:Ar ratio 1:800, 10 K. (d) MeOH:Ar ratio 0.5:800, 10K, (e) MeOH:Ar ratio 0.5:800 after annealing at 35K. Vibrational modes were assigned to NMF/MeOH complexes, respectively.

The C–N (ν_{10}) and C^m–N (ν_6) stretching modes of NMF are also perturbed due to the complexation. Weak broad bands were observed at 1219.2 and 1216.3 cm^{-1} , blue-shifted by 13.7 and 10.6 cm^{-1} from the unperturbed C–N (ν_{10}) stretching vibration mode of NMF at 1205.5 cm^{-1} . An additional a new band at 954.2 cm^{-1} blue-shifted by 6.5 cm^{-1} , is assigned to the C^m–N (ν_6) stretching mode of NMF in a 1:1 NMF – MeOH complex. (Figures 6.3.5 and 6.3.6)

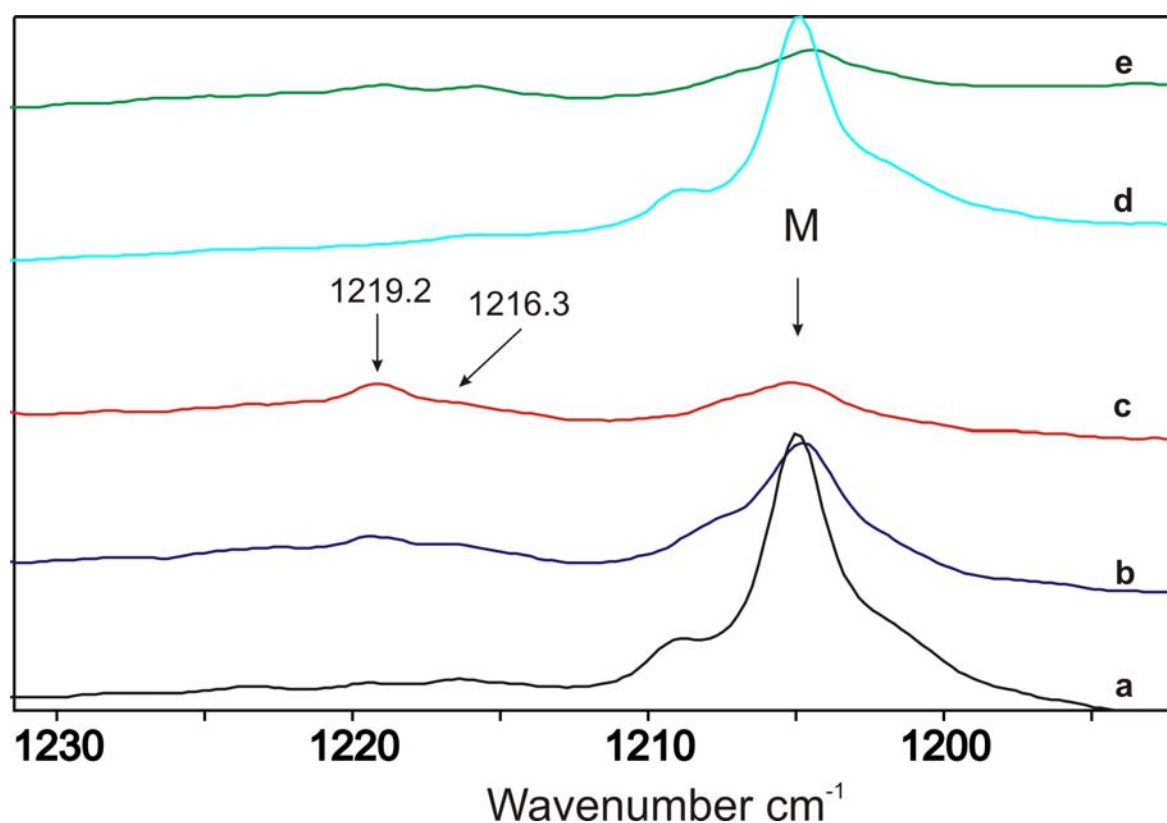


Figure 6.3.5. IR spectra in the range 1230 – 1190 cm⁻¹ of NMF/MeOH mixtures, matrix-isolated in argon: (a) NMF:MeOH:Ar ratio 1:1:800, 10 K; (b) NMF:MeOH:Ar ratio 1:1:800, after annealing at 35 K; (c) NMF:MeOH:Ar ratio 1:3:800, after annealing at 35 K. (d) NMF:Ar ratio 1:800, 10K, (e) NMF:Ar ratio 1:800 after annealing at 35K. Vibrational modes were assigned to NMF/MeOH complexes, respectively.

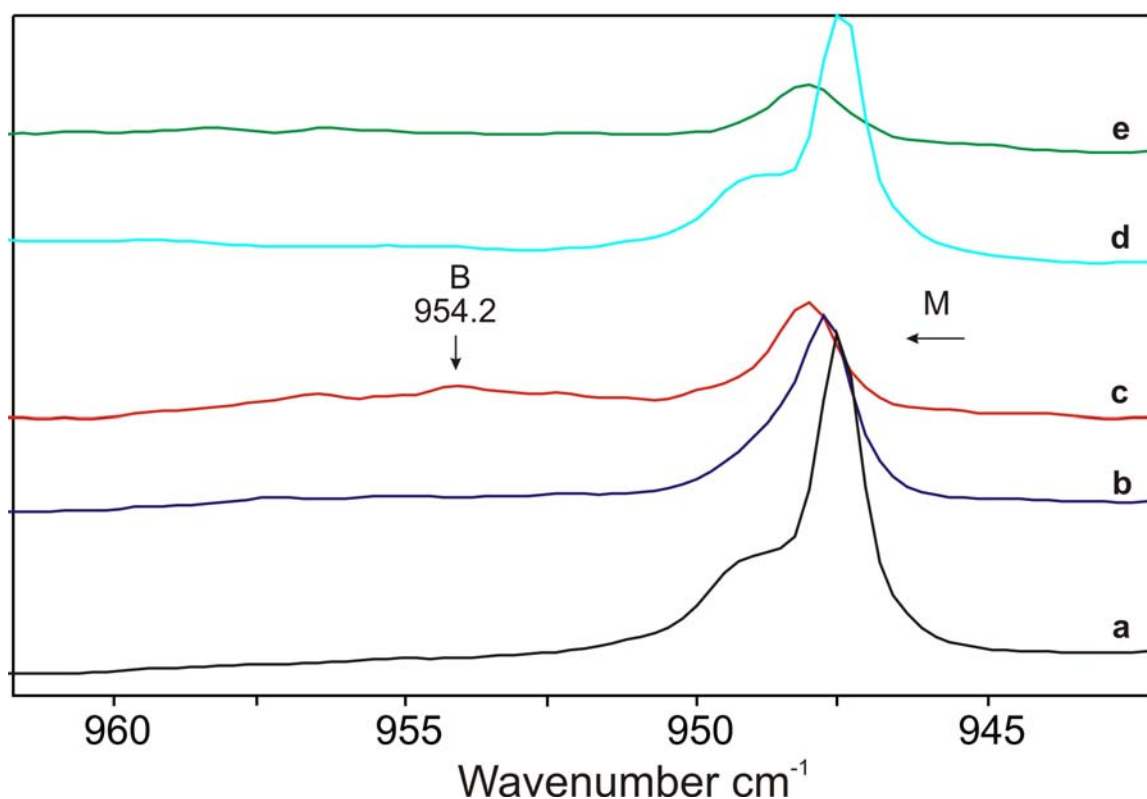


Figure 6.3.6. IR spectra in the range 960 – 940 cm^{-1} of NMF/MeOH mixtures, matrix-isolated in argon: (a) NMF:MeOH:Ar ratio 1:1:800, 10 K; (b) NMF:MeOH:Ar ratio 1:1:800, after annealing at 35 K; (c) NMF:MeOH:Ar ratio 1:3:800, after annealing at 35 K. (d) NMF:Ar ratio 1:800, 10K, (e) NMF:Ar ratio 1:800 after annealing at 35K. Vibrational modes were assigned to NMF/MeOH complexes, respectively.

6.3.3.3. Comparison of the Computed and the Experimental Vibrational Frequencies

The vibrational spectra of complexes were calculated and compared with the experimental data (Tables 6.3.3-6.3.5). The deviations between the calculated and observed vibrational modes result from matrix effects, anharmonicity of the vibrations, and deficiencies of the theoretical model. To correct these deviations scaling factors for each vibrational mode of the monomers (N-methylformamide and methanol) were calculated (Table 6.3.2). Applying these scaling factors to the calculated modes of the monomers exactly reproduces the experimental values of monomers. Applying the scaling to the modes of the complexes allows us a reliable prediction of the band positions of complexes.

Table 6.3.2. Calculated and experimental vibrational frequencies (cm^{-1}) of the NMF and MeOH monomers. Factor of correction.

Monomers and factor of correction				
Mode	Frequency (experimental) ^a	Frequency (calculated) ^b	Factor of correction	Assignment
Methanol (MeOH)				
12	3665.7	3886.6	0.943	$\nu(\text{O-H})$
2	1033.6	1042.9	0.991	$\nu(\text{C-O})$
1	-	302.8	-	$\nu(\text{O-H})$
N-methylformamide (NMF)				
21	3493.7	3697.7	0.945	$\nu(\text{N-H})$
16	1725.4	1744.9	0.989	$\nu(\text{C=O})$
10	1205.5	1235.1	0.976	$\nu(\text{C-N})$
6	947.7	967.6	0.979	$\nu(\text{C}^{\text{m}}-\text{N})$
4	535.5	476.9	1.122	$\tau(\text{N-H})$

[a] Experimental frequencies were observed in argon matrix. [b] Vibrational frequencies of the N-methylformamide and methanol monomers calculated at the MP2/TZ2P level of theory.

Dimer A. According to the calculations, the most perturbed mode in complex **A** is the O–H stretching vibration of methanol (Table 6.3.3). The predicted O–H stretching mode for dimer **A** (MP2/TZ2P level of theory) occurs at 3487.5 cm^{-1} and it is red-shifted by 178.2 cm^{-1} . The experimentally observed value at 3536.3 cm^{-1} is red-shifted by 129.4 cm^{-1} and it is assigned to the perturbed O–H mode of methanol in the NMF – MeOH complex **A**. This indicates that the methanol interacts with the NMF mainly via its hydroxyl hydrogen atom.

It is well known that the O–H stretching mode of methanol is hardly affected when methanol acts as a proton acceptor. On the other hand, it is very much red-shifted when methanol acts as a proton donor. For instance, the O–H mode of methanol in the acetone –

methanol complex^[248] is red-shifted by 148.6 cm^{-1} and in the methanol – water dimer^[240] is red-shifted by 128 cm^{-1} , where methanol acts as proton donor. The large red shift (-129.4 cm^{-1}) also indicates the formation of a strong hydrogen bond between the carbonyl group of the NMF and the hydroxyl group of the methanol. The band at 3536.3 cm^{-1} is assigned to the O–H stretching mode of methanol in complex **A**, which is in a good agreement with the calculated value at the MP2/TZ2P level of theory (Table 6.3.3).

Additional evidence for the role of methanol as a proton donor in NMF – MeOH complex is given by the blue-shift of the C–O stretching mode of methanol, although it is typically substantially less than the shift of the O–H stretching mode. (Table 6.3.3) The calculated frequency of the C–O stretching of methanol in dimer **A** (1050.8 cm^{-1} , MP2/TZ2P) is blue shifted by 17.2 cm^{-1} (Table 6.3.3). The experimental ν_2 mode of methanol monomer in argon appears at 1033.6 cm^{-1} . The band at 1051.4 cm^{-1} is consequently assigned to the C–O stretching mode of methanol in complex **A**, blue-shifted by 17.8 cm^{-1} (Figure 6.3.4).

This experimental C–O stretching shift is in a good agreement with the calculated shift for the NMF – MeOH complex **A** (17.2 cm^{-1}) (Table 6.3.3). On the other hand, it matches also with the C–O stretch shift for dimer **B** ($+18.6\text{ cm}^{-1}$) (Table 6.3.4). However, another weak absorption was found in this spectral region, which it is assigned to the C–O stretch in complex **B**, it will be discussed later. When methanol acts as a proton donor in the acetone – methanol^[248] and water – methanol^[249-252] complexes, blue shifts of 13.4 and 14 cm^{-1} are reported for the C–O stretching mode.

On codeposition of NMF and methanol in solid argon, a few absorptions that cannot be assigned to the parent species are observed in near to the modes of NMF. Those new bands appear close to the vibrational modes of NMF monomer. The perturbed modes corresponding to the complex formation are found at 1697.5 and 1219.2 (Figure 6.3.2-6.3.6). The corresponding parent modes appear at 1725.4 (C=O str.) and 1205.5 cm^{-1} (C–N str.). The frequency shifts in the complex are -27.9 and $+13.7$ for the C=O and C–N stretching vibrations, respectively.

Table 6.3.3. Experimental, calculated and predicted experimental vibrational frequencies (cm^{-1}) of the NMF – MeOH dimer **A**.^a

Dimer A									
Experimental					MP2/TZ2P				Assignment
Mode	In argon		Int.	Uncorrected		Corrected		Int.	
Methanol (MeOH)									
12	3536.3	−129.4	70	3698.3	−188.3	3487.5	−177.6	63	ν(O–H)
2	1051.4	+17.8	35	1060.4	+17.4	1050.8	+17.2	24	ν(C–O)
1	-	-	-	684.7	+381.9	-	-	17	τ(O–H)
N-methylformamide (NMF)									
21	-	-	-	3693.3	−4.4	3490.2	−4.2	90	ν(N–H)
16	1697.	−27.9	100	1733.3	−11.6	1714.2	−11.5	100	ν(C=O)
10	1219.	+13.7	12	1245.7	+10.6	1215.8	+10.3	8	ν(C–N)
6	-	-	-	963.8	−3.8	943.6	−3.7	2	ν(C ^m –N)
4	-	-	-	498.4	+21.5	559.7	+24.1	6	τ(N–H)

[a] The frequency shifts in dimer **A** compared to NMF and methanol (monomers **M**) are given in parentheses.

One characteristic of the formation of hydrogen bonded complexes of NMF is the red shift of the C=O stretching mode. The perturbed vibration of the carbonyl stretching mode was observed 27.9 cm^{-1} lower than the $\nu(\text{C=O})$ fundamental at 1725.4 cm^{-1} . The red shift in the C=O stretching vibration reflects the elongation of the C=O bond by 0.007 \AA (MP2/TZ2P) due to the complexation. The value predicted for the carbonyl-stretching mode of NMF in dimer **A** (MP2/TZ2P) is 1714.2 cm^{-1} . The agreement between the experimental and the calculated frequency shifts is not very good (-27.9 vs. -11.5 cm^{-1}). However, the band at 1697.5 cm^{-1} can be attributed to the C=O stretching vibration mode of NMF in complex **A** (Table 6.3.3).

The C–N stretching vibration at 1219.2 cm^{-1} is blue shifted by 13.7 cm^{-1} from the unperturbed molecule at 1205.5 cm^{-1} that is in good agreement with the calculated value of 10.3 cm^{-1} (Figure 6.3.5) (Table 6.3.3).

Series of experiments were carried out by varying the concentrations of NMF and methanol. All observed bands show the same kinetic. In order to know whether those bands are related to the 1:2 complexes of NMF and methanol, matrix-isolated spectra were taken with more diluted samples. No methanol dimers were identifiable in the spectra taken at NMF/MeOH/Ar ratio 1/0.03/800. However, perturbed O–H and C–O stretching peaks were seen again in the spectra. Their relative intensities were barely different from those of previous experiments. This suggests that those bands are not related to 1:2 complexes.

Dimer B. Our data is compatible with the existence of at least two NMF – MeOH complexes in argon matrix. The finding of two carbonyl shifts suggests that the carbonyl group of NMF is directly involved in these two complexes. The large shifts of the O–H and C–O stretches of methanol show that the complex is strongly hydrogen bonded.

The computed vibrational frequencies of dimer **B** (MP2/TZ2P) along with the experimental frequencies are listed in Table 6.3.4. The frequency shift for the C=O stretching mode is -20.7 cm^{-1} (MP2/TZ2P). The C–N and C^{m} –N stretching modes of NMF in complex **B** are blue-shifted by 10.0 and 5.5 cm^{-1} . The predicted frequencies for the C=O, C–N and C^{m} –N stretching modes in dimer **B** are 1705.0 , 1215.5 and 952.7 cm^{-1} , respectively (Table 6.3.4).

The calculated O–H stretching mode of methanol at 3464.7 cm^{-1} is red-shifted by 201.0 cm^{-1} (Table 6.3.4). The C–O stretching mode at 1052.2 cm^{-1} is blue shifted by 18.6 cm^{-1} . According to the calculations, the N–H stretching modes of NMF in dimers **A** and **B** do not affected upon compexation (Tables 6.3.3 and 6.3.4). The frequency shifts for the N–H stretching vibrational modes are -4.2 and 1.0 cm^{-1} , for dimers **A** and **B**, respectively.

The strong and broad band at 1684.0 cm^{-1} , which is red-shifted by 41.4 cm^{-1} is assigned to the C=O stretching vibration of NMF in dimer **B** (Figure 6.3.3) (Table 6.3.4). The C–N and C^{m} –N stretching modes of NMF (Figures 6.3.5 and 6.3.6) are blue shifted by 10.8 and 6.5 cm^{-1} in good agreement with the calculated values (Table 6.3.4).

The O–H stretching mode of methanol in dimer **B** was found at 3487.6 cm^{-1} , red-shifted by 178.1 cm^{-1} (Figure 6.3.4). The band at 1056.5 cm^{-1} is assigned to the C–O stretching mode of methanol in complex **B**, blue-shifted by 22.9 cm^{-1} (Table 6.3.4).

Table 6.3.4. Experimental, calculated and predicted experimental vibrational frequencies (cm^{-1}) of the NMF – MeOH dimer **B**.^a

Dimer B									
Mod e	Experimental			MP2/TZ2P				Assignment	
	In argon	Int.		Uncorrected	Corrected	Int.			
Methanol (MeOH)									
12	3487.6	-178.1	60	3674.2	-212.4	3464.8	-200.3	100	$\nu(\text{O-H})$
2	1056.5	+22.9	30	1061.8	+18.8	1052.2	+18.6	14	$\nu(\text{C-O})$
1	-	-	-	713.9	+411.1	-	-	26	$\tau(\text{O-H})$
N-methylformamide (NMF)									
21	-	-	-	3698.8	+1.1	3495.4	+1.0	7	$\nu(\text{N-H})$
16	1684.0	-41.4	100	1723.9	-21.0	1705.0	-20.7	63	$\nu(\text{C=O})$
10	1216.3	+10.8	10	1245.4	+10.3	1215.5	+10.0	6	$\nu(\text{C-N})$
6	954.2	+6.5	5	973.2	+5.6	952.7	+5.5	1	$\nu(\text{C}^{\text{m}}-\text{N})$
4	-	-	-	495.6	+18.7	556.5	+21.0	2	$\tau(\text{N-H})$

[a] The frequency shifts in dimer **B** compared to NMF and methanol (monomers **M**) are given in parentheses.

Dimer C. Dimer **C** is expected to be observed under matrix conditions. Table 6.3.5 shows its calculated vibrational frequencies (MP2/TZ2P). **C** stabilizes only by the H-O...H-N interaction (4) between the hydroxyl oxygen atom of methanol and the hydrogen atom linked to the nitrogen in NMF. According to the calculation, the most perturbed vibrational mode of NMF in complex **C** is the N-H stretching mode. The calculated N-H stretching mode appears at 3384.5 cm^{-1} , red shifted by 109.8 cm^{-1} . The other vibrational modes of NMF are almost not affected upon complexation.

Table 6.3.5. Experimental, calculated and predicted experimental vibrational frequencies (cm^{-1}) of the NMF – MeOH dimer **C**.^a

Dimer C									
Mod e	Experimental			MP2/TZ2P				Assignment	
	In argon	Int		Uncorrected	Corrected	Int.			
Methanol (MeOH)									
12	-	-	-	3881.7	-4.9	3660.4	-4.6	11	$\nu(\text{O-H})$
2	1030.7	-2.9	70	1033.6	-9.4	1024.3	-9.3	17	$\nu(\text{C-O})$
1	-	-	-	-	-	-	-	-	$\tau(\text{O-H})$
N-methylformamide (NMF)									
21	3399.4	-94.3	100	3581.5	-116.2	3384.5	-109.8	90	$\nu(\text{N-H})$
16	-	-	-	1737.9	-6.9	1718.9	-6.8	100	$\nu(\text{C=O})$
10	-	-	-	1257.0	+21.9	1226.8	+21.4	8	$\nu(\text{C-N})$
6	-	-	-	977.7	+10.1	957.2	+9.9	2	$\nu(\text{C}^{\text{m}}\text{-N})$
4	-	-	-	695.6	+218.7	781.2	+245.6	6	$\tau(\text{N-H})$

[a] The frequency shifts in dimer **C** compared to NMF and methanol (monomers **M**) are given in parentheses.

The weak absorption at 3399.4 cm^{-1} is assigned to the N–H stretching vibration mode of NMF in dimer **C**. This band appears only in presence both of NMF and methanol in argon matrix (Figure 6.2.2). The good agreement between the experimental (3399.4 cm^{-1}) and the calculated values (3384.5 cm^{-1} , MP2/TZ2P) indicates of the formation complex **C** in argon matrix as a minor product (Table 6.2.5).

6.3.3.4. Conclusion

The 1:1 hydrogen-bonded complexes of NMF and methanol (MeOH) have been studied by matrix isolation infrared spectroscopy and quantum chemical calculations. The two most stable complexes were observed in the argon matrix at 10 K. A number of intermolecular complex bands are found in both the NMF and MeOH fundamental regions. The C=O stretching of NMF is red shifted and the C–O stretching of MeOH is blue shifted due to the complexation. The O–H stretching mode of methanol also exhibits a large red shift. Structures, energies, and vibrational frequencies of the complexes were calculated at the MP2/TZ2P and B3LYP/6-311++G(2d,2p) levels of theory. Four NMF – MeOH minima were found at both levels of theory. Three are cyclic structures, involving the O–H...O, H–O...H and C–H...O=C interactions. The third most stable dimer is an open structure only stabilized by the H–O...H–N interaction. The binding energies of those complexes are –5.45, –4.92, –4.41 and –2.23 kcal/mol (MP2/TZ2P+BSSE+ZPE).

Chapter 7. Interaction and Reaction of Phenyl Radical with small molecules

7.1. Introduction (Phenyl Radical)

The phenyl radical (C_6H_5) (**1**) is a highly reactive 6-membered intermediate in combustion and soot formation^[249-252] and also play an important role in the chemistry of the formation polycyclic aromatic hydrocarbons (PAHs) of the interstellar gas and circumstellar envelopes.^[253] Indeed in addition they also play an important roles in oncogenesis and in tumor therapy by photoirradiation.^[254] Being among the simplest aromatic radical species, the phenyl radical is also often considered as a model for more complex aromatic radicals. Although numerous experimental studies with application of different techniques have been performed.^[253, 255-258] The phenyl radical can be formed by homolytic cleavage of a C-H bond in a benzene,^[256, 259, 260] $D_0(C_6H_5-H) = 112.0 \pm 0.6$ kcal mol⁻¹,^[261] as results of this loss, the symmetry drops from D_{6h} to C_{2v} (Figure 7.1.1). Indeed it is one of the simplest prototypes of an open-shell aromatic species, achieving stabilization of the radical due to resonance structures arising from electron delocalization around the ring.^[260, 262]

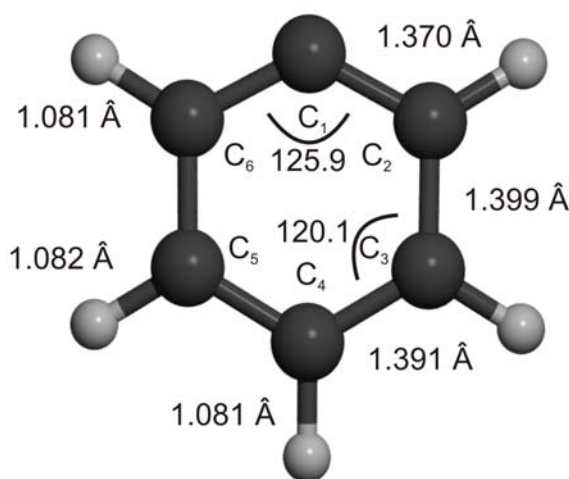


Figure 7.1.1. Optimized geometries of phenyl radical at the UB3LYP/cc-pVTZ level of theory. Bond lengths are given in angstrom and bond angle in degrees.

The phenyl radical has been studied by a variety of spectroscopic methods by means rotational, vibrational and electronic structure in the gas phase and in the solid state under low temperature conditions. First electron spin resonance studies of **1** were carried out by

Bennett *et al.*^[263, 264] revealed electron-proton spin multiplet structure of a C_{2v} radical and a 2A_1 ground electronic state. Later Kasai *et al.*^[265] have confirmed that unpaired electron resides primarily in a non-bonding σ -type orbital centered on the radical carbon (Figure 7.1.2). They generated phenyl radical by photolysis of phenyl iodine trapped in argon matrix at 4 K.

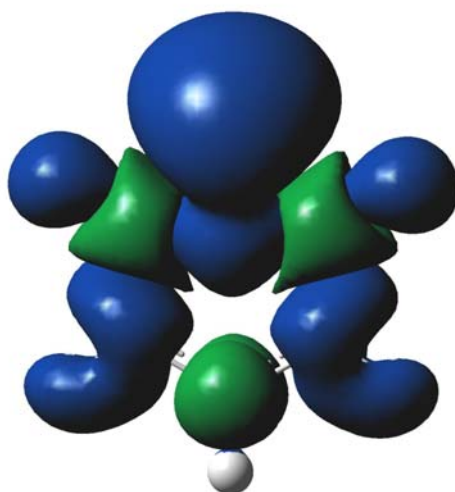


Figure 7.1.2. Spin density of **1** calculated at the UB3LYp/cc-pVTZ level of theory.

The accurate electronic absorption spectrum of matrix-isolated phenyl radical has been determined in the entire 52000–4000 cm^{-1} region by Radziszewski.^[266] It consists of three band systems corresponding to transitions to three excited electronic states: 2B_1 , with origin at 510.5 nm/ 2.43 eV ($\epsilon=2.8 \text{ L mol}^{-1} \text{ cm}^{-1}$); 2A_1 , with $\lambda_{\text{max}}=235.1 \text{ nm}/5.27 \text{ eV}$ ($\epsilon=220 \text{ L mol}^{-1} \text{ cm}^{-1}$); and 2B_2 with the origin at 211.5 nm/5.86 eV ($\epsilon=1650 \text{ L mol}^{-1} \text{ cm}^{-1}$). These transitions are attributed to the phenyl radical on the basis of the strict correlation of their intensity evolution in simultaneously measured IR and UV–visible spectra. Consistent results were obtained from several independent precursors. The transition symmetries were derived from polarization measurements on photo-oriented samples (Figure 7.1.3).

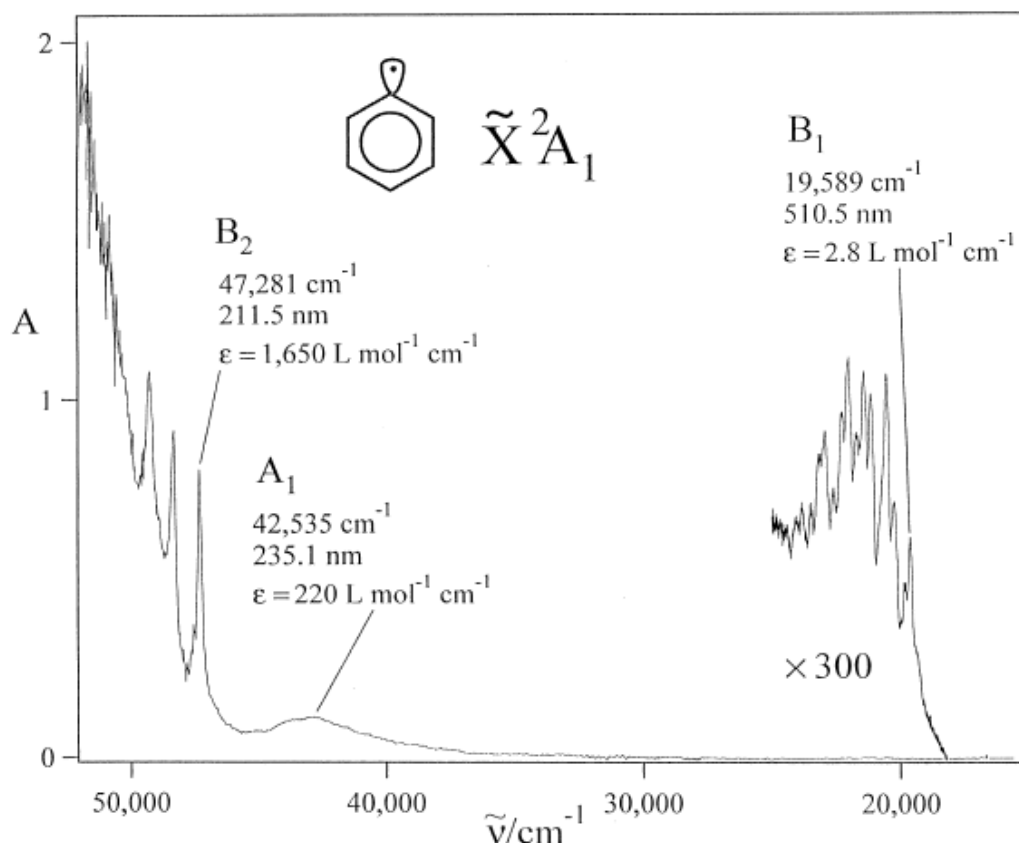
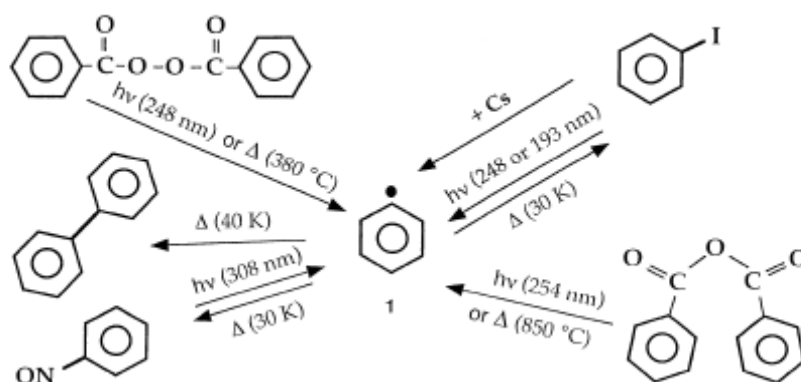


Figure 7.1.3. The electronic absorption spectrum of phenyl radical (**1**) prepared by irradiation of nitrosobenzene at 308 nm isolated in Ar matrix at 6 K. (This figure has been taken from referee).^[266]

In the gas phase phenyl radical was generated by a direct current discharge by removal of one hydrogen atom from benzene in the mixture with argon in a pulsed supersonic molecular beam by McMahon *et al.*^[260] Fourteen rotational transitions between 9 and 40 GHz and over 50 transitions between 150 and 330 GHz, each split by spin doubling; have been measured for the normal isotopic species. The rotational constants were assigned on the basis of post-Hartree-Fock CCSD(T)/cc-pVTZ level to be in an excellent agreement. Recently Sharp and coworkers reported the high resolution IR spectra of a jet-cooled phenyl radical were obtained via direct absorption laser spectroscopy in a stil-jet discharge supersonic expansion.^[258] Corresponding $v = 1 \leftarrow 0$ excitation of ν_{19} , the out-of-phase symmetric CH stretch mode and rigid asymmetric top A, B, C rotational constants were obtained.

The originally reported infrared spectra of **1** were obtained by photolysis of acetyl benzoyl peroxide in Ar matrix for out-of-plane CH bending region by Pacansky *et al.*^[267] The first a higher resolution IR spectra of **1**, was reported by Ellison and coworkers^[259]. They reported all 24 IR active transitions of **1**, following photodissociation of benzoyl

peroxide radical and benzoyl anhydride in cryogenic matrices (Scheme 7.1.1). Later in 2001 followed by a more systematic study they have completed of the IR absorption spectra of **1**, and several isotopically labeled isomers under low temperature conditions.^[256] In addition they measured the polarization of each of the bands as well as the intensities of the IR modes. The Raman active modes were assigned with the help of the isotopic shifts caused by ^{13}C substitution.^[268]



Scheme 7.1.1. Generations and reactions of the phenyl radical.^[266]

The restricted one-electron Kohn-Sham molecular orbital (MO) of **1**, in the upper valence region is depicted in Figure 7.1.4.^[262] In the benzene, the highest occupied molecular orbitals are doubly degenerated and of E_{1g} character. These two E_{1g} orbitals represent out-of-plane π -type combinations and are not affected by the breaking of the σ -type C-H bond: Upon formation of **1**, they become the $1a_2$ and $2b_1$ orbitals in the Figure 7.1.4. The nonbonding orbital of the C-H bond in the benzene are not largely affected or destabilized by the breaking of one of these bonds, it becomes the radical $7b_2$ orbital. The bonding molecular orbital in the benzene is due to the bonding combination of the six C-H σ -type C-H bond. As one of these bonds is broken, it will destabilized and consequently will become the highest single occupied molecular orbital (SOMO), shown as the $11a_1$ orbital (Figure 7.1.5).^[262]

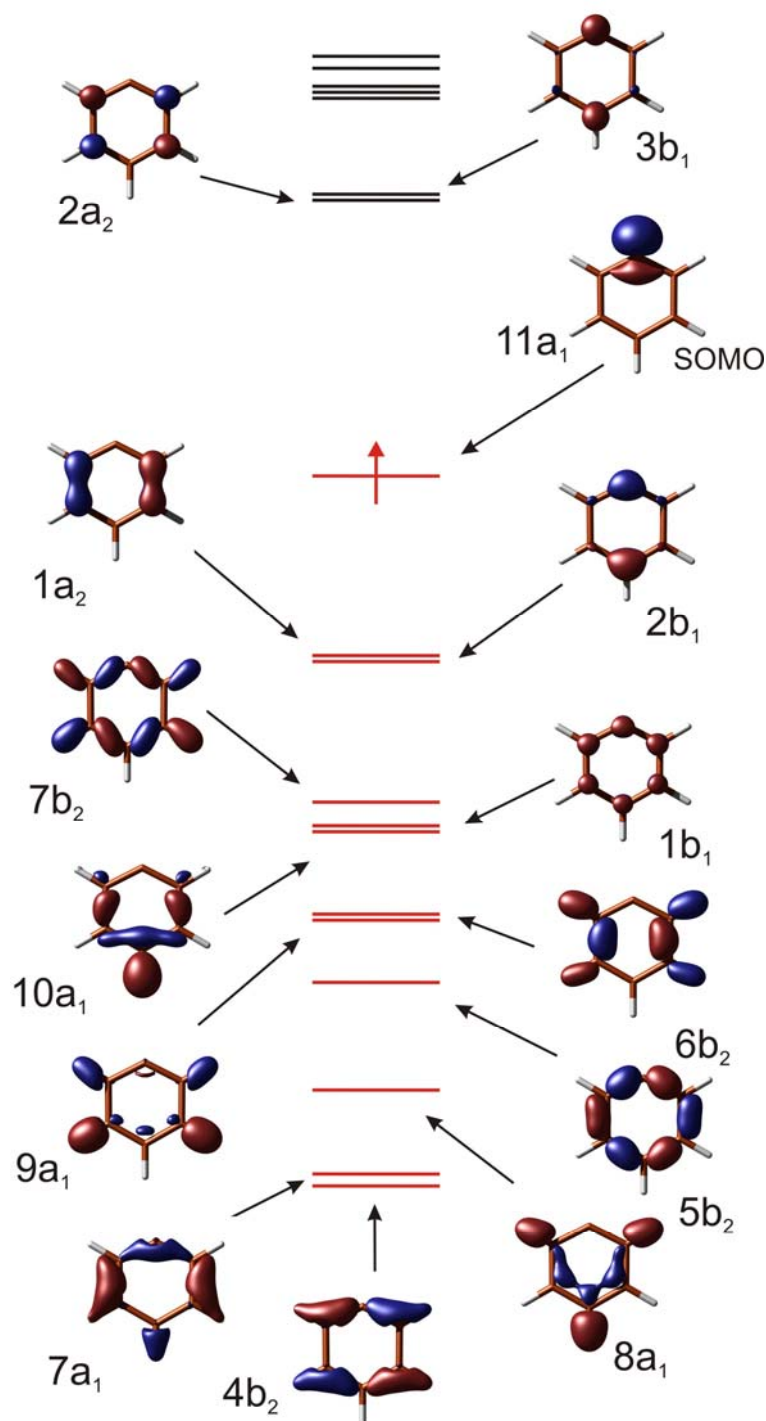


Figure 7.1.4. Quantitative one-electron Kohn-Sham molecular orbital diagram of **1**.^[262]

The phenyl radical is a σ -type radical. Therefore, its SOMO has no nodal plane. Its Löwdin populations, obtained from a restricted B1LYP/EPR-II calculations indicates that unpaired electron is largely C_1 character (70.5%) and also has a significant amount of *ortho* carbon and hydrogen atoms (16.6 and 3.4%, respectively).^[262]

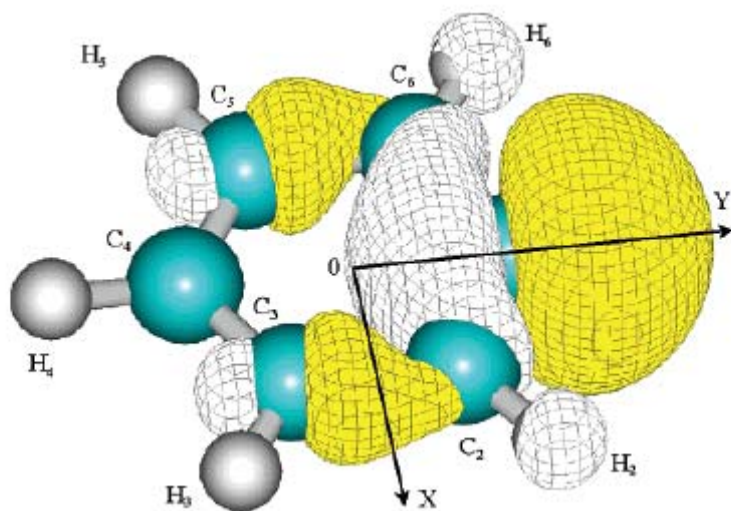


Figure 7.4.5. The **1** three-dimensional isosurface contour plot of ist 11a₁ SOMO. (This figure has been taken from referee.)^[262]

Chapter 7.2. Phenyl Peroxy Radical

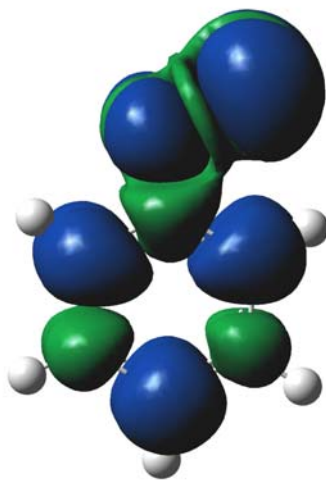
7.2.1. Introduction

The phenyl peroxy radical (**2**) is the primary product of the reaction of the phenyl radical (**1**) with molecular oxygen (equation 7.2.1). This reaction is considered to be of key importance in the combustion of aromatic hydrocarbons^[269, 270] and in the degradation of benzene in the troposphere.^[271, 272] Due to the high CH bond dissociation energy of 113 kcal/mol in benzene,^[273] the phenyl radical (**1**) is one of the most reactive organic radicals, and the reaction of **1** with molecular oxygen to give the peroxy radical (**2**) is exothermic by 46.3 kcal/mol according to ab-initio G2M calculations.^[274] This highly exothermic primary step of the oxidation of **1** is followed by a complex sequence of secondary reactions.^[274, 275] The kinetics of the **1** + ³O₂ reaction has been studied with the cavity-ring down method measuring the appearance of **2**,^[276] and from these data a small negative activation barrier of -0.32 kcal/mol was determined. Variation transition state theory reveals that the reaction of **1** with ³O₂ is barrierless,^[277] and thus the reaction rate should be at the diffusion limit. At very high temperatures the main fate of **2** is to lose an oxygen atom O(³P) and form the phenoxyl radical (**3**), which is still an exothermic reaction. The phenoxyl radical subsequently eliminates CO to yield the cyclopentadienyl radical C₅H₅. In cross-beam reactions between **1** and ³O₂ an oxygen atom is abstracted from molecular oxygen to produce **3** and O(³P) atoms.^[278] Under these conditions the phenyl peroxy radical **2** is an extremely short-lived intermediate with lifetimes below 10 fs.



By cavity ring-down spectroscopy a very weak and broad, structureless absorption in the visible region between 495 and 525 nm was found which could be used for kinetic measurements but which is not suitable for the spectroscopic identification of **2**.^[272, 277] In water solution, a broad peak with a maximum at 490 nm has been assigned to **2**.^[279, 280] According to DFT calculations the transitions of **2** in the visible region of the spectrum are due to intramolecular charge transfer and thus very sensitive to the solvent polarity.^[280]

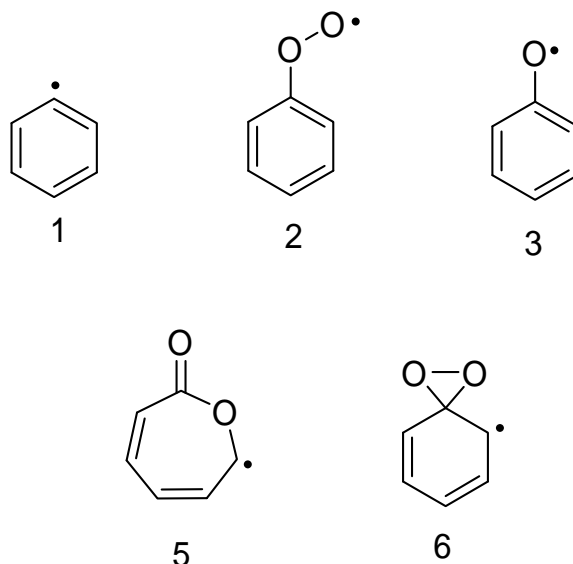
According to theoretical calculations, the lowest energy conformation of **2** has a planar C_s geometry and has a ²A'' electronic ground state. The unpaired electron of **2** is located on the terminal oxygen atom perpendicularly to the molecular plane (Figure 7.1.1).^[281, 282]



1

Figure 7.2.1. Spin density of **2** calculated at the UB3LYp/cc-pVTZ level of theory

The mechanism for the subsequent thermal decomposition of **2** has been extensively studied by different theoretical methods.^[274, 283, 284] In a computational study based on MP3 calculations, Carpenter proposed decomposition pathway of phenyl peroxy radical (**2**) through a dioxiranyl radical (**6**) intermediate, leading to the formation a very stable, seven-membered ring 2-oxepinoxy radical (**5**) than further decomposition to CO₂ and cyclopentadienyl radical.^[283] The structures and energies of 14 geometric isomers of **2** also have been calculated by *ab initio* molecular orbital methods.^[281] Fadden *et al.*^[284] have investigated various intermediates and transition states for unimolecular decomposition pathways of phenyl peroxy radical using hybrid density functional methods. They also explored the decomposition of 2-oxepinoxy radical (**5**) to variety products.^[285] Recently Tokmakov *et al.*^[274] have performed *ab initio* G2M calculations to investigate the potential energy surface for the reaction of **1** with O₂. They provided chemically accurate energetic and molecular parameters for various species of this reaction.



In contrast to **2**, the phenyl radical (**1**) has been trapped in inert gas matrices and characterized spectroscopically in great detail.^[266, 267, 286, 287] Basically, two methods can be used for the matrix isolation of **2**: the photodissociation of a matrix-isolated precursor or flash vacuum pyrolysis (FVP) of a precursor with subsequent trapping of the products in a low temperature matrices. To investigate the thermal reaction of **1** with $^3\text{O}_2$ in low temperature matrices, the matrix has to be annealed at approximately 2/3 of its melting point to allow for the diffusion of the trapped oxygen molecules. Since the matrix photodissociation necessarily produces radical pairs trapped in the same matrix cage, the subsequent annealing of these matrices results in unwanted radical recombination instead of reactions with other trapped molecules (e. g. oxygen) in most cases. FVP with subsequent trapping in matrices, on the other hand, produces radicals in individual matrix cages. Now the reaction with oxygen molecules can efficiently compete with radical recombination.

In this chapter, we report the matrix isolation and IR spectroscopic characterization of the phenyl peroxy radical (**2**) and several of its isotopomers. In addition, a second important isomer, the 2-oxepinoxy radical (**5**), could also be characterized.

7.2.2. Results and Discussion

Phenyl Radical. Various precursors, such as nitrosobenzene, iodobenzene, benzoyl peroxide, or benzoic anhydride, have been used as precursors for the matrix isolation of **2**.^[256, 288] In our experiments we use azobenzene (**4**) as a new thermal precursor of **1**. FVP of **4** at temperatures between 600 and 700°C with subsequent trapping with a large excess of argon at 10 K produces **1** in good yields. Byproducts found in these matrices are nitrogen (invisible in the IR), benzene (formed via hydrogen abstractions from **2**) and traces of acetylene (product of the thermal fragmentation of **2**). A second major product formed under these conditions is benzene **2**, obtained from **1** either via hydrogen abstraction from surface contaminations of the pyrolysis oven or via bimolecular reactions or rearrangements in the gas phase. Since pyrolysis of the perdeuterated d₁₀-**4** yields mainly d₆-**2**, the main source of hydrogen comes from **4**. The IR spectrum of matrix-isolated **1** with the strongest absorptions at 705.8 and 657.4 cm⁻¹ is in agreement with literature data. FVP of perdeuterated azobenzene d₁₀-**4** results in the formation of d₅-**2**, again its IR spectrum is in good agreement with the data reported in literature (Figure 7.2.2)

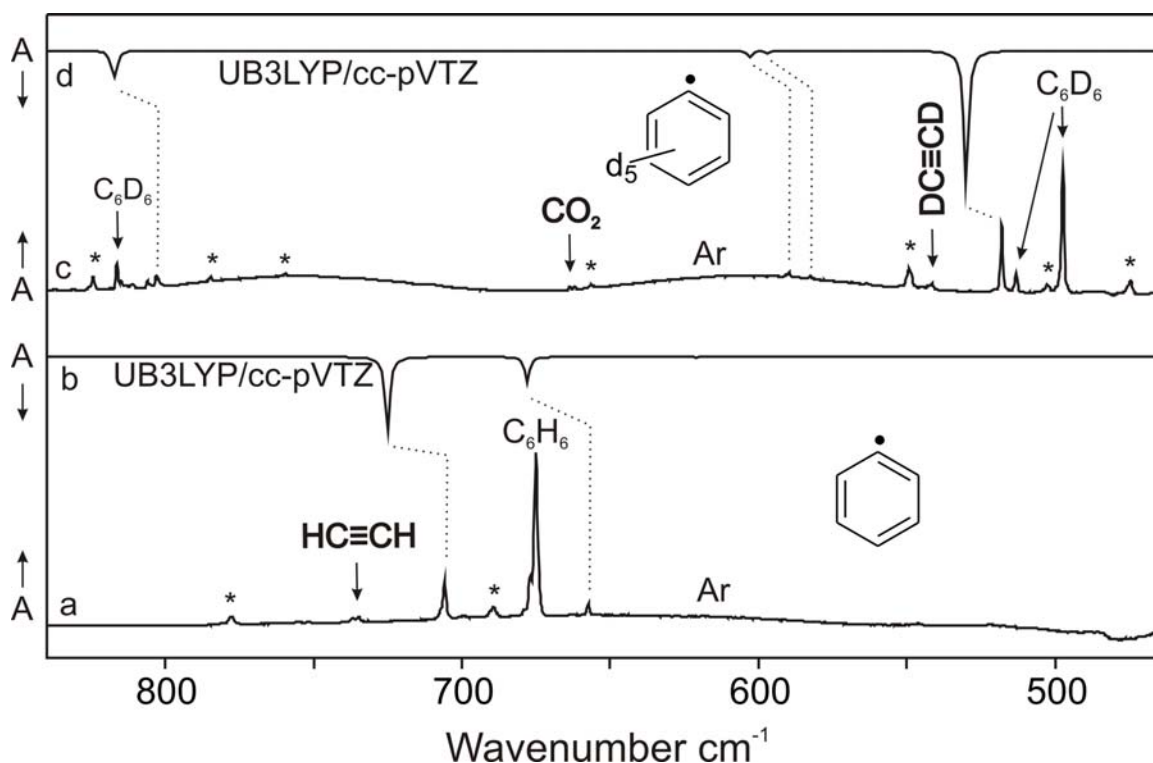


Figure 7.2.2. FVP products of azobenzene. (a) IR spectrum of a matrix (Ar at 10K) isolated the phenyl radical (**1**), containing products from VFP of azobenzene (**4**). Precursor bands are marked by asterisk (*). (b) Calculated vibrational spectrum (UB3LYP/cc-pVTZ) of **1**. (c) IR spectrum of a matrix (Ar at 10K) isolated the d_5 -**1**, containing products from FVP of d_{10} -**4**. Precursor bands are marked by asterisk (*) (d) Calculated vibrational spectrum (UB3LYP/cc-pVTZ) of d_5 -**1**.

Phenyl Peroxy Radical. In order to synthesize the oxygen trapping products of **2**, the argon was doped with 2% O_2 . FVP of **4** in O_2 -doped argon again resulted in the formation of **1**, benzene, and acetylene. In addition, new strong to medium IR absorptions are found at 1481.2, 1463.9, 905.1, 751.9, and 679.2 cm^{-1} (Figure 7.2.3, Table 7.2.1). If $^{18}O_2$ is used in the FVP, these bands show only very small isotopic shifts of less than 1 cm^{-1} . However, a weaker band at 1122.9 cm^{-1} shows a huge red-shift of -67.2 cm^{-1} which clearly indicates a OO stretching vibration. Other large red-shifts are found for a weak absorption at 793.9 cm^{-1} (-15.6 cm^{-1}) assigned to a $\nu(CO)$ stretching vibration and at 607.2 cm^{-1} (-11.8 cm^{-1}) assigned to a $\delta(COO)$ deformation mode. A comparison of the newly formed bands in O_2 -doped matrices with DFT calculations (UB3LYP/cc-pVTZ) of the phenyl peroxy radical **2** shows an excellent agreement. The two perdeuterated isotopomers d_5 -**2** and d_5 - $^{18}O_2$ -**2** were also synthesized and a careful analysis of their spectra confirms the assignment of the phenyl peroxy radical (Figure 7.2.4, Table 7.2.1). These experiments clearly show that the

phenyl radical **1** reacts with molecular oxygen in the gas phase to produce **2**. The phenoxy radical **3** was not observed under these conditions (Scheme 7.2.1).

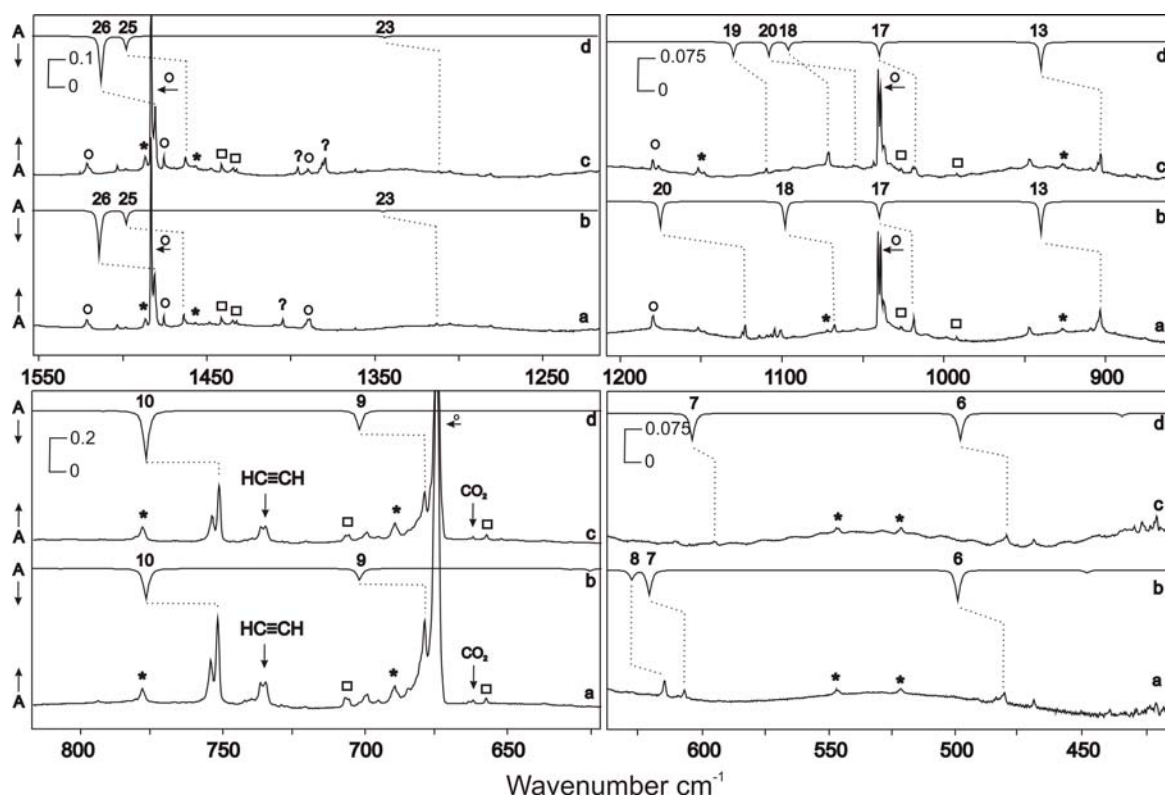


Figure 7.2.3. IR spectra showing the products of the FVP of **4** in 2% O₂-doped argon with subsequent trapping at 10 K. (a) Spectrum obtained after FVP with ¹⁶O₂. (b) Spectrum of **2** calculated at the UB3LYP/cc-pVTZ level of theory. (c) Spectrum obtained after FVP with ¹⁸O₂. (d) Spectrum of ¹⁸O₂-**2** calculated at the UB3LYP/cc-pVTZ level of theory. Bands of remaining precursor **4** are marked *, bands of the phenyl radical (**1**) are marked □ and bands of benzene are marked ○.

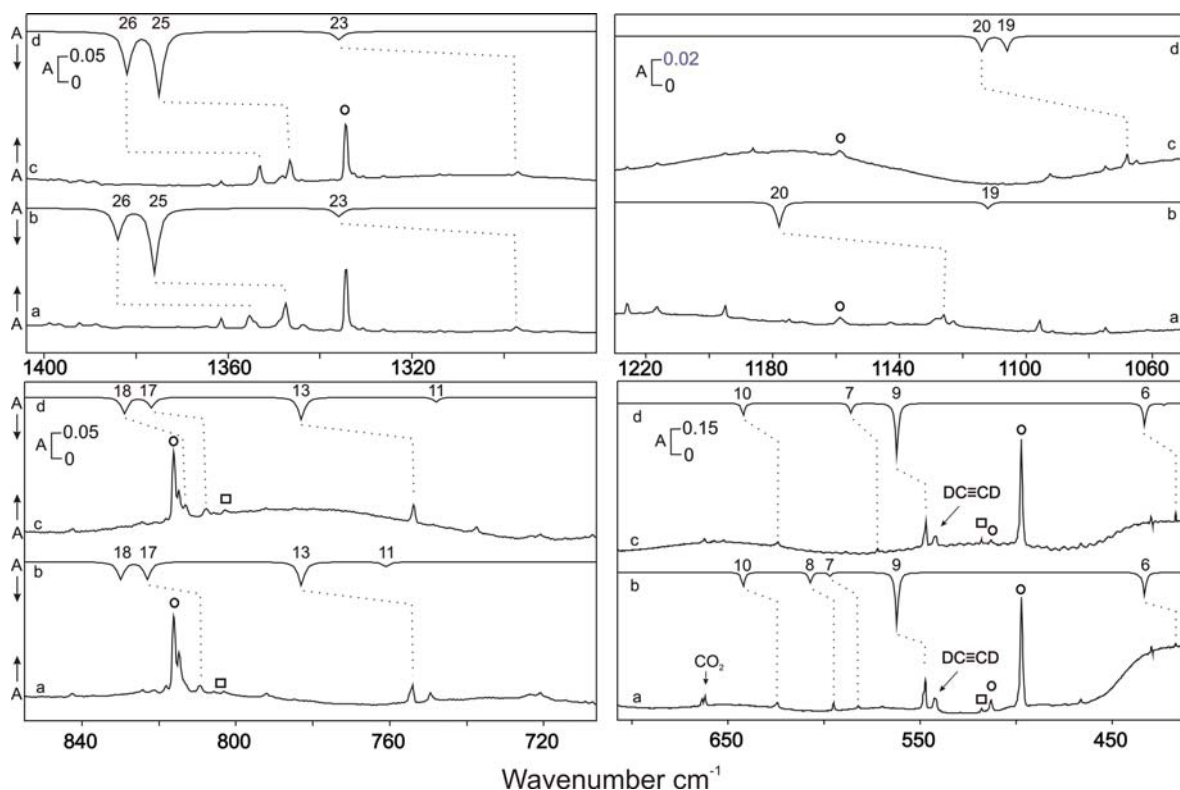
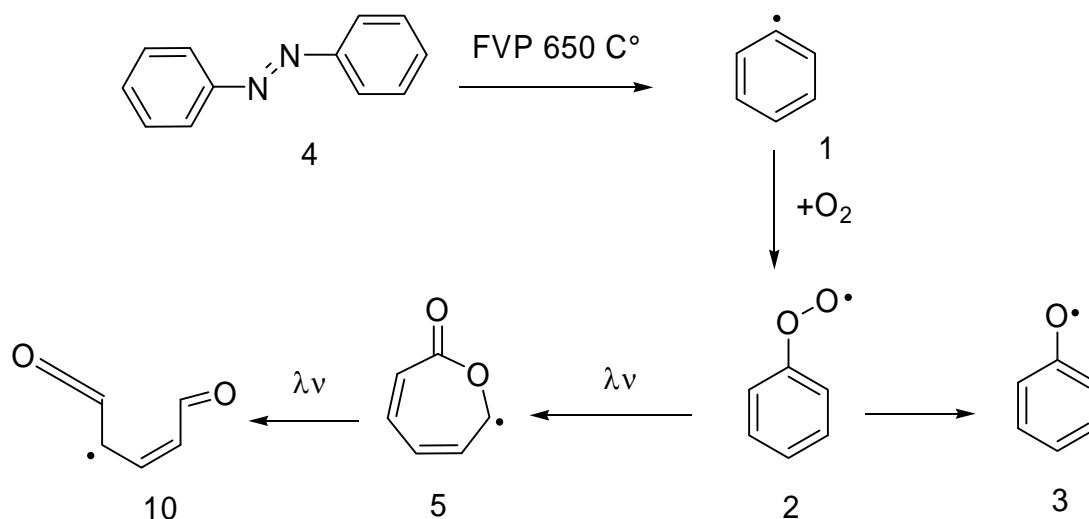


Figure 7.2.4. IR spectra showing the products of the FVP of d_5 -**4** in 2% O_2 -doped argon with subsequent trapping at 10 K. (a) Spectrum obtained after FVP with $^{16}O_2$. (b) Spectrum of d_5 -**2** calculated at the UB3LYP/cc-pVTZ level of theory. (c) Spectrum obtained after FVP with $^{18}O_2$. (d) Spectrum of d_5 - $^{18}O_2$ -**2** calculated at the UB3LYP/cc-pVTZ level of theory. Bands of remaining precursor **4** are marked *, bands of the phenyl radical (**1**) are marked \square and bands of benzene are marked \circ .



Scheme 7.2.1. Reaction of the phenyl radical **1** with molecular oxygen

The matrix produced after FVP of **4** in 2% O_2 -doped argon followed by trapping of the products at 10 K contains both the phenyl peroxy radical (**2**) and the phenyl radical

(1). At 10 K the matrix is very rigid and does not permit the diffusion of oxygen. However, annealing at 30 – 35 K results in the rapid diffusion of oxygen, which allows to investigate the thermal reaction of **2** with $^3\text{O}_2$ under the conditions of matrix isolation (Figure 7.2.5). In a similar way the reaction of triplet carbenes with $^3\text{O}_2$ had been investigated previously.^[289-291] These reactions proceed within several minutes and can be directly monitored by IR spectroscopy. Warming a matrix containing **1** and excess $^3\text{O}_2$ from 10 K to 35 K results in a rapid decrease of **1** and concurrently formation of **2**. The formation of **2** in a thermal reaction at temperatures as low as 30 K indicates a very small or no activation barrier for this reaction, in accordance with theoretical predictions.^[277]

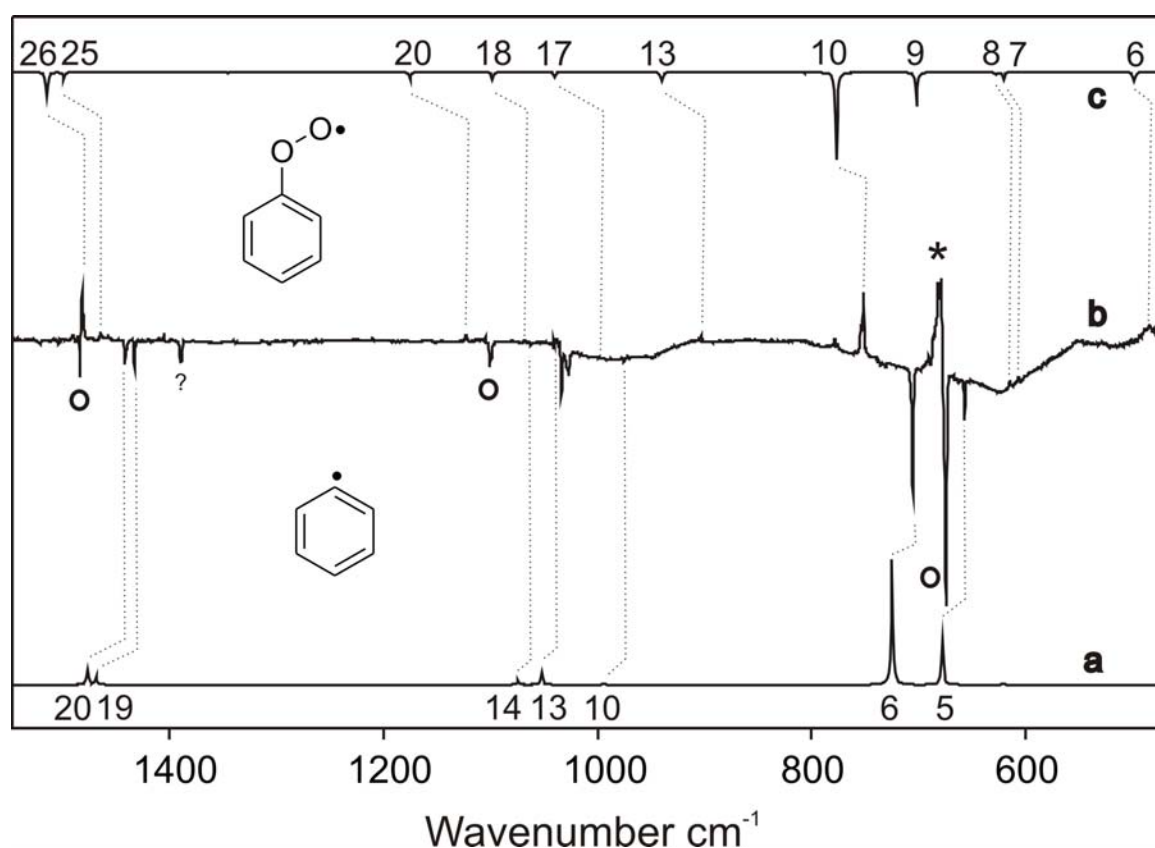


Figure 7.2.5. Difference IR spectra showing the annealing of **1** doped 0.1 % O_2 , matrix-isolated in argon at 10 K. Bands pointing downwards are disappearing during annealing and assigned to **1**. Bands pointing upwards are appearing and assigned to **2**. (a) IR spectrum of **1** calculated at the UB3LYP/cc-pVTZ level of theory. (b) Difference IR spectrum of the $^{16}\text{O}_2$ isotopomer. (c) IR spectrum of $^{16}\text{O}_2$ -**2** calculated at the UB3LYP/cc-pVTZ level of theory. Bands of benzene are marked \circ , bands of benzene dimers are marked *

Table 7.2.1. IR spectroscopic data of four isotopomers of the phenyl peroxy radical **2**

Mode ^a	C ₆ H ₅ ¹⁶ O ¹⁶ O (1)		C ₆ H ₅ ¹⁸ O ¹⁸ O (¹⁸ O ₂ - 1)		C ₆ D ₅ ¹⁶ O ¹⁶ O (d ₅ - 1)		C ₆ D ₅ ¹⁸ O ¹⁸ O (d ₅ - ¹⁸ O ₂ - 1)		Sym.	Assignment
	argon ^b	DFT ^c	argon ^b	DFT ^c	argon ^b	DFT ^c	argon ^b	DFT ^c		
33	3118.7	3227.7 (3)	3117.9	3227.7 (3)	-	2387.7 (3)	-	2387.7 (3)	A'	C ² -H str.
32	3189.1	3201.9 (8)	3187.2	3201.9 (8)	2318.9	2372.8 (15)	-	2372.8 (15)	A'	C ^{4,5,6} -H str.
31	3089.3	3193.8 (18)	3086.9	3193.8 (18)	-	2362.5 (19)	-	2362.5 (19)	A'	C ^{3,4,6} -H str.
30	3070.8	3183.4 (15)	3070.5	3183.4 (15)	2285.4	2351.2 (19)	-	2351.2 (19)	A'	C ^{3,5} -H str.
28	-	1643.9 (5)	-	1643.4 (5)	1583.4 (9)	1612.2 (3)	1582.4 (9)	1611.7 (3)	A'	CCC str. as.
26	1481.2 (52)	1514.2 (27)	1480.8 (55)	1513.9 (27)	1355.5 (17)	1384.1 (11)	1353.2 (30)	1382.4 (15)	A'	C ^{2,3,4,5} -H def.
25	1463.9 (12)	1498.6 (8)	1462.7 (10)	1498.1 (8)	1347.6 (32)	1376.0 (23)	1346.5 (37)	1375.7 (23)	A'	C ^{4,5} -H def.
23	1313.1 (3)	1345.6 (1)	1312.4 (2)	1344.6 (1)	1297.7 (7)	1336.8 (3)	1297.0 (7)	1336.6 (2)	A'	C ^{3,5} -H def./v srt.
20	1122.9 (8)	1175.1 (8)	1055.7 (8)	1108.1 (5)	1126.0 (8)	1178.3 (11)	1068.1 (14)	1114.6 (7)	A'	O-O str.
19	-	1129.2 (0)	1109.6 (3)	1130.2 (5)	-	1112.8 (3)	1007.6 (3)	1106.2 (7)	A'	C ¹ -O ⁷ str/C ^{2,6} -H def.
18	1067.7 (4)	1098.1 (8)	1071.1 (2)	1096.1 (3)	814.5 (9)	830.6 (11)	813.1 (18)	829.6 (11)	A'	C ^{2,4,6} -H def.
17	1018.5 (9)	1040.9 (5)	1017.3 (4)	1040.5 (5)	809.4 (9)	824.0 (11)	807.6 (14)	822.5 (7)	A'	C ^{2,3,5,6} -H def.
13	905.1 (12)	940.5 (10)	904.9 (14)	940.4 (10)	754.3 (21)	783.8 (15)	753.8 (26)	783.6 (15)	A''	C ^{2,4,6} -H wag.
11	793.9 (2)	807.9 (1)	778.3 (2)	792.3 (1)	-	761.6 (3)	-	748.6 (3)	A'	C ¹ -O ⁷ str/C ³ C ⁴ C ⁵ def.
10	751.9 (100)	777.3 (98)	751.3 (100)	777.1 (98)	624.3 (20)	642.7 (26)	624.4 (21)	642.6 (23)	A''	C ^{2,3,4,5,6} -H wag.
9	679.2 (22)	702.9 (38)	679.2 (24)	702.9 (38)	547.3 (100)	562.4 (96)	547.0 (100)	562.1 (100)	A''	C ^{2,4,6} -H wag.
8	615.1 (9)	628.5 (3)	-	626.7 (0)	595.0 (28)	608.0 (19)	572.3 (20)	586.6 (19)	A'	ring def. in plane
7	607.2 (5)	621.8 (8)	595.4 (3)	604.8 (10)	582.1 (11)	597.9 (7)	-	423.1 (3)	A'	C ¹ O ⁷ O ⁸ def.
6	480.8 (7)	499.3 (10)	479.7 (8)	498.4 (10)	429.3 (37)	433.8 (42)	429.5 (30)	433.2 (42)	A''	ring def. out of plane

[a] Mode numbers based on the C₆H₅¹⁶O¹⁶O isotopomer. [b] Argon matrix at 10 K. Vibrational numbers in cm⁻¹ and relative intensities in parenthesis. [c] Calculated at the UB3LYP/cc-pVTZ level of theory. Matrices containing **2** show a slightly orange color caused by a broad absorption with a maximum around 480 nm (Figure 7.2.6). This finding is in accordance with the broad band in the visible region observed in cavity-ring-down experiments.^[276] Irradiation into this band (argon, 10 K, λ > 400 nm) rapidly results in the disappearance of all bands assigned to **2** and formation of a new set of bands (Figure 7.2.6). The strongest IR band of the new compound at 1726.9 cm⁻¹ shows a strong ¹⁸O isotope shift of -30.7 cm⁻¹ and is thus assigned to a C=O stretching vibration (Figure 7.2.7). Other strong bands are found at 1307.9, 1095.8, and 724.9 cm⁻¹. The IR spectra of a number of isomers of **2** were calculated using DFT calculations, and an excellent agreement was found for the 2-oxepinoxy radical **5** (Figure 7.2.8 Table 7.2.2). The IR frequencies, intensities, and isotopic shifts of all four isotopomers very well match the calculated data.

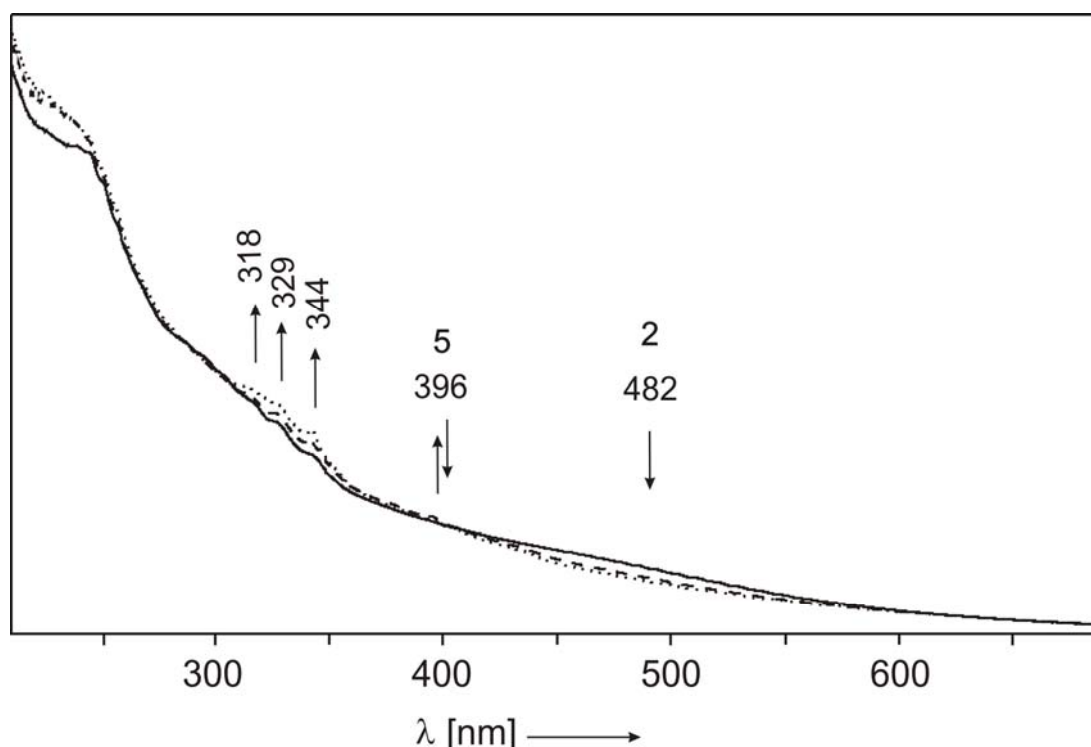


Figure 7.2.6. UV-vis spectrum of an argon matrix containing the FVP products of azobenzene doped 2 % oxygen (solid line). UV-vis spectrum of the same matrix after irradiation with $\lambda > 400$ nm (Hg high-pressure are lamp in combination with cut-off filter) during 15 minutes (dashed line). UV-vis spectrum of the same matrix after irradiation 120 minutes (dotted line).

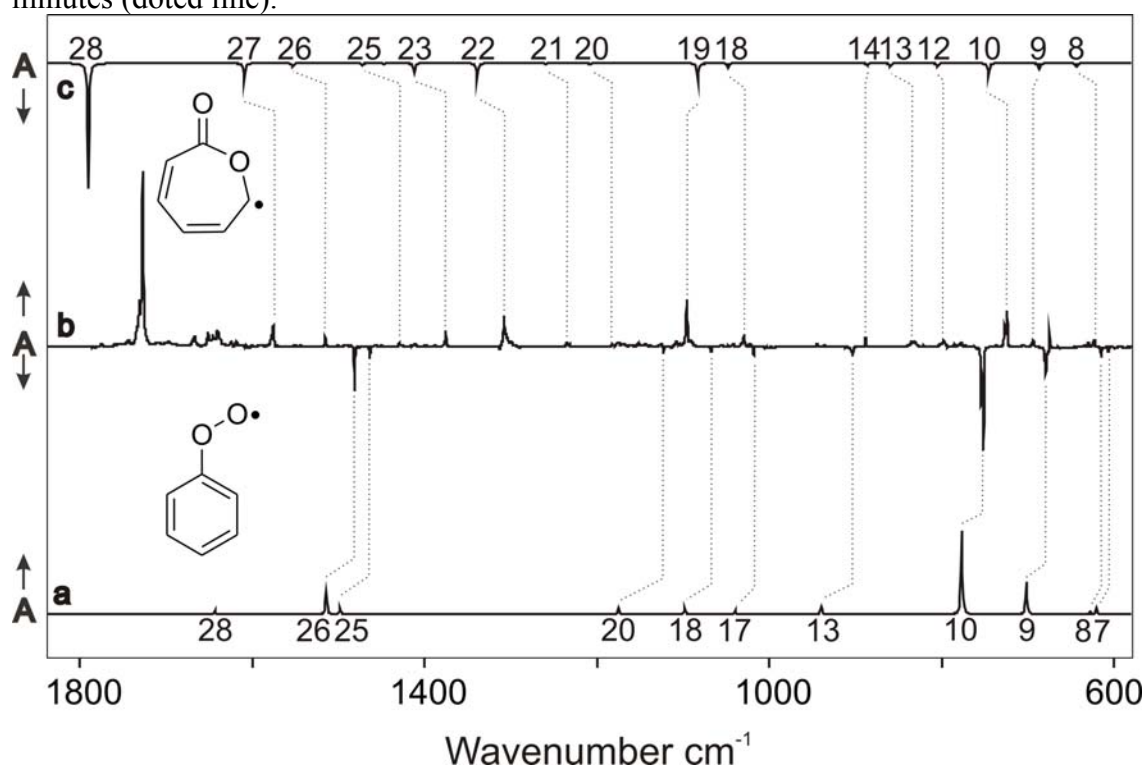


Figure 7.2.6. Difference IR spectra showing the photochemistry ($\lambda > 400$ nm) of **2**, matrix-isolated in argon at 10 K. Bands pointing downwards are disappearing during irradiation and assigned to **2**. Bands pointing upwards are appearing and assigned to **5**. (a) IR spectrum of **2** calculated at the UB3LYP/cc-pVTZ level of theory. (b) Difference IR spectrum of the $^{16}\text{O}_2$ isotopomer. (c) IR spectrum of **5** calculated at the UB3LYP/cc-pVTZ level of theory.

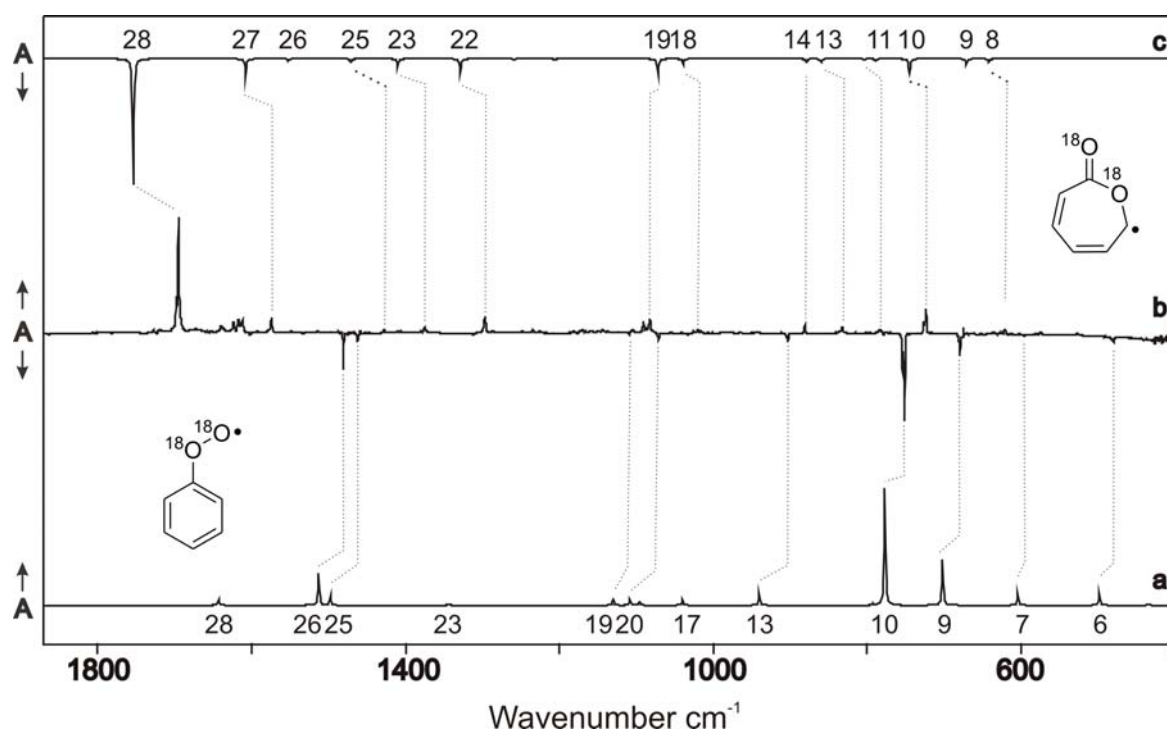


Figure 7.2.7. Difference IR spectra showing the photochemistry ($\lambda > 400$ nm) of $^{18}\text{O}_2$ -**2**, matrix-isolated in argon at 10 K. Bands pointing downwards are disappearing during irradiation and assigned to $^{18}\text{O}_2$ -**2**. Bands pointing upwards are appearing and assigned to $^{18}\text{O}_2$ -**5**. (a) IR spectrum of **2** calculated at the UB3LYP/cc-pVTZ level of theory. (b) Difference IR spectrum of the $^{18}\text{O}_2$ isotopomer. (c) IR spectrum of $^{18}\text{O}_2$ -**5** calculated at the UB3LYP/cc-pVTZ level of theory.

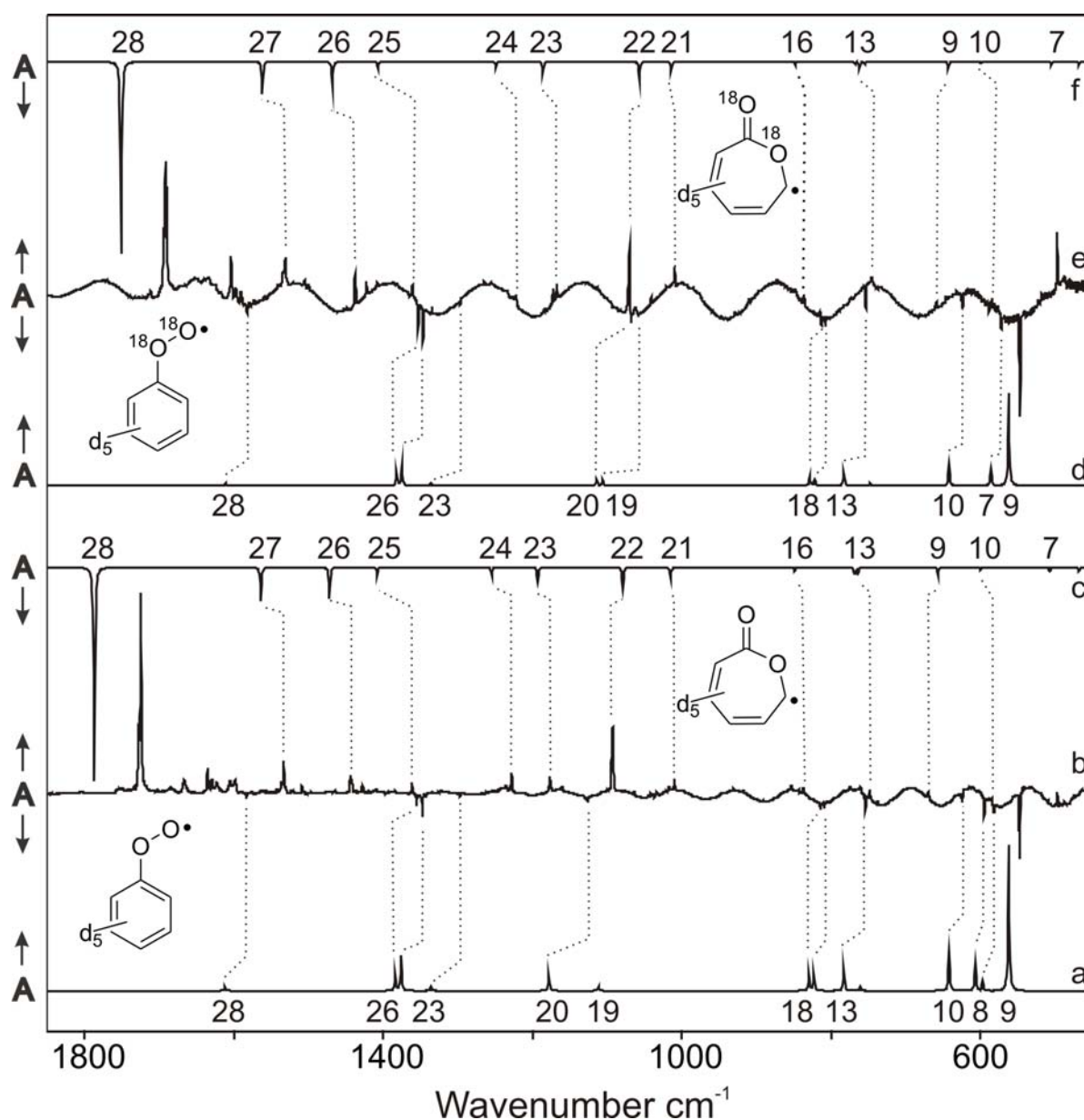


Figure 7.2.8. Difference IR spectra showing the photochemistry ($\lambda > 400$ nm) of d_5 -2, matrix-isolated in argon at 10 K. Bands pointing downwards are disappearing during irradiation and assigned to d_5 -2. Bands pointing upwards are appearing and assigned to d_5 -5. (a) IR spectrum of 2 calculated at the UB3LYP/cc-pVTZ level of theory. (b) Difference IR spectrum of the d_5 - $^{16}\text{O}_2$ isotopomer. (c) IR spectrum of d_5 -5 calculated at the UB3LYP/cc-pVTZ level of theory. (d) IR spectrum of d_5 - $^{18}\text{O}_2$ -2 calculated at the UB3LYP/cc-pVTZ level of theory. (e) Difference IR spectrum of the $^{18}\text{O}_2$ isotopomer. (f) IR spectrum of $^{18}\text{O}_2$ - d_5 -5 calculated at the UB3LYP/cc-pVTZ level of theory.

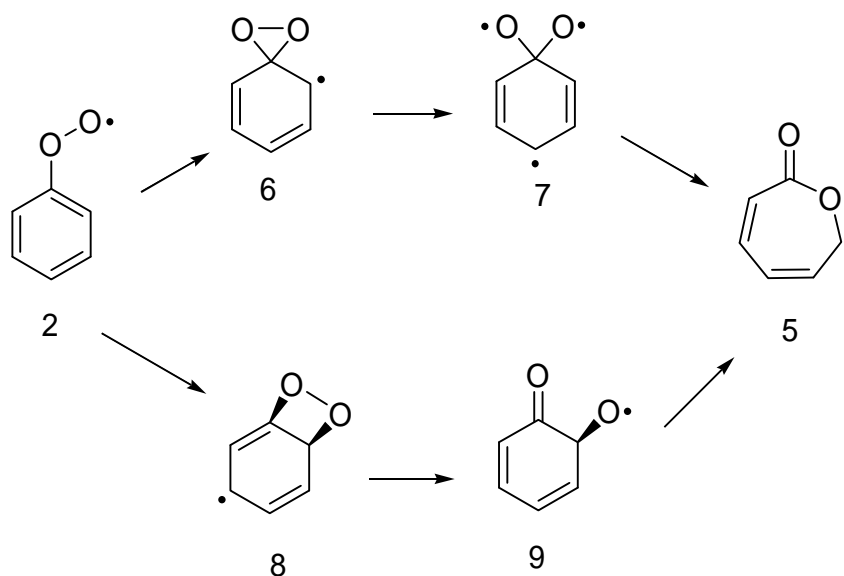
Table 7.2.2. IR spectroscopic data of four isotopomers of the 2-oxepinoxy radical **5**

Mode ^a	C ₆ H ₅ ¹⁶ O ¹⁶ O (5)		C ₆ H ₅ ¹⁸ O ¹⁸ O (¹⁸ O ₂ - 5)		C ₆ D ₅ ¹⁶ O ¹⁶ O (d ₅ - 5)		C ₆ D ₅ ¹⁸ O ¹⁸ O (d ₅ - ¹⁸ O ₂ - 5)		Sym.	Assignment
	argon ^b	DFT ^c	argon ^b	DFT ^c	argon ^b	DFT ^c	argon ^b	DFT ^c		
28	1726.9 (100)	1790.0 (99)	1696.2 (100)	1754.4 (99)	1724.8 (100)	1787.7 (99)	1691.7 (100)	1751.4 (99)	A	C=O str.
27	1575.8 (13)	1609.2 (14)	1574.8 (16)	1609.2 (14)	1533.3 (16)	1564.5 (16)	1531.3 (23)	1563.0 (17)	A	C ⁵ C ⁶ str
26	1515.8 (5)	1553.6 (3)	1514.6 (1)	1552.1 (2)	1443.8 (12)	1472.9 (15)	1438.1 (26)	1467.0 (13)	A	C ² C ³ str
25	1429.7 (~1)	1472.6 (2)	1428.3 (2)	1471.3 (3)	1361.6 (6)	1408.1 (4)	1360.7 (10)	1407.9 (4)	A	C ^{2,3} -H def./C ³ -C ⁴ str.
24	1415.8 (1)	1447.4 (1)	-	1446.6 (0)	1228.1 (10)	1255.5 (4)	1222.2 (8)	1249.9 (3)	A	C ^{5,6} -H def./ring str.
23	1375.8 (9)	1412.8 (8)	1375.4 (5)	1410.5 (6)	1177.2 (9)	1193.6 (7)	1167.4 (13)	1186.3 (6)	A	C ^{2,3,4} -H def./C ¹ C ² str.
22	1307.9 (18)	1339.6 (13)	1297.2 (15)	1329.8 (12)	1092.6 (33)	1079.2 (10)	1070.2 (52)	1057.5 (10)	A	C ^{5,6} -H def./C ¹ O ⁸ str.
21	1235.5 (2)	1259.2 (1)	1234.2 (2)	1259.2 (1)	1010.1 (6)	1015.8 (5)	1009.7 (15)	1014.4 (5)	A	C ^{2,3} -H def.
20	1177.4 (2)	1208.5 (1)	-	1206.1 (1)	-	909.9 (0)	-	905.1 (0)	A	C ^{4,5} -H def.
19	1095.8 (25)	1083.9 (14)	1083.4 (10)	1072.5 (13)	-	944.7 (0)	-	944.2 (0)	A	C ¹ O ⁸ str./C ^{4,5} - H def.
18	1029.6 (7)	1048.7 (4)	1016.7 (3)	1039.1 (5)	-	867.9 (0)	-	862.4 (0)	A	ring str.
17	-	1002.0 (0)	-	1001.9 (0)	-	809.6 (0)	-	809.5 (0)	A	C ^{2,3,4} -H wag.
16	-	953.6 (0)	-	952.4 (0)	837.2 (4)	849.9 (2)	836.8 (7)	848.4 (2)	A	ring str.
15	-	950.0 (0)	-	950.0 (0)	760.2 (3)	769.5 (2)	-	768.3 (1)	A	C ^{5,6} -H wag.
14	888.5 (6)	887.9 (2)	881.3 (8)	879.0 (3)	-	815.8 (0)	-	813.1 (0)	A	ring str.
13	833.4 (3)	860.5 (3)	832.5 (6)	860.1 (3)	748.5 (6)	764.2 (3)	746.4 (6)	762.1 (4)	A	ring str./C ^{2,4,6} - H wag.
12	797.9(2)	805.7 (1)	796.3 (~1)	804.1 (1)	-	671.1 (0)	-	670.1 (0)	A	C ^{2,3,4,5,6} -H wag
11	-	805.6 (2)	784.0 (4)	789.7 (2)	-	768.4 (3)	-	755.9 (1)	A	C ² C ¹ O ⁸ def
10	724.9 (19)	746.2 (11)	723.9 (22)	745.1 (12)	584.6 (3)	600.3 (1)	584.4 (6)	599.8 (1)	A	C ^{4,5,6} -H wag

9	694.2 (4)	687.5 (5)	-	671.6 (5)	669.8 (5)	657.7 (4)	659.2 (7)	643.0 (4)	A	C ¹ O ⁸ str
8	623.9 (5)	644.3 (3)	621.7 (5)	642.1 (3)	-	507.4 (2)	-	505.4 (2)	A	C ^{2,3,4,5} -H wag
7	527.8 (2)	550.6 (1)	-	549.4 (0)	450.9 (5)	468.5 (2)	450.6 (7)	468.2 (2)	A	ring def. out of plane
6	-	513.4 (0)	-	497.7 (0)	-	498.5 (0)	-	483.4 (0)	A	C ¹ O ⁷ def.

[a] Mode numbers based on the C₆H₅¹⁶O¹⁶O isotopomer. [b] Argon matrix at 10 K. Vibrational numbers in cm⁻¹ and relative intensities in parenthesis. [c] Calculated at the UB3LYP/cc-pVTZ level of theory.

The rearrangement of **2** to **5** is obviously a multi-step reaction. The formation of a spirodioxiranyl radical from **6** as an intermediate which rearranges to **5** via a dioxy triradical has been shown by computations to be a feasible mechanism.^[270, 283, 284] These and other proposed intermediates of the rearrangement are expected to be highly labile and are not observed during the photolysis of **2**. According to DFT calculations, the addition of a further molecule of oxygen at one of the three possible positions is endothermic by 9 – 13 kcal/mol with activation barriers of 17 – 18 kcal/mol. Thus, a further addition of molecular oxygen to **5** is not expected under the conditions of matrix isolation (Scheme 7.2.2).



Scheme 7.2.2. Unimolecular rearrangement pathways of **2** through a dioxiranyl and dioxetanyl intermediate resulting in **5** (B3LYP/6-311+G**).^[292]

Prolonged irradiation of matrix-isolated **5** at 10 K with visible light ($\lambda > 400$ nm) results in the complete photolysis of **5** and formation of a new compound with intense IR absorptions in the region between $2150 - 2050\text{ cm}^{-1}$ and $1650 - 1600\text{ cm}^{-1}$ (Figures 7.2.9, 7.2.10, Table 7.2.3). The bands in both regions show considerable ^{18}O -isotopic shifts which suggests ketene groups for the bands between $2150 - 2050\text{ cm}^{-1}$ and enones for the bands between $1650 - 1600\text{ cm}^{-1}$. Since some of these bands grow with different rates during the photolysis, we assume that a mixture of at least two compounds is formed. It is therefore tempting to assign ketoketene **10** and its conformers and configurational isomers to the photoproduct of **5**. However, since the IR spectra calculated for various geometrical isomers of **10** are very similar, an assignment to one of the isomers was not possible. In a study by Fadden and Hadad for the ring-opening of **5** to ketoketene **10** a thermal activation

barrier of 23.4 kcal/mol was calculated,^[285] while two other rearrangements of **5** were found to proceed via considerably higher activation barriers. Our experiments do not allow us to determine if the ring-opening is a photochemical or a hot ground state reaction. In any way, the product observed is that which is formed with the lowest predicted activation barrier.

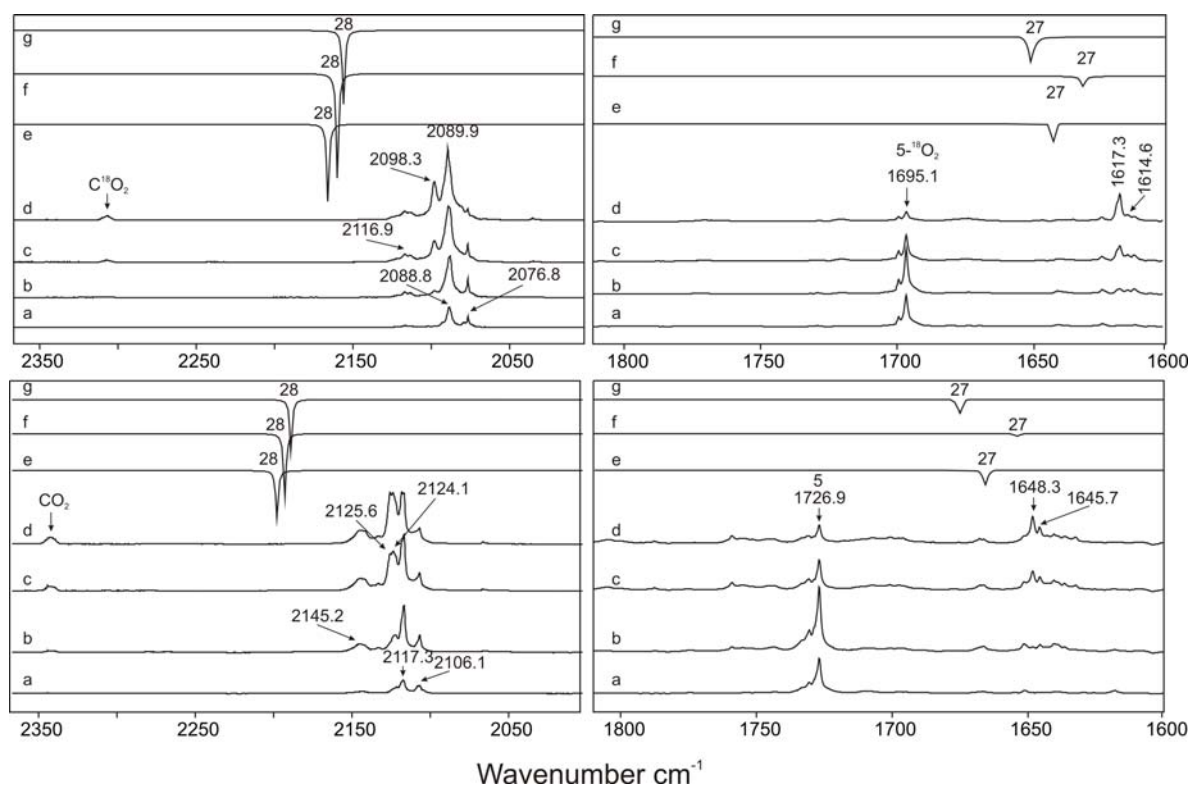


Figure 7.2.9. Difference spectra of FVP products of azobenzene doped 2% of O₂ (bottom) and ¹⁸O₂ (top) in an argon at 10K. (a) Difference spectra after 5 minutes irradiation $\lambda > 400$ nm (Hg high-pressure are lamp in combination with cut-off filter). (b) The same spectra after 30 minutes irradiation. (c) After 60 minutes irradiation. (d) After 180 minutes irradiation. (e) IR spectrum of **10c** and ¹⁸O₂-**10c** calculated at the UB3LYP/cc-pVTZ level of theory. (f) IR spectrum of **10a** and ¹⁸O₂-**10a** calculated at the UB3LYP/cc-pVTZ level of theory. (g) IR spectrum of **10b** and ¹⁸O₂-**10b** calculated at the UB3LYP/cc-pVTZ level of theory. The mode 28 due to vibration of the ketene group, the mode 27 due to vibration of the carbonyl group in the **10a-10c**, correspondingly.

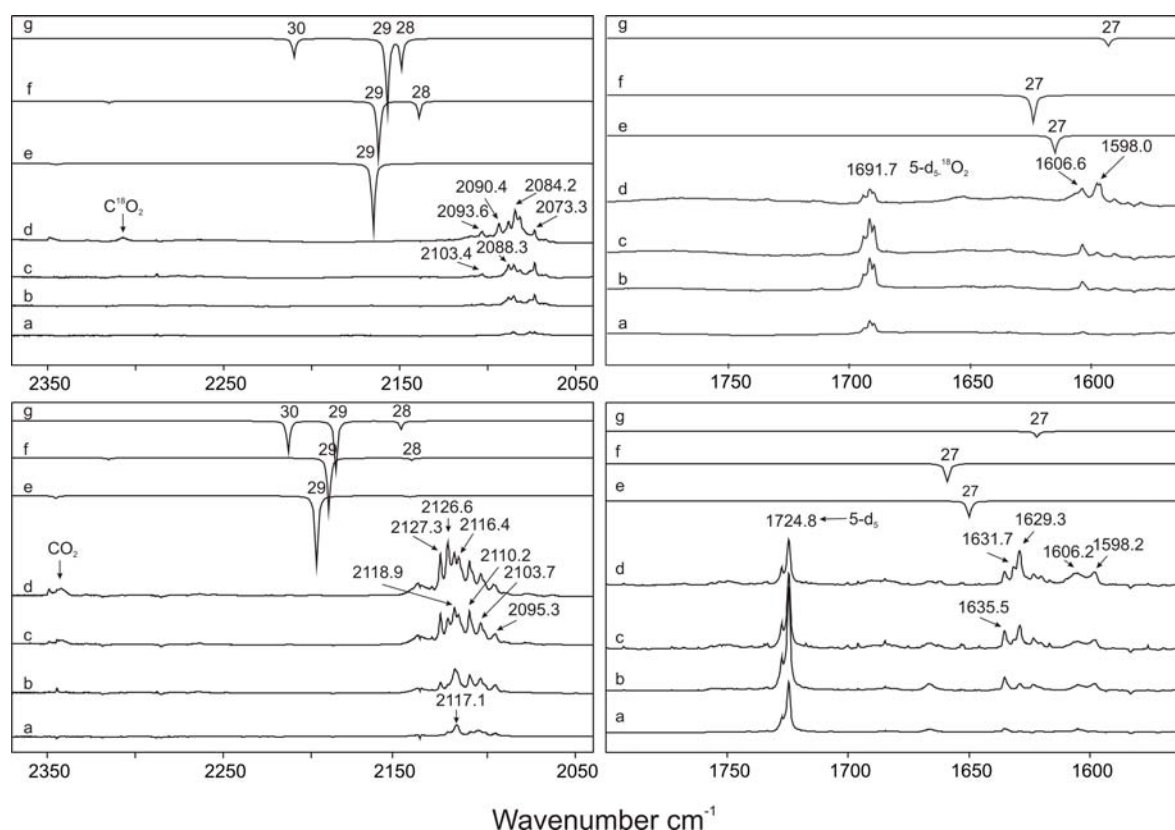


Figure 7.2.10. Difference spectra of FVP products of azobenzene- d_{10} doped 2% of O_2 (bottom) and $^{18}O_2$ (top) in an argon at 10K. (a) Difference spectra after 5 minutes irradiation $\lambda > 400$ nm (Hg high-pressure arc lamp in combination with cut-off filter). (b) The same spectra after 10 minutes irradiation. (c) After 30 minutes irradiation. (d) After 120 minutes irradiation. (e) IR spectrum of d_5-10c and $d_5-^{18}O_2-10c$ calculated at the UB3LYP/cc-pVTZ level of theory. (f) IR spectrum of d_5-10a and $d_5-^{18}O_2-10a$ calculated at the UB3LYP/cc-pVTZ level of theory. (g) IR spectrum of d_5-10b and $d_5-^{18}O_2-10b$ calculated at the UB3LYP/cc-pVTZ level of theory. Mode 28 due to vibration of the ketene group, mode 27 due to vibration of the carbonyl group in the **10a-10c**, correspondingly. Modes 30 and 28 due to C-H stretch of **10a-10c**, correspondingly.

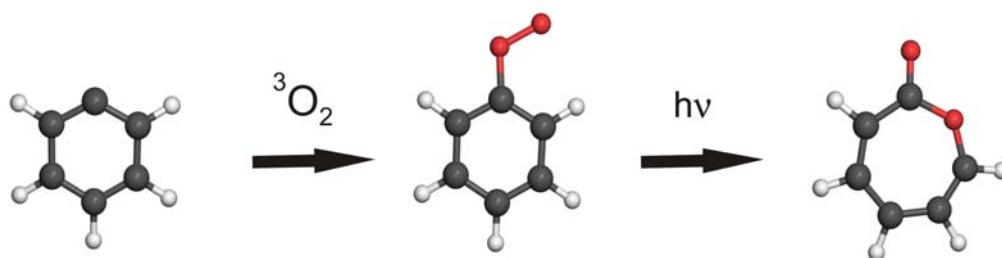
Table 7.2.3. Experimentally observed frequencies after photolysis of **2** and its isotopomers.

$^{16}\text{O}_2$	$^{18}\text{O}_2$	$^{16}\text{O}_2\text{-d}_5$	$^{18}\text{O}_2\text{-d}_5$
2145	2117	2127	2103
		2126	2093
2125	2098	2119	2090
		2117	
2124	2090	2116	2088
		2110	
2117	2089	2104	2084
		2095	
2106	2077		2073
		1635	
1648	1617		1606
		1632	
1645	1614	1629	1598
		1410	-
1489	1497	-	-
1471	1487	-	-
1468	-	-	-
1454	-	-	-
1384	-	-	-
1320	1225	-	-
1182	1180	1181	1180
1160	1160	1076	1040
1126	-	-	
948	947	-	910
900	-	-	
817	779	-	772
646	651	-	652
620	-	-	
593	590	518	497

7.2.3. Summary

We showed that the phenyl radical (**1**) rapidly reacts with molecular oxygen to produce the phenoxyl peroxy radical (**2**) both in the gas phase and in argon matrices. Phenoxyl radical (**3**) is not formed under these conditions. This indicates that the activation barrier for the oxygen addition to **1** is very low and that, despite the high exothermicity of this reaction, the primary product **2** can efficiently dissipate the excess energy without fragmentation. Loss of oxygen from **2** obviously requires a higher thermal excitation in high-temperature processes or in cross-beam experiments. This is of relevance to tropospheric chemistry, since the phenyl radical (**1**) can be produced in the troposphere from benzene via H-abstraction by OH radicals. The phenyl radical (**1**) will be efficiently quenched by oxygen to form peroxy radical (**2**). Under these conditions it is not expected that **2** cleaves to phenoxyl radical **3** and $\text{O}(^3\text{P})$. Formation of triplet oxygen atoms would

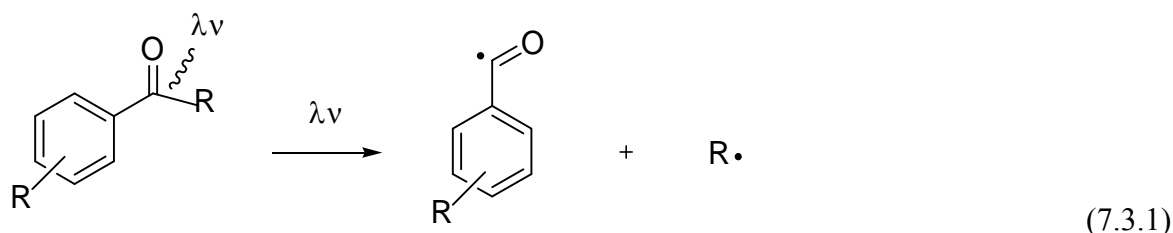
regenerate ozone and subsequently OH radicals. The photochemical rearrangement of **2** by visible light produces another intermediate of importance in the oxidation of benzene: the 2-oxepinoxy radical (**5**). This radical was also characterized by IR spectroscopy. Further irradiation finally leads to the cleavage of the ring and formation of a mixture of several conformers of ketoketene **10**. Our experiments do not allow us to determine if the photochemical steps which lead to **5** and **10** proceed on an excited surface or if these reactions are hot ground state reactions. Nevertheless, the products found in the matrix are the products that have been predicted by ab-initio and DFT calculations to be formed with the smallest activation barriers. These products are thus also relevant for the thermal combustion of benzene.



Chapter 7.3. Benzoyl Radical

7.3.1. Introduction

The benzoyl radical **11** is an important reactive intermediate that plays a role in the combustion of aromatic hydrocarbons and as an initiator in polymerization reactions.^[293] The direct interaction of **1** with carbon monoxide produces benzoyl radical (**11**), which is an essential importance in a large variety of chemical reactions. The great attention of the benzoyl radical was increased, when it has been shown that **11** plays an important role in the initiation processes of polymerization of methyl methacrylate (MMA).^[294, 295] Large number of aryl ketones have been synthesized to use as photoinitiators in free radical polymerizations.^[296, 297] Upon irradiation these ketones undergo classical Norrish type I cleavage to produce radical pairs with a high rate constant and good efficiency (eq. 7.3.1).^[298-300] Laser flash photolysis with transient UV/visible detection and also time-resolved IR spectroscopy were employed to detect the addition rate constants to alkenes for the aryl time radicals.

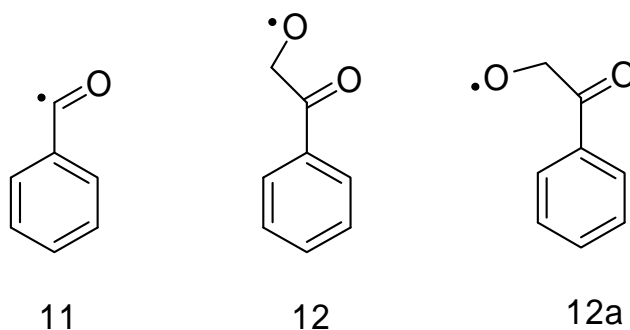


The kinetic of the reaction between phenyl radical and CO has been investigated by the cavity ring-down spectrometric technique under high pressure conditions. The second-order rate constant obtained at 397 K to be $1.70 \pm 0.38 \times 10^{-10} \text{ cm}^3 \text{ mole}^{-1} \text{ s}^{-1}$ by Nam and coworkers.^[301, 302] According to MP2 calculations the activation barrier for the reaction of **1** with CO is 3.33 kcal/mol while B3LYP predicts a very small activation barrier of only 0.73 kcal/mol.^[302]

The reaction of the benzoyl radical with molecular oxygen to yield the benzoylperoxy radical (**12**).^[298, 303] Peroxy radical and also their tetroxide dimers, play an important role in atmospheric chemistry.^[304]

From the original EPR. study of the benzoyl radical by Krusic and Rettig,^[305] it has become apparent that an unpaired electron is located on the sp^2 orbital (σ -orbital) of the carbonyl carbon. The EPR spectra of **11** and *para*-substituted species have been obtained

in solutions at low temperatures those are classified as σ -type radicals.^[306, 307] The EPR spectrum could also be obtained by time resolved EPR spectroscopy in solution.



The absorption spectra of the benzoyl radicals (**11**) have obtained by Matsuda *et al.*^[308] which also provides some additional support for the localization of an unpaired electron on the carbonyl group. The intensity of the absorption band of the benzoyl radical was very weak those are centered in the region 600-700 nm and was enhanced by the introduction of a substituent. These facts suggest the participation of a non-bonded orbital such as a σ -orbital in the transition. In the case of π -radicals such as the benzyl radical, the transition energy was small compared with that of the alkyl radicals since an unpaired electron conjugates with a π -orbital on the phenyl ring.^[308]

In this chapter, we report the synthesis and the first matrix isolated IR spectra of the benzoyl radical (**11**) in an argon matrix. This allows to record the complete mid IR spectrum of **11**, which has so far been unknown. The thermal reaction of **11** with molecular oxygen and the photochemistry of the intermediates is also reported. Finally we have performed density functional calculations (DFT) to provide the molecular and transition states parameters of the reaction between the phenyl radical and CO.

7.3.2. Results and Discussion

Benzoyl Radical. As mentioned above in order to synthesize phenyl radical (**1**) we carried out FVP of azobenzene (**4**) at temperatures above 600 °C in the gas phase with subsequent trapping of thermolysis products in large excess of argon at 15 K. Under this conditions the high yield of **1** can be produced.^[309, 310]

In order to synthesize benzoyl radical (**11**), FVP experiments was carry out in the presence of 2 % CO doped in argon at 10 K resulted in the formation of a new product with a strong IR band at 1824.4 cm⁻¹ that was not present in the absence of CO. At 10 K the matrix is very rigid and does not permit the diffusion of CO. If the matrix was annealed

at 30 – 35 K, all IR bands assigned to the new product increased (Figure 7.3.1) in intensity while that of phenyl radical **1** decreased. This indicates that the new compound is formed by a bimolecular reaction between **1** and CO with a very low or absent activation barrier. It is tempting to assign the new IR band at 1824.4 cm^{-1} to the C=O str. vibration of the benzoyl radical **11** (Figure 7.3.1). This is confirmed by comparison with the transient IR spectrum of **11** obtained by time resolved IR spectroscopy. The C=O stretching vibration of **11** in argon at 1824.4 cm^{-1} very nicely matches the corresponding absorption in CCl_4 at 1824 cm^{-1} .

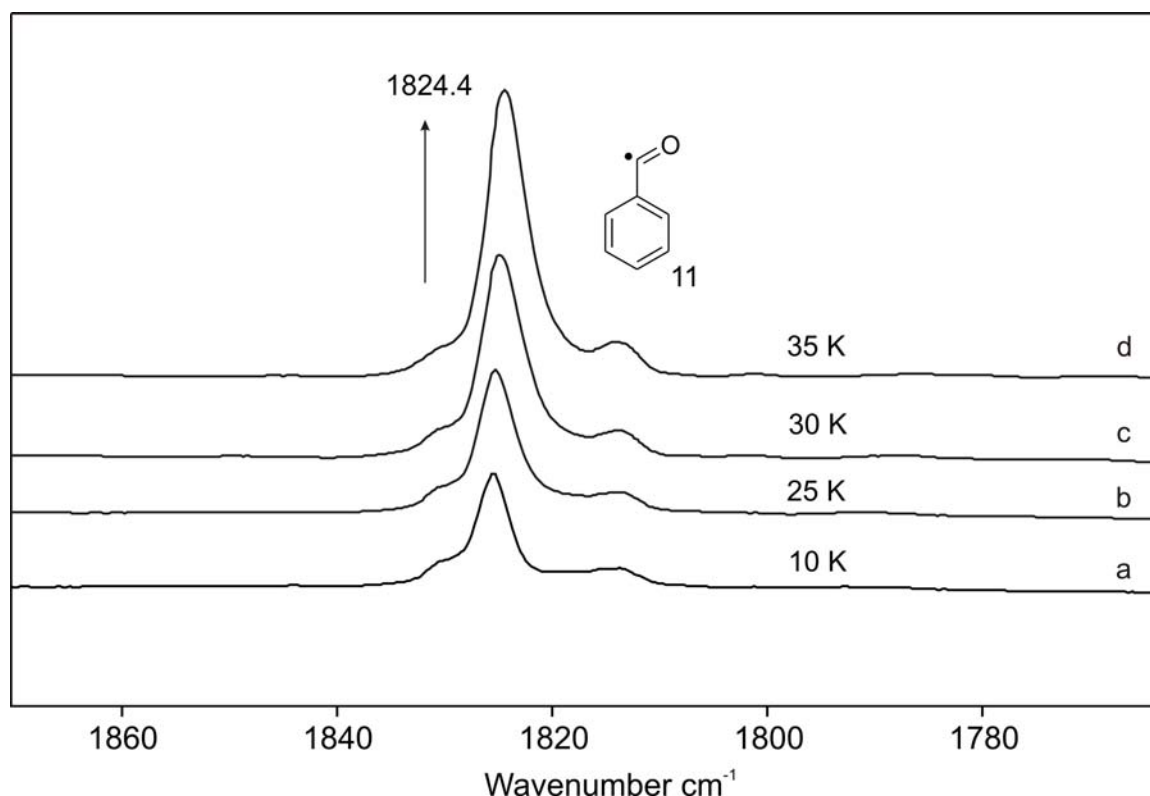


Figure 7.3.1. IR spectra showing the annealing of **1** doped 1 % CO, matrix-isolated in argon at 10 K. Band at 1824.4 cm^{-1} pointing upwards is appearing during annealing and assigned to **11**. (a) At 10 K (b) After annealing at 25 K for 10 min. (c) After annealing at 30 K for 10 min. (d) After annealing at 35 K for 10 min

The assignment of the IR spectrum of **11** was further confirmed by comparison of the spectrum in solid argon with calculations at the UB3LYP/cc-pVTZ level of theory, which nicely reproduce the experimental spectrum (Figure 7.3.2, Table 7.3.1). Matrix-isolated spectra of benzoyl radical (**d₅-11**) have also been obtained in argon matrix. Again expected spectra of **d₅-11** is in an excellent agreement with the results of DFT calculations (Figure 7.3.3, Table 7.3.1).

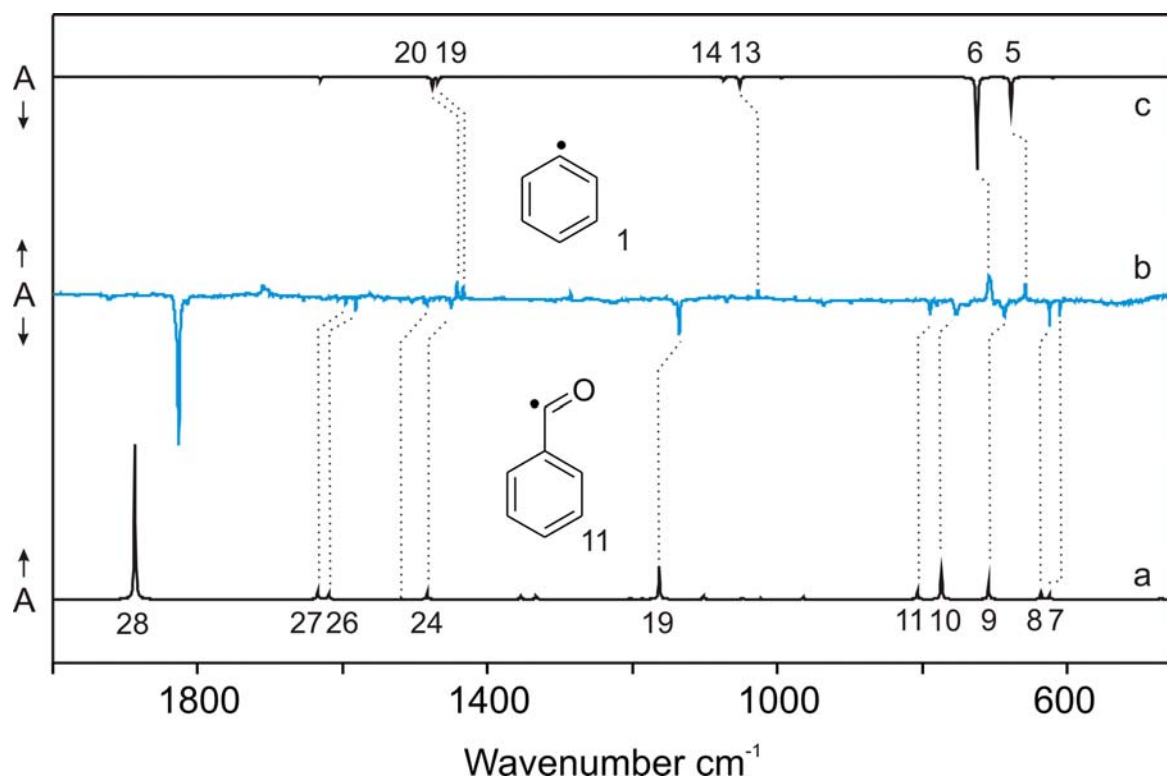


Figure 7.3.2. Difference IR spectra showing the photochemistry ($\lambda > 350\text{nm}$) of **11**, matrix-isolated in argon at 10 K. Bands pointing downwards are disappearing during irradiation and assigned to **11**. Bands pointing upwards are appearing and assigned to **1**. (a) IR spectrum of **11** calculated at the UB3LYP/cc-pVTZ level of theory. (b) Difference IR spectrum after 30 min irradiation. (c) IR spectrum of **1** calculated at the UB3LYP/cc-pVTZ level of theory.

Table 7.3.1. IR spectroscopic data of two isotopomers of the benzoyl radical **11**

Mode ^a	C ₆ H ₅ CO (1)		C ₆ D ₅ CO (d ₅ - 1)		Sym.	Assignment
	Argon ^b	DFT ^c	Argon ^b	DFT ^c		
28	1824.4 (100)	1886.2 (100)	1815.8 (100)	1885.9 (100)	A'	C=O str.
27	1594.8 (2)	1635.0 (6)	1556.8 (6)	1597.3 (6)	A'	C=C str.
26	1581.0 (9)	1619.0 (4)	1550.0 (8)	1579.3 (5)	A'	C=C str.
25	-	1518.8 (0)	1356.3 (<1)	1386.4 (1)	A'	C-H def.
24	1450.3 (4)	1484.0 (5)	1327.1 (7)	1357.7 (3)	A'	C-H def.
23	1307.8 (<1)	1354.6 (2)	-	1061.5 (0)	A'	C-H def.
22	1288.0 (1)	1333.8 (2)	1297.0 (3)	1328.9 (3)	A'	C-H def./C-C str
21	-	1203.4 (0)	866.6 (<1)	884.1 (0)	A'	C-H def.
20	-	1187.6 (0)	845.5 (2)	862.5 (1)	A'	C-H def.
19	1136.2 (21)	1163.5 (21)	1100.1 (32)	1124.3 (13)	A'	C-H def./C-C str.
18	1070.4 (3)	1102.0 (2)	817.2 (~1)	834.4 (1)	A'	C-H def.
17	-	1048.6 (1)	831.5 (13)	850.8 (6)	A'	C-H def.
16	-	1026.8 (0)	-	861.6 (0)	A''	C-H def.
15	-	1022.2. (0)	959.6 (5)	978.8 (0)	A'	ring str.
14	-	1007.0 (0)	-	820.8 (0)	A''	C-H def.
13	935.8 (2)	965.8 (1)	765.1 (3)	791.4 (1)	A''	C-H def.
12	-	872.4 (0)	-	678.0 (0)	A''	C-H def.
11	789.7 (11)	807.6 (5)	749.3 (6)	762.2 (3)	A'	C-O str./ ring str.
10	755.9 (12)	774.8 (18)	545.5 (27)	557.7 (11)	A''	C-H def.
9	687.8 (10)	709.3 (10)	624.9 (2)	643.5 (2)	A''	C-H def.
8	624.7 (16)	637.7 (4)	603.7 (15)	618.9 (5)	A'	CCO def./ring str.
7	610.4 (10)	625.9 (3)	587.0 (5)	602.0 (1)	A'	CCO def./ring str.
6	-	471.3 (1)	-	418.1 (2)	A''	C-H def.
5	-	442.2 (0)	-	431.2 (0)	A'	CCC def.
4	-	418.7 (0)	-	363.5 (0)	A''	C-H def.

[a] Mode numbers based on the C₆H₅¹²C¹⁶O isotopomer. [b] (Argon matrix at 10 K. Vibrational numbers in cm⁻¹ and relative intensities in parenthesis.) [c] Calculated at the UB3LYP/cc-pVTZ level of theory.

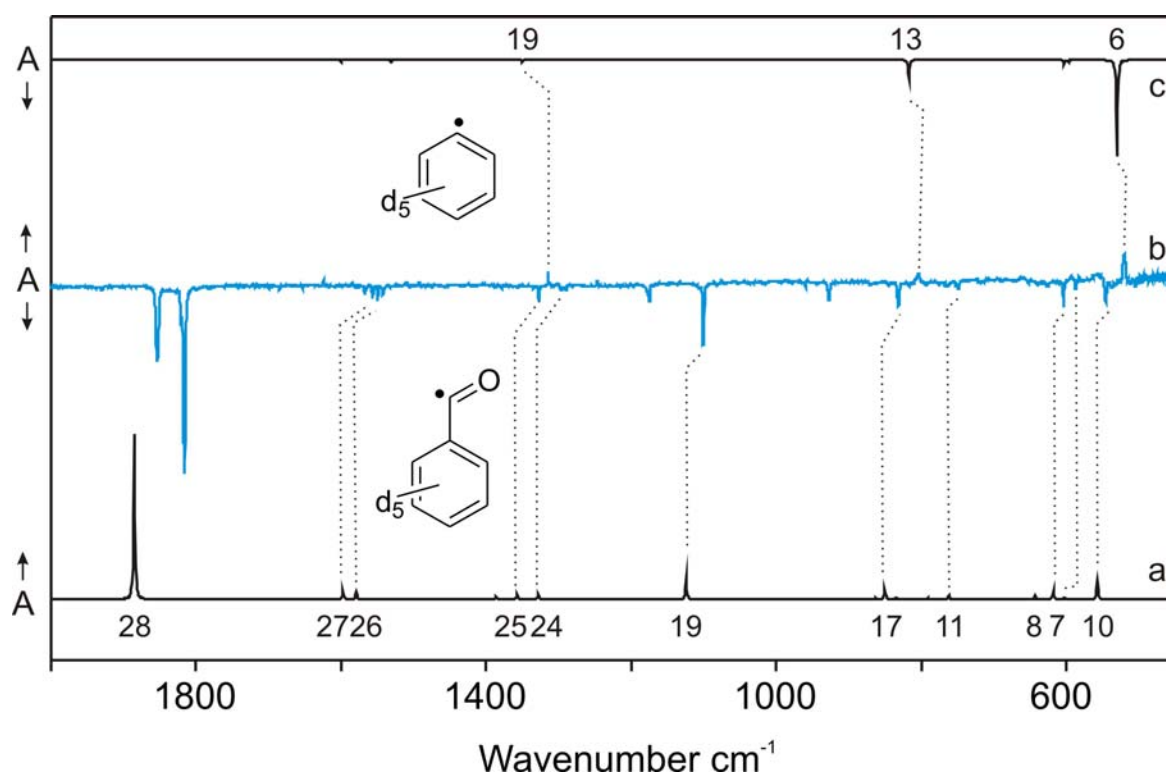
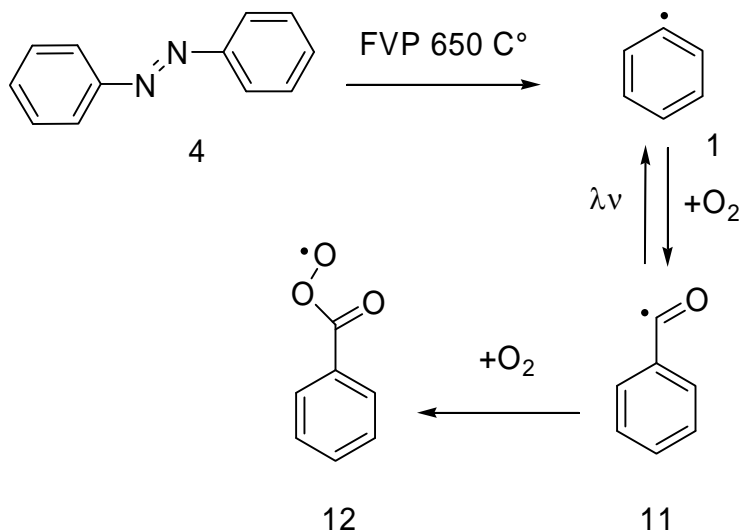


Figure 7.3.3. Difference IR spectra showing the photochemistry ($\lambda > 350\text{nm}$) of $d_5\text{-11}$, matrix-isolated in argon at 10 K. Bands pointing downwards are disappearing during irradiation and assigned to $d_5\text{-11}$. Bands pointing upwards are appearing and assigned to $d_5\text{-11}$. (a) IR spectrum of $d_5\text{-11}$ calculated at the UB3LYP/cc-pVTZ level of theory. (b) Difference IR spectrum after 30 min irradiation. (c) Difference IR spectrum after 15 min irradiation. (d) IR spectrum of $d_5\text{-1}$ calculated at the UB3LYP/cc-pVTZ level of theory.

According to DFT calculation the reaction $\mathbf{1} + \text{CO} \rightarrow \mathbf{11}$ is exothermic by 24.58 kcal/mol with a barrier of 0.7 kcal/mol at the B3LYP and 3.3 kcal/mol at the MP2 level of theory.^[311] The reaction between $\mathbf{1}$ and CO in solid argon is rapid at temperatures above 30 K where the diffusion of small molecules in argon becomes possible. From that we conclude that the thermal barrier for this reaction must be very small or absent, in agreement with the theoretical predictions.

However we performed potential energy surface (PES) calculation for the reactants and benzoyl radical using partial geometry optimization. The distance between C-C bond of the forming radical was kept constant at various values from 1.4 Å up to 5.0 Å, while other parameters were optimized. The plot of the potential energy curve against the length of the forming C–C bond is shown in Figure 7.3.4. The small barrier is predicted when CO approaches to $\mathbf{11}$ until the benzoyl radical is formed at the UB3LYP/cc-pVTZ level of theory.

The formation of **11** from **1** and CO is photochemically reversible. Irradiation of matrix-isolated **11** at 10 K with the UV light ($\lambda > 260$ nm) leads back to **1** and CO (Figure 7.3.2). Subsequent annealing at 35 K results again in the formation of **11** (Scheme 7.3.1).



Scheme 7.3.1. Reaction of the phenyl radical (**1**) with carbon monoxide and reaction of benzoyl radical (**11**) with $^3\text{O}_2$.

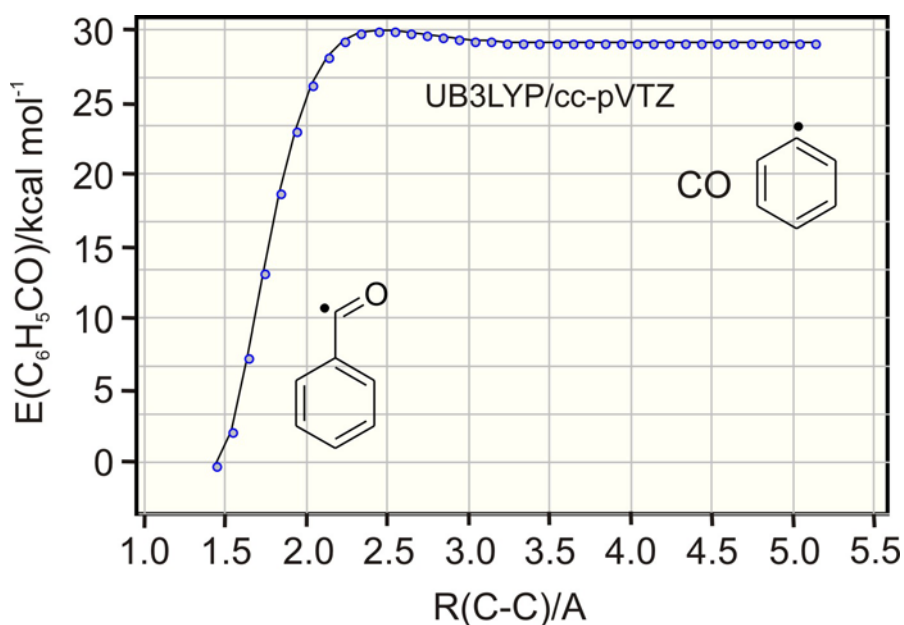


Figure 7.3.4. The $\text{C}_6\text{H}_5\text{-CO}$ dissociation potential energy surface calculated at the B3LYP/cc-pVTZ level of theory.

Benzoyl Peroxy Radical. Under the conditions of matrix isolation the formation of **12** requires that the phenyl radical **1** first reacts with CO to give **11**, which in a second thermal step reacts with O₂ to give **12**. Both thermal steps depend on the diffusion of CO and O₂, respectively, in the solid matrix. Since **1** is also highly reactive towards oxygen, mixtures of **12** and the phenylperoxy radical **2** are expected to be formed if mixtures of CO and O₂ are used as trapping reagents in argon. To increase the yield of **12** we therefore used an excess of CO with respect to O₂ in the experiments.

If a mixture approximately 0.5 % O₂ and 2 % CO doped in argon matrix containing of **1** and annealed up to 40 K results of the formation benzoyl peroxy radical (**12**) as major product. The formation of **12** takes place via **11** that monitored during annealing experiments. The formation of **12** was induced by either warming the argon matrix from 10 to 40 K with a rate of approximately 1 K min⁻¹ (free warming) or annealing the matrix at a defined temperature between 30 and 40 K for several minutes. In free warming experiments the intensity of the carbonyl stretching vibration of **11** at 1824.4 cm⁻¹ starts to increase at a temperature of 30 K up to 35 K. From 35 K the vibrational mode of **11** starts to decrease and simultaneously a new product with the prominent C=O stretching vibration at 1820.9 is formed (Figure 7.3.5, Table 7.3.2).

If ¹⁸O₂ is used, these bands show only very small isotopic shifts of less than 2 cm⁻¹, indicating that the oxygen atom of the C=O bond comes from CO and not from O₂. However, a band at 1107.0 cm⁻¹ shows a huge red-shift of -68.1 cm⁻¹ which clearly indicates a OO stretching vibration. Other large red-shifts are found for a absorption at 768.2 cm⁻¹ (-21.6 cm⁻¹) which is thus assigned to a CO stretching vibration. A comparison of the newly formed bands in O₂-doped matrices with DFT calculations (UB3LYP/cc-pVTZ) of the benzoyl peroxy radical (**12**) shows an excellent agreement. The two perdeuterated isotopomers d₅-**12** and d₅-¹⁸O₂-**12** were also synthesized and a careful analysis of their spectra confirms the assignment of the benzoyl peroxy radical (Figures 7.3.6-7.3.8) (Table 7.3.2). These experiments clearly show that the benzoyl radical (**1**) reacts with molecular oxygen in under matrix isolation conditions to produce **12**.

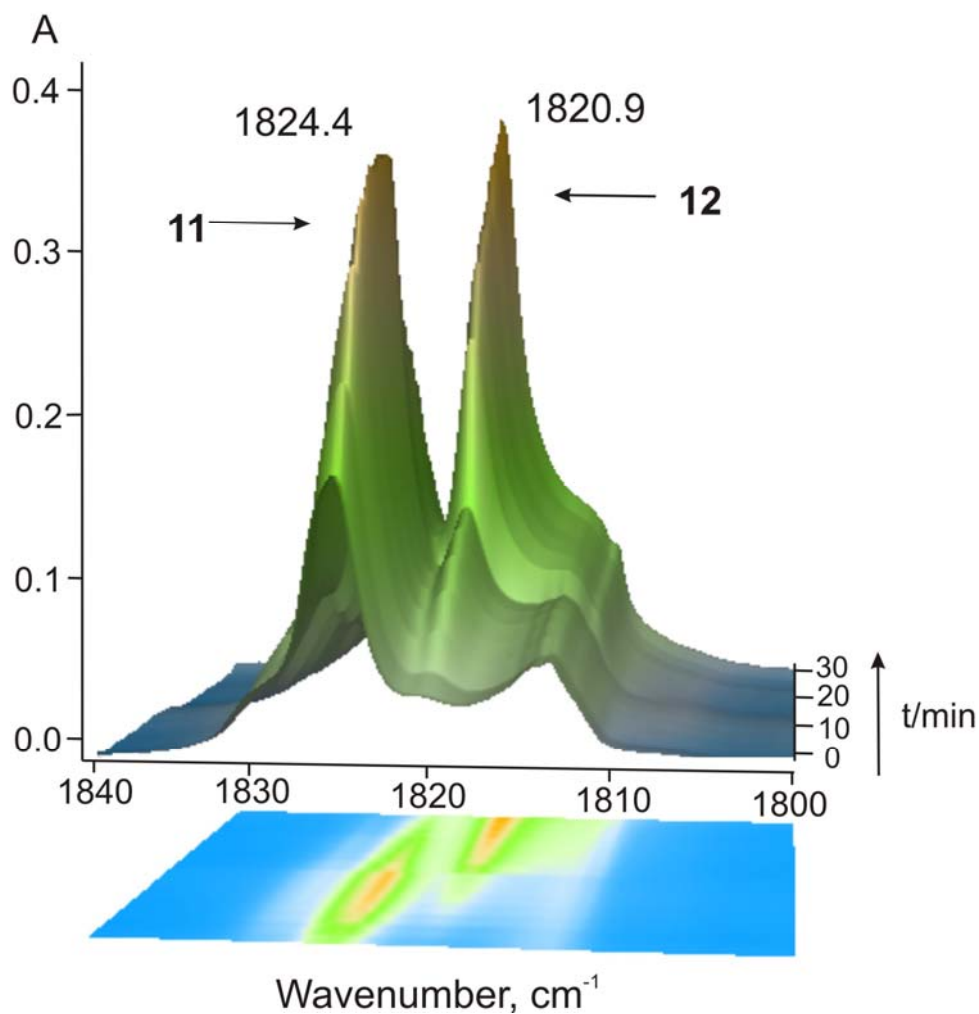


Figure 7.3.5. IR spectra of argon matrix containing phenyl radical (**1**) doped 2 % CO and 0.5 % O₂ during the slow warming from 10 K ($t=0$ min) to 40 K ($t=30$ min). Bands are assigned to benzoyl radical (**11**) and benzoyl peroxy radical (**12**).

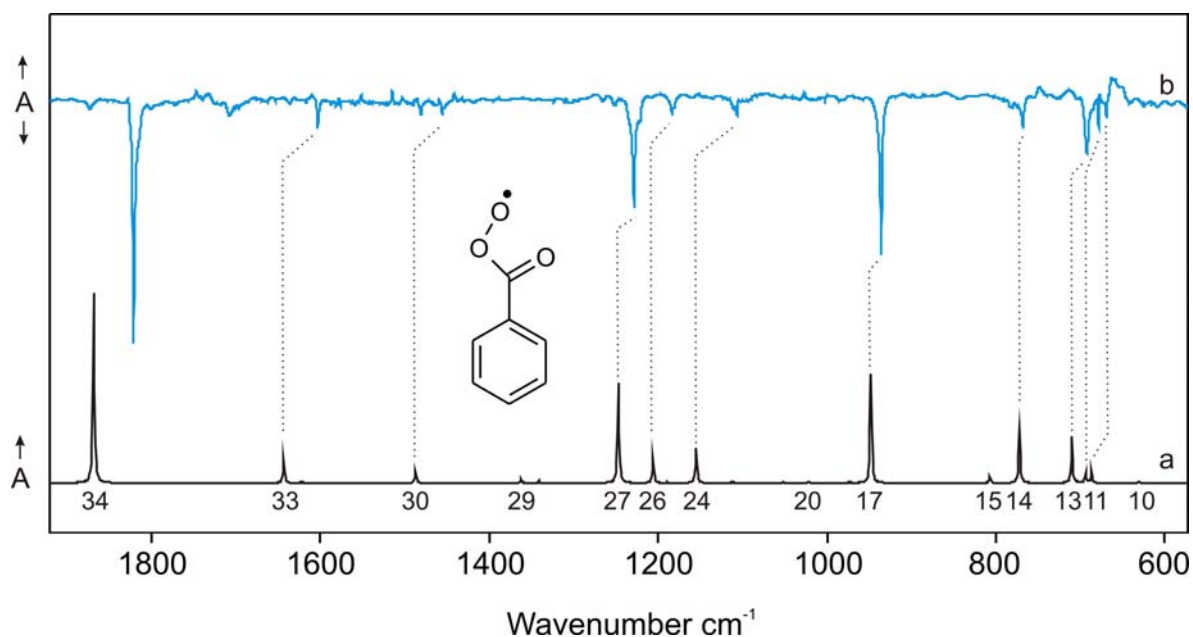


Figure 7.3.6. Difference IR spectra showing the photochemistry ($\lambda > 350\text{nm}$) of **12**, matrix-isolated in argon at 10 K. Bands pointing downwards are disappearing during irradiation and assigned to **12**. (a) IR spectrum of **12** calculated at the UB3LYP/cc-pVTZ level of theory. (b) Difference IR spectrum after 60 min irradiation.

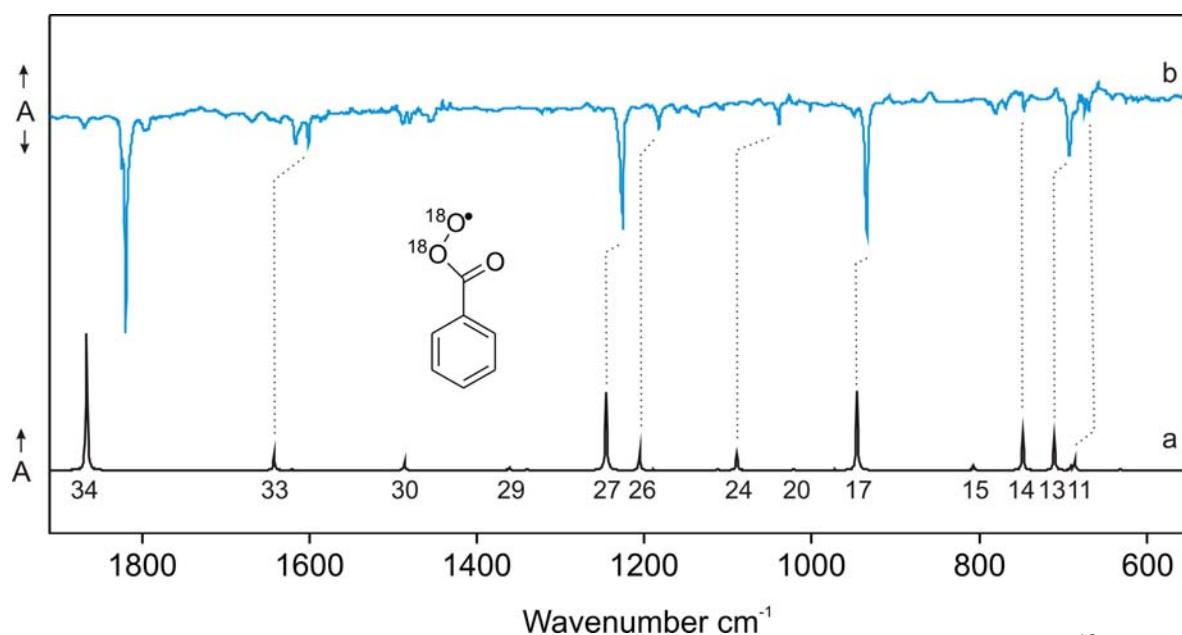


Figure 7.3.7. Difference IR spectra showing the photochemistry ($\lambda > 350\text{nm}$) of $^{18}\text{O}_2$ -**12**, matrix-isolated in argon at 10 K. Bands pointing downwards are disappearing during irradiation and assigned to $^{18}\text{O}_2$ -**12**. (a) IR spectrum of $^{18}\text{O}_2$ -**12** calculated at the UB3LYP/cc-pVTZ level of theory. (b) Difference IR spectrum after 60 min irradiation.

Table 7.3.2. IR spectroscopic data of four isotopomers of the benzoyl peroxy radical **12**

Mo de ^a	C ₆ H ₅ CO ¹⁶ O ¹⁶ O (3)		C ₆ H ₅ CO ¹⁸ O ¹⁸ O (3)		C ₆ D ₅ CO ¹⁶ O ¹⁶ O (3)		C ₆ D ₅ CO ¹⁸ O ¹⁸ O (3)		Assignment
34	1820.9 (100)	1868.2 (100)	1820.6 (100)	1867.9 (100)	1821.1 (100)	1867.8 (100)	1821.3 (100)	1867.6 (100)	C=O str.
33	1603.0 (10)	1643.1 (12)	1601.7 (13)	1643.1 (12)	1567.1 (22)	1605.1 (15)	1567.2 (48)	1605.1 (15)	C=C str.
32	-	1622.0 (1)	-	1622.0 (1)	-	1583.4 (1)	-	1583.4 (1)	C=C str.
31	-	1529.1 (0)	-	1529.1 (0)	1378.3 (10)	1404.8 (8)	1377.8 (20)	1404.6 (8)	C-H def.
30	1455.8 (<1)	1487.6 (6)	1455.2 (<1)	1487.6 (6)	1333.4 (5)	1364.0 (5)	1333.3 (12)	1363.9 (5)	C-H def.
29	-	1362.0 (2)	1322.7 (<1)	1362.0 (2)	1042.7 (3)	1066.3 (2)	1042.9 (4)	1064.8 (4)	C-H def.
28	-	1341.2 (1)	1309.8 (<1)	1340.9 (1)	1300.2 (4)	1336.6 (2)	1299.8 (8)	1336.5 (2)	C-H def./C-C str
27	1228.4 (38)	1247.8 (53)	1225.8 (63)	1246.6 (57)	1174.7 (49)	1195.6 (41)	1174.4 (54)	1192.8 (41)	C-C str./ C-H def.
26	1183.8 (8)	1206.6 (13)	1183.1 (10)	1206.6 (14)	866.8 (9)	883.4 (5)	866.7 (22)	883.3 (5)	C-H def.
25	-	1189.9 (0)	-	1189.9 (0)	846.2 (1)	862.7 (1)	846.6 (6)	862.6 (1)	C-H def.
24	1107.0 (7)	1155.2 (19)	1038.9 (8)	1090.6 (12)	1106.3 (12)	1154.0 (29)	1033.4 (18)	1092.2 (12)	O-O str.
23	-	1112.6 (1)	-	1112.7 (1)	824.3 (4)	842.3 (1)	824.3 (10)	842.2 (2)	C-H def.
22	-	1053.0 (0)	-	1052.9 (0)	-	839.2 (3)	813.7 (5)	838.7 (3)	C-H def.
21	-	1028.5 (0)	-	1028.5 (0)	-	867.6 (0)	-	867.6 (0)	C-H wag.
20	1002.3 (3)	1022.2 (1)	1002.3 (3)	1022.2 (1)	959.8 (7)	978.6 (1)	959.7 (14)	978.5 (1)	C-C str (ring)
19	-	1008.9 (0)	-	1008.9 (0)	-	822.7 (0)	-	822.7 (0)	C-H wag.
18	-	973.0 (1)	950.3 (<1)	973.0 (1)	-	815.3 (0)	-	815.2 (0)	C-H wag.
17	935.8 (65)	948.7 (57)	934.4 (67)	946.6 (58)	927.2 (60)	941.2 (49)	926.0 (98)	939.3 (49)	C-O str.
16	-	870.9 (0)	-	870.9 (0)	-	677.2 (0)	-	677.2 (0)	C-H wag.
15	783.6 (5)	807.5 (4)	788.5 (2)	807.3 (4)	701.7 (3)	719.6 (2)	701.6 (4)	719.0 (2)	C-H wag.
14	768.2 (10)	772.7 (28)	746.6 (10)	748.9 (28)	762.8 (9)	768.0 (26)	740.7 (12)	742.7 (24)	C-O str.
13	692.5 (27)	710.5 (25)	692.3 (20)	710.4 (24)	536.4 (14)	548.0 (16)	536.4 (32)	547.9 (16)	C-H wag.
12	678.6 (11)	694.7 (5)	678.6 (5)	690.0 (3)	651.8 (10)	666.8 (5)	648.9 (10)	663.9 (4)	ring skel.
11	668.5 (8)	687.2 (7)	668.2 (7)	686.4 (7)	604.0 (2)	620.6 (3)	604.4 (6)	620.2 (3)	ring out of plane
10	-	631.7 (1)	-	631.6 (1)	590.9 (<1)	605.5 (0)	591.2 (2)	605.5 (0)	ring skel.
9	-	462.2 (1)	-	456.2 (1)	-	452.0 (1)	-	446.1 (1)	C-C-O def.
8	-	443.2 (0)	-	442.8 (0)	-	398.8 (0)	-	398.5 (0)	ring out of plane

[a](Mode numbers based on the C₆H₅¹²C¹⁶O¹⁶O isotopomer.) [b] (Argon matrix at 10 K. Vibrational numbers in cm⁻¹ and relative intensities in parenthesis.) [c] (Calculated at the UB3LYP/cc-pVTZ level of theory.)

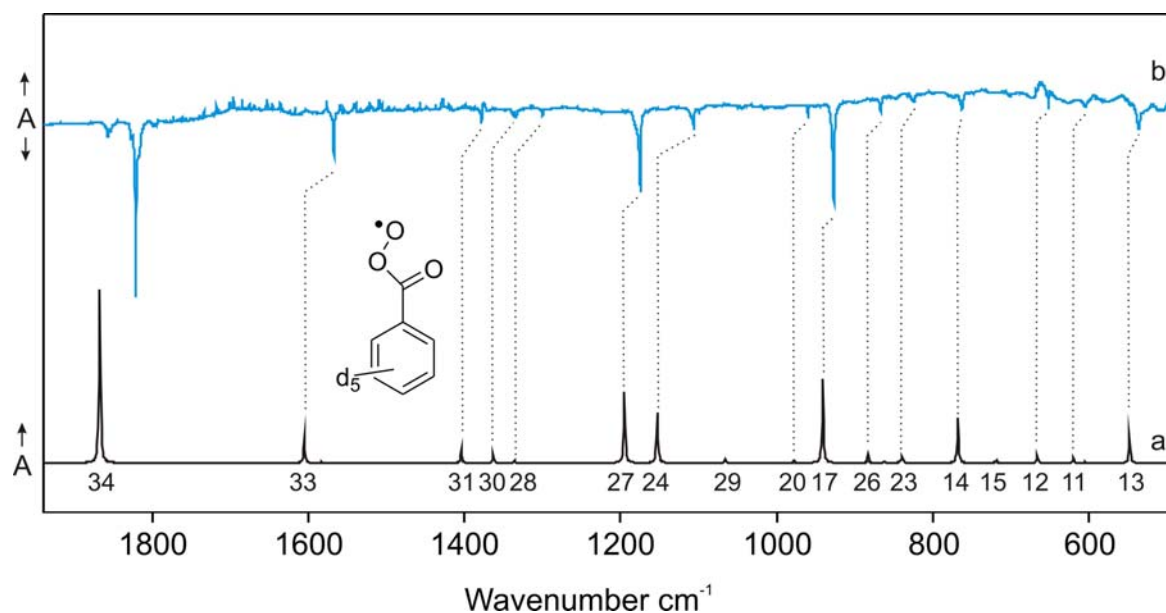


Figure 7.3.8. Difference IR spectra showing the photochemistry ($\lambda > 350\text{nm}$) of d_5 -**12**, matrix-isolated in argon at 10 K. Bands pointing downwards are disappearing during irradiation and assigned to d_5 -**12**. (a) IR spectrum of d_5 -**12** calculated at the UB3LYP/cc-pVTZ level of theory. (b) Difference IR spectrum after 60 min irradiation.

We also performed PES calculation using partial geometry optimization between reactants (**11** and O_2) and benzoyl peroxy radical (**12**). The length of the forming C-O bond was kept fixed (between 1.4 up to 5.0 Å) whereas all parameters were optimized (Figure 7.3.9). As you can see from the plot of the potential energy curve against the length of the forming bond, the energy smoothly decreases while benzoyl peroxy radical is formed. According to this result there is no definitive transition state exists of the reaction of **11** with O_2 .

Benzoyl peroxy radical (**12**) was obtained by quenching of benzoyl radical (**11**) in the solution with oxygen, decaying with a measured lifetime of $\tau = 5.2 \pm 0.2 \mu\text{s}$.^[298] Laser photolysis studies reveal that the rate constants for the reaction between the benzoyl radical and oxygen are ca. $4 \times 10^9 \text{ M}^{-1} \text{ s}^{-1}$ in toluene, acetone, and ethyl acetate.^[312]

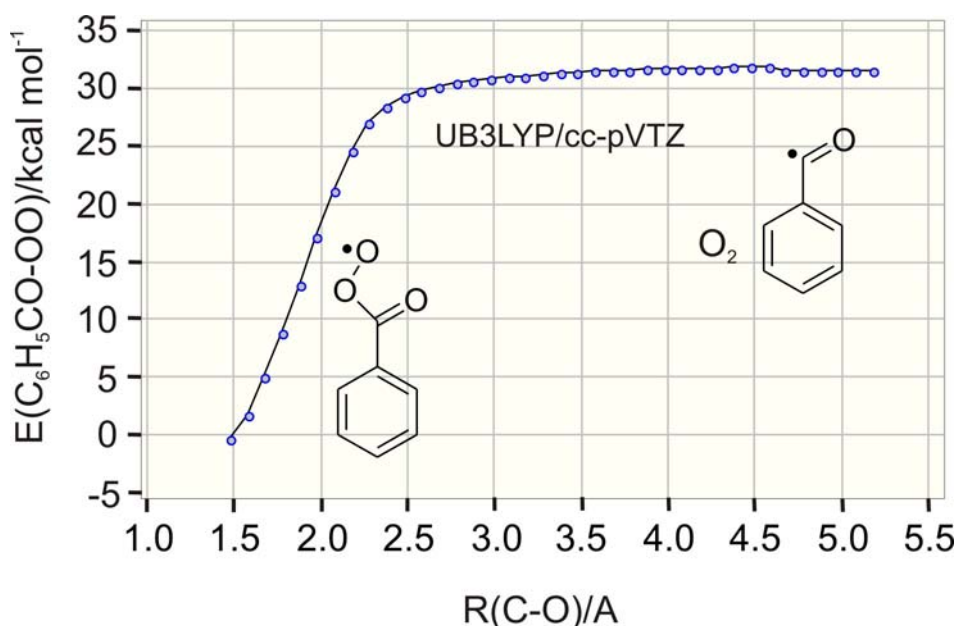


Figure 7.3.9. The $\text{C}_6\text{H}_5\text{CO-OO}$ dissociation potential energy surface calculated at the UB3LYP/cc-pVTZ level of theory.

Two rotamers **12a** and **12b** are possibly formed in the experiments. According to UB3LYP/cc-pVTZ calculations the *s*-*Z* conformer **12a** is by 3.47 kcal/mol (ZPE = 3.31 kcal/mol) more stable than the *s*-*E* conformer **12b**. The activation barrier for the **12a** → **12b** isomerization is calculated to 5.03 kcal/mol (Figure 7.3.10). The transition state structure is found to be nonplanar, exhibiting OCOO dihedral angle to be 84.29°. The calculated IR spectrum of **12a** is in good agreement with the experimental spectrum of **12a**, and there is no evidence for the formation of the less stable conformer **12b**.

UV irradiation ($\lambda > 260$ nm) of **12** at 10 K results in the disappearance of all bands assigned to **12** and formation of CO_2 and several other new bands, in particular very strong and broad absorption in the region between 2140 and 2120 cm^{-1} . If $^{18}\text{O}_2/^{16}\text{O}_2$ mixtures are used in the experiment new bands around 2089 cm^{-1} appear, which clearly indicates that one or several ketenes are formed. In addition, the three isotopomers C^{16}O_2 , $\text{C}^{18}\text{O}^{16}\text{O}$, and C^{18}O_2 are found (Figure 7.3.11). We assume that the photolysis of **12** results in ring-opening and formation of ketenes. However, due to the low intensity of other IR bands of the ketenes (presumably several isomers or conformers are formed) a definitive assignment was not possible.

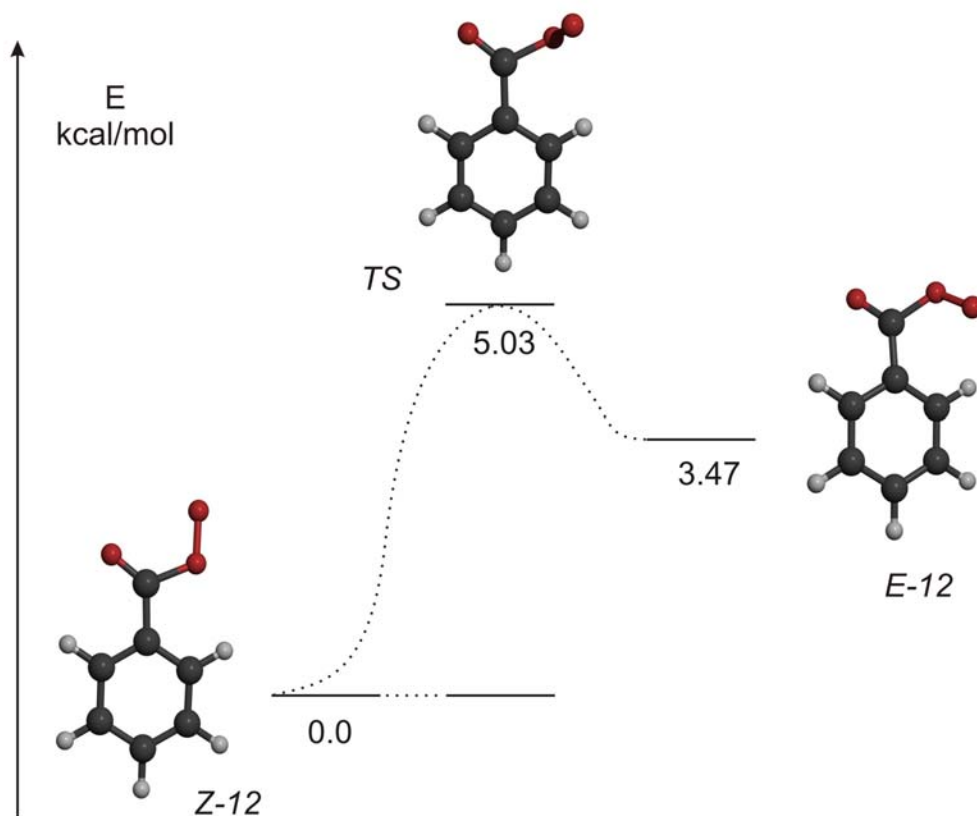


Figure 7.3.10. Theoretical isomerisation partway between two isomers of benzoyl peroxy radical (12). Stationary points and transition state were performed by use B3LYP/cc-pVTZ method.

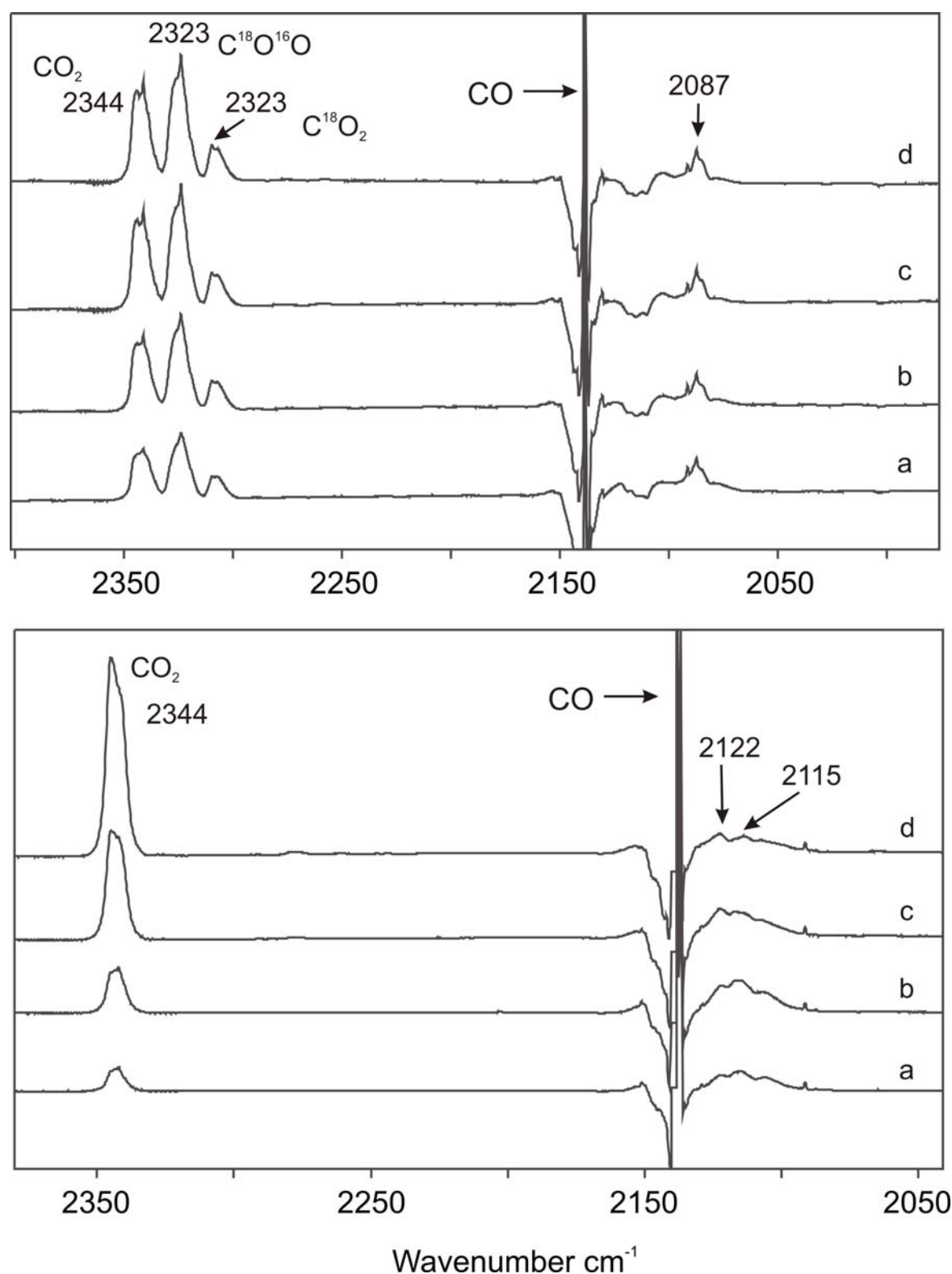


Figure 7.3.11. Bottom: Difference IR spectra showing the photochemistry ($\lambda > 350\text{nm}$) of **11**, matrix-isolated in argon at 10 K. Bands pointing downwards are disappearing during irradiation and assigned to **11**. (a) difference IR spectrum after 5 min irradiation (b) after 15 min. (c) after 30 min. (d) after 60 min. Top: Difference IR spectra showing the photochemistry ($\lambda > 350\text{nm}$) of $^{18}\text{O}_2$ -**11**, matrix-isolated in argon at 10 K. Bands pointing downwards are disappearing during irradiation and assigned to $^{18}\text{O}_2$ -**11**. (a) difference IR spectrum after 5 min irradiation (b) after 15 min. (c) after 30 min. (d) after 60 min.

7.3.3. Summary

The phenyl radical (**1**) is a highly reactive species that even under the conditions of matrix isolation rapidly reacts with CO and O₂ as long as diffusion of these small molecules in the solid matrix is possible. With CO the benzoyl radical **11** is formed which could be isolated and spectroscopically characterized. Interestingly, conditions could be found where mixtures of CO and O₂ in the same matrix produce good yields of the benzoyl peroxy radical **12** by subsequent reactions of the phenyl radical **1** with CO and O₂. Obviously, the reaction of **1** with CO can compete with the reaction with O₂. This is in line with DFT and ab initio calculations which predict very shallow or absent activation barriers for both reactions. The formation of the radicals **11** and **2** in argon matrices depends on the statistical distribution and rates of diffusion of CO and O₂. An excess of CO compared to O₂ thus results in the preferential formation of **11** which subsequently reacts with O₂ to **12**.

Chapter 7.4. Phenyl Radical - Water

7.4.1. Introduction

The phenyl radical (**1**) as well as the hydroxyl radical OH are highly reactive intermediates that play key roles in many reaction mechanisms. Gas phase reactions of these radicals are of particular importance to understand processes such as the combustion of hydrocarbons at high temperatures or the degradation of aromatics in the troposphere at ambient temperature. The reaction with the hydroxyl radical is the only known pathway for the removal of benzene (**13**) from the troposphere. Due to this fundamental importance, a large number of experimental and theoretical studies have been published in this field.^[313-320]

An interesting, not much studied aspect of radical chemistry is the role of weakly bound non-covalent complexes.^[321, 322] Complexes between radicals and water and other highly polar compounds are expected to be of importance to radical chemistry since these complexes might stabilize the radicals and thus modulate their reactivity.^[321]

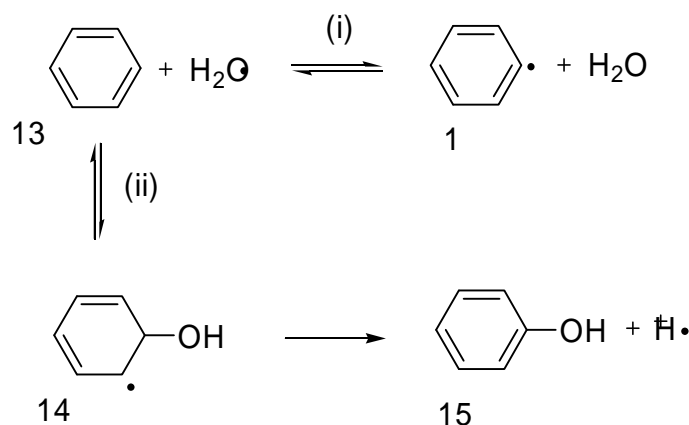
In this chapter, we present evidence that both the phenyl radical (**1**) and the hydroxyl radical form non-covalent complexes which are of importance for understanding the reactivity of these species. We described the formation of a weakly bound complex between the phenyl radical **1** and water under the conditions of matrix isolation.^[323] This complex proved to be photolabile, and with visible light irradiation reacted to a complex between the hydroxyl radical and benzene. We also found that this second complex is also photolabile and irradiation surprisingly results in ring-opening and formation of a highly unsaturated ketene.

Here we also describe a detailed mechanistic and computational study on the reaction between the phenyl radical and water. The sequence of reactions starts with the phenyl radical **1** interacting with water and ends with the complete destruction of the aromatic ring system under fairly mild irradiation conditions. A detailed knowledge of the elemental steps of this reaction sequence can contribute to the understanding of the highly complex processes involved in the combustion and degradation of aromatic compounds.

7.4.2. Results and Discussion

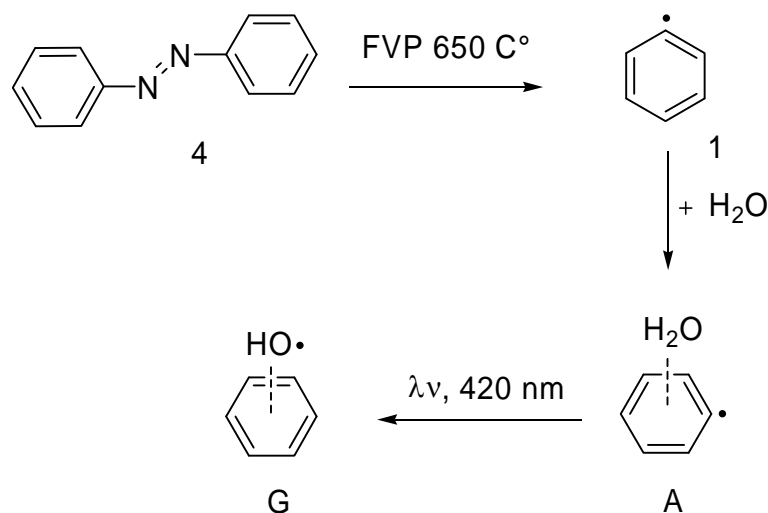
7.4.2.1 Matrix Isolation Studies the phenyl radical –water system

There are two pathways for the reaction of **13** with OH: (i) the hydrogen abstraction to give **1** and water and (ii) the addition to give the 2-hydroxy-cyclohexadienyl radical (**14**) (Scheme 7.4.1). At higher temperatures **14** can produce phenol (**15**) under loss of a hydrogen atom. The thermochemistry of these reactions was evaluated using G3 theory.^[319] According to this the hydrogen abstraction (i) is exothermic by 4.2 kcal/mol with an activation energy of 5.3 kcal/mol. The calculated reaction energy is in accordance with a simple estimation from the experimental bond enthalpies (DH₂₉₈) of the CH bond in benzene (112.9 kcal/mol) and the OH bond in water (118.8 kcal/mol), resulting in an enthalpy difference of 5.9 kcal/mol.^[273] The addition reaction (ii) is, according to the G3 calculation,^[319] more exothermic (–16.2 kcal/mol) and the barrier is shallower (2.8 kcal/mol) than that of reaction (i) (Scheme 7.4.1).



Scheme 7.4.1. Pathways of the reaction of the hydroxyl radical with benzene.

To gain insight into the systems benzene/OH and phenyl/H₂O we investigated the photochemical reaction of the phenyl radical with water in low-temperature argon matrices. As mentioned before, the phenyl radical (**1**) can be produced in high yields by flash vacuum pyrolysis of azobenzene **4** at 600°C and trapping of the products in argon at 10 K.^[310] The only by-products observed by IR spectroscopy in these matrices are benzene **13**, formed via hydrogen abstraction from surface contaminations of the pyrolysis oven and traces of acetylenes and other alkynes formed via ring-opening of the phenyl radical at higher temperatures.



Scheme 7.4.2. Synthesis of the phenyl radical (**1**) and its reaction with water

Complexes between **1** and water are generated by co-deposition of **1** and water with a large excess of argon at 10 K. In highly diluted matrices mainly the monomers – phenyl radical and water – are observed by IR spectroscopy. The monomers are easily identified by comparison with the literature data and pure samples of the matrix-isolated phenyl radical^[286, 324] and water^[84, 325, 326]. Water shows a high tendency of aggregation even in low temperature matrices. These aggregates have been extensively studied by IR spectroscopy.^[327-329] Matrices containing higher concentrations of both **1** and water show IR absorptions which are absent in matrices containing only one of these components. These absorptions are thus assigned to mixed complexes between phenyl radical and water. Annealing argon matrices containing phenyl radical and water at temperatures above 25 K allows small trapped molecules to diffuse and results in an increase of the aggregates. Dilution experiments in addition allow to differentiate dimers from higher aggregates. A combination of the results of all these experiments allows to confidently assigning sets of IR absorptions to mixed phenyl radical – water dimers.

Figure 7.4.1 shows the C–H wagging region of **1** in different sets of experiment. The spectrum marked (a) corresponds to a 1:800 molar ratio of water and argon deposited with the phenyl radical at 10 K. In this spectral region **1** has strong absorptions at 705.8 and 657.4 cm^{-1} , which have been assigned to the ν_6 and ν_5 modes, respectively (Figure 7.4.2). Water has no absorption in this region. After annealing the matrix for several minutes at 30 K new bands appear in the spectra at 711.4 and 659.8 cm^{-1} which are blue shifted from the unperturbed of phenyl radical by 5.6 and 2.4 cm^{-1} , assigned to the phenyl radical – water

dimer (Figure 7.4.1). These bands appear only when both monomers are co-deposited. Furthermore, the band intensity increases if the concentration of either of the two monomers is increased (Figure 7.4.2 spectra d). This clearly indicates that this band is due to a complex between **1** and water. Since this band appears at low concentrations of **1** and water it is assigned to a 1:1 complex. An additional band at 681.8 cm^{-1} is assigned to the benzene – water complex, in excellent agreement with the literature.^[17] Most notably main changes in the area of the out-of-plane CH deformation modes between 650 and 720 cm^{-1} (Figure 7.4.2).

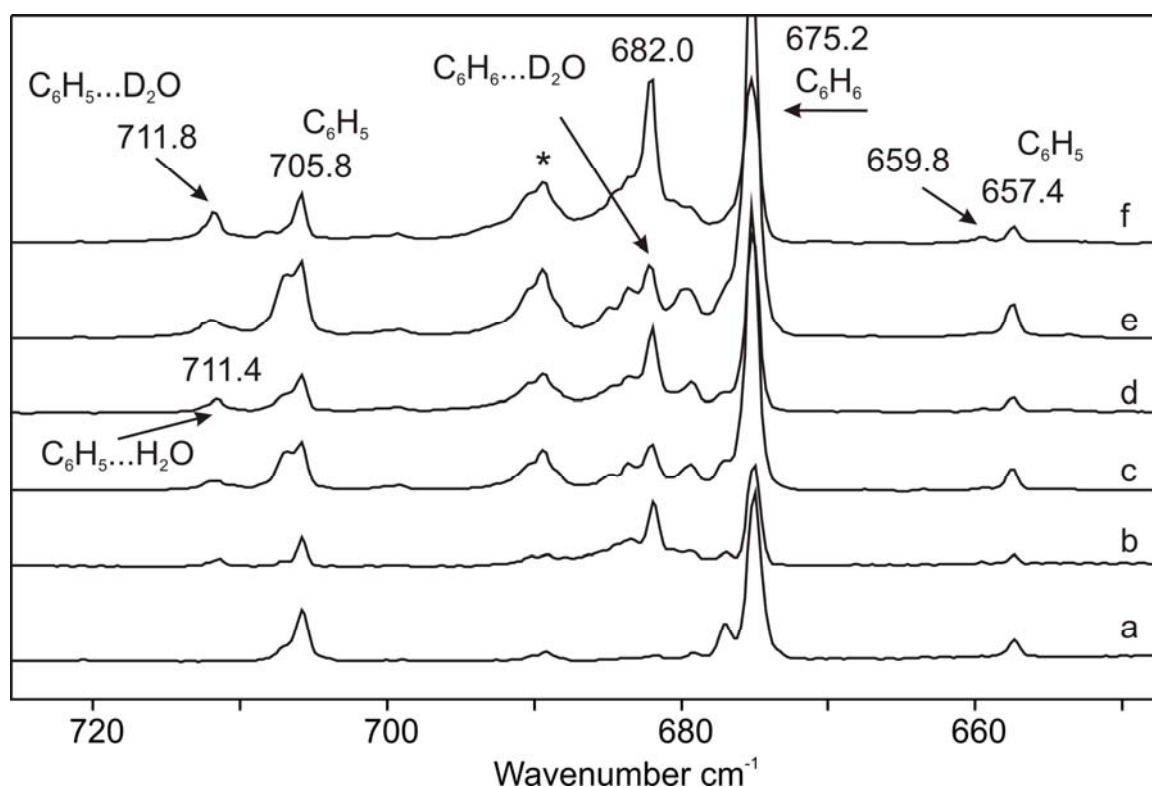


Figure 7.4.1. IR spectrum (in the range of C–H wagging mode of **1** showing the synthesis of phenyl radical in argon at 10 K. (a) IR spectrum of a matrix (Ar at 10 K) isolated the phenyl radical, containing products from FVP of **4** doped 0.1 % H_2O . (b) After annealing by free warm up to 40 K (c) IR spectrum of a matrix (Ar at 10K) isolated **1**, containing products from FVP of azobenzene doped 1 % H_2O . (d) After annealing by free warm up to 40K. (e) IR spectrum of a matrix (Ar at 10K) isolated **1**, containing products from FVP of azobenzene doped 1 % D_2O . (f) After annealing by free warm up to 40K. Precursor bands (**4**) are marked (*),

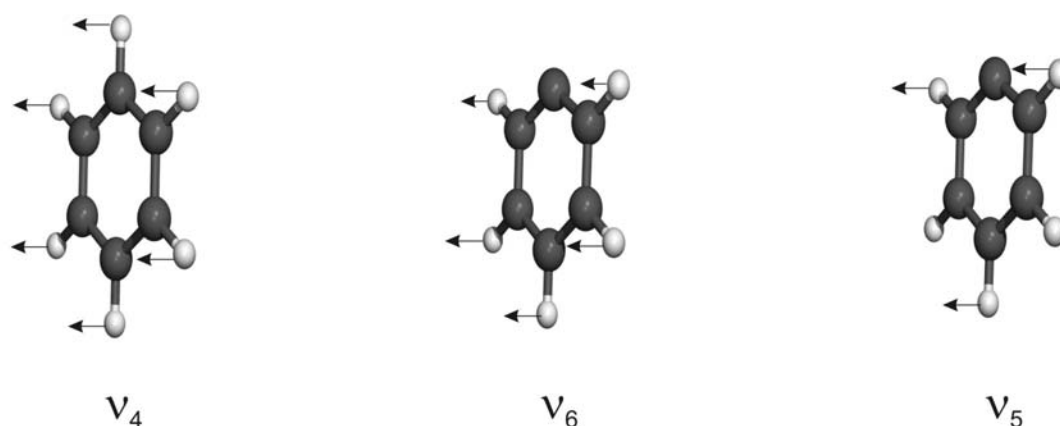


Figure 7.4.2. Displacement vectors showing some o.o.p. C-H deformation vibrations of benzene **13** and the phenyl radical **1**.

The experimentally frequency shifts of the vibrational modes of **1** interacting with H_2O and D_2O are basically identical (Figure 7.4.1 spectrums d and f). The v_6 mode of the phenyl radical at 711.4 cm^{-1} (H_2O) is shifted to 711.8 cm^{-1} (D_2O) and the v_5 mode at 659.8 cm^{-1} remains unchanged (Table 7.4.1). The experiments using $\text{d}_5\text{-1}$ confirmed the assignment of the phenyl radical – water dimer. The C–D wagging mode of the phenyl radical ($\text{d}_5\text{-1}$) (v_6) is observed at 518.0 cm^{-1} (Figure 7.4.3). On codeposition of **1** with the water and subsequently annealed above 30 K a new band appear at 522.3 cm^{-1} is blue-shifted by 4.3 cm^{-1} respect to the monomer. From the dependence of this new absorption on the concentration of both components, it is concluded that a 1:1 complex of **1** and water is formed.

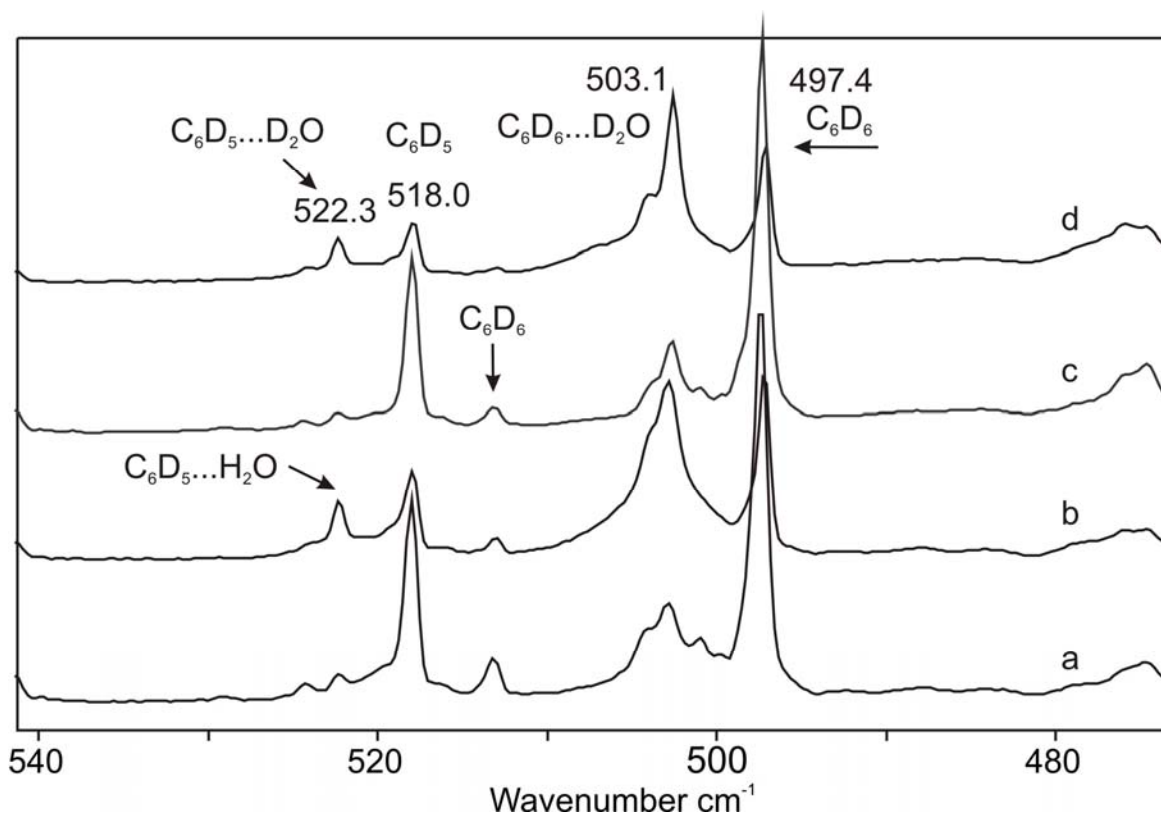


Figure 7.4.3. IR spectrum (in the range of C–D wagging mode of **1** showing the synthesis d_5 -**1** in argon at 10 K. (a) IR spectrum of a matrix (Ar at 10 K) isolated the d_5 -**1**, containing products from FVP of azobenzene doped 1 % H_2O . (b) After annealing by free warm up to 40 K (c) IR spectrum of a matrix (Ar at 10K) isolated the d_5 -**1**, containing products from FVP of azobenzene doped 1 % D_2O . (d) After annealing by free warm up to 40K.

Due to rotating and non-rotating monomer and high aggregates species of water in argon matrix, IR spectrum exhibits many bands even at high dilution, therefore the assignment of the absorptions of the phenyl radical – water complex in this region of spectrum is thus difficult. However the spectra of the water and its aggregates in a inert matrices has been studied in great detail.^[84, 328, 329] The ν_2 mode of the water monomer was found as reported at 3639.7 cm^{-1} .^[84] In the water OH stretching region the formation of a complex with **1** results in a new band at 3618.0 cm^{-1} that red-shifted by 21.7 cm^{-1} respect to the monomer. Its concentration dependency it is clearly shows that is due to a 1:1 phenyl radical – water complex (Figure 7.4.4A). Experiments using d_5 -**1** with H_2O shows basically identical experimental shift due to complexation therefore we tentatively assigned them to a complex between phenyl radical and water (Table 7.4.1). With deuterated water, the O–D stretching mode (ν_2) of D_2O is observed at 2645.1 cm^{-1} , red-shifted by 13.4 cm^{-1} from the unperturbed D_2O at 2658.5 cm^{-1} (Figure 7.4.4B).

Table 7.4.1. Experimental^a and Calculated (in italics)^b IR Spectroscopic Data of the C₆H₅...H₂O Complex.

	OH str.	CH o.o.p. def.	CH o.o.p. def.
H₂O	3639.4 ^c 3894.2		
D₂O	2658.8 ^c 2806.6		
H₂¹⁸O	3630.7 ^c 3886.1		
C₆H₅		705.8 ^d 734.0	657.4 ^d 681.8
C₆D₅		518.0 ^d 538.1	-
C₆H₅...H₂ O	3618.0 (- 21.4)	711.4 (+5.6)	659.8 (+2.4)
A	3863.5 (- 30.7)	739.3 (+5.3)	682.6 (+0.8)
B	3806.2 (- 88.0)	740.9 (+6.9)	680.5 (- 1.3)
C	3887.7 (- 6.5)	744.8 (+10.8)	684.1 (+2.3)
D	3887.8 (- 6.4)	746.6 (+12.6)	684.6 (+2.8)
C₆D₅...H₂ O	3618.0 (- 21.4)	522.3 (+4.3)	-
A	3864.5 (- 29.7)	540.2 (+2.1)	-
B	3806.2(- 88.0)	539.1 (+1.0)	-
C	3887.7 (- 6.5)	541.3 (+3.2)	-
D	3887.8 (- 6.4)	544.5 (+6.4)	-
C₆H₅...D₂ O	2645.1 (- 13.7)	711.8 (+6.0)	659.8 (+2.4)
A	2787.1 (- 19.5)	739.3 (+5.3)	682.6 (+0.8)
B	2862.0 (+56.0)	740.9 (+6.9)	680.4 (- 1.4)
C	2801.7(-	744.7(+1	684.1

	4.9)	0.7)	(+2.3)
D	2801.8 (- 4.8)	746.5 (+12.5)	684.5 (+2.7)
C₆D₅...D₂ O	2645.1 (- 13.7)	522.3 (+4.3)	-
A	2787.1 (- 19.5)	539.9 (+1.8)	-
B	2862.0 (+55.4)	539.1 (+1.0)	-
C	2801.7 (- 4.9)	541.2(+3. 1)	-
D	2801.7 (- 4.9)	544.3(+6. 2)	-
C₆H₅...H₂ ¹⁸O	3610.5 (- 20.2)	711.5 (+5.7)	659.5 (+2.1)
A	3854.7 (- 31.4)	739.3 (+5.3)	682.6 (+0.8)
B	3796.6 (- 89.5)	740.9 (+6.9)	680.5 (+21.0)
C	3879.6 (- 6.5)	744.8 (+10.8)	684.1(+2. 3)
D	3879.7 (- 6.4)	746.6 (+12.6)	684.6(+2. 8)

[a]Argon matrix [b] M05-2x/6-331++G(2d,2p) [c]References ^[17, 330, 331]. [d]Reference ^[286].
[e]Reference ^[332]

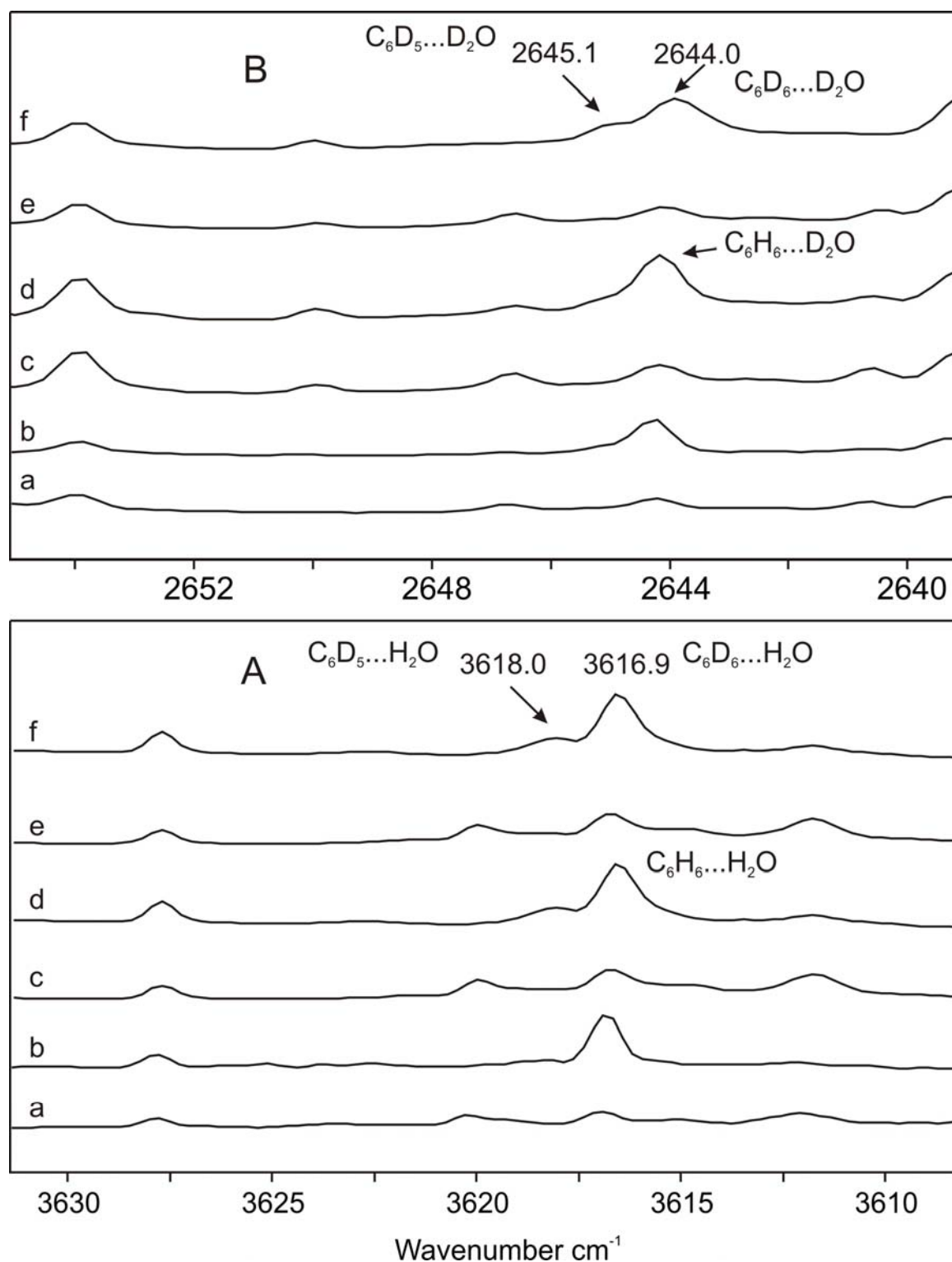


Figure 7.4.4. IR spectrum the ν_2 stretching region of water. (A) (a) IR spectrum of a matrix (Ar at 10 K) isolated **1**, doped 0.1 % H_2O . (b) After annealing by free warm up to 40 K (c) IR spectrum of a matrix (Ar at 10K) isolated **1**, 1 % H_2O . (d) After annealing by free warm up to 40K. (e) IR spectrum of a matrix (Ar at 10K) isolated d_5 -**1**, doped 1 % H_2O . (f) After annealing by free warm up to 40K. (B) (a) IR spectrum of a matrix (Ar at 10 K) isolated **1**, doped 0.1 % D_2O . (b) After annealing by free warm up to 40 K (c) IR spectrum of a matrix (Ar at 10K) **1**, doped 1 % D_2O . (d) After annealing by free warm up to 40K. (e) IR spectrum of a matrix (Ar at 10K) isolated the d_5 -**1**, doped 1 % D_2O . (f) After annealing by free warm up to 40K.

The experimentally observed frequencies and frequency shifts in the phenyl radical – water complex are similar to those for the benzene – water dimer in argon matrix.^[17] The shift of the ν_2 mode of H₂O in the phenyl radical complex indicates that the water forms a weak hydrogen bond with the phenyl radical. A comparison of the matrix IR spectrum of the phenyl radical – H₂O complex with the calculated for complex A (Figure 7.4.5) reveals an excellent agreement (Table 7.4.1).

7.4.2.2. Computational studies the phenyl radical –water dimers (by Elsa Sanchez-Garcia and Rachel Crespo-Otero)

The frequencies and the frequency shifts in the **1**...H₂O complex are similar to those of **13**...H₂O^[17] which suggests that both complexes have similar structures with the water molecule located on top of the aryl π system forming a weak OH... π hydrogen bond. On the other hand, the radical center in **1** could also act as hydrogen bond acceptor which should lead to a second complex with an in-plane water molecule and a OH...C(radical) hydrogen bond. We therefore systematically investigated the interactions between **1** and water using DFT methods. Since dispersion is important to describe these weakly bound complexes, we used the M05-2X functional of Truhlar^[333, 334] with a large 6-311++G(2d,2p) basis set. At this level of theory four **1**...H₂O complexes **A** – **D** were found (Figure 7.4.5) which are stabilized by the following intermolecular interactions:

- (1) The OH... π interaction between one hydrogen atom of the water molecule and the π system of the phenyl radical.
- (2) The OH...C (radical) interaction between one hydrogen atom of the water molecule and the radical center of the phenyl radical.
- (3) The CH...O interaction between one hydrogen atom of the phenyl radical and the oxygen atom of water.

In both complexes **A** and **B** the phenyl radical acts as a Lewis acid. For complex **A**, the interaction involves the electron donor capacity of the π system. In complex **B**, the unpaired electron is involved in the interaction. Complex **A** is the most stable complex (-2.39 kcal/mol CP and ZPE corrected) and is stabilized by interaction (1) between the OH

group of water and the π system of the phenyl radical. (Table 7.4.2) The calculated UB3LYP geometry of **A** is very similar to the calculated with UM05-2X.

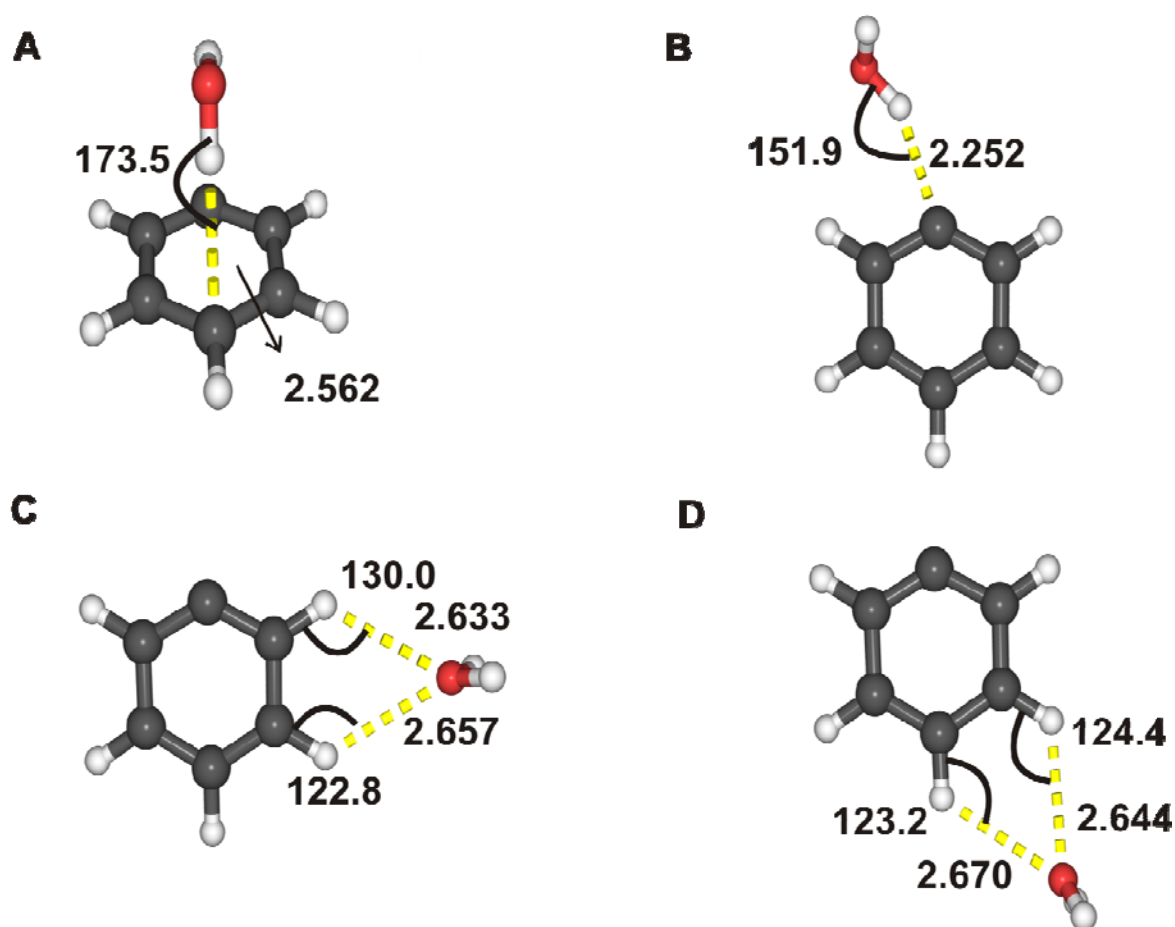


Figure 7.4.5. The calculated structures UM05-2X/6-311++G(2d,2p) with hydrogen bond lengths (Å) and angles (degree)

The non-symmetrical structure **B** follows in energy (-1.68 kcal/mol) and shows the interaction (2) where the OH group of the water molecule interacts with the radical center of the phenyl radical. The OHC angle is 151.9° and the hydrogen bonding distance 2.252 Å. When the B3LYP functional is used, the optimization of complex **B** leads to complex **BI**, with Cs symmetry, hydrogen bond distance of 2.247 Å and OHC hydrogen bond angle 173.6° (Figure 7.4.6). With the M05-2X functional, the **BI** geometry is a transition state (251 cm⁻¹) leading to **B**. This behavior is not surprising, since the potential energy surface of this kind of systems is very flat. The B3LYP functional predicts **BI** as the most stable complex (-0.79 kcal/mol).

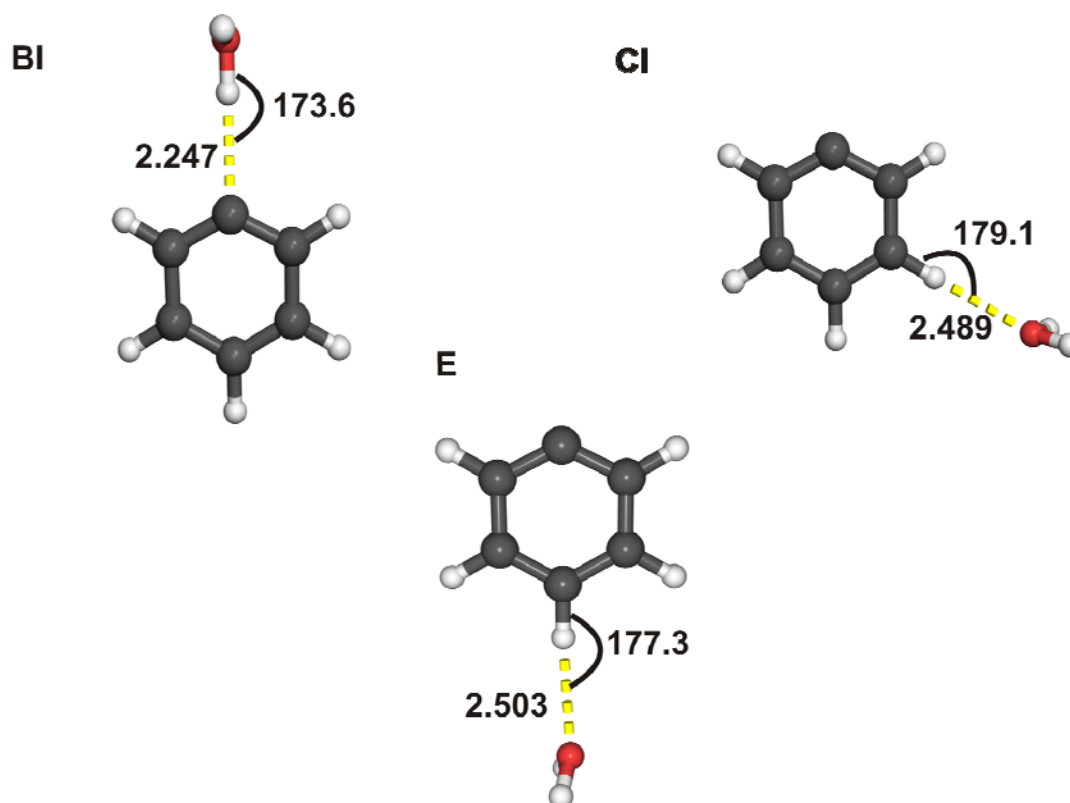


Figure 7.4.6. Additional calculated structures with hydrogen bond lengths (Å) and angles (degree) obtained at UB3LYP/6-311++G(2d,2p) level of theory.

Much less stable than **A** and **B**, are the Cs symmetrical complexes **C** and **D** (-1.09 and -1.03 kcal/mol, respectively) (Table 7.4.2). In these complexes, the phenyl radical acts as Lewis acid via its C-H antibonding orbitals. They are both stabilized by interaction (3) and differ to each other mostly in the position of the water molecule. In complex **C**, the water molecule is located between the ortho- and meta- hydrogen atoms of the phenyl radical. In complex **D**, the water is found between the meta- and para- hydrogen atoms of the phenyl radical.

When the B3LYP functional is used, complexes **CI** and **E** are found to be minima, although they are transition states with the UM05-2X functional. The geometry optimization of the **CI** and **E** structures at the UM05-2X level of theory leads to complexes **C** and **D**, respectively. (Figure 7.4.6) There are also differences between the UB3LYP and UM05-2X interaction energies. With B3LYP, the interaction energies of all complexes after CP and ZPE corrections take values extremely low (below 1 kcal/mol).

Table 7.4.2. Stabilization energies of the $C_6H_5 \dots H_2O$ complexes (kcal/mol)

UB3LYP ^a	UM05-2X ^b	RHF-UCCSD(T) ^c
---------------------	----------------------	---------------------------

Complex	ΔE	ΔE_{CP}	ΔE_{CP+ZPE}	ΔE	ΔE_{CP}	ΔE_{CP+ZPE}	ΔE	ΔE_{CP}
A	-1.71	-1.44	-0.67	-3.77	-3.26	-2.38	-3.69	-2.45
B	- ^e			-3.01	-2.76	-1.68	-2.71	-1.77
BI	-2.00	-1.74	-0.79	-2.88 ^d	-	-	-	-
C	-			-2.23	-2.04	-1.09	-2.38	-1.69
CI	-1.18	-1.02	-0.42	-	-	-	-	-
D	-1.09	-0.92	-0.27	-2.10	-1.91	-1.03	-2.27	-1.59
E	-1.11	-0.96	-0.37	-1.65 ^c				

[a] UB3LYP/6-311++G(2d,2p). [b] UM05-2X/6-311++G(2d,2p). [c] RHF-UCCSD(T)/6-311++G(2d,2p)//UM05-2X/6-311++G(2d,2p). [d] Optimization of **B** at the B3LYP level leads to **BI**. [e] At the M05-2X level **BI** is a transition state (TS) leading to **B** with one imaginary vibration at -25 cm^{-1} . [e] At the M05-2X level, E is a transition state (TS) leading to **D** with one imaginary vibration at $18i\text{ cm}^{-1}$.

The UM05-2X/6-311++G(2d,2p) vibrational frequencies of complex **A** show a good agreement with the experimental values (Table 7.4.1). Since we are dealing with weak interacting complexes, the frequency shifts from monomers are small. The largest shifts are found for the OH stretching mode of complex **B** (-88 cm^{-1}). In complex **B** there is a direct interaction of water with the unpaired electron of the radical, which involves spin transfer from the phenyl radical to the water molecule (Figure 7.4.7). The NBO calculations indicate that the spin density on the water molecule is 0.02 e and it is mainly localized on the oxygen atom. This spin transfer is related to the $n_{\text{O}}^{\sigma} \rightarrow \sigma_{\text{O-H}}^{*}$ donor-acceptor interaction, which it is contributing most to the stabilization of the complex. For the other complexes, the values of the spin densities do not differ significantly from the monomers. Their stabilization can be associated to the $\pi_{\text{C-C}} \rightarrow \sigma_{\text{O-H}}^{*}$ (**A** complex) and to $n_{\text{O}}^{\sigma} \rightarrow \sigma_{\text{C-H}}^{*}$ (**C** and **D** complexes) interactions. These donor-acceptor interactions have similar contributions from the alpha and beta orbitals. This behavior has been found in other radical – water complexes where the radical acts as a Lewis acid.^[321]

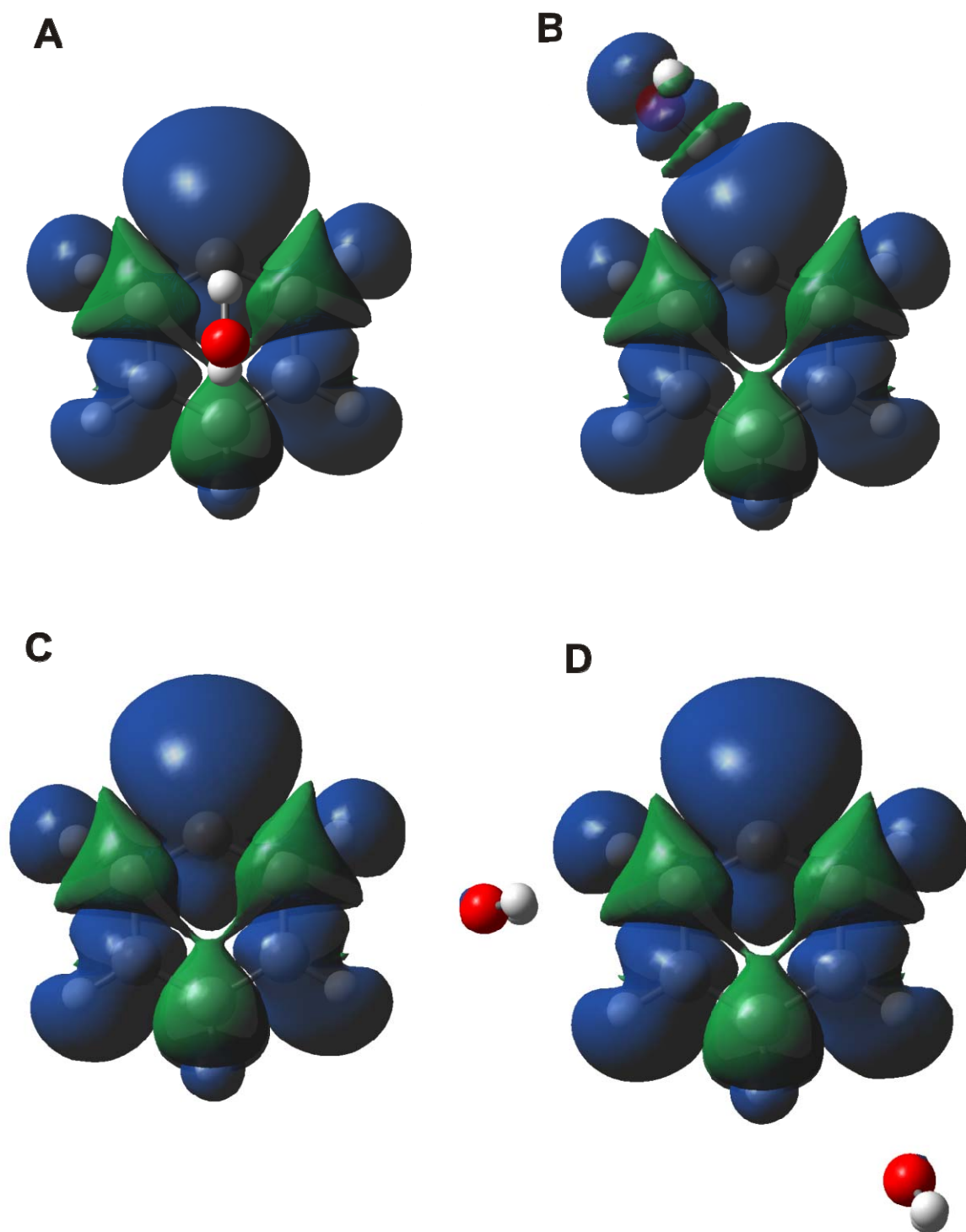


Figure 7.4.7. Spin Densities for phenyl – water complexes calculated at UM05-2X/6-311++G(2d,2p) level of theory.

7.4.2.3 Photochemistry of the phenyl radical – water complex

Complex **A** proved to be photolabile on near UV irradiation. Several minutes irradiation of the matrix with $\lambda > 350$ nm results in a bleaching of **A** (all three observed IR bands disappear simultaneously) and formation of a new compound **G** with IR bands at 3502.2, 1482.8, 1040.3, and 684.2 cm^{-1} (Figure 7.4.8, Table 7.4.3). Other bands in the spectrum are not affected (e. g. the benzene – water complex does not show any photochemistry). The 1482.8, 1041.2, and 684.2 cm^{-1} vibrations of **G** closely resemble vibrations of matrix-isolated **13** at 1483.3, 1040.8, and 675.0 cm^{-1} .^[17] In compound **G** the o.o.p. deformation mode of benzene is blue-shifted to 684.2 cm^{-1} in a similar way as in the benzene – water complex,^[17] and thus **G** is assigned to a benzene π complex. The other two benzene vibrations in **G** show very small red-shifts of less than 1 cm^{-1} (with respect to “free” matrix-isolated **13**) but can clearly be assigned to **G** and not to free benzene by monitoring the intensity changes during irradiation.

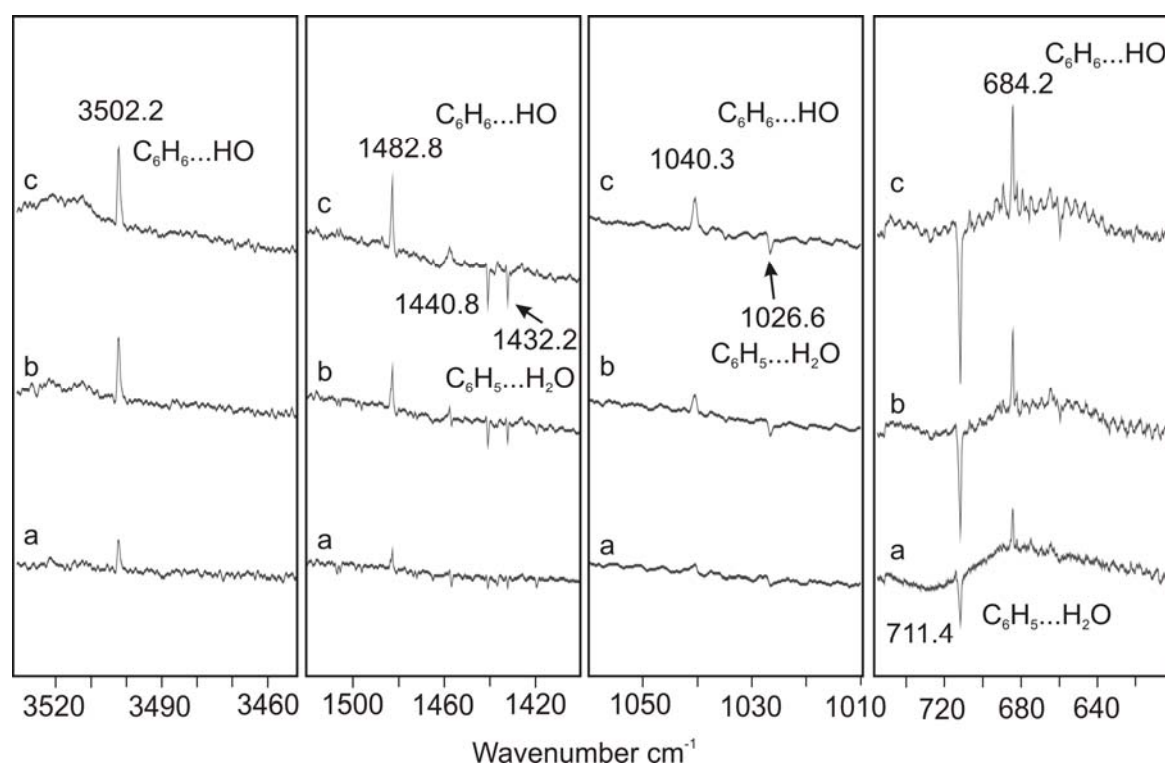


Figure 7.4.8. IR difference spectra showing photochemical transformation of **A** into **G**. a) bands pointing downwards assigned to **A** disappear and bands pointing upwards assigned to **G** appear after irradiation for 1 min with light of wavelength $\lambda > 420$ nm. b) after 2 min. c) after 5 min.

If D₂O is used in our experiments the ν_4 vibration of benzene (**13**) in **G** shows a very large isotope shift to 614.2 cm^{-1} as it is expected for d₁-**13** (Figure 7.4.9, Table 7.4.3). Compared to matrix-isolated d₁-**13** the band is blue-shifted by 6.0 cm^{-1} , indicating the formation of a π complex with d₁-**13** as one component. This clearly demonstrates that radical **1** is abstracting a deuterium atom from D₂O to give d₁-**13** during irradiation. What is left from the water molecule is an OD radical (or OH if normal water is used) and it is thus tempting to assign compound **G** to a weakly bound complex between **13** and the OH radical.

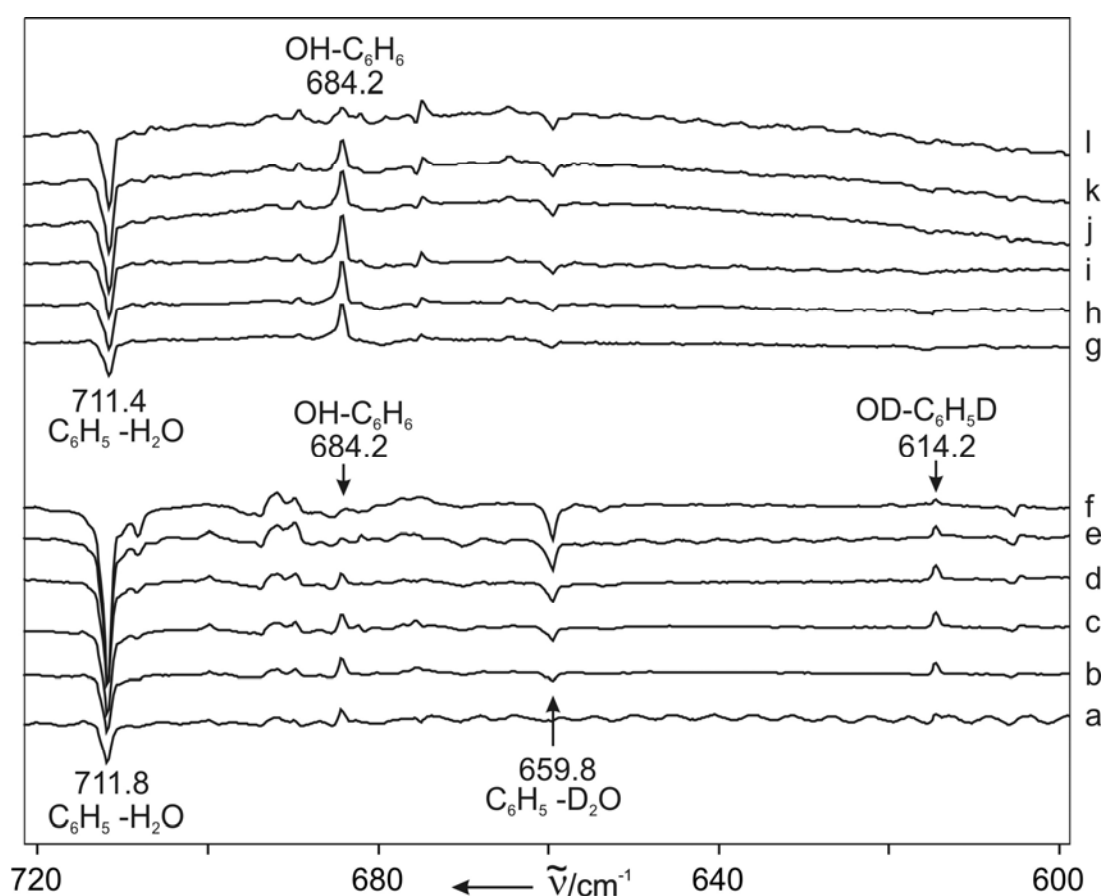


Figure 7.4.9. Difference IR spectra showing the photolysis ($\lambda > 350\text{ nm}$) of the phenyl radical – H₂O complex **A** and formation of the benzene – OH complex **G**. Bands pointing downwards are disappearing during photolysis, bands pointing upwards are appearing. The spectra (a) – (f) were taken after 0.5, 1, 2, 3, 4, and 10 min of irradiation using a mixture of D₂O and H₂O and show the formation of both benzene – OH (684.2 cm^{-1}) and d₁-benzene – OD (614.2 cm^{-1}). The spectra (g) – (l) were taken under similar conditions but using only H₂O. In this case only benzene – OH is formed.

Additional proves of the assignment is coming from the experiment using H_2O with $\text{d}_5\text{-1}$ (Figure 7.4.10). If hydrogen abstraction reaction takes place from the water to **1**, one has to expect formation of the $\text{d}_5\text{-13}$. In complex, the opp deformation mode of benzene exhibit blue shift by 7.4 cm^{-1} from unperturbed $\text{d}_5\text{-13}$ at 513.1 cm^{-1} . Other vibrational modes in the fingerprint region of $\text{d}_5\text{-13}$ at 1392.2, 927.4 and 818.8 considerably show small shifts ($1\text{-}4\text{ cm}^{-1}$) (Table 7.4.3). However the complete assignment of five isotopomers of complex **G** ($\text{C}_6\text{H}_6\cdots\text{HO}$, $\text{C}_6\text{H}_6\cdots\text{H}^{18}\text{O}$, $\text{C}_6\text{H}_5\text{D}\cdots\text{DO}$, $\text{C}_6\text{D}_6\cdots\text{DO}$ and $\text{C}_6\text{D}_5\text{H}\cdots\text{HO}$) are listed in Table 7.4.3 (See Figures 7.4.8-7.4.12).

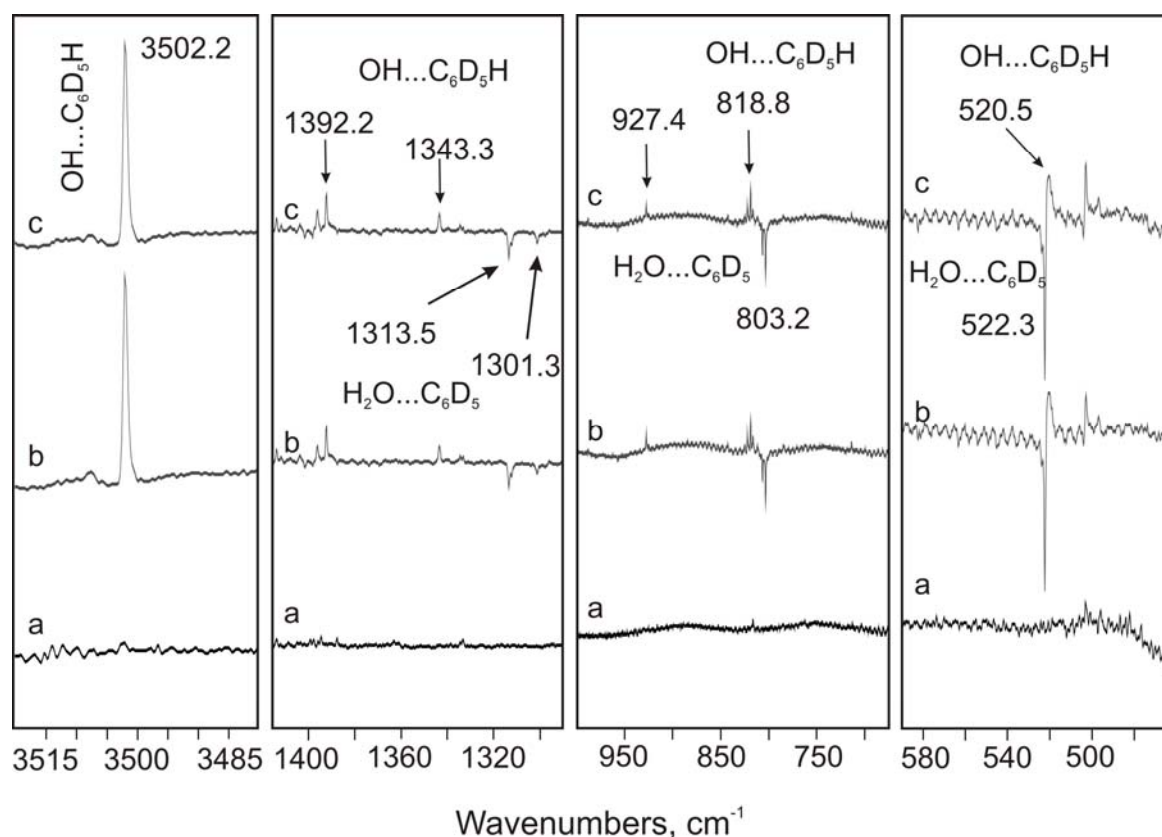


Figure 7.4.10. IR difference spectra showing photochemical transformation of **A**-($\text{d}_5\text{-1}\cdots\text{H}_2\text{O}$) into **G**-($\text{d}_5\text{-13}\cdots\text{OH}$). a) bands pointing downwards assigned to **A** disappear and bands pointing upwards assigned to **G** appear after irradiation for 1 min with light of wavelength $\lambda > 420\text{ nm}$. b) after 2 min. c) after 4 min.

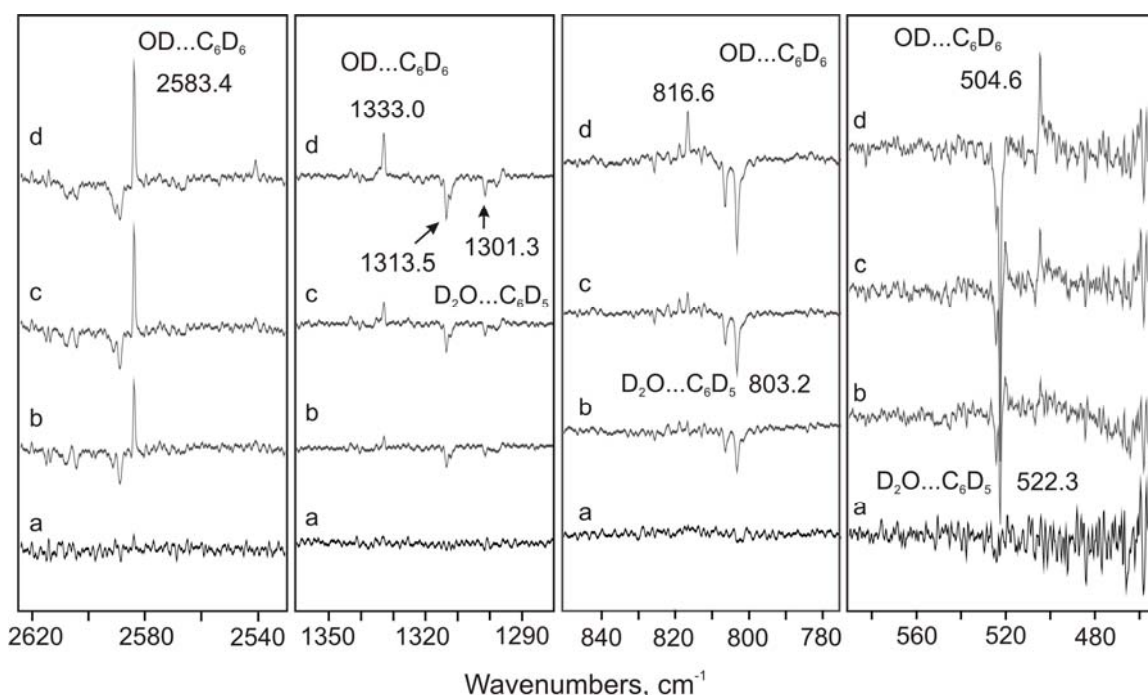


Figure 7.4.11. IR difference spectra showing photochemical transformation of **A**-(d₅-**1**...D₂O) into **G**-(d₆-**13**...OD). a) bands pointing downwards assigned to **A** disappear and bands pointing upwards assigned to **G** appear after irradiation for 0.5 min with light of wavelength $\lambda > 420$ nm. b) after 1 min. c) after 2 min. d) after 5 min.

This assignment is corroborated by analyzing the OH stretching region of the IR spectrum of **G**. The fourth observed IR absorption of **G** at 3502.2 cm^{-1} is red-shifted by 46 cm^{-1} with respect to the OH stretching vibration of the OH radical in solid argon at 3548.2 cm^{-1} .^[335, 336] This indicates the formation of a strong hydrogen bond, as expected for **G**. Isotopic substitution with deuterium as well as ^{18}O results in isotopic shifts of 918.8 and 11 cm^{-1} , respectively, proving that the 3502.2 cm^{-1} vibration is indeed an OH stretching vibration (Figure 7.4.12) (Table 7.4.3). Other OH containing compounds such as water or phenol can be excluded by comparison with their known matrix spectra.

The ^{18}O isotopic shift of the OH radical in **G** of -11 cm^{-1} is identical to that of the matrix-isolated OH radical and markedly different from that of H₂O, which provides additional evidence that **G** is a complex of the OH radical. Finally, the calculated IR spectrum of the **13**...OH π complex is in excellent agreement with the matrix IR spectrum of **G** (Table 7.4.3). In particular, the predicted shifts of the IR bands of the OH and the benzene fragments match the experimental values almost perfectly.

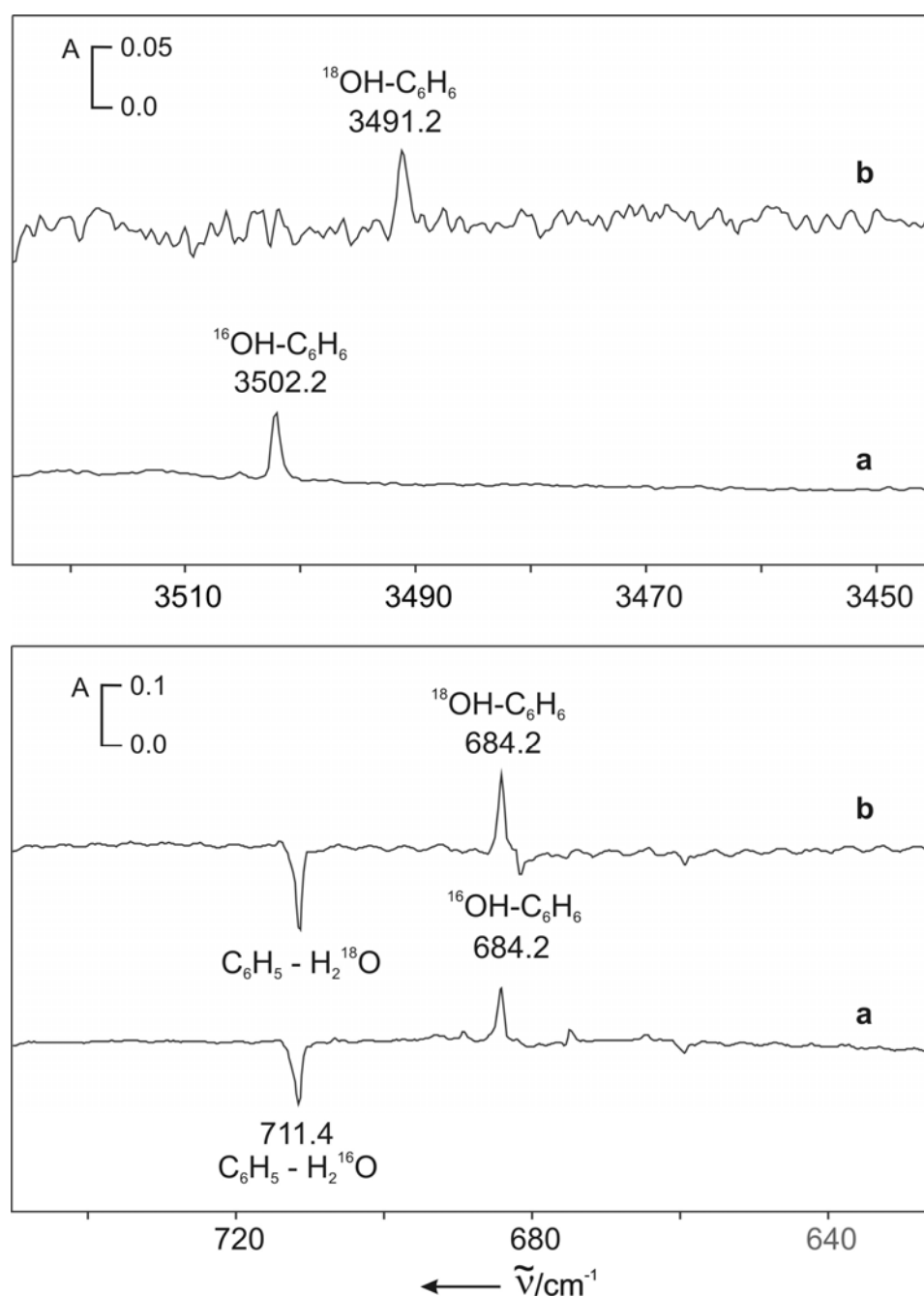


Figure 7.4.12. IR difference spectra showing the photochemistry transforming **1**...H₂O to **13**...OH. (a) Bands pointing downwards assigned to **1**...H₂O are disappearing and bands pointing upwards assigned to **13**...OH are appearing after 5 minutes irradiation with $\lambda > 420$ nm. (b) The same experiment using H₂¹⁸O.

Table 7.4.3. Experimental^a and Calculated (in italics)^b IR Spectroscopic Data of the C₆H₆...OH Complex

	OH str.	ring def.	ring def.	CH o.o.p. def.
OH^c	3548.2 3803.6			
OD^c	2616.1 2769.1			
¹⁸OH^c	3537.1 3791.1			
C₆H₆^d		1483.3 <i>1546.9</i>	1041.2 <i>1081.4</i>	675.0 <i>698.0</i>
C₆D₆^d		1334.7 <i>1395.4</i>	816.3 <i>839.6</i>	497.2 <i>512.5</i>
C₆H₅D^d		1480.2 <i>1539.3</i>	1036.9 <i>1076.8</i>	608.2 <i>628.5</i>
C₆HD₅^e		1392.6 1344.1	818.3	922.3 513.2
C₆H₆...OH	3502.2 (-46) 3759.5 (-44.1)	1482.8 (-0.5) 1545.5 (-1.4)	1040.3 (-0.9) 1080.8 (-0.6)	684.2 (+9.2) 711.7 (+13.7)
C₆HD₅...OH	3502.2 (-46)	1392.2 (-0.4) 1343.3 (-0.8)	818.8 (+0.5)	927.4 (+4.1) 520.5 (+7.3)
C₆H₅D...OD	2583.4 (-32.7)	-	-	614.2 (+6.0)
C₆D₆...OD	2583.4 (-32.7) 2737.1 (-32.0)	- -	816.6 (+0.3) -	504.6 (+7.4) 521.6 (+9.1)
C₆H₆...¹⁸OH	3491.2 (-45.9) 3748.6 (-42.5)	1482.7 (-0.4) <i>1545.1 (-1.8)</i>	1040.9 (-0.3) <i>1080.6 (-0.8)</i>	684.2 (+9.2) <i>708.9 (+10.9)</i>

[a] Argon matrix. [b] UM05-2X/6-311++G(2d,2p). [c] Reference^[337][d] Reference^[17] [e] Reference^[338]

7.4.2.4. Computational studies the Benzene – OH dimers (by Elsa Sanchez-Garcia and Rachel Crespo-Otero)

The $C_6H_6...OH$ complex was optimized at the UMP2, UM05-2X and UB3LYP levels of theory with the 6-311++G(2d,2p) basis set (Figure 7.4.13, Table 7.4.4). Several different structures were used as starting points. Stable complexes related to C-H...O-H interactions were not found. In the complex calculated with the B3LYP functional, the O atom of the hydroxyl radical is pointing towards one C atom of benzene. These results are in agreement with what has been previously reported.^[339, 340] The H atom of the OH^\bullet radical is pointing to the center of the benzene ring in the UMP2 and UM05-2X geometries. All structures have C_s symmetry and the UMP2 geometry comes near to a C_{6v} symmetric structure. The UMP2 and UM05-2X complexes are more stable than the obtained with the B3LYP functional (stabilization energies CP and ZPE corrected -3.08, -2.80 and -1.71 kcal/mol respectively, (Table 7.4.4)).

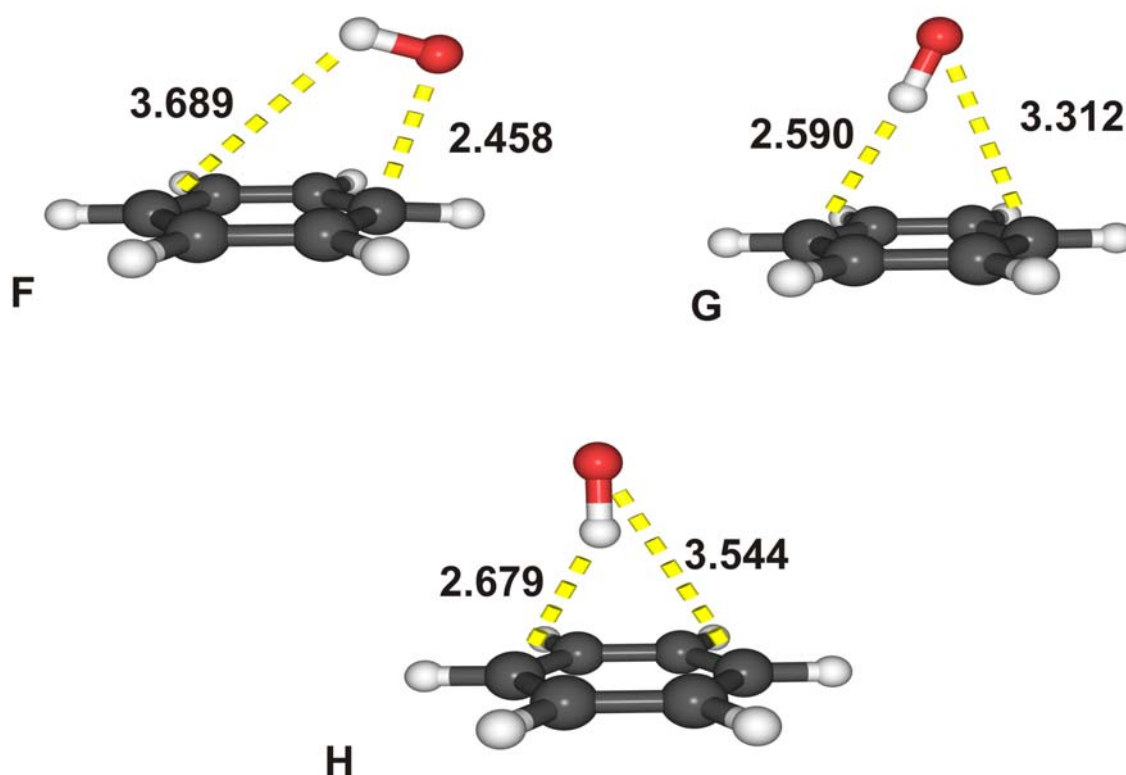


Figure 7.4.13. Calculated geometries for the $C_6H_6...OH$ complex. (F) UB3LYP/6-311++G(2d,2p) level of theory. (G.) UM05-2X/6-311++G(2d,2p) level of theory. (H) UMP2/6-311++G(2d,2p) level of theory.

The PES of this system is very shallow and the energy difference between the UMP2 and UM05-2X complexes is small. A definitive geometry cannot be unambiguously established in these circumstances. Nevertheless, the experimental data agrees very well with the frequencies calculated at the UM05-2X/6-311++G(2d,2p) level of theory. The calculated frequency shifts for this complex have similar signs and magnitude that the experimental ones. The formation of the $\text{C}_6\text{H}_6\cdots\text{OH}$ complex involves a shift of the O-H stretching frequency to smaller values (-46 cm^{-1}) (Table 7.4.3). The calculated frequency shifts with the UM05-2X, UMP2 and UB3LYP methods are -44.1 , -49.1 cm^{-1} , $+34.9\text{ cm}^{-1}$, respectively. The UB3LYP complex seems to be the worse of all considered geometries in agreement with previous studies reporting the limitations of the B3LYP functional to correctly treat dispersive interactions.^[321, 341]

Table 7.4.4. Stabilization energies of the $\text{C}_6\text{H}_6\cdots\text{OH}$ complexes

6-311++G(2d,2p)	ΔE	ΔE_{CP}	$\Delta E_{\text{CP+ZPE}}$
UM05-2X	-4.71	-4.31	-3.08
UB3LYP	-3.41	-2.97	-1.71
UMP2	-4.50	-3.29	-2.80

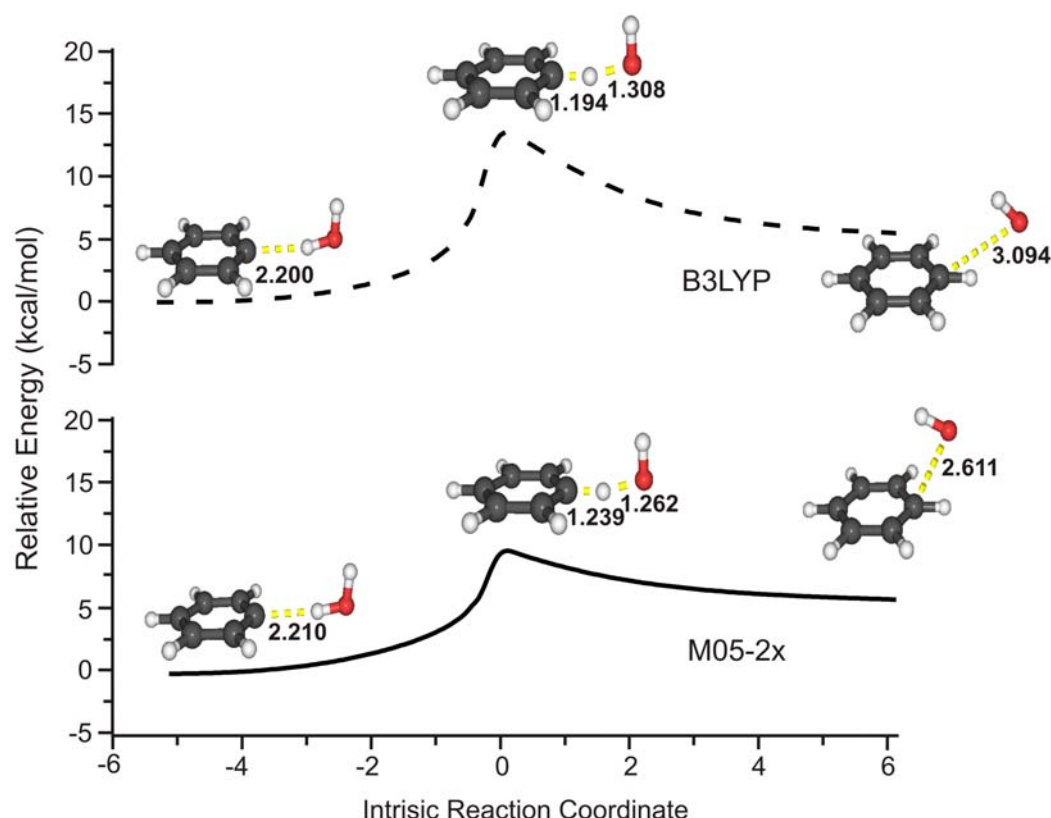


Figure 7.4.14. Intrinsic reaction coordinate for the water hydrogen abstraction from the phenyl radical to give the benzene – OH radical water complex.

The intrinsic reaction coordinate for the water hydrogen abstraction from the phenyl radical to give the benzene – OH radical water complex was also studied by us using the B3LYP and M05-2X functionals. It shows how after the reaction the OH radical leaves the plane of the benzene to adopt a position similar to that in the benzene – OH radical complexes calculated by us. More than 120 points were calculated in each case and although we would need more than 200 points to reach the exact geometry of our optimized complexes, it is clear that the hydrogen abstraction reaction leads to the structures discussed here. Especially since each optimization of non-planar $C_6H_6 - OH$ geometries converged to the complexes presented by us (Figure 7.4.14).

7.4.2.5. Photochemistry of the Benzene – OH dimer

The reaction between benzene and the hydroxyl radical has been very much investigated.^[339, 340, 342-344] In low-temperature regime conditions, the formation of radical **14** (2,4-cyclohexadieny, 6-hydroxy radical) dominates over other reaction channels. This reaction has been very well described.^[339, 340] It involves the formation of a pre-reactive complex and the barrier to radical **14** is 5.4 kcal/mol according G3 calculations.^[340] The role of pre-reactive complexes had been addressed by many authors.^[345, 346] In our conditions the intermolecular complex is stable,^[257] so the reactions take place only after irradiation.

Prolonged (5-30 minutes) irradiation at $\lambda > 420$ nm of the matrix containing the benzene – OH radical complex (**G**) results in a bleaching of bands of **G** and the appearance of new absorptions in the IR spectrum. Particularly, a well-defined band at 2130.8 cm^{-1} (Figure 7.4.15) and a set of bands which correlate with the band at 2130.8 cm^{-1} shows the same kinetic during the irradiation process (Table 7.4.5). All these bands observed in solid argon are assigned to butadienylketene (**16**). The formation of **16** in solid argon upon photolysis of **G** is particularly evidenced by the very strong band at 2130.8 cm^{-1} due to the $\text{R1R2C}=\text{C}=\text{O}$ ketene group. The experiments with H_2^{18}O confirmed the assignment of **16**. The band at 2130.8 cm^{-1} is shifted to 2079.8 cm^{-1} while other bands are not affected upon substitution with ^{18}O . This apply especially to the very characteristic bands at 904.7 and 588.9 cm^{-1} corresponding to the $\omega(\text{CH}_2)$ and $\omega(\text{CH})$ modes of **16**, which are only slightly shifted by less than 1 cm^{-1} upon substitution with ^{18}O (Figure 7.4.15).

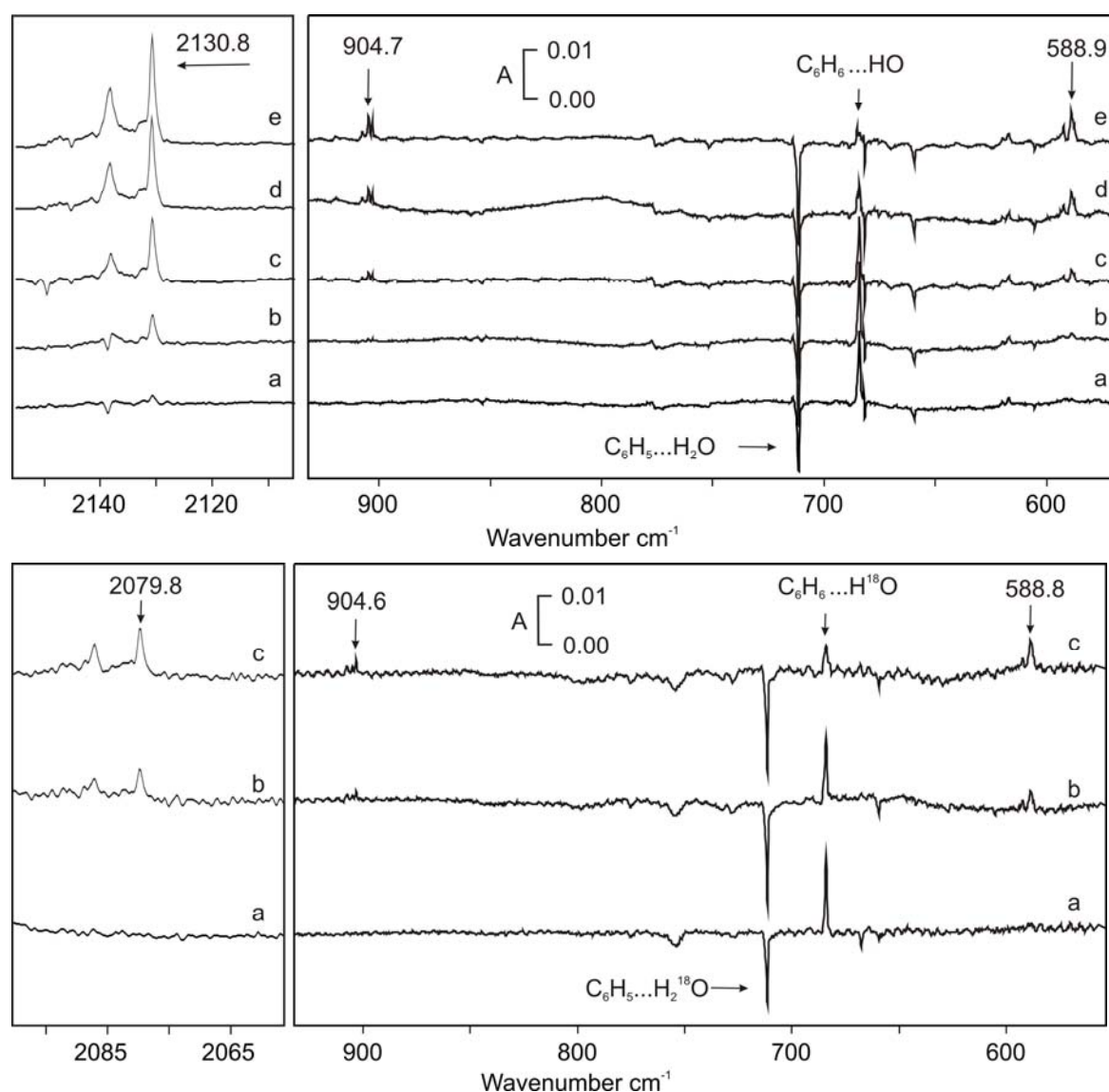
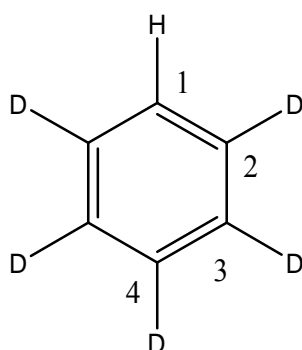


Figure 7.4.15. Top: IR difference spectra showing the photochemistry of $1...H_2O$ and $13...HO$ during irradiation with $\lambda > 420$ nm in argon at 10 K. (a) Bands pointing downwards assigned to $1...H_2O$ disappear and bands pointing upwards assigned to ketene **16** appear after 1 min irradiation time. (b) After 2 min irradiation time. (c) After 5 min irradiation time. (d) After 10 min irradiation time. (e) After 20 min irradiation time. Bottom: IR difference spectra showing photochemistry of $1...H_2^{18}O$ and $13...H^{18}O$ during irradiation with $\lambda > 420$ nm in argon at 10 K. (a) Bands pointing downwards assigned to $1...H_2^{18}O$ disappear and bands pointing upwards assigned to ketene ^{18}O -**16** appear after 2 min irradiation time. (b) After 5 min irradiation time. (c) After 15 min irradiation time.

Table 7.4.5: IR spectroscopic data of the ring opening product (Ar, 10K)

$\text{C}_6\text{H}_5 \cdot \text{H}_2\text{O}$	$\text{C}_6\text{H}_5 \cdot \text{H}_2^{18}\text{O}$	$\text{C}_6\text{H}_5 \cdot \text{D}_2\text{O}$	$\text{C}_6\text{D}_5 \cdot \text{H}_2\text{O}$	$\text{C}_6\text{D}_5 \cdot \text{D}_2\text{O}$	Assignment
2130.8	2079.8	2130.7	2130.6	2130.7	$\nu(\text{C}=\text{C}=\text{O})$
1375.3	1375.2	1396.0			$\delta(\text{C-H})$
1373.5	1373.5				
904.7	904.6	747.2	736.2	727.7	$\omega(\text{CH}_2)$
903.0	903.0				
592.4	592.4				$\omega(\text{CH})$
588.9	588.8				

The $\nu(\text{C}=\text{C}=\text{O})$ mode of **16** remains unchanged upon substitution with D_2O . The band at 2130.8 cm^{-1} is shifted to 2130.7 cm^{-1} , while in the fingerprint region the spectra changed drastically upon substitution with D_2O . The $\omega(\text{CH}_2)$ mode at 904.7 cm^{-1} is shifted to 747.2 cm^{-1} and is relatively low in intensity with respect to nondeuterated (Table 7.4.5). In order to form a ketene group, the OH radical must attack the benzene ring, which leads to the formation of **14**. We did not observe any peak that can be assigned to **14**, due to its high photolability ($\lambda > 420 \text{ nm}$). In the mixed isotopic experiments (for example $\text{d}_5\text{-13...HO}$) the OH radical in complex **G** can attack four different positions with respect to the hydrogen atom in $\text{d}_5\text{-13}$ (Scheme 7.4.3). This resulted in the formation of several isotopic conformers with a drastic variation of the IR spectra in the fingerprint region. The intensity of this mode is low due to the presence of several isotopomers. Although the $\omega(\text{CD}_2)$ mode at 727.7 cm^{-1} of $\text{d}_6\text{-16}$ ($\text{d}_6\text{-13...OD}$) is considerably high in intensity, indicating that only one isotopomer is formed in solid argon. We also computed the structures of the eight possible isomers of butadienylketene (**16**). The IR spectra of these isomers are different, which allow us to consider that only the most stable conformer is trapped in argon matrix (Figure 7.4.16). The unimolecular decomposition of **14** via different channels is discussed below.



Scheme 7.4.3. d₅-benzene

Gas-phase study of the reaction of OH radical with benzene carried out under atmospheric conditions reveal the formation phenol as major product.^[347, 348] At ambient temperatures this reaction proceeds almost exclusively via addition of OH radical to the benzene ring results in the formation of a hydroxycyclohexadienyl radical (**13**). Under atmospheric conditions the reaction follows different pathways, while the majority of phenol is formed via the reaction of **13** with oxygen. Klan et al.^[344] studied oxidation of aromatic hydrocarbons by OH radical in ice. There is no evidence for the formation phenol in our experiments.

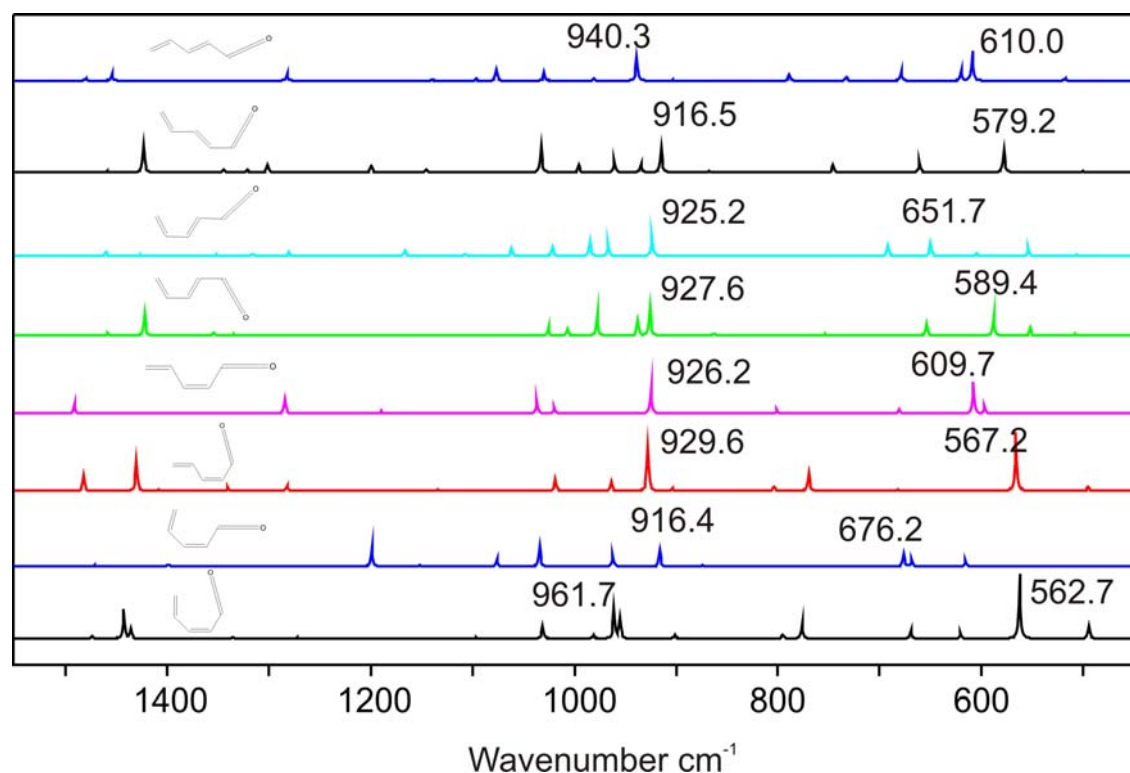


Figure 7.4.16. IR spectrum of seven isomers of Butadienylketene (BDK) at the UB3YLP/6-311++G** level of theory.

Referring the spectra obtaining after photolysis of OH...Benzene complex we found product band at 3409.4 cm^{-1} that can not be assigned either to **16** on the basis of their kinetic behaviour or to phenol on the basis to reference data from literature. The growth kinetics of this band suggests that it is a primary product of reaction OH radical with benzene, which is very stable under near UV irradiation. However the band at 3409.4 cm^{-1} indicates of the existence of an OH moiety which is shifted to 2509.8 cm^{-1} with D_2O instead of H_2O . This unknown compound is to be only one secondary product which formed upon photolysis of phenyl radical – water complex in solid argon.

7.4.2.6. Calculation of the ring opening (by Rachel Crespo-Otero and Elsa Sanchez-Garcia)

After irradiation of the $\text{C}_6\text{H}_6\cdots\text{OH}$ complex, a reaction takes place to form product (**16**) plus one hydrogen atom. This reaction can occur in the ground or the excited state. To analyze the different reaction paths from radical **14** to the product **16**, four reaction channels were considered at the ground state. The geometries of the reactants, intermediates, transition states and products are shown in Figures 7.4.17-7.4.19. The reaction is endothermic and many of the considered steps are also endothermic (Figures 7.4.20-7.4.22). Therefore and according to the Hammond principle, the transition states are more similar to the products than to the reactants.

Since the B3LYP functional have been already successfully used to obtain geometries of intermediates and transition states of similar reactions,^[349-352] we also employed it for our study. However, it is well known that the B3LYP functional tends to underestimate reaction barriers.^[353, 354] The energies obtained at the RHF-UCCSD(T)/6-311++G(2d,2p) level of theory are in most cases slightly larger than those calculated with B3LYP. Nevertheless, the energy profiles calculated by both methods are similar and valuable for interpretative purposes. Here the analysis is based on the ZPE corrected B3LYP/6-311++G(2d,2p) energies (Table 7.4.6).

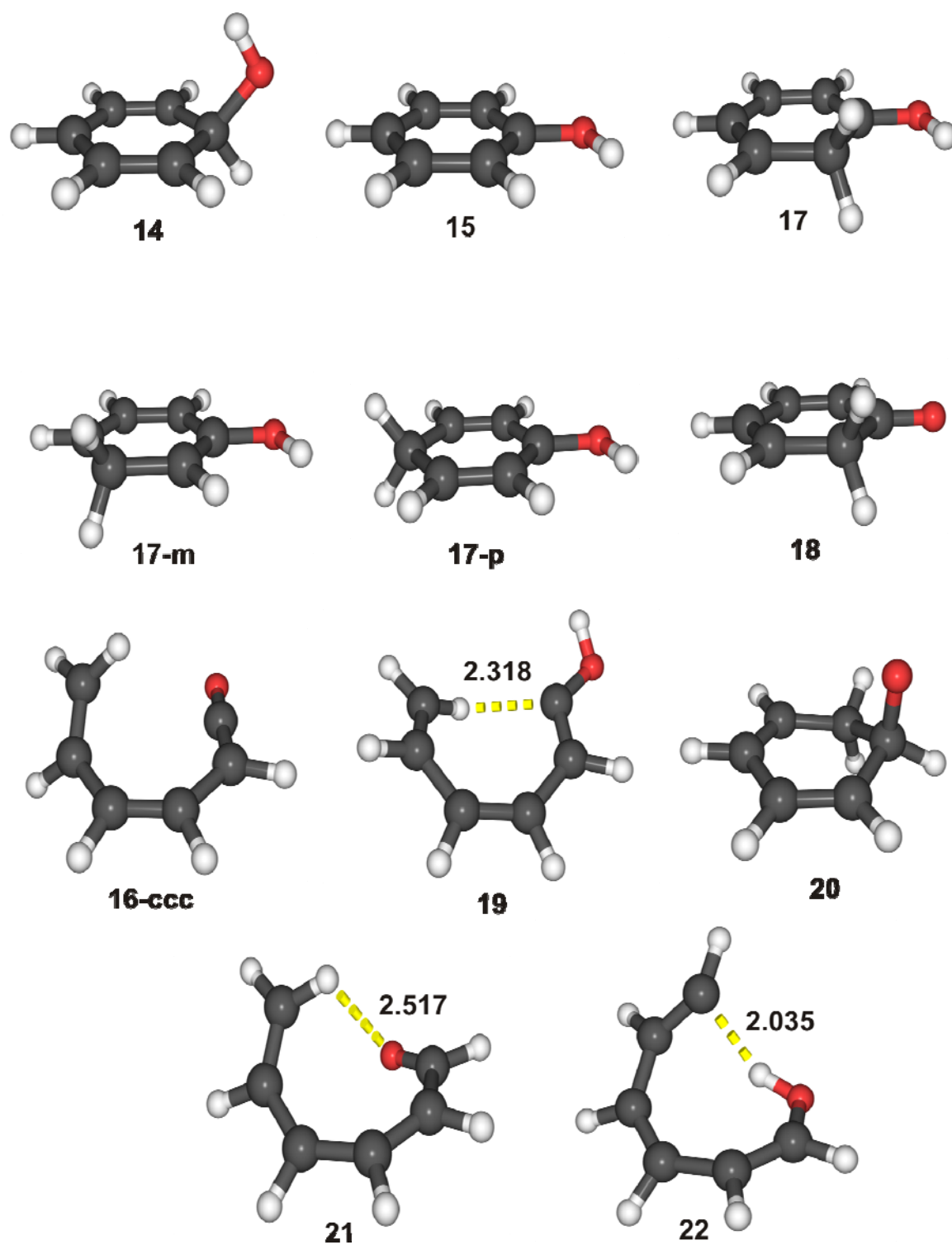


Figure 7.4.17. Calculated geometries for reactant, product and intermediates at UB3LYP/6-311++G(2d,2p) level of theory.

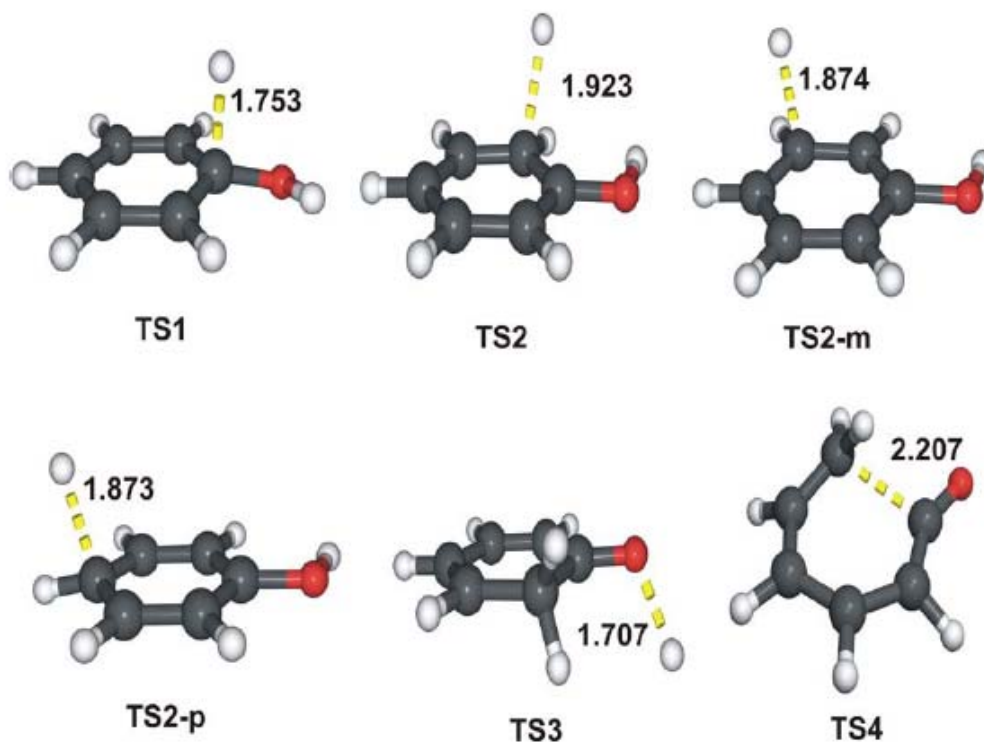


Figure 7.4.18. Calculated geometries for transition states at UB3LYP/6-311++G(2d,2p) level of theory.

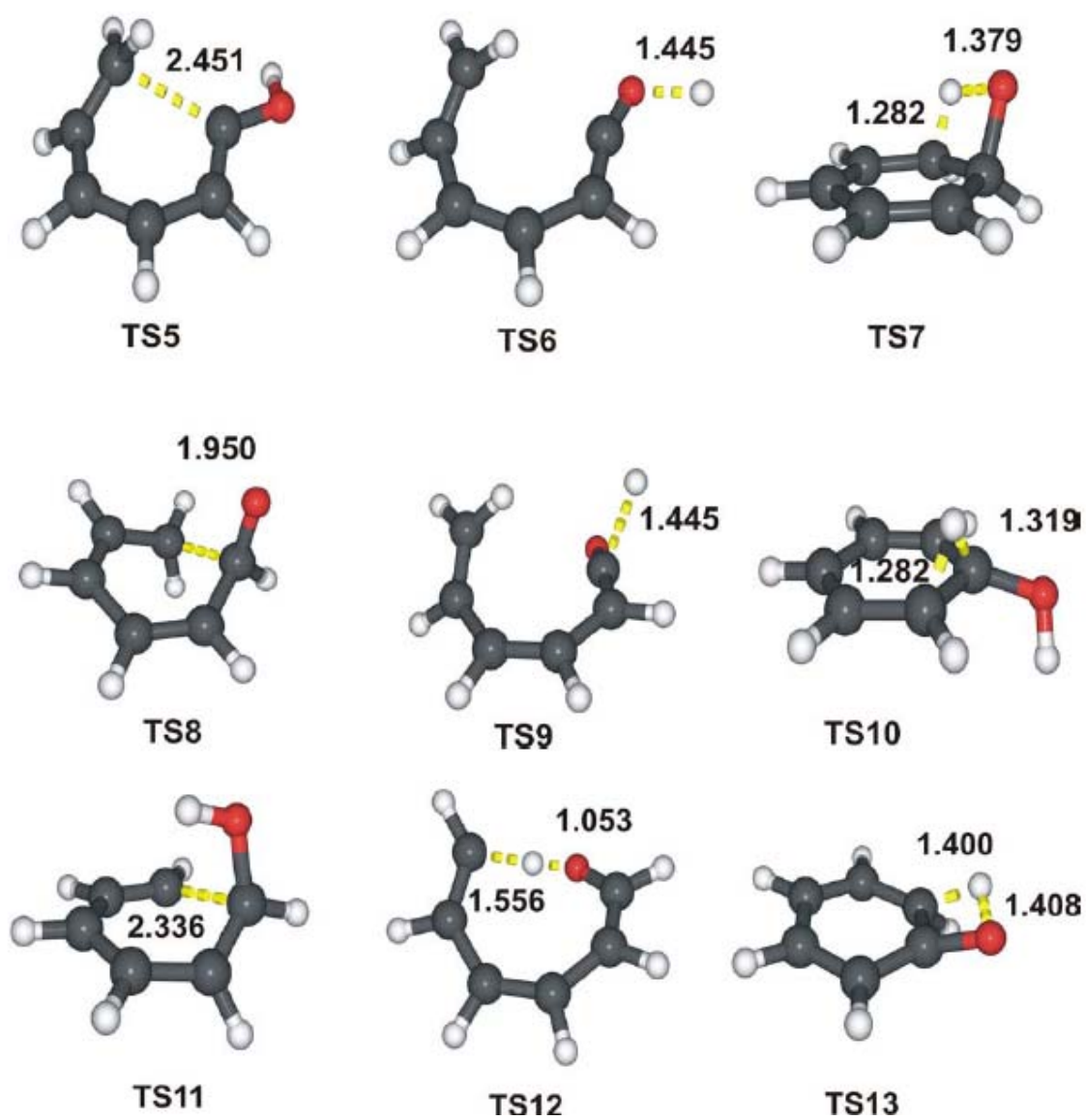


Figure 7.4.19. Calculated geometries for transition states at UB3LYP/6-311++G(2d,2p) level of theory.

Table 7.4.6. Energies of the intermediates (kcal/mol), reactant and products calculated with respect to radical **14**.

	UB3LYP ^a		UCCSD(T) ^b
	E	E _{ZPE}	E
14	0	0	0
15+H	23.97	18.23	23.99
17	-5.39	-5.74	-3.83
18	42.87	36.24	41.24
16-ccc+H	70.3	61.7	71.2
19	49.73	47.73	52.84
20	28.28	28.14	28.32
21	15.86	13.84	20.40
22	50.13	47.93	52.14
TS 1	29.74	25.20	31.27
TS 2	25.60	20.86	27.57
TS 3	44.57	38.79	46.64
TS 4	78.62	69.95	81.06
TS 5	51.73	49.45	54.74
TS 6	72.11	64.47	75.23
TS 7	49.53	46.65	51.21
TS 8	39.72	37.56	41.46
TS 9	81.84	73.83	89.04
TS 10	50.78	47.14	53.55
TS 11	57.61	55.04	58.00
TS 12	51.18	46.91	57.54
TS 13	94.73	84.75	97.37

[a]UB3LYP/6-311++G(2d,2p). [b]RHF-UCCSD(T)/6-311++G(2d,2p)//UB3LYP/6-311++G(2d,2p)

Reaction Channels I and II

The first and second reaction channels are related to the formation of phenol and the hydrogen radical (Figure 7.4.20). The formation of the phenol from radical **14** is well known and it has been studied,^[340] since it is a frequent thermal path in low-temperature

regime conditions. The B3LYP/6-311++G(2d,2p) calculated barrier is 29.74 kcal/mol (25.20 kcal/mol considering ZPE corrections) and 31.27 kcal/mol at the RHF-UCCSD(T)/6-311++G(2d,2p) level of theory. For the transition state **TS1** the distance between the H and C atoms is 1.753 Å. These values are similar to what have been previously obtained.^[339, 340] We have explored here the possibility of the formation of an stable intermolecular complex between phenol and hydrogen. With the B3LYP functional, this complex is unstable with respect to the isolated molecules. A complex between both molecules was not found with the UM05-2X functional. If a phenol – hydrogen complex is at all stabilized in matrix conditions, it would be probably very weak and it would not represent an important contribution to the reaction energy profile.

Thus, in the second step we have **15** and one hydrogen radical atom as reactants. Two possibilities were considered (Figure 7.4.20): The hydrogen radical attacks the phenol molecule (**15**) or it can diffuse through the matrix. If there is an attack of the hydrogen radical, then the ortho carbon radical **17** is produced. This radical **17** is -5.74 kcal/mol more stable than radical **14**. The calculated ΔE for the reaction between phenol and the hydrogen radical is -25.76 kcal/mol. The barrier for this step is very small ((B3LYP/6-311++G(2d,2p): 1.63 kcal/mol (2.63 kcal/mol with ZPE) and 3.58 kcal/mol at the RHF-UCCSD(T)/6-311++G(2d,2p) level of theory). The C-H distance for the transition state **TS2** is 1.923 Å and the ring is almost planar, which corresponds to an early transition state. An attack of the hydrogen radical to the meta or para carbon atoms of phenol is also considered here. The products are then the radicals **17-m** and **17-p**, which are -4.34 and -3.99 kcal/mol more stable than **14**. The corresponding barriers are slightly larger than the obtained for the ortho addition (**TS2-m** and **TS2-p**: 2.66 and 2.23 kcal/mol (3.65 and 3.29 kcal/mol considering ZPE), respectively). Therefore, the next steps are based in the ortho radical **17**, which leads straightforwardly to the product. The product can be obtained from the **17-m** and **17-p** radicals, too.

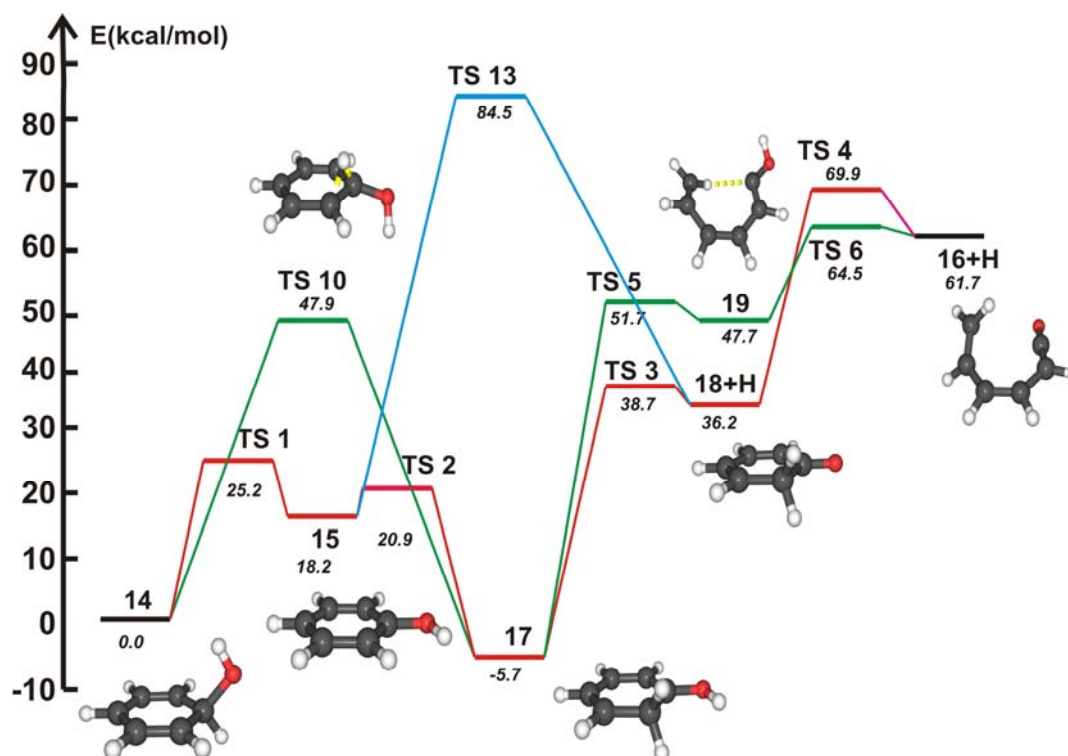


Figure 7.4.20. Energy profile (kcal/mol) of reaction channels I and II from radical **14** calculated at B3LYP/6-311++G(2d,2p) level of theory considering ZPVE.

The radical **17** can be formed in a single step from **14** via **TS10** (barrier 50.78 kcal/mol). The distances between the H atom and the ipso and meta carbons are 1.319 and 1.282 Å respectively. The breaking of the O-H bond in **17** needs an activation energy of 49.96 kcal/mol (44.53 considering ZPE and 50.53 kcal/mol at the RHF-CCSD(T) /6-311++G(2d,2p) level) to produce the intermediate **18** and one hydrogen atom. In the corresponding transition state, **TS3**, the O-H distance is 1.707 Å (Figures 7.4.19 and 7.4.20).

Phenol (**15**) isomerizes to **18** via **TS13**. The thermal decomposition of phenol produces cyclopentadiene (C_5H_6) and CO.^[355, 356] Zhu and Bozzelli^[349] studied theoretically the tautomeric equilibrium between phenol and 2,4 cyclohexadienone (**18**) and the ring opening reaction to form product **16**. Lin and Xu^[352] analyzed the phenol decomposition to C_5H_6 and CO. Three reaction channels were considered by these authors. The most feasible involves the phenol isomerization to **18** and the ring opening to produce **16**. Recently, Tseng *et al* studied^[351] the photodissociation dynamics of phenol employing multimass ion-imaging techniques and step-scan time-resolved Fourier-transform infrared spectroscopy. The products found by them are also cyclopentadiene and CO. They also analyzed the reaction channel from **15** to **16**. This reaction channel had also

been used to study the dynamics of O (1D)+C₆H₆ and C₆D₆ reactions, which produce C₅H₆ and CO.^[350]

For the **TS13** state, the O-H breaking (1.400 Å) and the C-H (1.408 Å) formation take place simultaneously. The calculated barrier for this step at the RHF-UCCSD(T)/6-311++G(2d,2p) level of theory is 73.47 kcal/mol, with B3LYP/6-311++G(2d,2p) is 70.76 kcal/mol (66.52 ZPE corrected). Both agree with the value of 68.7 kcal/mol obtained by Xu and Li at the G2//B3LYP/6-311G(d,p) level of theory.^[352]

The transition from **19** to **16** can occur via **TS4** and involves the breaking of the C-C bond. The calculated barrier for this step is 35.75 kcal/mol (ZPE corrected: 33.69 kcal/mol and RHF-UCCSD(T): 40.82 kcal/mol). The C-C distance changes from 1.527 in **18** to 2.207 in **TS4** to reach the value of 3.084 Å in **16**. The last step for all the reaction channels leads to the product in the completed closed conformation (**16-ccc**, Figure 7.4.17). The rotation around all bonds in **16** were considered and 8 isomers were found (Figures 7.4.23 and 7.4.24).

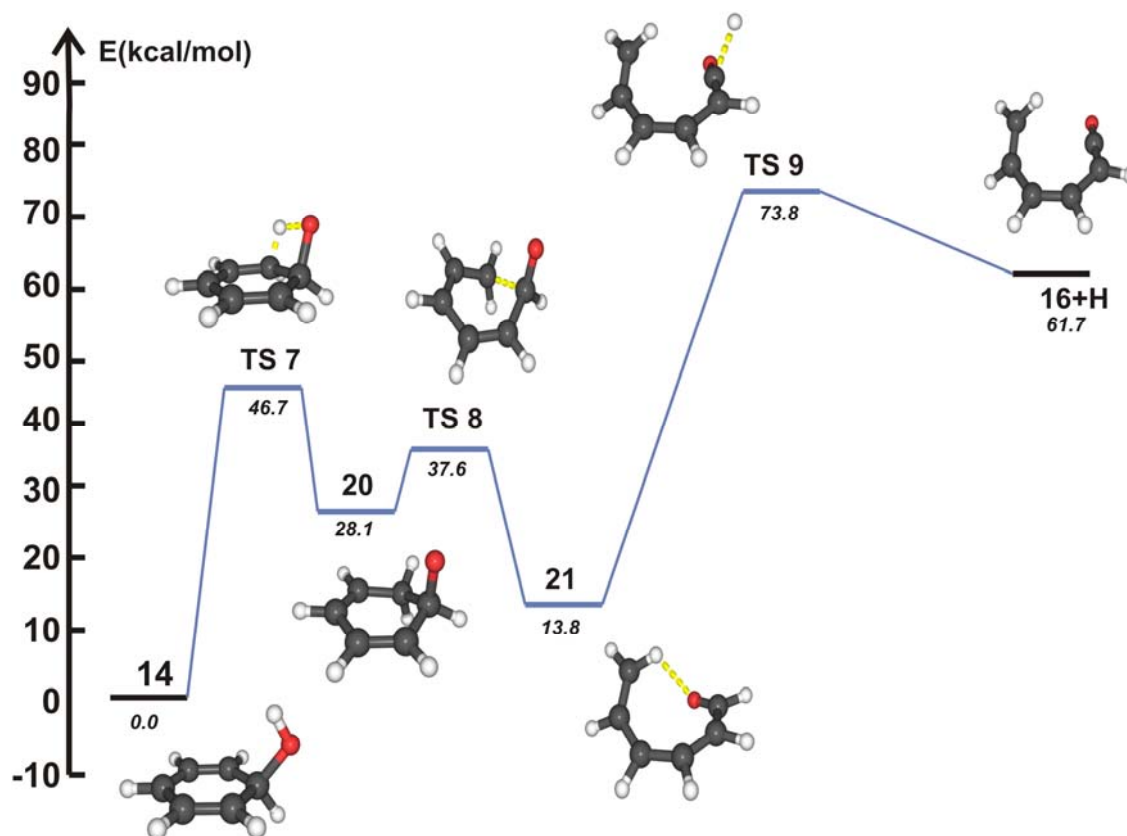


Figure 7.4.21. Energy profile (kcal/mol) of reaction channel III from radical **14** calculated at B3LYP/6-311++G(2d,2p) level of theory considering ZPVE.

In addition, another sub channel from **17** to **16** was considered. It implicates in the first step the ring opening to produce **19** via **TS5**. The barrier is 57.12 kcal/mol (ZPE corrected: 49.45 kcal/mol, RHF-UCCSD(T): 54.71 kcal/mol). The C-C distance (2.451 Å) is larger in **TS5** than in **TS4**. The barrier from **19** to **16** is 22.38 kcal/mol with the B3LYP functional (ZPE corrected: 16.74 kcal/mol) and 22.39 kcal/mol with RHF-UCCSD(T). The structure of **TS6** is similar to those of the final product **16** (Figures 7.4.17 and 7.4.19).

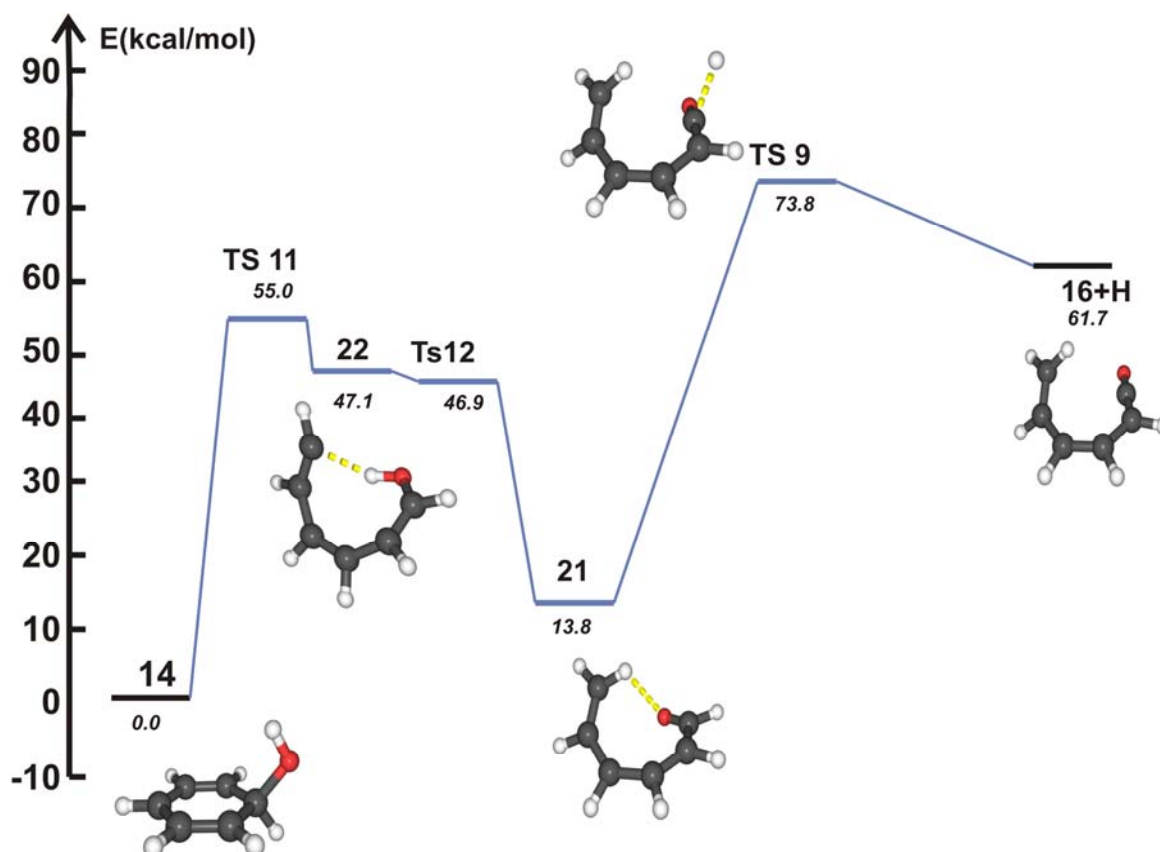


Figure 7.4.22. Energy profile (kcal/mol) of reaction channel IV from radical **14** calculated at B3LYP/6-311++G(2d,2p) level of theory considering ZPVE.

Reaction Channel III

Another reaction channel begins with the transfer of the H atom from the OH radical to the meta carbon atom of phenol. Intermediate **20** is produced through **TS7**. The barrier (49.53 kcal/mol, ZPE corrected: 46.65, RHF-UCCSD(T): 51.21 kcal/mol) is larger than the calculated for reaction channel I. The O-H bond is partially broken in **TS7** (1.379 Å) and the C-H bond is partially formed (1.282 Å). The next step is the ring opening to produce intermediate **21** via **TS8**. The barrier is small (B3LYP: 11.44 kcal/mol, ZPE corrected: 9.42 kcal/mol; RHF-UCCSD(T): 13.14 kcal/mol). The breaking of the O-H bond from **21** to form the product would require 56.25 kcal/mol through **TS9**. (Figures 7.4.20 and 7.4.21) The step from **21** to the products **16+H** has an ΔE of 54.48 kcal/mol (ZPE corrected: 47.85 kcal/mol and RHF-UCCSD(T): 50.79). Radical **21** is stabilized by the delocalization of the unpaired electron, since there are important spin densities on all atoms (NBO spin densities: 0.34, -0.13, 0.43, -0.14, 0.39 and 0.13 for C2, C3, C4, C5, C6 and O13 respectively). With the loss of the hydrogen atom in **16** the delocalization of the electron density decreases.

Reaction Channel IV

The fourth reaction channel involves the ring opening as the first step. The calculated barrier is 57.6 kcal/mol (55.4 considering ZPE correction and 58.0 kcal/mol with RHF-UCCSD(T)). This is the largest barrier from radical **14** and probably the less feasible path. The C-C length in the **TS11** geometry is 2.336 Å (Figure 7.4.19). Radical **22** is a reaction intermediate with a C...H distance of 2.035 Å (Figure 7.4.17). This distance is 1.556 Å in the transition state **TS12** (Figure 7.4.19) and decreases to 1.077 Å in radical **21**. We believe that the weak interaction found in radical **22** facilitates the simultaneous breaking of the O-H bond and the formation of the C-H bond in the next step. The barrier for this step is 1.05 kcal/mol with the B3LYP functional and 5.4 kcal/mol at the RHF-UCCSD(T) level of theory. If the ZPE correction is considered with B3LYP, the energy of **TS12** is smaller than the energy of **22**. Thus, the reaction would probably occur from **22** to **21**.

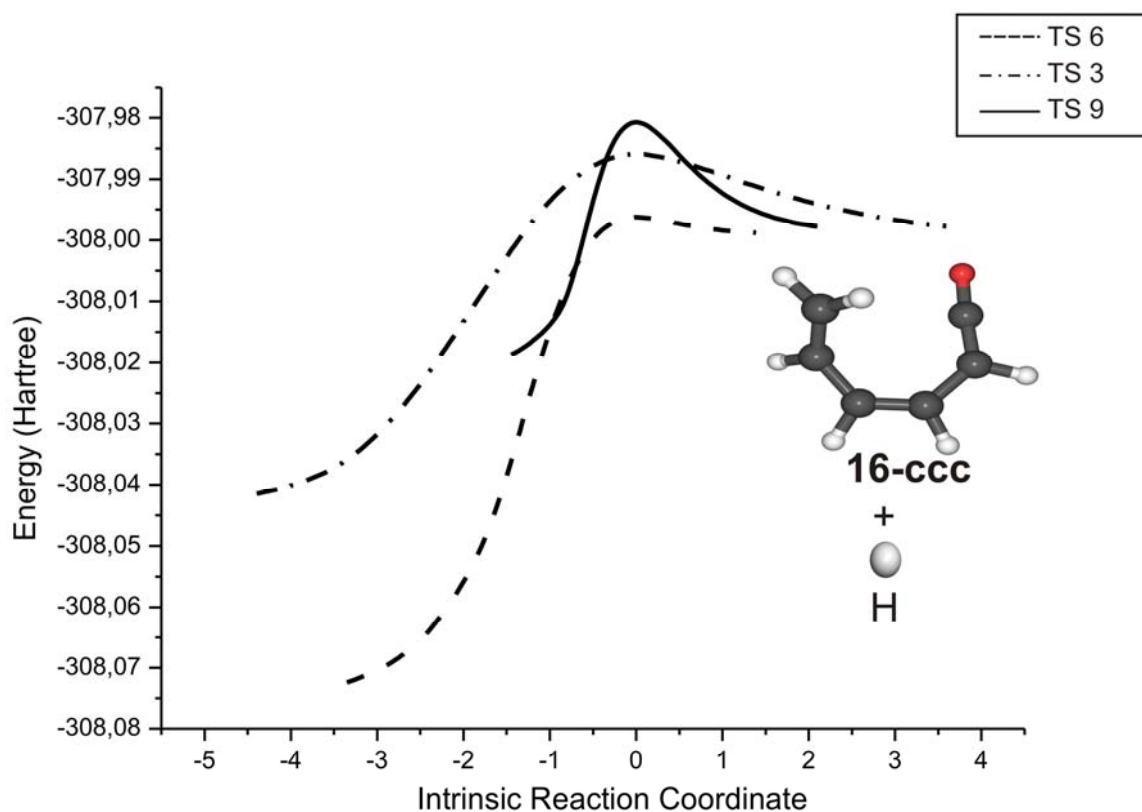


Figure 7.4.23. Intrinsic Reaction Coordinates (IRC) to the final product calculated at B3LYP/6-311++G(2d,2p)

In all reactions discussed above ketene **16** is formed in the *cis*- configuration and *s-cis* conformation **16-ccc** (Figure 7.4.17). The rotations around all bonds in **16** were

considered and 8 isomers were found (Figure 7.4.24). The most stable isomer is the *trans*-configuration and *anti*- conformation for all bonds (**16-ttt**). The next in energy (1.27 kcal/mol) is the isomer **16-tct** which differs in the configuration of the central bond. The barriers for the rotation around the bonds with the larger single bond character in the **16-ccc** isomer to produce **16-cct** and **16-tcc** are 11.9 and 8.9 kcal/mol, respectively. The barriers from **16-cct** and **16-tcc** to produce the **16-tct** isomer are 4.0 and 3.7 kcal/mol. The rotation around the bond with the larger double character in **16-tct** has a barrier of 65.5 kcal/mol to produce the most stable isomer **16ttt** . The spectra of all isomers are very similar (Table 7.4.7), therefore an unambiguous assignment is not possible.

Table 7.4.7. Calculated relative energies and IR frequencies for the ring opening product at B3LYP/6-311++G(2d,2p) level of theory

Isomers	16-ccc	16-cct	16-tcc	16-tct	16-ctc	16-ctt	16-ttc	16-ttt
Relative Energy (kcal/mol)	7.56	4.89	3.43	1.27	5.41	3.63	1.75	0.00
Vibrational Mode (cm ⁻¹)								
$\nu(\text{C}=\text{C}=\text{O})$	2173.6	2182.1	2170.5	2183.4	2176.8	2181.7	2176.6	2182.5
$\delta(\text{C}-\text{H})$	1443.7	1456.0	1432.8	1418.4	1424.3	1429.4	1425.9	1399.1
$\omega(\text{CH}_2)$	955.5	940.1	929.2	926.3	927.1	925.5	916.6	916.7
$\omega(\text{CH})$	562.2	610.8	567.9	609.1	655.8	606.4	579.2	615.2

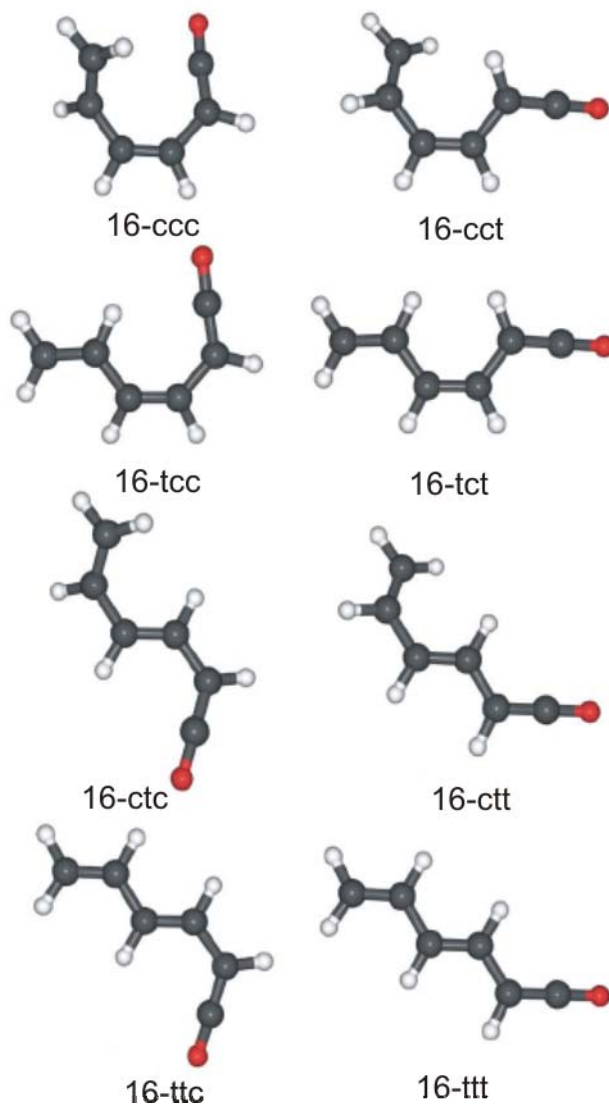


Figure 7.4.24. Isomers of product **16**, calculated at B3LYP/6-311++G(2d,2p) level of theory.

7.4.3. Summary

The phenyl radical **1** and water easily form a weakly bound π complex **1**...H₂O, with a structure **A** similar to that of the complex between benzene **13** and water. A second, according to our calculations slightly less stable complex **G** with a hydrogen bond to the radical center is not observed in the experiments. However, **G** is the pre-reactive complex leading to the abstraction of a hydrogen atom from water. The activation barriers for the rearrangements **A** \rightarrow **G** and **G** \rightarrow **A** have to be smaller than the binding energy of **A** and **G**, respectively, which explains that even under the conditions of matrix isolation only the

most stable complex is observed. On the other hand, **G** should be easily available on thermal or photochemical excitation of **A**.

According to our IRC calculations complex **G** is directly connected to the **13...HO** complex. The activation barrier of 13.63(9.84) kcal/mol at the M05-2X(B3LYP) level of theory is too high for a thermal reaction under the conditions of matrix isolation, however, visible light irradiation completely drives the reaction to the **13...HO** complex. This reaction is slightly endothermic, however, at room temperature calculated to be exergonic.^[320] Our experiments don't allow to differentiate between a photochemical reaction and a hot ground state reaction. However, it is most remarkable that the elusive complex between OH and benzene could be isolated and spectroscopically characterized, although it exists in a very shallow minimum and is both thermo- and photolabile.

The structure calculated for the **13...HO** complex depends much on the theoretical method used for the calculation. At the B3LYP level of theory the structure is as shown in Figure 7.4.13, in accordance with previous calculations.^[319, 320] This structure corresponds to an intermediate to the addition of OH to benzene **13** with the O atom interacting with one of the ring carbon atoms. The hydrogen atom of OH only weakly interacts with the benzene π system. In contrast, the structures obtained at the UM05-2X or UMP2 levels of theory shows a strong OH... π interaction as in the **1...H₂O** complex. The stabilization energy calculated with these methods is considerably higher than that calculated with B3LYP. It is therefore plausible to assume that the B3LYP calculated structure is an artifact which is confirmed by the comparison of the experimental IR spectrum of **13...OH** with the calculated spectra. The B3LYP calculations predict a blue-shift of the OH stretching vibration, which is in accordance with a C...O interaction and the OH hydrogen atom not involved in hydrogen bonding. In contrast, the M05-2X and UMP2 calculations predict a red-shift, as expected for the OH... π interaction, in excellent agreement with the experiment.

Irradiation of **13...HO** complex leads directly to ketene **16** as the major product while radical **14** or other intermediates are not observed. Radical **14** is the only plausible product formed from the **13...HO** complex, and all reasonable mechanisms for the formation of **16** require the formation of **14** as an intermediate. We therefore conclude that **14** is indeed formed, however, either with a large excess energy that leads to further reactions or it is photochemically unstable under the conditions of its formation. The formation of **16** and a hydrogen atom from radical **14** is calculated to be exothermic by 61.7 kcal/mol. If we

assume that the hydrogen atom dimerizes to give molecular hydrogen, this value is reduced by 52 kcal/mol.

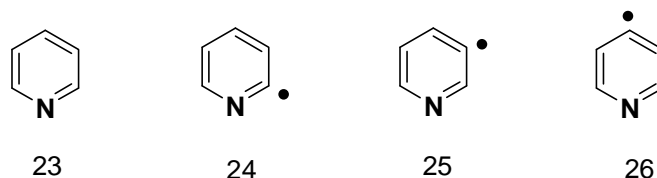
The most plausible reaction mechanism for the formation of ketene **16** is the sequence **14** → **15** + H → **7** → **17** + H → **16** + H. In the first step, phenol **15** and a hydrogen atom is formed from radical **17**. The hydrogen atom adds to the *ortho* position of phenol to give radical **17**. This loses the OH hydrogen atom to give **18** which finally ring-opens to **16**. Since we don't see experimentally any of the proposed intermediates, and since we not even know if the reaction proceeds on the ground state or an excited state, the mechanism remains speculative. However, the overall reaction is highly efficient and might be of relevance to atmospheric chemistry. Overall, the reaction between the phenyl radical **1** and water allows to gain insight into both reaction channels of the reaction between benzene **13** and the OH radical: the hydrogen abstraction, coming from the product side, and the addition, resulting in the complete destruction of the aromatic ring system.

Chapter 8. Pyridyl Radicals

8.1. Introduction.

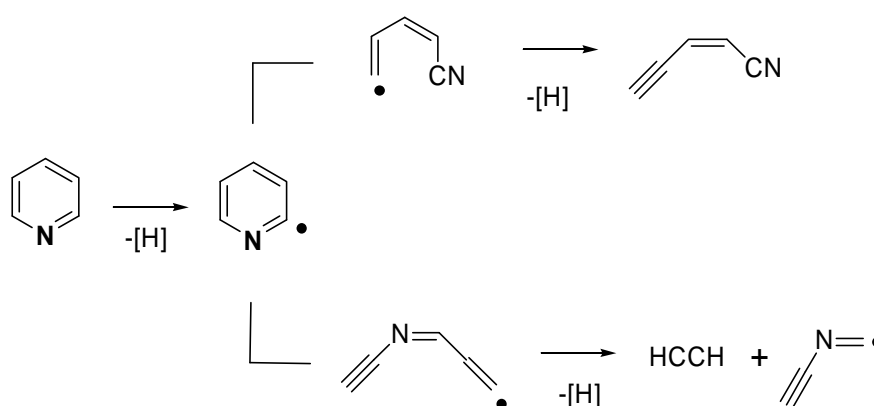
Heavy fuels, such as coal and coal-derived liquids are complex mixtures of aromatic hydrocarbons containing significant amount of nitrogen and sulfur.^[357] The combustion of those hydrocarbons produces oxides of these elements, which lead to environmental pollution, which constitute a class of the most widespread atmospheric pollutants.^[358-360] Different strategies of have been developed in order to reduce the oxides formation, because many of them are potent mutagens and carcinogens.^[361] However, completely satisfactory solution has not been found. It is well known that fuel bound nitrogen is predominantly in the form of aromatic heterocyclic such as pyrrole and pyridine rings.^[362-364]

Pyridine (**23**) is ideal model compound to study the complex chemical reactions that occurs when heavy fuels undergo pyrolysis and combustion. Therefore many theoretical and experimental investigations have been carried out.^[365-368] Thermal decomposition of **23** in the temperature range of 600 – 650 °C was carried out, and the major products of pyridine decomposition are atomic hydrogen and 2,2-bipyridine.^[369] In the higher temperature range the formation of hydrogen cyanide was observed as predominate product. A shock-tube pyrolysis study of **23** was studied by Mackie et al.^[365] They found that in the temperature range of 1300 – 1800 K the cyanoacetylene was the principal nitrogen-containing product. At elevated temperatures, hydrogen cyanide predominates. The thermal decomposition is interpreted as a chain reaction initiated by the C–H bond scission, which can lead to the formation of three possible pyridyl radical, the *o*-pyridyl radical (**24**) was predominate one.^[365]



Liu et al.,^[366] carried out a detailed quantum mechanical study of the unimolecular decomposition mechanism of **23**. DFT calculation indicates that the C–H bond scission in pyridine preferentially produces the *o*-pyridyl radical (**24**). The most energetically favourable decomposition channels of the pyridyl radicals is ring opening via C–N bond

cleavage and also the C–H bond cleavage leading to the formation of cyanovinylacetylene.^[366, 370-372] However, when activation entropies are taken into consideration, the most kinetically favourable pyrolysis pathway of pyridine (**23**) is the C–H bond dissociation producing *o*-pyridyl radical (**24**), followed by C–C bond fission producing acetylene and cyanovinyl radical (Scheme 8.1).^[366]



Scheme 8.1. Unimolecular decomposition channel of *o*-pyridyl radical (**24**).^[366]

Pyridine is the prototypical aromatic species that is encountered in many areas of pure chemistry, combustion chemistry, environmental chemistry and biochemical problems, than pyridyl radicals are equally fundamental molecules. Pyridyl radicals are formally can be derived from the homolytic cleavage of the C–H bond of pyridine. Three possible isomers 2-(*ortho*), 3-(*meta*) and 4-(*para*) pyridyl radical (**24**, **25** and **26**) can be obtained.

Kasai et al.^[373] have reported the ESR spectra of all three pyridyl radicals by photolysis of the corresponding iodides in argon matrices. Subsequently they have also succeeded to generate the ESR spectra of three pyridyl radicals in argon matrices by the method of dissociative electron capture, to be found that all three pyridyl radicals are σ -type radicals. 2-pyridyl radical (**24**) has been identified in γ -irradiation pyridine and show to be a σ -type radical by Bower et al.^[374]

Another interesting aspect has been expended in literature from the theoretical point of view of the interaction between single occupied molecular orbital (SOMO) of the broken bond and the lone-pair orbital of the nitrogen can be expected to affect the stability of these radicals.^[375, 376] The open-shell RHF and UHF methods were employed to study the orbital shape of pyridyl radicals. The RHF calculation showed that the SOMO of each

radical is localized mainly on the carbon atom at the radical center, and atomic spin population at the carbon atom is the highest for **26**.^[375]

Results introduced in this chapter are divided into two main parts; the first part is a brief analysis of the structures and orbitals of pyridyl radicals obtained by the DFT method. The density functional method has been applied to calculate the total energy of the pyridyl radical at the ground state. The second part, described the matrix isolation study of pyridyl radical. This allowed recording the complete mid IR spectrum, which has so far been unknown. In the infrared spectra the absorption frequencies are compared with the harmonic frequencies calculated with the UB3LYP hybrid functional using the cc-pVTZ basis set. The thermal reaction of pyridyl radicals with molecular oxygen and the photochemistry of the intermediates are also reported.

8.2. Molecular and electronic structure

Figures 8.2.1 and 8.2.2 show the optimized geometries and the spin densities of pyridyl radical **24**, **25** and **26** calculated at the UB3LYP/cc-pVTZ level of theory. The bond angles at the radical centers are deformed considerably from the original hexagonal angles. The CN bond length in **24** is 1.279 Å, which is very short in comparison with those in **25** and **26**, which are 1.343 and 1.329 Å, respectively.

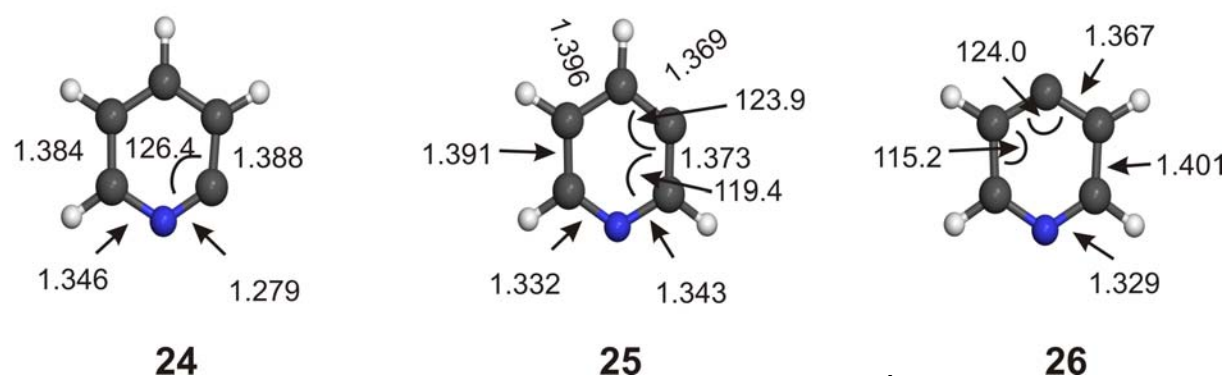


Figure 8.2.1. Selected structural parameters (bond lengths in Å) of pyridyl radicals calculated at the UB3LYP/cc-pVTZ level of theory.

NBO calculations indicate that the spin densities of the pyridyl radicals are mainly localized at the carbon atom of the radical center. The atomic spin densities of all three pyridyl radicals (**24** – **26**) predicted by DFT calculations are 0.80, 0.89 and 0.92, respectively (Figure 8.2.2). According to RHF calculations the *m*-pyridyl radical (**25**) has

the highest spin population at the carbon atoms 0.918, more than the *p*-pyridyl radical (**26**) – 0.916, and *o*-pyridyl radical (**24**) – 0.879.^[375]

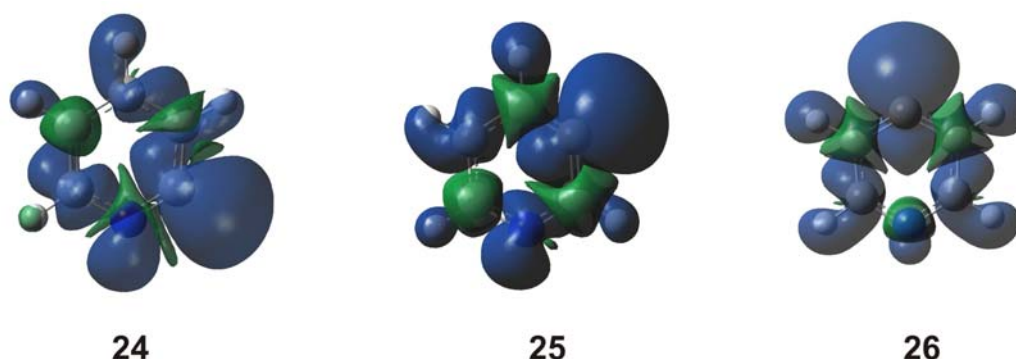


Figure 8.2.2. Spin densities in the **24** – **26** calculate at the UB3LYP/cc-pVTZ level of theory.

The energies of the three pyridyl radicals are presented in Table 8.2.1, in agreement with early semiempirical and ab initio calculation,^[375] the *o*-pyridyl radical (**24**) is about 5.17 and 6.32 kcal/mol more stable than *p*- and *m*-pyridyl radicals (**25** and **26**), respectively (Table 8.2.1). This is caused by the interaction between the nitrogen nonbonding orbital and the unpaired electron (SOMO) at the adjacent carbon atom in **24**. Kikuchi et al.,^[375] carried out RHF calculation, and found that the stability of **24** due to the interactions between the calculated orbital energies of the SOMO and the nonbonding orbital. According to the RHF calculations, the SOMO of **24** is higher than of **25** and **26**, while the nonbonding orbital of **24** lies lower than of **25** and **26**, which indicates an appreciable interaction between the two orbitals in **24**.^[375]

Table 8.2.1. Energies^a of **24**, **25** and **26**.

Method ^b	<i>o</i> -pyridyl (24)	<i>m</i> -pyridyl (25)	<i>p</i> -pyridyl (26)
UB3LYP	0.0	6.32	5.17
UB3LYP (ZPE)	0.0	6.18	4.88
UM052x	0.0	7.36	5.46
UM052x (ZPE)	0.0	7.03	5.02

[a] The energy are given in kcal/mol relative to **24**. [b] The cc-pVTZ basis set was used in the UB3LYP and UM052x calculations.

Pyridyl radicals are essentially pyridine molecules that lost the hydrogen atom, a result in the *o*-pyridyl radical (**24**), the symmetry drops from C_{2v} to C_s . The Kohn-Sham molecular orbital in the upper valence region calculated TD-DFT method is shown in Figure 8.2.3.

In the case of pyridine (**23**), the highest molecular orbital can be described as a combination of C–H σ bonds (Figure 8.3.4). When the C–H bond in the *ortho*-position is broken, it will destabilize and become the highest singly occupied molecular orbital (SOMO), shown in Figure 8.2.3. The second highest molecular orbital (HOMO-1) and the third highest molecular orbital (HOMO-2) of pyridine represent out-of-plane π -type combinations (Figure 8.3.4) that are not affected by the breaking of the σ -type C–H bond. Upon formation of **24** they remain unchanged (Figure 8.2.3).

Figure 8.2.3 shows the singly occupied MO (SOMO), second and third highest doubly occupied MO HOMO-1 and HOMO-2 of **25** and **26**, respectively. Similar to **24**, the MO which represent π -type combination do not affected at all by the breaking of the C–H bond.

The DFT calculations suggest that all three pyridyl radicals have 2A ground state.

Figure 8.2.3 shows the orbital energies of the pyridyl radicals (**24** – **26**) in the upper valence region. In **25** and **26**, HOMO-1 and SOMO energies are fairly constant, while the SOMO of **24** lies higher in energy than those of **25** and **26**. This is in agreement with previous semiempirical and ab initio studies. So far the origin of the stability of **24** among of all three pyridyl radicals is not clearly understood, although the interaction between the SOMO and the nonbonding orbital may have some contribution. Therefore, high level theoretical calculations are required to understand the origin of this stability.

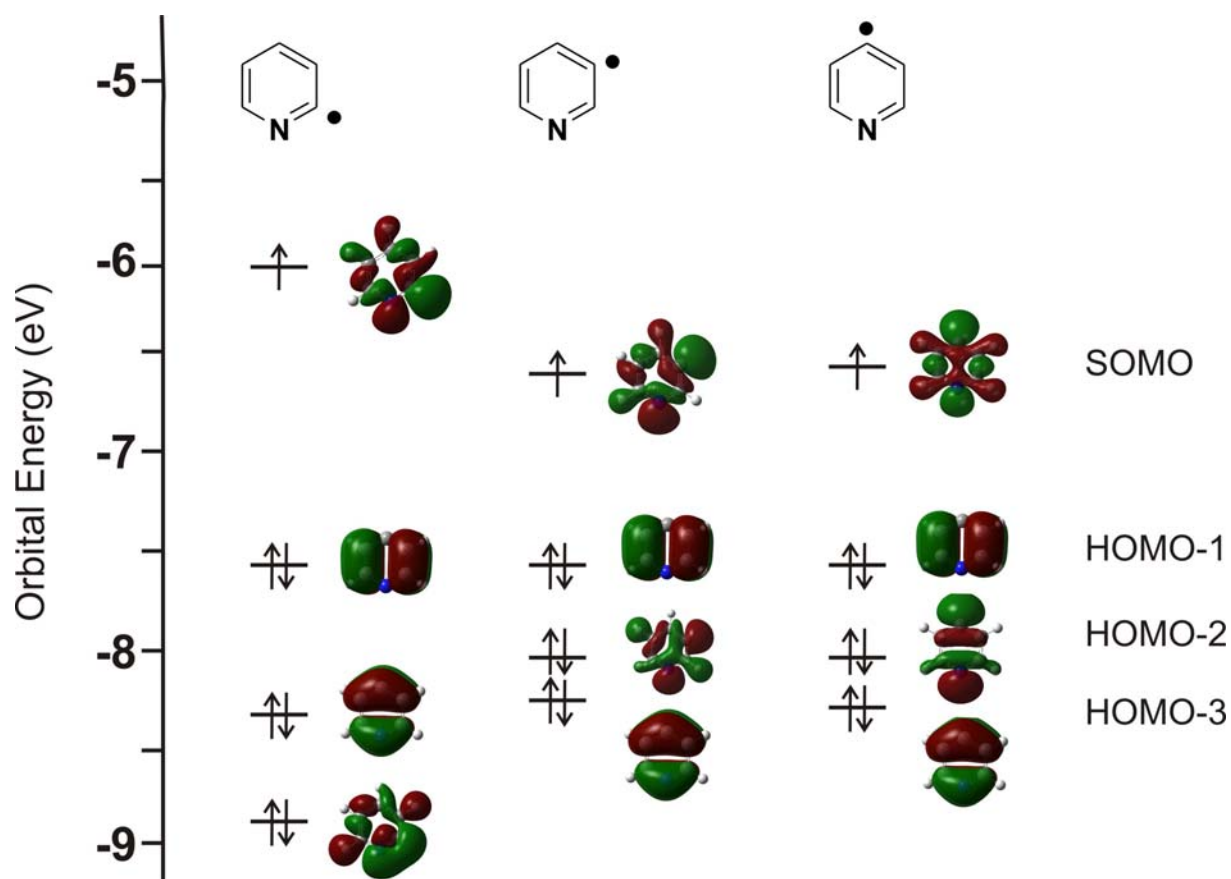


Figure 8.2.3. TD-B3LYP/cc-pVTZ SOMO, HOMO-1, HOMO-2 and HOMO-3 eigenvalues for the pyridyl radicals.

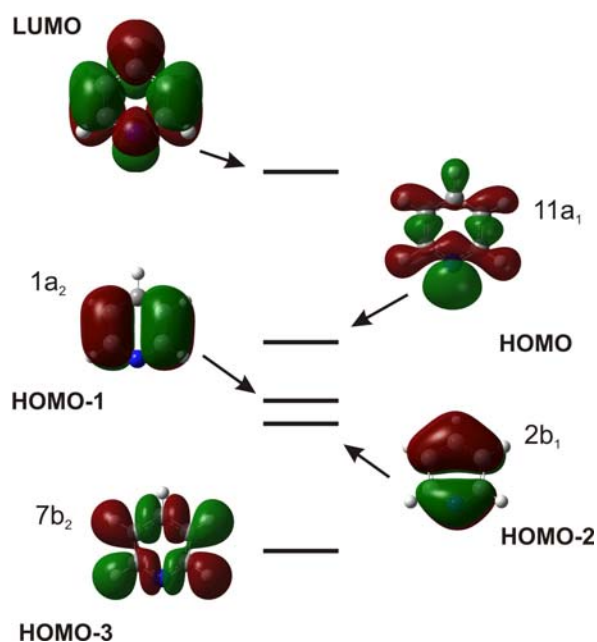


Figure 8.2.4. Selected Kohn-Sham molecular orbital of pyridine (**23**) calculated by means of TD-B3LYP/cc-pVTZ level of theory.

8.3. Matrix Isolation Study

8.3.1. o-Pyridyl Radical (**24**)

Due to the low C–I dissociation energy,^[377] 2-iodopyridine (**27**) has been used as precursor for the matrix isolation of **24**. FVP of **27** at temperatures between 620 and 700°C with subsequent trapping with a large excess of argon at 10 K produces **24** in good yields. Byproducts found in these matrices are iodine (invisible in the IR), pyridine (**23**) (formed via hydrogen abstractions from **24**) and traces of acetylene, diacetylene and HCN (product of the thermal fragmentation of **27**). A second major product formed under these conditions is pyridine **23**, obtained from **24** either via hydrogen abstraction from surface contaminations of the pyrolysis oven or via bimolecular reactions or rearrangements in the gas phase.

The IR spectrum of a matrix-containing the FVP products of **27** are shown in Figure 8.3.1.1. The strong absorptions at 735.1 and 564.5 cm⁻¹ are assigned to **24**, which are in excellent agreement with the IR spectrum of **24**, calculated at the UB3LYP/cc-pVTZ level of theory (Figure 8.3.1.1) (Table 8.3.1.1).

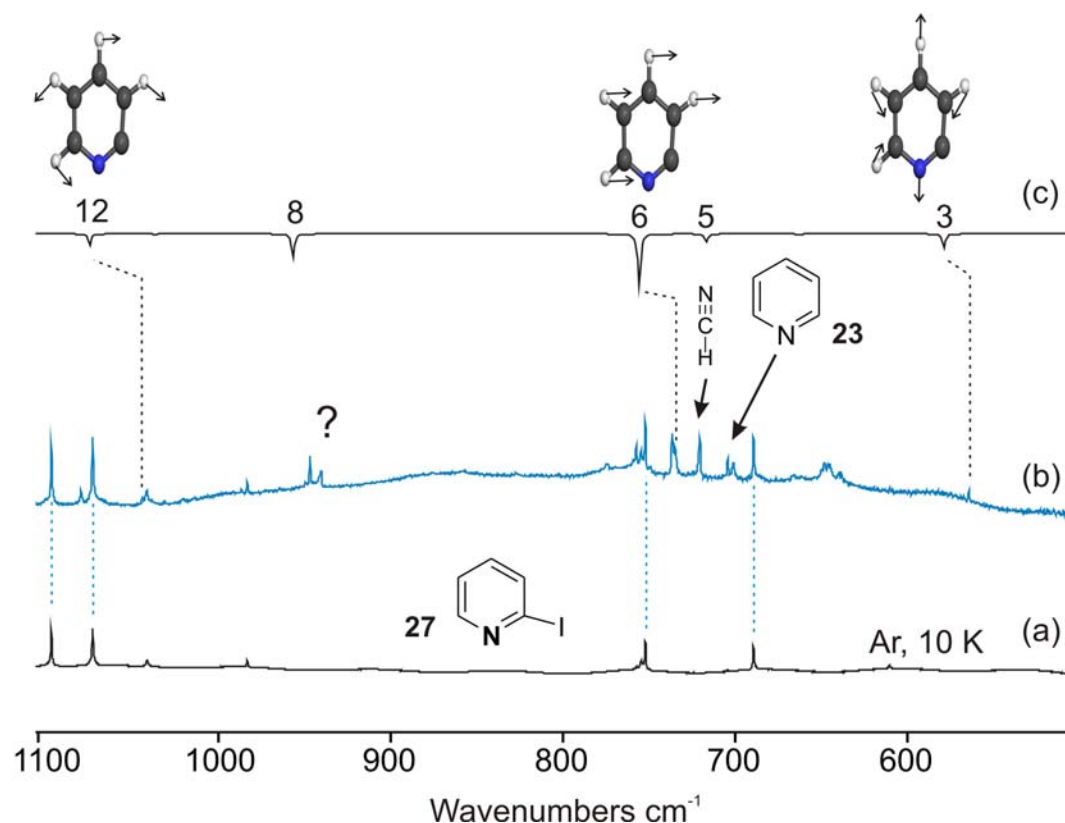


Figure 8.3.1.1. FVP products of **27**. (a) IR spectrum of a matrix (Ar at 10K) isolated **27**. (b) IR spectrum of a matrix (Ar at 10K) isolated the **24**, containing products from FVP of **27**. (c) Calculated vibrational spectrum (UB3LYP/cc-pVTZ) of **24**.

In order to provide clear assignments, we also investigated the photochemistry of **27** in argon matrix (Figure 8.3.1.2) (Table 8.3.1.1) UV irradiation (254 nm) 2-iodopyridine (**27**), matrix isolated in solid argon at 10 K, results in the decrease of IR bands of **27**, and simultaneously formation of several new compounds (Figure 8.3.1.2) Set of bands are assigned to **24** with the agreement with previous FVP experiments mentioned above. Subsequent annealing of the matrix containing photoproducts at 30 K for several minutes' results in a decrease of the bands assigned to **24** and subsequently the formation of **27**. The photolysis of a matrix-isolated **27** produces the **24** and an iodine atom in the matrix cages. Annealing of matrix containing radical pairs results almost exclusively in radical recombination. While other bands do not effected upon annealing, indicating the formation ring opening products (Figure 8.3.1.2) (Table 8.3.1.1).

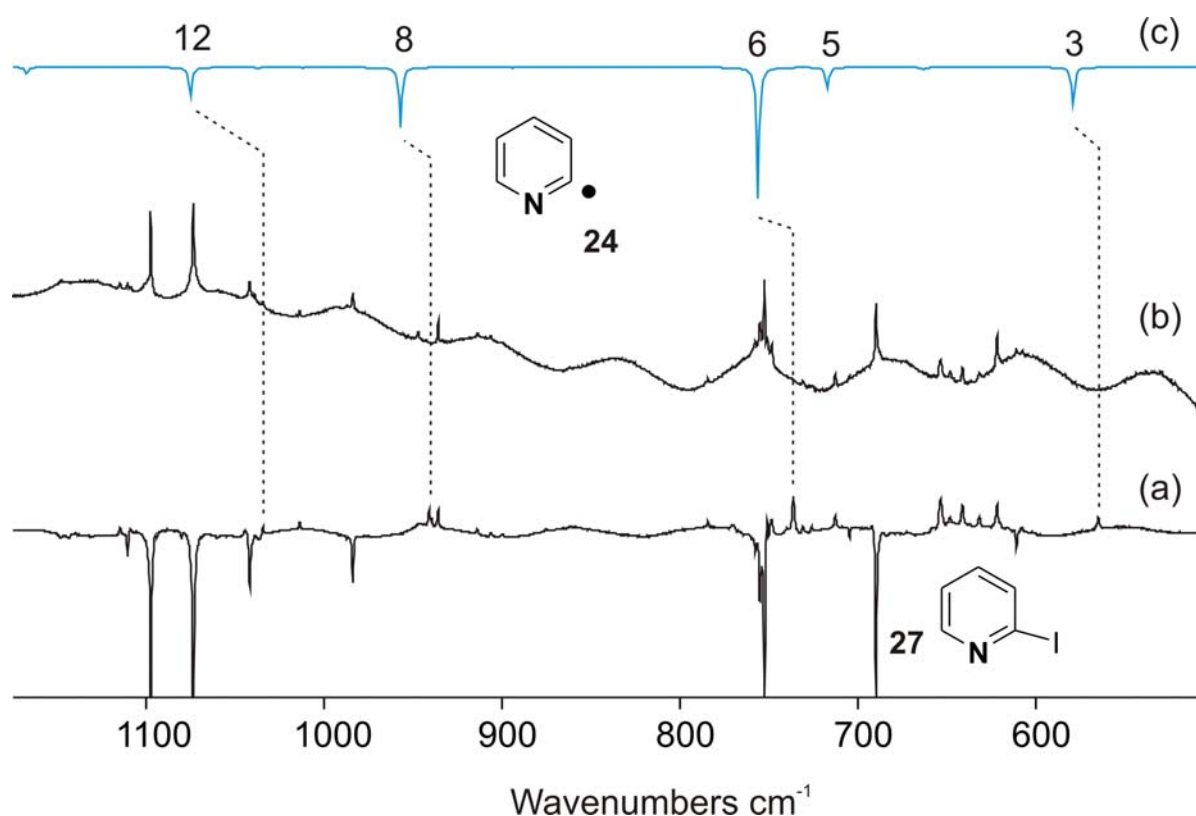


Figure 8.3.1.2. Photochemistry of **27** in solid argon. (a) Difference spectrum. Bands pointing downwards are disappearing during irradiation ($\lambda = 254$ nm) are belong to **27**. Bands pointing upwards are appearing and assigned to **24**. (b) IR spectra showing the annealing of **24** in argon after 15 min at 30 K. Bands that assigned to **24** are disappearing during annealing. (c) Calculated vibrational spectrum (UB3LYP/cc-pVTZ) of **24**.

Table 8.3.1.1. Observed and calculated IR bands of **24**.

Mode	$\nu_{\text{exp}}[\text{cm}^{-1}]^{[a]}$	$I_{\text{rel. exp.}}^{[b]}$	$\nu_{\text{calc}}[\text{cm}^{-1}]^{[c]}$	$I_{\text{rel. calc.}}$
12	1044.3	18	1075.1	22
10	-	-	1012.6	1
9	-	-	975.9	0
8	940.8	44	957.0	45
7	-	-	894.5	0
6	736.2	100	756.1	100
5	-	-	717.0	16
4	-	-	664.0	2
3	565.0	32	579.1	28

[a] Argon, 10 K. [b] Relative intensities based on the strongest absorption. [c] Calculated at the UB3LYP/cc-pVTZ level of theory.

8.3.2. *o*-Pyridyl Peroxy Radicals (**28a** and **28b**)

In order to synthesize the oxygen trapping products of **28a** and **28b**, the argon was doped with 2% O₂. FVP of **27** in O₂-doped argon again resulted in the formation of pyridine, HCN and acetylene. In addition, new strong to medium IR absorptions are found at 1598.7, 1464.7, 1428.6, 1310.1, 1260.1, 1176.5, 1125.4, 1038.8, 986.4, 803.5, 774.6, and 726.5 cm⁻¹ (Figure 8.3.2.1, Table 8.3.2.1). If ¹⁸O₂ is used in the FVP, these bands show only very small isotopic shifts of less than 1 cm⁻¹. However, a weaker band at 1125.4 cm⁻¹ shows a huge red-shift of -56.2 cm⁻¹ which clearly indicates a O–O stretching vibration. Other large red-shifts are found for a weak absorption at 803.5 cm⁻¹ (-12.4 cm⁻¹) assigned to a $\nu(\text{CO})$ stretching vibration. A comparison of the newly formed bands in O₂-doped matrices with DFT calculations (UB3LYP/cc-pVTZ) of the *o*-pyridyl peroxy radical **28a** shows an excellent agreement. These experiments clearly show that the *o*-pyridyl radical **24** reacts with molecular oxygen in the gas phase to produce **28a**.

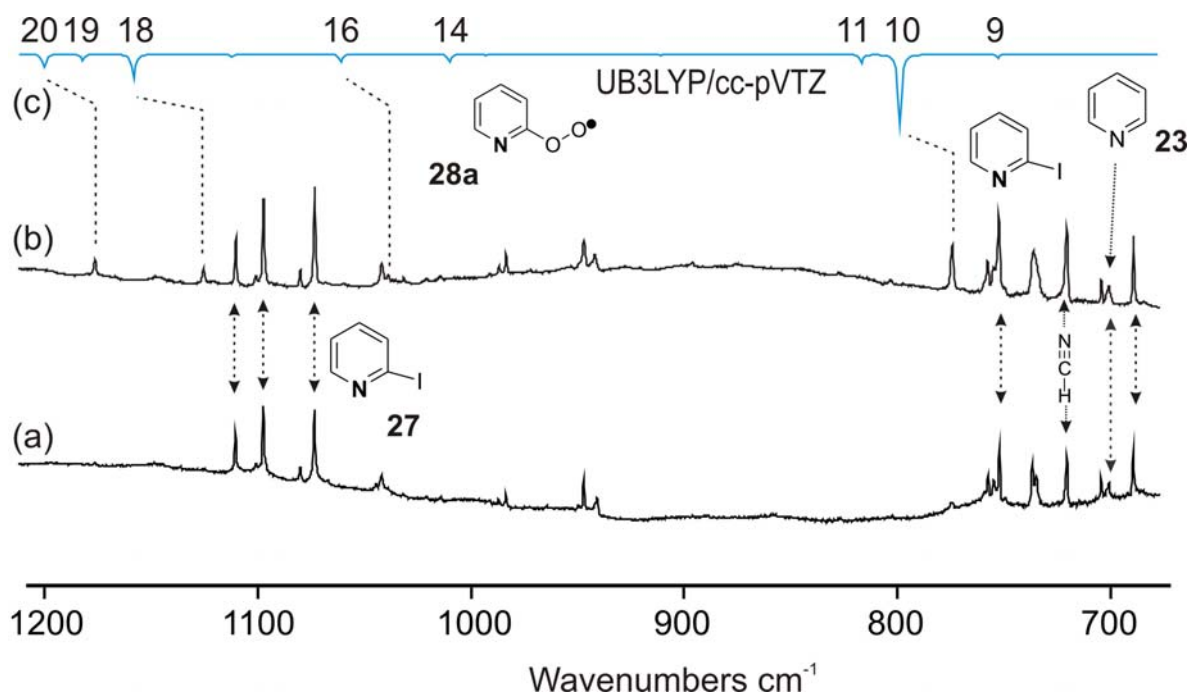
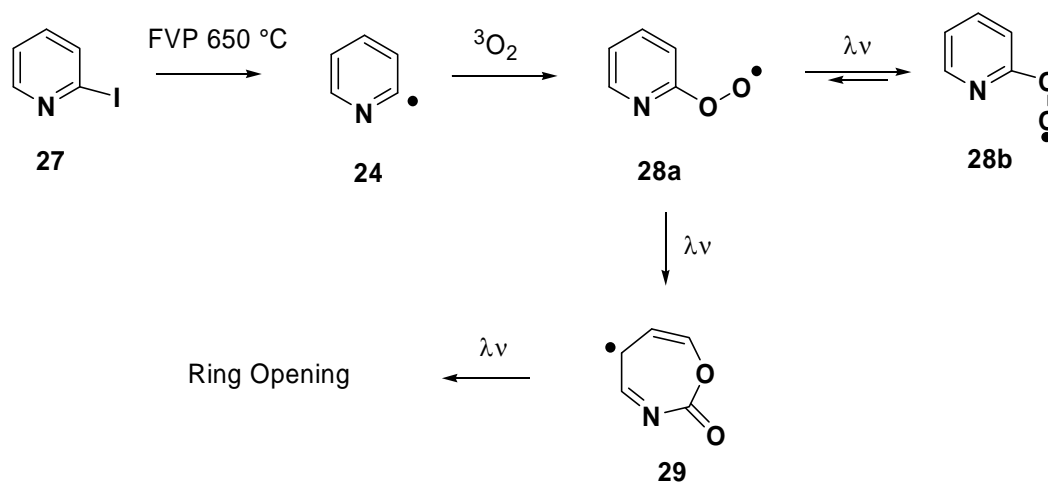


Figure 8.3.2.1. FVP products of **27**. (a) IR spectrum of a matrix (Ar at 10K) isolated the **24**, containing products from FVP of **27**. (b) IR spectrum of a matrix (Ar at 10K) isolated the **28a**, containing products from FVP of **27** in 2% O₂-doped argon with subsequent trapping at 10 K. (c) Calculated vibrational spectrum (UB3LYP/cc-pVTZ) of **28a**.



Scheme 8.3.2.1. Reaction of the *o*-pyridyl radical **24** with molecular oxygen

Table 8.3.2.1. IR spectroscopic data of the *o*-pyridyl peroxy radical **28a**.

Mode ^a	C ₅ NH ₄ OO (28a)		C ₅ NH ₄ ¹⁸ O ¹⁸ O (¹⁸ O ₂ - 28a)		Sym.	Assignment
	Argon ^b	DFT ^c	Argon ^b	DFT ^c		
26	1598.7 (27)	1637.6 (62)	1596.3 (59)	1636.8 (63)	A'	ring str.
25	1573.2 (5)	1613.4 (36)	1571.6 (17)	1613.5 (36)	A'	ring str.
24	1464.7 (10)	1500.2 (18)	1465.4 (37)	1500.0 (19)	A'	ring str./C C-H def.
23	1428.6 (84)	1464.0 (90)	1429.5 (46)	1463.5 (89)	A'	C-H def.(in plane)
22	1310.1 (4)	1340.7 (3)	1308.9 (1)	1339.7 (3)	A'	C-H def.(in plane)
21	1260.1 (6)	1312.1 (3)	1262.1 (3)	1311.1 (2)	A'	C-H def.(in plane)
20	1176.5 (41)	1200.9 (18)	1171.4 (33)	1191.1 (28)	A'	O-O str./C-H def.
19	-	1182.3 (8)	-	1168.7 (9)	A'	C-H def./O-O str
18	1125.4 (40)	1158.3 (34)	1069.2 (17)	1111.0 (13)	A'	O-O str/C-H def.
17	-	1113.0 (4)	-	1112.4 (0)	A'	C-H def.(in plane)
16	1038.8 (16)	1061.6 (11)	1036.3 (12)	1060.6 (12)	A'	C-H def.(in plane)
14	986.4 (5)	1010.1 (11)	985.9 (<1)	1009.8 (14)	A'	ring str.
13	-	993.4 (1)	-	993.2 (1)	A''	C-H def.(out-of- plane)
12	-	911.9 (2)	-	911.5 (2)	A''	C-H def.(out-of- plane).
11	803.5 (8)	817.8 (12)	791.1 (21)	804.7 (14)	A'	C-O str./ ring str.
10	774.6 (100)	799.7 (100)	775.2 (100)	799.1 (100)	A''	C-H def.(out-of- plane)
9	726.5 (1)	753.4 (6)	728.6 (7)	753.2(6)	A''	C-H def.(out-of- plane)
8	632.3 (2)	646.4 (3)	-	638.4 (3)	A'	ring str.
7	604.3 (4)	610.0 (11)	-	597.2 (9)	A'	ring def.

[a]Mode numbers based on the C₅NH₄¹⁶O¹⁶O isotopomer. [b]Argon matrix at 10 K. Wavenumbers in cm⁻¹ and relative intensities in parenthesis. [c]Calculated at the UB3LYP/cc-pVTZ level of theory

According to DFT calculations the reaction **24** with O₂ results in the formation of two possible conformers **28a** and **28b**. The experimental data indicate the presence of only one conformer in the argon matrix. UB3LYP/cc-pVTZ calculations show that conformer **28a** is by 2.01 kcal/mol (ZPE = 1.84 kcal/mol) more stable than conformer **28b**. The activation barrier for the **28a** → **28b** isomerization is calculated to be 4.74. kcal/mol (ZPE=4.45 kcal/mol) (Figure 8.3.2.2). The calculated IR spectrum of **28a** is in good agreement with the experimental spectrum of **28a**, and there is no evidence for the formation of the less stable conformer **28b**.

The reaction of **24** with O₂ is exothermic by 43.07 kcal/mol (UB3LYP/cc-pVTZ). We also performed PES calculation using partial geometry optimization between reactants (**24** and O₂) and *o*-pyridyl peroxy radical (**28a**). The length of the forming C-O bond was kept fixed (between 1.4 up to 5.0 Å) whereas all parameters were optimized (Figure 8.3.2.3). As seen from the plot of the potential energy curve against the length of the forming bond, the energy smoothly decreases while *o*-pyridyl peroxy radical (**28a**) is

formed. According to this there is no definitive transition state exists for the reaction of **24** with O_2 .

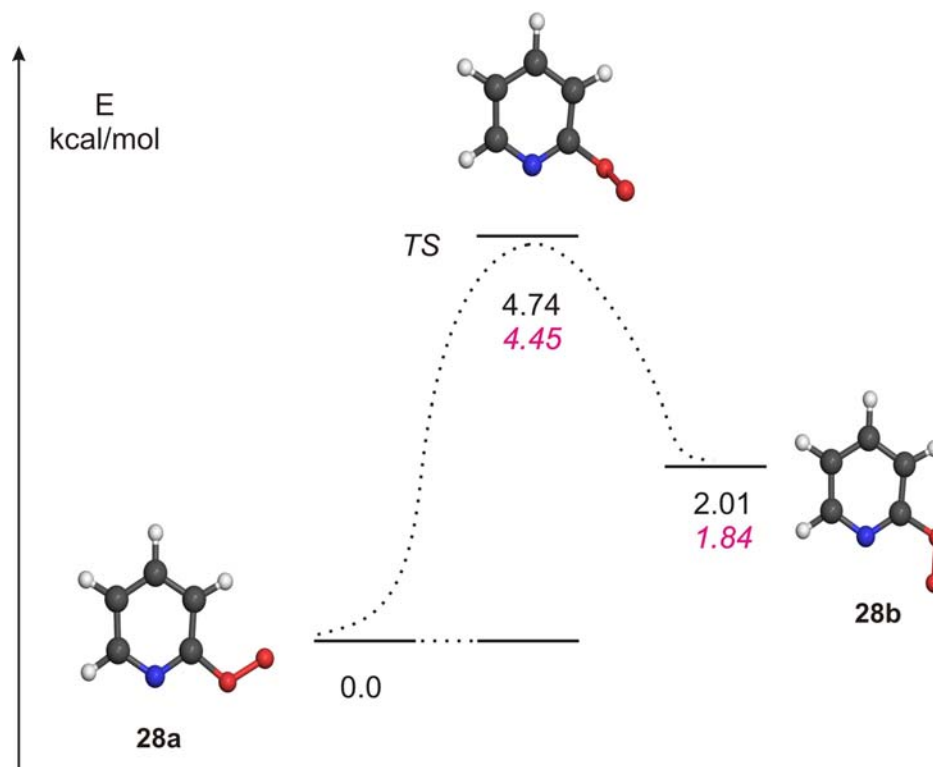


Figure 8.3.2.2. Theoretical isomerisation partway between two isomers of *o*-pyridyl peroxy radicals (**28a** and **28b**). Stationary points and transition state were performed by use B3LYP/cc-pVTZ method.

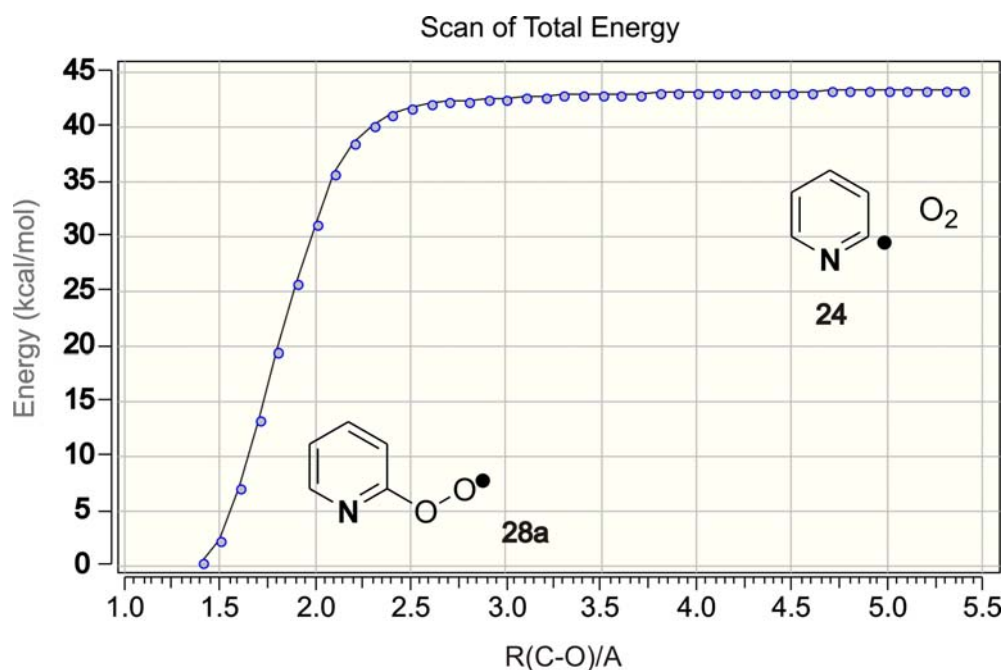


Figure 8.3.2.3. The **28a** dissociation potential energy surface calculated at the B3LYP/cc-pVTZ level of theory.

We also calculate PES for **28b**, again according to UB3LYP/cc-pVTZ there is no transition state for the reaction of **24** with O₂ (Figure 8.3.2.4).

According to DFT calculations the ground states of **28a** and **28b** are of Cs and ²A'' symmetry.

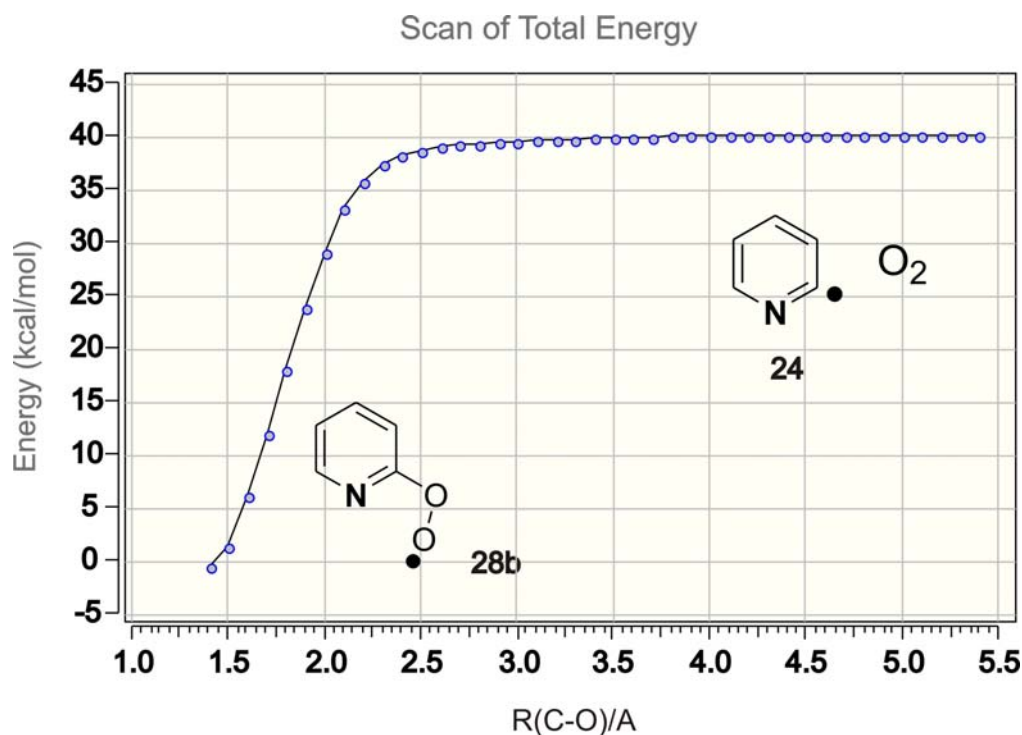


Figure 8.3.2.4. The **28b** dissociation potential energy surface calculated at the B3LYP/cc-pVTZ level of theory.

Now the question is, if there is no barrier between reactants (**24** and O₂) and products (**28a** and **28b**), then why **28a** formed in argon matrix while there is no evidence of the formation **28b**, even after annealing experiments. Before to begin to answer this question, we have performed the photochemical studies.

Irradiation of matrix-isolated **28a** at 10 K with visible light ($\lambda > 415$ nm) results in the complete photolysis of **28a** and formation of a new compound in a clean reaction (Figures 8.3.2.5 and 8.3.2.6) (Table 8.3.2.2). These new absorptions are in excellent agreement with the IR spectrum of **28b**, calculated at the UB3LYP/cc-pVTZ level of theory. This conformational reaction requires a photochemical activation and does not occur thermally on annealing the matrix at 30 K.

After annealing argon matrix containing predominantly **28b** at 30 K for several minutes results in rapid decrease of **28b** and **28a** is formed back again (Figure 8.3.2.7). The

formation of **28a** from **28b** in a thermal reaction at temperature 30 K indicates a very small activation barrier for this reaction. This observation is in agreement with the results mentioned above, that indicates if even **28b** formed in the gas phase from thermal reaction between **24** and O₂ is rapidly converted into **28a** due to the low activation barrier.

Table 8.3.2.2. IR spectroscopic data of the *o*-pyridyl peroxy radical **28b**.

Mode ^a	C ₅ NH ₄ OO (28b)		C ₅ NH ₄ ¹⁸ O ¹⁸ O (¹⁸ O ₂ - 28b)		Sym.	Assignment
	Argon ^b	DFT ^c	Argon ^b	DFT ^c		
26	1593.3 (28)	1637.1 (57)	1593.3 (32)	1636.5 (57)	A'	ring str.
25	1575.0 (9)	1615.2 (43)	1573.7 (31)	1614.9 (43)	A'	ring str.
24	1467.8 (27)	1504.3 (24)	1467.8 (23)	1503.7 (25)	A'	ring str./C C-H def.
23	1427.6 (48)	1463.5 (88)	1428.5 (70)	1462.9 (89)	A'	C-H def.(in plane)
22	1313.1 (7)	1342.9 (5)	1312.5 (2)	1342.0 (4)	A'	C-H def.(in plane)
21	-	1311.1 (1)	-	1310.3 (1)	A'	C-H def.(in plane)
20	1166.2 (75)	1186.2 (52)	1161.4 (54)	1182.8 (37)	A'	C-H def./C-O str
19	1143.9 (7)	1170.7 (21)	1073.5 (30)	1123.3 (6)	A'	O-O str /C-H def.
18	1121.3 (14)	1167.2 (18)	-	1167.8 (30)	A'	C-H def.
17	-	1116.7 (4)	1097.5 (21)	1123.3 (6)	A'	C-H def.(in plane)
16	1040.9 (7)	1063.4 (7)	-	1061.9 (4)	A'	C-H def.(in plane)
14	985.0 (2)	1009.8 (9)	983.5 (6)	1009.6 (8)	A'	Ring str.
13	961.1 (3)	991.8 (1)	-	991.3 (1)	A''	CH def.(out of plane)
12	-	901.1 (1)	-	900.8 (2)	A''	CH def.(out of plane).
11	807.9 (5)	822.3 (15)	792.7 (10)	806.8 (17)	A'	C-O str./ring str.
10	771.4 (100)	794.8 (100)	771.5 (100)	794.3 (100)	A''	CH def.(out of plane)
9	-	751.2 (7)	-	751.3 (7)	A''	CH def.(out-of- plane)
8	648.6 (9)	660.4 (5)	628.1 (<1)	641.2 (2)	A'	COO def./ring str.
7	614.3 (9)	629.7 (5)	613.5 (7)	628.5 (6)	A'	ring def.

[a]Mode numbers based on the C₅NH₄¹⁶O¹⁶O isotopomer. [b]Argon matrix at 10 K. Wavenumbers in cm⁻¹ and relative intensities in parenthesis. [c]Calculated at the UB3LYP/cc-pVTZ level of theory

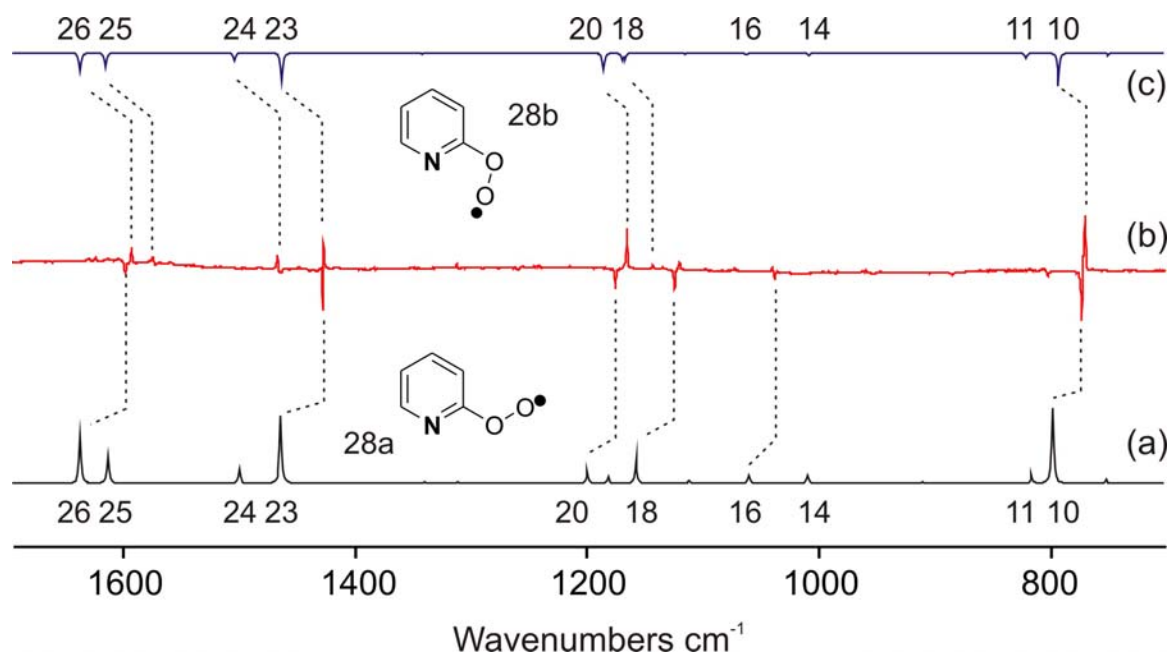


Figure 8.3.2.5. Photochemistry of **28** in solid argon. (a) Calculated vibrational spectrum (UB3LYP/cc-pVTZ) of **28a** (b) Difference spectrum. Bands pointing downwards are disappearing during irradiation ($\lambda > 515$ nm) are belong to **28a**. Bands pointing upwards are appearing and assigned to **28b**. (c) Calculated vibrational spectrum (UB3LYP/cc-pVTZ) of **28b**.

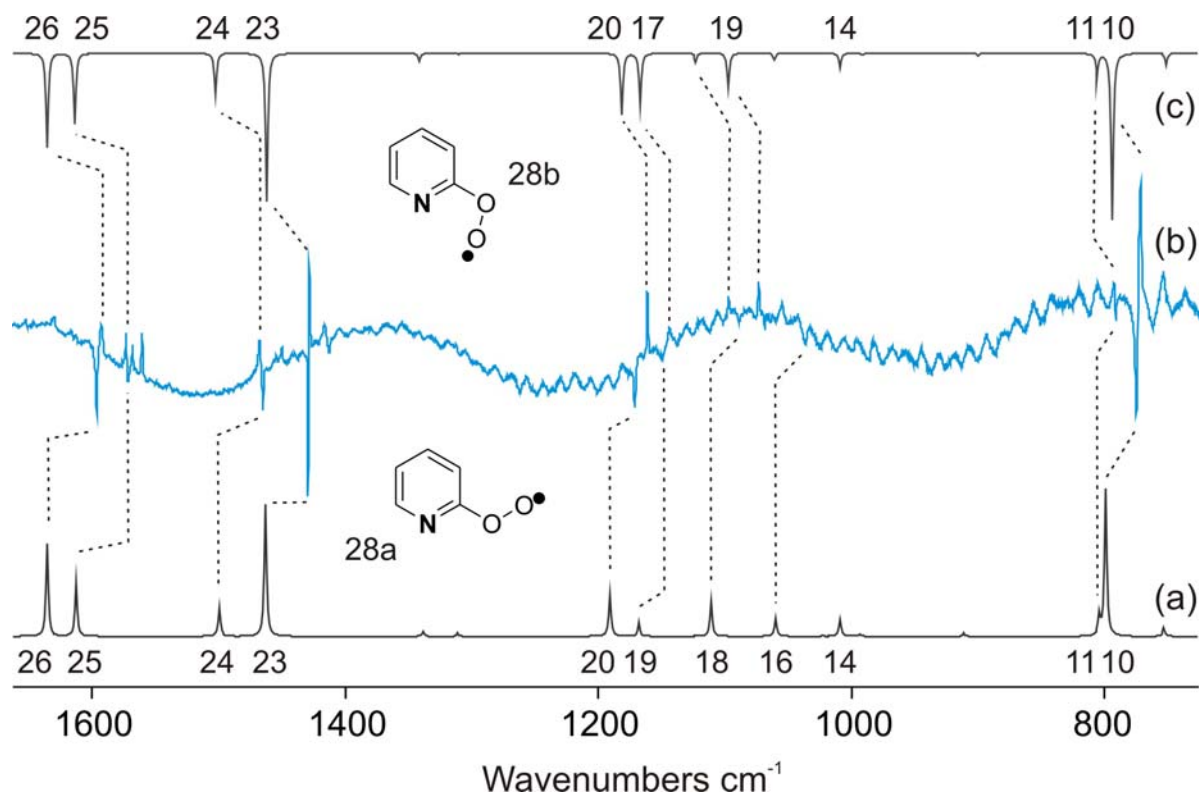


Figure 8.3.2.6. Photochemistry of $^{18}\text{O}_2$ -**28** in solid argon. (a) Calculated vibrational spectrum (UB3LYP/cc-pVTZ) of $^{18}\text{O}_2$ -**28a** (b) Difference spectrum. Bands pointing downwards are disappearing during irradiation ($\lambda > 515$ nm) are belong to $^{18}\text{O}_2$ -**28**. Bands

pointing upwards are appearing and assigned to $^{18}\text{O}_2\text{-28b}$. (c) Calculated vibrational spectrum (UB3LYP/cc-pVTZ) of $^{18}\text{O}_2\text{-28b}$.

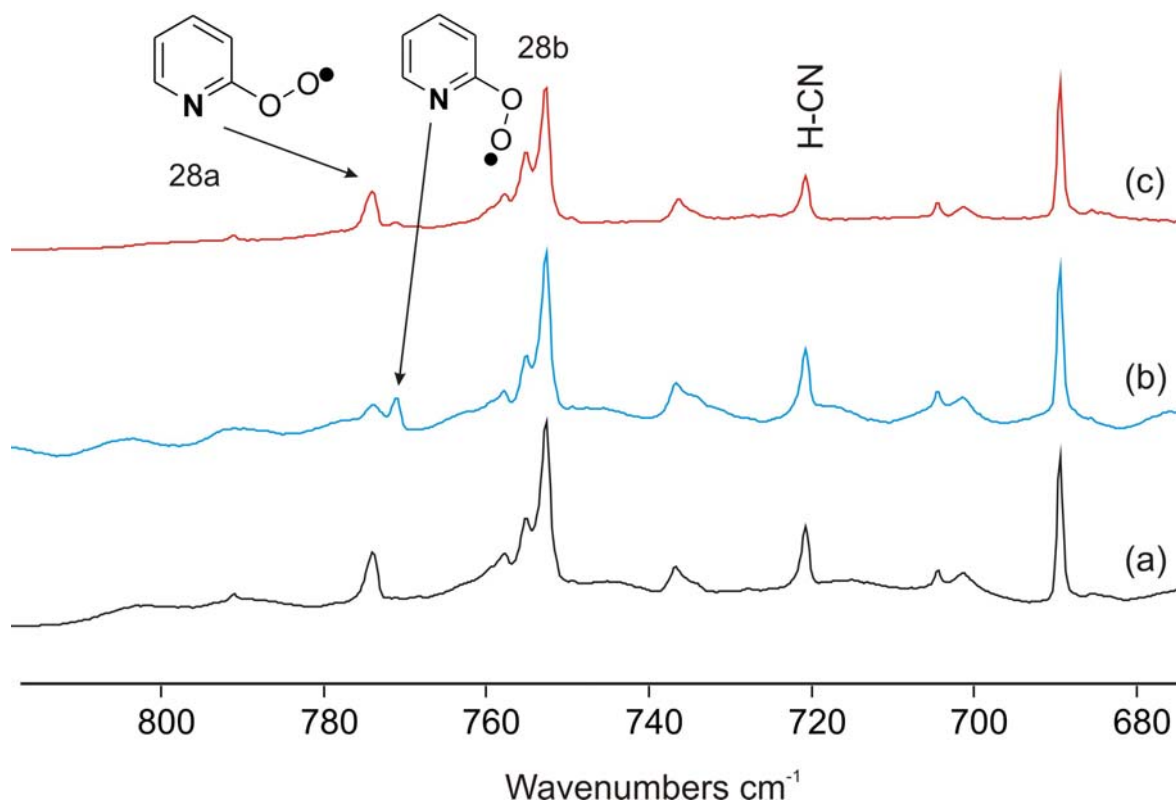


Figure 8.3.2.7. (a) IR spectrum of a matrix (Ar at 10K) isolated the **28a**, containing products from FVP of **27** in 2% O_2 -doped argon with subsequent trapping at 10 K. (b) IR spectrum recorded at 10 K after irradiation ($\lambda > 515$ nm) for 20 min. (c) IR spectrum recorded at 10 K after annealing at 30 K for 5 min.

It is well documented that aryl peroxy radicals have been observed to absorb in the visible region.^[378] It is shown that TD-DFT calculations produce good excitation energies for peroxy radicals.^[378] The UV spectrum of matrix isolated **28a** exhibits a broad absorption with a maximum around 373 nm along to the calculated UV spectrum of **28a** (Figure 8.3.2.8). As seen from Figure 8.3.2.8 the experimentally observed UV spectrum is in good agreement with the calculated spectrum obtained at the TD-UB3LYP/cc-pVTZ level of theory.

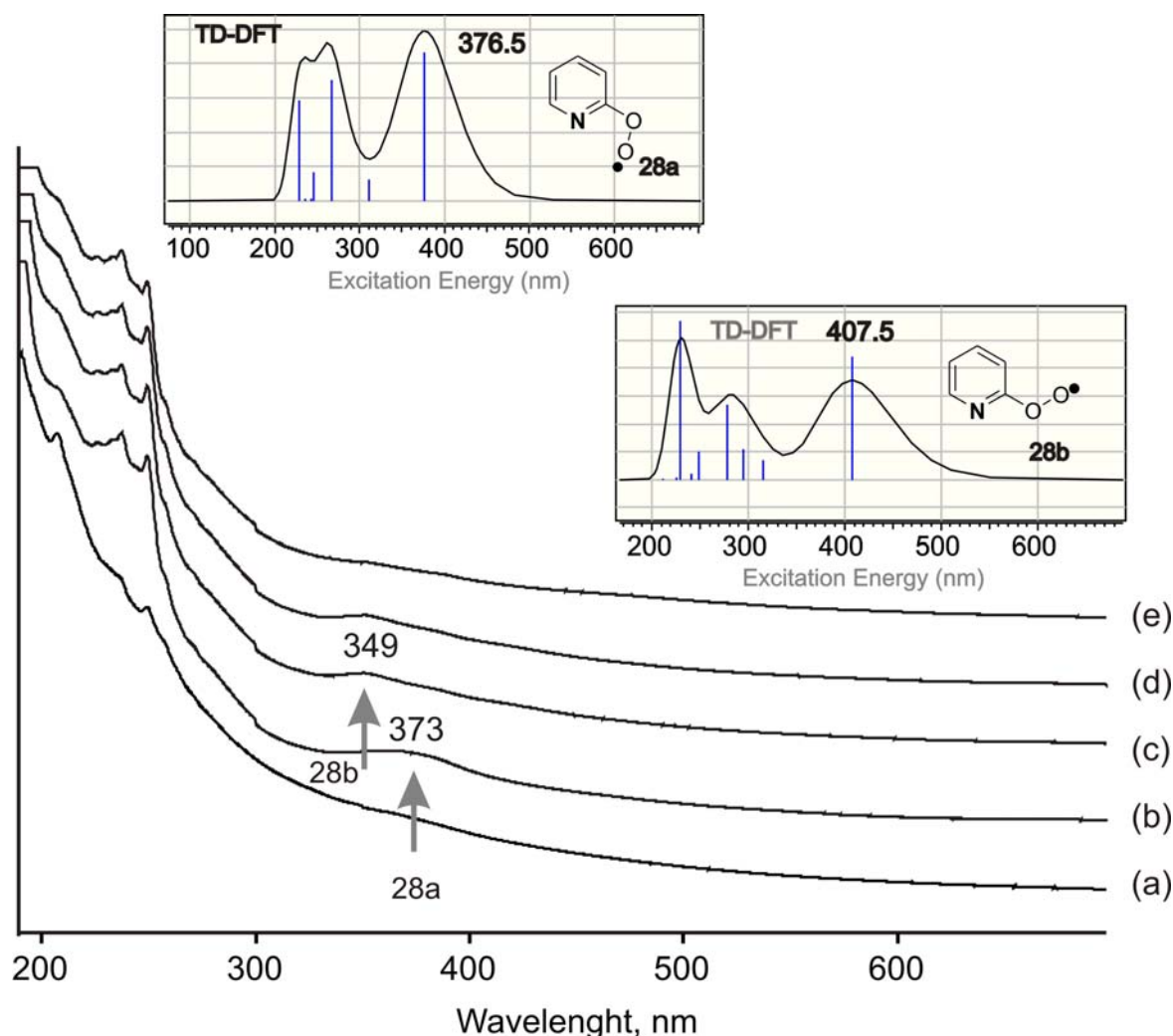


Figure 8.3.2.8. (a) UV spectrum of a matrix (Ar at 10K) isolated the **24**, containing products from FVP of **27** in argon at 10 K. UV spectrum of a matrix (Ar at 10K) isolated the **28a**, containing products from FVP of **27** in 2% O₂-doped argon with subsequent trapping at 10 K. (c) The same spectrum recorded at 10 K after irradiation ($\lambda > 515$ nm) for 30 min. (d) The same UV spectrum after irradiation ($\lambda > 420$ nm) for 5 min. (e) after 25 min.

Irradiation of matrix-isolated **28** at 10 K with the visible light ($\lambda > 420$ nm) results in the complete photolysis of **28** and formation of new compound with the intense band at 1700.6 cm^{-1} , which shows a substational red-shift (23.4 cm^{-1}) if $^{18}\text{O}_2$ is used (Figure 8.3.2.9). The newly formed compound is assigned to **29** based on DFT calculations (Scheme 8.3.2.1). Prolonged irradiation of **29** results in the disappearance of all bands assigned to **29** and formation several new bands in the region $2350 - 2050\text{ cm}^{-1}$, which

indicates of the formation several ring opening products. All these bands show different kinetics during photolysis, which makes a definitive assignment not possible.

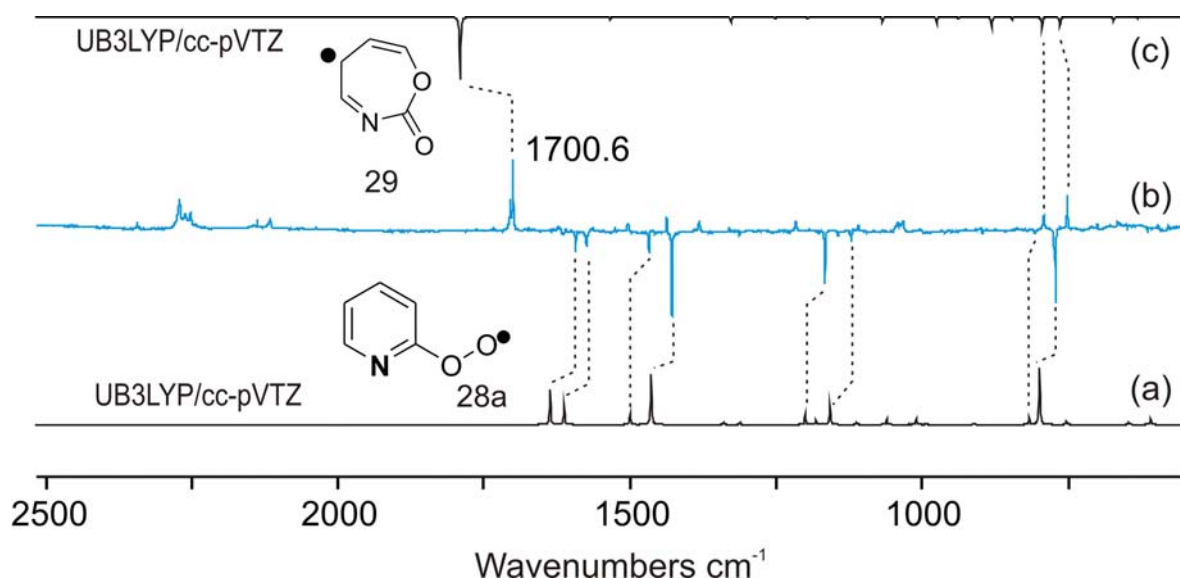


Figure 8.3.2.9. Photochemistry of **28** in solid argon. (a) Calculated vibrational spectrum (UB3LYP/cc-pVTZ) of **28a** (b) Difference spectrum. Bands pointing downwards are disappearing during irradiation ($\lambda > 420$ nm) are belong to **28a**. Bands pointing upwards are appearing and assigned to **29**. (c) Calculated vibrational spectrum (UB3LYP/cc-pVTZ) of **29**.
sl

8.4.1. *p*-Pyridyl Radical (**26**)

The second most stable pyridyl radical is the *p*-pyridyl radical (**26**). In order to synthesize **26** in argon matrix two different precursors (4-iodopyridine (**30**) and 4,4-azopyridine (**31**)) were used. FVP of **30** and **31** at temperatures between 620 and 700°C with subsequent trapping with a large excess of argon at 10 K produces **26** in good yields.

Figure 8.4.1.1 shows matrix-isolated IR spectra of **26** in the spectral region between 900 – 650 cm^{-1} . The most intense absorption in the IR spectrum of **26** is due to an out-of-plane (o.o.p) combined CH vibration mode at 749.8 cm^{-1} . These absorptions are in good agreement with the IR spectrum of **26**, calculated at the UB3LYP/cc-pVTZ level of theory (Table 8.4.1.1).

Photolysis of **30** in argon matrix at 10 K with UV light produces new set of bands, which are assigned to **26**. It should be mentioned that the IR bands of **26** produced photochemically are slightly different (shifted and broadness) those compared to produced in the FVP experiments. Similar effects were reported in literature, and attributed to the interaction of radicals with iodine atoms, isolated in the same matrix cage (Figure 8.4.1.2).

Subsequent annealing of the matrix at 30 K for several minutes again results in the formation of **30**.

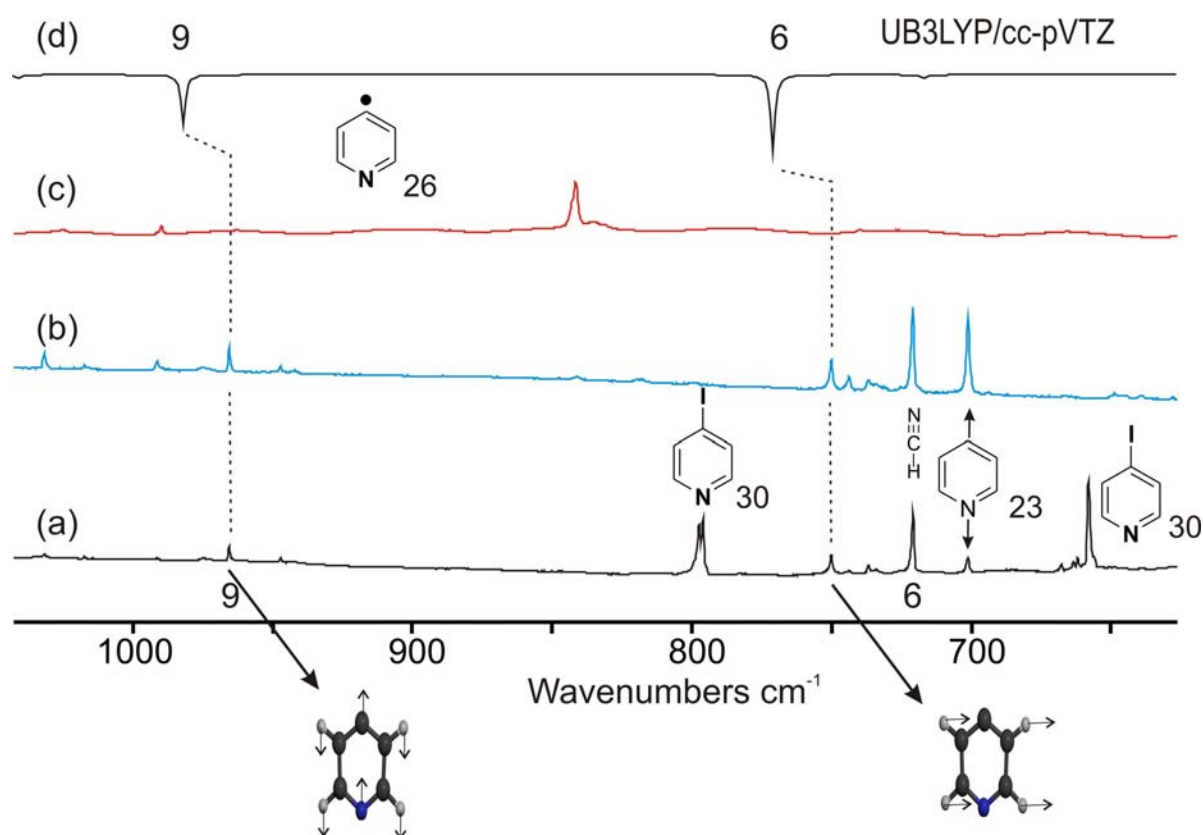


Figure 8.4.1.1. FVP products of **30** and **31**. (a) IR spectrum of a matrix (Ar at 10K) isolated the **26**, containing products from FVP of **30**. (b) IR spectrum of a matrix (Ar at 10K) isolated the **26**, containing products from FVP of **31**. (c) IR spectrum of a matrix (Ar at 10K) isolated the **31**. (d) Calculated vibrational spectrum (UB3LYP/cc-pVTZ) of **26**.

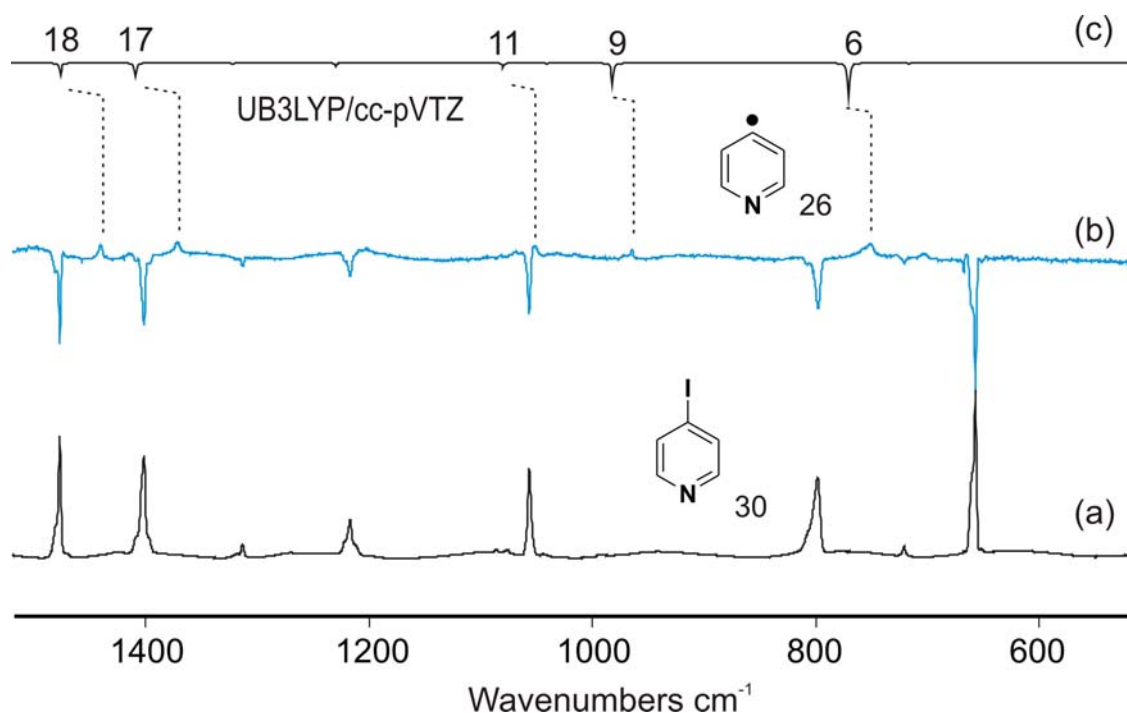


Figure 8.4.1.2. Photochemistry of **30** in solid argon. (a) IR spectrum of a matrix (Ar at 10K) isolated **30** (b) Difference spectrum. Bands pointing downwards are disappearing during irradiation ($\lambda = 254$ nm) are belong to **30**. Bands pointing upwards are appearing and assigned to **26**. (c) Calculated vibtrational spectrum (UB3LYP/cc-pVTZ) of **26**.

Table 8.4.1.1. Observed and calculated IR bands of **26**.

Mode	$\nu_{\text{exp}}[\text{cm}^{-1}]^{[a]}$	$I_{\text{rel. exp.}}^{[b]}$	$\nu_{\text{calc}}[\text{cm}^{-1}]^{[c]}$	$I_{\text{rel. calc.}}$
20	1570.9	50	1618.3	49
19	1496.5	27	1539.1	98
18	1439.8	- ^d	1476.5	36
17	1373.2	12	1409.6	38
16	-	-	1322.9	3
15	-	-	1266.1	1
14	-	-	1230.6	9
13	1147.8	12	1081.0	16
12	1031.9	- ^d	1075.6	2
11	1017.3	11	1041.6	6
10	-	-	990.6	0
9	965.6	20	982.7	64
8	-	-	968.2	0
7	-	-	830.8	0

6	749.8	100	771.2	99
5	-	-	717.4	6

[a] Argon, 10 K. [b] Relative intensities based on the strongest absorption. [c] Calculated at the UB3LYP/cc-pVTZ level of theory. [d] Overlaps with the bands of precursor

8.4.2. *p*-Pyridyl Peroxy Radical (32)

In contrast to the *o*-pyridyl radical (24), the interaction of **26** with molecular oxygen leads to the formation of only one conformer, *p*-pyridyl peroxy radical (32). In order to synthesize **32**, FVP experiments were carried out in the presence of 2 % oxygen doped in argon. FVP of **31** and **32** again resulted in the formation of pyridine (**23**), acetylene, diacetylene and HCN as side products. In addition, new absorptions at 1600.0, 1572.3, 1484.3 1410.8, 1220.0, 1149.5, 1119.2, 990.1, 817.1 and 807.7 cm^{-1} are found. By comparison of the experimentally observed frequencies with the calculated spectrum (UB3LYP/cc-pVTZ) the absorptions are assigned to the *p*-pyridyl peroxy radical (32) (Figure 8.4.2.1 and Table 8.4.2.1). If $^{18}\text{O}_2$ is used, the band at 1119.2 shows a huge red-shift of 57.7 cm^{-1} indication of the O–O stretching mode. Another band at 807.7 cm^{-1} shows only small red-shift of 16.2 cm^{-1} , which is assigned to the C–O stretching mode based on DFT calculations (UB3LYP/cc-pVTZ). Band positions, relative intensities, and isotopic shifts are nicely agree with the calculated data (Table 8.4.2.1).

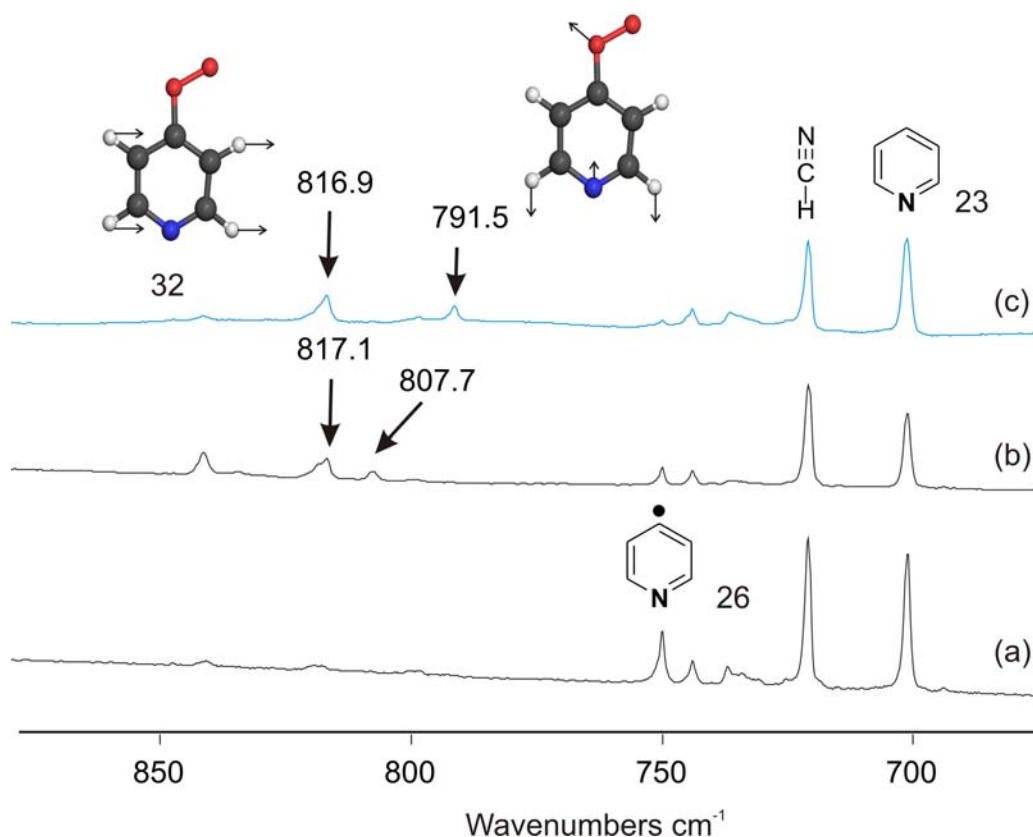


Figure 8.4.2.1. FVP products of **31**. (a) IR spectrum of a matrix (Ar at 10K) isolated the **26**, containing products from FVP of **31**. (b) IR spectrum of a matrix (Ar at 10K) isolated the **32**, containing products from FVP of **31** in 2% O_2 -doped argon with subsequent trapping at 10 K.

(c) IR spectrum of a matrix (Ar at 10K) isolated the $^{18}\text{O}_2\text{-32}$, containing products from FVP of **31** in 2% $^{18}\text{O}_2$ -doped argon with subsequent trapping at 10 K.

These experiments clearly show that the thermal reaction of **26** with O_2 results in the formation of **32**. DFT calculations do not indicate the existence of any activation barrier for this reaction (Figure 8.3.2.2). The exothermicity of this reaction is 44.68 kcal/mol (UB3LYP/cc-pVTZ).

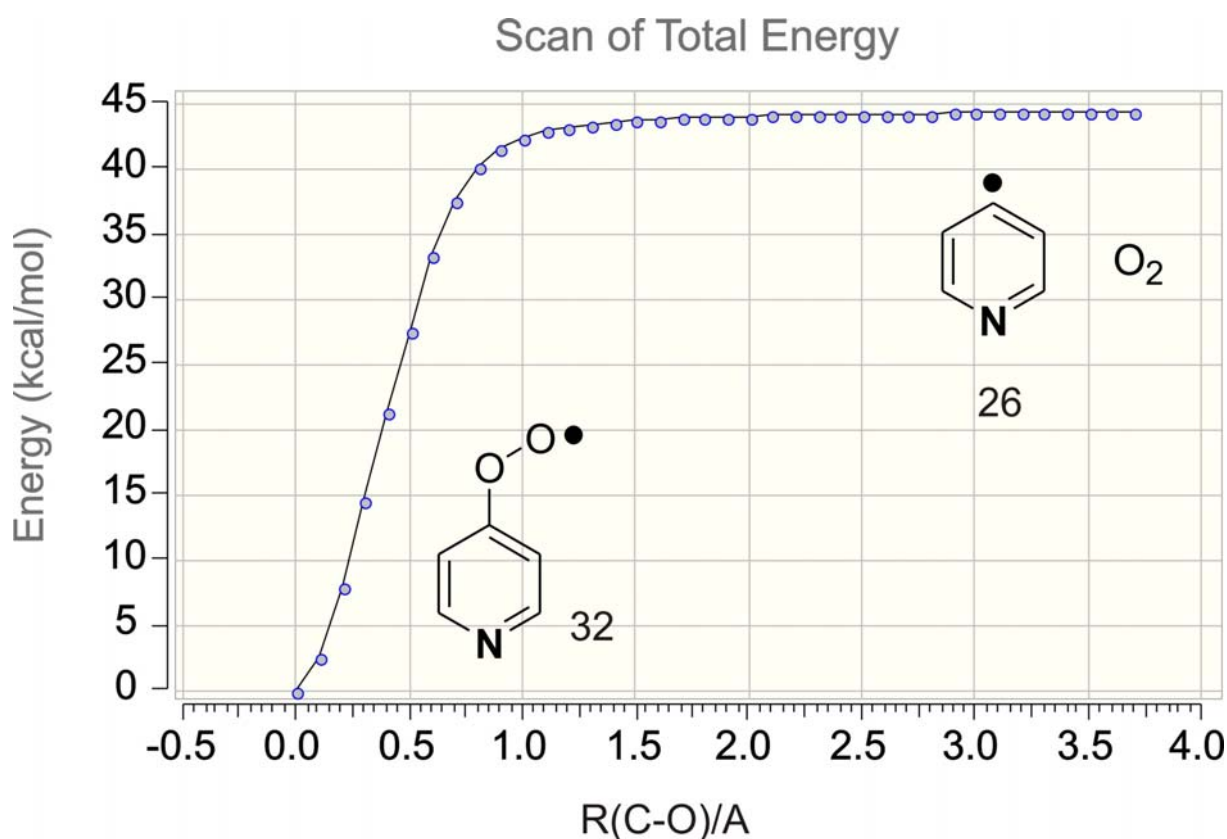


Figure 8.4.2.2. The **32** dissociation potential energy surface calculated at the B3LYP/cc-pVTZ level of theory.

Table 8.4.2.1. IR spectroscopic data of the *p*-pyridyl peroxy radical **32**.

Mode ^a	C ₅ NH ₄ OO (32)		C ₅ NH ₄ ¹⁸ O ¹⁸ O (¹⁸ O ₂ - 32)		Sym.	Assignment
	Argon ^b	DFT ^c	Argon ^b	DFT ^c		
26	1600.0 (62)	1635.8 (53)	1699.8 (58)	1635.0 (53)	A'	ring str.
25	1572.3 (100)	1607.4 (100)	1569.6 (51)	1607.4 (100)	A'	ring str.
24	1484.3 (31)	1514.6 (29)	1484.3 (37)	1514.3 (29)	A'	ring str./C C-H def.
23	1410.8 (60)	1445.7 (42)	1411.2 (53)	1445.2 (42)	A'	C-H def.(in plane)
22	-	1360.4 (0)	-	1359.1 (1)	A'	C-H def.(in plane)
21	-	1285.4 (3)	-	1285.0 (3)	A'	Ring str.
20	1220.0 (1)	1243.3 (2)	1220.0 (2)	1242.2 (2)	A'	C-H def. (in plane)
19	1119.2 (31)	1172.6 (19)	1061.5 (16)	1108.7 (14)	A'	O-O str.
18	1149.5 (31)	1164.7 (10)	1142.9 (16)	1159.4 (9)	A'	C-O str./ring str..
17	-	1099.7 (0)	-	1098.4 (3)	A'	C-H def.(in plane)
16	-	1069.1 (1)	-	1067.7 (1)	A'	C-H def.(in plane)
15	-	1014.2 (0)	-	1013.8 (0)	A''	CH def.(out of plane)
14	990.1 (14)	1010.5 (10)	990.1 (9)	1010.4 (10)	A'	Ring str.
13	-	990.5 (2)	-	990.1 (2)	A''	CH def.(out of plane).
12	-	874.9 (4)	-	874.7 (4)	A''	CH def.(out of plane)
11	817.1 (80)	848.2 (92)	816.9 (100)	847.7 (92)	A''	CH def.(out of plane)
10	807.7 (46)	818.4 (35)	791.5 (56)	801.8 (39)	A'	C-O str./ring str.
9	-	746.5 (1)	-	746.4 (1)	A''	ring def.
8	-	674.5 (1)	-	674.2 (0)	A'	Ring str.
7	-	622.5 (23)	-	604.4 (18)	A'	COO def./ring str.
6	-	525.4 (27)	-	524.6 (27)	A''	ring def.

[a]Mode numbers based on the C₅NH₄¹⁶O¹⁶O isotopomer. [b]Argon matrix at 10 K. Wavenumbers in cm⁻¹ and relative intensities in parenthesis. [c]Calculated at the UB3LYP/cc-pVTZ level of theory

Irradiation of **32** with blue light ($\lambda > 420$ nm) at 10 K results in the disappearance of all bands assigned to **32** and formation of CO₂ and several other new bands, in particular a very strong and broad absorption at 2144 cm⁻¹ (Figure 8.4.2.3). If ¹⁸O₂ is used in the experiment new bands at 2118 and 2089 cm⁻¹ appear, which clearly indicates that one or several ketenes are formed. In addition, C¹⁸O₂ is found at 2310 cm⁻¹ (Figure 8.4.2.4). We assume that the photolysis of **32** results in ring-opening and formation of ketenes. However, due to the low intensity of other IR bands of the ketenes (presumably several isomers or conformers are formed) a definitive assignment was not possible.

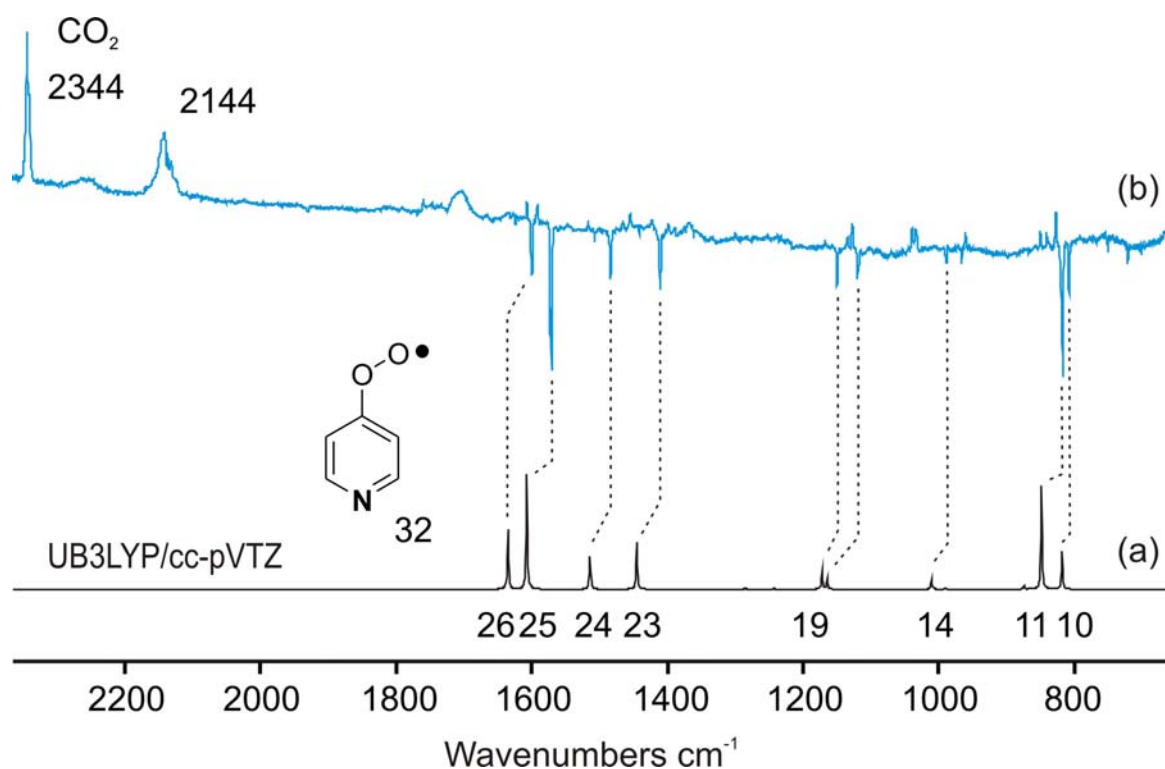


Figure 8.4.2.3. Photochemistry of **32** in solid argon. (a) Calculated vibrational spectrum (UB3LYP/cc-pVTZ) of **32** (b) Difference spectrum. Bands pointing downwards are disappearing during irradiation ($\lambda > 420$ nm) for 15 min are belong to **32**. Bands pointing upwards are appearing due to ring opening products.

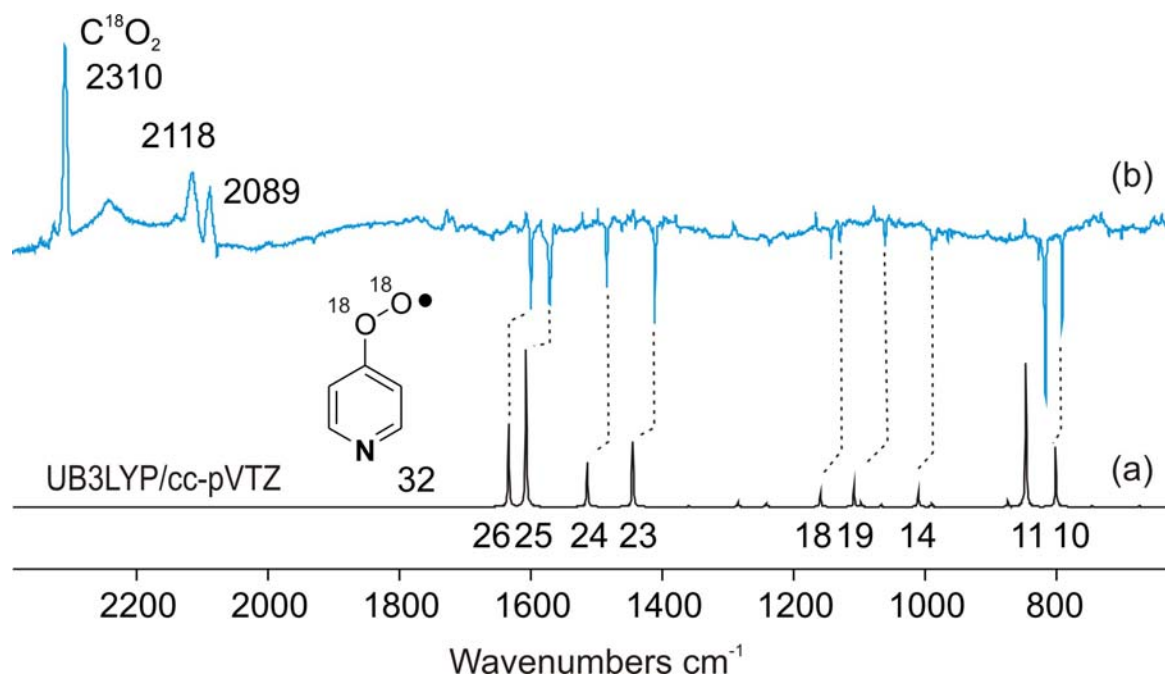


Figure 8.4.2.4. Photochemistry of $^{18}\text{O}_2$ -**32** in solid argon. (a) Calculated vibrational spectrum (UB3LYP/cc-pVTZ) of $^{18}\text{O}_2$ -**32** (b) Difference spectrum. Bands pointing downwards are disappearing during irradiation ($\lambda > 420$ nm) for 15 min are belong to $^{18}\text{O}_2$ -**32**. Bands pointing upwards are appearing due to ring opening products.

8.5.1. *m*-Pyridyl Radical (**25**)

In order to synthesize *o*-pyridyl radical (**25**) we carried out FVP experiments of 3-iodopyridine (**33**) at temperatures above 600 °C in the gas phase with subsequent trapping of the thermolysis products in the large excess of argon at 10 K. Besides of some unreacted starting material (**33**) and side products such as acetylene, diacetylene and HCN several new absorptions are detected that can not be assigned to any previously known species (Figure 8.5.1.1) (Table 8.5.1.1). The strong band at 671.7 cm⁻¹ which is due to out-of-plane wagging mode of **25** and other less intense bands in the mid-IR region rapidly decrease if the matrix is irradiated with visible light ($\lambda > 420$ nm) (Figure 8.5.1.2). Simultaneously, a few strong bands in the spectral region between 3300 – 3100 cm⁻¹ and 700 – 600 cm⁻¹ are appearing, indicating the formation of acetylenic compounds. From the decay kinetics of these bands and based on DFT calculations (UB3LYP/cc-pVTZ), the photolabile compound is assigned to **25**.

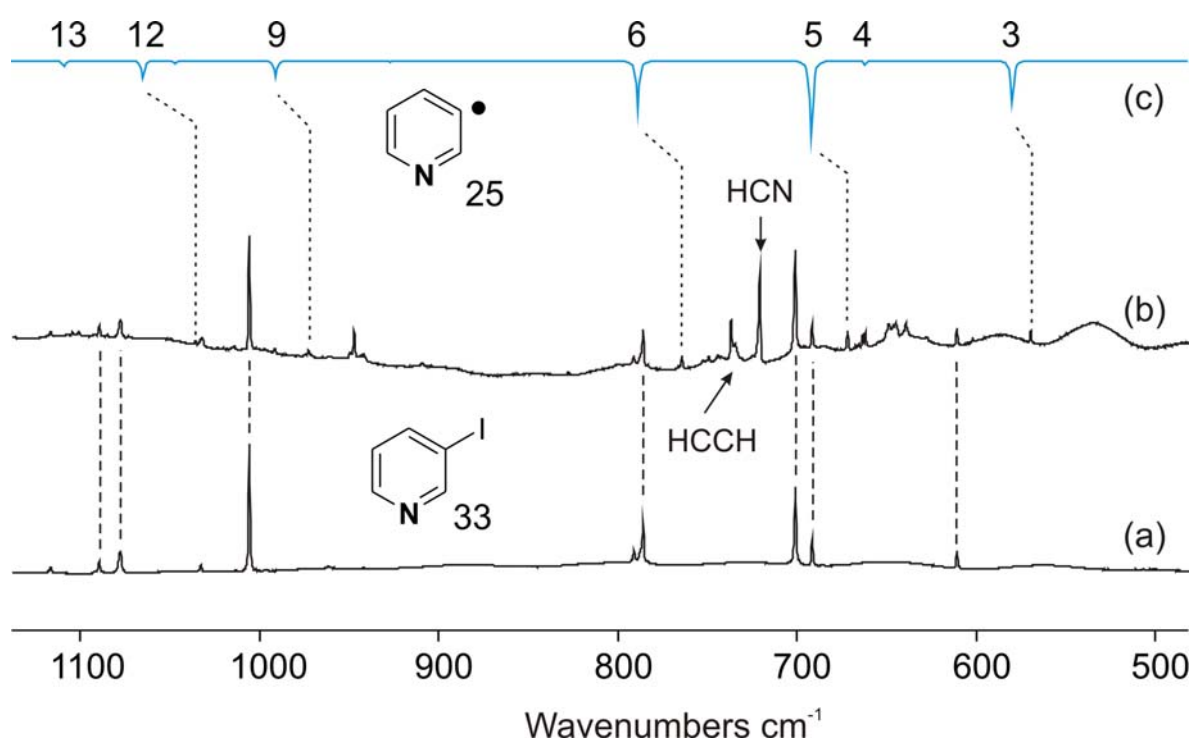


Figure 8.5.1.1. FVP products of **33**. (a) IR spectrum of a matrix (Ar at 10K) isolated **33**. (b) IR spectrum of a matrix (Ar at 10K) isolated the **25**, containing products from FVP of **33**. (c) Calculated vibrational spectrum (UB3LYP/cc-pVTZ) of **25**.

As mentioned above, the photolysis of **25** results in the formation of ring opening products. However, due to the low intensity of other IR bands (presumably several isomers or conformers are formed) a definitive assignment was not possible (Figure 8.5.1.2)

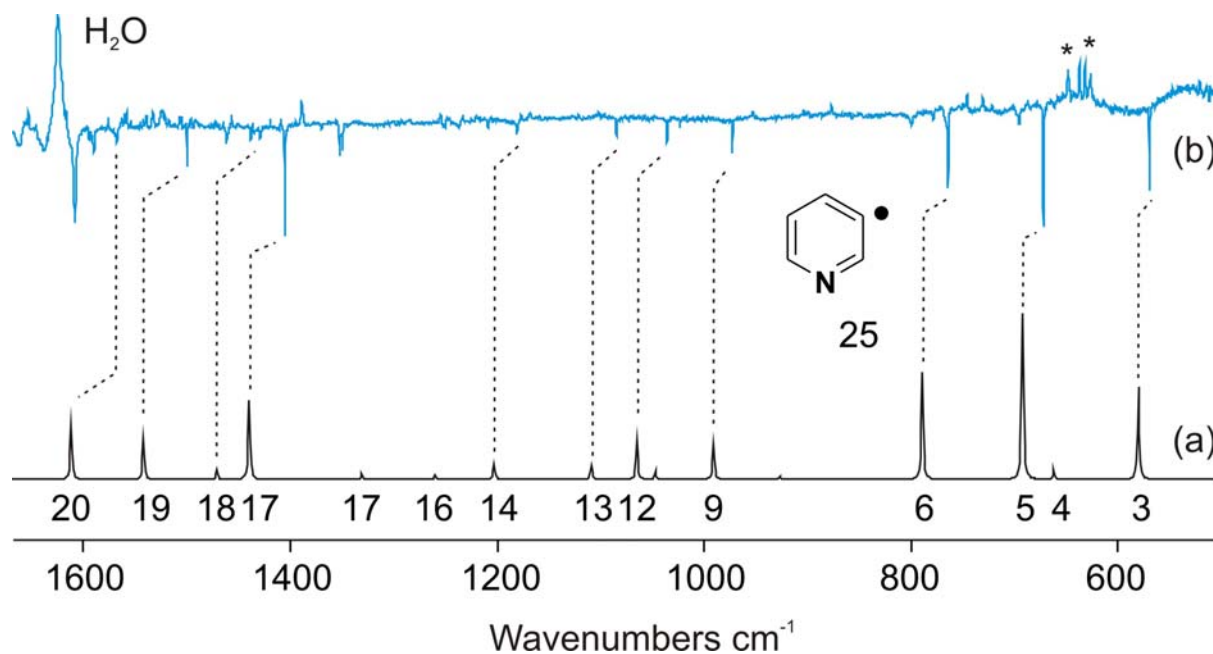


Figure 8.5.2.2. Photochemistry of **25** in solid argon. (a) Calculated vibrational spectrum (UB3LYP/cc-pVTZ) of **25** (b) Difference spectrum. Bands pointing downwards are disappearing during irradiation ($\lambda > 420$ nm) for 15 min are belong **25**. Bands pointing upwards are appearing due to ring opening products (*).

Table 8.5.1.1. Observed and calculated IR bands of **25**.

Mode	$\nu_{\text{exp}}[\text{cm}^{-1}]^{[a]}$	$I_{\text{rel. exp.}}^{[b]}$	$\nu_{\text{calc}}[\text{cm}^{-1}]^{[c]}$	$I_{\text{rel. calc.}}$
20	1567.8	13	1612.5	32
19	1499.9	33	1542.5	24
18	1438.6	11	1471.7	6
17	1405.4	94	1440.4	48
16	1297.8	3	1331.6	4
15	1209.4	7	1260.3	3
14	1181.2	9	1203.8	9
13	1084.8	16	1109.9	8
12	1035.8	24	1066.0	24
11	1023.5	8	1047.7	5
10	-	-	998.7	0
9	972.7	30	991.1	21
8	-	-	950.8	0
7	-	-	927.2	2
6	764.4	60	789.0	65
5	671.7	100	692.7	100
4	646.2	9	662.6	6
3	569.6	71	580.5	56

[a] Argon, 10 K. [b] Relative intensities based on the strongest absorption. [c] Calculated at the UB3LYP/cc-pVTZ level of theory.

8.5.2. *m*-Pyridyl Peroxy Radicals (**34a** and **34b**)

To investigate bimolecular reactions between **25** and O₂ FVP experiments were carried out with small amounts of oxygen (0.5 – 2 %). This resulted in the formation of new products with strong IR absorptions at 799.2 and 795.9 cm⁻¹ which were not present in the absence of oxygen (Figure 8.5.2.1). If the matrix was annealed at 30 – 35 K for several minutes, all IR bands assigned to the new products started to increase in intensity, while the bands of the *m*-pyridyl radical (**25**) decreased. This indicates that new compounds are formed by a bimolecular reaction between **25** and oxygen and that this reaction has a very low or no barrier. These new band are assigned to out-of-plane (o.o.p)

deformation modes of *m*-pyridyl peroxy radicals (**34a** and **34b**) (Tables 8.5.2.1 and 8.5.2.2). The assignments of IR spectra were also confirmed by comparison with IR spectra of **34a** and **34b** calculated at the UB3LYP/cc-pVTZ level of theory.

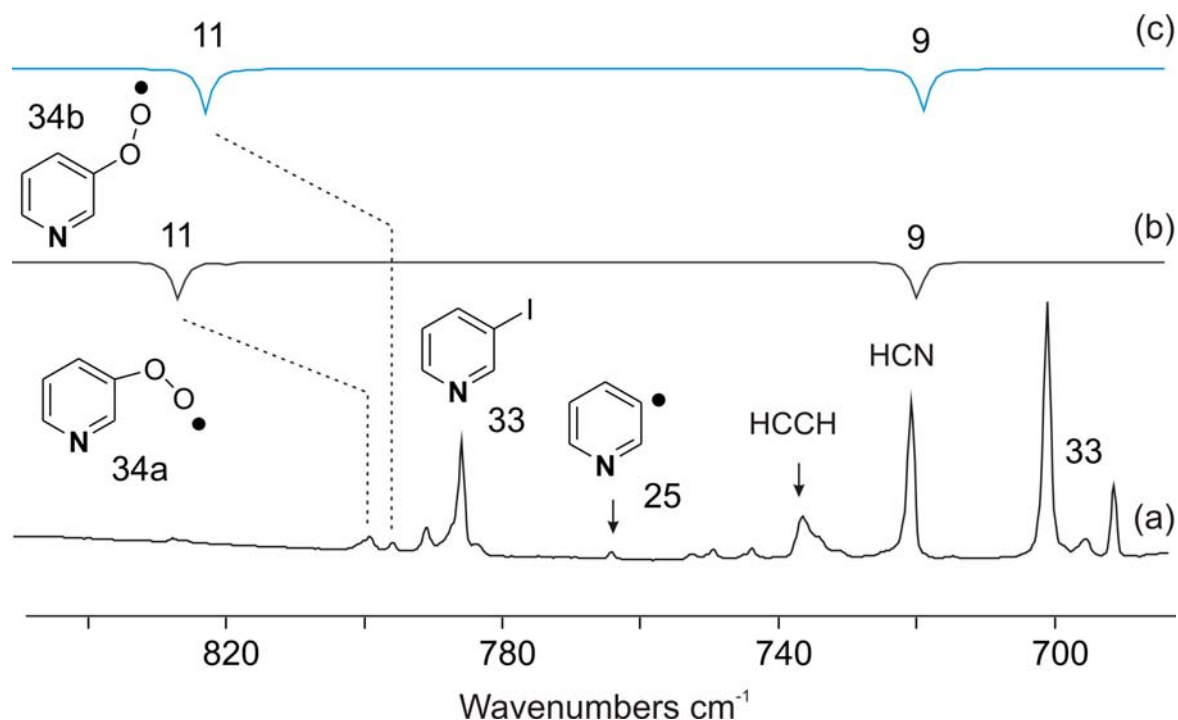


Figure 8.5.2.1. FVP products of **33**. (a) IR spectrum of a matrix (Ar at 10K) isolated **34a** and **34b**, containing products from FVP of **33** in 2% O₂-doped argon with subsequent trapping at 10 K. (b) Calculated vibrational spectrum (UB3LYP/cc-pVTZ) of **34a**. (c) Calculated vibrational spectrum (UB3LYP/cc-pVTZ) of **34b**.

According to DFT calculations, the reaction of **25** with O₂ produces two possible conformers **34a** and **34b**. The reactions of **25** with O₂ are exothermic by 44.94 and 44.23 kcal/mol. UB3LYP/cc-pVTZ calculations show that conformer **34a** is more stable than the conformer **34b** by 0.71 kcal/mol. The activation barrier for the **34a** → **34b** isomerization is calculated to 4.19 kcal/mol (Figure 8.5.2.2).

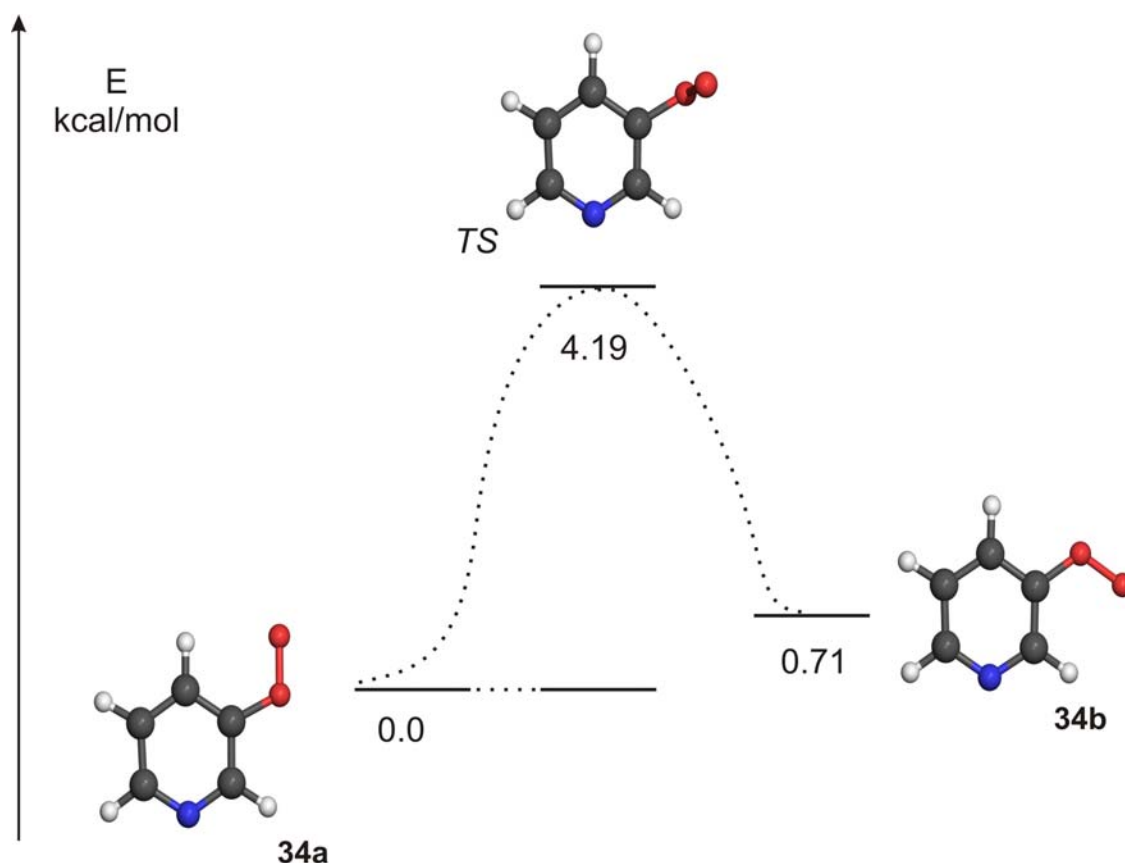


Figure 8.5.2.2. Theoretical isomerisation pathway between two isomers of *o*-pyridyl peroxy radicals (**34a** and **34b**). Stationary points and transition state were performed by use B3LYP/cc-pVTZ method.

Irradiation of **34a** and **34b**, matrix isolated in argon matrix at 10 K for several minutes with the visible light ($\lambda > 550$ nm) results in the decrease of the IR bands of **34b**, and simultaneously in the increase of IR bands of **34a** (Figures 8.5.2.3 and 8.5.2.4). The reverse reaction **34b** \rightarrow **34a** also can be achieved by photolysis of matrix with the light $\lambda > 515$ nm. Prolonged irradiation results in the complete photolysis of **34a** and **34b**, and formation of new compound with the intense bands in the spectral region between $1750 - 1680$ cm^{-1} , indicating of the formation of ring expanded products. If $^{18}\text{O}_2$ is used latter mentioned bands are shifted in low frequency region, which clearly indicates the existence of carbonyl group. Molecular mechanism of photodissociation of **34a** and **24b** is currently under progress in our laboratory.

Table 8.5.2.1. IR spectroscopic data of the *m*-pyridyl peroxy radical **34a**.

Mo de ^a	C ₅ NH ₄ OO (34a)		C ₅ NH ₄ ¹⁸ O ¹⁸ O (¹⁸ O ₂ - 34a)		Sym.	Assignment
	Argon ^b	DFT ^c	Argon ^b	DFT ^c		
26	1594.6 (17)	1627.8 (24)	1592.6 (11)	1627.3(24)	A'	ring str.
25	1565.6 (21)	1606.2 (25)	1565.5 (25)	1606.0 (25)	A'	C-H def.(in plane).
24	1473.9 (25)	1507.5 (19)	1473.3 (29)	1507.0 (20)	A'	C-H def.(in plane).
23	1429.4 (100)	1462.0 (100)	1428.8 (69)	1461.7 (100)	A'	C-H def.(in plane)
22	-	1356.1 (1)	1319.8 (7)	1355.5 (2)	A'	C-H def.(in plane)
21	-	1293.7 (2)	-	1293.2 (2)	A'	ring str./ C-H def
20	1191.0 (27)	1223.3 (28)	1190.1 (14)	1221.4 (27)	A'	C-H def. (in plane)
19	1155.7 (21)	1175.0 (31)	1150.6 (17)	1169.6 (22)	A'	C-H def./ C-O str
18	-	1166.5 (2)	1189.2 (19)	1103.5 (14)	A'	O-O str.
17	-	1114.2 (16)	1085.9 (10)	1112.8 (13)	A'	C-H def.(in plane)
16	-	1059.8 (1)	1077.7 (23)	1059.3 (2)	A'	ring str.
15	1016.5 (42)	1035.6 (35)	1015.5 (25)	1035.2 (35)	A'	ring def.
14	-	1014.1 (1)	-	1014.1 (1)	A''	CH def.(out of plane).
13	-	977.9 (8)	-	977.8 (8)	A''	CH def.(out of plane).
12	-	941.0 (5)	-	941.0 (5)	A''	CH def.(out of plane)
11	799.4 (72)	827.8 (86)	799.5 (52)	827.7 (86)	A''	CH def.(out of plane)
10	-	820.1 (5)	-	806.8 (4)	A'	C-O str./ring str.
9	701.6 (30)	720.4 (83)	701.9 (100)	720.3 (83)	A''	ring def.
8	623.4 (22)	646.4 (17)	611.1 (23)	636.0 (19)	A'	COO def./ring str
7	-	618.9 (5)	-	609.1 (2)	A'	ring str.
6	-	495.5 (0)	-	494.4 (0)	A''	ring def.

[a]Mode numbers based on the C₅NH₄¹⁶O¹⁶O isotopomer. [b]Argon matrix at 10 K. Wavenumbers in cm⁻¹ and relative intensities in parenthesis. [c]Calculated at the UB3LYP/cc-pVTZ level of theory

Table 8.5.2.1. IR spectroscopic data of the *m*-pyridyl peroxy radical **34b**.

Mode ^a	C ₅ NH ₄ OO (34b)		C ₅ NH ₄ ¹⁸ O ¹⁸ O (¹⁸ O ₂ - 34b)		Sym.	Assignment
	Argon ^b	DFT ^c	Argon ^b	DFT ^c		
26	1590.1 (7)	1629.4 (15)	-	1629.0 (15)	A'	ring str.
25	1569.5 (10)	1607.1 (34)	-	1606.8 (34)	A'	ring str.
24	1468.0 (39)	1502.5 (27)	-	1502.3 (28)	A'	C-H def.(in plane).
23	1434.3 (55)	1466.4 (93)	1432.7 (100)	1465.5 (93)	A'	C-H def.(in plane)
22	-	1355.7 (0)	-	1354.9 (0)	A'	C-H def.(in plane)
21	-	1288.0 (4)	-	1287.7 (3)	A'	ring str./ C-H def
20	1189.4 (22)	1219.5 (20)	-	1219.2 (19)	A'	C-H def. (in plane)
19	1151.2 (30)	1174.8 (28)	-	1104.6 (4)	A'	O-O str.
18	-	1163.8 (13)	1144.4 (15)	1160.2 (17)	A'	C-H def./ C-O str
17	1119.0 (16)	1125.4 (22)	-	1127.6 (38)	A'	C-H def.(in plane)
16	-	1060.7 (0)	-	1059.9 (0)	A'	ring str.
15	1014.7 (42)	1033.8 (34)	1014.2 (42)	1033.6 (35)	A'	ring def.
14	-	1008.8 (0)	-	1008.8 (0)	A''	CH def.(out of plane).
13	-	976.3 (13)	-	976.2 (12)	A''	CH def.(out of plane).
12	-	945.4 (2)	-	945.4 (2)	A''	CH def.(out of plane)
11	795.9 (100)	823.9 (100)	796.5 (82)	823.8 (100)	A''	CH def.(out of plane)
10	-	818.6 (1)	-	806.2 (2)	A'	C-O str./ring str.
9	696.0 (45)	719.6 (96)	695.9 (60)	719.6 (96)	A''	ring def.
8	627.2 (18)	639.9 (18)	616.8 (21)	630.4 (16)	A'	COO def./ring str
7	599.1 (16)	613.2 (22)	591.0 (9)	602.1 (21)	A'	COO def.
6	-	489.5 (0)	-	488.6 (0)	A''	ring def.

[a]Mode numbers based on the C₅NH₄¹⁶O¹⁶O isotopomer. [b]Argon matrix at 10 K. Wavenumbers in cm⁻¹ and relative intensities in parenthesis. [c]Calculated at the UB3LYP/cc-pVTZ level of theory

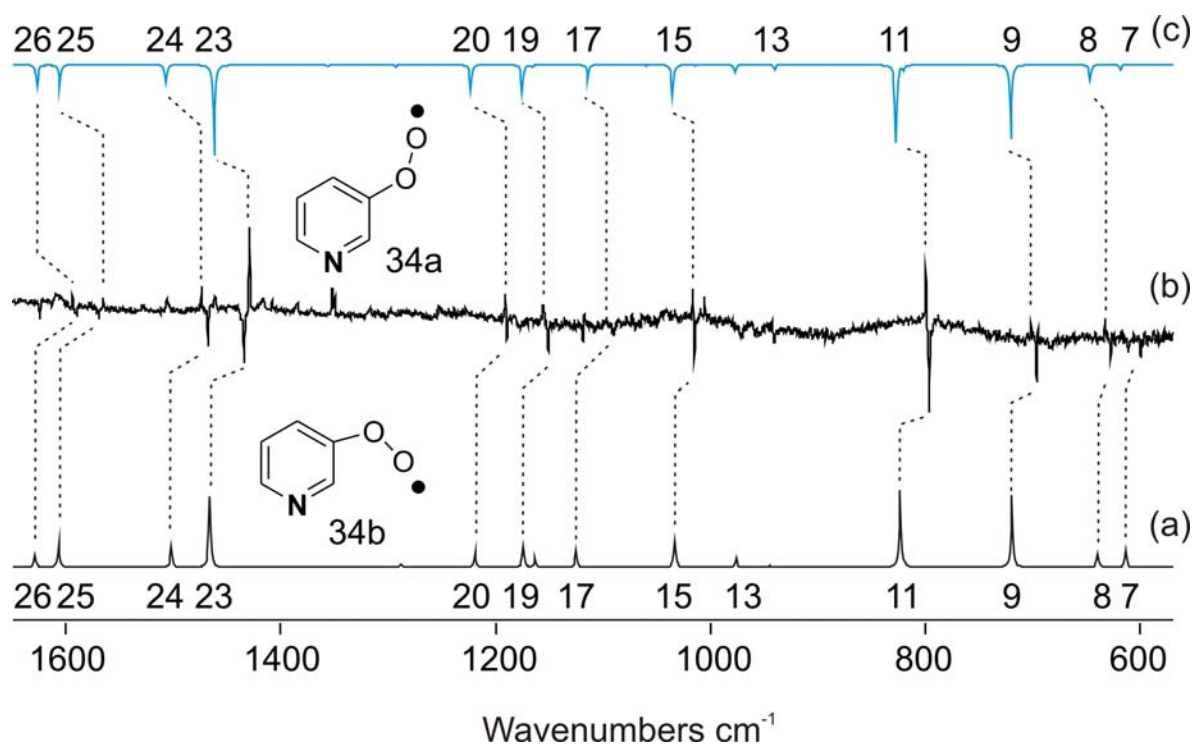


Figure 8.5.2.3. Photochemistry of **34** in solid argon. (a) Calculated vibrational spectrum (UB3LYP/cc-pVTZ) of **34b** (b) Difference spectrum. Bands pointing downwards are disappearing during irradiation ($\lambda > 550 \text{ nm}$) are belong to **34b**. Bands pointing upwards are appearing and assigned to **34a**. (c) Calculated vibrational spectrum (UB3LYP/cc-pVTZ) of **34a**.

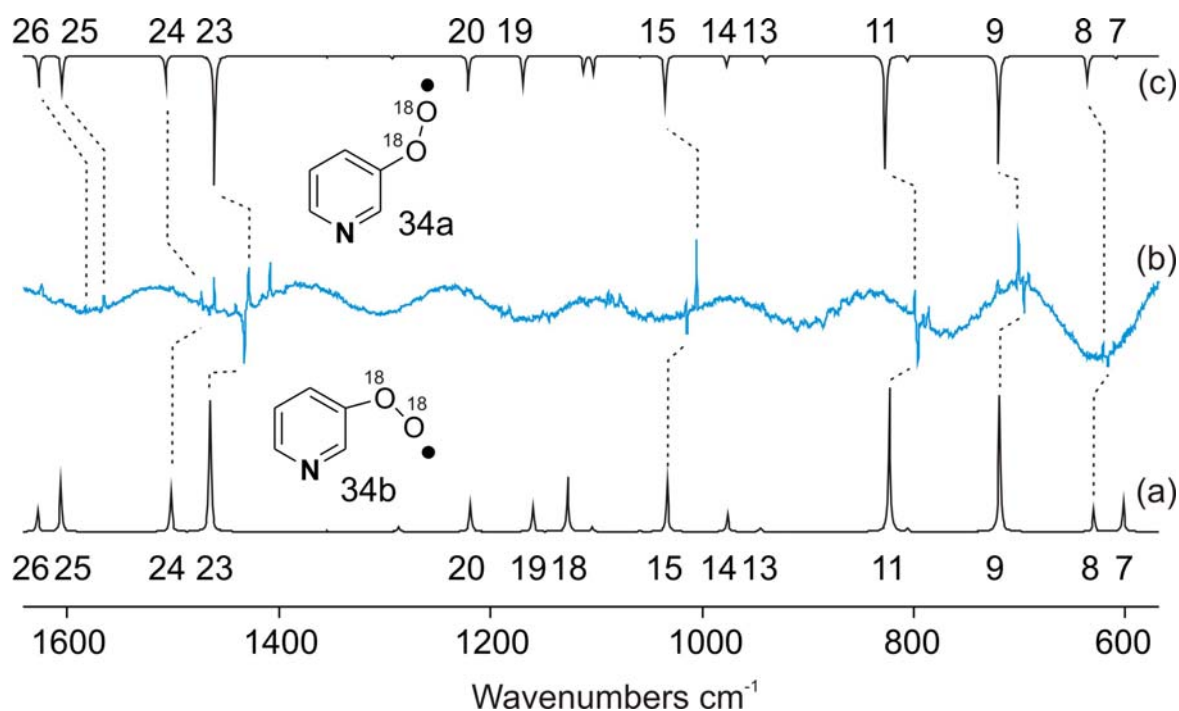


Figure 8.5.2.3. Photochemistry of $^{18}\text{O}_2$ -**34** in solid argon. (a) Calculated vibrational spectrum (UB3LYP/cc-pVTZ) of $^{18}\text{O}_2$ -**34b** (b) Difference spectrum. Bands pointing downwards are disappearing during irradiation ($\lambda > 550 \text{ nm}$) are belong to $^{18}\text{O}_2$ -**34b**. Bands

pointing upwards are appearing and assigned to $^{18}\text{O}_2$ -**34a**. (c) Calculated vibrational spectrum (UB3LYP/cc-pVTZ) of $^{18}\text{O}_2$ -**34a**.

8.4. Summary

In this chapter we reported the synthesis and IR spectroscopic characterization of three pyridyl radicals in argon matrix from different precursors. Two general approaches were used to synthesize pyridyl radicals in solid argon. (i) Photolysis of matrix-isolated iodo-precursors result in the cleavage of C–I bonds. In this case radical pairs are formed in the same matrix cage, and annealing of the matrix results in recombination of these radical pairs. (ii) FVP with subsequent trapping in matrices, on the other hand, produces radicals in individual matrix cages, which allows to investigate bimolecular reactions of those radicals with small molecules such as oxygen, CO etc.

Ortho-pyridyl radical (**24**), the most stable among the three pyridyl radicals, has been generated by FVP and photochemically of 2-iodopyridine. The assignment was achieved by comparison between experimentally observed IR spectrum and calculated spectrum at the UB3LYP/cc-pVTZ level of theory, which has been proved to be very good for the predictions of IR spectra. The compound **24** does not show any photochemistry by irradiation with UV-vis light. Bimolecular reaction between **24** and oxygen has been studied, experimentally and theoretically. According to DFT calculations, two possible conformers (**28a** and **28b**) can be obtained. UB3LYP method predicts no activation barrier for these reactions. The compounds **28a** and **28b** are shown to be photochemically very labile. Irradiation with the light ($\lambda > 420$ nm) results a rapid rearrangement into ring expansion product.

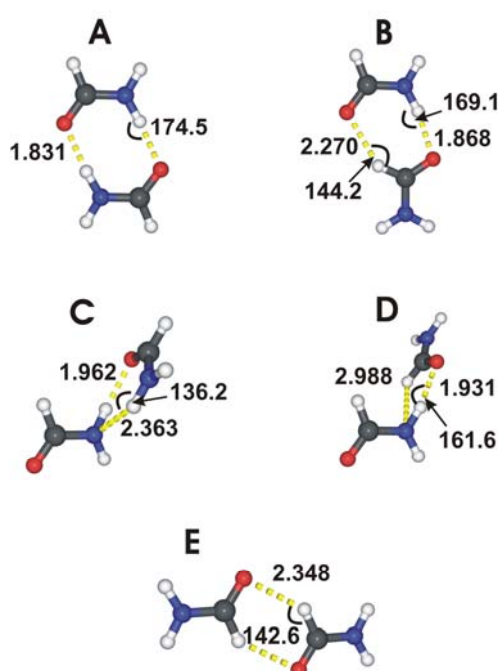
The second most stable pyridyl radical is *p*-pyridyl radical **25** was synthesized and spectroscopically characterized from two different precursors (4-iodopyridine and 4,4-azopyridine) using FVP experiments. The compound **25** is a very reactive species and rapidly reacts with O_2 to give *p*-pyridyl peroxy radical (**32**), which can be isolated and spectroscopically characterized in argon matrix.

The least stable *m*-pyridyl radical (**26**) is shown to be photolabile under matrix isolation conditions. Irradiation of matrix-isolated **26** with the light ($\lambda > 420$ nm) results a complete photolysis of **26** and formation of the ring opening products. In analogy to the previous experiments, the reaction between **26** and oxygen produces corresponding peroxy radicals **34a** and **34b**. The **34a** and **34b** are photolabile and rapidly rearrange to the ring expansions products upon $\lambda > 420$ nm irradiation.

9. General Summary

9.1. Aggregation of formamide in inert matrices at low temperature conditions

The dimerization of FMA monomer **M** in argon matrices leads to two products: the thermodynamically more stable dimer **A** with two strong NH...O hydrogen bonds and the less stable **C/D** with only one strong hydrogen bond. In solid xenon evidence for an additional labile dimer **B** is found. A systematic computational study using the MMH method produces five dimers **A** – **E** which are minima at the MP2/cc-pVTZ level of theory. With the calculated dimerization energy of -10.4 kcal/mol **A** is, as expected, the most stable dimer found. In dimer **B** one of the FMA molecules is rotated in a way that a strong NH...O interaction is replaced by a weaker CH...O interaction reducing the complex stabilization compared to **A** by about 4 kcal/mol. With FMA dimer **B** is not observed after annealing and instead the even less stable (-4.7 kcal/mol) dimer **C/D** is formed. The dynamics simulations also reveal that the structurally and energetically similar dimers **C** and **D** rapidly interconvert even at low temperature. Thus, just three distinct dimers remain : **A**, **B**, and **C/D**, which are indeed observed in the experiment, **B** having been observed before annealing when high FMA concentrations had been deposited.



The formation of both dimers **A** and **C/D** in the argon matrix is a consequence of the first step of the dimerization of **M** in which the carbonyl oxygen atom of one FMA molecule interacts with an amino hydrogen atom of the second molecule. There are two possible arrangements for this interaction leading to different dimers: (i) The *trans* hydrogen atom of the first FMA molecule interacts with the carbonyl oxygen atom of the second molecule. This can only lead to dimers **C** or **D**. (ii) The *cis* hydrogen atom of one FMA molecule interacts with the carbonyl oxygen atom of the second molecule leading to dimers **A** or **B**. The rearrangement of **C/D** to **A** or **B** requires breaking the strong N- $H_{cis} \cdots O$ hydrogen bond, which is energetically not possible under the conditions of matrix isolation. Thus, once one strong $NH \cdots O$ hydrogen bond is formed, the further reaction leads either to **C/D** or **A/B** which do not interconvert. In case (ii) obviously the energetically more stable complex **A** is formed rather than **B**.



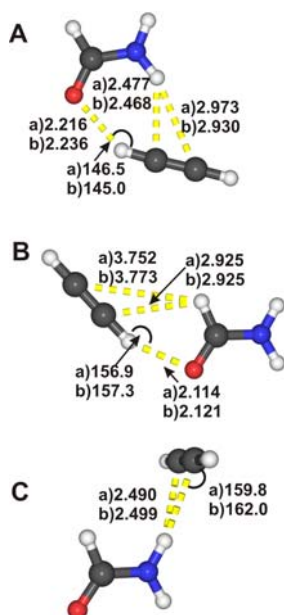
9.2. Formamide –Acetylene complexes

Using matrix isolation techniques and *ab initio* calculations, we found that FMA – acetylene dimers are formed in the matrix and there is an evidence of the formation of one FMA – acetylene trimer when increasing the acetylene concentration.

Three stable FMA – acetylene dimers were identified at the MP2 level of theory with the aug-cc-pVDZ and cc-pVTZ basis sets. Their binding energies are between -2.96 and -1.79 kcal/mol.(MP2/cc-pVTZ +ZPE+BSSE) The most stable dimer **A** is stabilized by the $N-H_{FMA} \cdots \pi$ and $C=O_{FMA} \cdots H_{acet}$ interactions between FMA and acetylene. Dimer **B** shows the $C-H_{FMA} \cdots \pi$ and $C=O_{FMA} \cdots H_{acet}$ interactions while dimer **C** is stabilized only by the $N-H_{FMA} \cdots \pi$ interactions. By comparing the experimental and calculated frequencies, the dimers **A** and **B** were identified in argon and nitrogen matrices. In both complexes the stronger $C=O_{FMA} \cdots H_{acet}$ interaction occurs as it is evidenced by the large shifts of the $\equiv C-H$ stretching modes.

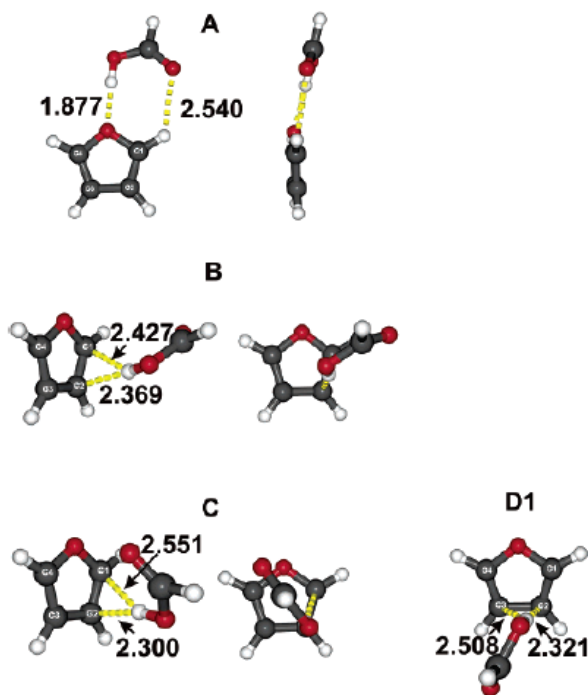
Eight, 1:2 FMA – acetylene trimers (**T-A** to **T-H**) with binding energies between -5.44 and -2.62 kcal/mol were identified. (MP2/aug-cc-pVDZ + ZPE +BSSE). The trimers **T-A** and **T-B** are close in energy. Weak bands observed under matrix isolation conditions

at higher concentrations of acetylene suggest the formation of a trimer. Nevertheless, the spectra could not be clearly assigned as corresponding to the trimer T-**B** or T-**A**.



9.3. Furan–Formic Acids

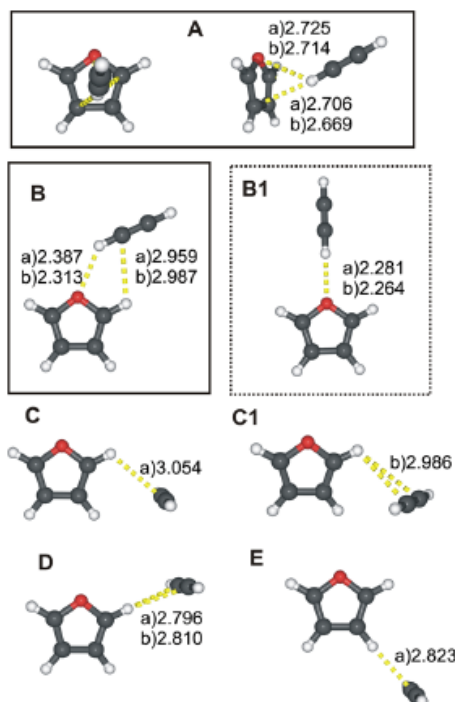
Furan is an interesting heterocyclic system that is able to accept hydrogen bonds both in the molecular plane at the basic oxygen atom and perpendicular to the molecular plane at its electron-rich σ -system. Formic acid, on the other hand, can act as hydrogen bridge donor either via its acidic OH group or via the less acidic CH group. In addition, it can serve as hydrogen bridge acceptor via its two oxygen atoms. The combination of furan and formic acid thus results in a variety of noncovalently bound dimers which are systematically studied.



The binding energy of the most stable complex **A** is -3.91 kcal/mol (MP2/6-311++G(d,p) + PE+ BSSE). Although the OH...O interaction is dominating in dimer **A**, the secondary C=OFA...HFu interaction between the carbonyl oxygen atom of FA and the hydrogen atom of furan leads to an additional significant stabilization of this complex. The matrix isolation experiments reveal that dimer **A** is the major, if not only, complex formed if the two monomers are allowed to diffuse slowly in solid argon. The additional IR absorptions that appear in the matrix spectra under these conditions nicely match the theoretical predictions for complex **A**.

9.4. Acetylene-Furan

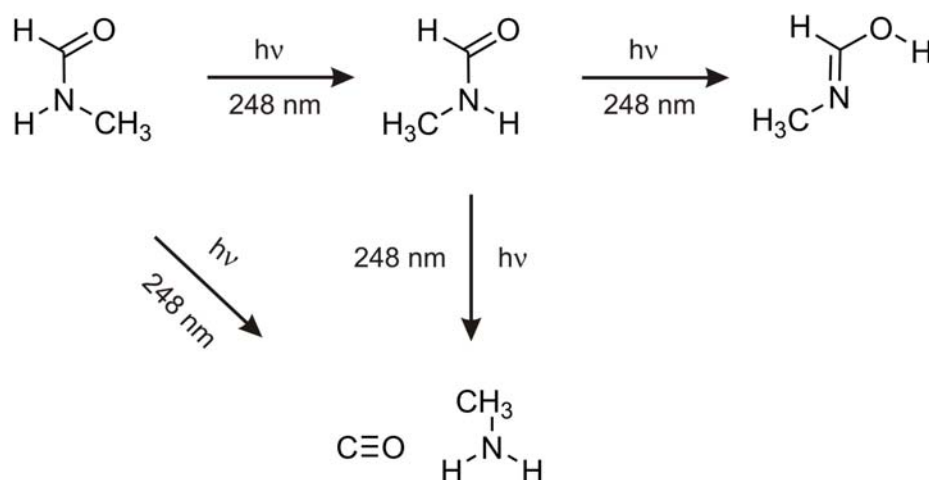
Five structures were identified to be minima on the potential energy surface of the acetylene–furan dimer in MP2/6-311++G(d,p) geometry optimizations. One of these **A** is characterized by a $\text{CH}_{\text{Ac}}\dots\pi_{\text{Fu}}$ interaction. The nearly isoenergetic structure **B** is characterized by a $\text{CH}_{\text{Ac}}\dots\text{O}_{\text{Fu}}$ interaction and an additional, presumably very weak, interaction of a hydrogen atom with the π system of the acetylene.



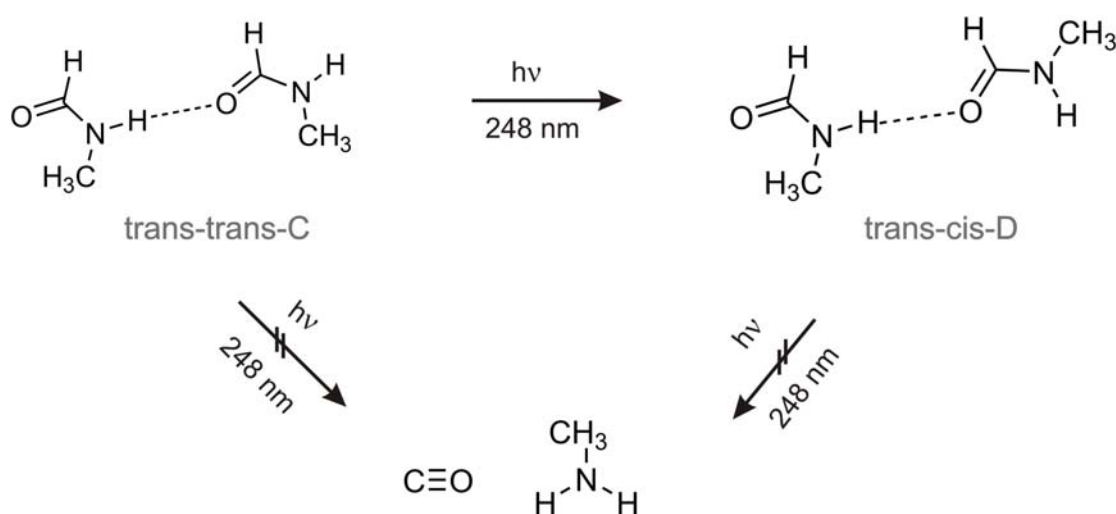
Comparison between calculated and measured IR spectra of acetylene–furan deposited in an argon matrix, however, makes it likely that structure **B** is formed in the matrix.

9.5. *N*-methylformamide: Monomers and Dimers

Ultraviolet irradiation (wavelength $\lambda=248$ nm) of NMF in argon and nitrogen matrices at 10 K leads to the formation several primary photoproducts. According to B3LYP calculations the *cis*–NMF is less stable by 0.948 kcal/mol than the *trans*–NMF, was generated during irradiation from the *trans*– form of NMF. This *cis*– conformer is an intermediate in the ultraviolet photolysis, leading to intramolecular proton transfer from the amino group to the carbonyl oxygen atom in the formation of *N*-methylformimidic acid which is a tautomer of NMF. With the support of theoretical calculation we demonstrated that *N*-methylformimidic acid is isolated in argon and nitrogen matrices in its energetically most stable (*s*-Z)-(*E*) configuration. At the same time decomposition products such as H_2NCH_3 –CO and HNCO – CH_4 have also been trapped in the matrix cage during the photolysis.

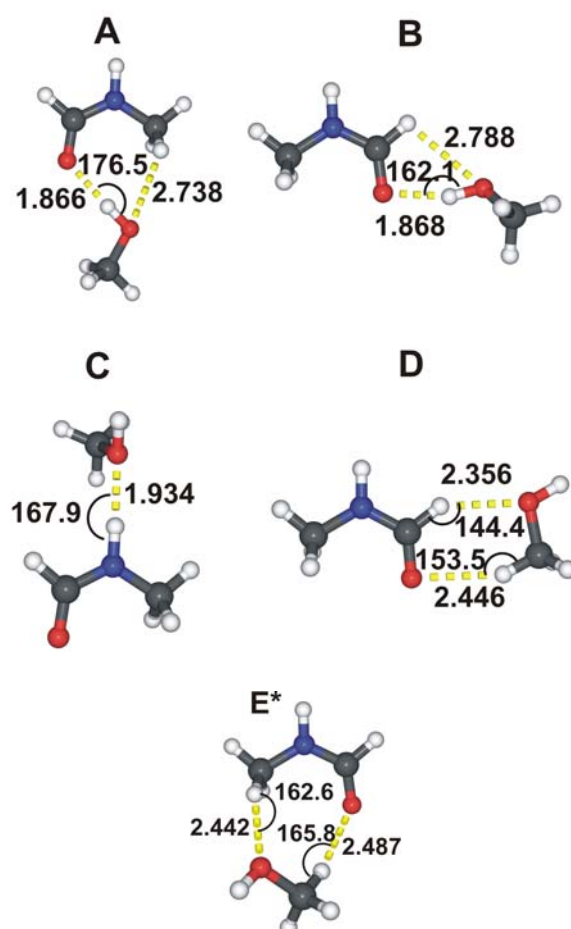


We have investigated the aggregation of the NMF in argon matrix in combination with DFT calculations that provide fruitful information to differentiate the dimers at low temperature conditions. After careful analyses of infrared spectra we are able to identify only one dimer (t-t-C). However, some weak bands that appear in the whole spectral region can be assigned to the *trans-cis*- types of dimers in argon matrix. The possibilities of finding the *cis-cis* type of dimers will be quite low in contrast to their large thermodynamic stability. These findings can be explained by the consideration that the population of the *cis*- conformer of the NMF is very low. Even if the dimers of the *cis*- NMF would be more stable, they will not be produced by rotation of the *trans*- to the *cis*- isomers during the aggregation at low temperature conditions. Therefore, upon annealing the *trans*- isomer of NMF mainly produces dimers.



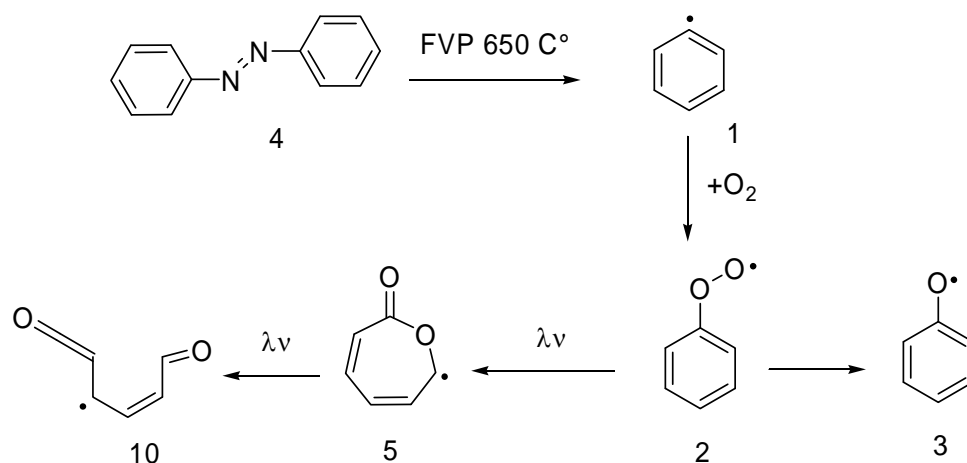
9.6. NMF–Methanol

The 1:1 hydrogen-bonded complexes of NMF and methanol (MeOH) have been studied by matrix isolation infrared spectroscopy and quantum chemical calculations. The two most stable complexes were observed in the argon matrix at 10 K. A number of intermolecular complex bands are found in both the NMF and MeOH fundamental regions. The C=O stretching of NMF is red shifted and the C–O stretching of MeOH is blue shifted due to the complexation. The O–H stretching mode of methanol also exhibits a large red shift. Structures, energies, and vibrational frequencies of the complexes were calculated at the MP2/TZ2P and B3LYP/6-311++G(2d,2p) levels of theory. Four NMF – MeOH minima were found at both levels of theory. Three are cyclic structures, involving the O–H...O, H–O...H and C–H...O=C interactions. The third most stable dimer is an open structure only stabilized by the H–O...H–N interaction. The binding energies of those complexes are –5.45, –4.92, –4.41 and –2.23 kcal/mol (MP2/TZ2P+BSSE+ZPE).



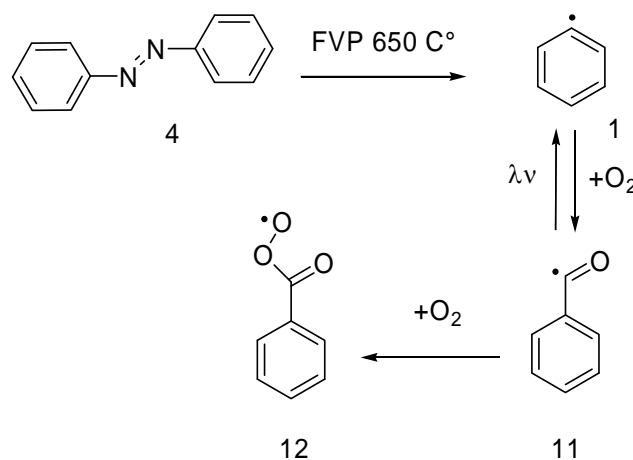
9.7. Phenyl Peroxy Radical

We showed that the phenyl radical (**1**) rapidly reacts with molecular oxygen to produce the phenoxyl peroxy radical (**2**) both in the gas phase and in argon matrices. Phenoxyl radical (**3**) is not formed under these conditions. This indicates that the activation barrier for the oxygen addition to **1** is very low and that, despite the high exothermicity of this reaction, the primary product **2** can efficiently dissipate the excess energy without fragmentation. Loss of oxygen from **2** obviously requires a higher thermal excitation in high-temperature processes or in cross-beam experiments. This is of relevance to tropospheric chemistry, since the phenyl radical (**1**) can be produced in the troposphere from benzene via H-abstraction by OH radicals. The phenyl radical (**1**) will be efficiently quenched by oxygen to form peroxy radical (**2**). Under these conditions it is not expected that **2** cleaves to phenoxyl radical **3** and O(3P). Formation of triplet oxygen atoms would regenerate ozone and subsequently OH radicals. The photochemical rearrangement of **2** by visible light produces another intermediate of importance in the oxidation of benzene: the 2-oxepinoxy radical (**5**). This radical was also characterized by IR spectroscopy. Further irradiation finally leads to the cleavage of the ring and formation of a mixture of several conformers of ketoketene **10**. Our experiments do not allow us to determine if the photochemical steps which lead to **5** and **10** proceed on an excited surface or if these reactions are hot ground state reactions. Nevertheless, the products found in the matrix are the products that have been predicted by ab-initio and DFT calculations to be formed with the smallest activation barriers. These products are thus also relevant for the thermal combustion of benzene.



9.8. Benzoyl Radical

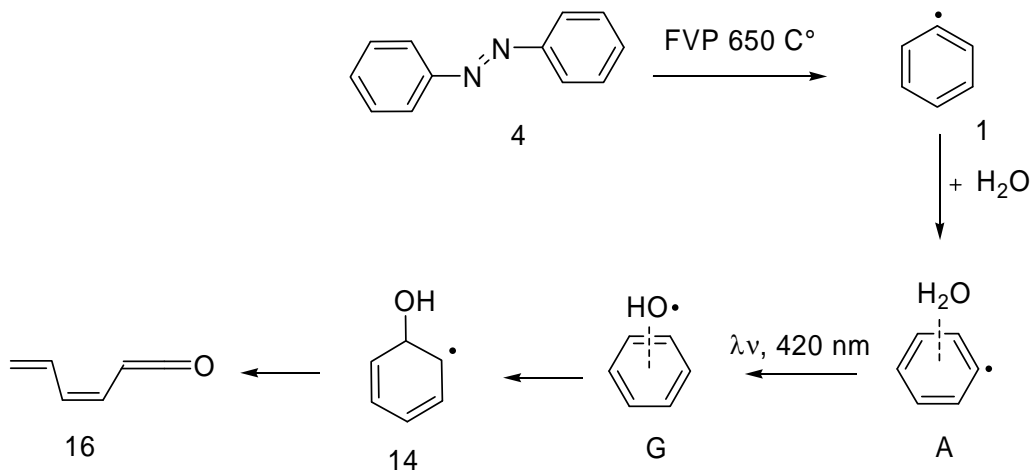
The phenyl radical (**1**) is a highly reactive species that even under the conditions of matrix isolation rapidly reacts with CO and O₂ as long as diffusion of these small molecules in the solid matrix is possible. With CO the benzoyl radical **11** is formed which could be isolated and spectroscopically characterized. Interestingly, conditions could be found where mixtures of CO and O₂ in the same matrix produce good yields of the benzoyl peroxy radical **12** by subsequent reactions of the phenyl radical **1** with CO and O₂. Obviously, the reaction of **1** with CO can compete with the reaction with O₂. This is in line with DFT and ab initio calculations which predict very shallow or absent activation barriers for both reactions. The formation of the radicals **11** and **12** in argon matrices depends on the statistical distribution and rates of diffusion of CO and O₂. An excess of CO compared to O₂ thus results in the preferential formation of **11** which subsequently reacts with O₂ to **12**.



9.9. Phenyl radical –water. A pre-reactive complex

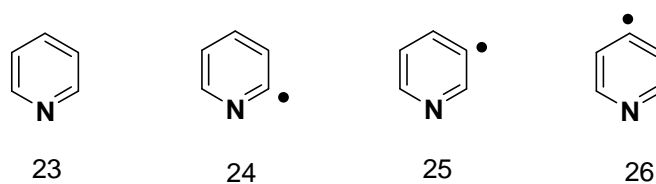
We have isolated and characterized complexes between the phenyl radical and water and between the hydroxyl radical and benzene for the first time. We observed light-driven hydrogen-atom transfer from water to the phenyl radical within these complexes. Our results demonstrate the importance of radical complexes for the radical reactivity. Irradiation of **G** complex leads directly to ketene **16** as the major product while radical **14** or other intermediates are not observed. We therefore conclude that **14** is indeed formed,

however, either with a large excess energy that leads to further reactions or it is photochemically unstable under the conditions of its formation.



9.10. Pyridyl radicals

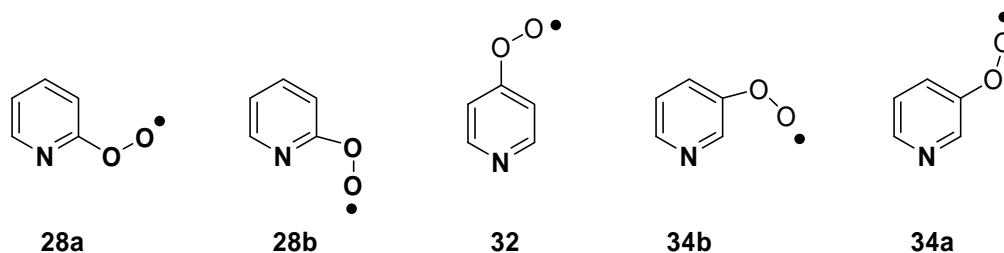
In this chapter we reported the synthesis and IR spectroscopic characterization of three pyridyl radicals in argon matrix from different precursors. Two general approaches were used to synthesize pyridyl radicals in solid argon. (i) Photolysis of matrix-isolated iodo-precursors result in the cleavage of C–I bonds. In this case radical pairs are formed in the same matrix cage, and annealing of the matrix results in recombination of these radical pairs. (ii) FVP with subsequent trapping in matrices, on the other hand, produces radicals in individual matrix cages, which allows to investigate bimolecular reactions of those radicals with small molecules such as oxygen, CO etc.



Ortho-pyridyl radical (**24**), the most stable among the three pyridyl radicals, has been generated by FVP and photochemically of 2-iodopyridine. The assignment was achieved

by comparison between experimentally observed IR spectrum and calculated spectrum at the UB3LYP/cc-pVTZ level of theory, which has been proved to be very good for the predictions of IR spectra. The compound **24** does not show any photochemistry by irradiation with UV-vis light. Bimolecular reaction between **24** and oxygen has been studied, experimentally and theoretically. According to DFT calculations, two possible conformers (**28a** and **28b**) can be obtained. UB3LYP method predicts no activation barrier for these reactions. The compounds **28a** and **28b** are shown to be photochemically very labile. Irradiation with the light ($\lambda > 420$ nm) results a rapid rearrangement into ring expansion product.

The second most stable pyridyl radical is *p*-pyridyl radical **25** was synthesized and spectroscopically characterized from two different precursors (4-iodopyridine and 4,4-azopyridine) using FVP experiments. The compound **25** is a very reactive species and rapidly reacts with O₂ to give *p*-pyridyl peroxy radical (**32**), which can be isolated and spectroscopically characterized in argon matrix.



The least stable *m*-pyridyl radical **26** is shown to be photolabile under matrix isolation conditions. Irradiation of matrix-isolated **26** with the light ($\lambda > 420$ nm) results in complete photolysis of **26** and formation of the ring opening products. In analogy to the previous experiments, the reaction between **26** and oxygen produces corresponding peroxy radicals **34a** and **34b**. The **34a** and **34b** are photolabile and rapidly rearrange to the ring expansions products upon $\lambda > 420$ nm irradiation.

Chapter 10. Methods and materials

10.1. Synthesis

All solvents were distilled and dried as standard procedure before use. TLC analysis were carried out using Polygram Sil G/UV₂₅₄ silica gel pre-coated plates and the spots were analyzed using UV lamp (CAMAG). Column chromatography was carried out using ICN silica 32-63 (60 Å).

10.2. Analytical equipments

NMR spectroscopy: NMR spectra were recorded on Bruker DPX-200 (200.13 MHz: ¹H-NMR and 50.3 MHz: ¹³C-NMR) spectrometers.

Mass spectrometer: Mass spectra were recorded on Varian MAT-CH5 spectrometer at 70eV EI. Characteristic peaks were given with their relative intensities.

Melting point apparatus: Melting point were measured on Büchi melting point apparatus of Dr. Tottoti.

10.3. Matrix Isolation Set-up

10.3.1. Apparatus

Matrix isolation experiments were performed by standard techniques using an APD CSW-202 Displex closed cycle helium refrigerator.

10.3.2. Deposition

Matrixes were produced by co-deposition of the compound with a large excess of argon (Messer Griesheim, 99.99%) or xenon (Messer Griesheim, 99.99%) on top of a cold CsI window with a rate of approximately 0.11 mmol/min. Volatile compounds were premixed with inert gas (argon, xenon or nitrogen) in a steel-mixing chamber using standard manometric methods. About 0.5-2 mbar of compound was mixed with 1000-1500 mbar of inert gas in a 2L glass bulb. Nonvolatile precursors were deposited from a side-arm using a furnace (Büchi GKR-51).

10.3.3. Flash vacuum pyrolysis (FVP)

Flash vacuum pyrolysis (FVP) was carried out by slowly subliming precursor through a 7 cm quartz tube heated electrically with a tantalum wire. The sample at a pressure of about 10–5 mbar is sublimed into the pyrolysis zone and condensed afterwards with inert gas and deposited on the spectroscopic window. The temperature of the pyrolysis zone is measured using a PT100-sensor, which is placed in such a way that there is no direct contact with quartz surface.

10.3.4. IR- and UV- spectrometers

Matrix infrared spectra were recorded with Bruker IFS66 and IFS66s FTIR spectrometers with a standard resolution of 0.5 cm^{-1} using a liquid nitrogen cooled MCT detector in the range of $400\text{--}4000\text{ cm}^{-1}$. UV spectra were recorded using Hewlett-Packard HP8452 Diodearray spectrophotometer for a range 190–820 nm with a resolution of 2 nm or Varian Cary 5000 UV-Vis-NIR spectrophotometer.

10.3.5. Light Sources

Broad band UV/Vis- irradiations were carried out using a 500 W high pressure mercury lamps (Ushio) having a quartz optics (L.O.T. Oriel). The housing of the lamp contains a collimator to get parallel beams, a 10 cm long water filter to avoid heat radiation and a slit to adjust the beam profile. The wavelength can be chosen by varying dichroic mirrors or by using cut-off filters (Schott and Balzers). Irradiation at 254 nm was carried out with a Gräntzel low-pressure mercury arc lamp. Laser photolyses were accomplished with a Compex100 Excimer-Laser (Lambda Physik LPX 105 SD) for $\lambda = 248\text{ nm}$ (Kr/F2) and for $\lambda = 193\text{ nm}$ (Ar/F2) or Compex110 Excimer-Laser (Lambda Physik) for $\lambda = 308\text{ nm}$ (Xe/Cl₂).

10.4. Quantum chemical calculations

Optimized geometries and vibrational frequencies of all species were calculated at the UB3LYP^[379–381] level of theory using the 6-311+G(d,p) polarized valence-triple- ξ basis set^[382, 383] and Dunning's cc-pVTZ^[384–386] basis sets. All DFT calculations were carried out with Gaussian 03.^[387]

Chapter 11. Synthesis

Azobenzene-d₁₀

Azobenzene-d₁₀ was synthesized according to a literature procedure.^[388] In the flask are placed 2.5 g. (2.08 ml., 0.02 moles) of nitrobenzene-d₅ (Acros Organics), 25 ml. of methanol, and a solution of 3.25 g. (0.081 moles) of sodium hydroxide in 7.5 ml. of distilled water. To the mixture is added 2.65 g. (0.041 moles) of zinc dust, the stirred and the mixture is refluxed for 12 hours. The mixture is filtered while hot, and the precipitate of sodium zincate is washed on the filter with a little warm methanol. All the methanol is distilled from the filtrate, the residue is chilled, and the crystalline azobenzene is filtered. In order to remove zinc salts from the crude azobenzene, the latter is added to 5 ml. of 2% hydrochloric acid, the mixture is warmed to about 70° in order to melt the azobenzene and is stirred rapidly for about 5 minutes. Stirring is continued while the mixture is chilled to solidify the azobenzene. The product is filtered, washed well with water, and recrystallized from a mixture of 7.2 ml. of 95% ethanol and 0.6 ml. of water. The yield of azobenzene melting at 67-68° is 1.5–1.6 g. (84–86%). ¹³C NMR (50.33 MHz, CDCl₃) δ_C 152.99, 78.06, 77.43, 76.79; MS (RI, 70 eV) (m/z, %) 192 (M⁺), 110, 82, 54, 45.

Chapter 12. Appendix

12.1. Quantum chemical calculations

This section contains the information comprising the optimized geometry (in Cartesian co-ordinates), energy values (in hartrees), zero-point energy correction (in hartrees) and the imaginary frequencies of the computed structures.

Phenyl radical (1) 2A_1 UB3LYP/cc-pVTZ

C	-1.31854000	0.00000000	0.00000000	E=-231.64410935 ZPE=0.087244
C	-0.62984600	-1.20909300	0.00000000	
C	0.76917000	-1.22106400	0.00000000	
C	1.39156700	-0.00000100	0.00000000	
C	0.76917000	1.22106600	0.00000000	
C	-0.62984600	1.20909300	0.00000000	
H	-2.40024100	0.00000000	0.00000000	
H	-1.17342400	-2.14548600	0.00000000	
H	1.31852600	-2.15319400	0.00000000	
H	1.31852500	2.15319400	0.00000000	
H	-1.17342500	2.14548400	0.00000000	

Phenyl Peroxyl radical (2) 2A_1 UB3LYP/cc-pVTZ

C	0.00000000	0.55729700	0.00000000	E=-231.64410935 ZPE= 0.095947
C	-1.02796800	-0.37313700	0.00000000	
C	-0.69097100	-1.71995000	0.00000000	
C	0.64283600	-2.11921900	0.00000000	
C	1.65469000	-1.16428700	0.00000000	
C	1.33827000	0.18688000	0.00000000	
H	-2.05276300	-0.03776400	0.00000000	
H	-1.47712700	-2.46268100	0.00000000	
H	0.89194900	-3.17136400	0.00000000	
H	2.69176700	-1.47036300	0.00000000	
H	2.10295300	0.95081700	0.00000000	
O	-0.22050000	1.93806100	0.00000000	
O	-1.48674000	2.31017000	0.00000000	

Phenoxy radical (**3**) 2B_1 UB3LYP/cc-pVTZ

C	0.000000	0.000000	-1.777911	E=-306.9391303 ZPE= 0.091418
C	0.000000	1.220511	-1.082954	
C	0.000000	1.235503	0.288228	
C	0.000000	0.000000	1.044998	
C	0.000000	-1.235503	0.288228	
C	0.000000	-1.220511	-1.082954	
H	0.000000	0.000000	-2.859523	
H	0.000000	2.148833	-1.638958	
H	0.000000	2.157575	0.853028	
H	0.000000	-2.157575	0.853028	
H	0.000000	-2.148833	-1.638958	
O	0.000000	0.000000	2.295712	

2-oxepinoxy radical (**5**) 2A_1 UB3LYP/cc-pVTZ

C	-1.75756000	-0.75548500	0.00000000	E=-382.1742301 ZPE= 0.089423
C	-1.86151600	0.65054200	0.00000000	
C	-0.79494000	1.55215900	0.00000000	
C	-0.64245300	-1.52841900	0.00000000	
C	0.55502800	1.30328400	0.00000000	
C	1.29947700	0.05434300	0.00000000	
H	-2.68097400	-1.32020800	0.00000000	
H	-2.85931700	1.06708200	0.00000000	
H	-1.06784800	2.60126100	0.00000000	
H	-0.73717200	-2.60533300	0.00000000	
H	1.22983400	2.14697400	0.00000000	
O	2.49801500	0.01041900	0.00000000	
O	0.66789300	-1.20395900	0.00000000	

Dioxiranyl radical (**6**) 2A_1 UB3LYP/cc-pVTZ

C	2.09379700	0.00000000	0.00000000	E=-382.1486936 ZPE= 0.093892
C	1.39223100	1.22501900	0.00000000	
C	0.02982300	1.25061100	0.00000000	
C	-0.73466200	0.00000000	0.00000000	
C	0.02982400	-1.25061100	0.00000000	
C	1.39223100	-1.22501900	0.00000000	
H	3.17452700	0.00000000	0.00000000	
H	1.94761300	2.15344400	0.00000000	
H	-0.53925600	2.16885500	0.00000000	
H	-0.53925600	-2.16885500	0.00000000	
H	1.94761300	-2.15344400	0.00000000	
O	-1.95066900	0.00000000	0.74115200	
O	-1.95066900	0.00000000	-0.74115200	

1,6-dioxo-2,4-hexadienyl radical (**10a**) ²A UB3LYP/cc-pVTZ

C	-1.86212300	0.72980600	-0.03433800	E=-382.0616841 ZPE= 0.091951
C	-0.67866200	1.45906000	0.01065200	
C	0.66201200	1.08933600	0.02949000	
C	-2.07586800	-0.69243800	0.07599900	
C	1.22902000	-0.21517100	-0.09103900	
C	2.53745000	-0.44008200	-0.02321200	
H	-2.78281800	1.29335900	-0.12935300	
H	-0.82112700	2.53419300	0.02058900	
H	1.37219700	1.90081700	0.12303900	
H	0.63369700	-1.10019200	-0.26808500	
O	3.67117400	-0.65161600	0.03710400	
O	-3.18016900	-1.20809800	-0.01669400	
H	-1.20095800	-1.33352600	0.28521200	

1,6-dioxo-2,4-hexadienyl radical (**10b**) ²A UB3LYP/cc-pVTZ

C	-1.35644300	0.89548200	-0.28676400	E=-382.1438815 ZPE= 0.092024
C	-0.25452800	1.73525400	-0.21528200	
C	1.07602900	1.52061000	0.13963600	
C	-1.51268000	-0.42178700	0.28118100	
C	1.84183900	0.32558300	0.29954600	
C	1.55437400	-0.92136100	-0.06457800	
H	-2.26179900	1.29317500	-0.72985700	
H	-0.45683600	2.76565500	-0.48951400	
H	1.66953900	2.41525200	0.27460300	
H	2.86057000	0.41270300	0.66243500	
O	1.37734500	-2.02326700	-0.35917000	
O	-2.53036500	-1.08730700	0.16704700	
H	-0.67886700	-0.80488200	0.89687700	

1,6-dioxo-2,4-hexadienyl radical (**10c**) ²A UB3LYP/cc-pVTZ

C	-1.93514300	0.72336300	-0.00000900	E=-382.1538384 ZPE= 0.091783
C	-0.58492500	1.04333700	-0.00003100	
C	0.49414300	0.16981100	0.00106600	
C	-2.50075900	-0.60439700	-0.00003100	
C	1.84591400	0.62256900	-0.00016900	
C	2.90370200	-0.18271100	0.00111300	
H	-2.65923200	1.52824500	-0.00035400	
H	-0.34287000	2.10209800	-0.00102800	
H	0.32735500	-0.89829000	0.00264100	
H	2.08015000	1.68096600	-0.00198300	
O	3.83210200	-0.87195900	-0.00099600	
O	-3.70135400	-0.82713300	-0.00038500	
H	-1.78898300	-1.45211100	0.00013800	

Benzoyl radical (**11**) 2A_1 UB3LYP/cc-pVTZ

C	0.59065700	-2.10318300	0.00000000	E=-345.0457829 ZPE= 0.097497
C	1.62317100	-1.17167500	0.00000000	
C	1.32849600	0.18493300	0.00000000	
C	0.00000000	0.60808300	0.00000000	
C	-1.03792300	-0.33175900	0.00000000	
C	-0.73872900	-1.68416000	0.00000000	
H	0.81989800	-3.16058300	0.00000000	
H	2.65250300	-1.50307500	0.00000000	
H	2.11567300	0.92660000	0.00000000	
H	-2.06207600	0.01510800	0.00000000	
H	-1.53627800	-2.41505000	0.00000000	
C	-0.29718700	2.05554500	0.00000000	
O	-1.35007900	2.59878800	0.00000000	

Benzoyl Peroxyl radical-Z (**12**) 2A UB3LYP/cc-pVTZ

C	2.90798900	-0.27958500	0.00000000	E=-495.4783215 ZPE= 0.105877
C	2.04119400	-1.36680100	0.00000000	
C	0.66855800	-1.16458300	0.00000000	
C	0.15943900	0.13824800	0.00000000	
C	1.03544300	1.22884900	0.00000000	
C	2.40402700	1.01838100	0.00000000	
H	3.97741200	-0.44270400	0.00000000	
H	2.43446400	-2.37395700	0.00000000	
H	-0.00301100	-2.00897300	0.00000000	
H	0.62463300	2.22822600	0.00000100	
H	3.07941700	1.86276600	0.00000000	
C	-1.28447900	0.43473100	0.00000000	
O	-1.82169400	1.49224800	-0.00000100	
O	-2.04384500	-0.80089900	0.00000000	
O	-3.34770300	-0.60644900	0.00000100	

Benzoyl Peroxyl radical-E (**12a**) ²A UB3LYP/cc-pVTZ

C	-2.74644800	-0.29291300	0.03246500	E=-495.4727917 ZPE= 0.1056225
C	-1.86252600	-1.30366300	-0.32952600	
C	-0.49866800	-1.05618800	-0.37534900	
C	-0.01436100	0.21922300	-0.07061100	
C	-0.90919000	1.23778800	0.27321200	
C	-2.26844000	0.97820000	0.33530200	
H	-3.80834100	-0.49489400	0.07496500	
H	-2.23567700	-2.28848900	-0.57416200	
H	0.17986500	-1.84619100	-0.65619400	
H	-0.52262900	2.22359900	0.48846700	
H	-2.95504700	1.76559100	0.61388800	
C	1.40624600	0.60107300	-0.17879300	
O	1.84904200	1.68907500	-0.36639300	
O	2.40021200	-0.45199200	-0.10565300	
O	2.08851500	-1.44467500	0.71365000	

TS-for benzoyl peroxyl radical ²A UB3LYP/cc-pVTZ

C	-2.80638200	-0.34961300	0.08382100	E=-495.4702984 ZPE= 0.1053643 Imaginary freq. (-90.50)
C	-1.89718600	-1.38588400	-0.09610900	
C	-0.53977500	-1.11302500	-0.18566500	
C	-0.09069000	0.20739300	-0.09297200	
C	-1.00977500	1.24794200	0.08846100	
C	-2.36219800	0.96748700	0.17604700	
H	-3.86387000	-0.56699700	0.15283100	
H	-2.24538400	-2.40699700	-0.16616600	
H	0.16779500	-1.91584500	-0.32399800	
H	-0.64421200	2.26237100	0.15870200	
H	-3.07202200	1.77090000	0.31648400	
C	1.33195600	0.56053500	-0.17911900	
O	1.83872700	1.62967600	-0.09200700	
O	2.19401000	-0.59401300	-0.45834100	
O	2.70501200	-1.02971700	0.68726900	

N-methylformamide (**trans**) ¹A UB3LYP/6-311++G(2d,2p)

C	-0.86954300	0.42688500	-0.00001400	E=-209.2725666 ZPE= 0.073862
O	-1.41171900	-0.66059900	-0.00016600	
N	0.47384000	0.64127400	0.00010400	
H	-1.43947400	1.37437600	0.00004700	
H	0.79205200	1.59807400	0.00021300	
C	1.45726700	-0.43191300	0.00005100	
H	2.08996400	-0.38431400	-0.89035400	
H	2.08993200	-0.38442200	0.89048300	
H	0.91806100	-1.37766900	-0.00001800	

N-methylformamide (**cis**) ¹A UB3LYP/6-311++G(2d,2p)

C	-0.73379800	0.34554600	0.00000000	E=-209.2708365 ZPE= 0.073784
O	-1.86645800	-0.09261000	0.00000000	
N	0.39694200	-0.40944700	0.00000000	
H	-0.51440000	1.43059500	0.00000000	
H	0.25713300	-1.41093200	0.00000000	
C	1.75044400	0.11738500	0.00000000	
H	1.70456200	1.20781400	0.00000000	
H	2.30295100	-0.19903000	0.88936700	
H	2.30295100	-0.19903100	-0.88936600	

N-methylformamide (**TS**) ¹A UB3LYP/6-311++G(2d,2p)

C	-0.83129000	-0.37452200	0.23119200	E=-209.2533692 ZPE= 0.072810
O	-1.46890400	0.56584000	-0.15166800	
N	0.51330500	-0.68941000	-0.17210100	
H	-1.24841000	-1.09355000	0.95537400	
H	0.49379700	-0.84621400	-1.17647300	
C	1.45883600	0.40959400	0.11048200	
H	1.54968200	0.53283200	1.18963100	
H	2.43712300	0.12871200	-0.27477400	
H	1.16063400	1.36693800	-0.32575100	

N-methylformimidic acid (s-Z)-(E) (**3a**) ¹A UB3LYP/6-311++G(2d,2p)

C	0.53064100	0.36101200	0.00000000	E=-209.2670 ZPE= 0.073754
O	1.82709800	-0.01841200	0.00000000	
N	-0.42012200	-0.46301800	0.00000000	
H	0.44389900	1.45118200	0.00000000	
C	-1.78056000	0.04589200	0.00000000	
H	-1.84029600	1.14391600	0.00000000	
H	-2.30996700	-0.33032900	-0.87980100	
H	-2.30996700	-0.33032900	0.87980100	
H	1.83992200	-0.98743500	0.00000000	

N-methylformimidic acid (s-E)-(E) (**3b**) ¹A UB3LYP/6-311++G(2d,2p)

C	0.53064100	0.36101200	0.00000000	E=-209.25880 ZPE= 0.073544
O	1.82709800	-0.01841200	0.00000000	
N	-0.42012200	-0.46301800	0.00000000	
H	0.44389900	1.45118200	0.00000000	
C	-1.78056000	0.04589200	0.00000000	
H	-1.84029600	1.14391600	0.00000000	
H	-2.30996700	-0.33032900	-0.87980100	
H	-2.30996700	-0.33032900	0.87980100	
H	2.47357884	0.70355237	-0.00000000	

Trans-trans-A dimer NMF (**t-t-A**) ¹A UB3LYP/6-311++G(2d,2p)

C	-1.87039300	0.33373000	-1.93119300	E=-418.5502735 ZPE= 0.148761
O	-1.83609200	0.75035000	-0.78580800	
N	-0.78902500	0.05314200	-2.69331100	
H	-2.82188200	0.13745000	-2.45988300	
H	-0.95351900	-0.24505400	-3.64187500	
C	0.58467000	0.24871300	-2.23524000	
H	1.25801700	-0.25548200	-2.92833600	
H	0.84069900	1.31187900	-2.20103100	
H	0.72338700	-0.17399100	-1.24044300	
O	1.83609200	-0.75035000	0.78580800	
C	1.87039300	-0.33373000	1.93119300	
N	0.78902500	-0.05314200	2.69331100	
H	2.82188200	-0.13745000	2.45988300	
H	0.95351900	0.24505400	3.64187500	
C	-0.58467000	-0.24871300	2.23524000	
H	-0.72338700	0.17399100	1.24044300	
H	-1.25801700	0.25548200	2.92833600	
H	-0.84069900	-1.31187900	2.20103100	

Trans-trans-B dimer NMF (**t-t-B**) ¹A UB3LYP/6-311++G(2d,2p)

C	2.55964600	-0.97738200	-0.30098500	E=-418.5515547 ZPE= 0.149124
O	1.63629000	-1.45115800	0.34171200	
N	2.90180400	0.32931800	-0.32256700	
H	3.21674100	-1.59923800	-0.93629100	
H	3.67413300	0.60045800	-0.91029200	
C	2.17712600	1.35618500	0.42458600	
H	2.16555400	1.10913900	1.48855100	
H	2.69128900	2.30758800	0.28937200	
H	1.14564500	1.44923900	0.07585200	
O	-1.20101900	1.14256300	-0.24914000	
C	-1.37647000	-0.02348600	0.07281100	
N	-2.58969500	-0.63057400	0.15454400	
H	-0.54206900	-0.69513000	0.32916900	
H	-2.59988700	-1.60199400	0.42494100	
C	-3.84790000	0.03645100	-0.14122000	
H	-3.62573400	1.07646400	-0.37465500	
H	-4.52157100	0.00103900	0.71925200	
H	-4.34545600	-0.42061500	-1.00146700	

Trans-trans-C dimer NMF (**t-t-C**) ¹A UB3LYP/6-311++G(2d,2p)

C	-2.55224500	-0.89265000	-0.16983300	E=-418.5552019 ZPE= 0.149252
O	-3.76437600	-1.03251500	-0.14806700	
H	-1.86586500	-1.75011100	-0.29936700	
N	-1.87880000	0.27453900	-0.04480700	
H	-0.86348400	0.24553200	-0.08364100	
C	1.94846200	-0.21234200	0.70219500	
O	1.11758700	0.16483800	-0.11077900	
H	1.67121800	-0.54548600	1.71677500	
N	3.27998900	-0.27576400	0.48068700	
H	3.86129500	-0.59846600	1.23926300	
C	-2.54549600	1.55505600	0.12132700	
H	-2.28590200	2.23871300	-0.69216300	
H	-2.26974000	2.02189400	1.07180500	
H	-3.62104200	1.38414700	0.11144500	
C	3.90947400	0.10661600	-0.77712000	
H	4.54925200	0.98276000	-0.64383500	
H	4.50747600	-0.71756300	-1.17229900	
H	3.12161000	0.34848900	-1.48779400	

Trans-trans-D dimer NMF (**t-t-D**) ¹A UB3LYP/6-311++G(2d,2p)

C	2.56862800	-0.86617000	-0.22160800	E=-418.5552148 ZPE= 0.149312
O	3.78292600	-0.98757200	-0.21794500	
H	1.89486800	-1.72480800	-0.40102500	
N	1.87785600	0.27879500	-0.01427900	
H	0.86307200	0.23766400	-0.05571600	
C	-1.94758100	-0.38085900	0.63362200	
O	-1.11760100	0.15084800	-0.08884100	
H	-1.66681700	-0.93229300	1.54700300	
N	-3.28264100	-0.36807600	0.42460500	
H	-3.86132900	-0.85256100	1.09385800	
C	2.52567800	1.55719200	0.22639500	
H	2.18531300	1.99430100	1.16946700	
H	2.31588100	2.26380200	-0.58240200	
H	3.60073100	1.39119800	0.27923700	
C	-3.91643800	0.28563800	-0.71355600	
H	-4.42511300	-0.44436100	-1.34812300	
H	-4.63865300	1.03249900	-0.37575500	
H	-3.13877800	0.77851200	-1.29365600	

Trans-trans-E dimer NMF (**t-t-E**) ¹A UB3LYP/6-311++G(2d,2p)

C	1.73468900	-0.13303300	0.00000000	E=-418.5512688 ZPE= 0.148930
O	1.47141000	1.06033200	0.00000000	
N	2.99126300	-0.65041200	0.00000000	
H	0.94918000	-0.90580000	0.00000000	
H	3.07575600	-1.65522300	0.00000000	
C	4.19811700	0.16194100	0.00000000	
H	4.80266400	-0.03214300	0.89027800	
H	4.80266500	-0.03214400	-0.89027700	
H	3.89441800	1.20748000	-0.00000100	
O	-1.47140300	-1.06032300	0.00000000	
C	-1.73469100	0.13304100	0.00000000	
N	-2.99126800	0.65041000	0.00000000	
H	-0.94918700	0.90581200	0.00000000	
H	-3.07576800	1.65522000	0.00000000	
C	-4.19811600	-0.16195200	0.00000000	
H	-3.89440900	-1.20748900	0.00000000	
H	-4.80266500	0.03212800	-0.89027700	
H	-4.80266400	0.03212800	0.89027800	

Trans-cis-A dimer NMF (**t-c-A**) ¹A UB3LYP/6-311++G(2d,2p)

C	2.11393200	-1.17166100	-0.23207800	E=-418.5561658 ZPE= 0.149644
O	0.93482500	-1.38684600	0.01363600	
N	2.74285900	0.01246800	-0.09999300	
H	2.78178700	-1.96860500	-0.60326500	
C	-2.01560700	1.04011900	-0.14241900	
N	-1.80007800	-0.27898600	0.03778500	
H	-0.83078300	-0.59781700	0.05676400	
O	-1.14723300	1.89089800	-0.27473400	
H	-3.09151700	1.30159200	-0.16003000	
C	-2.85527200	-1.26453000	0.18261400	
H	-2.78432600	-1.78166200	1.14387200	
H	-3.82591900	-0.76647300	0.13336700	
H	-2.81207400	-2.01078800	-0.61598900	
H	3.73192700	0.02811500	-0.29580600	
C	2.10528400	1.22831100	0.40464800	
H	1.08853500	1.31699800	0.02123600	
H	2.06895400	1.22876200	1.49824000	
H	2.68318300	2.08965000	0.06926500	

Trans-cis-B dimer NMF (**t-c-B**) ¹A UB3LYP/6-311++G(2d,2p)

C	-1.42237500	0.60526400	-0.05269400	E=-418.5501475 ZPE= 0.149058
O	-0.99648900	1.72643100	-0.28671800	
N	-2.73276400	0.25618000	-0.10935700	
H	-0.76029100	-0.23115900	0.22631500	
H	-3.37946200	0.99077600	-0.36399600	
C	-3.24048300	-1.07878500	0.15965700	
H	-2.40008200	-1.73032000	0.40329200	
H	-3.93263600	-1.07993300	1.00682400	
H	-3.75224300	-1.49381500	-0.71359100	
C	2.20745700	-1.17950500	-0.31743700	
N	2.82163300	0.02252100	-0.27034100	
O	1.18508700	-1.47017300	0.28341400	
H	2.73485800	-1.90117500	-0.96779700	
H	3.64884000	0.14669000	-0.83227500	
C	2.31164600	1.14979900	0.50908500	
H	2.20371700	0.86262500	1.55734100	
H	3.02804300	1.96819900	0.44006500	
H	1.34092100	1.48650100	0.13647700	

Trans-cis-C dimer NMF (**t-c-C**) ¹A UB3LYP/6-311++G(2d,2p)

C	2.04830700	-0.56507400	-0.74474000	E=-418.5533553 ZPE= 0.149387
O	3.05264700	-1.20821900	-0.49298200	
H	1.47349600	-0.70820500	-1.67898300	
N	1.48988300	0.37100400	0.06172000	
H	0.70387100	0.90926700	-0.29820000	
C	-2.09202700	0.80486900	-0.43762200	
O	-1.14484500	1.52255700	-0.72530700	
H	-3.13222700	1.09579000	-0.66549200	
N	-2.00066300	-0.39608200	0.17541600	
H	-1.06572500	-0.71164300	0.40503700	
C	2.13357300	0.79993200	1.29557900	
H	1.40044600	1.31079900	1.92089100	
H	2.96872600	1.48107500	1.10195200	
H	2.52402800	-0.06787200	1.82806200	
C	-3.13191100	-1.24893800	0.50530600	
H	-3.06403300	-2.21089800	-0.00912400	
H	-4.05236900	-0.75588400	0.18892000	
H	-3.19082600	-1.42632900	1.58214900	

Trans-cis-D dimer NMF (**t-c-D**) ¹A UB3LYP/6-311++G(2d,2p)

C	-2.58383200	-0.94292300	-0.13708200	E=-418.5535838 ZPE= 0.149103
O	-3.77092800	-1.15058000	0.05703000	
H	-1.88318000	-1.74978800	-0.42395100	
N	-1.96718000	0.25386900	-0.02647500	
H	-0.97645500	0.31353700	-0.24482300	
C	1.92468300	-0.02601700	0.05370500	
O	0.97467500	0.45205900	-0.54757200	
H	1.79923400	-0.66001700	0.94921300	
N	3.21844600	0.15372800	-0.28820200	
H	3.38268700	0.72594800	-1.10634100	
C	-2.69662300	1.46451500	0.31565000	
H	-1.98272700	2.23732900	0.60179500	
H	-3.37417100	1.27121200	1.14913500	
H	-3.29429200	1.82844800	-0.52644900	
C	4.35592600	-0.41579600	0.41730100	
H	5.01756200	0.36766200	0.79536500	
H	3.99219900	-0.99511900	1.26709300	
H	4.92937900	-1.08289700	-0.23140700	

Trans-cis-D1 dimer NMF (**t-c-D1**) ¹A UB3LYP/6-311++G(2d,2p)

C	2.55741300	-0.94419700	-0.13739600	E=-418.5535584 ZPE= 0.149126
O	3.73435100	-1.20963800	0.04617100	
H	1.81925300	-1.71911500	-0.41711000	
N	1.98595400	0.27761700	-0.03152800	
H	0.99054200	0.35570000	-0.22188600	
C	-1.92780200	-0.02229000	0.06840000	
O	-0.97115600	0.47439300	-0.50637900	
H	-1.81280000	-0.68226700	0.94642100	
N	-3.21762700	0.16565500	-0.28431200	
H	-3.37266700	0.76158400	-1.08716600	
C	2.73931600	1.47362800	0.30613700	
H	2.30327400	1.97372400	1.17547700	
H	2.75691400	2.17872000	-0.53060200	
H	3.76152400	1.17959500	0.54013300	
C	-4.36284800	-0.42562600	0.39000400	
H	-5.02918900	0.34549500	0.78486100	
H	-4.92852800	-1.07215200	-0.28579000	
H	-4.00866000	-1.03132000	1.22533500	

Trans-cis-E dimer NMF (**t-c-E**) ¹A UB3LYP/6-311++G(2d,2p)

C	1.65741700	0.18272300	0.00000000	E=-418.5498114 ZPE= 0.148963
O	1.20197800	-0.95154500	0.00000000	
N	2.98152400	0.48715200	0.00000000	
H	1.00915900	1.07380600	0.00000000	
C	-1.80323600	0.48091400	0.00000000	
N	-3.12595400	0.17615600	0.00000000	
H	-3.76308300	0.96156100	0.00000000	
O	-1.35727100	1.61824800	0.00000000	
H	-1.14769300	-0.40636600	0.00000000	
C	-3.66176200	-1.17442300	0.00000000	
H	-4.27011100	-1.36268600	-0.88941800	
H	-2.83083100	-1.88141400	0.00000000	
H	-4.27011100	-1.36268600	0.88941800	
H	3.22928600	1.46462100	0.00000000	
C	4.03952500	-0.51139900	0.00000000	
H	3.56964300	-1.49353800	0.00000000	
H	4.66771400	-0.41848600	-0.89022600	
H	4.66771300	-0.41848700	0.89022700	

Cis-trans-B dimer NMF (**c t-B**) ¹A UB3LYP/6-311++G(2d,2p)

C	2.29964900	0.93718300	-0.00000600	E=-418.5573042 ZPE= 0.149798
O	1.46770300	1.83499100	-0.00002100	
N	2.02789600	-0.38348600	0.00000900	
H	3.38510700	1.15452300	-0.00000500	
O	-0.87031700	-0.83193900	0.00000700	
C	-1.38666200	0.28229300	-0.00000800	
N	-2.71988600	0.50716700	-0.00001300	
H	-0.77660200	1.19827800	-0.00001900	
H	-3.02252200	1.46922100	-0.00002400	
C	-3.72213500	-0.54876100	-0.00000100	
H	-3.20111800	-1.50441600	0.00000500	
H	-4.35358100	-0.48745100	-0.89025400	
H	-4.35357400	-0.48743700	0.89025600	
H	1.03897100	-0.65426200	0.00000900	
C	3.04183600	-1.42154200	0.00002700	
H	2.95965800	-2.05571000	0.88770100	
H	2.95966600	-2.05573200	-0.88763200	
H	4.03269500	-0.96222900	0.00002500	

Cis-cis-A dimer NMF (**c c-A**) ¹A UB3LYP/6-311++G(2d,2p)

C	-1.02854300	1.75664100	0.00000000	E=-418.5637328 ZPE= 0.150281
O	-1.66655700	0.70412500	0.00000000	
N	0.30841200	1.85720700	0.00000000	
H	-1.54680100	2.73218100	0.00000000	
H	0.84470700	0.97971700	0.00000000	
C	1.02854300	3.11822900	0.00000000	
H	0.31642100	3.94604900	0.00000000	
H	1.66083000	3.20811700	0.88751000	
H	1.66083000	3.20811700	-0.88751000	
C	1.02854300	-1.75664100	0.00000000	
N	-0.30841200	-1.85720700	0.00000000	
H	-0.84470700	-0.97971700	0.00000000	
O	1.66655700	-0.70412500	0.00000000	
H	1.54680100	-2.73218100	0.00000000	
C	-1.02854300	-3.11822900	0.00000000	
H	-1.66083000	-3.20811700	-0.88751000	
H	-0.31642100	-3.94604900	0.00000000	
H	-1.66083000	-3.20811700	0.88751000	

Cis-cis-B dimer NMF (**c c-B**) ¹A UB3LYP/6-311++G(2d,2p)

C	-1.37931900	-0.40566100	0.00000600	E=-418.5559423 ZPE= 0.149756
O	-0.60169200	-1.35584000	0.00000800	
N	-2.72372600	-0.53175100	0.00000900	
H	-1.01742400	0.63486700	0.00000100	
H	-3.08347400	-1.47722200	0.00001300	
C	-3.65703400	0.58351500	0.00000700	
H	-3.09086700	1.51566900	0.00000200	
H	-4.29270600	0.56796600	-0.88955600	
H	-4.29270300	0.56797300	0.88957200	
C	2.02281800	1.14597500	-0.00001100	
N	2.08839700	-0.20039500	-0.00000400	
H	1.19786800	-0.70912700	0.00000100	
O	0.99316800	1.80850400	-0.00001100	
H	3.01968200	1.62722700	-0.00001600	
C	3.32840600	-0.95418900	-0.00000400	
H	3.40575900	-1.58898300	-0.88761600	
H	4.17436800	-0.26351600	-0.00001000	
H	3.40576400	-1.58897500	0.88761300	

Cis-cis-E dimer NMF (**c c-E**) ¹A UB3LYP/6-311++G(2d,2p)

C	1.20806300	-1.24480100	0.00000000	E=-418.54 83593 ZPE= 0.148940
O	1.80778100	-0.18025000	0.00000000	
H	0.10618500	-1.29778100	0.00000000	
N	1.80778100	-2.46221100	0.00000000	
H	2.81911200	-2.45960100	0.00000000	
C	-1.20806300	1.24480100	0.00000000	
O	-1.80778100	0.18025000	0.00000000	
H	-0.10618500	1.29778100	0.00000000	
N	-1.80778100	2.46221100	0.00000000	
H	-2.81911200	2.45960100	0.00000000	
C	-1.09975500	3.73112300	0.00000000	
H	-0.02666900	3.53423700	0.00000000	
H	-1.33846000	4.32144000	-0.88943700	
H	-1.33846000	4.32144000	0.88943700	
C	1.09975500	-3.73112300	0.00000000	
H	0.02666900	-3.53423700	0.00000000	
H	1.33846000	-4.32144000	-0.88943700	
H	1.33846000	-4.32144000	0.88943700	

Chapter 13. References

- [1] G. A. Jeffrey, *An Introduction to Hydrogen Bonding*, New York, **1997**.
- [2] G. R. Desiraju, *Accounts of Chemical Research* **2002**, 35, 565.
- [3] A. C. Legon, D. J. Millen, *Chemical Society Reviews* **1987**, 16, 467.
- [4] A. E. Reed, L. A. Curtiss, F. Weinhold, *Chemical Reviews (Washington, DC, United States)* **1988**, 88, 899.
- [5] L. Pauling, *The Nature of the Chemical Bond.*, Cornell University Press, Ithaca, NY, **1939**.
- [6] M. Nishio, M. Hirota, Y. Umezawa, *CH/p Interaction: Evidence, Nature, and Consequences*, **1998**.
- [7] Z. Ciunik, S. Jarosz, *Journal of Molecular Structure* **1998**, 442, 115.
- [8] S. Sarkhel, G. R. Desiraju, *Proteins: Structure, Function, and Bioinformatics* **2003**, 54, 247.
- [9] A. Werner, *Liebigs Annalen der Chemie* **1902**, 261.
- [10] A. Hantzsch, *Ber.* **1911**, 43, 3049.
- [11] W. M. Latimer, W. H. Rodebush, *Journal of the American Chemical Society* **1920**, 42, 1419.
- [12] G. C. Pimentel, A. L. McClellan, *The Hydrogen Bond*, Freeman, San Francisco, **1960**.
- [13] F. Fillaux, N. Leygue, J. Tomkinson, A. Cousson, W. Paulus, *Chemical Physics* **1999**, 244, 387.
- [14] Y. Maréchal, **2007**.
- [15] C. E. S. Bernardes, M. E. Minas da Piedade, *Journal of Physical Chemistry A* **2008**, 112, 10029.
- [16] T. Steiner, *Angewandte Chemie, International Edition* **2002**, 41, 48.
- [17] A. Engdahl, B. Nelander, *Journal of Physical Chemistry* **1985**, 89, 2860.
- [18] S. Suzuki, P. G. Green, R. E. Bumgarner, S. Dasgupta, W. A. Goddard, III, G. A. Blake, *Science (Washington, DC, United States)* **1992**, 257, 942.
- [19] J. F. Malone, C. M. Murray, M. H. Charlton, R. Docherty, A. J. Lavery, *Journal of the Chemical Society, Faraday Transactions* **1997**, 93, 3429.
- [20] T. Steiner, G. Koellner, *Journal of Molecular Biology* **2001**, 305, 535.
- [21] G. R. Desiraju, *Accounts of Chemical Research* **1991**, 24, 290.
- [22] G. R. Desiraju, T. Steiner, *The Weak Hydrogen Bond in Structural Chemistry and Biology*, Oxford University Press, **1999**.
- [23] G. R. Desiraju, *Chemical Communications (Cambridge, United Kingdom)* **2005**, 2995.
- [24] M. Budesinsky, P. Fiedler, Z. Arnold, *Synthesis* **1989**, 858.
- [25] I. E. Boldeskul, I. F. Tsymbal, E. V. Ryltsev, Z. Latajka, A. J. Barnes, *Journal of Molecular Structure* **1997**, 436-437, 167.
- [26] P. Hobza, V. Spirko, H. L. Selzle, E. W. Schlag, *Journal of Physical Chemistry A* **1998**, 102, 2501.
- [27] P. Hobza, V. Spirko, Z. Havlas, K. Buchhold, B. Reimann, H.-D. Barth, B. Brutschy, *Chemical Physics Letters* **1999**, 299, 180.
- [28] P. Hobza, Z. Havlas, *Chemical Physics Letters* **1999**, 303, 447.
- [29] M. Pitonak, P. Neogady, J. Rezac, P. Jurecka, M. Urban, P. Hobza, *Journal of Chemical Theory and Computation* **2008**, 4, 1829.
- [30] P. Hobza, *Physical Chemistry Chemical Physics* **2001**, 3, 2555.
- [31] P. Hobza, Z. Havlas, *Chemical Reviews (Washington, D. C.)* **2000**, 100, 4253.

- [32] M. Ortlieb, M. Havenith, *Journal of Physical Chemistry A* **2007**, *111*, 7355.
- [33] S. T. Shipman, P. C. Douglass, H. S. Yoo, C. E. Hinkle, E. L. Mierzejewski, B. H. Pate, *Physical Chemistry Chemical Physics* **2007**, *9*, 4572.
- [34] Z. Smedarchina, A. Fernandez-Ramos, W. Siebrand, *Journal of Chemical Physics* **2005**, *122*, 134309/1.
- [35] M. Gantenberg, M. Halupka, W. Sander, *Chemistry--A European Journal* **2000**, *6*, 1865.
- [36] J. Bournay, Y. Marechal, *Journal of Chemical Physics* **1973**, *59*, 5077.
- [37] H. Ratajczak, W. J. Orville-Thomas, C. N. R. Rao, *Chemical Physics* **1976**, *17*, 197.
- [38] P. Gilli, V. Bertolasi, V. Ferretti, G. Gilli, *Journal of the American Chemical Society* **1994**, *116*, 909.
- [39] D. Hadzi, *Chimia* **1972**, *26*, 7.
- [40] S.-Y. Yen, C.-H. Mou, W.-P. Hu, *Chemical Physics Letters* **2004**, *383*, 606.
- [41] L. Pauling, R. B. Corey, H. R. Branson, *Proceedings of the National Academy of Sciences of the United States of America* **1951**, *37*, 205.
- [42] J. D. Watson, F. H. C. Crick, *Nature (London, United Kingdom)* **1953**, *171*, 737.
- [43] G. E. Schulz, R. H. Schirmer, *Principles of Protein Structure*, **1979**.
- [44] J. Sponer, J. Leszczynski, P. Hobza, *Journal of Biomolecular Structure & Dynamics* **1996**, *14*, 117.
- [45] J. Sponer, J. Leszczynski, P. Hobza, *Journal of Computational Chemistry* **1996**, *17*, 841.
- [46] J. Sponer, J. Leszczynski, P. Hobza, *Journal of Physical Chemistry* **1996**, *100*, 5590.
- [47] J. Sponer, J. Leszczynski, P. Hobza, *Journal of Physical Chemistry* **1996**, *100*, 1965.
- [48] J. Sponer, J. Leszczynski, V. Vetterl, P. Hobza, *Journal of Biomolecular Structure & Dynamics* **1996**, *13*, 695.
- [49] J. Sponer, J. Leszczynski, P. Hobza, *Biopolymers* **2001**, *61*, 3.
- [50] J. Sponer, J. Leszczynski, P. Hobza, in *Biopolymers*, Vol. 61, **2001**, pp. 3.
- [51] A. C. Legon, D. J. Millen, *Chemical Reviews (Washington, DC, United States)* **1986**, *86*, 635.
- [52] A. C. Legon, D. J. Millen, *Accounts of Chemical Research* **1987**, *20*, 39.
- [53] A. C. Legon, D. J. Millen, *Molecular Spectroscopy (Chemical Society, London)* **1973**, *1*, 1.
- [54] S. G. Batten, A. G. Ward, A. C. Legon, *Journal of Molecular Structure* **2006**, *780-781*, 300.
- [55] A. M. Andrews, K. W. Hillig, II, R. L. Kuczkowski, A. C. Legon, N. W. Howard, *Journal of Chemical Physics* **1991**, *94*, 6947.
- [56] A. C. Legon, L. C. Willoughby, *Chemical Physics Letters* **1983**, *95*, 449.
- [57] A. Di Michele, M. Freda, G. Onori, A. Santucci, *J. Phys. Chem. A FIELD Full Journal Title:Journal of Physical Chemistry A* **2004**, *108*, 6145.
- [58] P. R. G. a. J. A. d. Haseth, **2007**.
- [59] A. Engdahl, B. Nelander, P. O. Aastrand, *Journal of Chemical Physics* **1993**, *99*, 4894.
- [60] E. Liepins, M. V. Petrova, E. Gudriniece, J. Paulins, S. L. Kuznetsov, *Magn. Reson. Chem. FIELD Full Journal Title:Magnetic Resonance in Chemistry* **1989**, *27*, 907.

- [61] H. Benedict, I. G. Shenderovich, O. L. Malkina, V. G. Malkin, G. S. Denisov, N. S. Golubev, H.-H. Limbach, *J. Am. Chem. Soc. FIELD Full Journal Title:Journal of the American Chemical Society* **2000**, 122, 1979.
- [62] S. N. Smirnov, H. Benedict, N. S. Golubev, G. S. Denisov, M. M. Kreevoy, R. L. Schowen, H.-H. Limbach, *Can. J. Chem. FIELD Full Journal Title:Canadian Journal of Chemistry* **1999**, 77, 943.
- [63] H. Benedict, H.-H. Limbach, M. Wehlan, W.-P. Fehlhammer, N. S. Golubev, R. Janoschek, *J. Am. Chem. Soc. FIELD Full Journal Title:Journal of the American Chemical Society* **1998**, 120, 2939.
- [64] H. Benedict, C. Hoelger, F. Aguilar-Parrilla, W.-P. Fehlhammer, M. Wehlan, R. Janoschek, H. H. Limbach, *J. Mol. Struct. FIELD Full Journal Title:Journal of Molecular Structure* **1996**, 378, 11.
- [65] A. R. Ubbelohde, K. J. Gallagher, *Acta Crystallogr. FIELD Full Journal Title:Acta Crystallographica* **1955**, 8, 71.
- [66] D. Mootz, M. Schilling, *J. Am. Chem. Soc. FIELD Full Journal Title:Journal of the American Chemical Society* **1992**, 114, 7435.
- [67] D. L. Wyatt, C. M. G. de Godoy, S. Cukierman, *J. Phys. Chem. B* **2009**, 113, 6725.
- [68] Y. C. Kim, M. Wikstrom, G. Hummer, *Proc. Natl. Acad. Sci. U. S. A.* **2009**, 106, 13707.
- [69] T. Langenbacher, D. Immeln, B. Dick, T. Kottke, *J. Am. Chem. Soc.* **2009**, 131, 14274.
- [70] J. P. Ceron-Carrasco, A. Requena, E. A. Perpete, C. Michaux, D. Jacquemin, *Chem. Phys. Lett.* **2009**, 484, 64.
- [71] S. Kim, T. Karl, D. Helmig, R. Daly, R. Rasmussen, A. Guenther, *Atmos. Meas. Tech.* **2009**, 2, 99.
- [72] J. M. Anglada, S. Olivella, A. Sole, *J. Phys. Chem. A* **2006**, 110, 1982.
- [73] A. Gutberlet, G. Schwaab, O. Birer, M. Masia, A. Kaczmarek, H. Forbert, M. Havenith, D. Marx, *Science (Washington, DC, U. S.)* **2009**, 324, 1545.
- [74] M. Rini, D. Pines, B.-Z. Magnes, E. Pines, E. T. J. Nibbering, *J. Chem. Phys.* **2004**, 121, 9593.
- [75] B. S. Ault, G. C. Pimentel, *J. Phys. Chem.* **1973**, 77, 57.
- [76] J. D. C. D. Coyle, **1989**.
- [77] M. Rini, A. Kummrow, J. Dreyer, E. T. J. Nibbering, T. Elsaesser, *Faraday Discuss.* **2002**, 122, 27.
- [78] I. Dunkin, *Matrix Isolation Techniques: A Practical Approach*, **1998**.
- [79] E. Whittle, D. A. Dows, G. C. Pimentel, *J. Chem. Phys.* **1954**, 22, 1943.
- [80] W. Sander, H. Wandel, G. Bucher, J. Graefenstein, E. Kraka, D. Cremer, *Journal of the American Chemical Society* **1998**, 120, 8480.
- [81] M. Winkler, W. Sander, *Angewandte Chemie, International Edition* **2000**, 39, 2014.
- [82] A. Mardyukov, W. Sander, *Chem.--Eur. J. FIELD Full Journal Title:Chemistry--A European Journal* **2009**, 15, 1462.
- [83] A. Mardyukov, E. Sanchez-Garcia, P. Rodziewicz, N. L. Doltsinis, W. Sander, *J. Phys. Chem. A* **2007**, 111, 10552.
- [84] G. P. Ayers, A. D. E. Pullin, *Spectrochimica Acta, Part A: Molecular and Biomolecular Spectroscopy* **1976**, 32A, 1641.
- [85] F. Jensen, *Introduction to Computational Chemistry*, John Wiley and Sons, **1999**.
- [86] J. B. Foresman, A. Frisch, *Exploring Chemistry with Electronic Structure Methods*, Second ed., Gaussian, Inc., Pittsburgh, **1996**.
- [87] S. Scheiner, *Hydrogen Bonding: A Theoretical Perspective*, Oxford University Press, New York, **1997**.

- [88] M. C. H. Wolfram Koch, *Wiley-VCH Verlag GmbH* **2001**
- [89] R. Vargas, J. Garza, R. A. Friesner, H. Stern, B. P. Hay, D. A. Dixon, *Journal of Physical Chemistry A* **2001**, *105*, 4963.
- [90] E. M. Cabaleiro-Lago, M. A. Rios, *Journal of Chemical Physics* **1999**, *110*, 6782.
- [91] P. Hobza, Z. Havlas, *Theoretical Chemistry Accounts* **1998**, *99*, 372.
- [92] M. Rasanen, *Journal of Molecular Structure* **1983**, *101*, 275.
- [93] M. Rasanen, *Journal of Molecular Structure* **1983**, *102*, 235.
- [94] A. C. Gomez Marigliano, E. L. Varetti, *Journal of Physical Chemistry A* **2002**, *106*, 1100.
- [95] G. V. Papamokos, I. N. Demetropoulos, *Journal of Physical Chemistry A* **2004**, *108*, 7291.
- [96] S. J. Grabowski, W. A. Sokalski, J. Leszczynski, *J. Phys. Chem. A FIELD Full Journal Title:Journal of Physical Chemistry A* **2006**, *110*, 4772.
- [97] J. Lundell, M. Krajewska, M. Raesaenen, *Journal of Physical Chemistry A* **1998**, *102*, 6643.
- [98] M. Albrecht, C. A. Rice, M. A. Suhm, *J. Phys. Chem. A FIELD Full Journal Title:Journal of Physical Chemistry A* **2008**, *112*, 7530.
- [99] J. A. Frey, S. Leutwyler, *Journal of Physical Chemistry A* **2006**, *110*, 12512.
- [100] A. Bende, A. Vibok, G. J. Halasz, S. Suhai, *International Journal of Quantum Chemistry* **2001**, *84*, 617.
- [101] S. J. Grabowski, W. A. Sokalski, J. Leszczynski, *Journal of Physical Chemistry A* **2006**, *110*, 4772.
- [102] E. Tsuchida, *Journal of Chemical Physics* **2004**, *121*, 4740.
- [103] E. S. Garcia, **2006**.
- [104] M. Halupka, W. Sander, *Spectrochimica Acta, Part A: Molecular and Biomolecular Spectroscopy* **1998**, *54A*, 495.
- [105] M. Gantenberg, M. Halupka, W. Sander, *Chemistry-a European Journal* **2000**, *6*, 1865.
- [106] A. Mardyukov, E. Sanchez-Garcia, W. Sander, *J. Phys. Chem. A* **2009**, *113*, 1086.
- [107] R. B. Homer, C. D. Johnson, *Chem. Amides* **1970**, 187.
- [108] H. Sigel, R. B. Martin, *Chemical Reviews (Washington, DC, United States)* **1982**, *82*, 385.
- [109] R. B. Bohn, L. Andrews, *Journal of Physical Chemistry* **1989**, *93*, 5684.
- [110] P. W. Schultz, G. E. Leroi, A. I. Popov, *Journal of the American Chemical Society* **1995**, *117*, 10735.
- [111] G. Maier, J. Endres, *European Journal of Organic Chemistry* **2000**, 1061.
- [112] K. Sundararajan, V. Vidya, K. Sankaran, K. S. Viswanathan, *Spectrochimica Acta, Part A: Molecular and Biomolecular Spectroscopy* **2000**, *56A*, 1855.
- [113] M. Hartmann, S. D. Wetmore, L. Radom, *Journal of Physical Chemistry A* **2001**, *105*, 4470.
- [114] S. Tsuzuki, K. Honda, T. Uchimaru, M. Mikami, K. Tanabe, *Journal of the American Chemical Society* **2000**, *122*, 3746.
- [115] M. L. H. Jeng, A. M. DeLaat, B. S. Ault, *Journal of Physical Chemistry* **1989**, *93*, 3997.
- [116] A. M. DeLaat, B. S. Ault, *Journal of the American Chemical Society* **1987**, *109*, 4232.
- [117] M. L. H. Jeng, B. S. Ault, *Journal of Physical Chemistry* **1990**, *94*, 4851.
- [118] S.-T. King, *Journal of Physical Chemistry* **1971**, *75*, 405.
- [119] E. S. Kline, Z. H. Kafafi, R. H. Hauge, J. L. Margrave, *Journal of the American Chemical Society* **1985**, *107*, 7559.

- [120] S. A. McDonald, G. L. Johnson, B. W. Keelan, L. Andrews, *Journal of the American Chemical Society* **1980**, *102*, 2892.
- [121] K. V. Jovan Jose, R. Gadre Shridhar, K. Sundararajan, K. S. Viswanathan, *J Chem Phys FIELD Full Journal Title: The Journal of chemical physics FIELD Publication Date: 2007*, *127*, 104501. FIELD Reference Number: FIELD Journal Code: 0375360 FIELD Call Number:.
- [122] E. D. Jemmis, K. T. Giju, K. Sundararajan, K. Sankaran, V. Vidya, K. S. Viswanathan, J. Leszczynski, *Journal of Molecular Structure* **1999**, *510*, 59.
- [123] K. Sundararajan, K. Sankaran, K. S. Viswanathan, A. D. Kulkarni, S. R. Gadre, in *Journal of Physical Chemistry A*, Vol. *106*, **2002**, pp. 1504.
- [124] A. Mardyukov, E. Sanchez-Garcia, P. Rodziewicz, N. L. Doltsinis, W. Sander, *Journal of Physical Chemistry A* **2007**, *111*, 10552.
- [125] A. Engdahl, B. Nelander, *Chemical Physics Letters* **1983**, *100*, 129.
- [126] K. Sundararajan, K. S. Viswanathan, *Journal of Molecular Structure* **2006**, *798*, 109.
- [127] A. Karpfen, *Journal of Physical Chemistry A* **1999**, *103*, 11431.
- [128] I. L. Alberts, T. W. Rowlands, N. C. Handy, *Journal of Chemical Physics* **1988**, *88*, 3811.
- [129] T. Aoyama, O. Matsuoka, N. Nakagawa, *Chemical Physics Letters* **1979**, *67*, 508.
- [130] R. G. A. Bone, N. C. Handy, *Theoretica Chimica Acta* **1990**, *78*, 133.
- [131] J. S. Craw, W. B. De Almeida, A. Hinchliffe, *Theochem* **1989**, *60*, 69.
- [132] D. G. Prichard, R. N. Nandi, J. S. Muentner, *Journal of Chemical Physics* **1988**, *89*, 115.
- [133] K. Shuler, C. E. Dykstra, *Journal of Physical Chemistry A* **2000**, *104*, 11522.
- [134] K. Shuler, C. E. Dykstra, *Journal of Physical Chemistry A* **2000**, *104*, 4562.
- [135] E. Sanchez-Garcia, L. George, L. A. Montero, W. Sander, *Journal of Physical Chemistry A* **2004**, *108*, 11846.
- [136] K. V. Jovan Jose, S. R. Gadre, K. Sundararajan, K. S. Viswanathan, *Journal of Chemical Physics* **2007**, *127*, 104501/1.
- [137] K. Sundararajan, N. Ramanathan, *Journal of Molecular Structure* **2007**, *833*, 150.
- [138] N. R. Brinkmann, G. S. Tschumper, G. Yan, H. F. Schaefer, *Journal of Physical Chemistry A* **2003**, *107*, 10208.
- [139] H. Ushiyama, K. Takatsuka, in *Journal of Chemical Physics*, Vol. *115*, **2001**, pp. 5903.
- [140] F. Madeja, M. Havenith, *Journal of Chemical Physics* **2002**, *117*, 7162.
- [141] L. George, E. Sanchez-Garcia, W. Sander, *Journal of Physical Chemistry A* **2003**, *107*, 6850.
- [142] L. George, E. Sanchez-Garcia, W. Sander, *J. Phys. Chem. A FIELD Full Journal Title: Journal of Physical Chemistry A* **2003**, *107*, 6850.
- [143] E. Sanchez-Garcia, M. Studentkowski, L. A. Montero, W. Sander, *ChemPhysChem* **2005**, *6*, 618.
- [144] J. Lundell, M. Rasanen, *J. Phys. Chem.* **1995**, *99*, 14301.
- [145] M. Pettersson, J. Lundell, L. Khriachtchev, M. Raesaenen, *J. Am. Chem. Soc.* **1997**, *119*, 11715.
- [146] E. Sanchez-Garcia, L. A. Montero, W. Sander, *Journal of Physical Chemistry A* **2006**, *110*, 12613.
- [147] E. Sanchez-Garcia, A. Mardyukov, M. Studentkowski, L. A. Montero, W. Sander, *J. Phys. Chem. A* **2006**, *110*, 13775.
- [148] K. Pei, H. Li, in *Journal of Molecular Structure*, Vol. *693*, **2004**, pp. 141.
- [149] A. C. Legon, P. Ottaviani, *Physical Chemistry Chemical Physics* **2004**, *6*, 488.

- [150] D.-M. Huang, Y.-B. Wang, L. M. Visco, F.-M. Tao, in *Journal of Physical Chemistry A*, Vol. 108, **2004**, pp. 11375.
- [151] E. V. Gromov, A. B. Trofimov, N. M. Vitkovskaya, H. Koppel, J. Schirmer, H. D. Meyer, L. S. Cederbaum, *Journal of Chemical Physics* **2004**, 121, 4585.
- [152] G. C. Cole, A. C. Legon, P. Ottaviani, *Journal of Chemical Physics* **2002**, 117, 2790.
- [153] B. S. Ault, in *Journal of Molecular Structure*, Vol. 127, **1985**, pp. 343.
- [154] S. A. Cooke, G. K. Corlett, J. H. Holloway, A. C. Legon, *Journal of the Chemical Society, Faraday Transactions* **1998**, 94, 2675.
- [155] I. D. Reva, A. M. Plokhotnichenko, E. D. Radchenko, G. G. Sheina, Y. P. Blagoi, *Spectrochimica Acta, Part A: Molecular and Biomolecular Spectroscopy* **1994**, 50A, 1107.
- [156] L. George, W. Sander, *Spectrochimica Acta* 2004, in press.
- [157] L. George, W. Sander, *Spectrochimica Acta* 2004, in press.
- [158] L. George, W. Sander, *Spectrochimica Acta* 2004, in press.
- [159] E. Sanchez-Garcia, A. Mardyukov, A. Tekin, R. Crespo-Otero, L. A. Montero, W. Sander, G. Jansen, *Chem. Phys.* **2008**, 343, 168.
- [160] R. E. Miller, P. F. Vohralik, R. O. Watts, *Journal of Chemical Physics* **1984**, 80, 5453.
- [161] G. T. Fraser, R. D. Suenram, F. J. Lovas, A. S. Pine, J. T. Hougen, W. J. Lafferty, J. S. Muenter, *Journal of Chemical Physics* **1988**, 89, 6028.
- [162] Y. Ohshima, Y. Matsumoto, M. Takami, K. Kuchitsu, *Chemical Physics Letters* **1988**, 147, 1.
- [163] K. Matsumura, F. J. Lovas, R. D. Suenram, *Journal of Molecular Spectroscopy* **1991**, 150, 576.
- [164] I. L. Alberts, T. W. Rowlands, N. C. Handy, in *Journal of Chemical Physics*, Vol. 88, **1988**, pp. 3811.
- [165] D. Prichard, J. S. Muenter, B. J. Howard, *Chem. Phys. Lett.* **1987**, 135, 9.
- [166] R. G. A. Bone, C. W. Murray, R. D. Amos, N. C. Handy, *Chem. Phys. Lett.* **1989**, 161, 166.
- [167] A. Metzethin, O. Birer, E. Sanchez-Garcia, M. Havenith, *J. Chem. Phys. FIELD Full Journal Title:Journal of Chemical Physics* **2008**, 129, 114307/1.
- [168] T. Steiner, E. B. Starikov, A. M. Amado, J. J. C. Teixeira-Dias, *Journal of the Chemical Society, Perkin Transactions 2: Physical Organic Chemistry* **1995**, 1321.
- [169] K. Sundararajan, K. S. Viswanathan, A. D. Kulkarni, S. R. Gadre, in *Journal of Molecular Structure*, Vol. 613, **2002**, pp. 209.
- [170] R. D. Pendley, G. E. Ewing, *Journal of Chemical Physics* **1983**, 78, 3531.
- [171] M. Tasumi, M. Nakata, *Journal of Molecular Structure* **1985**, 126, 111.
- [172] S. Ataka, H. Takeuchi, I. Harada, M. Tasumi, *Journal of Physical Chemistry* **1984**, 88, 449.
- [173] S. Shin, A. Kurawaki, Y. Hamada, K. Shinya, K. Ohno, A. Tohara, M. Sato, *Journal of Molecular Structure* **2006**, 791, 30.
- [174] A. D. Headley, J. Nam, *Theochem* **2002**, 589-590, 423.
- [175] S. Ataka, H. Takeuchi, M. Tasumi, *Journal of Molecular Structure* **1984**, 113, 147.
- [176] I. Harada, M. Tasumi, *Chemical Physics Letters* **1980**, 70, 279.
- [177] N. A. Besley, M. T. Oakley, A. J. Cowan, J. D. Hirst, *J. Am. Chem. Soc. FIELD Full Journal Title:Journal of the American Chemical Society* **2004**, 126, 13502.
- [178] N. A. Besley, J. D. Hirst, *Trends Phys. Chem. FIELD Full Journal Title:Trends in Physical Chemistry* **1999**, 7, 139.

- [179] J. D. Hirst, D. M. Hirst, C. L. Brooks, III, *J. Phys. Chem. FIELD Full Journal Title:Journal of Physical Chemistry* **1996**, 100, 13487.
- [180] H. Basch, M. B. Robin, N. A. Kuebler, *J. Chem. Phys. FIELD Full Journal Title:Journal of Chemical Physics* **1967**, 47, 1201.
- [181] J. M. Gingell, N. J. Mason, H. Zhao, I. C. Walker, M. R. F. Siggel, *Chem. Phys. FIELD Full Journal Title:Chemical Physics* **1997**, 220, 191.
- [182] E. B. Nielsen, J. A. Schellman, *J. Phys. Chem. FIELD Full Journal Title:Journal of Physical Chemistry* **1967**, 71, 2297.
- [183] N. L. Doltsinis, M. Sprik, *Chem. Phys. Lett. FIELD Full Journal Title:Chemical Physics Letters* **2000**, 330, 563.
- [184] V. Pajcini, S. A. Asher, *J. Am. Chem. Soc. FIELD Full Journal Title:Journal of the American Chemical Society* **1999**, 121, 10942.
- [185] P. R. Taylor, *J. Am. Chem. Soc. FIELD Full Journal Title:Journal of the American Chemical Society* **1982**, 104, 5248.
- [186] R. L. Jones, *Journal of Molecular Spectroscopy* **1958**, 2, 581.
- [187] H. E. Hallam, C. M. Jones, *Transactions of the Faraday Society* **1969**, 65, 2607.
- [188] T. Miyazawa, *Journal of Molecular Spectroscopy* **1960**, 4, 155.
- [189] I. Suzuki, *Bulletin of the Chemical Society of Japan* **1962**, 35, 540.
- [190] M. Kitano, K. Kuchitsu, *Bulletin of the Chemical Society of Japan* **1974**, 47, 631.
- [191] J. D. Baldeschwieler, G. C. Pimentel, *Journal of Chemical Physics* **1960**, 33, 1008.
- [192] R. T. Hall, G. C. Pimentel, *Journal of Chemical Physics* **1963**, 38, 1889.
- [193] S. Coussan, C. Manca, Y. Ferro, P. Roubin, *Chemical Physics Letters* **2003**, 370, 118.
- [194] A. Trivella, P. Roubin, P. Theule, M. Rajzmann, S. Coussan, C. Manca, *Journal of Physical Chemistry A* **2007**, 111, 3074.
- [195] A. Aspiala, T. Lotta, J. Murto, M. Rasanen, *Journal of Chemical Physics* **1983**, 79, 4183.
- [196] K. Marushkevich, L. Khriachtchev, J. Lundell, M. Raesaenen, *Journal of the American Chemical Society* **2006**, 128, 12060.
- [197] K. Marushkevich, L. Khriachtchev, M. Raesaenen, *Journal of Physical Chemistry A* **2007**, 111, 2040.
- [198] C. N. R. Rao, K. G. Rao, A. Goel, D. Balasubramanian, *Journal of the Chemical Society [Section] A: Inorganic, Physical, Theoretical* **1971**, 3077.
- [199] D. P. Chong, P. Aplincourt, C. Bureau, *Journal of Physical Chemistry A* **2002**, 106, 356.
- [200] C. H. Langley, N. L. Allinger, *Journal of Physical Chemistry A* **2002**, 106, 5638.
- [201] A. C. Fantoni, W. Caminati, *Journal of the Chemical Society, Faraday Transactions* **1996**, 92, 343.
- [202] Y. Li, R. L. Garrell, K. N. Houk, *J. Am. Chem. Soc. FIELD Full Journal Title:Journal of the American Chemical Society* **1991**, 113, 5895.
- [203] I. Azumaya, H. Kagechika, Y. Fujiwara, M. Itoh, K. Yamaguchi, K. Shudo, *J. Am. Chem. Soc. FIELD Full Journal Title:Journal of the American Chemical Society* **1991**, 113, 2833.
- [204] F. Duvernay, A. Trivella, F. Borget, S. Coussan, J.-P. Aycard, T. Chiavassa, *Journal of Physical Chemistry A* **2005**, 109, 11155.
- [205] F. Duvernay, T. Chiavassa, F. Borget, J.-P. Aycard, *Journal of Physical Chemistry A* **2005**, 109, 6008.
- [206] X. C. Wang, J. Nichols, M. Feyereisen, M. Gutowski, J. Boatz, A. D. J. Haymet, J. Simons, *Journal of Physical Chemistry* **1991**, 95, 10419.

- [207] M. W. Wong, K. B. Wiberg, M. J. Frisch, *Journal of the American Chemical Society* **1992**, *114*, 1645.
- [208] H. Basch, M. B. Robin, N. A. Kuebler, *Journal of Chemical Physics* **1968**, *49*, 5007.
- [209] J. M. Gingell, N. J. Mason, H. Zhao, I. C. Walker, M. R. F. Siggel, *Chemical Physics* **1997**, *220*, 191.
- [210] N. A. Besley, M. T. Oakley, A. J. Cowan, J. D. Hirst, *Journal of the American Chemical Society* **2004**, *126*, 13502.
- [211] L. Serrano-Andres, M. P. Fuelscher, *Journal of the American Chemical Society* **1996**, *118*, 12190.
- [212] N. L. Doltsinis, M. Sprik, *Chemical Physics Letters* **2000**, *330*, 563.
- [213] J. D. Hirst, D. M. Hirst, C. L. Brooks, III, *Journal of Physical Chemistry A* **1997**, *101*, 4821.
- [214] H. Basch, M. B. Robin, N. A. Kuebler, *Journal of Chemical Physics* **1967**, *47*, 1201.
- [215] E. B. Nielsen, J. A. Schellman, *Journal of Physical Chemistry* **1967**, *71*, 2297.
- [216] X.-B. Chen, W.-H. Fang, D.-C. Fang, *Journal of the American Chemical Society* **2003**, *125*, 9689.
- [217] D. Liu, W. H. Fang, X. Y. Fu, *Chemical Physics Letters* **2000**, *318*, 291.
- [218] C. J. Purnell, A. J. Barnes, S. Suzuki, D. F. Ball, W. J. Orville-Thomas, *Chem. Phys. FIELD Full Journal Title:Chemical Physics* **1976**, *12*, 77.
- [219] J. Lundell, M. Krajewska, M. Rasanen, *Journal of Molecular Structure* **1998**, *448*, 221.
- [220] M. E. Jacox, D. E. Milligan, *J. Chem. Phys. FIELD Full Journal Title:Journal of Chemical Physics* **1964**, *40*, 2457.
- [221] V. E. Bondybey, J. H. English, C. W. Mathews, R. J. Contolini, *J. Mol. Spectrosc. FIELD Full Journal Title:Journal of Molecular Spectroscopy* **1982**, *92*, 431.
- [222] J. H. Teles, G. Maier, B. A. Hess, Jr., L. J. Schaad, M. Winnewisser, B. P. Winnewisser, *Chem. Ber. FIELD Full Journal Title:Chemische Berichte* **1989**, *122*, 753.
- [223] S. Raunier, T. Chiavassa, F. Marinelli, A. Allouche, J.-P. Aycard, *J. Phys. Chem. A FIELD Full Journal Title:Journal of Physical Chemistry A* **2003**, *107*, 9335.
- [224] A. J. Barnes, *J. Mol. Struct. FIELD Full Journal Title:Journal of Molecular Structure* **1983**, *100*, 259.
- [225] S. R. Davis, L. Andrews, *J. Mol. Struct. FIELD Full Journal Title:Journal of Molecular Structure* **1987**, *157*, 103.
- [226] Z. Mielke, K. G. Tokhadze, M. Hulkiewicz, L. Schriver-Mazzuoli, A. Schriver, F. Roux, *J. Phys. Chem.* **1995**, *99*, 10498.
- [227] S. Ataka, H. Takeuchi, M. Tasumi, *J. Mol. Struct.* **1984**, *113*, 147.
- [228] S. Shin, A. Kurawaki, Y. Hamada, K. Shinya, K. Ohno, A. Tohara, M. Sato, *J. Mol. Struct.* **2006**, *791*, 30.
- [229] J. D. Dunitz, *X-Ray Analysis and the Structure of Organic Molecules*, **1979**.
- [230] J. D. Dunitz, Editors, et al., *Structure and Bonding, Vol. 36: Inorganic Chemistry and Spectroscopy*, **1979**.
- [231] D. G. Truhlar, Editor, *ACS Symposium Series, Vol. 263: Resonances in Electron-Molecule Scattering, van der Waals Complexes, and Reactive Chemical Dynamics*, **1984**.
- [232] R. L. Jones, *Journal of Molecular Spectroscopy* **1963**, *11*, 411.
- [233] A. C. Fantoni, W. Caminati, H. Hartwig, W. Stahl, *Journal of Molecular Structure* **2002**, *612*, 305.

- [234] P. R. Rablen, J. W. Lockman, W. L. Jorgensen, *Journal of Physical Chemistry A* **1998**, *102*, 3782.
- [235] S. Aloisio, P. E. Hintze, V. Vaida, in *Journal of Physical Chemistry A*, Vol. 106, **2002**, pp. 363.
- [236] W. Qian, S. Krimm, in *Journal of Physical Chemistry A*, Vol. 106, **2002**, pp. 6628.
- [237] B. Nelander, *Journal of Chemical Physics* **1980**, *72*, 77.
- [238] L. Andrews, G. L. Johnson, S. R. Davis, *Journal of Physical Chemistry* **1985**, *89*, 1710.
- [239] X. K. Zhang, E. G. Lewars, R. E. March, J. M. Parnis, *Journal of Physical Chemistry* **1993**, *97*, 4320.
- [240] S. W. Han, K. Kim, *Journal of Physical Chemistry* **1996**, *100*, 17124.
- [241] S. W. Han, K. Kim, *Journal of Molecular Structure* **1999**, *475*, 43.
- [242] M. Wierzejewska Hnat, H. Ratajczak, *Bulletin of the Polish Academy of Sciences, Chemistry* **1988**, *36*, 179.
- [243] N. Bakkas, Y. Bouteiller, A. Loutellier, J. P. Perchard, S. Racine, *Chemical Physics Letters* **1995**, *232*, 90.
- [244] S. Coussan, Y. Bouteiller, J. P. Perchard, V. Brenner, P. Millie, W. Q. Zheng, F. Talbot, *Journal of Chemical Physics* **1999**, *110*, 10046.
- [245] S. Coussan, Y. Bouteiller, A. Loutellier, J. P. Perchard, S. Racine, A. Peremans, W. Q. Zheng, A. Tadjeddine, *Chemical Physics* **1997**, *219*, 221.
- [246] K. V. Jovan Jose, R. Gadre Shridhar, K. Sundararajan, K. S. Viswanathan, *J Chem Phys* **2007**, *127*, 104501.
- [247] R. N. Perutz, J. J. Turner, *J. Chem. Soc., Faraday Trans. 2*, *69*(4), 452-61 **1973**.
- [248] N. Bakkas, Y. Bouteiller, A. Loutellier, J. P. Perchard, S. Racine, *J. Chem. Phys.* **1993**, *99*, 3335.
- [249] I. Glassman, **1996**.
- [250] J. A. Miller, C. F. Melius, *Combust. Flame FIELD Full Journal Title:Combustion and Flame* **1992**, *91*, 21.
- [251] N. M. Marinov, W. J. Pitz, C. K. Westbrook, M. J. Castaldi, S. M. Senkan, *Combust. Sci. Technol. FIELD Full Journal Title:Combustion Science and Technology* **1996**, *116-117*, 211.
- [252] M. J. Castaldi, S. M. Senkan, *Combust. Sci. Technol. FIELD Full Journal Title:Combustion Science and Technology* **1996**, *116-117*, 167.
- [253] X. Gu, R. I. Kaiser, *Acc. Chem. Res. FIELD Full Journal Title:Accounts of Chemical Research* **2009**, *42*, 290.
- [254] W. M. Harspool, **1995**.
- [255] T. Yu, M. C. Lin, *J. Am. Chem. Soc.* **1994**, *116*, 9571.
- [256] A. V. Friderichsen, J. G. Radziszewski, M. R. Nimlos, P. R. Winter, D. C. Dayton, D. E. David, G. B. Ellison, *J. Am. Chem. Soc.* **2001**, *123*, 1977.
- [257] A. Mardyukov, E. Sanchez-Garcia, R. Crespo-Otero, W. Sander, *Angew. Chem., Int. Ed.* **2009**, *48*, 4804.
- [258] E. N. Sharp, M. A. Roberts, D. J. Nesbitt, *Phys. Chem. Chem. Phys.* **2008**, *10*, 6592.
- [259] J. G. Radziszewski, M. R. Nimlos, P. R. Winter, G. Barney Ellison, *J. Am. Chem. Soc.* **1996**, *118*, 7400.
- [260] R. J. McMahon, M. C. McCarthy, C. A. Gottlieb, J. B. Dudek, J. F. Stanton, P. Thaddeus, *Astrophys. J.* **2003**, *590*, L61.
- [261] G. E. Davico, V. M. Bierbaum, C. H. DePuy, G. B. Ellison, R. R. Squires, *J. Am. Chem. Soc.* **1995**, *117*, 2590.
- [262] S. M. Mattar, *J. Phys. Chem. A* **2007**, *111*, 251.

- [263] J. E. Bennett, B. Mile, A. Thomas, *Proc. R. Soc. London, Ser. A FIELD Full Journal Title:Proceedings of the Royal Society of London, Series A: Mathematical, Physical and Engineering Sciences* **1966**, 293, 246.
- [264] J. E. Bennett, B. Mile, A. Thomas, *Chem. Commun. (London) FIELD Full Journal Title:Chemical Communications (London)* **1965**, 265.
- [265] P. H. Kasai, E. Hedaya, E. B. Whipple, *J. Amer. Chem. Soc. FIELD Full Journal Title:Journal of the American Chemical Society* **1969**, 91, 4364.
- [266] J. G. Radziszewski, *Chem. Phys. Lett.* **1999**, 301, 565.
- [267] J. Pacansky, J. Bargon, *J. Am. Chem. Soc.* **1975**, 97, 6896.
- [268] A. Lapinski, J. Spanget-Larsen, M. Langgard, J. Waluk, J. G. Radziszewski, *J. Phys. Chem. A FIELD Full Journal Title:Journal of Physical Chemistry A* **2001**, 105, 10520.
- [269] C. Barckholtz, M. J. Fadden, C. M. Hadad, *Journal of Physical Chemistry A* **1999**, 103, 8108.
- [270] M. J. Fadden, C. Barckholtz, C. M. Hadad, *Journal of Physical Chemistry A* **2000**, 104, 3004.
- [271] G. D. Edwards, C. A. Cantrell, S. Stephens, B. Hill, O. Goyea, R. E. Shetter, R. L. Mauldin, III, E. Kosciuch, D. J. Tanner, F. L. Eisele, *Analytical Chemistry* **2003**, 75, 5317.
- [272] K. Tonokura, Y. Norikane, M. Koshi, Y. Nakano, S. Nakamichi, M. Goto, S. Hashimoto, M. Kawasaki, M. P. S. Andersen, M. D. Hurley, T. J. Wallington, *Journal of Physical Chemistry A* **2002**, 106, 5908.
- [273] S. J. Blanksby, G. B. Ellison, *Accounts of Chemical Research* **2003**, 36, 255.
- [274] I. V. Tokmakov, G.-S. Kim, V. V. Kislov, A. M. Mebel, M. C. Lin, *Journal of Physical Chemistry A* **2005**, 109, 6114.
- [275] J. K. Merle, C. M. Hadad, *Journal of Physical Chemistry A* **2004**, 108, 8419.
- [276] T. Yu, M. C. Lin, *Journal of the American Chemical Society* **1994**, 116, 9571.
- [277] G. da Silva, J. W. Bozzelli, *Journal of Physical Chemistry A* **2008**, 112, 3566.
- [278] X. Gu, F. Zhang, R. I. Kaiser, *Chemical Physics Letters* **2007**, 448, 7.
- [279] X. Fang, R. Mertens, C. von Sonntag, *Journal of the Chemical Society, Perkin Transactions 2: Physical Organic Chemistry* **1995**, 1033.
- [280] S. Naumov, C. von Sonntag, *Journal of Physical Organic Chemistry* **2005**, 18, 586.
- [281] A. M. Mebel, M. C. Lin, *Journal of the American Chemical Society* **1994**, 116, 9577.
- [282] J. L. Weisman, M. Head-Gordon, *Journal of the American Chemical Society* **2001**, 123, 11686.
- [283] B. K. Carpenter, *Journal of the American Chemical Society* **1993**, 115, 9806.
- [284] C. Barckholtz, M. J. Fadden, C. M. Hadad, *Journal of Physical Chemistry A* **1999**, 103, 8108.
- [285] M. J. Fadden, C. M. Hadad, *Journal of Physical Chemistry A* **2000**, 104, 8121.
- [286] A. V. Friderichsen, J. G. Radziszewski, M. R. Nimlos, P. R. Winter, D. C. Dayton, D. E. David, G. B. Ellison, *Journal of the American Chemical Society* **2001**, 123, 1977.
- [287] A. Lapinski, J. Spanget-Larsen, M. Langgard, J. Waluk, J. G. Radziszewski, *Journal of Physical Chemistry A* **2001**, 105, 10520.
- [288] J. G. Radziszewski, M. R. Nimlos, P. R. Winter, G. B. Ellison, *J. Am. Chem. Soc.* **1996**, 118, 7400.
- [289] W. Sander, *Angew. Chem.* **1986**, 98, 255.
- [290] W. W. Sander, *J. Org. Chem.* **1989**, 54, 333.
- [291] W. Sander, G. Bucher, S. Wierlacher, *Chem. Rev.* **1993**, 93, 1583.

- [292] C. Barckholtz, M. J. Fadden, C. M. Hadad, *J. Phys. Chem. A* **1999**, *103*, 8108.
- [293] R. F. Sawyer, *Symp. (Int.) Combust., [Proc.] FIELD Full Journal Title: Symposium (International) on Combustion, [Proceedings]* **1992**, *24th*, 1423.
- [294] N. S. Allen, M. C. Marin, M. Edge, D. W. Davies, J. Garrett, F. Jones, S. Navaratnam, B. J. Parsons, *J. Photochem. Photobiol.* **1999**, *126*, 135.
- [295] A. Ajayaghosh, S. Das, M. V. George, *J. Polym. Sci., Part A: Polym. Chem.* **1993**, *31*, 653.
- [296] J. Eichler, C. P. Herz, I. Naito, W. Schnabel, *J. Photochem.* **1980**, *12*, 225.
- [297] C. P. Herz, J. Eichler, *Farbe Lack* **1979**, *85*, 933.
- [298] C. Kolano, G. Bucher, H. H. Wenk, M. Jaeger, O. Schade, W. Sander, *J. Phys. Org. Chem.* **2004**, *17*, 207.
- [299] C. S. Colley, D. C. Grills, N. A. Besley, S. Jockusch, P. Matousek, A. W. Parker, M. Towrie, N. J. Turro, P. M. W. Gill, M. W. George, *J. Am. Chem. Soc.* **2002**, *124*, 14952.
- [300] G. W. Sluggett, P. F. McGarry, I. V. Koptug, N. J. Turro, *J. Am. Chem. Soc.* **1996**, *118*, 7367.
- [301] G.-J. Nam, W. Xia, J. Park, M. C. Lin, *Chem. Phys. Processes Combust.* **1999**, 304.
- [302] G.-J. Nam, W. Xia, J. Park, M. C. Lin, *J. Phys. Chem. A* **2000**, *104*, 1233.
- [303] C. E. Brown, A. G. Neville, D. M. Rayner, K. U. Ingold, J. Luszyk, *Aust. J. Chem.* **1995**, *48*, 363.
- [304] T. J. Wallington, P. Dagaut, M. J. Kurylo, *Chem. Rev. FIELD Full Journal Title: Chemical Reviews (Washington, DC, United States)* **1992**, *92*, 667.
- [305] P. J. Krusic, T. A. Rettig, *J. Amer. Chem. Soc.* **1970**, *92*, 722.
- [306] L. Grossi, G. Placucci, *Chem. Commun.* **1985**, 943.
- [307] J. E. Bennett, B. Mile, *Trans. Faraday Soc.* **1971**, *67*, 1587.
- [308] O. Ito, T. Sakaguchi, M. Matsuda, *J. Chem. Soc., Faraday Trans.* **1978**, *74*, 1188.
- [309] A. Mardyukov, E. Sanchez-Garcia, R. Crespo-Otero, W. Sander, *Angew. Chem., Int. Ed.* **2009**, *48*, 4804.
- [310] A. Mardyukov, W. Sander, *Chem.--Eur. J.* **2009**, *15*, 1462.
- [311] G.-J. Nam, W. Xia, J. Park, M. C. Lin, *J. Phys. Chem. A* **2000**, *104*, 1233.
- [312] M. Hoshino, R. Konishi, H. Seto, H. Seki, H. Sonoki, T. Yokoyama, H. Shimamori, *Res. Chem. Intermed.* **2001**, *27*, 189.
- [313] T. Seta, M. Nakajima, A. Miyoshi, *Journal of Physical Chemistry A* **2006**, *110*, 5081.
- [314] B. Bohn, C. Zetzsch, *Physical Chemistry Chemical Physics* **1999**, *1*, 5097.
- [315] R. Volkamer, B. Klotz, I. Barnes, T. Imamura, K. Wirtz, N. Washida, K. H. Becker, U. Platt, *Physical Chemistry Chemical Physics* **2002**, *4*, 1598.
- [316] C.-C. Chen, J. W. Bozzelli, J. T. Farrell, *Journal of Physical Chemistry A* **2004**, *108*, 4632.
- [317] S. Raoult, M.-T. Rayez, J.-C. Rayez, R. Lesclaux, *Physical Chemistry Chemical Physics* **2004**, *6*, 2245.
- [318] J. S. Poole, X. Shi, C. M. Hadad, M. S. Platz, *Journal of Physical Chemistry A* **2005**, *109*, 2547.
- [319] I. V. Tokmakov, M. C. Lin, *Journal of Physical Chemistry A* **2002**, *106*, 11309.
- [320] M. P. DeMatteo, J. S. Poole, X. Shi, R. Sachdeva, P. G. Hatcher, C. M. Hadad, M. S. Platz, *J. Am. Chem. Soc.* **2005**, *127*, 7094.
- [321] R. Crespo-Otero, E. Sanchez-Garcia, R. Suardiaz, L. A. Montero, W. Sander, *Chem. Phys.* **2008**, *353*, 193.
- [322] S. Hammerum, *J. Am. Chem. Soc.* **2009**, *131*, 8627.

- [323] A. Mardyukov, E. Sanchez-Garcia, R. Crespo-Otero, W. Sander, *Angew. Chem., Int. Ed.* **2009**, *48*, 4804.
- [324] J. G. Radziszewski, M. R. Nimlos, P. R. Winter, G. B. Ellison, *Journal of the American Chemical Society* **1996**, *118*, 7400.
- [325] G. P. Ayers, A. D. E. Pullin, *Chemical Physics Letters* **1974**, *29*, 609.
- [326] J. P. Perchard, *Chemical Physics* **2001**, *273*, 217.
- [327] Y. Bouteiller, J. P. Perchard, *Chemical Physics* **2004**, *305*, 1.
- [328] J. Ceponkus, G. Karlstroem, B. Nelander, *Journal of Physical Chemistry A* **2005**, *109*, 7859.
- [329] A. Engdahl, B. Nelander, *Journal of Chemical Physics* **1987**, *86*, 4831.
- [330] G. P. Ayers, A. D. E. Pullin, *Spectrochim. Acta, Part A* **1976**, *32A*, 1641.
- [331] G. P. Ayers, A. D. E. Pullin, *Spectrochim. Acta, Part A* **1976**, *32A*, 1629.
- [332] G. P. Ayers, A. D. E. Pullin, *Spectrochim. Acta, Part A* **1976**, *32A*, 1689.
- [333] Y. Zhao, D. G. Truhlar, *Acc. Chem. Res.* **2008**, *41*, 157.
- [334] Y. Zhao, D. G. Truhlar, *J. Phys. Chem. A* **2008**, *112*, 1095.
- [335] B. M. Cheng, Y. P. Lee, J. F. Ogilvie, *Chem. Phys. Lett.* **1988**, *151*, 109.
- [336] A. Engdahl, G. Karlstrom, B. Nelander, *Journal of Chemical Physics* **2003**, *118*, 7797.
- [337] A. Engdahl, B. Nelander, *J. Chem. Phys. FIELD Full Journal Title:Journal of Chemical Physics* **2005**, *122*, 126101/1.
- [338] L. H. P. Weldon, C. L. Wilson, *J. Chem. Soc.* **1946**, 235.
- [339] C.-C. Chen, J. W. Bozzelli, J. T. Farrell, *J. Phys. Chem. A FIELD Full Journal Title:Journal of Physical Chemistry A* **2004**, *108*, 4632.
- [340] I. V. Tokmakov, M. C. Lin, *J. Phys. Chem. A FIELD Full Journal Title:Journal of Physical Chemistry A* **2002**, *106*, 11309.
- [341] Y. Zhao, D. G. Truhlar, *J. Chem. Theory Comput. FIELD Full Journal Title:Journal of Chemical Theory and Computation* **2007**, *3*, 289.
- [342] M. P. DeMatteo, J. S. Poole, X. Shi, R. Sachdeva, P. G. Hatcher, C. M. Hadad, M. S. Platz, *J. Am. Chem. Soc. FIELD Full Journal Title:Journal of the American Chemical Society* **2005**, *127*, 7094.
- [343] T. H. Lay, J. W. Bozzelli, J. H. Seinfeld, *J. Phys. Chem. FIELD Full Journal Title:Journal of Physical Chemistry* **1996**, *100*, 6543.
- [344] J. Dolinova, R. Ruazicka, R. Kurkova, J. Klanova, P. Klan, *Environ. Sci. Technol. FIELD Full Journal Title:Environmental Science & Technology* **2006**, *40*, 7668.
- [345] J. R. Alvarez-Idaboy, N. Mora-Diez, R. J. Boyd, A. Vivier-Bunge, *J. Am. Chem. Soc. FIELD Full Journal Title:Journal of the American Chemical Society* **2001**, *123*, 2018.
- [346] J. R. Alvarez-Idaboy, N. Mora-Diez, A. Vivier-Bunge, *J. Am. Chem. Soc. FIELD Full Journal Title:Journal of the American Chemical Society* **2000**, *122*, 3715.
- [347] R. Volkamer, B. Klotz, I. Barnes, T. Imamura, K. Wirtz, N. Washida, K. H. Becker, U. Platt, *Phys. Chem. Chem. Phys. FIELD Full Journal Title:Physical Chemistry Chemical Physics* **2002**, *4*, 1598.
- [348] B. Klotz, R. Volkamer, M. D. Hurley, M. P. S. Andersen, O. J. Nielsen, I. Barnes, T. Imamura, K. Wirtz, K.-H. Becker, U. Platt, T. J. Wallington, N. Washida, *Phys. Chem. Chem. Phys. FIELD Full Journal Title:Physical Chemistry Chemical Physics* **2002**, *4*, 4399.
- [349] L. Zhu, J. W. Bozzelli, *J. Phys. Chem. A FIELD Full Journal Title:Journal of Physical Chemistry A* **2003**, *107*, 3696.

- [350] H.-F. Chen, C.-W. Liang, J. J. Lin, Y.-P. Lee, J. F. Ogilvie, Z. F. Xu, M. C. Lin, *J. Chem. Phys. FIELD Full Journal Title:Journal of Chemical Physics* **2008**, *129*, 174303/1.
- [351] C.-M. Tseng, Y. T. Lee, M.-F. Lin, C.-K. Ni, S.-Y. Liu, Y.-P. Lee, Z. F. Xu, M. C. Lin, *J. Phys. Chem. A FIELD Full Journal Title:Journal of Physical Chemistry A* **2007**, *111*, 9463.
- [352] Z. F. Xu, M. C. Lin, *J. Phys. Chem. A FIELD Full Journal Title:Journal of Physical Chemistry A* **2006**, *110*, 1672.
- [353] R. L. Bell, D. L. Taveras, T. N. Truong, J. Simons, *Int. J. Quantum Chem. FIELD Full Journal Title:International Journal of Quantum Chemistry* **1997**, *63*, 861.
- [354] M. N. Glukhovtsev, R. D. Bach, A. Pross, L. Radom, *Chem. Phys. Lett. FIELD Full Journal Title:Chemical Physics Letters* **1996**, *260*, 558.
- [355] R. Cypres, B. Bettens, *Tetrahedron FIELD Full Journal Title:Tetrahedron* **1974**, *30*, 1253.
- [356] A. B. Lovell, K. Brezinsky, I. Glassman, *Int. J. Chem. Kinet. FIELD Full Journal Title:International Journal of Chemical Kinetics* **1989**, *21*, 547.
- [357] J. F. Unsworth, D. J. Barratt, P. T. Roberts, Editors, *Coal Science and Technology, Vol. 19: Coal Quality and Combustion Performance, An International Perspective*, **1992**.
- [358] P. C. Painter, M. M. Coleman, *Fuel* **1979**, *58*, 301.
- [359] D. W. Turner, R. L. Andrews, C. W. Siegmund, *AIChE Symposium Series* **1972**, *68*, 55.
- [360] D. W. Turner, C. W. Siegmund, R. L. Andrews, *Combustion (New York, 1929)* **1972**, *44*, 21.
- [361] R. A. Perry, D. L. Siebers, *Nature (London)* **1986**, *324*, 657.
- [362] L. R. Snyder, *Anal. Chem.* **1969**, *41*, 1084.
- [363] G. W. Mushrush, G. O. Spencer, E. J. Beal, J. H. Wynne, J. M. Hughes, D. R. Hardy, *Pet. Sci. Technol.* **2000**, *18*, 901.
- [364] A. Lifshitz, C. Tamburu, A. Suslensky, *J. Phys. Chem.* **1989**, *93*, 5802.
- [365] J. C. Mackie, M. B. Colket, III, P. F. Nelson, *J. Phys. Chem.* **1990**, *94*, 4099.
- [366] R. Liu, T. T. S. Huang, J. Tittle, D. Xia, *J. Phys. Chem. A* **2000**, *104*, 8368.
- [367] E. Ikeda, P. Nicholls, J. C. Mackie, *Proc. Combust. Inst.* **2000**, *28*, 1709.
- [368] M. E. Vaschetto, B. A. Retamal, A. P. Monkman, M. Springborg, *J. Phys. Chem. A* **1999**, *103*, 11096.
- [369] S. Ruhemann, *Braunkohlle* **1929**, *28*, 749.
- [370] X. Cheng, *THEOCHEM* **2005**, *731*, 89.
- [371] X. L. Cheng, Y. Y. Zhao, Z. Y. Zhou, *THEOCHEM* **2004**, *678*, 17.
- [372] X. Cheng, L. Niu, Y. Zhao, Z. Zhou, *Spectrochimica Acta, Part A: Molecular and Biomolecular Spectroscopy* **2004**, *60A*, 907.
- [373] P. H. Kasai, D. McLeod, Jr., *J. Amer. Chem. Soc.* **1972**, *94*, 720.
- [374] H. J. Bower, J. A. McRae, M. C. R. Symons, *Chem. Commun.* **1967**, 542.
- [375] O. Kikuchi, Y. Hondo, K. Morihashi, M. Nakayama, *Bull. Chem. Soc. Jpn.* **1988**, *61*, 291.
- [376] O. Kikuchi, Y. Hondo, Y. Yokoyama, K. Morihashi, M. Nakayama, *Bull. Chem. Soc. Jpn.* **1991**, *64*, 3448.
- [377] S. J. Blanksby, G. B. Ellison, *Acc. Chem. Res.* **2003**, *36*, 255.
- [378] J. L. Weisman, M. Head-Gordon, *J. Am. Chem. Soc.* **2001**, *123*, 11686.
- [379] A. D. Becke, *Journal of Chemical Physics* **1993**, *98*, 5648.
- [380] C. Lee, W. Yang, R. G. Parr, *Physical Review B: Condensed Matter and Materials Physics* **1988**, *37*, 785.

-
- [381] B. Miehlich, A. Savin, H. Stoll, H. Preuss, *Chemical Physics Letters* **1989**, 157, 200.
- [382] A. D. McLean, G. S. Chandler, *Journal of Chemical Physics* **1980**, 72, 5639.
- [383] R. Krishnan, J. S. Binkley, R. Seeger, J. A. Pople, *Journal of Chemical Physics* **1980**, 72, 650.
- [384] D. E. Woon, T. H. Dunning, Jr., *Journal of Chemical Physics* **1993**, 98, 1358.
- [385] R. A. Kendall, T. H. Dunning, Jr., R. J. Harrison, *Journal of Chemical Physics* **1992**, 96, 6796.
- [386] T. H. Dunning, Jr., *Journal of Chemical Physics* **1989**, 90, 1007.
- [387] M. J. e. a. G. G. Frisch, Inc.: Pittsburgh, PA, 2003.
- [388] H. E. Bigelow, D. B. Robinson, *Organic Syntheses* **1942**, 22, 28.

Acknowledgement

This thesis arose in part out of years of research that has been done since I joined to group of Prof. Sander. During my work I had a deal with a great number of people whose contribution in assorted ways to the research. And it is pleasure to convey my gratitude to them all in my acknowledgment.

I would also like to thank Prof. Dr. Martina Havenith for kindly acting as referee.

I would like to express my special thanks to Dr. Elsa Sanchez-Garcia for her fruitful suggestion at various stages of this research work. Especialy, her crutial contribution in the theoretical part of this work. Also I would like to thank Dr Rachel Otero-Crespo for theoretical calculations; it was great to work with you.

Especially, I expend my appreciation to Dr. Sugumar Venkataramani for gave me a lot of suggestion during my thesis, writing and later carefully read and corrected my thesis and of course for his constructive comments on this thesis.

Special thanks to all as well former and current members with whom I spent my research time in Bochum. In this regard, I would like to thank Dr. Torres-Alacan, Patrik, Christopher, Melanie, Andre, Dr. Christina.Toenshof, Y-am, Fee, Alex, Sandra, Saouli, Björn, Arun, Tuhin, Stefan, Andreas, Matthias, Matthias Böhm, Arndt Richter, Dr. Dirk Grote, Laura, Magdalena, Dr. Kavitha Velappan, Sunanda, Rafael.

I would like to thank to Dr. Dirk Grote for reading and corrected my thesis.

I would like to thank Sandra Müller for helping me to format my thesis.

I would like to thank to Torsten Poerschke and Anja Metzelthin from the group of Pr. Dr. Martina Havenith, for the collaboration work and showing me the Helium Cluster Machine.

Thanks to Prof. Dr. Götz Bucher and Prof. Dr. Holger Bettinger for their great scientific contribution during time in Bochum.

I would like to thank Herr Torsten Haenschke for his huge help computer related problems and for keeping the computers running all the time. I express my thanks to Frau Urlike Steger for help in the administrative work. I wish to thank Frau Heidemarie Joppich and Herr Klaus Goman for their great work, assistance, help, and maintenance of the laboratory equipments. I also thank to Frau Barbara Schröder for help related with chemicals.

I would like to thank to Research School for assistance and financial support.

Thanks to Mrs. Talbot and Mr. Koch of the Graduate school of Chemistry and Biochemistry for the administrative works.

Last, but certainly not least, my special thanks to my mother and for bring me to this wonderful world, and to my brother supporting and encouraging me to get the good educations, and also to my wife for her patience, understanding and accompanying, and also to my wonderful daughter Meline. I dedicate his thesis to them.

CURRICULUM VITAE

PERSONAL DATA

Name : Artur Mardukov
Date of Birth : 15. 10. 1977
Parents : N. Mardukov and S. Arzumanyan
Marital status : Married
Nationality : Armenian

EDUCATION

1984-1994 : Yerevan's school №171
1997-2001 : Yerevan State University, Faculty of Chemist-
Bachelors of Science obtained.
2001-2003 : Yerevan State University, Faculty of Chemist-
Master of Science obtained.
2003-2005 : Senior Researcher in the Molecule Structure
Research Center, NAS Armenia
since 2005 : Ruhr-Universität-Bochum, PhD-student

LANGUAGES

Armenian and Russian – fluently, English – well, German – Basic.

PUBLICATIONS

1. Kurtikyan T. S., Mardukov A. N., Kazaryan R.K., Goodwin J. A. 'Microporous porphyrin assemblies. Interaction of NO₂ gas with sublimed layers of *meso*-mono -4-pyridyl-triphenylporphyrinato cobalt (II)'; "Journal of Porphyrins and Phthalocyanines", 2003, vol. 7, p. 775-779.
2. Kurtikyan T. S., Mardukov A. N., Goodwin J. A. 'Interaction of Nitrogen Oxides with Sublimed Layers of (*meso*-Tetraphenylporphyrinatocobalt (II); IR Evidence of Oxo-Transfer from (Nitro) porphyrinatocobalt (III) to Free Nitric Oxide'; "Inorganic Chemistry", 2003, vol. 45, No. 25, p. 8489-8493.
3. Goodwin, John; Kurtikyan, Tigran; Standard, Jean; Walsh, Rosa; Zheng, Bin; Parmley, Diedre; Howard, James; Green, Shaun; Mardukov, Arthur; Przybyla, David E. Variation of Oxo-Transfer Reactivity of (Nitro)Cobalt Picket Fence Porphyrin with Oxygen-Donating Ligands. *Inorganic Chemistry* (2005), 44(7), 2215-2223.
4. Elsa Sanchez-García, Arthur Mardukov, Marc Studentkowski, Luis A. Montero, Wolfram Sander. Furan-Formic Acid Dimers: An ab Initio and Matrix Isolation Study . *J. Phys. Chem. A*, 110 (51), 13775 -13785, 2006.

5. Kurtikyan, Tigran S.; Markaryan, Emil R.; Mardyukov, Artur N.; Goodwin, John A. Low-Temperature Spectral Observation of the First Six-Coordinate Nitrosyl Complexes of Cobalt(II) meso-Tetratolylporphyrin with Trans Nitrogen Base Ligands. *Inorganic Chemistry* (2007), 46(5), 1526-1528.
6. Mardyukov, Artur; Sanchez-Garcia, Elsa; Rodziewicz, Pawel; Doltsinis, Nikos L.; Sander, Wolfram. Formamide Dimers: A Computational and Matrix Isolation Study. *Journal of Physical Chemistry A* (2007), 111(42), 10552-10561.
7. Sanchez-Garcia, Elsa; Mardyukov, Artur; Tekin, Adem; Crespo-Otero, Rachel; Montero, Luis A.; Sander, Wolfram; Jansen, Georg. Ab initio and matrix isolation study of the acetylene-furan dimer. *Chemical Physics* (2008), 343(2-3), 168-185.
8. Kurtikyan, T. S.; Mardyukov, A. N.; Goodwin, J. A. Direct synthesis of six-coordinate nitro complexes of cobalt meso-tetraphenylporphyrinate with trans-O-donor ligands. *Russian Journal of Coordination Chemistry* (2008), 34(8), 606-611.
9. Mardyukov, Artur; Sanchez-Garcia, Elsa; Sander, Wolfram. Matrix Isolation and Ab Initio Study of the Noncovalent Complexes between Formamide and Acetylene. *Journal of Physical Chemistry A* (2009), 113(6), 1086-1095.
10. Mardyukov, Artur; Sander, Wolfram. Matrix isolation and spectroscopic characterization of the phenylperoxy radical and its rearranged products. *Chemistry--A European Journal* (2009), 15(6), 1462-1467.
11. Mardyukov, Artur; Sanchez-Garcia, Elsa; Crespo-Otero, Rachel; Sander, Wolfram. Interaction and Reaction of the Phenyl Radical with Water: A Source of OH Radicals. *Angewandte Chemie, International Edition* (2009), 48(26), 4804-4807,
12. Mardyukov, Artur; Sander Wolfram. Matrix Isolation and IR Characterization of the Benzoyl and Benzoyl Peroxy Radicals. *European Journal of Organic Chemistry* (2010), 15, 2904-2909.
13. Mardyukov, Artur; Crespo-Otero, Rachel; Sanchez-Garcia, Elsa; Sander Wolfram. Photochemistry and reactivity of the phenyl radical – water system: A matrix isolation and computational study. *Chemistry--A European Journal* (2010) accepted (inside cover).

Conferences Attended:

1. "Aggregation of small molecules in cryogenic matrices. Non-covalent complexes of Formamide-Acetylene and Formamide-Formic Acid"

Mardyukov, Artur; Sanchez-Garcia, Elsa; Sander, Wolfram. At the International Symposium of Reactive Intermediates and Unstable Molecules (ISRIUM 2007), Ascona, Switzerland, (19-24 August 2007).

2. "Matrix Isolation and Photochemistry of Phenyl Peroxy Radical"

Artur Mardyukov, Wolfram Sander. 19th IUPAC Conference on Physical Organic Chemistry, The Royal University of Santiago de Compostela, Spain, (13-18 July 2008).

3. "Matrix-Isolated Spectra of Phenyl Peroxy Radical"

Artur Mardyukov, Wolfram Sander. 7th International Conference of Low Temperature Chemistry, Helsinki, Finland, (24-29 August 2008).

4. "Photochemistry of N-methylformamide: Monomers, Dimers"

Mardyukov, Artur; Sanchez-Garcia, Elsa; Sander, Wolfram. On non-covalent interactions in chemistry and biochemistry. Czocha castle, Poland (21-28 September 2008) (**oral presentation**).

5. "Complete Story of the Reaction of Phenyl Radical with Water: A Matrix Isolation Study."

Mardyukov, Artur; Sanchez-Garcia, Elsa; Sander, Crespo-Otero, Rachel; Sander, Wolfram. At the International Symposium of Reactive Intermediates and Unstable Molecules (ISRIUM 2009), Liblice Castle near Prague, Czech Republic, (5-10 July 2009).

6. "Matrix Isolation and Photochemistry of Phenyl Radical – Water System"

Mardyukov, Artur; Sanchez-Garcia, Elsa; Sander, Crespo-Otero, Rachel; Sander, Wolfram. 7th Seminars of Advanced Studies on Molecular Design and Bioinformatics: Molecular Interactions, Havana, Cuba, (22-28 August 2009).

Workshops Attended:

1. Workshop Forschergruppe 618. Ruhr-University Bochum, (13 February 2006) (Oral presentation).
2. Workshop Forschergruppe 618. Ruhr-University Bochum, (06 November 2006) (Oral presentation).
3. Workshop Forschergruppe 618. Ruhr-University Bochum, 12 October 2007 (Oral presentation).
4. Workshop Forschergruppe 618. Ruhr-University Bochum, 10 February 2010 (Oral presentation).

Chemistry Skills:

Experience in various synthetic and separation techniques involved in a several synthesis of desire molecules, in yield improvement and process development.

Experience in matrix isolation techniques and Flash Vacuum Pyrolysis methods.

Knowledge in vacuum techniques and usage of LASER.

Experience in quantum chemical calculations (Density Functional Theory and ab initio methods)

Knowledge in Mass spectrometry, NMR, IR and UV-Visible spectroscopic techniques
Computer Skills:

Expertise in Windows, worked in Linux operating systems

Handled various scientific packages such as Gaussian (98/03 Windows version and Linux versions), Molpro, Gauss view, Molden, Molekel, Pov Ray, Povchem, Chemdraw, ISIS Draw, WinNMR and OPUS.

Experience in MS-Office and CorelDraw

Instruments Handled:

Bruker IFS/66 and IFS/66s FTIR spectrometers

Bruker DPX-200 NMR spectrometer equipped with auto-sampler

Hewlett Packard 8452A Diode-array Spectrophotometer

Lambda Physics Excimer lasers

Applied Photophysics UK KN-020 Flash Kinetic Spectrometer

Applied Photophysics SP- Quanta Ray GCR-2 Nd-YAG LASER Flash Kinetic Spectrometer

Hewlett Packard 5892 Series II Gas Chromatography equipped with HP5972 Series Mass Selective Detector (GCMS)